NASA CONTRACTOR REPORT

NASA CR-66897-3

NASA CR-66897-3

SUBSTANTIATION DATA FOR

HYPERSONIC CRUISE VEHICLE WING STRUCTURE EVALUATION

Volume 3, Sections 23 through 27

by P. P. Plank, I. F. Sakata, G. W. Davis, and C. C. Richie

Prepared by
LOCKHEED MISSILES & SPACE COMPANY
Sunnyvale, California
for Langley Research Center

NATIONAL AERONAUTICS AND SPACE ADMINISTRATION • WASHINGTON, D.C.
FEBRUARY 1970

NASA CR-66897-3

SUBSTANTIATION DATA FOR

HYPERSONIC CRUISE VEHICLE

WING STRUCTURE EVALUATION

Volume 3, Sections 23 through 27

15 February 1970

by

P. P. Plank, I. F. Sakata, G. W. Davis, and C. C. Richie

Prepared under Contract No. NAS 1-7573
Lockheed Missiles & Space Company
Sunnyvale, California

for Langley Research Center

NATIONAL AERONAUTICS AND SPACE ADMINISTRATION

PRECEDING PAGE BLANK NOT FILMED.

CONTENTS

PRECEDING PAGE BLANK NOT FILMED.

SUMMARY

An analytical and experimental evaluation was performed for several promising structural concepts to provide the basis of minimum total-system-cost for selection of the best concepts for the design of a hypersonic vehicle wing.

Results, procedures, and principal justification of results are presented in reference 1. Detailed substantiation data are given herein. Each major analysis is presented in a separate section. Vehicle loads and temperatures are given with each structural analysis that influences weight. In addition to the weight analysis, fabrication cost, performance penalties (surface roughness drag), reliability, and total-system-cost analyses are presented.

Reference 1. Plank, P. P.; Sakata, I. F.; Davis, G. W.; and Richie, C. C.: Hypersonic Cruise Vehicle Wing Structure Evaluation, NASA CR-1568, 1970.

PRECEDING PAGE BLANK NOT FILMED.

INTRODUCTION

The utility of a hypersonic cruise vehicle depends upon a low structural mass fraction in a high-temperature environment. Unfortunately, this requirement exceeds the limits of state-of-the-art structures. The only hypersonic structures flown to date have been the X-15 research airplane and the ASSET unmanned lifting reentry test vehicle, both of which are unsuitable for cruising flight.

For the past several years, the NASA Langley Research Center and other agencies have been investigating promising structural concepts, such as those discussed in references 2, 3, and 4, and the 1967 Conference on Hypersonic Aircraft Technology (ref. 5) was devoted to the subject.

An evaluation was performed of promising wing structure concepts to the same in-depth analyses, including all known environmental structural considerations that could affect the four evaluation factors: weight, cost, performance, and reliability. These factors were then interacted in a total-system-cost study for a system range-payload capability of 205 billion ton-miles to provide the basis for selecting the best structural concept for the wing structure of minimum total-system-cost.

Results of this structural evaluation are reported in reference 1. This reference also includes the procedures and principal justification of results, whereas this report gives detailed substantiation of the results in reference 1. Principal analytical and test efforts are presented in separate sections. This report is bound as three separate volumes.

REFERENCES

2. Heldenfels, R. R.: Structural Prospects for Hypersonic Air Vehicle ICAS paper, 1966.

3. Plank, P. P.; and MacMiller, C. I.: Analytical Investigation of Candidate Thermal-Structural Concepts Applicable to Wing, Fuselage, and Inlet Structure of a Manned Hypersonic Vehicle. AFFDL-TR-66-15, 1966 (conf).

4. Plank, P. P.: Hypersonic Thermal-Structural Concept Trends. SAE paper 660678, 1966.

5. NASA-SP-148 (Conf). Conference on Hypersonic Technology, Ames Research Center, 1967.

PRECEDING PAGE BLANK NOT FILMED.

ACKNOWLEDGEMENT

This investigation was conducted under NASA Contract No. NAS1-7573, Research and Development Program for Development and Validation of Structural Concepts for a Hypersonic Cruise Vehicle Wing Structure. The study was originated at the Lockheed-California Company, Burbank, California and completed at Lockheed Missiles & Space Company, Sunnyvale, California. P. P. Plank was the Program Technical Manager, I. F. Sakata and G. W. Davis the Project Engineers, and C. C. Richie was head of structural concept optimization. The other contributors to the program are acknowledge at each section.

Four Lockheed-California Company personnel acted in an advisory capacity. They are L. W. Nelson, Structure Division Engineer, Structures Division; E. J. Himmel, Department Manager, Stress Analysis; W. J. Crichlow, Department Manager, Advanced Materials and Structural Mechanics; and M. G. Childers, Manager, Physical Sciences Laboratory Development Engineer.

Dr. M. S. Anderson, L. R. Jackson, and J. C. Robinson of the Structures Research Division, NASA Langley Research Center, Hampton, Virginia, were the Program Manager, Technical Representative of the Contracting Officer (TRCO), and Assistant TRCO, respectively, for the project.

Section 23

COST ANALYSIS

by

E. W. Reed, D. E. Sherwood, and I. F. Sakata

PRECEDING PAGE BLANK NOT FILMED.

CONTENTS

PRECEDING PAGE BLANK NOT FILMED.

TABLES

PRECEDING PAGE BLANK NOT FILMED.

ILLUSTRATIONS

PRECEDING PAGE BLANK NOT FILMED.

SYMBOLS

A,B,C,D,E	Costing zones defined in figure 23-17
a,b	x and y distances between simply supported edges of plate
a/b	Panel aspect ratio
BL	Butt line
CER	Cost estimating relationship
ECM	Electrochemical milling
GW	Gross weight
L	Length
S	Surface area
Sta	Wing station

Subscripts

ℓe	Denotes leading edge
P	Denotes panel
S	Denotes substructure
T	Denotes total

Section 23

COST ANALYSIS

The basis for evaluating and rating the structure concepts is minimum total system cost; therefore, manufacturing cost information for the various vehicle components of the baseline vehicle (gross weight = 550 000 lb). The cost estimates (expressed in 1968 dollars) were determined for engineering purposes only, using current labor rates and material prices. The data generated are considered sufficiently accurate to provide valid cost information so that a relative comparison of concepts can be made.

Facilities and process development costs were not included. It was further assumed that clean-room conditions would be available for fabricating the vehicle components, that suitable controlled-atmosphere furnaces and process baths have been installed, and that required special equipment and machine tools will have been developed and installed.

Initial Panel Screening Costs

Comparative costs for the candidate structural panels and heat shield combinations, as applicable, were determined on the basis of the aforementioned premise. These costs were determined by a detailed production cost analysis of typical panels sized for representative hypersonic cruise vehicle loads and included recurring and nonrecurring costs encompassing material, labor, and tooling for 1000 production units. The costs presented in table 23-1 include panel closeouts and applicable manufacturing methods using René 41 and Haynes 25 alloys. The semimonocoque spanwise concept panel costs reflect representative values for the statically determinate concept. The manufacturing methods for the monocoque waffle and honeycomb are discussed earlier in the monocoque weights section (section 13). The semimonocoque concepts reflect production techniques discussed in section 27.

Heat Shield Costs

Cost information was determined for two refurbishable and two permanently attached heat shield concepts discussed in detail in the heat shield sizing and weights section (section 20). All heat shield concepts were evaluated on the tubular panel (size: 92 inch x 46 inch).

The refurbishable heat shield included the following:

1. Corrugated skin with multiple supports

2. Flat skin dimpled-stiffened clip-supported

The permanently attached heat shields included the two variations of the modular heat shield concept:

1. Modular, simply supported

2. Modular, cantilevered

This cost study was conducted in sufficient detail to estimate the tooling required for fabrication and assembly. Figure 23-1 indicates relative costs of the four concepts evaluated, including labor and material. Table 23-2 presents costs in dollars per square foot for 100 vehicles. The results of this cost evaluation indicate that the corrugated heat shield is lowest in cost.

Leading Edge Costs

The evaluation of leading edge concepts was made for both the continuous and segmented designs. The leading edge cost data encompassing labor, material and total cost requirements considering 100 vehicles is presented in table 23-3 in terms of $/lb and $/linear foot. These data indicate that the segmented leading edge concept provides the lower cost.

Wing Segment Costs

Manufacturing costs of the wing structure concepts were determined on the basis of detailed analysis of a typical manufacturing segment using 1968 labor rates and material prices. The detailed cost analysis included (1) substructure fabrication and assembly; (2) panel fabrication, assembly, and installation; and (3) heat shield fabrication, assembly, and installation with tooling requirements amortized over 100 vehicles.

To facilitate costing, the vehicle structure was divided into typical manufacturing segments as shown in figure 23-2, with the detailed analysis confined to the main wing manufacturing segment. A typical arrangement and geometry for the main wing manufacturing segment is shown in figure 23-3. This segment (one-half shown) consists of 1874 square feet of planform area located between Station 2136 and Station 2506. The segment is further divided into 3 zones (A, B, and C). These zones represent typical types of structures found in the segment as determined by detailed structural analysis. The basic elements consist of the substructure, structural panels, and heat shields (including insulation). This latter was costed in detail for the heat shield cost evaluation presented earlier and the results applied to each structure concept, as applicable. The distribution of the substructure costs to the various zones is based on the volume contained by each zone (i.e. the product of surface area and depth). These distribution factors are 44.5 percent, 31.1 percent, and 24.4 percent for zones A, B, and C, respectively. The structural panel costs are distributed on the basis of planform area with distribution factors of 33.4 percent, 27.9 percent, and 38.7 percent for zones A, B, and C, respectively. The heat shield costs are distributed in proportion to the area of applicability of the heat shields. The basic arrangement for the six structural concepts is presented in figure 23-4, showing ribs, spars, number of intersections, etc. The weights for each zone are based on unit weight results of the detailed structural analysis presented in section 13 and summarized in table 23-4.

Substructure Costs. - The substructure costs consist of (1) chordwise ribs, (2) spanwise spars, (3) a leading edge spar, and (4) a breakline spar. The assembly costs for the substructure are based on the number of spar-rib intersections in the main wing segment and a costing factor used to account for the type and complexity of the joint involved.

To determine substructure costs for all concepts, a detailed cost analysis of the monocoque waffle concept was made. These data were then applied as applicable (i.e., linear feet of spar, rib) to determine the appropriate cost for the fabrication and assembly of the substructure for the main wing manufacturing segment.

For the substructure of the monocoque concepts, the chordwise ribs were considered continuous from Station 2136 to Station 2506 (30.8 feet). The rib assembly consisted of continuous caps of 30.8-foot length, with the web elements running between the spanwise elements. Each of the web elements was considered to be fabricated in a sequence of operations as shown in figure 23-5. Fabrication of the caps was based on the assumption that the material was purchased as coil stock and slit to appropriate width. This stock would be straightened, formed, and cut to a 30.8-foot length. The chordwise rib fabrication involved joining of the segmented webs and continuous caps by melt-through welding the cap to the webs, using a tracer-controlled gantry-mounted welded head. The fixture for this operation was also used as the assembly fixture for the webs and caps as illustrated in figure 23-6. After the melt-through welding operation, the overlapping edges of the webs are spotwelded for the depth of the beam.

Fabrication of the spars was planned to follow a procedure similar to that described above, except that the web had a slightly different configuration and the length of the spar segment, as assembled, was a function of the spacing of the chordwise ribs (figure 23-7).

The substructure assembly was fabricated by loading the chordwise ribs and spanwise spar segments into a horizontal fixture, and locating these elements at appropriate places to maintain contour and spar/rib spacing. Figures 23-8 through 23-10 present typical intersections used for this study. The various substructure elements were secured at the intersections by resistance welding supplemented in certain areas by mechanical fasteners. An estimated total of 14 200 resistance spotwelds and 1 015 mechanical fasteners were required in the study area. Appropriately designed splice plates were added to the upper and lower spar/rib at each intersection. An additional 6 800 resistance welds were required to secure the splice plates. It was assumed that the substructure would be aged and oxidized as a unit prior to fit-up and assembly of the structural panels.

The structural panel costs, including fabrication assembly and installation, were determined for each concept based on panel details presented in the primary structure sizing and weights section (section 13). The manufacturing cost for the monocoque waffle is based on electrochemical milling (ECM), "stresskin" panels for the noneycomb sandwich, and the manufacturing techniques discussed in section 27 for the semimonocoque and statically determinate concepts.

Monocoque Concept Costs. – The wing substructure costs for the minimum-weight waffle concept (AR = 1.8) and the honeycomb concept were obtained from the following data developed for the monocoque waffle aspect ratio study.

Aspect ratio study: Aspect ratios of 1, 2, 3, and 4, as well as 1.8 and 3.6, were investigated to determine the sensitivity of this parameter with respect to weight and cost. A schematic for the various aspect ratios studied is shown in figure 23-11. The substructure, panel, and total weight variation with aspect ratio is shown in figure 23-12. For all aspect ratios evaluated, a constant chordwise rib spacing of 22.3 inches was assumed (b = 20.0 + 2.3). The aspect ratio of 1.8 and 3.6 minimizes the complexity at the breakline spar intersection by providing repeatable panels and substructure details.

The substructure costs were developed in detail for the aspect ratio of 1.8. These costs were then factored to develop costs for each of the other aspect ratios. Substructure fabrication labor and material costs were factored as a ratio of linear feet of structural elements to the linear feet in the 1.8 aspect ratio. Substructure assembly labor and material costs were factored as a ratio of the number of structure intersections. Tooling costs for the spanwise, diagonal (one-third high point), and leading edge beams were assumed to be constant. Tooling for the chordwise members was factored by the ratio of linear feet of structure, compensating for the impact that the similarity of the ribs within the fuselage area would have on this tooling cost. Substructure assembly tooling costs were assumed to be constant, since the major part of this cost results from the massive assembly fixture required to mate the various structure elements.

The monocoque waffle substructure manufacturing costs are presented in table 23-5. These data show the increase in total cost with the decrease in aspect ratio due to the increase in number of spars, as well as assembly complexity. Further comparison of substructure costs for aspect ratio 1.8 to 2.0 indicates that the increase in spanwise beam cost exceeds the cost due to the complexity of the substructure assembly, for AR = 2.0; thus total substructure costs for AR = 1.8 is 1 percent to 2 percent greater than for AR = 2.0. Substructure weight shows a similar trend with the lowest weight coming from the aspect ratio of 4.

The waffle panels were assumed to be machined from plate stock, utilizing electrochemical milling (ECM) equipment with a power of 20 000 amperes available at the cutting surface. A cutting rate of 0.1 in./in.^{2}/1000 amperes was used to establish ECM machining costs. A study of a panel layout used for the

45° by 45° pattern indicated that a minimum of five ECM tools would be required for a regular sized panel. Special panels, such as occur along the leading edge beam, would require additional tooling. After ECM machining of the panel pockets, a secondary machining operation was performed to remove the risers in the flanged attaching areas. After aging, panels were fitted to the substructure, trimmed to size, drilled, and assembled, using Rene' 41 plate nuts and flush screws on the lower surface with Hi-Lok fasteners for the upper surface attachment. Table 23-6 presents the panel fabrication and installation costs, with tooling costs amortized over 100 units. Minimum-cost results from the aspect ratio 1 panels, which also result in minimum panel weight. Comparison of panel manufacturing costs for $AR = 1.8$ and $AR = 2.0$ indicates that, although the panel fabrication cost is less for the former, the installation costs due to the increased linear feet for attachments more than offset the gains for panel repeatability.

The total manufacturing cost variation with aspect ratio was obtained by combining the information for the substructure (table 23-5) with panel fabrication and installation data (table 23-6) and heat shield data (table 23-2). The elemental costs for the substructure, panel, and heat shield/insulation are presented for the various aspect ratios in table 23-7. The total cost variation with aspect ratio indicates a decreasing cost trend for the greater aspect ratios. This difference, however, is small, indicating minimum-weight considerations to be more important than cost for the waffle concept.

A summary of cost data for the waffle concept aspect ratio study is presented in table 23-8. Labor, material, and nonrecurring costs are itemized separately to show the effect of each on total cost. The data are presented in dollars, dollars per square foot, and dollars per pound. For the minimum-weight arrangement ($AR = 1.8$), labor costs account for approximately 31 percent of the total cost, with material cost accounting for 65 percent. Tooling costs amortized over 100 units account for 4 percent of the total cost.

The effects of number of vehicles on these costs are presented in figures 23-13, 23-14, 23-15, and 23-16. The decrease in labor costs with increase in aspect ratio is indicated in figure 23-13. That the material cost increases with aspect ratio is evident in figure 23-14. The tooling cost variance with the number of vehicles is small for all numbers considered and becomes almost negligible with 100 or more vehicles, as shown in figure 23-15. Total manufacturing cost variance with aspect ratio is shown in figure 23-16. When 100 or more vehicles are considered, the decrease in labor cost with aspect ratio is offset by the increase in material cost with aspect ratio, resulting in approximately the same cost for all aspect ratios.

Concept costs: The substructure fabrication and labor cost for the minimum-weight waffle concept ($AR = 1.8$), which is used as the basis for determining substructure costs for the other arrangements, is presented in table 23-9. The total honeycomb concept substructure cost for the main wing manufacturing segment is approximately 60 percent of the waffle concept cost. This cost is attributed to a 50 percent reduction in linear feet of ribs and spars, coupled with the reduced substructure assembly costs due to the lower number of rib-spar intersections.

The monocoque concept panel fabrication and installation costs are presented in table 23-10. The waffle concept costs are the results of the aspect ratio study (table 23-6). The honeycomb concept costs reflect basic panel costs (as purchased from Stresskin Products Co., Santa Ana, California) with subsequent panel processing and installation accomplished in a major fabrication and assembly area. This processing entails the machining of the core to accept the inner closer channel, channel fabrication, spotwelding, and chem-milling the face sheets to the specified thickness. Panel installation includes locating the panels in the substructure, locating the cover strips, drilling, deburring, final trimming to size, installating the plate nuts (as specified) and installing the flush fasteners. Panel fabrication cost reflects the major impact of labor for the honeycomb, whereas the material cost provided the major cost for the waffle panels. Panel installation costs are a function of the substructure grid arrangement, accounting for the added complexity involved in the honeycomb closeout design. Total panel costs indicate honeycomb costs to be approximately 60 percent of the ECM waffle panels with a 36 percent weight reduction.

The combined substructure, panel, and heat shield fabrication, assembly, and installation costs for the monocoque concepts are shown in table 23-11. This table summarizes the information on tables 23-9 and 23-10, in addition to providing heat shield data. Total cost comparison indicates that the honeycomb concept is approximately 62 percent of the waffle concept. The summary on table 23-12 presents the main wing manufacturing segment costs in terms of labor, material, and tooling for the substructure, panels, and heat shields. For the waffle concept, labor accounts for approximately 31 percent and material approximately 64 percent of the total, with 5 percent for tooling. For the honeycomb design, labor is approximately 45 percent of the total cost, 48 percent for materials, and 7 percent for tooling. For both concepts, the tooling cost is insignificant.

To provide cost information for each zone (A, B, and C) of the wing, appropriate distribution factors are applied to the total costs previously calculated. Substructure costs for labor, material, and tooling for each zone are presented in table 23-13. These costs with appropriate weights and areas, as indicated, provide unit costs for each zone. The average cost for the waffle concept is $90 per square foot, with unit cost variance between $57 per square foot for the outboard area to $120 per square foot for the center area. Honeycomb concept unit costs ($/ft^2) are approximately 63 percent of the waffle costs.

Panel fabrication and installation costs, including heat shield information, is provided in table 23-14. The distribution factor is a function of area; thus the resulting unit costs ($/ft^2) are constant for each concept. Since both the cost and weight for the honeycomb concept are approximately 64 percent of the waffle concept, the resulting unit costs are similar with the average being approximately $90 per pound.

A summary of the monocoque concept total manufacturing costs for each zone is presented in table 23-15. For the main wing segment, the honeycomb concept cost is approximately $500 per square foot compared to the waffle concept cost of $779 per square foot. The cost difference is attributed primarily to material cost which is directly associated with weight; thus, the importance of minimum weight is emphasized.

Semimonocoque concept costs. — The wing substructure costs for the spanwise-tubular, spanwise-beaded, and chordwise convex beaded/tubular concepts were obtained from the detailed costing information developed for the monocoque waffle concept reported earlier.

The substructure fabrication labor and material costs were factored as a ratio of the linear feet of structural elements, as indicated in figure 23-4 and table 23-16, to the linear feet in the AR = 1.8 monocoque arrangment (table 23-5. Substructure assembly labor and material costs were factored as a ratio of the number of structure intersections (tables 23-5 and 23-16) considering the complexity of the joint involved (figure 23-4). Tooling costs for the spanwise, breakline, and leading edge spars were assumed to be constant. Tooling costs for the chordwise ribs were factored by the ratio of linear feet of structure, compensating for the impact that the similarity of the spars within the fuselage area would have on this tooling cost. Substructure assembly tooling costs were assumed to be constant, since the major part of this cost results from the massive assembly fixture required to mate the various structural elements.

The lowest substructure cost is associated with the spanwise concepts, the chordwise concept is 26 percent costlier, due to its closely spaced spars which result in a large number of spars and rib-spar joints.

The fabricated sheetmetal structural panels were costed in detail with variations appropriate to the uniqueness of each panel concept. For example, the tubular panel designs were assumed to be formed in two halves with each requiring a three-stage forming operation with two interstage anneals. Annealing was assumed to be performed in a controlled-atmosphere furnace with subsequent bath cooling. Panel halves, as formed, were assembled with blanked doublers and spotwelded to form a complete structural panel. Heat shield components were added as appropriate, and the complete assembly aged and oxidized. Panel assemblies were fitted to the substructure, trimmed, drilled, and assembled. Typical panels with appropriate heat shields were costed for each zone (A,B, and C) of the wing surface, considering changes in material usage and shape of panel. Other panel manufacturing was accomplished in a similar manner with appropriate variations for the particular panel concept (i.e., one formed panel for the beaded concept, or special forming tools along the leading edge of the panel for the chordwise concept). Although very high initial tooling costs are required for the beaded panels, this panel results in lowest cost, with approximately 21 percent of the fabrication cost attributed to labor, 64 percent for materials, and 15 percent for tooling. Since the material costs are related directly to weight, the importance of minimum weight is indicated by these data. The data also indicate at approximately 60 percent of the panel fabrication and installation costs are for installation. Concepts with larger substructure grids result in fewer fasteners and minimize installation costs. Cost comparison of the total panel fabrication and installation requirements indicates that the beaded concept is lowest in cost, with the tubular concept 2.5 percent greater and the chordwise concept 41 percent greater than the beaded concept. The latter is attributed to the impact of closely spaced spars requiring more closeouts per linear foot of panel, as well as greater installation costs due to the increased linear feet of attachments.

A summary of the semimonocoque concept manufacturing costs encompassing substructure, panel, and heat shield (including insulation) fabrication, assembly, and installation is presented in table 23-17. The substructure and panel cost data are from tables 23-16 and 23-18, respectively. The heat shield (insulation) cost is based on the data from table 23-2, with heat shield being used on the exposed wing for the spanwise concepts and lower surface only for the chordwise concept. Minimum cost results for the spanwise beaded concept, with the spanwise tubular being approximately 2 percent costlier and the chordwise concept being 23 percent costlier.

A labor, material, and tooling cost summary is presented in table 23-19 for the semimonocoque concepts. For the lowest cost beaded concept, the labor costs account for approximately 40 percent of the total; material costs 45 percent and amortized nonrecurring costs 15 percent. Total unit costs range from $\$291/ft^2$ to $\$358/ft^2$ and $\$58/lb$ to $\$53/lb$ for the minimum-weight to maximum-weight concepts, considering the basic structural elements of the main wing manufacturing segment.

The substructure manufacturing costs for each of the zones (A, B, and C) are presented in table 23-20. Appropriate distribution factors, weight, and geometry data are used to develop unit costs for each zone as indicated. Basic data from table 23-17 and appropriate weight tables are used (table 23-4).

The panel fabrication and installation costs for each zone are presented in table 23-21. Cost data from table 23-18 are used with the appropriate distribution factors noted and appropriate panel weight data from table 23-4 to obtain the unit cost data.

The heat shield and insulation manufacturing cost data for each zone is presented in table 23-22. Distribution factors are based on area of applicability (i.e., zone A represents heat shield on the lower surface only) with weight information taken from tables 23-4 to obtain the unit cost data for the heat shields.

A summary of manufacturing costs and unit costs for each zone is presented in table 23-23. These manufacturing costs are based on data from tables 23-20 23-21 and 23-22. The costs reflect the manufacturing requirements for the basic structural elements only. Additional cost factors are essential to develop unit costs that would be representative of the total wing.

Statically determinate concept costs. - The wing substructure manufacturing costs, excluding the impact of the slip-joint assemblies, are presented in table 23-24. The basic arrangement of substructure is represented by the grid presented in figure 23-4 and includes additional spars as indicated. The detail costing information for the substructure presented earlier is used with appropriate linear feet and number of intersection ratios to obtain the cost data presented. Comparing the substructure cost data with the spanwise beaded concept indicates a 16 percent increase in cost with a 12 percent increase in substructure weight. The cost increase is attributed to an increase in spar requirement and resulting increase in the effective number of spar-rib intersections. A further iteration of the statically determinate concept could possibily yield an increase in spar spacing and a corresponding cost reduction. The impact of the slip-joint assemblies is not included in the aforementioned percentages.

The statically determinate concept panel manufacturing costs presented in table 23-25 indicate similar fabrication costs and slightly greater installation cost in comparison to the semimonocoque spanwise beaded concept. Increase in installation costs is the result of panel attachment details in which additional fasteners are used along the panel spanwise joints.

A summary of substructure, panel, and heat shield (including insulation) costs for labor, material, and tooling is presented in table 23-26. Total manufacturing costs for the basic structural elements excluding the slip-joint assemblies are approximately 18 percent greater than for the minimum-cost semimonocoque concept. The impact of labor, materials, and tooling on the manufacturing cost of this concept is presented in table 23-27. Labor and material dollars each account for approximately 43 percent of the total, with heat shield cost approximately 13 percent of the total manufacturing cost. The unit cost ($/ft^2) of the basic structure (less slip-joint assemblies) is 18 percent greater than the minimum-cost semimonocoque concept with a dollars-per-pound increase of 12 percent also indicated.

The manufacturing costs encompassing labor, materials, and tooling for each zone (A,B, and C) are presented in table 23-28 for the substructure, panel and heat shields. The data are based on results shown in table 23-26, using appropriate distribution factors discussed earlier and weight information from table 23-4. Table 23-29 summarizes the labor, material, and tooling costs for the main wing segment, as well as presenting the unit costs ($/lb and $/ft^2) for each zone. These data, with appropriate cost factors to account for the slip-joint assemblies and other cost items to reflect total wing costs, are used as inputs to the interaction analysis discussed in section 26.

Wing segment cost summary. - A summary of manufacturing costs for the main wing segment is presented in tables 23-30 and 23-31. These costs are total costs for the combination of concepts including primary structure and heat shields/insulation. Total cost, weight and unit costs ($/lb, $/ft^2) are presented for each zone (table 23-31) as well as for the total main wing segment.

The statically determinate costs do not include the impact of the slip-joint assemblies; and encompass the basic elements of the wing structure only.

The minimum-cost concept is the semimonocoque-beaded at $291 per square foot with the semimonocoque-tubular next at $5.00 per square foot greater. The monocoque concepts are the costliest, with the waffle and honeycomb being 168 percent and 65 percent greater, respectively, than the lowest-cost beaded concept. It is emphasized that these costs reflect manufacturing costs for only the basic structure of a representative manufacturing segment (main wing) and only provide a cost comparison for a relative ranking of the concepts. It is further noted that the statically determinate concept costs do not include the impact of the slip-joint assemblies. Factors to account for machined and sheetmetal parts, as well as other machined parts and miscellaneous structures are added to these costs to provide cost data to obtain the total wing manufacturing costs discussed later.

Total Wing Costs

Cost estimating relationships (CERs)for labor, material, and tooling were developed for each concept, using the detailed main wing segment manufacturing costs as the bases. These CERs, presented in $/lb, provide a factor which, when multiplied by the estimated weight of the total wing, results in the incremental manufacturing cost (i.e., labor, material, tooling) of the total wing. Wing geometry for the baseline vehicle, with reference areas, is presented in figure 23-17. Wing weights for the baseline vehicle are itemized in table 23-32, and are used to obtain the manufacturing costs for the total wing.

Experience has indicated that for a given material and design concept selection, there is a predictable relationship between total vehicle manufacturing hours and hours required to perform various activities during this period of manufacturing. The main wing segment costing is as detailed as possible considering the depth of design available. The costing involves the fabrication and assembly of the basic structure of the wing (i.e., panels, substructure, heat shield) which for most concepts are sheetmetal components, the exception being the ECM waffle concept panels and the slip-joint assemblies of the statically determinate concept. The actual manufacturing of the complete wing would introduce other sheetmetal and machined parts, particularly at the interfaces between manufacturing segments of the vehicle (i.e., wing-to-wing, wing-to-fuselage, etc.). The developed CERs for the wing include factors which account for these unknown elements.

The detailed costing relationships developed for the supersonic transport (SST), which, from a technological standpoint was quite similar to the hypersonic cruise vehicle, indicated an estimated cumulative average cost at 100 units of 768 100 total manufacturing hours. A breakdown of this total included 357 000 hours for machined parts, or 49 percent of the total manufacturing hours. For the purpose of this study, it was assumed that this relationship would exist for the semimonocoque chordwise concept, since it is the most similar to the construction proposed for the SST (i.e., multispar, chordwise stiffened). Other assumptions made to develop the CERs for each concept include the following:

(1) To provide a more common basis of comparison of HCV (chordwise concept) to SST, the heat shield/insulation labor and material costs were deleted from the chordwise concept costs to arrive at the machined parts cost.

(2) Labor and material costs were increased by 25 percent to account for additional sheetmetal parts (i.e. stiffeners, clips, etc.) but were not costed in detail.

(3) Calculated weights were increased by 10 percent to account for the uncosted items. These sheetmetal parts are assumed to be relatively light in weight.

(4) A labor rate of $12/hr was used to obtain the time involved in machining.

(5) A material removal rate for Rene′41 of 0.266 lb/hr was used. An overall titanium machining material removal rate of 1.33 lb/hr has been developed from actual experience with titanium. An analysis of the comparative machinability of Rene′41 versus 6Al-4V titanium for the various types of machining done during aircraft manufacture indicates that Rene′41 is approximately five times as difficult to machine as titanium. Therefore, a material removal rate of (1.33/5) pounds per hour was assumed for Rene′41.

(6) A buy-to-net factor of 2 for sheetmetal costs was used to account for losses due to rejected parts and other scrap.

(7) A buy-to-net factor of 11 was used for machined parts.

(8) Net material after machining was estimated as 10 percent of estimated material removed.

(9) Total raw material purchased was estimated as equal to the product of the net-to-buy factor for machined parts and the estimated net material, or 1.10 times the estimated material removed.

(10) Machined parts raw material cost was based on $25/lb.

The machined parts estimated labor and material costs are presented in table 23-33. These cost estimates are for the semimonocoque chordwise concept based on the assumptions made above. The total costs for labor and materials for the machined parts are $262 614. Since the machined parts required are primarily a function of substructure arrangement and complexity, the machined parts labor and material costs for the other concepts are assumed to be proportional to the substructure labor and material costs for each concept (table 23-34). The statically determinate concept machined parts and added sheetmetal costs include the cost for the special slip-joint fitting assemblies at each spar-rib interface, special furselage-to-wing interface fittings, and the required sheetmetal elements as calculated in table 23-35. The labor and material costs for the slip-joint assemblies are $\$73/ft^2$ and $\$39/ft^2$, respectively, based on cost results of table 23-35.

Labor and material cost estimating relationship. – The total labor and material costs are determined (table 23-34) for each concept by estimating cost increases (25 percent) due to additional sheetmetal elements and appropriate factors for machined parts labor and material. Unit costs ($/lb) are calculated, using the costed structure weight increased by factors used to account for the additional sheetmetal elements as well as machined part weights. The final labor and material CERs presented in table 23-34) are used to determine the cost for manufacturing the complete wing. The CERs result in approximately twice the labor costs and 2.5 times the material cost developed for the main wing manufacturing segment.

Wing structure labor costs. – The total wing structure labor costs for each zone (A,B, and C) are presented in table 23-36. The labor factor is the ratio of the labor cost relationship determined for the overall wing to the labor cost for the main wing manufacturing segment. The labor factor is used as a multiplying factor to determine total labor costs for each zone of the wing. Total labor costs for the wing concepts vary between 2.36 million dollars for the minimum-weight beaded concept to 4.25 million dollars for the monocoque waffle concept.

Wing structure material costs. – The total wing structure material costs for each zone are presented in table 23-37. The material factor is the ratio of the material cost relationship determined for the overall wing to the material cost for each zone of the wing. Total material costs for the wing concepts vary from 3.96 million dollars for the minimum-weight beaded concept to 11.1 million dollars for the monocoque waffle concept.

Tooling cost estimating relationship. – The tooling cost estimates determined for the main wing manufacturing segment are used to calculate the tooling unit cost ($/lb) for the various structure concepts (table 23-38). Tooling costs for the estimated sheetmetal and machined parts are based on this same unit cost; thus, the total tooling cost is increased approximately 15 percent above initial calculated values. The wing tooling CER for each concept (table 23-38) is used to compute overall tooling costs.

Tooling CERs for the fuselage and empennage are based on estimates available from the SST program. Estimated tooling costs on the SST program were 85 hours per pound for the wing, 131 hours per pound for the fuselage, and 185 hours per pound for the empennage. As in the case of machined parts costs, these estimates are assumed to be directly applicable to the semimonocoque chordwise concept. Appropriate values for the tooling CER for the fuselage and empennage for this concept, based on the estimated tooling cost for the SST, are shown in table 23-39. This tooling CER was assumed to be constant for the fuselage and empennage for the various concepts.

The total structure tooling cost (table 23-39) for each structural segment (wing, fuselage, and empennage) was determined by the product of the tooling CER and the respective segment weight. The structure CER, as indicated, is obtained by dividing the summation of tooling cost by the total weight.

In addition to the above tooling costs, final mate and assembly (FM & A) tooling costs must be included in the overall tooling costs. Experience on the P-3 program and the estimate for the SST program indicate that about 19 percent of the total tooling costs result in this area; thus, FM & A tooling costs are assumed to be 19/81 or 23.4 percent of the structure CER.

The tooling costs estimated to this point represent what is usually referred to as initial tooling. This is the basic tooling required to produce the vehicle prototypes. Once a production program is begun, additional tooling (production tooling) is required to meet an established production rate. On past programs, a ratio of total tooling (initial tooling plus production tooling) to initial tooling has been estimated, using a Rand formula, at about 2.2. The SST program extimates indicated a ratio of 2.82. Since it appears that the tooling required for this program is simpler, a ratio of 2 has been assumed. The resulting data indicate that the overall tooling cost estimating relationship (overall tooling CER) varies between $1416 per pound for the monocoque waffle concept to approximately $2000 per pound for the statically determinate concept.

Total wing cost summary. – The manufacturing costs for the total wing structure for each concept were determined for the baseline airplane (GW = 550 000 lb). The total wing costs (table 23-40) are based on the cost estimating relationships for labor, material, and tooling, and the total wing weights, as shown in table 23-37, 23-38, and 23-39.

Results given in Table 23-40 indicate that the semimonocoque spanwise tubular is the next lowest-cost concept. This concept is 6 percent heavier than the beaded concept for the baseline vehicle, but the wing cost is only 2 percent greater than the beaded concept. The cost results for the other concepts, in order of the cost, are semimonocoque chordwise; monocoque honeycomb statically determinate and monocoque waffle. The cost order is similar to that calculated for the main wing segment (table 23-30) except for change in order of the honeycomb and statically determinate concepts.

Vehicle Production Costs

To determine vehicle production costs, a comparison of the overall wing structure cost estimating relationships with those developed for the SST program was made. These data provide a ratio indicating the relative complexity of the structural technologies between the SST and hypersonic cruise vehicle. Using this ratio and value-engineering estimating techniques, cost estimating relationships were developed for each of the structural and subsystem segments of the hypersonic cruise vehicle typified by figure 23-18. Development of other subsystem requirements (i.e., avionics, controls, etc.) were obtained from data taken from the Electra, P-3, F-104, FX, and SST programs. These relationships, as presented in table 23-41, are in terms of labor and material, and were developed from historical data accumulated from previous production and development contracts.

For each of the structural concepts studied, it was assumed that these cost estimating factors would remain constant for all segments other than the wing and leading edge table 23-42). It was assumed that overall cost differences associated with the various structural concepts would be reflected by the application of these cost estimating factors to varying vehicle segment weights.

Total vehicle production costs (labor and material only), less engines, were developed, utilizing these cost estimating factors. Total vehicle costs shown in table 23-43 indicate that the semimonocoque spanwise beaded concept is minimum cost. The semimonocoque spanwise tubular concept is next, being less than 1 percent costlier. The other concepts, in order of cost, are the semimonocoque chordwise, monocoque honeycomb statically determinate, and the monocoque waffle.

The calculated dollars per pound ($/16) main wing manufacturing costs information for each zone, as discussed in the concept cost sections and summarized in tables 23-15, 23-23, and 23-29, are used with the appropriate cost factors as inputs to the interaction analysis discussed in section 26.

TABLE 23-1

INITIAL SCREENING COSTS OF STRUCTURAL PANELS

Primary structure concepts		Material	Cost 1000 Units $\$/ft^2$
Monocoque[a]	Waffle grid unflanged - 45° x 45°	René 41 Haynes 25	229
	Waffle grid flanged - 45° x 45°	René 41 Haynes 25	291
	Waffle grid unflanged - 0° x 90°	René 41 Haynes 25	254
	Waffle grid flanged - 0° x 90°	René 41 Haynes 25	293
	Honeycomb sandwich	René 41 Haynes 25	354
	Truss-core sandwich	René 41 Haynes 25	123
Semimonocoque[b] (spanwise)	Tubular	René 41 Haynes 25	69 55
	Corrugation stiffened	René 41 Haynes 25	74 82
	Trapezoidal corrugation	René 41 Haynes 25	45 44
	Beaded	René 41 Haynes 25	56 55
Semimonocoque[b] (chordwise)	Convex beaded	René 41 Haynes 25	55 50
	Trapezoidal corrugation	René 41 Haynes 25	54 47
	Beaded	René 41 Haynes 25	56 54

Notes:

[a] $S_{ref} = 9.0\ ft^2$; Panel size: 26 in. x 49.8 in.

[b] $S_{ref} = 9.0\ ft^2$; Panel size: 30 in. x 43.2 in.

TABLE 23-2

SUMMARY OF HEAT SHIELD COST EVALUATION FACTOR DATA
FOR 100-VEHICLE PRODUCTION RUN

Cost evaluation factor	Heat-shield concept			
	Refurbishable		Permanently attached	
	Corrugated skin multiple supports	Flat-skin dimple-stiffened clip-supported	Simply supported	Canti-levered
Material and labor, \$ per ft^2	24.50	40.10	44.20	36.40

TABLE 23-3

LEADING-EDGE COST EVALUATION FOR WING EVALUATION AREA WITH 100-VEHICLE PRODUCTION RUN

Leading-Edge Concept	Primary structure	Dollars/lb			Dollars/linear ft		
		Labor	Material[b]	Total	Labor	Material	Total
Segmented[a]	Monocoque	22.90	77.55	100.45	97.40	329.60	427.00
	Semimonocoque and Statically determinate	19.90	67.40	87.30	97.40	329.60	427.00
Continuous	Monocoque	51.33	199.13	250.46	387.01	501.34	888.35
	Semimonocoque and Statically determinate	47.50	180.22	227.72	394.79	497.68	892.47

[a]20-in. segments.

[b]TD NiCr.

TABLE 23-4

WEIGHTS FOR MAIN WING MANUFACTURING SEGMENT

Primary structure concept	W, lb/ft^2			W^a, lb			
	A	B	C	A	B	C	Σ
Monocoque waffle concept							
Panel	7.81	9.13	6.68	2 324	2 269	2 294	6 887
Substructure	2.90	2.90	1.69	976	821	690	2 493
Thermal protection	0	0	1.07	0	0	380	380
Heat shield			(0.92)			(330)	
Insulation			(0.15)			(50)	
Total	10.71	12.03	9.44	3 300	3 090	3 370	9 760
Monocoque honeycomb concept							
Panel	4.73	4.83	4.76	1 460	1 240	1 700	4 400
Substructure	1.52	1.52	0.92	470	390	330	1 190
Thermal protection	0	0	1.07	0	0	380	380
Heat shield			(0.92)			(330)	
Insulation			(0.15)			50)	
Total	6.25	6.35	6.75	1 930	1 630	2 410	5 970
Semimonocoque, spanwise tubular							
Panel	2.89	2.91	2.78	891	748	992	2 631
Substructure	1.37	1.57	1.08	422	404	386	1 212
Thermal protection	0.56	1.13	1.83	172	290	653	1 115
Heat shield	(0.56)	(1.13)	(1.53)			(546)	
Insulation			(0.30)			(107)	
Total	4.82	5.61	5.69	1 485	1 442	2 031	4 985
Semimonocoque, spanwise beaded							
Panel	2.52	2.68	2.46	776	689	878	2 343
Substructure	1.37	1.57	1.08	422	404	386	1 212
Thermal protection	0.56	1.13	1.83	172	290	653	1 115
Heat shield	(0.56)	(1.13)	(1.53)			(546)	
Insulation			(0.30)			(107)	
Total				1 370	1 383	1 917	4 670

[a] $S_A = 308$ ft^2; $S_B = 257$ ft^2; $S_C = 357$ ft^2; $S_{Total} = 922$ ft^2.

TABLE 23-4

MAIN WING SEGMENT WEIGHTS (CONCLUDED)

Primary structure concept	W, lb/ft^2			W, lb			
	A	B	C	A	B	C	Σ
Semimonocoque chordwise convex beaded tubular							
Panel	3.47	3.39	3.52	1 070	870	1 260	3 200
Substructure	2.85	2.78	1.54	880	720	550	2 150
Thermal protection	0.61	0.61	1.28	180	160	460	800
Heat shield	(0.61)	(0.61)	(0.99)	(180)	(160)	(350)	(690)
Insulation	0	0	(0.29)			(110)	(110)
Total	6.93	6.78	6.34	2 130	1 750	2 270	6 150
Statically determinate spanwise beaded							
Panel	2.76	2.89	2.46	850	743	878	2 471
Substructure	1.56	1.63	1.29	481	419	460	1 360
Thermal protection	0.56	1.13	1.54	172	290	550	1 012
Heat shield	(0.56)	(1.13)	(1.54)				
Insulation	(0)	(0)	(0)				
Total	4.88	5.65	5.29	1 503	1 452	1 888	4 843

TABLE 23-5

WAFFLE CONCEPT SUBSTRUCTURE MANUFACTURING COSTS[a] (DOLLARS)

Structural element		Aspect ratio, a/b					
		1.0	1.8	2.0	3.0	3.6	4.0
1. Chordwise ribs							
Linear feet	ft	505	502	502	503	500	504
Labor	$	3 950	3 930	3 930	3 940	3 920	3 950
Material	$	21 430	21 300	21 300	21 340	21 210	21 390
Nonrecurring	$	1 298 390	1 290 650	1 290 650	1 293 230	1 285 490	1 295 810
Subtotal[b]	$	38 364	38 136	38 136	38 212	37 985	38 298
2. Spanwise beams							
Linear feet	ft	509	273	242	159	116	119
Labor	$	6 010	3 220	2 850	1 880	1 370	1 400
Material	$	22 600	12 120	10 740	7 060	5 150	5 280
Nonrecurring	$	313 080	313 080	313 080	313 080	313 080	313 080
Subtotal[b]	$	31 741	18 471	16 721	12 071	9 651	9 811
3. Leading edge and breakline beams							
Linear feet	ft	68	68	68	68	68	68
Labor	$	380	380	380	380	380	380
Material	$	1 850	1 850	1 850	1 850	1 850	1 850
Nonrecurring	$	156 190	156 190	156 190	156 190	156 190	156 190
Subtotal[b]	$	3 792	3 792	3 792	3 792	3 792	3 792

TABLE 23-5

WAFFLE CONCEPT SUBSTRUCTURE MANUFACTURING COSTS[a] (DOLLARS) (Concluded)

Structural element		Aspect ratio, a/b					
		1 0	1.8	2.0	3.0	3.6	4.0
4. Substructure assembly							
No. intersections		1 242	613	630	412	329	346
Labor	$	14 080	6 950	7 150	4 670	3 730	3 920
Material	$	7 130	3 520	3 620	2 370	1 890	1 990
Nonrecurring	$	1 217 450	1 217 450	1 217 450	1 217 450	1 217 450	1 217 450
Subtotal	$	33 384	22 644	22 944	19 214	17 794	18 084
5. Total cost[b]	$	107 281	83 043	81 593	73 289	69 222	69 985
6. Substructure weight	lb	3 215	2 493	2 356	1 995	1 919	1 880

[a]For one-half of main wing area = 922 ft^2.

[b]Nonrecurring costs amortized over 100 units.

TABLE 23-6

WAFFLE PANEL FABRICATION AND INSTALLATION COSTS[a] (DOLLARS)

Manufacturing operation		Aspect ratio, a/b					
		1.0	1.8	2.0	3.0	3.6	4.0
1 Fabrication							
Labor	$	63 320	65 300	64 340	66 170	67 700	68 210
Material	$	287 180	358 500	365 870	387 860	395 970	394 980
Nonrecurring	$	192 400	186 500	191 130	188 330	190 880	194 440
Subtotal[b]	$	352 424	425 665	432 121	455 913	465 579	465 134
2. Installation							
Linear feet	ft	1 082	843	812	730	684	691
Labor	$	178 670	139 150	134 000	120 500	112 850	114 060
Material	$	70 440	54 860	52 753	47 510	44 430	44 970
Nonrecurring	$	68 980	53 720	51 730	46 520	43 570	44 030
Subtotal[b]	$	249 800	194 547	187 270	168 475	157 716	159 470
3. Total panel costs[b]	$	602 224	620 212	619 391	624 388	623 295	624 604
4. Panel weights	lb	6 372	6 884	7 031	7 802	8 178	8 417

[a]For one-half of main wing area = 922 ft^2.

[b]Nonrecurring costs amortized over 100 units.

TABLE 23-7

WAFFLE CONCEPT
SUBSTRUCTURE, PANEL, AND HEAT SHIELD FABRICATION, ASSEMBLY AND INSTALLATION COSTS[a] (DOLLARS)

Structural elements		Aspect ratio, a/b					
		1.0	1.8	2.0	3.0	3.6	4.0
1. Substructure							
Labor	$	24 420	14 480	14 310	10 870	9 400	9 650
Material[b]	$	53 010	38 790	37 510	32 620	30 100	30 510
Amort NR[b]	$	29 851	29 773	29 773	29 799	29 722	29 825
Subtotal[b]	$	107 281	83 043	81 593	73 289	69 222	69 985
2. Panel							
Labor	$	241 990	204 450	198 340	186 670	180 550	182 270
Material[b]	$	357 620	413 360	418 623	435 370	440 400	439 950
Amort NR[b]	$	2 614	2 402	2 428	2 348	2 345	2 384
Subtotal[b]	$	602 224	620 212	619 391	624 388	623 295	624 604
3. Heat shield/insula.							
Labor	$	3 100	3 100	3 100	3 100	3 100	3 100
Material[b]	$	9 250	9 250	9 250	9 250	9 250	9 250
Amort NR[b]	$	2 950	2 950	2 950	2 950	2 950	2 950
Subtotal[b]	$	15 300	15 300	15 300	15 300	15 300	15 300
4. Total cost	$	724 805	718 555	716 284	712 977	707 817	709 889

[a]For one-half of main wing area = 922 ft^2.

[b]NR. nonrecurring costs amortized over 100 units.

TABLE 23-8

SUMMARY-WAFFLE CONCEPT
MAIN WING SEGMENT COSTS FOR VARIOUS ASPECT RATIOS

Aspect ratio	a/b	1.0	1.8	2.0	3.0	3.6	4.0
Planform area	ft^2	922	922	922	922	922	922
Total weight	lb	9 970	9 760	9 770	10 180	10 480	10 680
Labor	$	269 510	222 030	215 750	200 640	193 050	195 020
	$/ft^2$	292	241	234	217	209	211
	$/lb	27	23	22	20	18	18
Material	$	419 880	461 400	465 383	477 240	479 750	479 710
	$/ft^2$	455	500	504	517	520	520
	$/lb	42	47	48	47	46	45
Nonrecurring (amort over 100 units)	$	35 415	35 125	35 151	35 097	35 017	35 159
	$/ft^2$	38	38	38	38	38	38
	$/lb	4	4	4	3	3	3
Total cost	$	724 805	718 555	716 284	712 977	707 817	709 889
	$/ft^2$	786	779	776	773	767	770
	$/lb	73	73	73	70	68	66

TABLE 23-9

MONOCOQUE CONCEPT SUBSTRUCTURE MANUFACTURING COST[a] (DOLLARS)

(Main Wing Segment)

Structure concept		Monocoque	
		Waffle	Honeycomb
1. Chordwise ribs			
Linear feet	ft	502	263
Labor	$	3 930	2 060
Material	$	21 300	11 160
Nonrecurring	$	1 290 650	835 050
Subtotal[b]	$	38 136	21 570
2. Spanwise beams			
Linear feet	ft	273	142
Labor	$	3 220	1 670
Material	$	12 120	6 300
Nonrecurring	$	313 080	313 080
Subtotal[b]	$	18 471	11 101
3. Leading edge and breakline beams			
Linear feet	ft	68	68
Labor	$	380	380
Material	$	1 850	1 850
Nonrecurring	$	156 190	156 190
Subtotal[b]	$	3 792	3 792
4. Substructure assembly			
No. of intersections		613	212
Labor	$	6 950	2 410
Material	$	3 520	1 220
Nonrecurring	$	1 217 450	1 217 450
Subtotal[b]	$	22 644	15 804
5. Total Cost	$	83 043	52 267
6. Substructure			
Weight	lb	2 493	1 190

TABLE 23-10

MONOCOQUE CONCEPT PANEL FABRICATION AND INSTALLATION COSTS[a] (DOLLARS)

(Main Wing Segment)

Structure concept		Monocoque	
		Waffle	Honeycomb
1. Fabrication			
Labor	$	65 300	83 130
Material	$	358 500	151 994[c]
Nonrecurring	$	186 500	--
Subtotal[b]	$	425 665	235 124
2. Installation			
Linear feet	ft	843	473
Labor	$	139 150	105 990
Material	$	54 860	32 190
Nonrecurring	$	53 720	34 033
Subtotal[b]	$	194 547	138 520
3. Total panel cost	$	620 212	373 664
4. Panel weight	lb	6 884	4 400

[a]For one-half of the main wing segment = 922 ft^2

[b]Nonrecurring costs amortized over 100 units.

[c]Includes basic honeycomb panel purchased from Stresskin Products Co., Santa Ana, Calif.

TABLE 23-11

MONOCOQUE CONCEPT SUBSTRUCTURE, PANEL, HEAT SHIELD (INCLUDING INSULATION) FABRICATION, ASSEMBLY AND INSTALLATION COSTS[a] (DOLLARS)

(Main Wing Segment)

Structure concept		Monocoque	
		Waffle	Honeycomb
1. Substructure	$		
Labor	$	14 480	6 520
Material	$	38 790	20 530
Amort. NR	$	29 773	25 217
Subtotal	$	83 043	52 267
2. Panel	$		
Labor	$	204 450	189 120
Material	$	413 360	184 184
Amort. NR	$	2 402	340
Subtotal	$	620 212	373 644
3. Heat shield/insul.	$		
Labo.	$	3 100	3 100
Material	$	9 250	9 250
Amort. NR	$	2 950	2 950
Subtotal	$	15 300	15 300
4. Total cost	$	718 555	441 211
5. Total weight	lb	9 760	5 970

[a]For one-half the main wing segment.

TABLE 23-12

MONOCOQUE CONCEPT
MAIN WING SEGMENT COST

Structure concept		Monocoque	
		Waffle	Honeycomb
Planform area	ft^2	922	922
Total weight	lb	9 760	5 970
Labor	$	222 030	198 740
	$/ft^2$	241	216
	$/lb	23	33
Material	$	461 400	213 964
	$/ft^2$	500	232
	$/lb	47	36
Nonrecurring	$	35 125	28 507
(Amort over 100 units)	$/ft^2$	38	31
	$/lb	4	5
Total cost	$	718 555	441 211
	$/ft^2$	779	480
	$/lb	73	74

TABLE 23-13

MONOCOQUE CONCEPT SUBSTRUCTURE MANUFACTURING COSTS[a]

(Main Wing Segment)

Concept	Zone	Distrib. factor	Labor, $	Material, $	Amort[b] Nonrecurr, $	Total $	Weight, lb	Area, ft^2	$\frac{\$}{lb}$	$\frac{\$}{ft^2}$
Waffle	A	0.445	6 444	17 261	13 249	36 954	976	308	38	120
	B	0.311	4 503	12 064	9 259	25 826	821	257	31	100
	C	0.244	3 533	9 465	7 265	20 263	696	357	29	57
	Σ	1.000	12 480	38 790	29 773	83 043	2 493	922	33	90
Honeycomb	A	0.445	2 900	9 140	11 200	23 240	470	308	50	76
	B	0.311	2 030	6 380	7 840	16 250	390	257	42	63
	C	0.244	1 590	5 010	6 177	12 777	330	357	39	36
	Σ	1.000	6 520	20 530	25 217	52 267	1 190	922	44	57

[a]For one-half of main wing segment = 922 ft^2.

[b]Nonrecurring costs amortized over 100 units.

TABLE 23-14

MONOCOQUE CONCEPT PANEL FABRICATION AND INSTALLATION COSTS[a]

(Main Wing Segment)

Concept	Zone	Distrib. factor	Labor, $	Material $	Amort[b] Nonrecurr, $	Total $	Weight lb	Area, ft^2	$\frac{\$}{lb}$	$\frac{\$}{ft^2}$
Waffle	A	0.334	68 286	138 062	802	207 150	2 324	308	89	672
	B	0.279	57 042	115 327	670	173 039	2 269	257	76	672
	C	0.387	79 122	159 970	930	240 022	2 294	357	105	672
	Σ	1.000	204 450	413 360	2 402	620 212	6 887	922	90	672
Honeycomb	A	0.334	163 200	61 517	113	124 830	1 460	308	86	405
	B	0.279	52 720	51 388	95	104 203	1 240	257	84	405
	C	0.387	73 200	71 279	132	144 611	1 700	357	85	405
	Σ	1.000	189 120	184 184	340	373 644	4 400	922	85	405
Heat shield (typical for both concepts)	A	–	–	–	–	–	–	–	–	–
	B	–	–	–	–	–	–	–	–	–
	C	1.000	3 100	9 250	2 950	15 300	380	357	40	43
	Σ	1.000	3 100	9 250	2 950	15 300	380	357	40	43

TABLE 23-15

MONOCOQUE CONCEPT TOTAL MANUFACTURING COSTS[a]

(Main Wing Segment)

Concept	Zone	Labor, \$	Material, \$	Amort. NR \$[b]	Total, \$	Weight, lb	Area, ft^2	\$/lb	\$/ft^2
Waffle	A	74.730	155 324	14 051	244 105	3 300	308	74	793
	B	61 545	127.391	9 929	198 865	3 090	257	65	773
	C	85 755	178 685	11 145	275 585	3 370	357	82	772
	Σ	222 030	461 400	35 125	718 555	9 760	922	73	779
Honeycomb	A	66 100	70 657	11 313	148 070	1 930	308	77	481
	B	54 750	57 768	7 935	120 453	1 630	257	74	469
	C	77 890	85 539	9 259	172 688	2 410	357	72	483
	Σ	198 740	231 964	28 507	441 211	5 970	922	74	480

[a]For one-half of the main wing segment = 922 ft^2 .

[b]NR, nonrecurring costs amortized over 100 units.

TABLE 23-16

SEMIMONOCOQUE SUBSTRUCTURE MANUFACTURING COSTS[a] (DOLLARS)

(Main Wing Segment)

Structure concept		Spanwise		Chordwise
		Tubular	C Beaded	Convex beaded (U) Tubular (U)
1. Chordwise ribs				
Linear feet	ft	259	259	146
Labor	$	2 030	2 030	1 144
Material	$	10 990	10 990	6 198
Nonrecurring	$	902 420	902 420	653 070
Subtotal[b]	$	22 044	22 044	13 873
2. Spanwise beams				
Linear feet	ft	119	119	434
Labor	$	1 400	1 400	5 120
Material	$	5 280	5 280	19 270
Nonrecurring	$	313 080	313 080	313 080
Subtotal[b]	$	9 811	9 811	27 52[illegible]
3. Leading edge and breakline beams				
Linear feet	ft	68	68	68
Labor	$	380	380	380
Material	$	1 850	1 850	1 850
Nonrecurring	$	156 190	156 190	156 190
Subtotal[b]	$	3 792	3 792	3 792
4. Substructure assembly				
No. of intersections		186	186	400
Labor	$	2 106	2 106	4 531
Material	$	1 067	1 067	2 295
Nonrecurring	$	1 217 450	1 217 450	1 217 450
Subtotal[b]	$	15 347	15 347	19 000
5. Total cost[b]		50 994	50 994	64 186
6. Substructure weight	lb	1 212	1 212	2 150

[a]For one-half of main wing area = 922 ft^2.

[b]Nonrecurring costs amortized over 100 units.

TABLE 23-17

SEMIMONOCOQUE

SUBSTRUCTURE, PANEL, HEAT SHIELD (INCL INSULATION)
FABRICATION, ASSEMBLY AND INSTALLATION COSTS[a] (DOLLARS)

(Main Wing Segment)

Structure concept		Spanwise		Chordwise
		Tubular	Beaded	Convex Beaded (U), Tubular (L)
1. Substructure				
Labor	\$	5 916	5 916	11 175
Material	\$	19 187	19 197	29 613
Amort. NR[b]	\$	25 891	25 891	23 398
Subtotal[b]	\$	50 994	50 994	64 186
2. Panel				
Labor	\$	90 151	84 598	126 830
Material	\$	75 199	69 252	1 100 680
Amort. NR[b]	\$	3 362	10 576	3 230
Subtotal[b]	\$	168 712	164 426	230 740
3. Heat shield/Insula.				
Area	ft^2	1 536	1 536	922
Labor	\$	16 375	16 375	10 033
Material	\$	32 514	32 514	20 448
Amort. NR[b]	\$	4 458	4 455	4 455
Subtotal[b]	\$	53 344	53 344	34 936
4. Total cost	\$	273 050	268 764	329 862

[a]For one-half of main wing area = 922 ft^2.

[b]NR. nonrecurring costs amortized over 100 units.

TABLE 23-18

SEMIMONOCOQUE PANEL FABRICATION AND INSTALLATION COSTS[a] (DOLLARS)

(Main Wing Segment)

Structure concept		Spanwise		Chordwise
		Tubular	Beaded	Convex beaded (U) Tubular (L)
1. Fabrication				
Labor	$	16 531	13 448	19 860
Material	$	45 939	41 202	58 510
Nonrecurring	$	301 900	1 024 300	274 900
Subtotal[b]	$	65 489	64 893	81 119
2. Installation				
Linear feet	ft	446	431	648
Labor	$	73 620	71 150	106 970
Material	$	29 260	28 050	42 170
Nonrecurring	$	34 260	33 300	48 140
Subtotal[b]	$	103 223	99 533	149 621
3. Total panel costs	$	168 712	164 426	230 740
4. Panel weights	lb	2 631	2 343	3 200

[a]For one-half of main wing area = 922 ft^2.

[b]Nonrecurring costs amortized over 100 units.

TABLE 23-19

SEMIMONOCOQUE CONCEPTS MAIN WING SEGMENT COSTS

Structure concept		Spanwise Tubular	Spanwise Beaded	Chordwise Convex beaded (U) Tubular (L)
Planform area	ft^2	922	922	922
Total weight	lb	4 958	4 670	6 150
Labor	$	112 412	106 889	148 038
	$/$ft^2$	122	116	160
	$/lb	23	23	24
Material	$	126 900	120 953	150 741
	$/$ft^2$	138	131	164
	$/lb	26	26	24
Nonrecurring (Amort. over 100 units)	$	33 708	40 922	31 083
	$/$ft^2$	36	44	34
	$/lb	7	9	5
Total cost	$	273 050	268 764	329 862
	$/$ft^2$	296	291	358
	$/lb	55	58	53

TABLE 23-20

SEMIMONOCOQUE CONCEPT SUBSTRUCTURE MANUFACTURING COSTS[a]

(Main Wing Segment)

Concept	Zone	Distrib. factor	Labor, $	Material, $	Amort.[b] Nonrecurr, $	Total, $	Weight, lb	Area, ft^2	$\frac{\$}{lb}$	$\frac{\$}{ft^2}$
Spanwise tubular	A	0.445	2 633	8 538	11 521	22 692	422	308	54	74
	B	0.311	1 840	5 967	8 052	15 859	404	257	39	62
	C	0.244	1 443	4 682	6 318	12 443	386	357	32	35
	Σ	1.000	5 916	19 187	25 891	50 994	1 212	922	42	55
Spanwise beaded	A	0.445	2 633	8 538	11 521	22 692	422	308	54	74
	B	0.311	1 840	5 967	8 052	15 859	404	257	39	62
	C	0.244	1 443	4 682	6 318	12 443	386	357	32	35
	Σ	1.000	5 916	19 187	25 891	50 994	1 212	922	42	55
Chordwise Convex beaded(U) tubular(L)	A	0.445	4 973	13 178	10 412	28 563	880	308	32	93
	B	0.311	3 475	9 210	7 277	19 962	720	257	28	78
	C	0.244	2 727	7 225	5 709	15 661	550	357	28	44
	Σ	1.000	11 175	29 613	23 398	64 186	2 150	922	30	70

[a]For one-half of main wing area = 922 ft^2.

[b]Nonrecurring costs amortized over 100 units.

TABLE 23-21

SEMIMONOCOQUE CONCEPT PANEL FABRICATION AND INSTALLATION COSTS[a]

(Main Wing Segment)

Concept	Zone	Distrib. factor	Labor, $	Material, $	Amort[b] Nonrecurr, $	Total, $	Weight, lb	Area, ft^2	$/lb	$/ft^2
Spanwise tubular	A	0.334	30 110	25 116	1 123	56 349	891	308	63	183
	B	0.279	25 152	20 980	938	47 070	748	257	63	183
	C	0.387	34 889	29 103	1 301	65 293	992	357	66	183
	Σ	1.000	90 151	75 199	3 362	168 712	2 631	922	64	183
Spanwise beaded	A	0.334	28 256	23 130	3 532	54 918	776	308	71	178
	B	0.279	23 603	19 321	2 951	45 875	689	257	67	178
	C	0.387	32 739	26 801	4 093	63 633	878	357	72	178
	Σ	1.000	84 598	69 252	10 576	164 426	2 343	922	70	178
Chordwise Conve bea ed (U) tubular (L)	A	0.334	42 361	33 627	1 079	77 067	1 070	308	72	250
	B	0.279	35 386	28 090	901	64 377	870	257	74	250
	C	0.387	49 083	38 963	1 250	89 296	1 260	357	71	250
	Σ	1.000	126 830	100 680	3 230	230 740	3 200	922	72	250

[a]For one-half of main wing area = 922 ft2

[b]Non-recurring costs amortized over 100 units.

TABLE 23-22

SEMIMONOCOQUE CONCEPT HEAT SHIELD/INSULATION FABRICATION AND INSTALLATION COSTS[b]

(Main Wing Segment)

Concept	Zone	Distrib. factor	Labor, $	Material, $	Amort.[b] Nonrecurr, %	Total, $	Weight, lb	Area, ft^2	$\frac{\$}{lb}$	$\frac{\$}{ft^2}$
Spanwise	A	0.200	3 275	6 503	891	10 669	172	308	61	35
	B	0.335	5 486	10 892	1 492	17 870	290	257	59	70
	C	0.465	7 614[c]	15 119[c]	2 072	24 805	653	357	39	70
	Σ	1.000	16 375	32 514	4 455	53 344	1 115	922	48	58
Spanwise beaded	A	0.200	3 275	6 503	891	10 669	172	308	61	35
	B	0.335	5 486	10 892	1 492	17 870	290	257	59	70
	C	0.465	7 614[c]	15 119[c]	2 072	24 805	653	357	39	70
	Σ	1.000	16 375	32 514	4 455	53 344	1 115	922	48	58
Chordwise Convex beaded (U) tubular (T)	A	0.334	3 351	6 830	1 488	11 629	180	308	65	38
	B	0.279	2 799	5 705	1 243	9 747	160	257	61	38
	C	0.387	3 883	7 913	1 724	13 520	460	357	29	29
	Σ	1.000	10 033	20 448	4 455	34 936	800	922	44	38

[a]For one-half of main wing area = 922 ft^2.

[b]Nonrecurring costs amortized over 100 units.

[c]Insulation applied to zone C only, weight = 105 lb.

TABLE 23-23

SEMIMONOCOQUE CONCEPT TOTAL MANUFACTURING COSTS[a]

(Main Wing Segment)

Concept	Zone	Labor, $	Material, $	Amort. NR $[b]	Total, $	Weight, lb	Area ft^2	$/lb	$/$ft^2$
Spanwise tubular	A	36 018	40 157	13 535	89 710	1 485	308	60	291
	B	32 478	37 839	10 482	80 799	1 442	257	56	314
	C	43 946	48 904	9 691	102 541	2 031	357	50	287
	Σ	112 442	126 900	33 708	273 050	4 958	922	55	296
Spanwise beaded	A	34 164	38 171	15 944	88 279	1 370	308	64	286
	B	30 929	36 180	12 495	79 604	1 383	257	58	310
	C	41 796	46 602	12 483	100 881	1 917	357	53	282
	Σ	106 889	120 953	40 922	268 764	4 670	922	58	292
Chordwise convex beaded(U) tubular(L)	A	50 685	53 635	12 979	117 299	2 130	308	55	382
	B	41 660	43 005	9 421	94 086	1 750	257	54	366
	C	55 693	54 101	8 683	118 477	2 270	357	52	332
	Σ	148 038	150 741	31 083	329 862	6 150	922	54	358

[a]For one-half of main wing area = 922 ft^2.

[b]Nonrecurring costs amortized over 100 units.

TABLE 23-24

STATICALLY DETERMINATE SUBSTRUCTURE MANUFACTURING COSTS[a]

(Main Wing Segment)

Structure concept		Spanwise
		Beaded
1. Chordwise ribs		
Linear feet	ft	227
Labor	$	1 774
Material	$	9 620
Nonrecurring	$	946 180
Subtotal[b]	$	20 856
2. Spanwise beams		
Linear feet	ft	274
Labor	$	3 240
Material	$	12 200
Nonrecurring	$	313 800
Subtotal[b]	$	18 578
3. Leading edge and breakline beams		
Linear feet	ft	68
Labor	$	380
Material	$	1 850
Nonrecurring	$	156 190
Subtotal[b]	$	3 792
4. Substructure assembly		
No. of intersections		221
Labor	$	2 510
Material	$	1 270
Nonrecurring	$	1 217 450
Subtotal[b]		15 954
5. Total cost		59 180
.. Substructure weight	lb	1 360

[a]For one-half of main wing segment = 922 ft^2 .

[b]Nonrecurring costs amortized over 100 units.

TABLE 23-25

STATICALLY DETERMINATE PANEL FABRICATION AND INSTALLATION COSTS[a] (DOLLARS)

(Main Wing Segment)

Structure concept		Spanwise
		Beaded
1. Fabrication		
Labor	$	13 784
Material	$	43 500
Nonrecurring	$	1 121 852
Subtotal[b]	$	68 502
2. Installation		
Linear feet	ft	599
Labor	$	98 900
Material	$	39 000
Nonrecurring	$	43 300
Subtotal[b]	$	138 333
3. Total panel costs	$	206 835
4. Panel weights	lb	2 471

[a]For one-half of main wing segment = 922 ft^2.

[b]Nonrecurring costs amortized over 100 units.

TABLE 23-26

STATICALLY DETERMINATE CONCEPT TOTAL SUBSTRUCTURE, PANEL, HEAT-SHIELD FABRICATION, ASSEMBLY, AND INSTALLATION COSTS[a] (DOLLARS)

(Main Wing Segment)

Structure concept			Spanwise Beaded
1.	Substructure		
	Labor	$	7 904
	Material	$	24 940
	Amort. NR[b]	$	26 336
	Subtotal	$	59 180
2.	Panel		
	Labor	$	112 [illegible]84
	Material	$	82 500
	Amort. NR[b]	$	11 651
	Subtotal	$	206 835
3.	Heat Shields		
	Labor	$	15 865
	Material	$	30 184
	Amort. NR[b]	$	4 455
	Subtotal	$	50 504
4.	Total cost	$	316 519

[a]one-half of main wing area = 922 ft^2 .

[b]Nonrecurring costs amortized over 100 units.

TABLE 23-27

SUMMARY
STATICALLY DETERMINATE CONCEPT
MAIN WING SEGMENT COSTS

Structure concept		Spanwise Beaded
Planform area	ft^2	922
Total weight	lb	4 843
Labor	$	136 453
	$\$/ft^2$	148
	$/lb	28
Material	$	137 624
	$\$/ft^2$	149
	$/lb	28
Nonrecurring	$	42 442
(Amort. over	$\$/ft^2$	46
100 units	$/lb	9
Total cost	$	316 519
	$\$/ft^2$	344
	$/lb	65

TABLE 23-28

STATICALLY DETERMINATE CONCEPT DISTRIBUTED
SUBSTRUCTURE, PANEL, HEAT-SHIELD FABRICATION ASSEMBLY
AND INSTALLATION COSTS[a]

(Main Wing)

Element	Zone	Distrib factor	Labor, $	Material, $	Amort.[b] Nonrecurr, $	Total, $	Weight, lb	Area, ft^2	$ \frac{\$}{lb}$	$\frac{\$}{ft^2}$
Substructure	A	0.445	3 518	11 098	11 720	26 336	481	308	55	85
	B	0.311	2 458	7 756	8 190	18 404	419	257	44	73
	C	0.244	1 928	6 086	6 426	14 440	460	357	31	40
	Σ	1.000	7 904	24 940	26 336	59 180	1 360	922	44	64
Panel	A	0.334	37 636	27 555	3 891	69 082	850	308	81	224
	B	0.279	31 439	23 018	3 251	57 708	743	257	73	224
	C	0.387	43 609	31 927	4 509	80 045	878	357	91	224
	Σ	1.000	112 684	82 500	11 651	206 835	2 471	922	84	224
Heat shield	A	0.200	3 173	6 037	891	10 101	172	308	59	33
	B	0.335	5 320	10 147	1 492	16 959	290	257	59	66
	C	0.465	7 372	14 000	2 072	23 444	550	357	43	66
	Σ	1.000	15 865	30 184	4 455	50 504	1 012	922	50	55

[a]For one-half of main wing area = 922 ft^2.

[b]Nonrecurring costs amortized over 100 units.

TABLE 23-29

SUMMARY
STATICALLY DETERMINATE CONCEPT TOTAL MANUFACTURING COSTS[a]

(Main Wing)

Concept	Zone	Labor, $	Material, $	Amort.[b] Nonrecurr, $	Total $	Weight $	Area, ft²	$/lb	$/ft²
Spanwise beaded	A	44 327	44 690	16 502	105 519	1 503	308	70	342
	B	39 217	40 921	12 933	93 071	1 452	257	64	362
	C	52 909	52 013	13 007	117 929	1 888	357	62	330
	Σ	136 453	137 624	42 442	316 519	4 843	922	66	344

[a]For one-half of main wing segment = 922 ft².
[b]Nonrecurring costs amortized over 100 units.

TABLE 23-30

STRUCTURE CONCEPT MANUFACTURING COSTS
FOR MAIN WING SEGMENT

Structure concept	Monocoque		Semimonocoque			Statically determinate
			Spanwise		Chord-wise	Spanwise
	Waffle	Honeycomb-core	Tubular	Beaded	Convex beaded tubular	Beaded
Labor, $	$222 030	$198 740	$112 442	$106 889	$148 038	$136 453
Material, $	461 400	213 964	126 900	120 953	150 741	137 624
Tooling, $	35 125	28 507	33 708	40 922	31 083	42 442
Total cost per unit, $	718 555	441 211	273 050	268 764	329 862	316 519
Weight, lb	9 760	5 970	4 958	4 670	6 150	4 843
Dollars per lb	73	74	55	58	53	65
Dollars per ft^2	779	480	296	291	358	343

[a]Costed area = 922 ft^2.

TABLE 23-31

SUMMARY – STRUCTURE CONCEPT[a] MANUFACTURING COSTS

(Main Wing Manufacturing Segment)

Structure concept	Zone	Total cost, $	Weight, lb	Area, ft^2	$\frac{\$}{lb}$	$\frac{\$}{ft^2}$
Monocoque waffle	A	244 105	3 300	308	74	793
	B	198 865	3 090	257	65	773
	C	275 585	3 370	357	82	772
	Σ	718 555	9 760	922	73	779
Monocoque honeycomb	A	148 070	1 930	308	77	481
	B	120 453	1 630	257	74	469
	C	172 688	2 410	357	72	483
	Σ	441 211	5 970	922	74	480
Semimonocoque spanwise tubular	A	89 710	1 485	308	60	291
	B	80 799	1 442	257	56	314
	C	102 541	2 031	357	50	287
	Σ	273 050	4 958	922	55	296
Semimonocoque spanwise beaded	A	88 279	1 370	308	64	285
	B	79 604	1 383	257	58	310
	C	100 881	1 917	357	53	282
	Σ	268 764	4 670	922	58	292
Semimonocoque chordwise convexbeaded/ tubular	A	117 299	2 130	308	55	382
	B	94 086	1 750	257	54	366
	C	118 477	2 270	357	52	332
	Σ	329 862	6 150	922	54	358
Statically determinate[b] spanwise beaded	A	105 519	1 503	308	70	342
	B	93 071	1 452	257	64	362
	C	117 929	1 888	357	62	330
	Σ	316 519	4 843	922	66	344

[a]Primary structure and heat shield/insulation.

[b]Does not include the impact of the slip-joint assemblies.

TABLE 23-32

TOTAL WING WEIGHT SUMMARY[a]

(Baseline – G. W. = 550,000 lb)

Structure concept	Location (ref figure 23-17)				Total[b]
	A	B	C	D	
Monocoque waffle	23 213	38 780	21 054	16 829	99 876
Monocoque honeycomb	13 539	20 472	15 098	13 539	61 568
Semimonocoque spanwise tubular	13 421	22 853	12 408	12 089	60 771
Semimonocoque spanwise beaded	12 436	21 934	11 682	11 339	57 391
Semimonocoque chordwise beaded/tubular	15 461	24 764	14 023	14 409	68 657
Statically Determ. spanwise beaded	14 513	24 686	12 052	11 919	63 170

[a]Pounds.

[b]Does not include leading edge.

TABLE 23-33

MACHINE PARTS ESTIMATED LABOR AND MATERIAL COSTS FOR OVERALL WING STRUCTURE[a]

	Item	Operation/ref.	Results
1	Total labor costs – main wing	(Table 23-19)	$148 038
2	Heat shield/insulation labor costs	(Table 23-17)	10 033
3	Labor costs – basic structure	($\boxed{1}$ – $\boxed{2}$)	138 005
4	Estimate total labor costs	(1.25 $\boxed{3}$)	172 506
5	Total material costs – main wing)	(Table 23-19)	150 741
6	Heat shield/insulation material costs	(Table 23-17)	20 448
7	Material costs – basic structure	($\boxed{5}$ – $\boxed{6}$)	130 293
8	Estimated net material	(1.25 $\boxed{7}$)	162 870
9	Buy-to-net factor	–	2
10	Total estimated material	($\boxed{8}$ x $\boxed{9}$)	325 740
11	Total labor and material – basic structure	($\boxed{3}$ + $\boxed{10}$)	$498 246
12	Total machined parts labor	(49/51 $\boxed{4}$)	$165 726
13	Total machined parts hours	Rate of $12/hr	13 810 hr
14	Estimated material removed	Rate of 0.266 lb/hr	3 673 lb
15	Buy-to-net factor	–	11
16	Estimated net material	(0.10 $\boxed{14}$)	367 lb
17	Estimated total raw material purchased	($\boxed{15}$ x $\boxed{16}$)	4 037 lb
18	Machined parts raw material costs	–	$24/lb
19	Machined parts estimated material costs	($\boxed{17}$ x $\boxed{18}$)	$ 96 888
20	Total labor and material – machined parts	($\boxed{12}$ + $\boxed{19}$)	$262 614[a]

[a]Estimated cost for semimonocoque chordwise concept based on assumptions specified.

TABLE 23-34

LABOR AND MATERIAL COST ESTIMATING RELATIONSHIPS FOR OVERALL WING STRUCTURE COST

	Primary-structure concept	Units	Monocoque		Semimonocoque			Statically Determinate Beaded
			Waffle	Honeycomb	Spanwise		Chordwise	
					Tubular	Beaded	a	
	Labor costs	Units						Ref tbl 23-35
1	Basic (Table 23-12 and 23-19)	$	222 030	198 740	112 442	106 889	148 038	140 153
2	Estimated (1.25 $\boxed{1}$)	$	278 000	248 000	140 552	133 500	185 048	175 000
3	Labor factor for mach parts[b]	–	1.296	0.585	0.529	0.529	1.0000	0.708
4	Machine parts ($\boxed{3}$ x c)	$	214 700	97 000	87 700	87 700	165 726	117 200
5	Total labor ($\boxed{2}$ + $\boxed{4}$)	$	492 700	345 000	228 252	221 200	350 774	359 400[g]
	Material costs							
6	Basic (Table 23-12 and 23-19)	$	461 400	213 964	126 900	120 953	150 741	141 324
7	Estimated (1.25 $\boxed{6}$)	$	576 000	267 000	158 625	151 000	188 426	177 000
8	Buy-to-net factor	–	2	2	2	2	2	2
9	Estimated net ($\boxed{7}$ x $\boxed{8}$)	$	1 152 000	534 000	317 250	302 000	376 852	354 000
10	Matl. factor for mach. parts[d]	–	1.310	0.693	0.648	0.623	1.0000	0.928
11	Machine parts ($\boxed{10}$ x e)	$	126 900	67 200	62 800	60 300	96 888	90 000
12	Total material ($\boxed{9}$ + $\boxed{11}$)	$	1 278 900	601 200	380 050	362 300	473 740	483 300[g]
	Weights							
13	Costed basic structure (23-4)	lb	9 760	5 970	4 958	4 670	6 150	4 843
14	Miscellaneous (0.10 $\boxed{13}$)	lb	976	597	496	467	615	616[h]
15	Machine parts ($\boxed{10}$ x f)	lb	480	254	238	228	367	489[i]
16	Estimated weight ($\boxed{13}$ + $\boxed{14}$ + $\boxed{15}$)	lb	11 216	6 821	5 692	5 365	7 132	5 948

TABLE 23-34

LABOR AND MATERIAL COST ESTIMATING RELATIONSHIPS FOR OVERALL WING STRUCTURE COST (CONCLUDED)

Primary-structure concept		Monocoque		Semimonocoque			Statically Determinate Beaded
		Waffle	Honeycomb	Spanwise		Chordwise	
				Tubular	Beaded	a	
Weights (Cont.)	Units						Ref tbl 23-35
17 Labor CER ($\boxed{5} \div \boxed{16}$)	\$/lb	44	51	40	41	49	60
18 Material CER ($\boxed{12} \div \boxed{16}$)	\$/lb	114	88	67	68	67	81

[a] Convex beaded, upper; tubular, lower.

[b] Substructure labor cost ratio: $\left(\frac{\text{Labor cost for concept X}}{\text{Labor cost, chordwise concept}}\right)$ (ref. tables 23-16, 23-17, and 23-26).

[c] Machine part labor cost for chordwise concept.

[d] Substructure material cost ratio: $\left(\frac{\text{Matl cost for concept X}}{\text{Matl. cost, chordwise concept}}\right)$ (ref. table 23-16, 23-17, and 23-26).

[e] Machine part material cost for chordwise concept.

[f] Machine part weight for chordwise concept

[g] Includes machine parts labor or material as applicable (ref. table 23-33).

[h] Assume 10 percent of costed basic structure plus sheetmetal parts weight of slip-joint assemblies.

[i] Assume machine parts weight includes ship-joint assembly weights.

TABLE 23-35

STATICALLY DETERMINATE CONCEPT SLIP-JOINT ASSEMBLY COSTS

N	Option		Results	Remark/Reference
1	Net material weight for slip-joint assemblies	–	281 lb	Table 23-4
2	Machined parts weight for slip-joint assy.	–	149 lb	Table 23-4
3	Sheetmetal parts weight for slip-joint assy.	($\boxed{1}$ – $\boxed{2}$)	132 lb	
4	Unit labor cost – basic structure	–	$28/lb	Table 23-27
5	Labor cost – sheet metal parts of slip-joint assy.	($\boxed{3}$ x $\boxed{4}$)	$ 3 700	Add to basic labor cost
6	Labor cost – basic structure	–	$136 453	Table (23-27)
7	Calculated labor cost – basic	($\boxed{5}$ + $\boxed{6}$)	$140 153	
8	Estimated labor cost – basic	(1.25 $\boxed{7}$)	$175 000	
9	Unit material cost – basic structure	–	$28/lb	Table 23-27
10	Material cost – sheetmetal parts of slip-joint assy.	($\boxed{3}$ x $\boxed{9}$)	$ 3 700	
11	Material cost – basic structure	–	$137 624	Table 23-27
12	Calculated material cost – basic	($\boxed{10}$ + $\boxed{11}$)	$141 324	
13	Estimated material cost – basic	(1.25 $\boxed{12}$)	$177 000	
14	Machined parts buy-to-net factor	–	11	(See assumptions made to develop CERs)
15	Total raw material purchased for machined parts	($\boxed{2}$ x $\boxed{14}$)	1640 lb	
16	Machined parts raw material cost	–	$24/lb	
17	Estimated machined parts material cost	($\boxed{15}$ x $\boxed{16}$)	$ 39 300	
18	Estimated material removed	(10 $\boxed{2}$)	1 490 lb	
19	Total machined parts hours	($\boxed{18}$ 0.266)	5.600 hr	
20	Total machined parts labor	(12 $\boxed{14}$)	$67 200	

TABLE 23-36

TOTAL WING STRUCTURE LABOR COSTS
($/lb AND $)

1	2	3	4	5	6	7	8	9	10	11
Structure concept	Labor costs	Labor CER	Labor factor	Zone	Main wing weight; lb	Labor costs		LCER	Total wing weight; lb	Total wing cost, $
	$/lb	$/lb				$	$/lb	$/lb		
	(a)	(Table 23-34)	③ ÷ ②	--	(Table 23-4)	(a)	⑦ ÷ ⑥	④ x ⑧	(Table 23-32)	⑨ x ⑩
Monocoque waffle	23	44	1 913	A	3 300	74 730	23	44	40 042	$1\ 762 \times 10^3$
				B	3 090	61 545	20	38	38 780	1 474
				C	3 370	85 755	25	48	21 054	1 011
				Σ	9 760	222 030	23	44	99 876	$4\ 247 \times 10^3$
Monocoque honeycomb	33	51	1 548	A	1 930	66 100	34	53	25 998	$1\ 378 \times 10^3$
				B	1 630	54 750	34	53	20 472	1 085
				C	2 410	77 890	32	50	15 098	755
				Σ	5 970	198 740	33	51	61 568	$3\ 218 \times 10^3$
Semimonocoque spanwise tubular	23	40	1 739	A	1 485	36 018	24	42	25 510	$1\ 071 \times 10^3$
				B	1 442	32 478	23	40	22 853	914
				C	2 031	43 946	22	38	12 408	472
				Σ	4 958	112 442	23	40	60 771	$1\ 457 \times 10^3$
Semimonocoque spanwise beaded	23	41	1 780	A	1 370	34 164	25	44	23 775	$1\ 046 \times 10^3$
				B	1 383	30 929	22	39	21 934	855
				C	1 917	41 796	22	39	11 682	456
				Σ	4 670	106 553	23	41	57 391	$2\ 357 \times 10^3$
Semimonocoque chordwise convex bead/tubular	24	49	2 040	A	2 130	50 685	24	48	30 870	$1\ 482 \times 10^3$
				B	1 750	41 660	24	46	24 764	1 189
				C	2 270	55 693	25	51	14 023	715
				Σ	6 150	148 038	24	48	69 657	$3\ 386 \times 10^3$
Statically determinate spanwise beaded	28	60	2 140	A	1 503	44 327	30	64	26 432	$1\ 691 \times 10^3$
				B	1 452	39 217	27	58	24 686	1 432
				C	1 888	52 909	28	60	12 052	723
				Σ	4 843	136 453	28	60	63 170	$3\ 846 \times 10^3$

[a] Ref table 23-12, 23-19 and 23-27.

TABLE 23-37

TOTAL WING STRUCTURE MATERIAL COSTS
($/lb AND $)

1	2	3	4	5	6	7	8	9	10	11
Structure concept	Matl costs	Matl CER	Matl factor	Zone	Main wing weight, lb	Material costs		MCER	Total wing weight, lb	Total wing cost, $
	$/lb	$/lb				$	$/lb	$/lb		
	(a)	(Table 23-34)	3 ÷ 2	-	(Table 23-4)	(a)	7 ÷ 6	4 x 8	(Table 23-32)	9 x 10
Monocoque waffle	47	114	2 425	A	3 300	155 324	47	114	40 042	$4\ 565 \times 10^3$
				B	3 090	127 391	41	100	38 780	3 873
				C	3 370	178 685	53	128	21 054	2 695
				Σ	9 760	461 400	47	114	99 876	$11\ 138 \times 10^3$
Monocoque honeycomb	36	88	2 440	A	1 930	70 657	37	89	25 998	$2\ 314 \times 10^3$
				B	1 630	57 768	35	85	20 472	1 740
				C	2 410	85 539	35	85	15 098	1 283
				Σ	5 970	213 964	36	88	61 568	$5\ 337 \times 10^3$
Semimonocoque spanwise tubular	26	67	2 577	A	1 485	40 157	27	70	25 510	$1\ 786 \times 10^3$
				B	1 442	37 839	26	67	22 853	1 531
				C	2 031	48 904	24	62	12 408	769
				Σ	4 958	126 900	26	67	60 771	$4\ 086 \times 10^3$
Semimonocoque spanwise beaded	26	68	2 615	A	1 370	38 171	28	73	23 775	$1\ 736 \times 10^3$
				B	1 383	36 180	26	68	21 934	1 492
				C	1 917	46 602	24	63	11 682	736
				Σ	4 670	120 953	26	68	57 391	$3\ 964 \times 10^3$
Semimonocoque chordwise convex bead/tubular	24	67	2 790	A	2 130	53 635	25	70	30 870	$2\ 161 \times 10^3$
				B	1 750	43 005	25	70	24 764	1 733
				C	2 270	54 100	24	67	14 023	940
				Σ	6 150	150 741	24	67	69 657	$4\ 834 \times 10^3$
Statically determinate spanwise beaded	28	81	2 900	A	1 503	44 690	30	87	26 432	$2\ 300 \times 10^3$
				B	1 452	40 921	28	81	24 686	2 000
				C	1 888	52 013	28	81	12 052	976
				Σ	4 843	137 624	28	81	63 170	$5\ 276 \times 10^3$

[a] Ref. table 23-12, 23-19, and 23-27.

TABLE 23-38

TOOLING COST ESTIMATING RELATIONSHIP FOR OVERALL WING STRUCTURE

Primary-structure concept		Monocoque		Semimonocoque			Statically determinate
		Waffle	Honeycomb	Spanwise		Chordwise	
				Tubular	Beaded	a	Beaded
1 Costed basic structure wt[b]	lb	9 760	5 970	4 958	4 670	6 150	4 843
2 Estimated fab and assy.[c]	$	3 512 500	2 350 700	3 370 800	4 092 200	3 108 300	4 244 200
3 Basic unit cost ($\boxed{2} \div \boxed{1}$)	$/lb	360	478	679	875	506	878
4 Weight of misc & mach parts[b]	lb	1 456	851	734	695	982	1 105
5 Misc & mach parts tool cost[d]	$	524 000	407 000	498 000	607 000	496 000	970 000
6 Total tooling cost ($\boxed{2} + \boxed{5}$)	$	4 036 500	4 357 700	3 868 800	4 699 200	3 604 300	5 214 200
7 Estimate weight[b]	lb	11 2[illegible]	6 821	5 692	5 365	7 132	5 948
8 Tooling CER	$/lb	360	478	679	875	506	878

[a] Convex beaded, upper, tubular, lower.

[b] Ref. Table 23-34.

[c] Ref. Tables 23-12, 23-19, and 23-27 for nonrecurring costs.

[d] $\boxed{3} \times \boxed{4}$

TABLE 23-39

OVERALL TOOLING COST ESTIMATING RELATIONSHIP

1	2	3	4	5	6	7	8	9	10	11
Structure concept	Structure segment	Est. tool cost-SST	Tooling CER	Total weight	Structure tool. cost	Structure CER ($/lb)	FM & AT CER ($/lb)	Initial tool CER ($/lb)	Overall tooling CER ($/lb)	Overall wing tool cost ($)
		hr/lb	$/lb	lb	$	Σ6 Σ5	.234 7[c]	7 + 8	2 9	$
Monocoque waffle	Wing		360	99 876	35 955 360					$1\ 414 \times 10^5$
	Fuselage		780[a]	86 289	67 305 420					
	Empennage		1100[b]	6 990	7 689 000					
	Σ			193 155	110 949 780	574	1343	708	1416	
Monocoque honeycomb	Wing		478	61 568	29 429 504					1.024×10^5
	Fuselage		780	86 289	67 305 420					
	Empennage		1100	6 990	7 689 000					
	Σ			154 847	104 423 924	674	158	832	1664	
Semimonocoque spanwise tubular	Wing		679	60 771	41 263 509					$1\ 133 \times 10^5$
	Fuselage		780[a]	86 289	67 305 420					
	Empennage		1100[b]	6 990	7 689 000					
	Σ			154 050	116 257 929	755	177	932	1864	
Semimonocoque spanwise beaded	Wing		875	57 391	50 217 125					$1\ 176 \times 10^5$
	Fuselage		780[a]	86 289	67 305 420					
	Empennage		1100[b]	6 990	7 689 000					
	Σ			150 670	125 211 545	831	194	1025	2050	
Semimonocoque chordwise	Wing	85	506	69 657	35 246 442					$1\ 186 \times 10^5$
	Fuselage	131	780[a]	86 289	67 305 420					
	Empennage	185	1100[b]	6 990	7 689 000					
	Σ			162 936	110 240 862	690	161	851	1702	
Statically determinate spanwise beaded	Wing		878	63 170	55 463 260					$1\ 299 \times 10^5$
	Fuselage		780[a]	89 984	70 187 570					
	Empennage		1100[b]	6 990	7 689 000					
	Σ			160 144	133 339 780	833	195	1028	2056	

[a] Tooling CER for fuselage = (Wing CER for Semimono. Chordwise) (131/85).
[b] Tooling CER for empennage = (Wing CER for Semimono Chordwise) (185/85).
[c] FM & AT, final mate and assembly tooling cost est. relationship = 19/81 (struc CER).
[d] Convex beaded, upper; tubular, lower.
[e] Fuselage weight includes increase in body weight of 3695 lb.
[f] Overall wing tooling costs = (Wing weight) (Overall tooling CER).

TABLE 23-40

TOTAL WING STRUCTURE MANUFACTURING COSTS
BASELINE 550,000 LB AIRPLANE
(100 VEHICLES)

Primary structure concept	Monocoque		Semimonocoque			Statically determinate
			Spanwise		Chordwise	Spanwise
	Waffle	Honeycomb-core	Tubular	Beaded	Convex-beaded/tubular	Beaded
Labor, $\$ \times 10^3$	4 247	3 218	2 457	2 357	3 386	3 846
Material, $\$ \times 10^3$	11 138	5 337	4 086	3 964	4 834	5 276
Tooling, $\$ \times 10^3$	1 414	1 024	1 133	1 176	1 186	1 299
Total cost, cost, $\$ \times 10^3$	16 799	9 579	7 676	7 497	9 406	10 421
Weight, lb	99 876	61 568	60 771	57 391	69 657	63 170
Dollars/lb	168	156	126	131	135	165
Dollars/ft^2	1 719	980	785	767	962	1 066

[a]Total costed wing area = 9774 ft^2.

TABLE 23-41

VEHICLE COST ESTIMATING FACTORS

Costing factors	Units	Value
CPAV = cost per pound of avionics	$/lb	1590
CECSL = labor cost for ECS	$/lb	30
CECSM = material cost for ECS	$/lb	192
CEL = labor cost for elevons	$/lb	63
CEM = material cost for elevons	$/lb	110
CELRL = labor cost for electrical	$/lb	89
CELRM = material cost for electrical	$/lb	93
CFEQL = labor cost for furnishings and equipment	$/lb	44
CFEQM = material cost for furnishings and equipment	$/lb	48
CFCL = labor cost for flight controls	$/lb	75
CFCM = material cost for flight controls	$/lb	385
CFINL = labor cost for fins	$/lb	153
CFINM = material cost for fins	$/lb	126
CFSL = labor cost for fuel system	$/lb	151
CFSM = material cost for fuel system	$/lb	289
CFUSL = labor cost for body structure	$/lb	65
CFUSM = material cost for body structure	$/lb	46
CHYDL = labor cost for hydraulic	$/lb	120
CHYDM = material cost for hydraulic	$/lb	342
CINLL = labor cost for inlet	$/lb	219
CINLM = material cost for inlet	$/lb	325

TABLE 23-41
(Concluded)

Costing factors	Units	Value
CINTL = labor cost for instruments	$/lb	29
CINTM = material cost for instruments	$/lb	186
CLEL = labor cost for wing leading edges	$/lb	*
CLEM = material cost for wing leading edges	$/lb	*
CMWLA = labor cost for wing structures - A	$/lb	*
CMWLB = labor cost for wing structures - B	$/lb	*
CMWLC = labor cost for wing structures - C	$/lb	*
CMWMA = material cost for wing structures - A	$/lb	*
CMWMB = material cost for wing structures - B	$/lb	*
CMWMC = material cost for wing structures - C	$/lb	*
CNCL = labor cost for nose cap	$/lb	105
CNCM = material cost for nose cap	$/lb	350
CPLG = labor cost for landing gear	$/lb	2
CPLGM = material cost for landing gear	$/lb	29
ICPAV = installation cost per pound of avionics	$/lb	154.0
NTRJ = number of engines per vehicle		4.0

*Reference table 23-42.

TABLE 23-42

OVERALL WING COST ESTIMATING FACTORS ($/LB)

Structure concept	Monocoque		Semimonocoque			Statically determinate
	Biaxial		Spanwise		Chordwise	Spanwise
	Waffle	Honeycomb	Tubular	Beaded	a	Beaded
Wing A						
Labor	44	53	42	44	48	64
Material	114	89	70	73	70	87
Wing B						
Labor	38	53	40	39	48	58
Material	100	85	67	68	70	81
Wing C						
Labor	48	50	38	39	51	60
Material	128	85	62	63	67	81
Leading edge						
Labor	23	23	20	20	20	20
Material	78	78	67	67	67	67
Overall tooling	1416	1664	1864	2050	1702	2056

TABLE 23-43

TOTAL VEHICLE PRODUCTION COSTS[a]
(100 VEHICLES)

Primary structure concept	Dollars ($)
Monocoque waffle	51.745×10^6
Monocoque honeycomb	46.273
Semimonocoque spanwise tubular	44.255
Semimonocoque spanwise beaded	44.032
Semimonocoque chordwise convex beaded, upper; tubular, lower	45.814
Statically determinate spanwise beaded	46.835

[a]Labor and material, less engines.

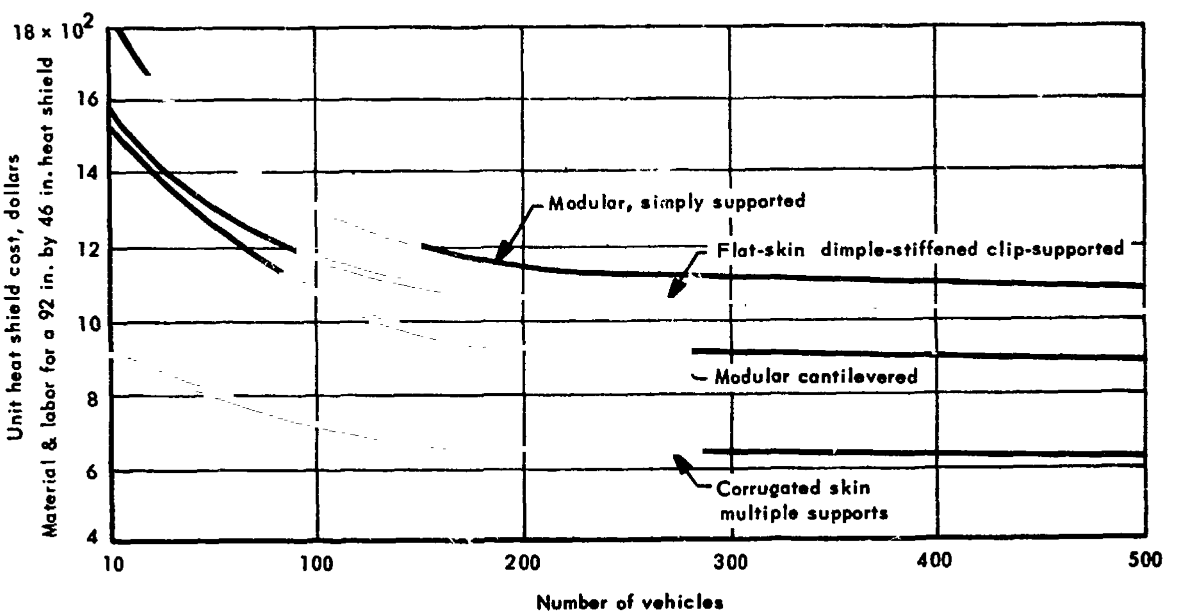

F71

Figure 23-1. Unit heat shield cost versus number of aircraft

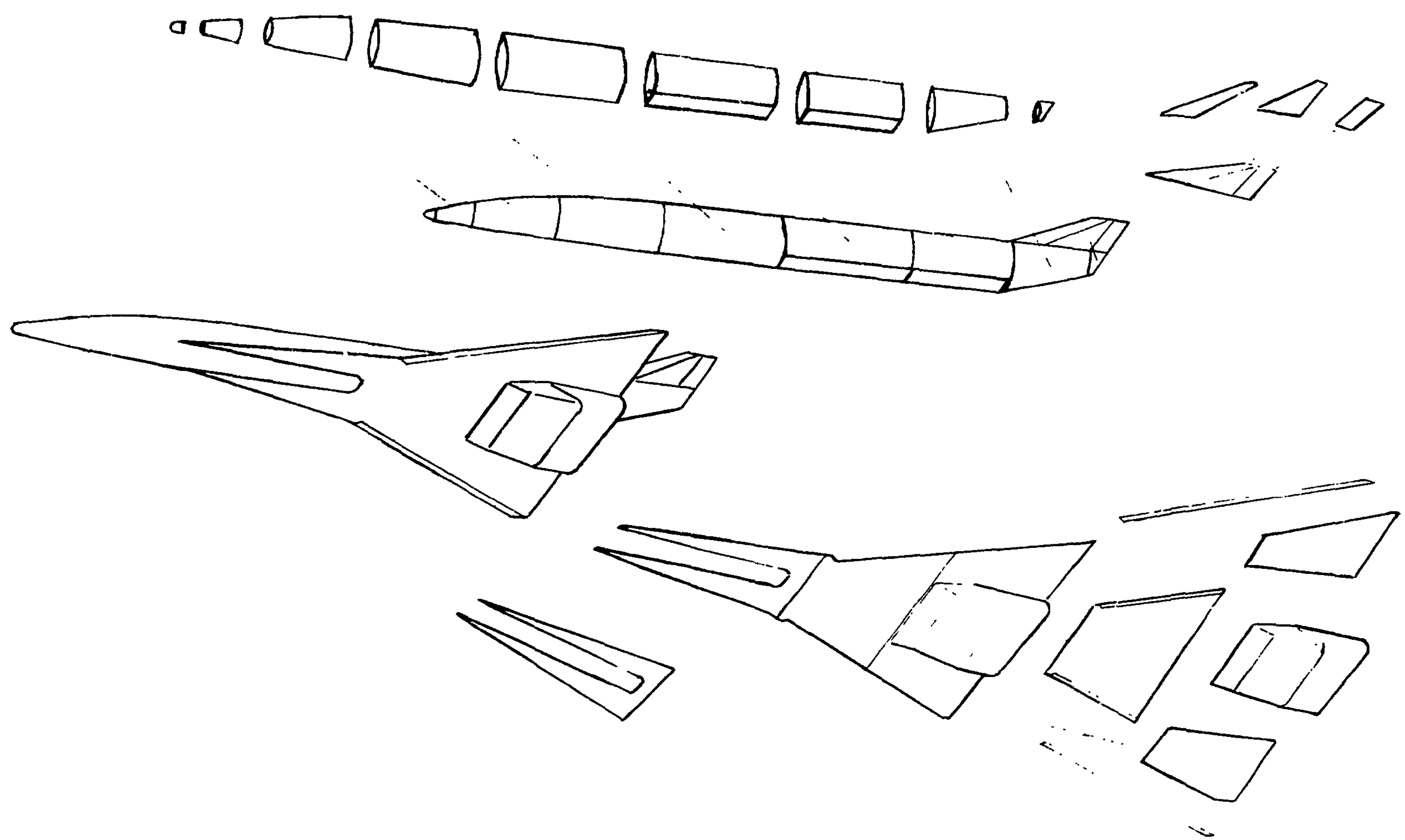

Figure 23-2. Hypersonic cruise airplane - manufacturing segments

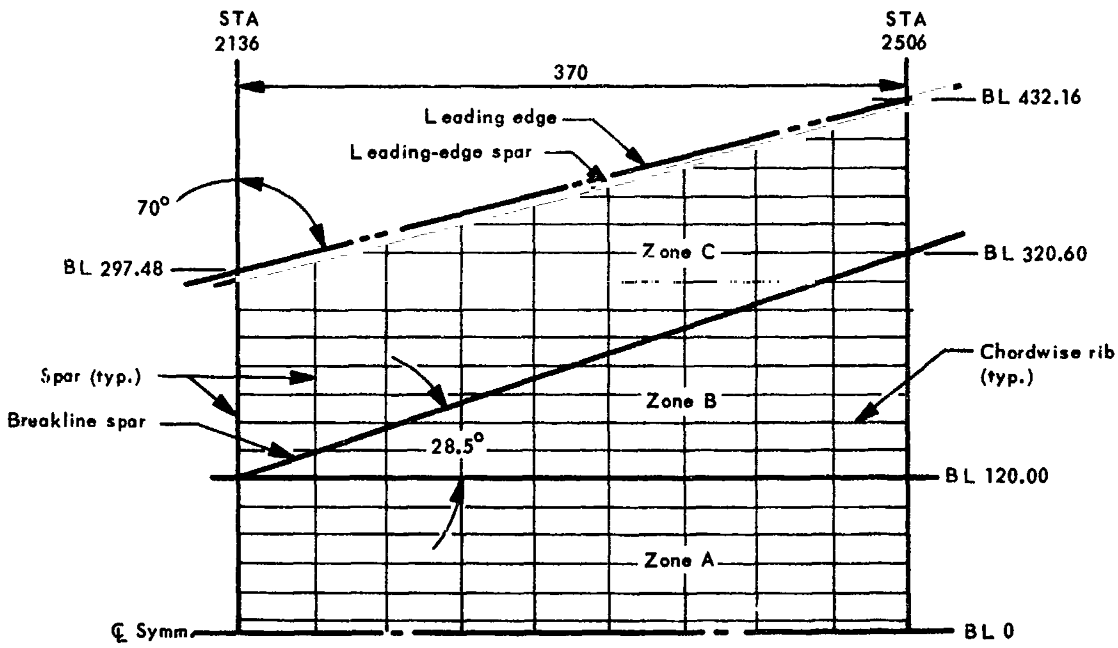

Zone	Area (ft^2)	
A	616	
B	515	
C	743	includes leading edge (S_{1e} = 30 ft^2)
Total	1874	

Figure 23-3. Manufacturing segment, main wing

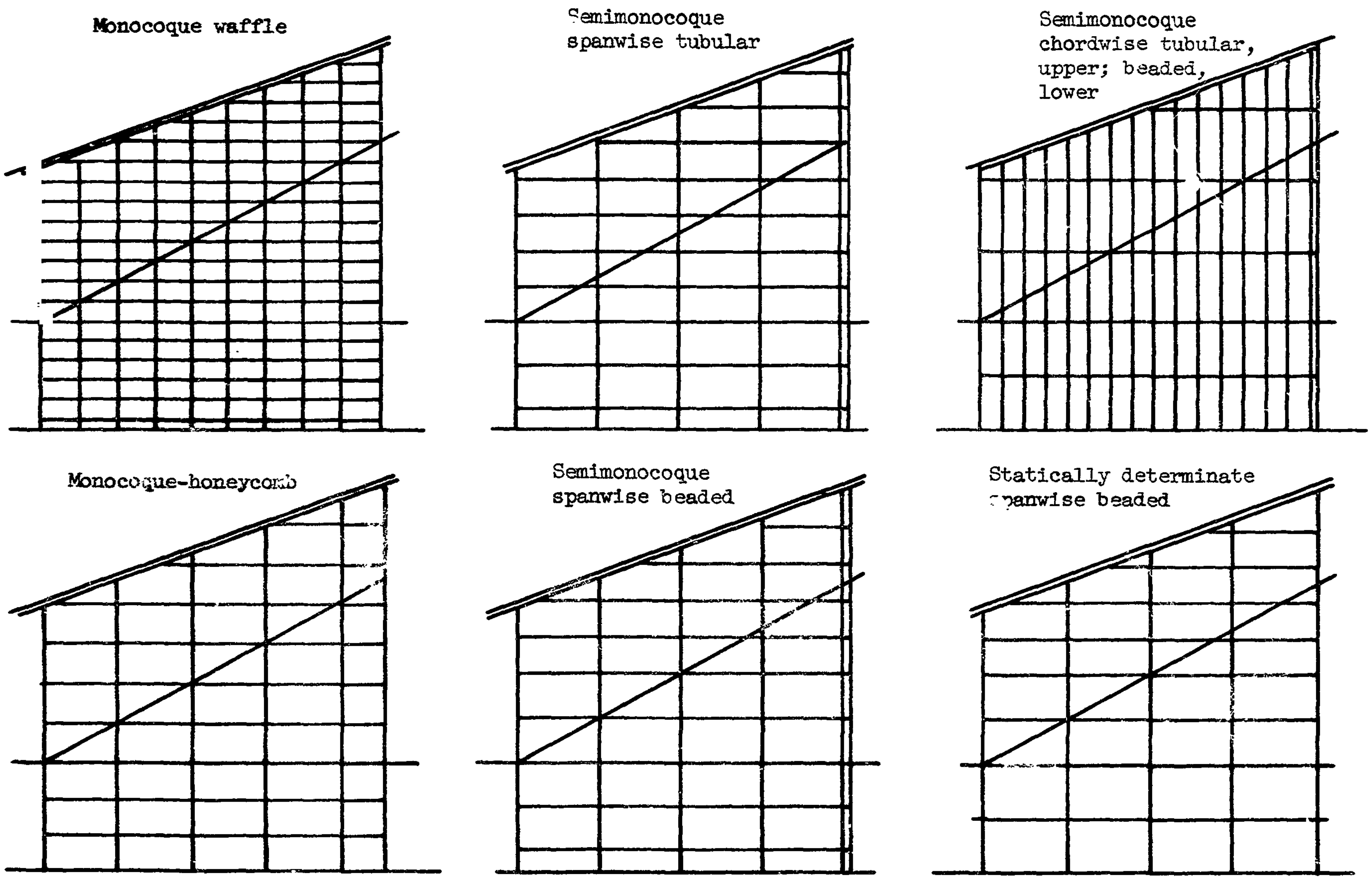

Figure 23-4. Structure concept arrangement

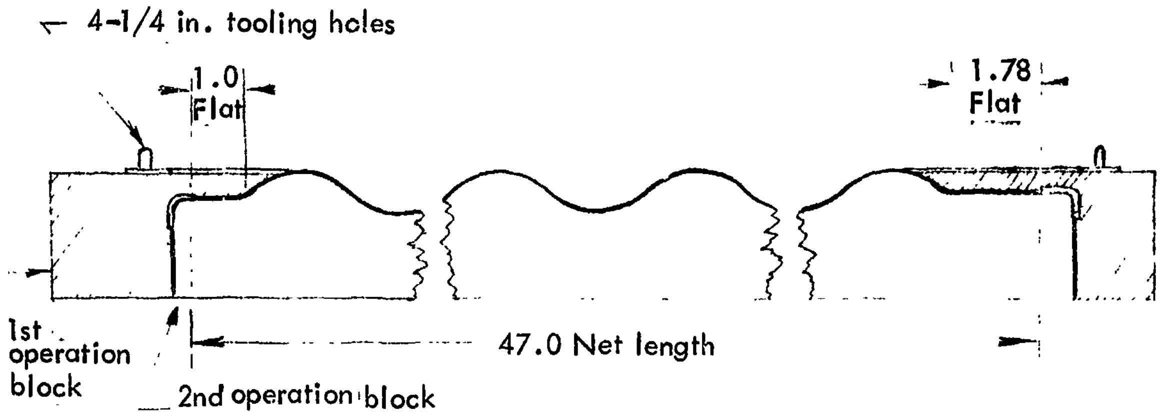

Amount of material

Develop blank,

0.02 in. x 44.4 x 49 inches^2 x 0.298 lb/in.^{3} = 12.97 lb

Net part

0.02 in. x 2087 inches^2 x 0.298 lb/in.^{3} = 12.44 lb

Material cost

2176 inches^2 x 0.0808* \$/in.^{2} = \$175.82

Production time

ECH Ref.	Operation	Set-up time	Run time
10.220	Shear strip, blank and pierce, burr, clean, and ID	3.43	0.348
10.220	Verson form 1st block	0.05	0.085
10.220	Verson form 2nd block	0.05	0.085
1.106	Shear ends to net trim (remove added trim and T.H.'s)	0.13	0.145
	Total (hours)	3.66	0.663 (hours)

* Ref: Engineering Cost Handbook (ECH)

Figure 23-5. Circular-arc Corrugation Web element Fabrication

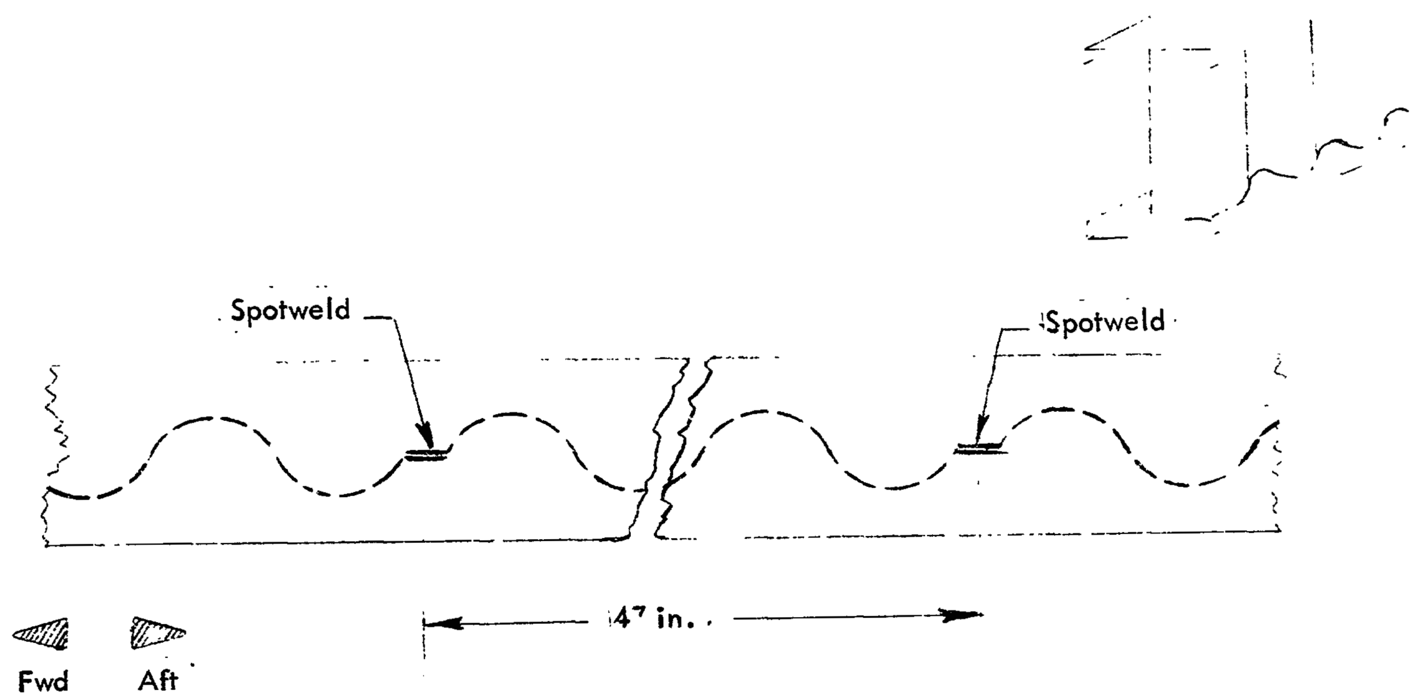

Note: This is a representative drawing and is not drawn to scale. Sections of web lie between the spanwise beams spaced 47 inches apart.

Figure 23-6. Typical chordwise rib assembly

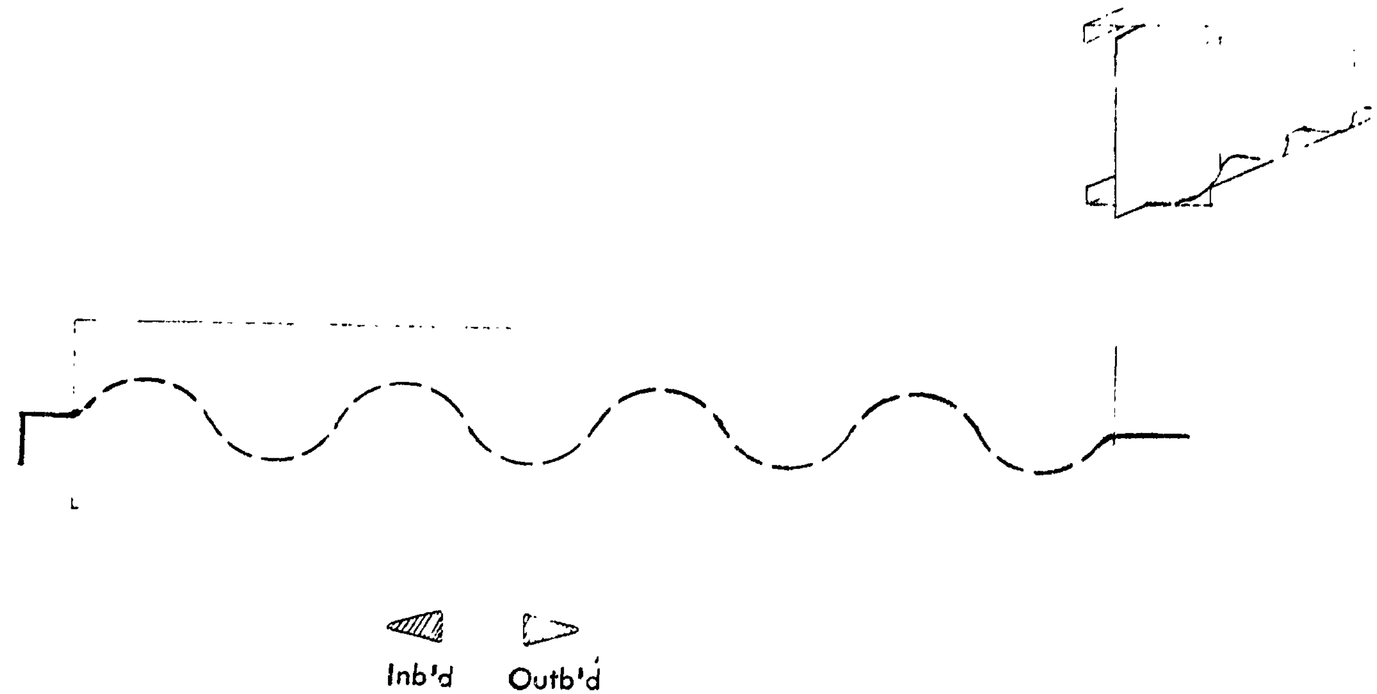

Note: This is a representative drawing and is not drawn to scale. Sections of web and cap lie between chordwise beams.

Figure 23-7. Typical spanwise beam segment

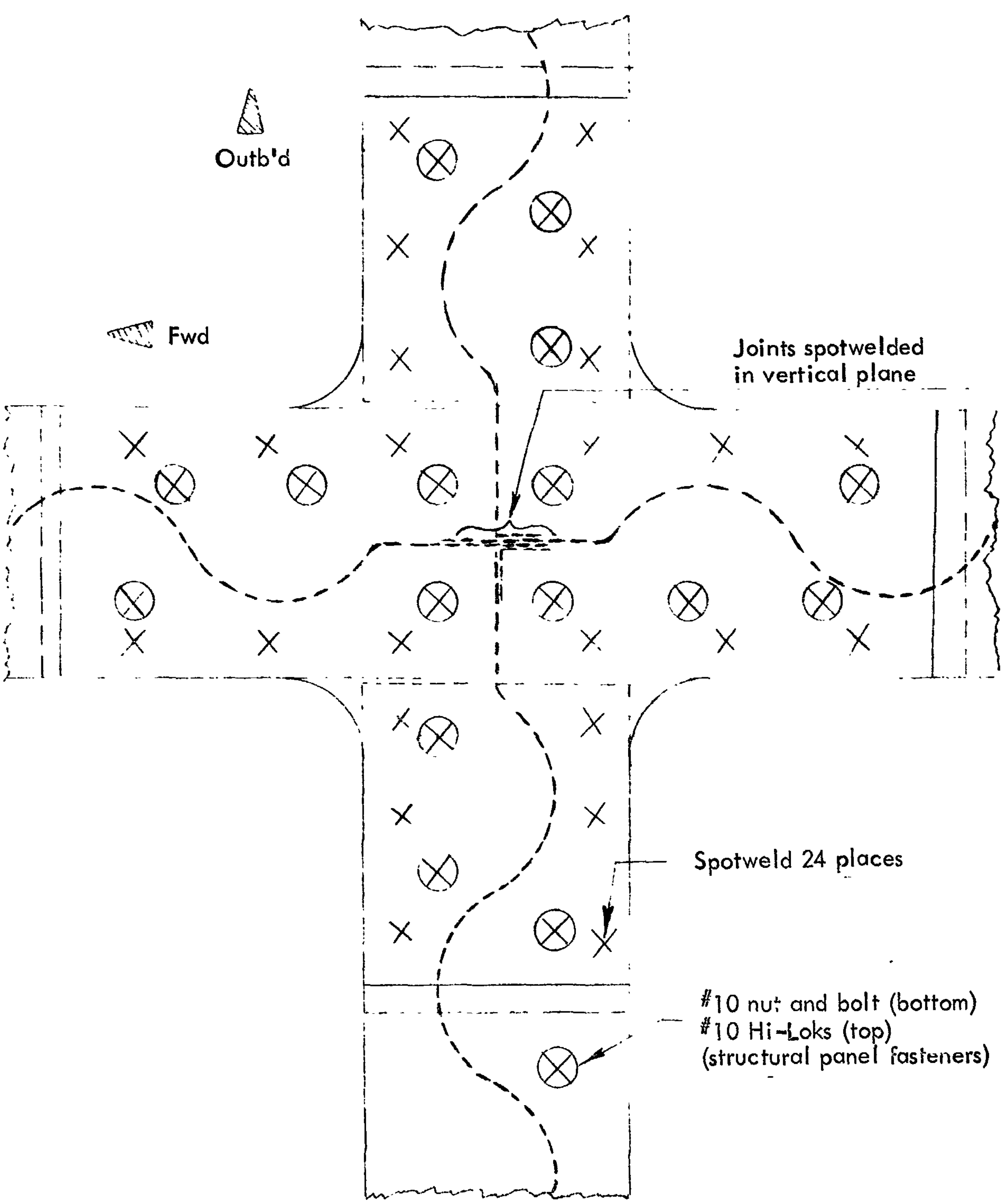

Figure 23-8. Typical intersection detail

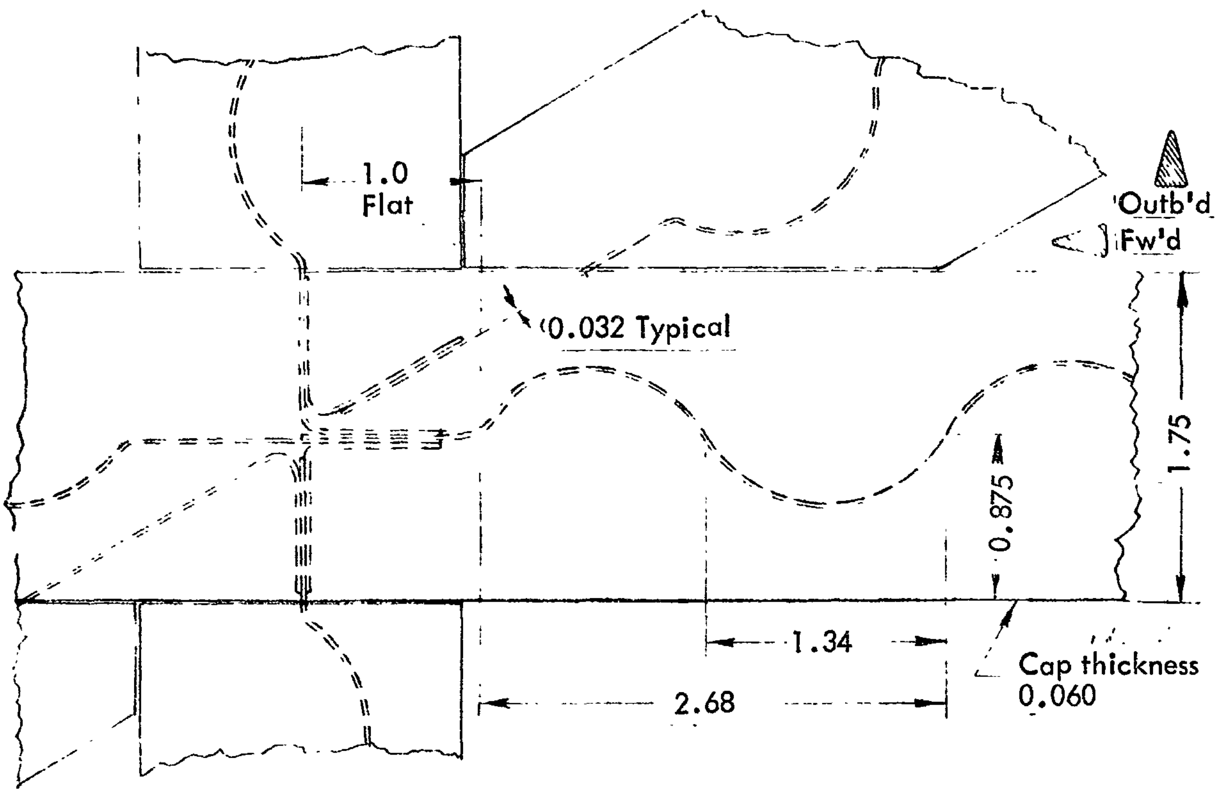

1.34	Linear dim./node	44.22	Linear node length
x 33	Nodes/panel	+1.00	Flat 1st end
44.22	Linear length/33 nodes	+1.78	Flat 2nd end
		47.00	Inches = Total linear length

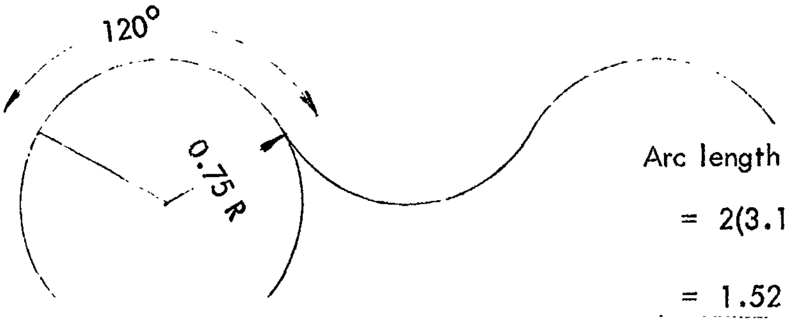

Web circular
Arc corrugation

$$\text{Arc length} = 2 \cdot R \cdot \frac{\text{Arc}}{360^\circ} \cdot \pi$$

$$= 2(3.1416)(0.75)\frac{120}{360}$$

$$= 1.52 \text{ inches}$$

Figure 23-9. Typical web and beam cap intersection detail

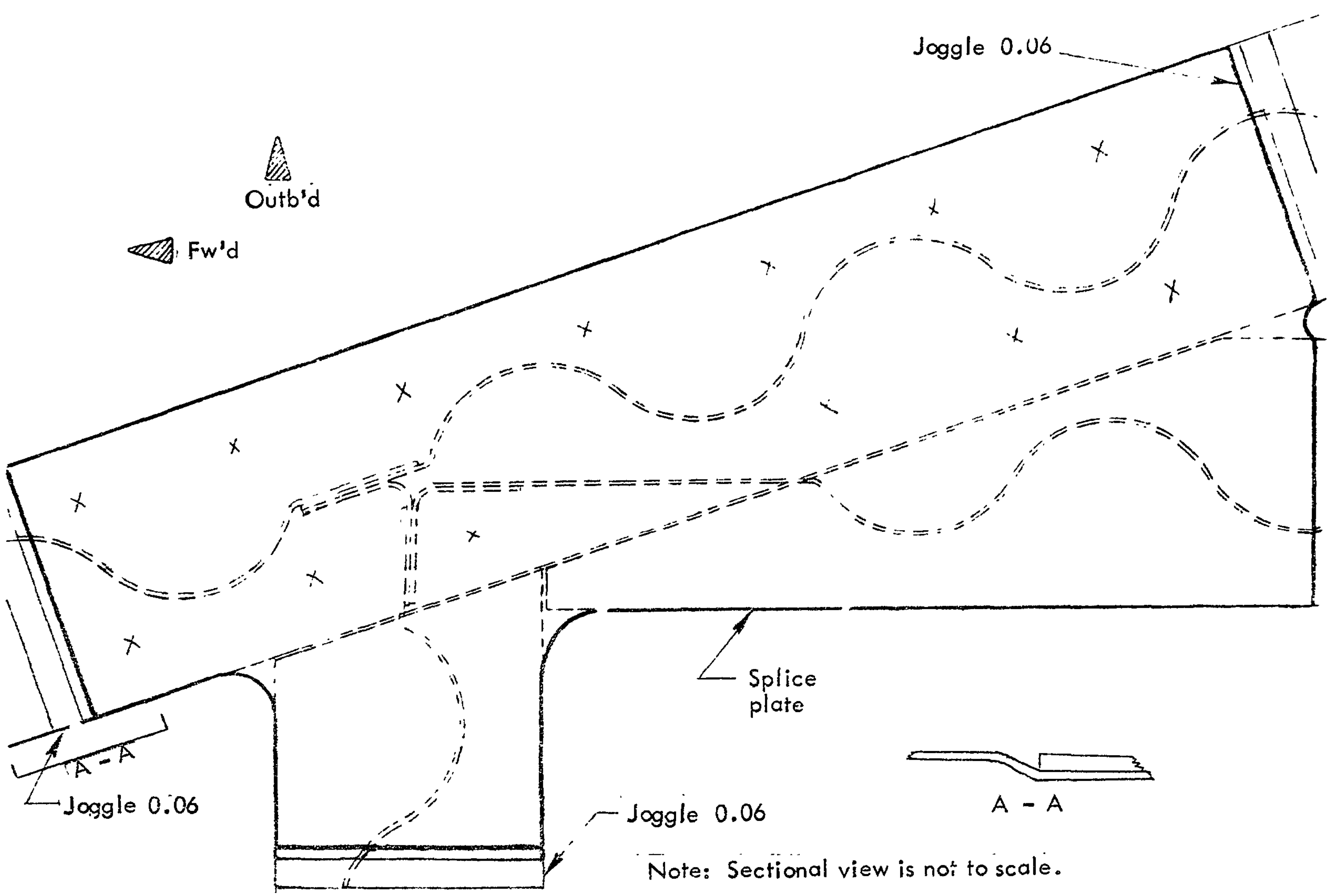

Figure 23-10. Right wing leading-edge cap

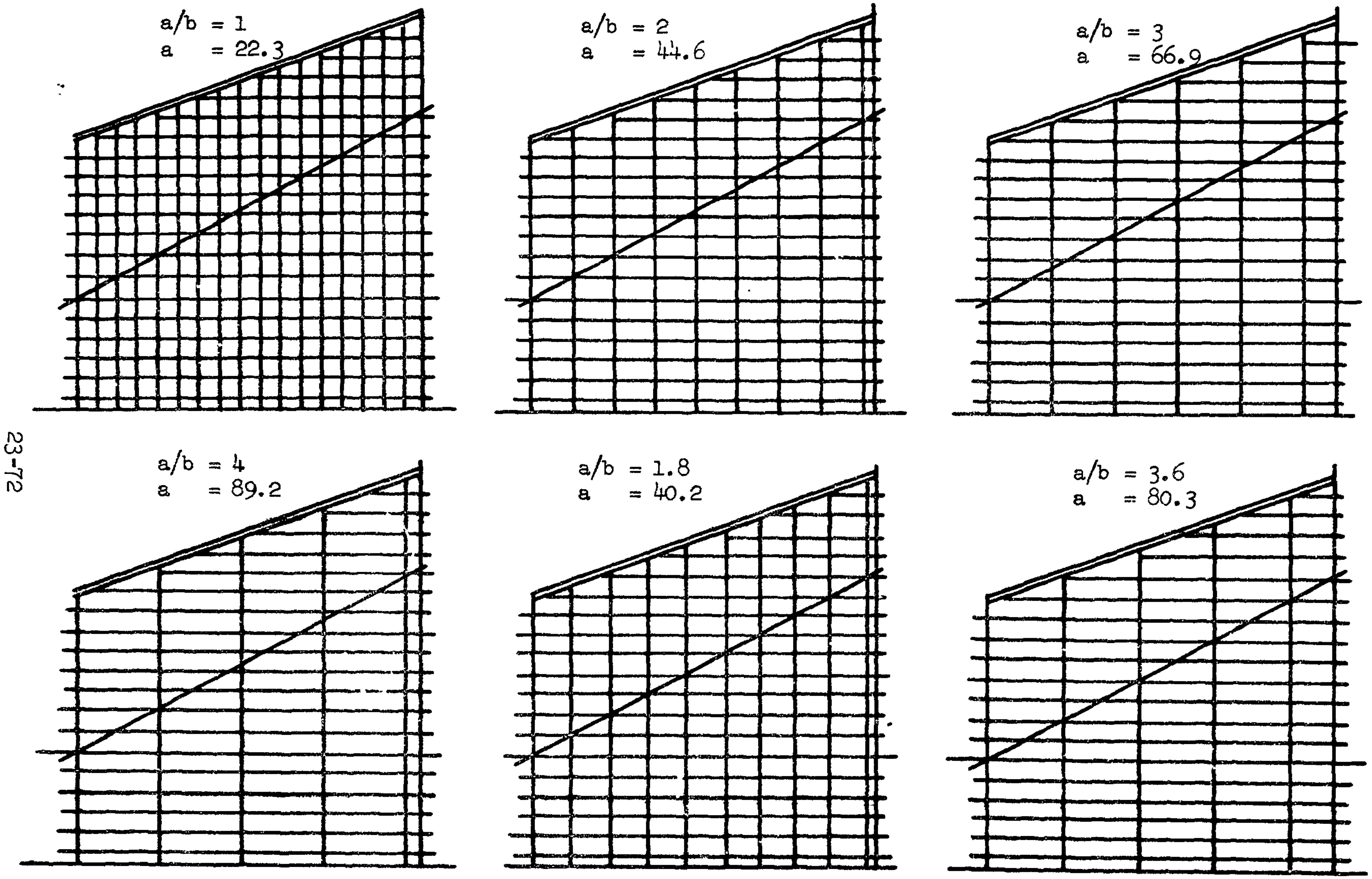

Figure 23-11. Panel aspect ratio study, monocoque waffle primary structure concept (b = 22.3)

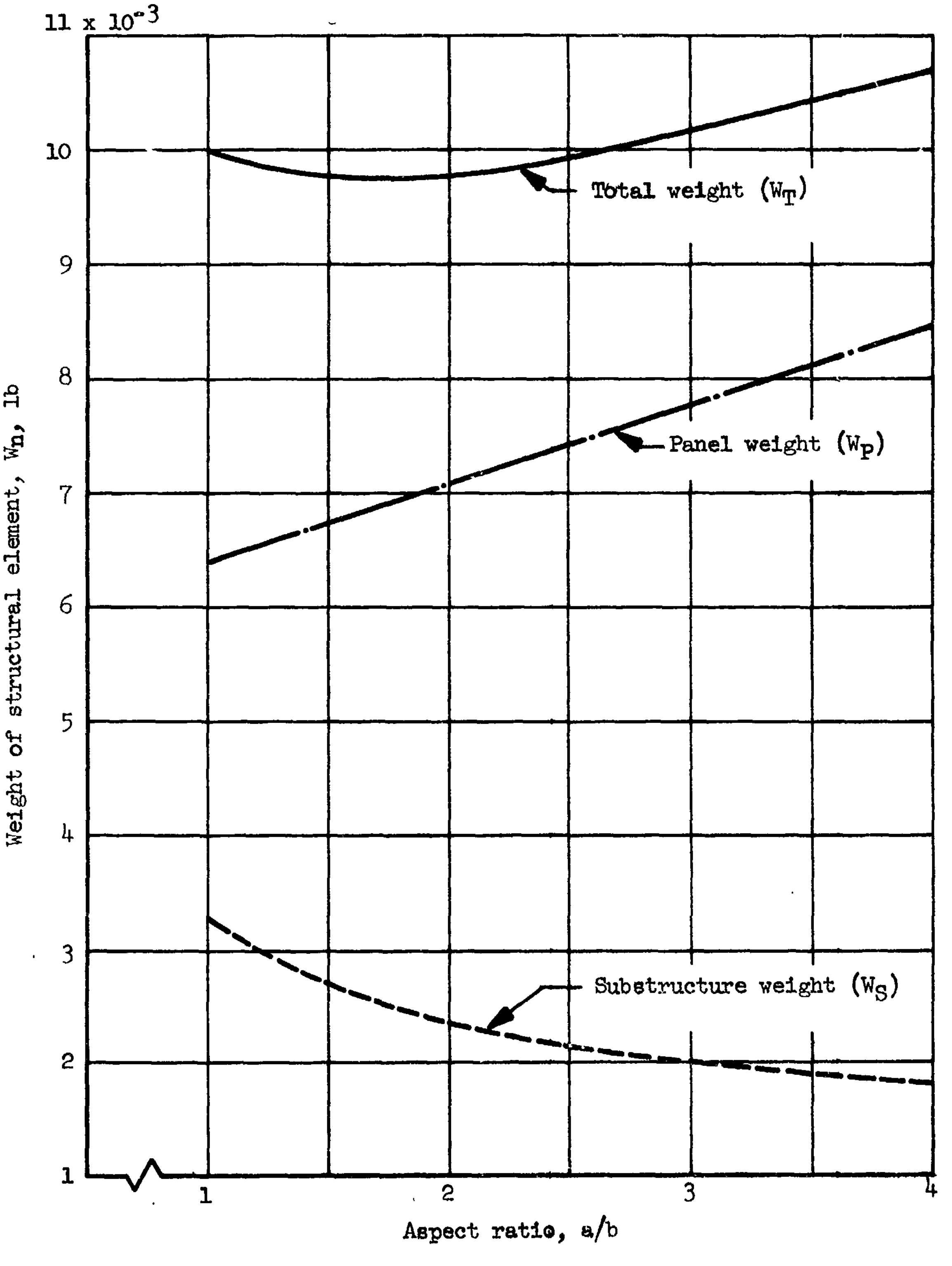

Figure 23-12. Main wing segment weight variation with aspect ratio

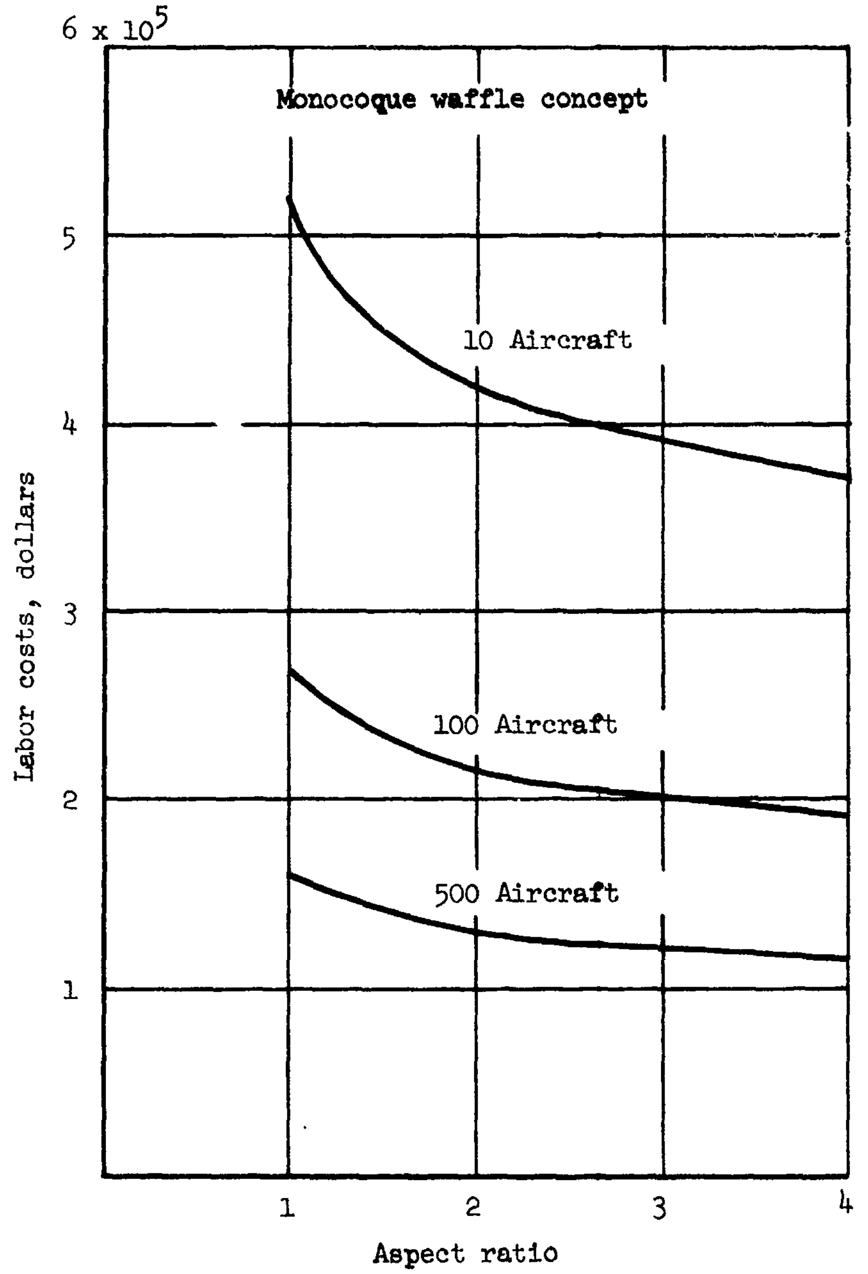

Figure 23-13. Labor cost vs aspect ratio

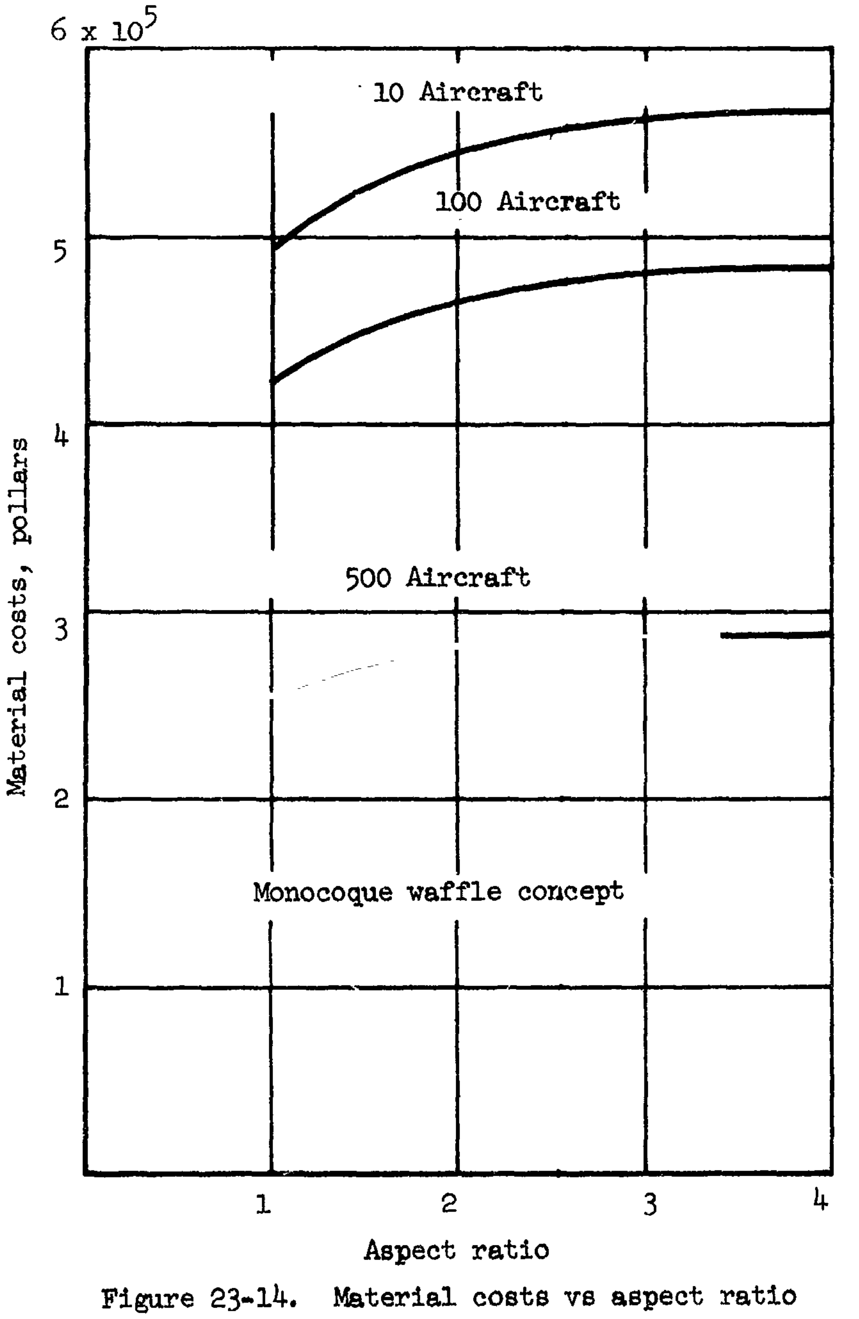

Figure 23-14. Material costs vs aspect ratio

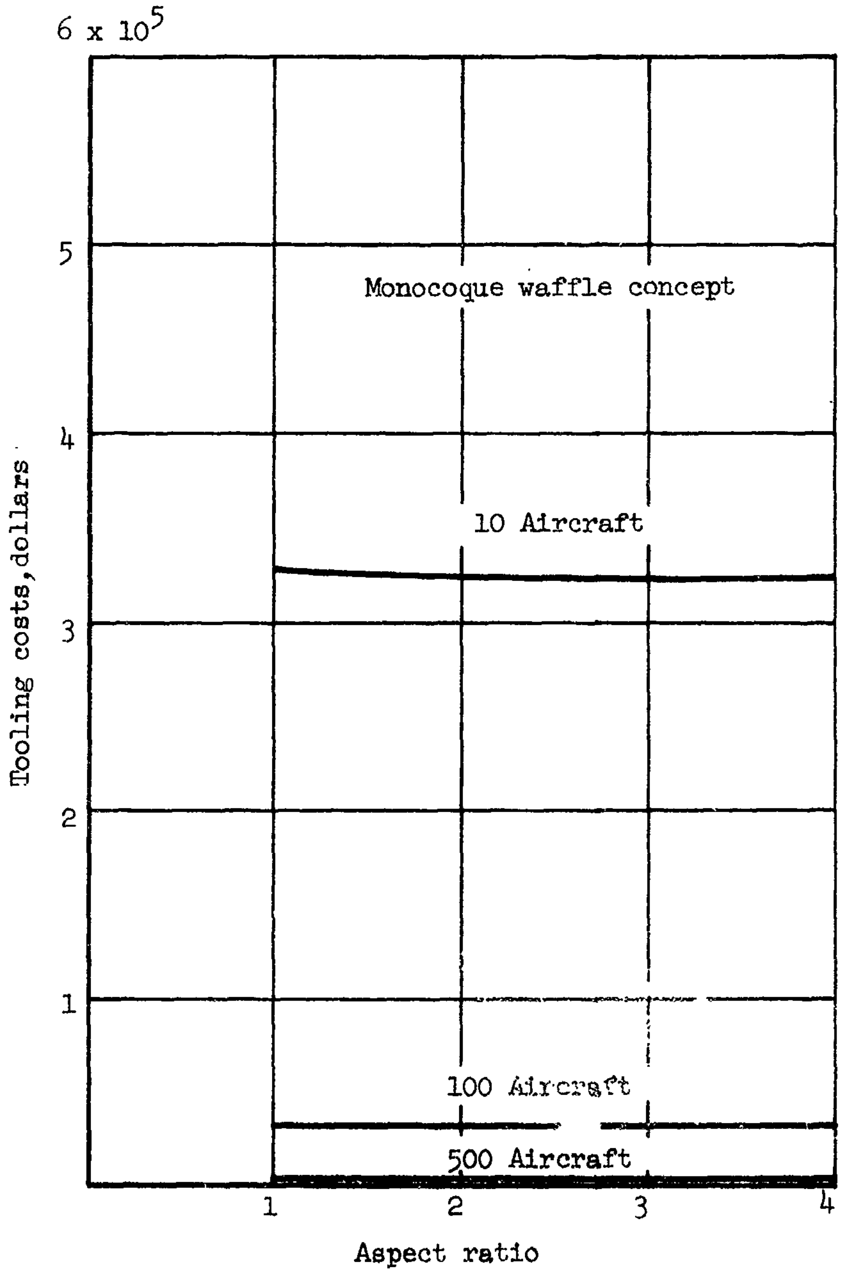

Figure 23-15. Tooling costs vs aspect ratio

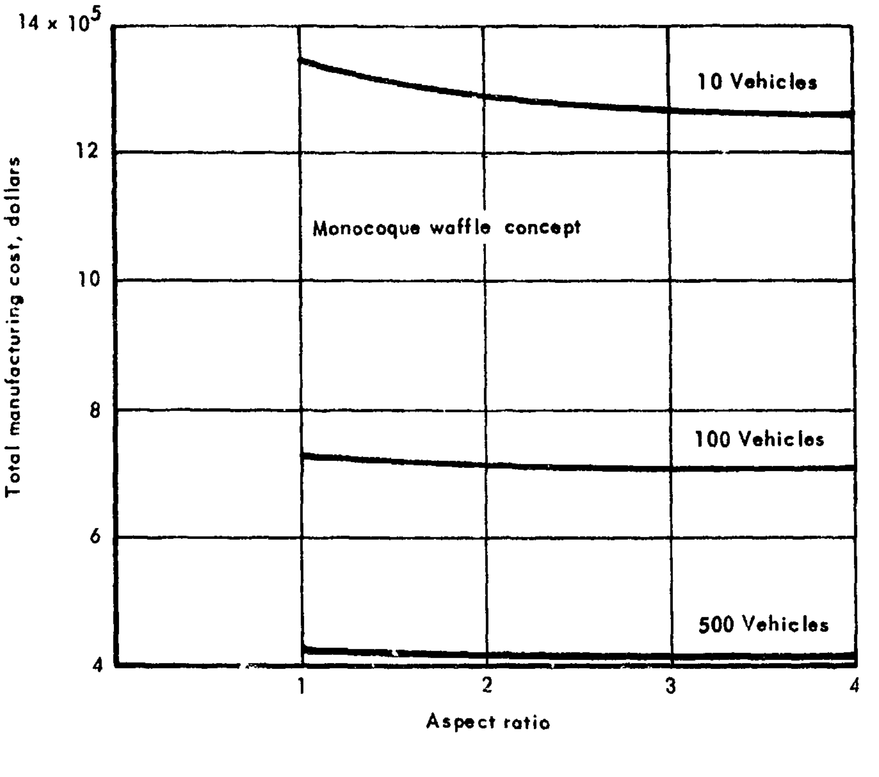

Figure 23-16. Total manufacturing cost vs aspect ratio

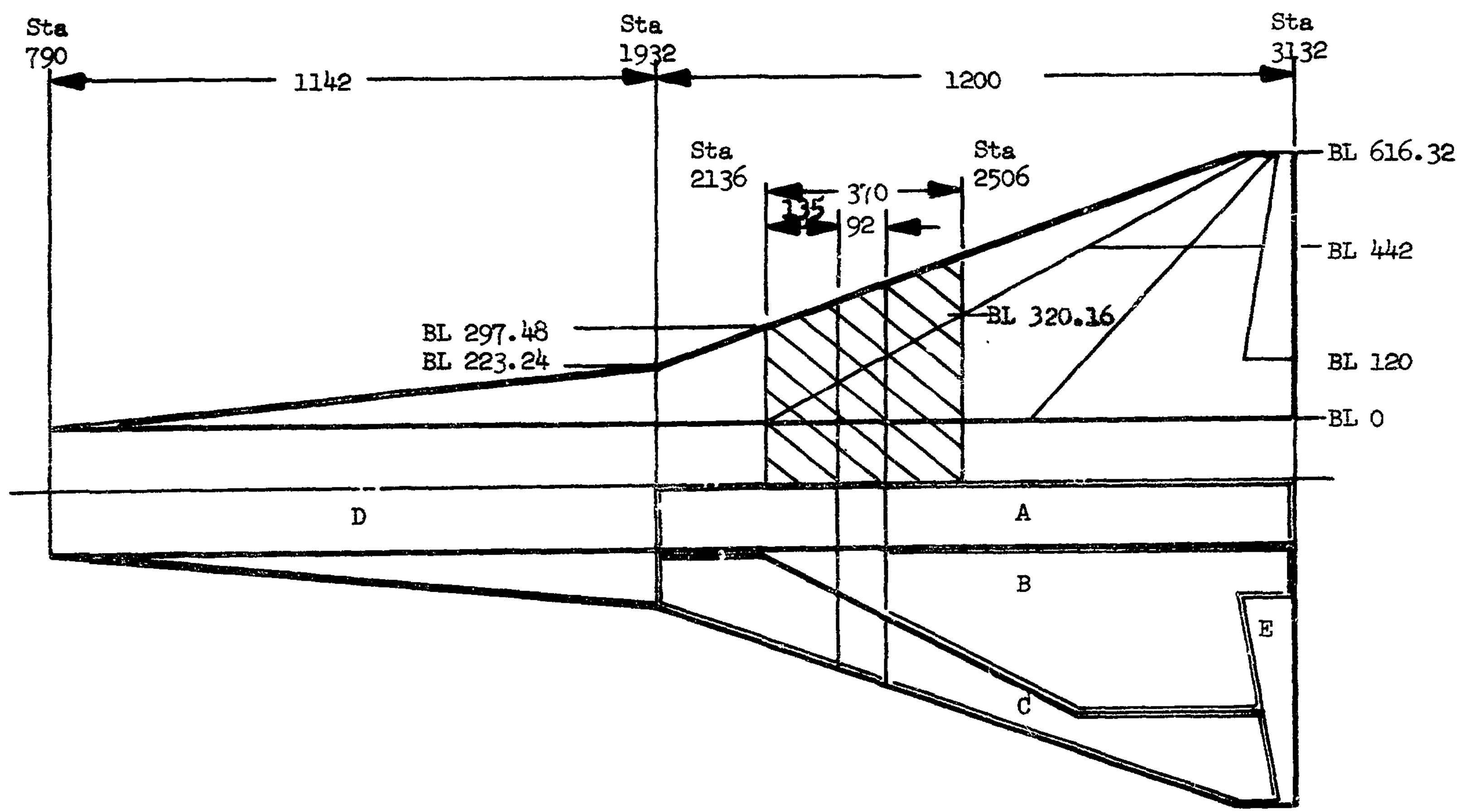

Figure 23-17. Wing geometry and reference areas for baseline vehicle

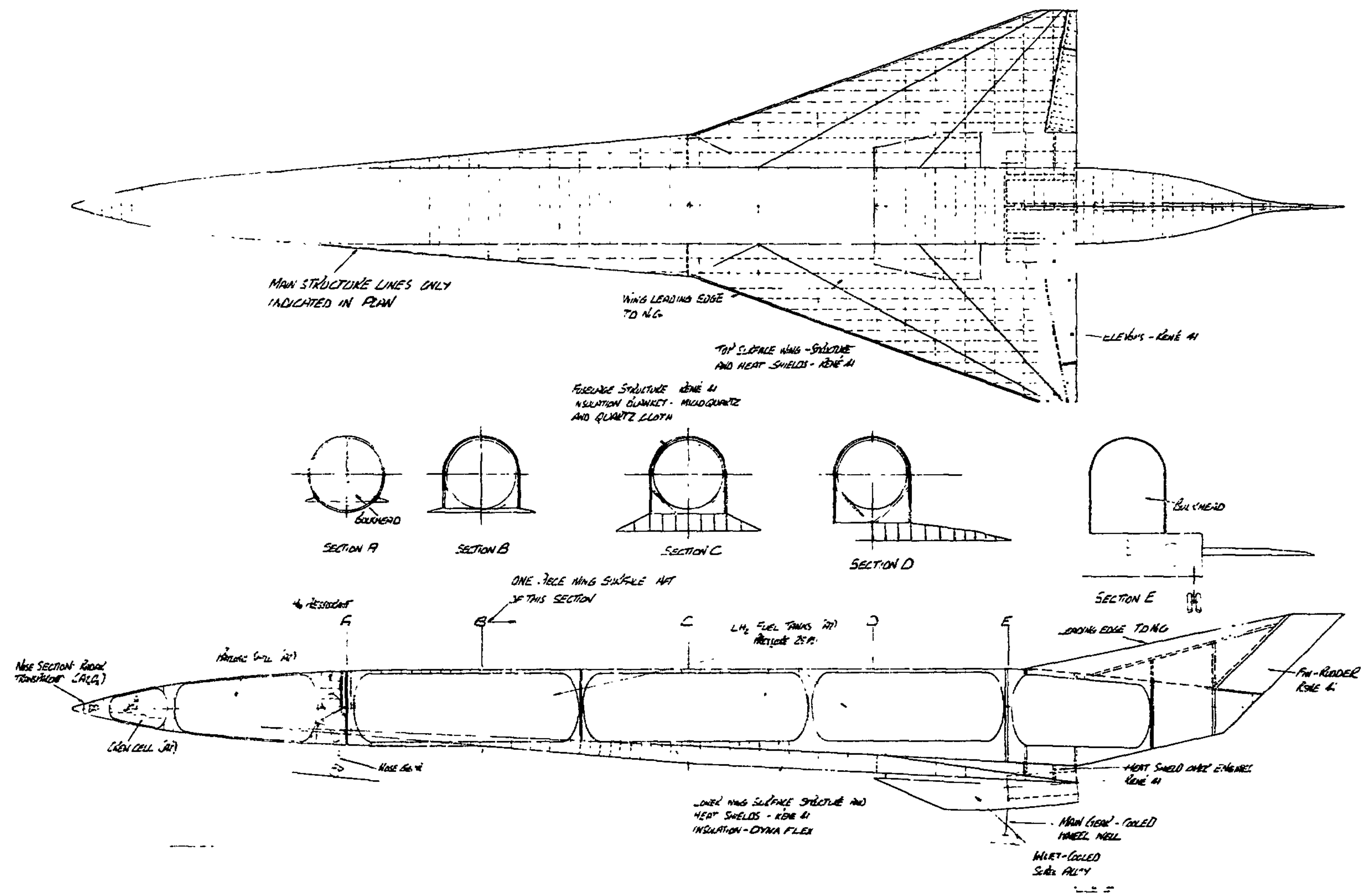

Figure 23-18. Structure general assembly

Section 24

PERFORMANCE ANALYSIS

by

R. S. Peyton

PRECEDING PAGE BLANK NOT FILMED.

CONTENTS

PRECEDING PAGE BLANK NOT FILMED.

TABLES

PRECEDING PAGE BLANK NOT FILMED.

ILLUSTRATIONS

Figure		Page

SYMBOLS

BL	Butt line
FS	Fuselage station
g	Gravitational acceleration
L	Distance between end closeouts
ϵ	Maximum height or depth of surface wave
λ	Wave length of surface perturbation
μ	Wave length of surface perturbation normal to airflow

Section 24

PERFORMANCE ANALYSIS

The performance analyses consisted of evaluating the primary structures, heat shields, and leading edges for performance degradation (aerodynamic drag losses) due to surface roughness and wing distortion.

METHODS AND PARAMETRIC DESIGN DATA

Methods and parametric design data were established for evaluating performance degradation (aerodynamic drag loss) in terms of fuel increment due to surface roughness and wing distortion (due to deflection). Performance degradation was investigated for the following types of roughness and distortion of the wing

Uniformly Distributed or Equivalent Sand Grain Roughness

This type of roughness results from the unpolished condition of the wing skin, coatings on the wing skin, spotwelds, or anything else that mars the finish of the wing skin. The uniformly distributed roughness increases the friction drag throughout the entire flight regime.

The incremental drag contribution due to the uniformly distributed (sand grain) roughness was assessed with the computer program described in reference 24-1. This program, which was developed at NASA Langley Research Center, combines the Sommer and Short T' method (ref. 24-2) and Goddard's method (ref. 24-3) to compute skin friction drag coefficients on a flat plate with variable and sand grain roughness. All portions of the wing were presumed to have the same surface roughness. The drag increments due to various degrees of surface roughness were assessed over the nominal flight profile. Performance losses due to partial areas of roughness are determined by reducing the fuel increment using the ratio of the partial area to the total surface of the wing.

Sheet Metal Joints and Fasteners

Surface protrusions and cavities are produced by various sheet metal joints and fasteners. These surface imperfections produce pressure drag at all flight speeds.

As suggested by Hoerner in reference 24-4 (Chapters 5 and 17), the estimation of the drag contributions due to the sheet metal joints and fasteners was based on the local flow properties within that part of the boundary layer affecting the protuberance or cavity. An appropriate form drag coefficient based on the shape of the surface imperfection and the local Mach number was determined. This drag coefficient, combined with the local dynamic pressure, was used to estimate the drag contributions of the sheet metal joints and fasteners.

Two-dimensional Surface Waviness in Which the Wave Crests are Perpendicular to the Wing Chord

This type of wing distortion may result from fabrication tolerances and deflections in the wing skin due to air loads and thermal effects. The surface waviness contributes pressure drag primarily during transonic and supersonic flight.

The pressure drag contributions of the surface waves were estimated with the linearized inviscid theory presented in reference 24-5. The drag estimates produced by the inviscid theory are expected to be slightly conservative. Test data reported in reference 24-6 indicate that the drag contributed by two-dimensional surface waviness on an ogive cylinder decreases from values predicted by the inviscid linearized theory as the ratio of the boundary layer height to the wavelength is increased. Unfortunately, there is insufficient test data available at this time to quantitatively establish the effects of the boundary layer on the drag contribution of the surface waviness. However, the ratio of the average depth of the boundary layer to the length of the surface waves (distance between spars) for the candidate wing concepts of this program is less than the ratio that existed for the tests of reference 24-6. Therefore, the effects of the boundary layer upon the drag produced by the surface waviness should be less than those observed by the test results. Thus, the inviscid theory, although slightly conservative, will produce valid estimates of the drag due to surface waviness for the candidate wing concepts.

The performance degradation due to two-dimensional surface waves with wave crests perpendicular to the wing chord was determined. The surface waves were taken to be sinusoidal in cross section shape. If the waves assumed the shape of a circular-arc, the performance degradation would be 8 percent greater than that produced by the sinusoidal waveform. The additional fuel required to perform the fixed range mission is parametrically illustrated as a function of the height of the wave, ϵ , and the wavelength, λ . Surface waves with constant values of ϵ/λ were assumed to exist over the entire wetted area of the wing. Performance degradation due to partial areas of surface waviness are calculated by multiplying the fuel increment by the ratio of the area of the distorted portion of the wing to the total wing surface area.

Three-Dimensional Surface Bumps or Depressions

Air loads, thermal effects, or fabrication tolerances may produce this type of distortion in surface panels whose outer edges are attached to rigid structure. Pressure drag in the transonic and supersonic speed regime is produced by the surface bumps.

Performance losses due to three-dimensional depressions or bumps were defined using the linearized inviscid theory of reference 24-5. The fuel increment required to compensate for the surface distortion is presented as a function of ϵ/λ, where λ is the length of the depression measured parallel to the wing chord (the chordwise length of the wing panel) and ϵ is the displacement of the wing surface at the center of the panel. Again, the bumps or depressions were assumed to exist over the entire wing surface. If only a portion of the wing surface area is distorted by the depressions, the performance losses are calculated by applying the distorted area/total area ratio to the fuel increments.

Surface Corrugations Parallel to the Wing Chord

This source of roughness is the result of the beading or corrugations incorporated into the design of the wing skin and heat shield. These surface corrugations contribute pressure drag at transonic and supersonic speeds and increase friction drag at all speeds.

The performance degradation due to the corrugations incorporated into the wing skin was determined for the applicable concepts, using the linearized inviscid theory of reference 24-5. The corrugations are parallel to the wing chord. The wave drag due to this form of roughness is generated at the front and rear face of the end closeout of the bead or trough. Skin friction drag is increased due to the increase in wetted area resulting from the corrugations. The fuel increment required to compensate for the drag caused by this class of roughness is presented as a function of ϵ/λ and L/λ, where λ is the width and ϵ is the height or depth of the bead or trough and L is the distance between the end closeouts. When the end closeouts occur at the leading and trailing edge of the wing, an effective length of 80 ft is used to determine the L/λ value. If there are no end closeouts, a value of ∞ is taken for L/λ parameter. Constant values of ϵ/λ and L/λ were assumed to exist continuously over the entire wing surface. When a flat area exists between adjacent beads or troughs, the fuel penalty is determined by multiplying the fuel increment by the corrugated area/total wing surface area ratio. The corrugated surface area is the sum of areas of the individual corrugations, where the area of a single bead or trough is $L\lambda$. In the case of the corrugated heat shield, the corrugations incorporated a single low drag end closeout on or near the leading edge. The performance degradation due to this type of closeout was determined for each individual candidate wing concept based on linearized inviscid theory.

Deformation of the Primary Wing Structure

Thermal and air loads produce spanwise and chordwise deflections of the primary wing structure. This type of wing distortion increases the zero-lift drag and alters the induced drag characteristics of the vehicle throughout the flight regime.

Distortions of the wing were determined at the Mach 8 cruise condition. These distortions were assumed to exist throughout the entire mission. The increased drag due to the various types of roughness and wing distortion were assessed over the entire speed regime, using the computer program described in reference 24-7. The performance penalties resulting from the increased drag were determined for the vehicle using the nominal acceleration schedule for the climb-acceleration flight mode and the nominal speed-altitude schedule for all phases of the mission. The takeoff weight of the vehicle remained at 550 000 lb.

Parametric Design Data

Parametric design curves for various types of roughness, as discussed earlier, are shown in figures 24-1 through 24-4.

Evaluation Approach

The incremental drag changes due to the six types of roughness and distortion represent the drag difference between the rough, distorted wing and an ideally smooth wing. The wing of the nominal vehicle was defined to have an amount of roughness and distortion that would produce a drag increase equal to 10 percent of the smooth wing friction drag.

The nominal wing roughness would be equivalent to a fuel penalty of 1110 lb, and was compensated for the nominal mission performance. Therefore, the fuel penalty used in the concepts evaluation procedure is the difference between the fuel increment determined for the candidate wing concept and the fuel increment of 1110 lb resulting from the roughness and distortion that was assumed for the nominal wing.

Performance degradation due to surface roughness and waviness was evaluated for the heat shield and leading edge concepts, such that a final selection of the heat shield and leading edge concepts could be accomplished.

A performance degradation evaluation was conducted for each of the six structural concepts, including the thermal protection system and leading edge for constant mission range. A performance comparison was conducted by comparing all of the structural concepts in terms of fuel/payload increment. The fuel increment for each of the six concepts was input into the interaction factor evaluation.

PRIMARY STRUCTURES

The performance penalties resulting from the combined roughness and distortion of the wing are summarized in table 24-1 for the candidate structural concepts.

Monocoque Waffle

The surface finish of the wing skin of the concepts evaluated is smooth enough to result in no performance losses due to uniformly distributed (sand-grain) roughness. The waffle panels undergo three-dimensional surface distortion, which results in a fuel increment of 31 lb. The waffle panels are connected with a butt joint every 43 in., measured in the chordwise direction. The corrugated heat shield has a lap joint every 43 in. These sheet-metal joints, plus those of the segmented leading edge, produce a fuel penalty of 19 lb. The corrugated heat shield and the end closeouts for the heat-shield corrugations result in a fuel loss of 118 lb. The wing deflections (figs. 24-5 through 24-8) for the cruise-limit loads were used to determine the fuel penalty due to wing deformation, which is 611 lb. The total fuel increment due to the combined roughness and distortion of the monocoque wing concept is 779 lb.

Monocoque Honeycomb Sandwich

The fuel penalty caused by three-dimensional distortion of the honeycomb panels is 282 lb. This value is larger than that for the monocoque waffle concept because of larger thermal deflections (thermal gradients) imposed on the honeycomb sandwich. The joints, fasteners, and the segmented leading edge cause a fuel penalty of 155 lb. The corrugated heat shield in the lower outboard surface results in a fuel increment of 118 lb. The fuel penalty attributed to the wing distortion is 458 lb (figs. 24-9 through 24-12). The total fuel increment required to compensate for the roughness and deformation of this wing concept is 1013 lb.

Semimonocoque Spanwise Tubular

This concept has corrugated heat shields on all exposed surfaces and a segmented leading edge. The fuel penalty caused by three-dimensional panel distortion is 73 lb. The lap joints of the heat shield, spaced every 90.0 in., and the sheetmetal joints of the leading-edge have a fuel penalty of 23 lb. The fuel penalty due to the corrugations on the upper and lower heat shield is 427 lb. The fuel penalty attributed to the wing distortion is 314 lb (figs. 24-13 through 24-16). The total fuel penalty for the combined roughness and wing distortion is 837 lb.

Semimonocoque Spanwise Beaded Skin

This primary structure concept incorporates the corrugated heat shield and a segmented leading edge. The fuel penalties resulting from the sheet-metal joints, corrugations, and primary-structure deformations are identical to those of the previous primary-structure concept. The surface panels of these wing concepts are subject to three-dimensional distortion, which introduces an 81-lb fuel penalty. The total fuel penalty for the concept due to the roughness and distortion of the wing is 845 lb.

Semimonocoque Chordwise Convex-Beaded/Tubular

This candidate wing concept has convex-beaded panels on the upper surface of the wing, which require no heat shield, and tubular panels with a corrugated heat shield on the lower wing surface. The fuel penalty produced by three-dimensional distortion is 159 lb. The lap joints of the heat shield, spaced every 24 in., and the sheet metal joints of the segmented leading edge installation introduce a fuel loss of 32 lb. The convex beads of the upper wing skin have an end closeout every 24 in. The fuel penalty due to the corrugations of the upper wing skin and the corrugations of the lower surface heat shield is 1841 lb. The fuel increment attributed to the wing distortion is 521 lb (figs. 24-17 to 24-20). The total fuel increment required to compensate for the roughness and deformation of this wing concept is 2553 lb.

Statically Determinate

This concept has the leading edge and corrugated heat shield employed by the spanwise-stiffened semimonocoque concepts. The lap joints of the heat shield result in a fuel penalty of 30 lb for the sheet metal joints and fasteners. The surface panels distort three-dimensionally, producing a fuel penalty of 195 lb. The fuel penalty for the wing deformation (figures 24-21 to 24-24) is 383 pounds, and the total fuel increment required to compensate for the roughness and distortion of the wing is 1040 lb.

Fuel Increment Summary

The performance penalties resulting from the various types of roughness and distortion of the wing are summarized for the six candidate wing concepts in table 24-1. The total fuel increment for the combined roughness and distortion of each of the candidate wing concepts is compared to the fuel increment of 1110 lb, allowed to compensate for the assumed roughness of the nominal wing. The net difference between the fuel increment determined for a wing and the nominal 1110-lb fuel increment is also listed in table 24-1 for each of the candidate wing concepts. As shown in table 24-1, the concept fuel in increments are less than the nominal fuel increment except for the chordwise concept

The fully heat-shielded surfaces have no appreciable drag increase over a relatively smooth (partially shielded) concept, such as the waffle. However, unshielded upper surface panels with beads (chordwise concept) protruding into the air stream provide the most drag, even though the beads are oriented in the direction of flow.

Using the net fuel increments for each concept, the fuel mass fractions for the baseline vehicle shown in table 24-1 were determined for input into the interaction evaluation factor investigation.

HEAT SHIELDS

The performance degradation resulting from the surface roughness, sheet-metal joints and fasteners, surface waviness, corrugations, and deformation of the primary wing structure has been evaluated for the four heat shields used with the spanwise tubular structure. The evaluations are summarized in table 24-2. Wing deflection drag (deformation of primary structure) is included to indicate relative drag of heat shields.

The corrugated sheet metal heat shield on the upper and lower wing surfaces was considered first. The surface finish on this and all of the other heat shield concepts is sufficiently smooth to cause no performance penalties, but the surface of the corrugated heat shields suffers three-dimensional wave distortion, resulting in a fuel penalty of 73 lb. In addition, the skin of this heat shield has a rear-facing lap joint every 90 in., which along with the joints and fasteners associated with the segmented leading edge, cause a fuel penalty of 23 lb. The corrugations of the heat shield and the end close-outs of the corrugations near the leading edge result in a fuel penalty of 427 lb. Since all heat-shield concepts were applied to the same primary structure, the fuel increment of 314 lb due to the deformation of the primary structure is common to all concepts. The total fuel increment due to the roughness and distortion of the wing for the corrugated heat shield concept is 837 lb.

The second concept considered has a flat, dimple-stiffened skin on the upper and lower surfaces. These panels are subject to three-dimensional wave distortion, and the fuel increment due to this surface waviness is 43 lb. The panels also have a chordwise butt joint every 15.3 in. The fuel penalty due to these sheet-metal joints and those of the segmented leading edge is 31 lb. The total fuel increment for the combined roughness and distortion of the wing with the flat skin, dimple-stiffened heat shield is 388 lb.

The third heat shield concept consists of the simply supported, modular heat shield on the upper wing surface and the corrugated heat shield on the lower surface of the wing. Again, the panels incur three-dimensional wave distortion. The fuel penalty resulting from the surface waviness is 5 lb. The skin of the modular concept has a rear-facing chordwise lap joint every 10.4 in., and the lower surface has a lap joint every 90 in. These sheet-metal joints, combined with the joints and fasteners of the segmented leading edge, result in a fuel penalty of 58 lb. The corrugations on the lower surface heat shield cause a fuel penalty of 231 lb. The total wing fuel penalty for the simply supported modular heat shield is 608 pounds.

The fourth arrangement, the cantilevered modular heat shield, is used on the upper surface. The surface waviness is identical to that of the third concept. The cantilevered modular heat shield has a rear-facing chordwise lap joint every 2.61 in. The fuel penalty for the lap joints and the sheet-metal joints of the leading edge is 149 lb. The total fuel increment resulting from the roughness and distortion of this wing concept is 699 lb.

The fuel increments required to compensate for the combined roughness and distortion of the four wing concepts are all less than the 1110-lb fuel increments initially allowed to compensate for the assumed roughness and distortion of the nominal wing. As a result, the net fuel increments c. payload decrements used in the evaluation procedures have negative values for each of the candidate heat-shield systems.

LEADING EDGE

The performance degradation resulting from the sheet-metal joints and fasteners, and the corrugation and closeouts have been evaluated for the segmented and the continuous leading-edge concepts. The end closeouts for the corrugated heat shield are located in the leading edge for the continuous leading-edge concepts. The segmented leading edge is cylindrical in shape, requiring that the end closeouts of the corrugations be located in the heat shield just behind the leading edge. The geometric characteristics of the end closeouts are the same for both of the leading-edge concepts and result in identical performance degradation. Because of a joggle joint at the attachment of the leading edge with the wing panel, there is a fuel penalty of 10 lb for either concept. In addition to the joggle joint, the segmented leading edge has an expansion gap between each 20-in. segment. Each segment is fastened to the wing structure with flush-mounted screws. Because of the drag contributed by the expansion gaps and the flush-mounted screws as well as load deflection, the fuel penalty associated with the segmented leading edge adds another 10.2 lb. Therefore, the fuel/payload increments for the continuous and segmented leading edges are 10 lb and 20.2 lb, respectively.

REFERENCES

24-1 Aker, L. J.: A Digital Computer Program for Calculating Airplane Turbulent Skin Friction Drag. LR 19620, April 1966.

24-2 Peterson, J. B.: A Comparison of Experimental and Theoretical Results for the Compressible Turbulent-Boundary-Layer Skin Friction with Zero Pressure Gradient. NASA TN D-1795, March 1968.

24-3 Goddard, F. E.: Effect of Uniformly Distributed Roughness on Turbulent Skin-Friction Drag at Supersonic Speeds. Journal of the Aero-Space Sciences, January 1959.

24-4 Hoerner, S. F.: Fluid-Dynamic Drag. Published by the author, 1965.

24-5 Smith, K. G.: The Increase in Wave Drag at Supersonic Speeds Due to Surface Waviness. Royal Aircraft Establishment Technical Report No. No. 65173, August 1965.

24-6 Czarnecki, K. R.; and Monta, W. J.: Pressure Drags Due to Two-Dimensional Fabrication-Type Surface Roughness on an Ogive Cylinder at Transonic Speeds. NASA TN D-3519, August 1966.

24-7 Elliot, R. D.: A Digital Computer Program for Calculating Pressure Distributions and Aerodynamic Coefficients of Warped Wings of Arbitrary Planform in Supersonic Flow. LR 18764, February 1966.

TABLE 24-1. – PRIMARY-STRUCTURE CONCEPT PERFORMANCE EVALUATION
(Fuel increment required to perform constant-range mission)

Primary structure concept	Monocoque waffle	Monocoque honeycomb-core sandwich	Semimonocoque spanwise tubular	Semimonocoque spanwise beaded skin	Semimonocoque chordwise tubular/convex beaded	Statically determinate beaded skin
Fuel increment due to uniformly distributed roughness, lb	0	0	0	0	0	0
Fuel increment due to sheetmetal joints and fasteners, lb	19	155	23	23	32	30
Fuel increment due to surface waviness, lb	31	282	73	81	159	195
Fuel increment due to corrugation, lb	118	118	427	427	1841	427
Fuel increment due to deformation of primary structure, lb	611	458	314	314	521	388
Total fuel increment for wing-structure concept, lb	779	1013	837	845	2553	1040
Total fuel increment due to nominal wing roughness and distortion, lb	1110	1110	1110	1110	1110	1110
Net fuel increment due to wing roughness and distortion, lb	-331	-97	-273	-265	+1443	-70
Fuel mass fraction	0.3994	0.3998	0.3995	0.3995	0.4026	0.3999

TABLE 24-2. – HEAT-SHIELD CONCEPT PERFOI IANCE EVALUATION

(Semimonocoque spanwise tubular primary-structure fuel increment required to perform constant-range mission)

Upper surface heat-shield concept	Corrugated	Flat-skin dimple-stiffened	Simply supported modular	Cantilevered modular
Lower surface heat-shield concept	Corrugated	Flat-skin dimple-stiffened	Corrugated	Corrugated
Fuel increment due to uniformly distributed roughness, lb	0	0	0	0
Fuel increment due to sheet-metal joints and fasteners, lb	23	31	58	149
Fuel increment due to surface waviness, lb	73	43	5	5
Fuel increment due to corrugations, lb	427	0	231	231
Fuel increment due to deformation of primary structure, lb	314	314	314	314
Total fuel increment due to wing roughness and distortion, lb	837	388	608	699
Total fuel increment due to nominal wing roughness and distortion, lb	1110	1110	1110	1110
Net fuel increment due to wing roughness and distortion,, lb	-273	-722	-502	-411

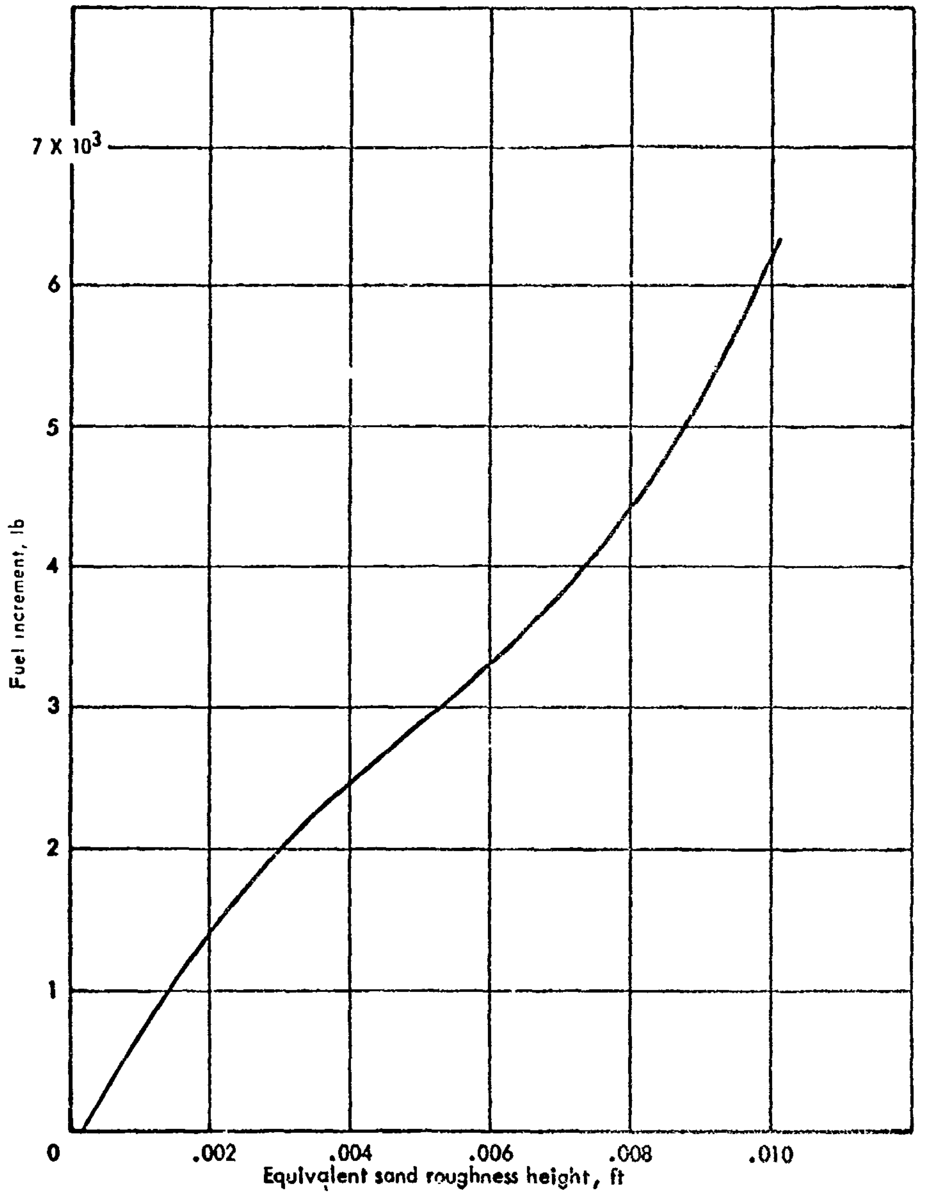

Figure 24-1. Fuel increment required to compensate for uniformly distributed roughness on wing surface for constant mission range

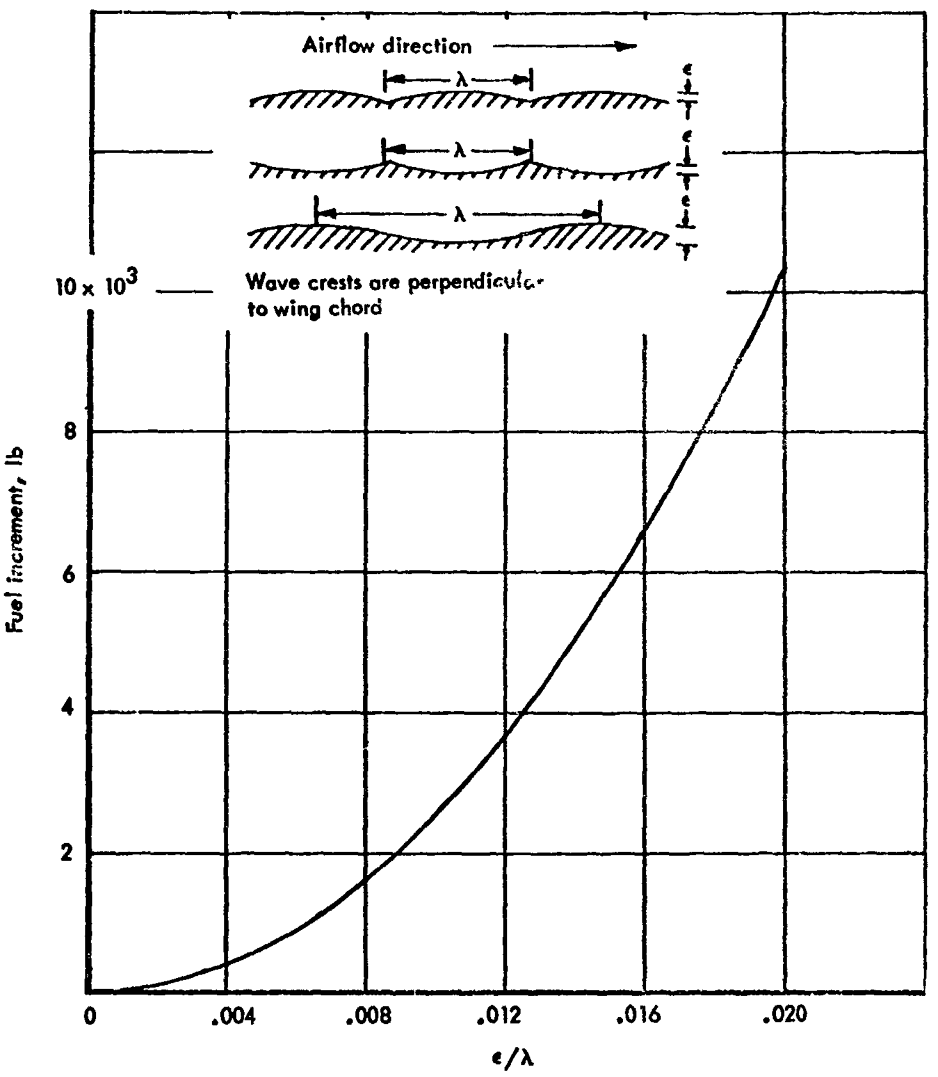

Figure 24-2. Fuel increment required to compensate for uniform waviness over wing surface for constant mission range

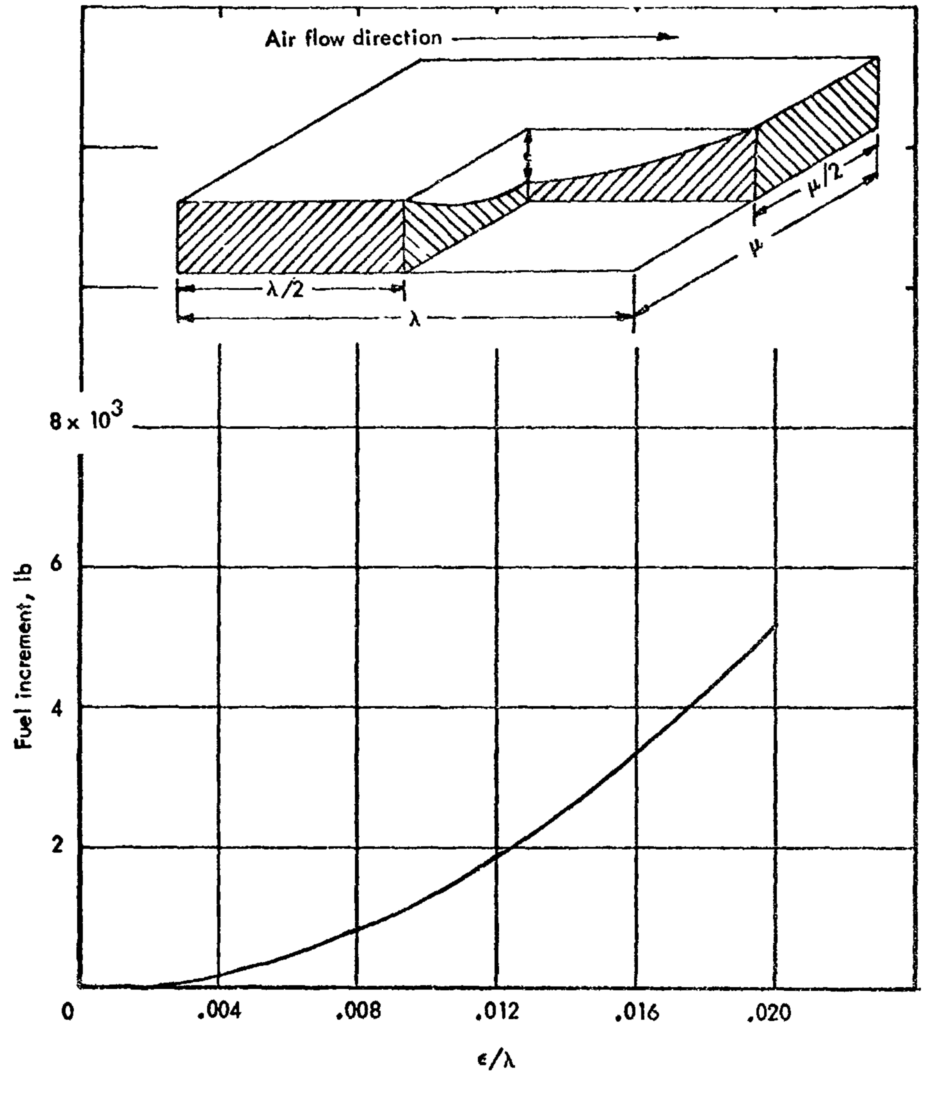

Figure 24-3. Fuel increment required to compensate for uniform three dimensional waviness over wing surface for constant range

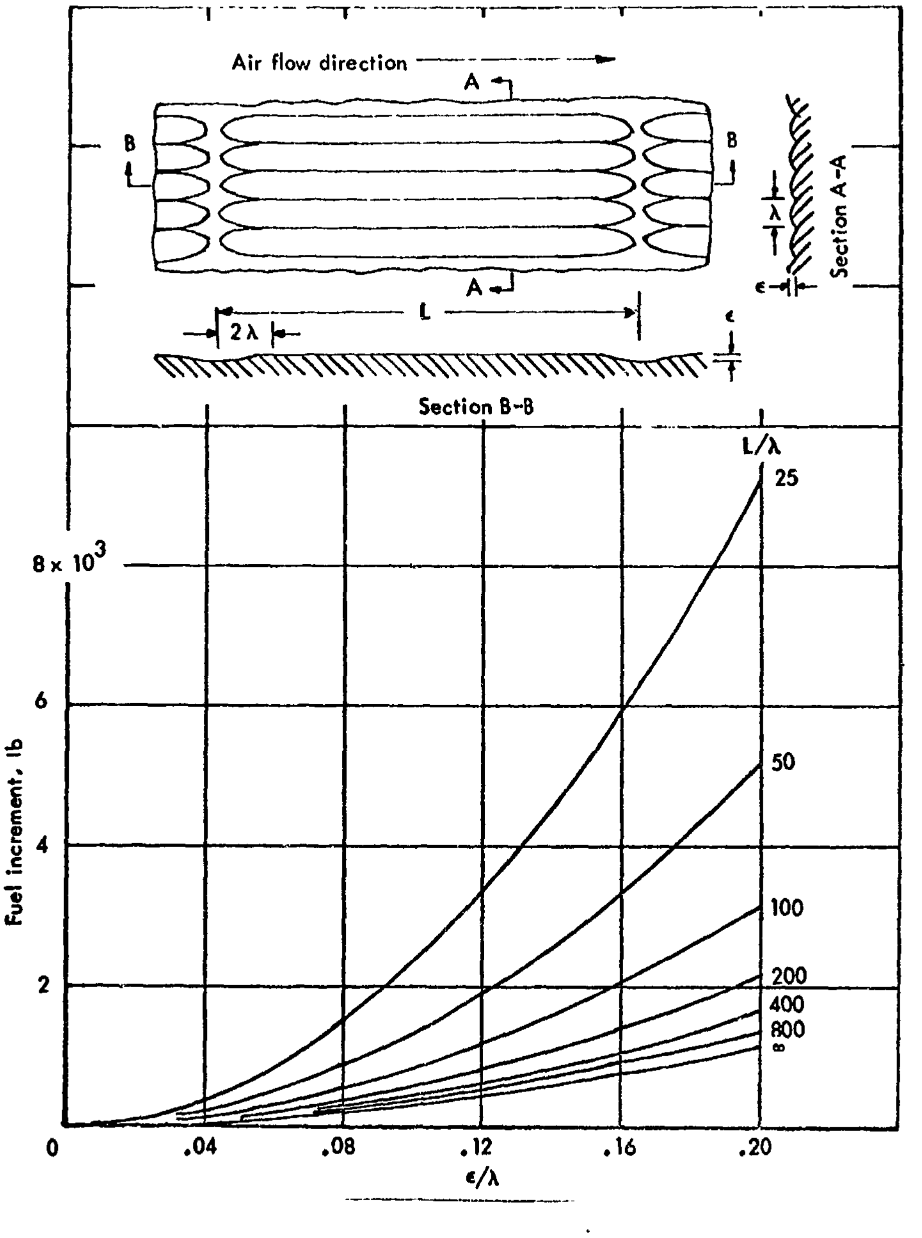

Figure 24-4. Fuel increment required to compensate for uniform corrugation in wing surface for constant mission range

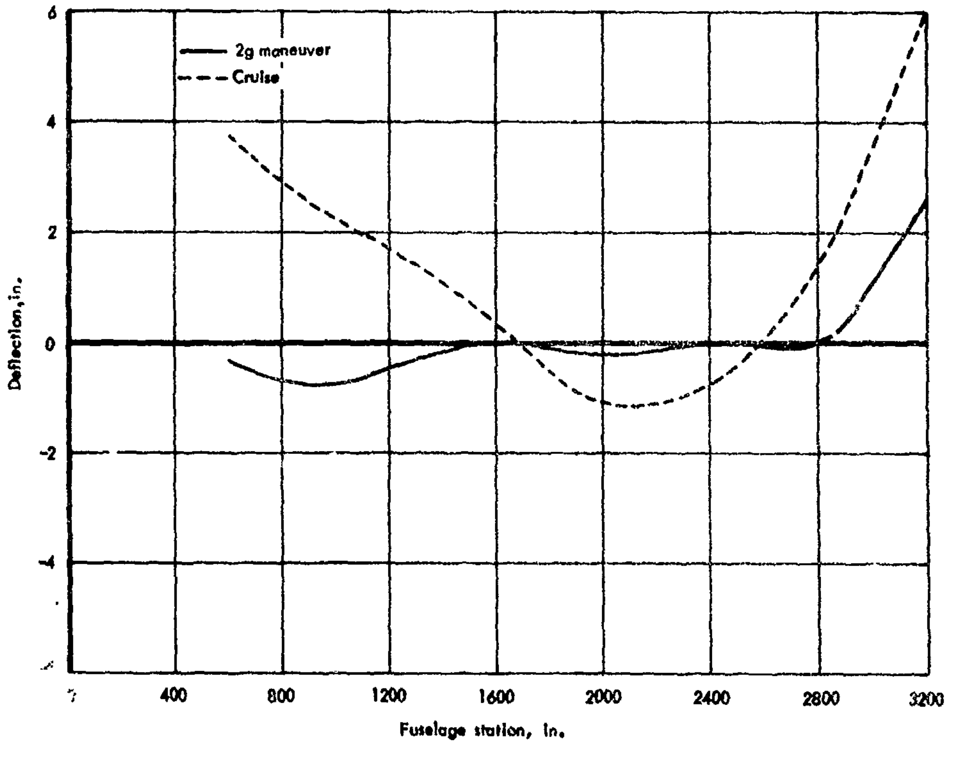

Figure 24-5. Fuselage deflections net due to limit loads along BL 120 (intersection of fuselage and wing), monocoque waffle concept

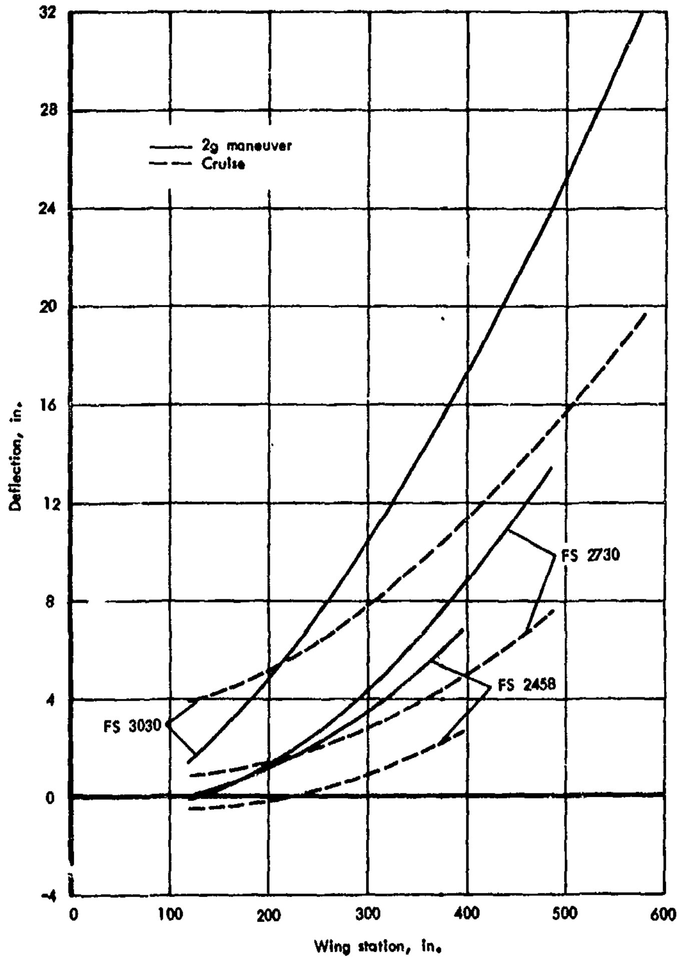

Figure 24-6. Wing deflections net due to limit loads, monocoque waffle concept

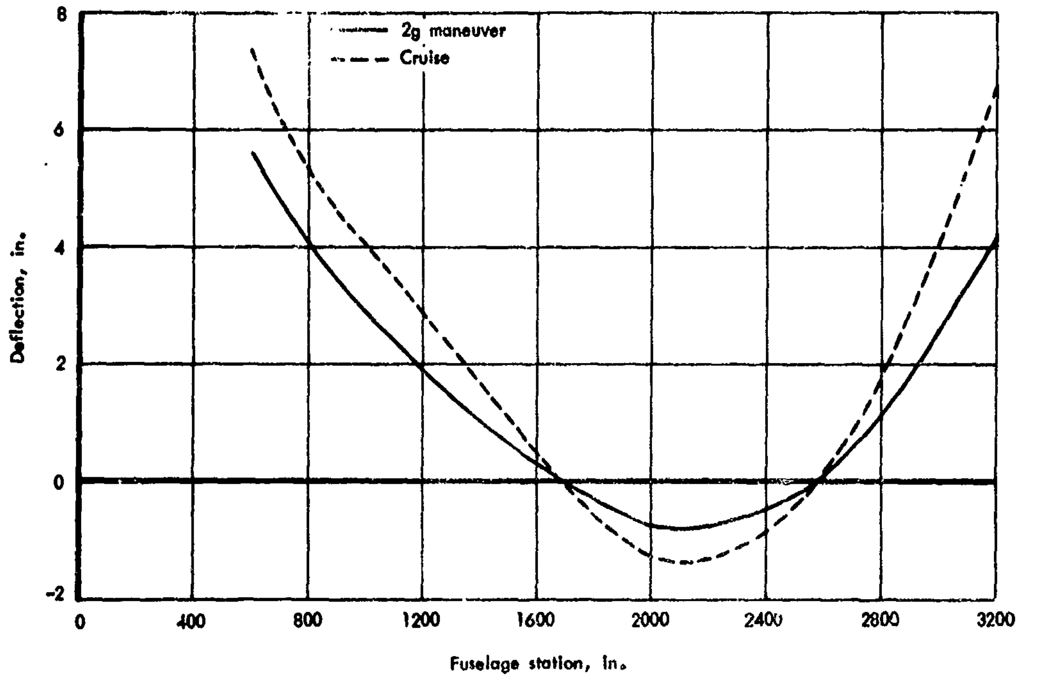

Figure 24-7. Fuselage deflection due to thermal stresses along BL 120 (intersection of fuselage and wing), monocoque waffle concept

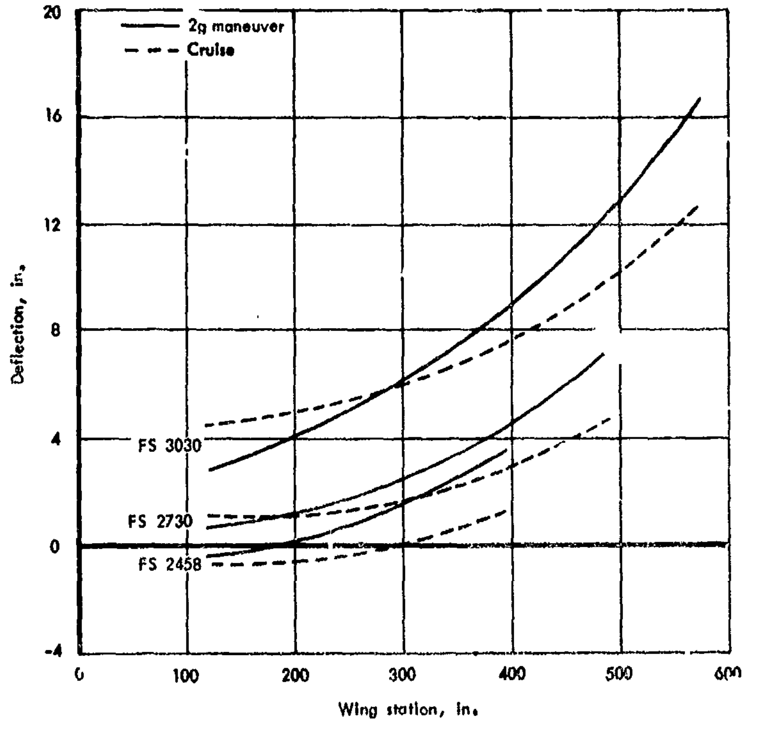

Figure 24-8. Wing deflections due to thermal stresses, monocoque waffle concept

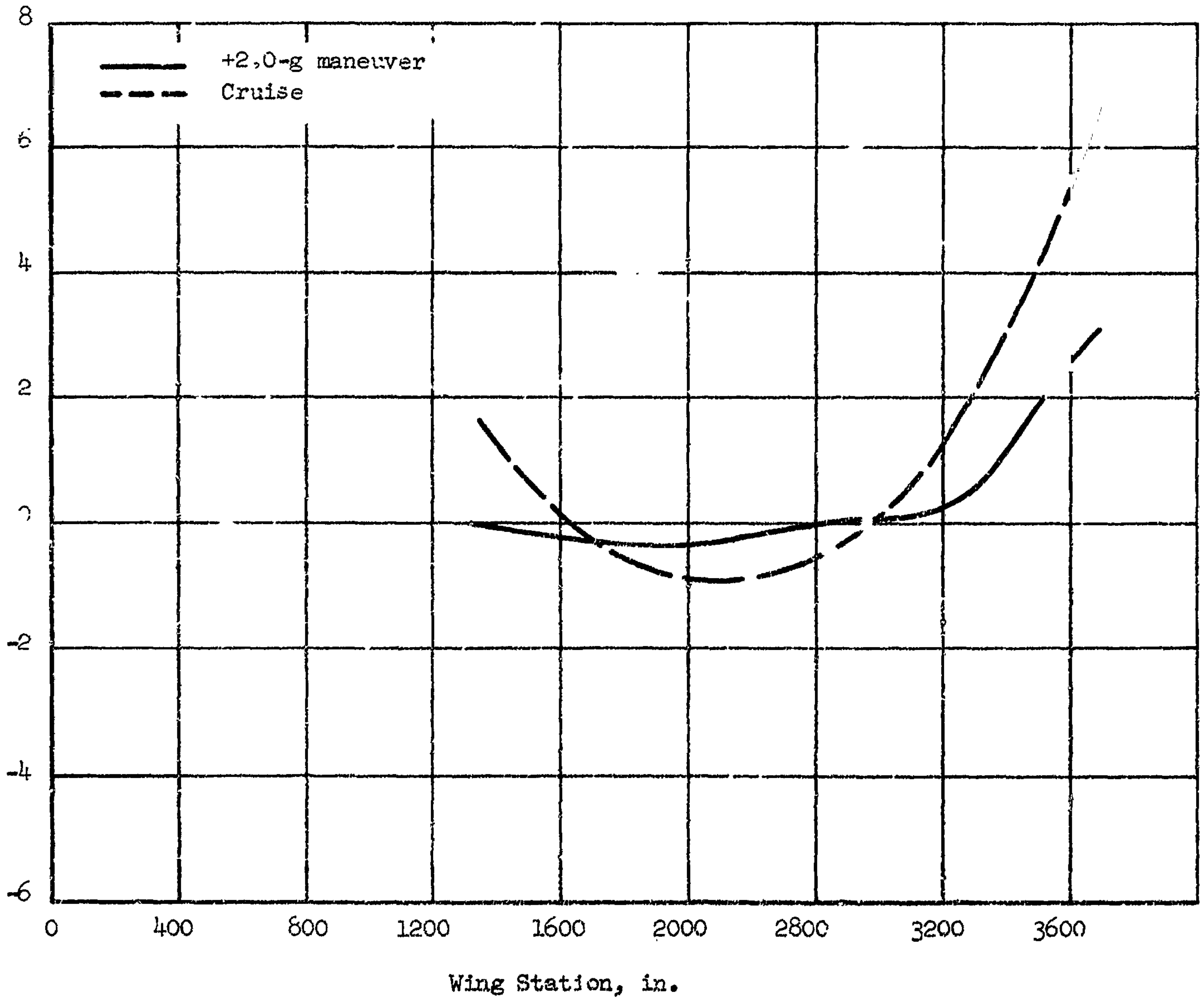

Figure 24-9. Fuselage deflections net due to limit loads along BL 120 (intersection of fuselage and wing) honeycomb concept

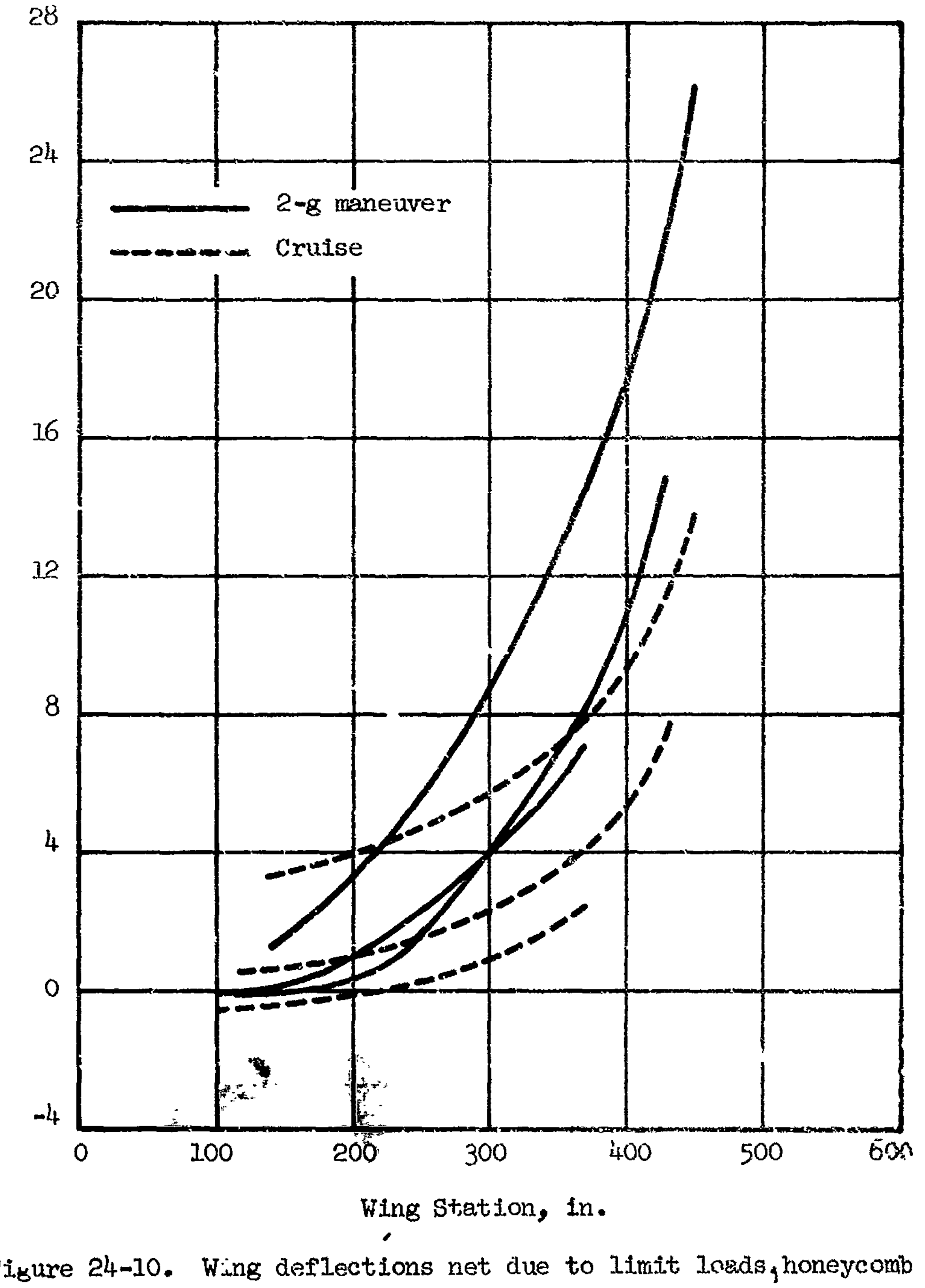

Figure 24-10. Wing deflections net due to limit loads, honeycomb concept

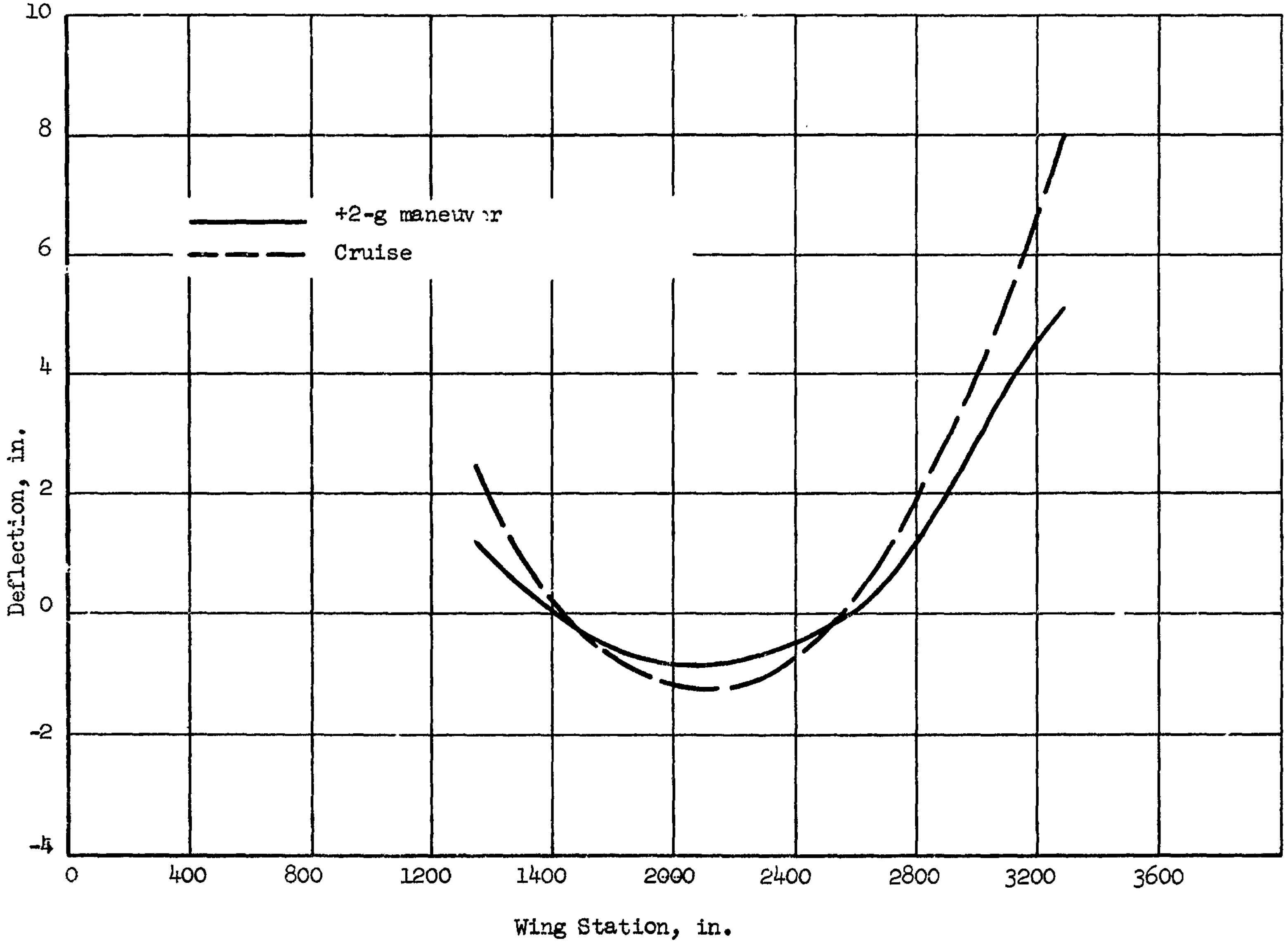

Figure 24-11. Fuselage deflections due to thermal stresses along BL 120 (intersection of fuselage and wing), honeycomb concept

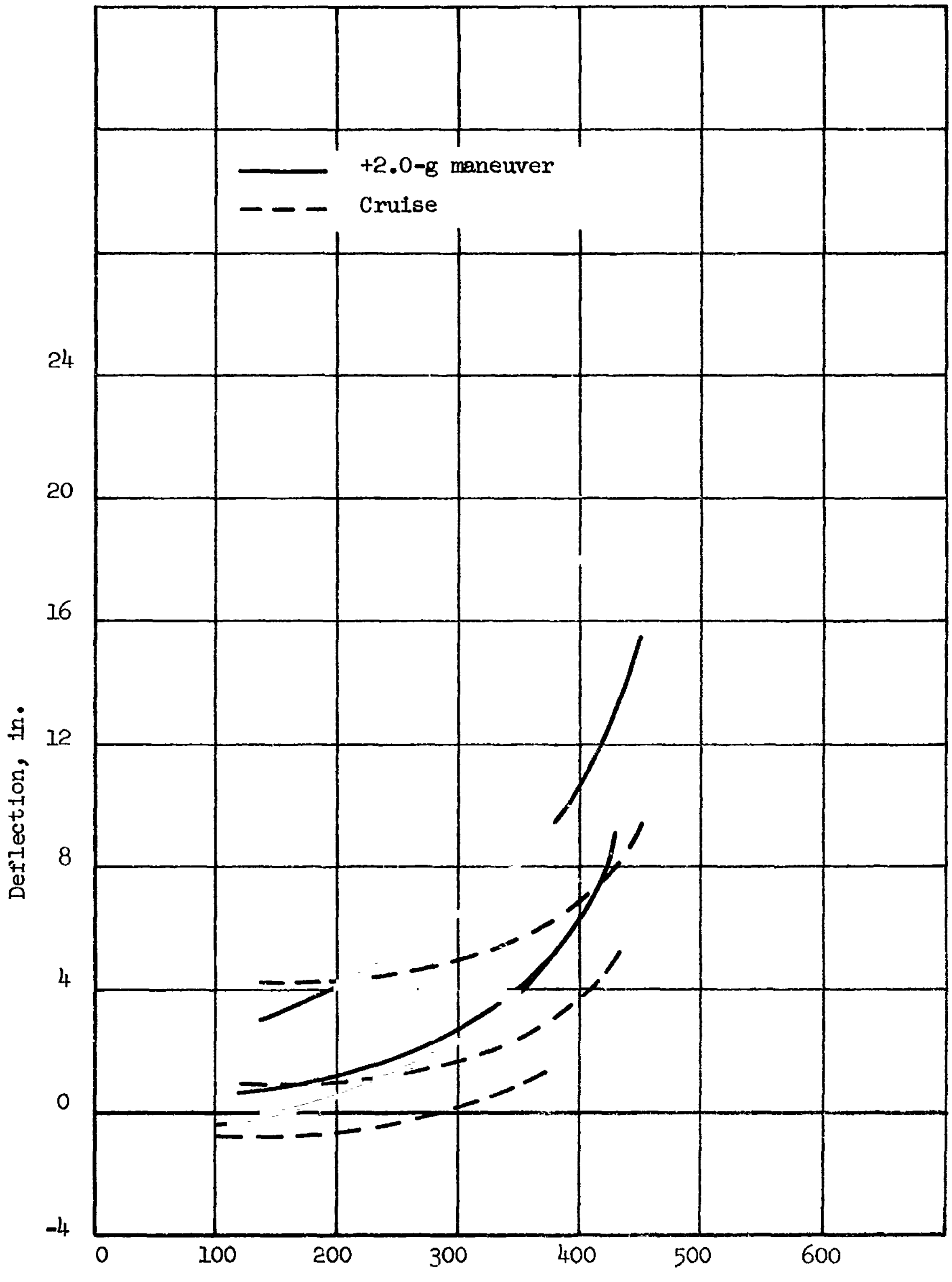

Figure 24-12. Wing deflections due to thermal stresses, honeycomb concept

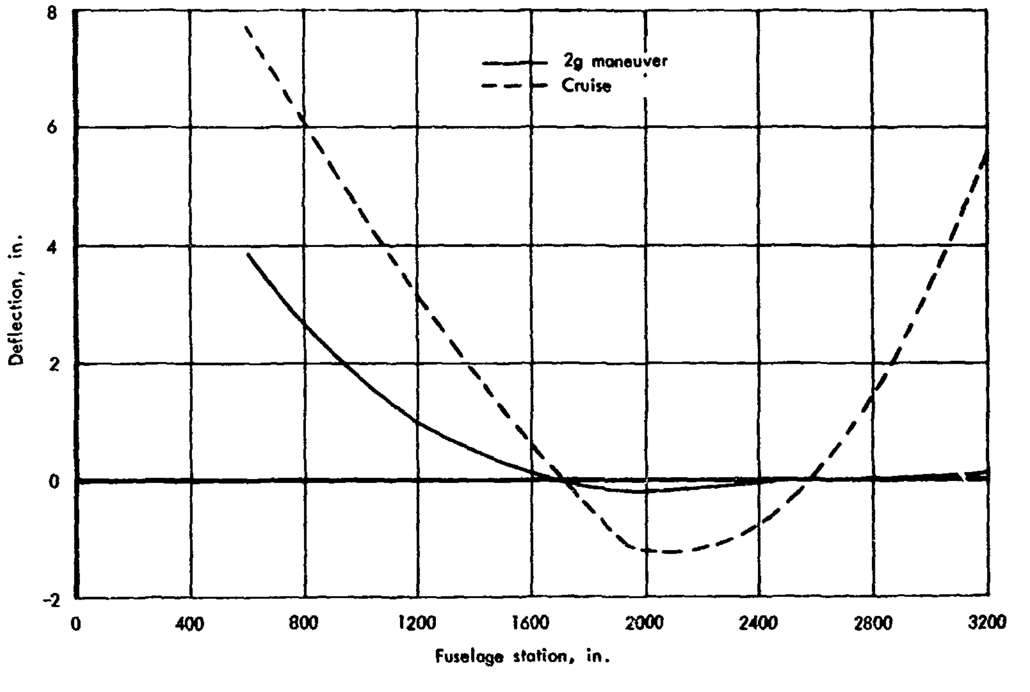

Figure 24-13. Fuselage deflections net due to limit loads along BL 120 (intersection of fuselage and wing), semimonocoque (spanwise) concept

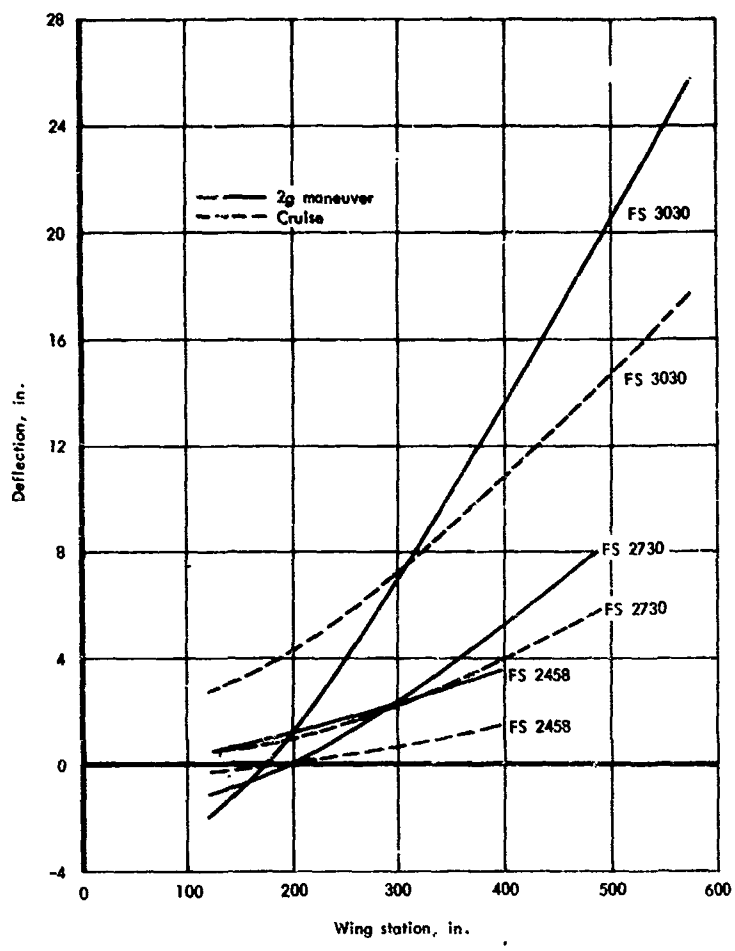

Figure 24-1?. Wing deflections net due to limit loads, semimonocoque (spanwise) concept

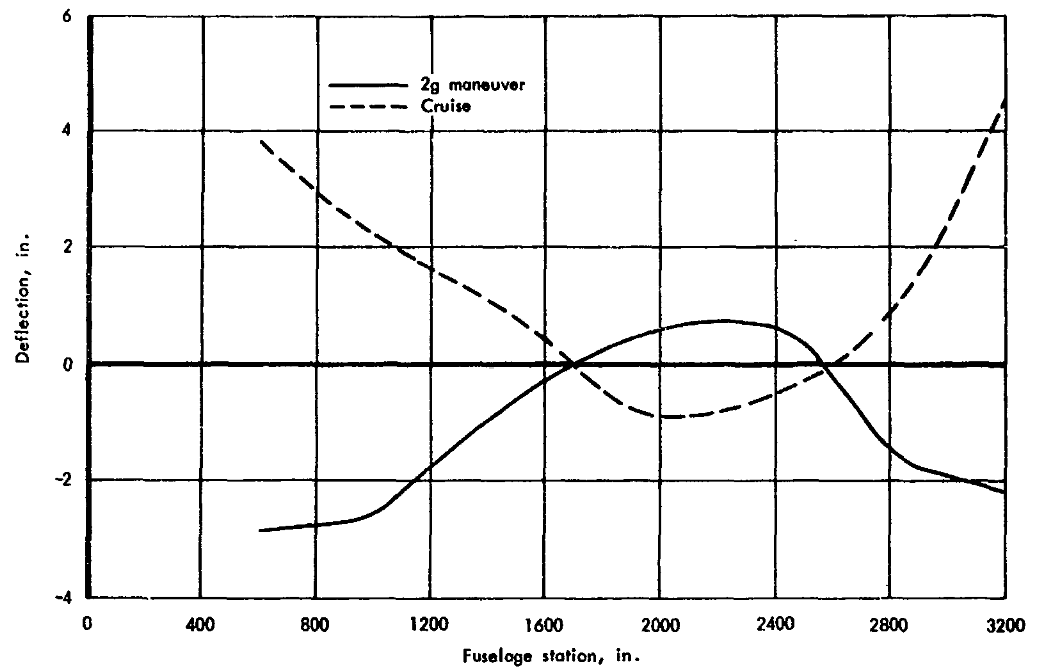

Figure 24-15. Fuselage deflections due to thermal stresses along BL 120 (intersection of fuselage and wing), semimonocoque (spanwise) concept

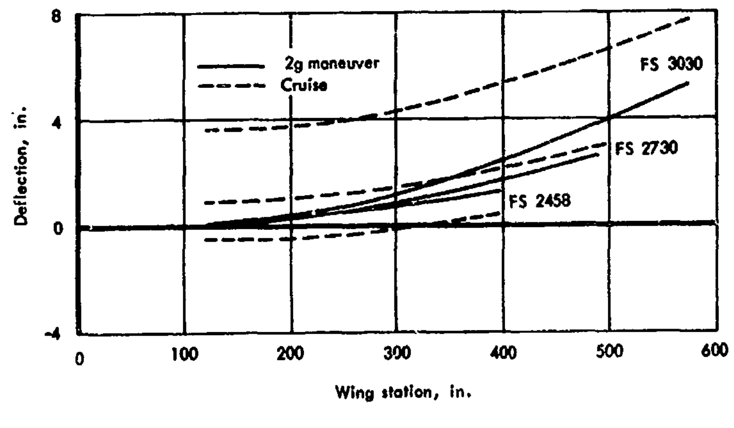

Figure 24-16. Wing deflections due to thermal stresses, semimonocoque (spanwise) concept

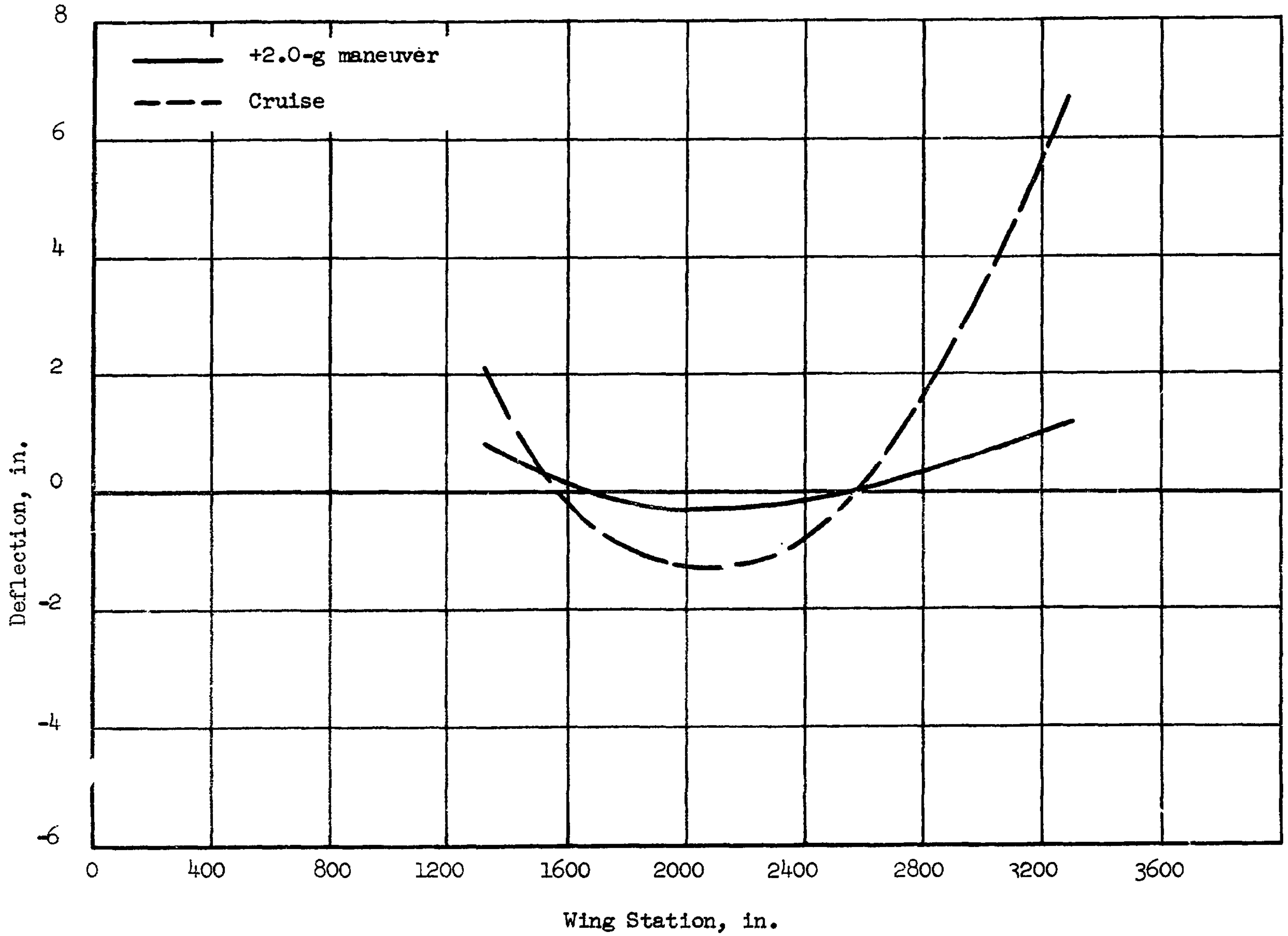

Figure 24-17. Fuselage deflection net due to limit loads along BL 120 (intersection of fuselage and wing) semimonocoque (chordwise) concept

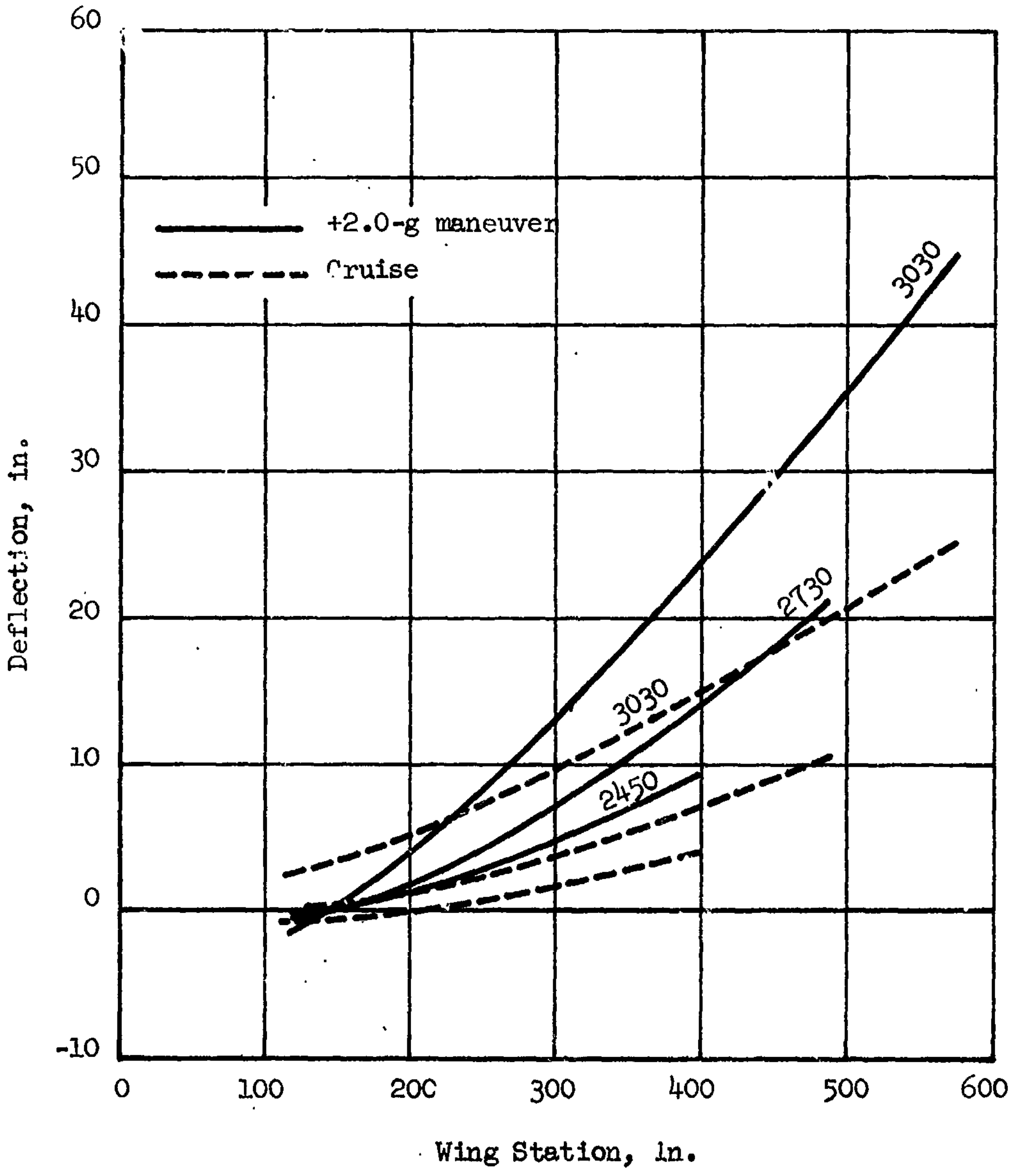

Figure 24-18. Wing deflections net due to limit loads, semimonocoque (chordwise) concept

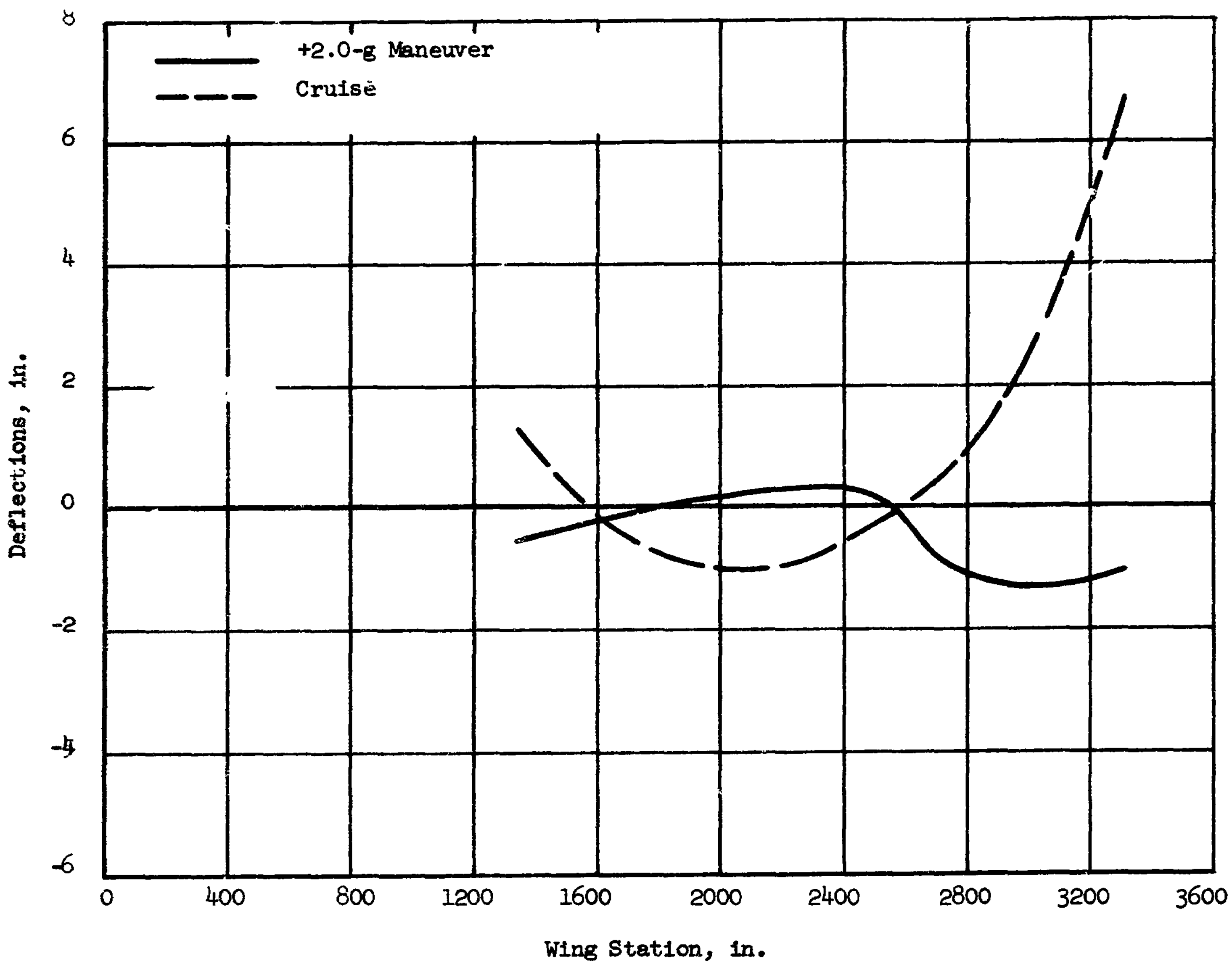

Figure 24-19. Fuselage deflection net due to limit loads along BL 120 (intersection of fuselage and end wing) semimonocoque (chordwise) concept

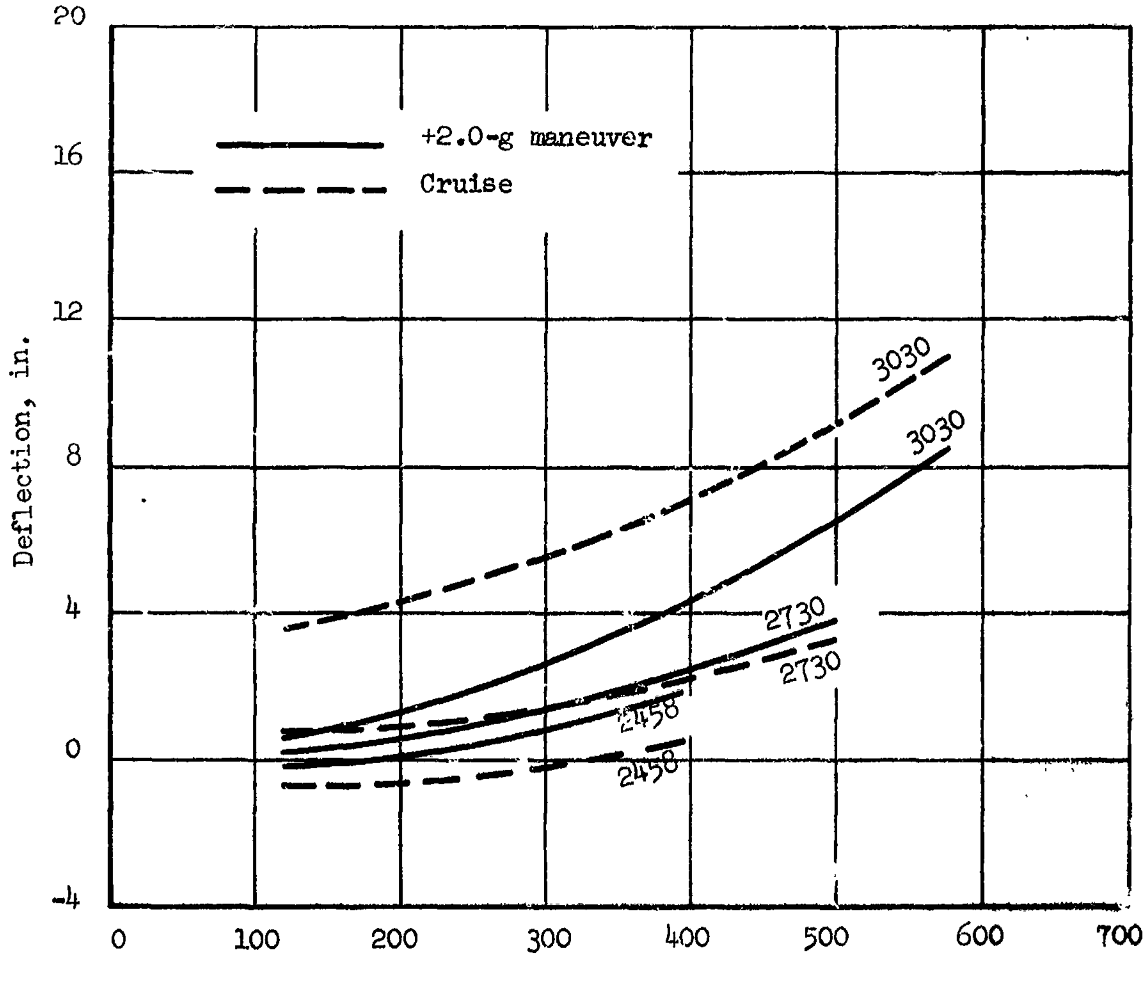

Figure 24-20. Wing deflections due to thermal stresses semimonocoque (chordwise) concept

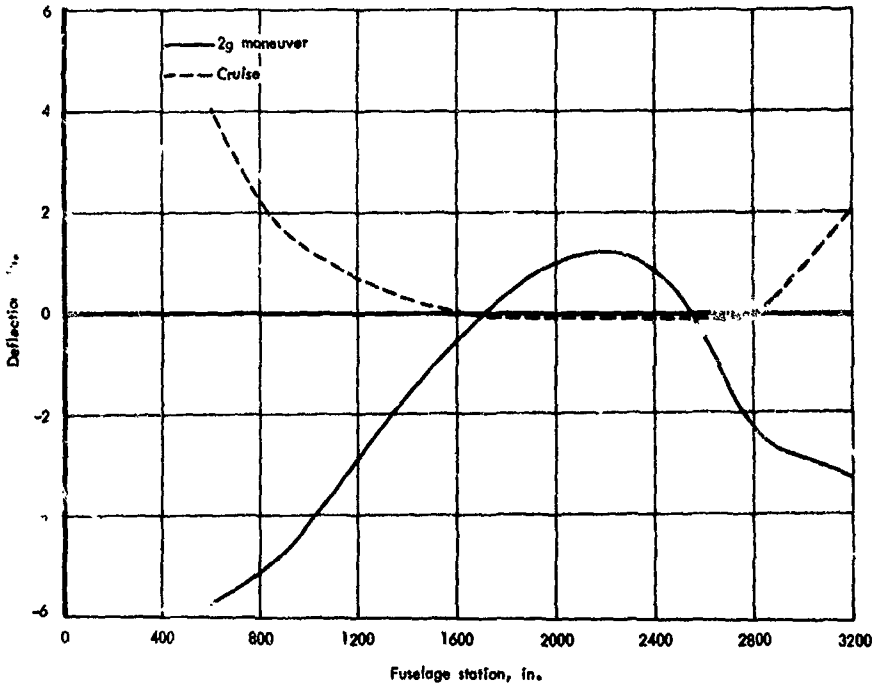

Figure 24-21. Fuselage deflections net due to limit loads along BL 120 (intersection of fuselage and wing), statically determinate concept.

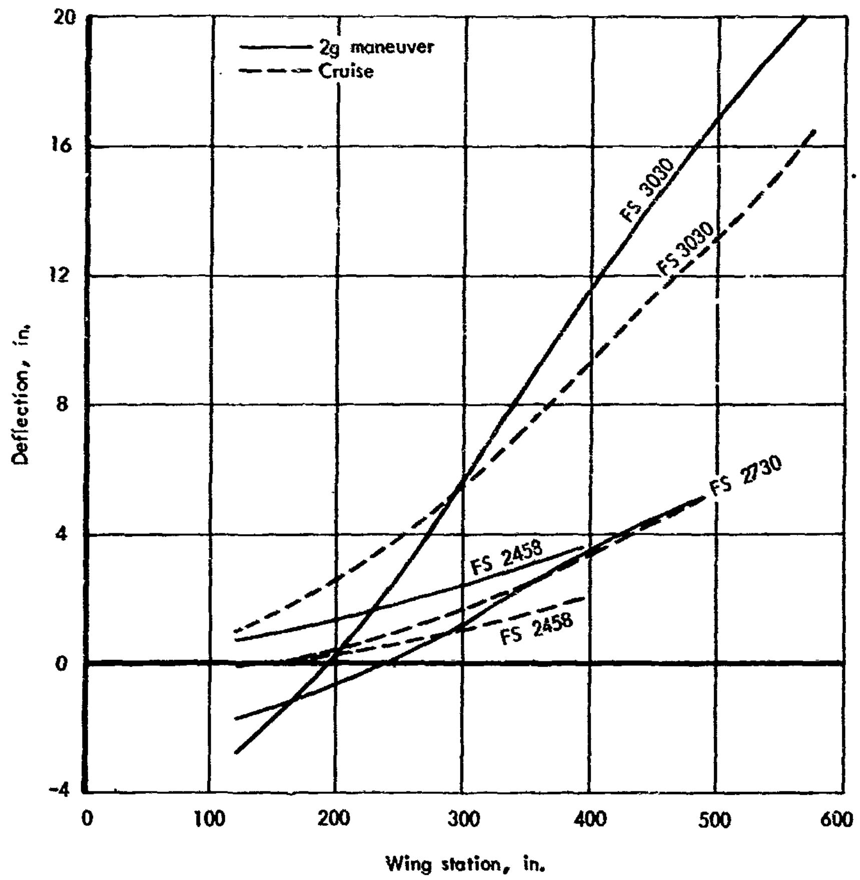

Figure 24-22. Wing deflections net due to limit loads, statically determinate concept

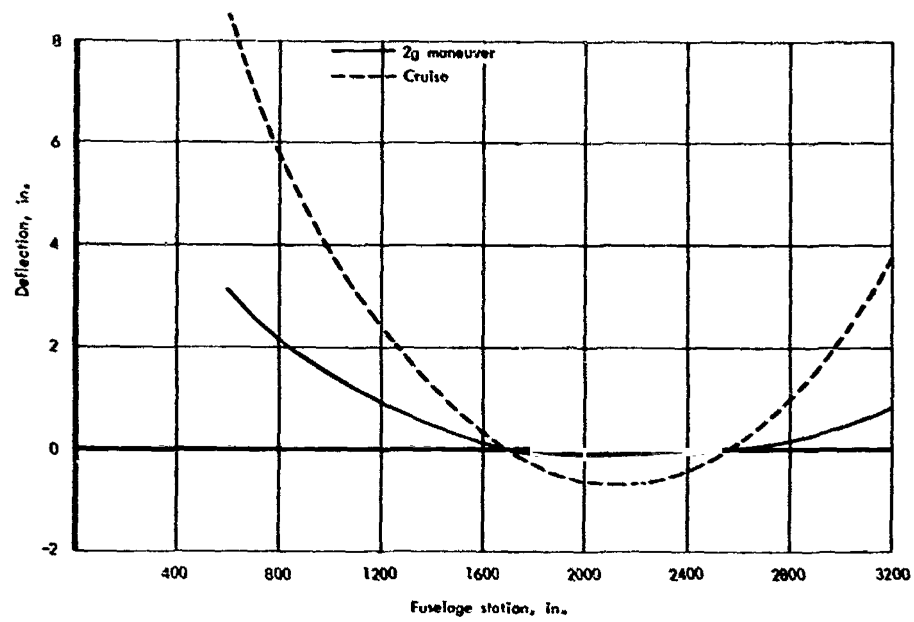

Figure 24-23. Fuselage deflections due to thermal stresses along BL 120 (intersection of fuselage and wing), statically determinate concept

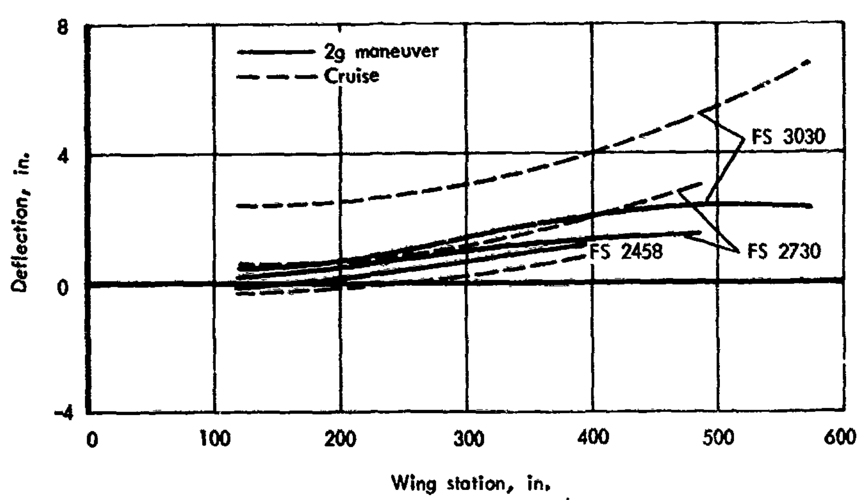

Figure 24-24. Wing deflections due to thermal stresses, statically determinate concept

Section 25

RELIABILITY

by

C. C. Richie, G. W. Davis, I. F. Sakata, B. C. Wollner

PRECEDING PAGE BLANK NOT FILMED.

CONTENTS

PRECEDING PAGE BLANK NOT FILMED.

TABLES

PRECEDING PAGE BLANK NOT FILMED.

ILLUSTRATIONS

PRECEDING PAGE BLANK NOT FILMED.

SYMBOLS

a, b	X and y distance between simply supported edges of panel
F_{tu}	Ultimate tensile strength
F_{1g}	Fatigue allowable tensile stress
g	Gravitational acceleration
K_Q	Fatigue quality index
N_Z	Inertia load factor in Z directions
p	Pressure
p_{limit}	Limit pressure
$p_{ult.}$	Ultimate pressure
t_{FLAT}	Flat thickness of leading edge
t_{NOSE}	Nose thickness of leading edge
$\bar{t}$	Equivalent thickness
RT	Room temperature

Section 25

RELIABILITY

The reliability analysis consisted of selecting a range for factor of safety and calculating structural weight for low, nominal, and high levels of factor of safety. The key factors, involving safety, creep, fatigue, and maintainability were evaluated in this study.

METHOD OF EVALUATION

The primary factors affecting structural reliability are:

1. The physical environment within the operating limits of the vehicle

2. Design accuracy, including accountability for all possible contingencies

3. Consistency of the reproduced articles to engineering requirements

4. Maintainability.

A numerical approach to a statistical probability evaluation is not possible because data do not exist to substantiate this approach. Instead, the basic approach must establish a consistent reliability standard, adequate for mission performance over the vehicle life span, which all concepts must satisfy. Therefore, to satisfy the primary reliability factors discussed above, a structural reliability evaluation method was established which consists of parametric variation of the key factors affecting the relative reliability (sensitivity) of the structural concepts, as measured by weight. These key factors, involving factors of safety, creep, fatigue, and maintainability, were used for three levels of structural reliability (low, nominal design, and high) and three flight load conditions (-0.5-g, +2.0-g, and cruise) as shown in table 25-1. Also, figure 25-1 presents the overload and operative boundaries for the low, nominal, and high levels of factors of safety.

The design limit load factor of safety of 1.30 was specified for the flight load conditions. Normal aircraft design practice sets this factor at a value of 1.00. Normal aircraft factors were considered the minimum (low) acceptable level; the required value of 1.30 was the nominal value; and an arbitrary design limit load factor of safety of 1.67 was chosen for the high value. Similarly, factors of safety on thermal strain of 1.10, 1.30 (required), and 1.50 were used. Creep and fatigue factors of safety operating time were selected at 1 (low), 1.5 (nominal), and 2 (high).

The fourth primary reliability factor, maintainability, concerned with long life, damage tolerance, and slow crack growth (for long inspection intervals), is provided for by the sensitivity measured by the design factors of safety variations discussed above. In addition, repairability was assessed by evaluating refurbishment requirements of leading edges and heat shields. Accessibility for interior wing inspection and repair was satisfied by using mechanical fasteners that permitted the wing panels to be removed.

Using the established reliability method, a parametric evaluation was conducted to establish the sensitivity of each concept (weight) for the three levels of reliability (low, nominal design, and high). After evaluating one concept (waffle) for the key sensitivity factors listed in table 25-1, it was determined that the 2.0-g load condition was the most critical load condition, with creep and fatigue not governing the design. Therefore, all the concepts were evaluated for the 2.0-g load condition and the three levels of factors of safety. These concepts encompassed heat shields, leading edges, and primary structures.

HEAT SHIELD RELIABILITY

Results of the heat shield reliability evaluations are shown in table 25-2, with heat shields applicable to a typical spanwise tubular panel (46 in. by 92 in.). For each load factor, the optimum heat shield consists of minimum-gage skin with the support spacing decreased to allow for increased pressure loading. Thus, variation in the equivalent thickness panel ($\bar{t}$) is due only to changes in support spacing. The multisupported corrugated heat shield, for example, has support spacing of 15.3 in., 13.1 in., and 11.5 in. for the three levels of reliability.

Panel sizes for the flat-skin, dimple-stiffened concept are 23 in., 15.3 in., and 15.3 in. Because only heat shield sizes that are multiples of the primary-structure panel size are considered in the heat shield evaluation, the support spacing and $\bar{t}$ for nominal and high factors of safety are identical. The next larger size (23 in.) would have larger bending moments than allowed by minimum-gage design.

The weights of the two modular concepts are not affected by variations in factor of safety, since they are not influenced by the support spacing of the primary structural panel.

The results indicate that reliability (sensitivity) had little influence upon final selection of the heat shield concept.

LEADING EDGE RELIABILITY

The leading edge reliability evaluation results are shown in table 25-3. As indicated, the segmented leading edge provides considerably more flights than the continuous concept; and the nominal design for the segmented leading edge more than satisfies the vehicle design life of 8110 flights. The continuous leading-edge concept does not meet the life requirements for any level of reliability studied.

PRIMARY STRUCTURE RELIABILITY

Relative structural reliability (sensitivity) was based on average unit weights for the entire wing cross section. To determine average unit wing weights, a spanwise distribution based on total wing cross section weights in the center (A), inboard (B), and outboard (C) wing areas was used for the wing-investigation area. Then total weights were obtained. The wing weights include upper and lower surface panels, spar caps and webs, rib caps and webs, heat shields, insulation, panel closeouts, oxidation penetration, corner posts, fasteners. As an example, tables 25-4 through 25-6 present a summary of component weights for the monocoque waffle concept for the three levels of reliability.

The reliability evaluation results for the six primary structures are shown in table 25-7 for the wing-investigation area and the total wing. The monocoque waffle results show constant variation in average wing weight of about 1.0 lb/ft^2 between levels of reliability. For the monocoque honeycomb-sandwich concept, the constant variation in average wing weight is about 0.20 lb/ft^2 between levels of reliability. For the spanwise tubular concept, the results indicate variations in wing weight of about 0.30 lb/ft^2, For the beaded-skin concept, a constant variation of about 0.40 lb/ft^2 was indicated.

The chordwise concept results indicate variations in wing weight of about 0.65 lb/ft^2 between the low and nominal reliability levels and about 0.45 lb/ft^2 between the nominal and high reliability levels. The statically determinate concept results indicate variations in wing weight of about 0.40 lb/ft^2.

For the fatigue reliability evaluation, discrete loading spectra were used to arrive at a loading distribution (actual number of cycles applied at discrete load levels) for cumulative damage analysis. A fatigue-life versus allowable stress plot, based on the Palmgren-Miner cumulative damage theory, provided a direct-reading method of determining the potential penalty (reduced allowable stress) for increase in lifetime. Results of the fatigue-reliability evaluation are shown in figure 25-2. Fatigue life requirements for low, nominal, and high levels of reliability were based on scatter factors of 1.0, 1.5, and 2.0, respectively, applied to the specified vehicle life of 10 000 hours at 1400°F. Between low and nominal levels of reliability, the allowable mean stress at cruise decreased 6 ksi.

The effect of creep on primary structural panel design was determined for the cruise condition loads and temperatures, and scatter factors corresponding to low and high levels of reliability were applied to the total cruise time. The resulting structures, optimized for creep only, accounted for only 70 percent of the weight of structures designed for the maneuver conditions and checked for creep life. Therefore, creep conditions must be evaluated, although they are not critical to the design.

SUMMARY OF CONCEPT RELIABILITY EVALUATION

Reliability-evaluation results for the selected monocoque, semimonocoque, and statically determinate primary structure concepts are summarized in figure 25-3 for the wing investigation area and in figure 25-4 for the total wing. As shown, for low, nominal, and high levels of reliability, they represent ultimate factors of safety of 1.5, 2.0, and 2.5, respectively. Average unit wing weights were based on loads for the +2.0-g maneuver condition.

As shown in figure 25-3, the chordwise concept is lower in weight than the honeycomb-sandwich for the low, but not high, reliability. This is due to the minimum-gage restraint of the honeycomb-sandwich.

The total wing weight evaluation of figure 25-4 indicates that the minimum-gage honeycomb-sandwich is heavier than the statically determinate concept for the low reliability. However, the honeycomb-sandwich is lower in weight than both the statically determinate and tubular concepts at high (2.5) factors of safety, which indicates greater honeycomb efficiency in the higher load ranges.

REFERENCE

25-1 Heldenfels, R. R.: The Effect of Nonuniform Temperature Distributions on the Stresses and Distortions of Stiffened-Shell Structures. NACA TN 2240, Nov. 1950.

TABLE 25-1

SUMMARY OF RELIABILITY PARAMETERS

-0.5-g and +2.0-g load conditions (applied to operating limit loads)			Life criteria for primary structure (fatigue and creep allowables)		
Reliability level	Ultimate load factor	Ultimate thermal strain factor	Reliability level	Fatigue[a] scatter factor	Creep[b] scatter factor
Low	1.5	1.1	Low	1.0	1.0
Nominal	2.0	1.3	Nominal	1.5	1.5
High	2.5	1.5	High	2.0	2.0

[a]Applied to fatigue spectra.

[b]Cruise limit loads; 0.5-percent total creep tensile strain; creep buckling based on isochronous stress-strain curves.

TABLE 25-2

HEAT-SHIELD RELIABILITY EVALUATION[a]

Heat-shield concept		Equivalent panel thickness, $\bar{t}$, in.		
		Low ultimate load factor = 1.5 p_{ult} = 0.75 psi	Nominal ultimate load factor = 2.0 p_{ult} = 1.0 psi	High ultimate load factor = 2.5 p_{ult} = 1.25 psi
Refurbishable	Corrugated, multisupported	0.0127	0.0131	0.0135
	Flat-skin dimple-stiffened, clip-supported	0.0291	0.0298	0.0298
Permanently	Modular simply supported	0.0118	0.0118	0.0118
	Modular cantilevered	0.0123	0.0123	0.0123

[a] p_{limit} = 0.5 psi

TABLE 25-3

LEADING-EDGE RELIABILITY EVALUATION

Structural arrangement	Leading-edge life (number of flights)		
	Level of reliability [a] [b] [c]		
	Low scatter factor = 1.0	Nominal scatter factor = 1.5	High scatter factor = 2.0
Segmented leading edge t_{NOSE} = 0.125 in. t_{FLAT} = 0.030 in. Length = 20.0 in. [d]	10.0×10^6	11.9×10^5	2.5×10^5
Continuous leading edge t_{NOSE} = 0.625 in. t_{FLAT} = 0.060 in.	74	12	2

[a] Scatter factor applied to low-cycle fatigue strain allowable.

[b] Fatigue quality index, K_Q = 2, applied to limit elastic thermal strain.

[c] Analysis of end effect based on reference 41.

[d] For cumulative fatigue damage analysis, -0.5-g and +2.0-g conditions are assumed to occur for one of ten flights.

TABLE 25-4

SUMMARY OF COMPONENT WING WEIGHTS FOR LOW, NOMINAL, AND HIGH LEVELS OF RELIABILITY, CENTER AREA (A)

(Monocoque waffle concept: partial heat shield at outboard area lower surface with insulation; a = 40 in., b = 20 in.)

Item		Equivalent Thickness, in. Low factor	Nominal factor	High factor
Panels	Upper	0.06173	0.07082	0.07925
	Lower	0.05624	0.06575	0.07511
	Total	0.11797	0.13657	0.15436
Cap and closeout - single shear	Upper rib direction	0.01643	0.01827	0.01985
	Upper spar direction	0.00821	0.00913	0.00993
	Total	0.02464	0.02740	0.02978
	Lower rib direction	0.01345	0.01543	0.01708
	Lower spar direction	0.00672	0.00772	0.00854
	Total	0.02017	0.02315	0.02562
	Total	0.04481	0.05055	0.05540
Rib and spar webs	Rib web	0.0363	0.0363	0.0363
	Spar web	0.0182	0.0182	0.0182
	Total	0.0545	0.0545	0.0545
Web intersection	Total	0.00225	0.00225	0.00225
Dynaflex insulation	Insulation	-	-	-
	Packaging	-	-	-
	Total	-	-	-
Corrugated heat shield	Corrugation	-	-	-
	Clip	-	-	-
	Total	-	-	-
Oxidation	Total	0.000498	0.000498	0.000498
Fastener	Total	0.00541	0.00541	0.00541
Total equivalent thickness		0.22544	0.24975	0.27130
Total unit weight, lb/ft^2		9.67	10.72	11.64

TABLE 25-5

SUMMARY OF COMPONENT WING WEIGHTS FOR LOW, NOMINAL, AND HIGH LEVELS OF RELIABILITY, INBOARD AREA (B)

(Monocoque waffle concept: partial heat shield at outboard area lower surface with insulation; a = 40 in., b = 20 in.)

Item		Equivalent Thickness in. Low factor	Nominal factor	High factor
Panels	Upper	0.06889	0.07904	0.08852
	Lower	0.07035	0.08224	0.09395
	Total	0.13924	0.16128	0.18247
Cap and closeout - single shear	Upper rib direction	0.01776	0.01975	0.02147
	Upper spar direction	0.00888	0.00988	0.01074
	Total	0.02664	0.02963	0.03221
	Lower rib direction	0.01560	0.01791	0.01981
	Lower spar direction	0.00780	0.00895	0.00991
	Total	0.02340	0.02686	0.02972
	Total	0.05004	0.05649	0.06193
Rib and spar webs	Rib web	0.0363	0.0363	0.0363
	Spar web	0.0182	0.0182	0.0182
	Total	0.0545	0.0545	0.0545
Web intersection	Total	0.00225	0.00225	0.00225
Dynaflex insulation	Insulation	-	-	-
	Packaging	-	-	-
	Total	-	-	-
Corrugated heat shield	Corrugation	-	-	-
	Clip	-	-	-
	Total	-	-	-
Oxidation	Total	0.000498	0.000498	0.000498
Fastener	Total	0.00541	0.00541	0.00541
Total equivalent thickness		0.25194	0.28043	0.30594
Total unit weight, lb/ft^2		10.63	12.03	13.13

TABLE 25-6

SUMMARY OF COMPONENT WING WEIGHTS FOR LOW, NOMINAL, AND HIGH LEVELS OF RELIABILITY, OUTBOARD AREA (C)

(Monocoque waffle concept: partial heat shield at outboard area lower surface with insulation, a = 40 in., b = 20 in.)

Item		Equivalent Thickness, in. Low factor	Nominal factor	High factor
Panels	Upper	0.05962	0.06840	0.07660
	Lower	0.03871	0.04525	0.05169
	Total	0.09833	0.11365	0.12829
Cap and closeout-angle shear	Upper rib direction	0.01551	0.01725	0.01859
	Upper spar direction	0.00775	0.00862	0.00930
	Total	0.02326	0.02587	0.02789
	Lower rib direction	0.00927	0.01065	0.01178
	Lower spar direction	0.00464	0.00532	0.00589
	Total	0.01391	0.01597	0.01767
	Total	0.03717	0.04184	0.04556
Rib and spar webs	Rib web	0.0182	0.0182	0.0182
	Spar web	0.0091	0.0091	0.0091
	Total	0.0273	0.0273	0.0273
Web intersection	Total	0.001125	0.001125	0.001125
Dynaflex insulation	Insulation	0.00146	0.00146	0.00146
	Packaging	0.00202	0.00202	0.00202
	Total	0.00348	0.00348	0.00348
Corrugated heat shield	Corrugation	0.01660	0.01660	0.01660
	Clip	0.00485	0.00485	0.00485
	Total	0.02145	0.02145	0.02145
Oxidation	Total	0.005664	0.005664	0.005664
Fastener	Total	0.00541	0.00541	0.00541
Total equivalent thickness		0.19993	0.21992	0.23828
Total unit weight, lb/ft^2		8.58	9.44	10.23

TABLE 25-7

RELIABILITY EVALUATION WING WEIGHTS FOR BASELINE VEHICLE

Structural concept	Investigation Area		Total wing weight, lb [a]	Total wing average unit weight, lb/ft^2 [b]
	Reliability level	Avg. unit weight, lb/ft^2		
Monocoque waffle	Low	9.446	94 388	9.350
	Nominal	10.494	103 086	10.212
	High	11.402	110 373	10.933
Monocoque honeycomb sandwich	Low	6.285	63 254	6.266
	Nominal	6.473	64 778	6.417
	High	6.739	66 756	6.613
Spanwise tubular	Low	5.058	61 114	6.054
	Nominal	5.376	63 981	6.338
	High	5.755	67 418	6.678
Spanwise beaded-skin	Low	4.640	56 753	5.622
	Nominal	5.060	60 601	6.003
	High	5.519	64 766	6.416
Semimonocoque chordwise	Low	5.959	67 000	6.637
	Nominal	6.666	72 867	7.218
	High	7.134	76 742	7.602
Statically determinate	Low	5.139	62 607	6.202
	Nominal	5.550	66 380	6.575
	High	5.912	69 763	6.911

[a] Includes elevon and basic wing weights less leading-edge weight.

[b] Wing area = 10,095 ft^2.

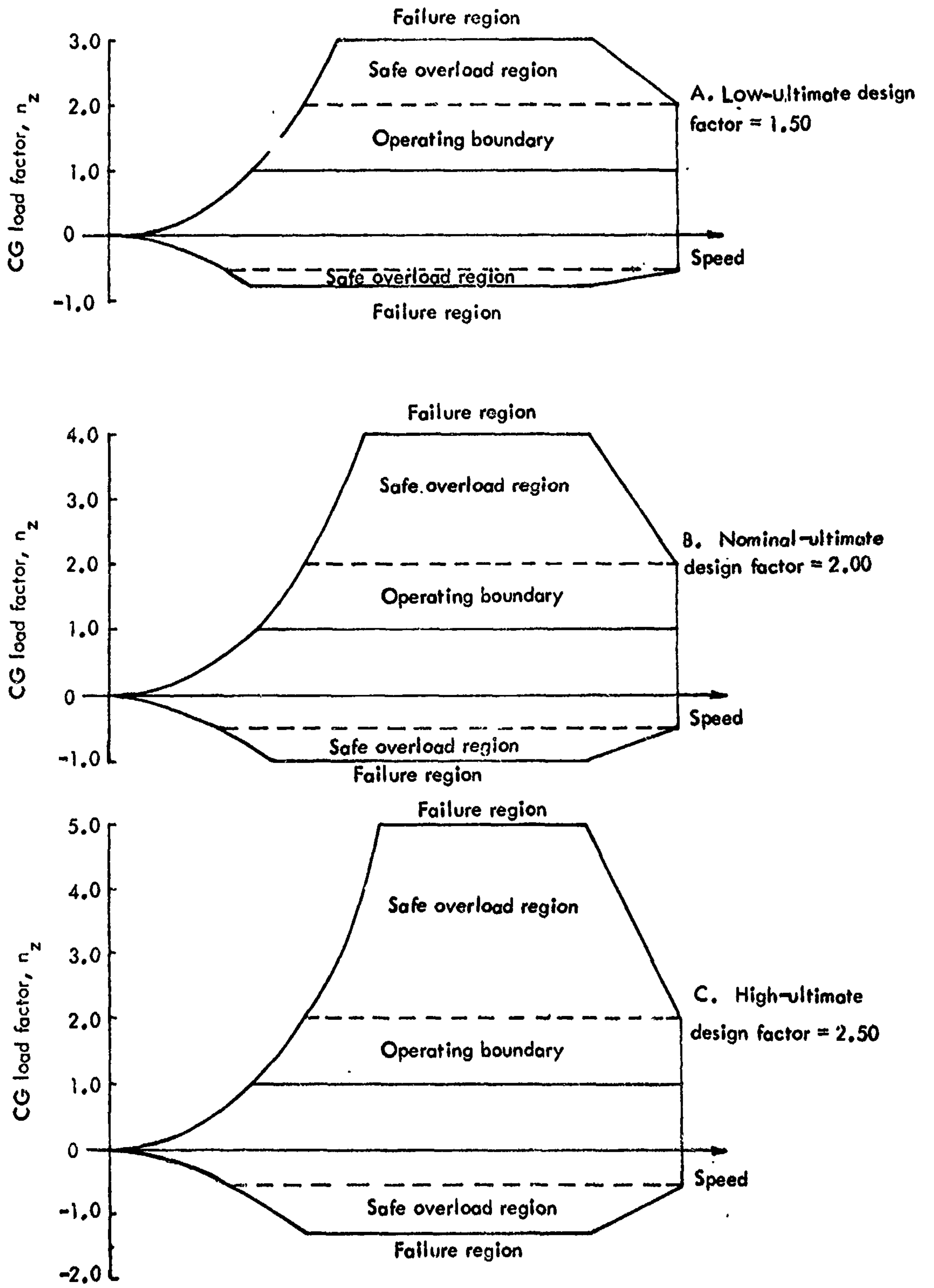

Figure 25-1 Safe overload boundaries and operating boundaries for low, nominal, and high level increase in structural reliability

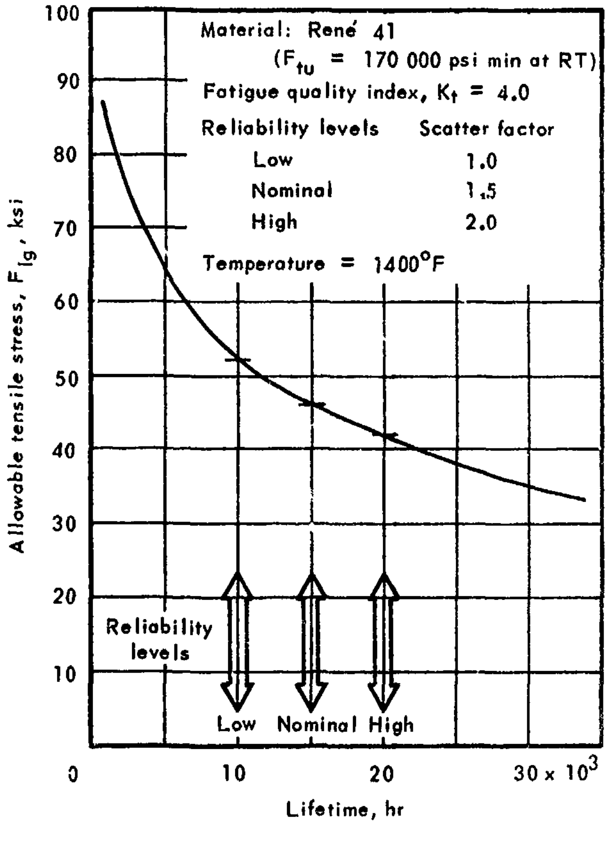

Figure 25-2 Allowable tensile stress for fatigue, René 41

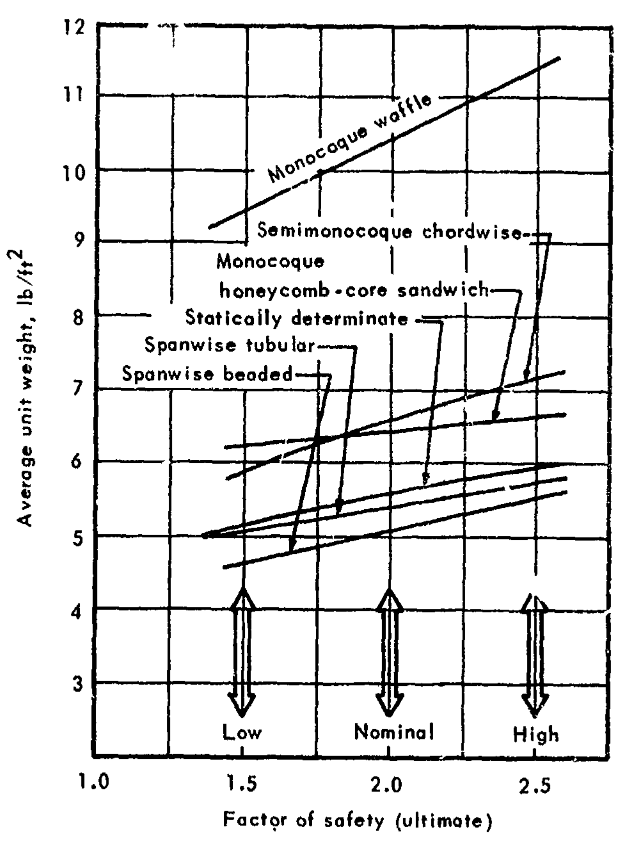

Figure 25-3 Wing investigation area: average unit rates vs factor of safety

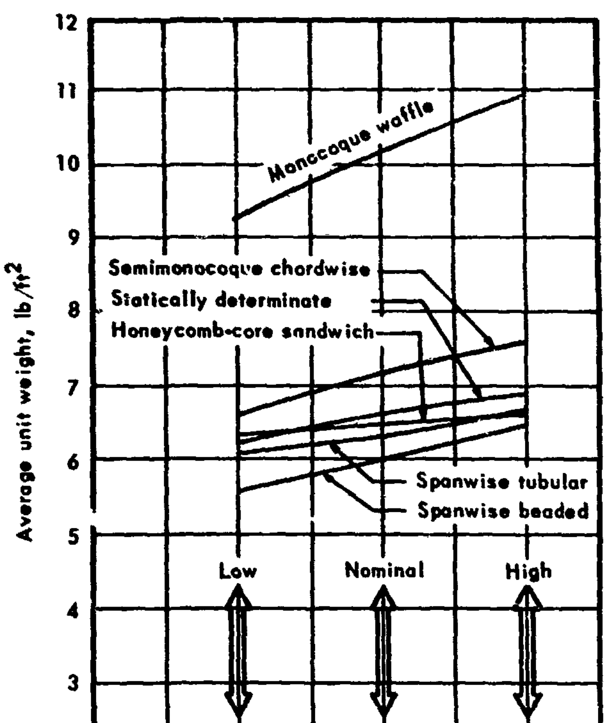

F

Figure 25-4 Total wing: aver ... ht vs factors of safety

Section 26

RATING FACTOR INTERACTION

by

I.F. Sakata, R.D. Mijares, D.E. Sherwood

PRECEDING PAGE BLANK NOT FILMED.

CONTENTS

PRECEDING PAGE BLANK NOT FILMED.

TABLES

PRECEDING PAGE BLANK NOT FILMED.

ILLUSTRATIONS

ILLUSTRATIONS (Cont.)

SYMBOLS

DOC	Direct operating cost
GTOW	Gross takeoff weight
IOC	Indirect operating cost
IV	Initial investment cost
OV	Operational vehicle
RDT&E	Research, development, test and evaluation cost
S	Actual wing area
S_{REF}	Reference wing area
TOC	Total operation cost
TSC	Total system cost
W	Vehicle weight
W_{PL}	Weight of payload
w	Unit wing weight expressed in lb/ft^2
ΔTSC	Difference in total system cost

Section 26

RATING FACTOR INTERACTION

A rating factor interaction evaluation was conducted by interrelating the total wing factors of weight, cost, performance, and reliability to a total vehicle system cost for each wing structural concept.

INTERACTION PROCEDURE

A common denominator, minimum total system cost (TSC), was selected as the basis for evaluating and comparing the wing-structure concepts. The baseline mission range requirement of 4000 nautical miles and a fleet size of 200 vehicles (550 000 lb each) with a payload of 55 000 pounds satisfying 10 000 hours of life (8110 missions) for 10 years resulted in a fleet payload-range requirement of 205 billion ton-miles (statute) for each concept.

The total wing weights and costs for the three levels of reliability and fuel mass fractions associated with roughness drag performance (resulting in payload changes for the wing structure concept of the baseline 500 000-lb vehicle) were submitted for integration into a whole vehicle system. Except for the statically determinate concept, which requires additional fuselage weight, identical weight and cost scaling relationships were used for the remaining portion of the vehicle. The vehicle integration was simulated by an analytical vehicle weight-cost sizing evaluation model.

Vehicle Weight-Cost Sizing Method

A vehicle weight-sizing analysis procedure (ref. 26-1) was coupled with a cruise transport economics model (ref. 26-2). Basic input data included weight and volume coefficients, propulsion-system data, specific geometrical characteristics, and cost coefficients.

For the vehicle weight-sizing analysis, the baseline vehicle gross weight (W), reference wing area (SREF), and total fuel weight to vehicle gross weight (fuel fraction) were used. These baseline vehicle data are presented in section 22. The vehicle configuration was assumed to be geometrically similar and to have a constant take-off wing-loading for all sizes of vehicles.

Airplane procurement costs were established through use of the economics model of reference 26-2 and an economics subroutine employing supersonic transport cost model techniques to determine the direct and indirect operating costs.

The established baseline-vehicle cumulative cost estimates per unit for 100 vehicles was used. The labor cost was then factored along a learning curve to obtain labor costs for any required number of aircraft. Material costs were similarly factored along a learning curve. (A learning curve is an expression of the rate at which production cost per unit decreases as the number of units produced increases.) The learning curves cited here are based on airframe industry standards (ref. 26-3). Total tooling costs were amortized over the appropriate production quantity. A summation of airframe manufacturing labor and material, avionic, and propulsion costs provided total vehicle costs for the established production quantity. One-time investment costs, including spares, facilities, and production tooling required to bring the system to operational status were then added to obtain the initial investment cost for the established number of operational vehicles.

In addition to these data, payload (W_{PL}) extreme values were bounded, as presented in figure 26-1. All these constraints were put into the weight-scaling synthesis model loop, in which wing reference area is the primary scaling parameter. As the vehicle gross weight parameter varied, variations in fuel requirements to perform the 4000-mile nautical mission resulted in payload capability variations. Once the weight and sizing conditions were satisfied for the basic mission requirements, the data were put into the economics (fig. 26-1), in which each element cost was varied linearly with vehicle weight change. Then, the vehicle procurement (including anticipated spares), direct operating cost, indirect operating cost, and total system cost were computed in detail for the specified mission. Because of structural efficiency variations between the wing concepts, the output provided variable fleet sizes and vehicle gross weights to satisfy the 205 billion ton-mile (statute) fleet payload range requirement, as well as total system cost.

Cost Model Summary

The three major categories which make up the cost model for the cruise airplane are:

1. Research, Development, Test and Evaluation -- (RDT&E)

2. Initial Investment – (IV)

3. Total Operation Cost – (TOC)

For this study, however, only the latter two categories were used and are considered to make up the cruise airplane total system cost (TSC). Thus, TSC = IV + TOC.

Initial Investment

This category consists of all one-time investment costs required to bring the system to an operational status. The elements comprising this category are noted in table 26-1. The major elements are the operational vehicles, spares, and facilities. A learning factor on materials and on labor for fabrication, as discussed earlier, is taken into consideration in determining the flight vehicle manufacturing cost (ref. 26-3).

Total Operation Cost

The costs of operating the system (both direct and indirect operating) for a 10-year period are included in this category. Both the direct operating cost (DOC) and indirect operating cost (IOC) are based on the Air Transport Association (ATA) method.

The ATA method, developed from reference 26-4, is a universally recognized method for estimating operating expenses. This method has been revised, updated and used as a part of the FAA's economic model ground value for the U.S. Supersonic Transport Development Program. The costing factors required for the ATA method of determining direct and indirect operating costs for various size vehicles are obtained from cost analysis work described in reference 26-2.

Direct Operating Cost. – The direct operating expenses are calculated in accordance with reference 26-5.

Fuel Cost: The cost of hydrogen fuel is a critical factor in the future economic feasibility of the hypersonic transport. Reference 26-6 presents the results of a study made of liquid hydrogen production cost based upon projection of the increased demand associated with hydrogen-fueled aircraft. Production costs were estimated at 10 important international locations. Variables investigated were plant capabity, production methods, probable technological advances, and the effect of the geographical location of raw materials and energy sources.

The results of this study indicated that future production cost of liquid hydrogen may range from 8 to 13 cents per pound, depending on the location and quantity produced. This price includes amortization of the LH_2 plant cost. For this study, 11 cents per pound was selected as the cost of the liquid hydrogen fuel.

Indirect Operating Cost. – The U. S. Scheduled Airlines Indirect Operating Expense Constants have been updated from the 1966 expense reported on Form 41 to the Civil Aeronautics Board (ref. 26-7). These constants are used in conjunction with the formula outlined in reference 26-8.

The operating expenses composition and indirect expense subjects, considered in this research program, for the U.S. International Airlines are presented in table 26-2.

Cost Model Program

The various elements of the cost model computer program are presented in table 26-3 and the nomenclature defining the model is shown in table 26-4.

INTERACTION RESULTS

The various structural concepts at each level of reliability were evaluated and compared using the results of the interaction computer program. The segmented leading edge and multiple-support corrugated heat shield concepts were used with each structure. The results include cruise vehicle weight and geometry data, as well as vehicle procurement, direct and indirect operating costs, and total system costs. Data were obtained for a range of vehicle, payload, and fleet sizes to meet the basic mission-payload-range requirements of 205 billion ton-miles (statute) so that the minimum total system cost for each concept could be defined.

Results are given in tables 26-5 and 26-6 in dollars and in cents per ton-mile, respectively, for the minimum total system cost vehicles. These tables indicate that the semimonocoque spanwise beaded-skin concept is the minimum TSC wing structure. The spanwise tubular concept is the next lowest cost concept. These tables also show that the minimum TSC is about $74.7 billion dollars (36.4 cents per ton-mile) for the fleet requirement specified and that the fleet procurement cost are $5.7 billion or $9.35 billion with spares. The tables also show a significant cost difference of $6 billion (3 cents per ton-mile) between the minimum cost and next lowest cost primary structure. In addition, improved reliability from low to nominal or nominal to high for any of the concepts adds approximately $5 billion to the TSC, except for the honeycomb sandwich low-to-nominal reliability, which is about $3 billion. The differences in roughness drag and initial cost between concepts have insufficient effect on total system cost to change the effect of weight differences. One exception is that at high levels of reliability, honeycomb, even though it is more costly to fabricate than the next heavier concept, offers lower TSC; consequently their ratings change with reliability level.

A plot of minimum TSC (in terms of cents per ton-mile) as it varies with wing unit weight for the optimum-size vehicle and the corresponding baseline-size vehicle for the various structural concepts (at nominal factor of safety) is given in figure 26-2. The waffle concept costs are large because at the waffle-concept weight, the vehicle has little payload. Consequently 1023 vehicles (see table 26-5A) instead of 129 for the minimum-weight beaded-skin concept are required to perform the fleet mission requirements. Figure 26-2 shows the effect of increasing unit wing weight, which if extrapolated to about 12.0 lb/ft^2, would show the TSC approaching infinity, since at this weight the payload is zero.

Baseline-vehicle-size wing weights are shown in addition to the optimum-size vehicle data because the unit wing weights for the baseline vehicle are comparable to one another, whereas the optimum-size vehicle unit weights vary as a function of vehicle size. This consistency for baseline-size vehicle wing unit weights enables estimates to be made of how other concepts calculated for the baseline-size vehicle, such as those dropped out by intermediate screening, compare with the listed concepts. For instance, the semimonocoque spanwise trapezoidal corrugation concept wing average weight is 7.45 lb/ft^2 (see section 13), which from figure 28-2 indicates a weight and a TSC that are greater than all but the waffle concept.

A plot of TSC (in terms of cents/ton-mile) as it varies with vehicle size (expressed as gross takeoff weight) is given in figure 26-3 for the different structural concepts. The minimum-cost beaded panel concept permits a vehicle length variation of 350 to 488 ft or, expressed as a variation of from 620 000 to 1 200 000 pounds, at less cost than the next-lowest cost tubular wing structure vehicle. Moreover, the order of structure selection remains unchanged regardless of vehicle size for the range given in figure 26-3.

Total system cost, payload, and fleet size variation with vehicle size for low, nominal, and high levels of reliability (factor of safety) are presented in figures 26-4 and 26-5 for the monocoque waffle concept. Because of large wing weights and resulting small payload capability, the monocoque waffle concept requires large fleets to accomplish the basic mission, as shown in figures 26-4 and 26-5. For the monocoque honeycomb concept shown in figures 26-6 and 26-7, the variation is cost with vehicle size and for the three levels of reliability the variation is small (less the ±5%). Also, for the high level of reliability, the system cost is less than the cost of the vehicle with the semimonocoque tubular wing.

For the semimonocoque tubular concept, the cost variance is approximately ±8 percent for the minimum-cost vehicles for the various levels of reliability, as indicated in figure 26-8. Fleet size varies from 132 to 166 between the low and high level of reliability, as shown in figure 26-9. For the minimum cost system, cost variation between low and high levels of reliability is approximately ± 10 percent of the nominal level, as indicated in figure 26-10 for the beaded concept. The fleet size varies between 115 to 149 for the low and high level of reliability, with the nominal being 129 for the nominal 882 621-pound vehicle of the beaded concept (figure 26-11).

The data for the semimonocoque chordwise concept are given in figures 26-12 and 26-13. A greater spread in cost and fleet size results, as shown. Fleet size varies from 168 to 244, respectively, for the low and high level of reliability designs. For the statically determinate concept, the cost variations between low and high level reliabilities vehicles are similar to the minimum-cost vehicle, semimonocoque spanwise beaded, resulting in a ±10 percent variation from the nominal, as shown in figure 26-14. The spread in fleet size for the minimum-cost vehicle is between 153 to 199 with the nominal being 175 vehicles (figure 26-15).

Baseline Vehicle
(Gross Takeoff Weight = 550 000 Pounds)

A group weight statement for the 550 000-pound gross weight vehicle of each concept is presented in table 26-7. These vehicles satisfy the specified mission-payload-range and fuel fraction requirements for the nominal level of reliability. The results indicate a tradeoff between wing weight and payload, which in turn affects the number of operational vehicles required to perform the payload-range schedule. The structure and payload mass fractions vary from the initially assigned values, given in table 26-8. The increase in the structure mass fraction is attributed to the increase in wing unit weights for the various structure concepts evaluated. It is noted that the semimonocoque spanwise beaded concept is the only concept with a payload mass fraction equal to the assigned value of 0.10. Both semimonocoque tubular and monocoque honeycomb concepts have payload mass fractions of 0.09, whereas monocoque waffle has only 0.02 payload mass fraction.

A summary of vehicle geometry data as well as pertinent design parameters are shown in table 26-9. Of significance are the wing weights (table 26-7) which when divided by the total wing area results in the nominal wing unit weights used for concept comparison. For the statically determinate concept, the fuselage weight increase is included with the wing weight to obtain an effective wing unit weight, so that the wing design concepts can be compared on a common basis. Table 26-9 shows that the semimonocoque, spanwise beaded skin concept has the least weight, with the next least weight being the semimonocoque, spanwise tubular concept (5.4 percent heavier).

Cost results for the operational vehicles are presented in table 26-10, including initial investment costs for the specified number of vehicles required to perform the basic payload-range schedule. Total operational costs (includes direct and indirect operating costs), and total system costs for each concept are shown. The individual flight vehicle costs, regardless of concept, do not vary appreciably ($30.9 million to $32.2 million). The fleet cost (OV – operational vehicles) varies directly with the number of vehicles required to perform the specified payload-range schedule. Since unit vehicle costs do not vary appreciably, the primary influence on operational-vehicle and initial-investment costs is the fleet size requirement. Similarly, fleet size has the major impact on the total operational cost (TOC), which is the primary factor influencing TSC. The total operational costs are approximately 88 percent of the total system costs, as indicated. The importance of weight is indicated, for the design of the vehicles, and lesser influence of initial cost. For the given gross weight (550 000 lb), an increase in structure weight decreases the payload carrying capability. This decrease directly affects the fleet size required to perform the specified mission. Since, in general, operating costs (DOC plus IOC) are nearly the same for all concepts (except monocoque waffle) regardless of fleet size, the total system cost varies directly with wing weight.

Table 26-10 indicates that the semimonocoque, spanwise-beaded skin concept is the lowest TSC wing structure. The semimonocoque, spanwise tubular concept is the next lowest cost concept, with the monocoque honeycomb being the third lowest cost. The cost increase of the tubular and honeycomb concepts over the minimum-cost beaded concept, which is approximately $86.3 billion, is 6.9 percent and 9.0 percent, respectively. For the tubular concept, this increase almost equals the procurement cost for the beaded concept and the increase for the honeycomb concept exceeds it.

Minimum Total System Cost Vehicles
(Gross Takeoff Weight = Variable)

A group weight statement for the vehicle sized to achieve minimum system cost is presented in table 26-11. The gross takeoff weights vary between 562 904 lb to 882 621 lb for the minimum cost systems. The trend for vehicles with larger payloads and consequently smaller fleet sizes is noted. The resulting mass fraction for the various components is given in table 26-12, which indicates a structure-payload variation. The heavier wing weights result in large structure mass fraction with the decrease in payload fraction. The decrease in propulsion as well as equipment mass fractions are attributed to constants used in the computer program. Although the main engine and propellant distribution system are sized and weighted to satisfy the thrust requirements for change in variable gross weight, the air induction system is assumed constant (44 689 lb). Thus, with increase in vehicle size, the propulsion mass fraction tends to decrease. This assumption was made to avoid an air induction system design exercise, which was considered unwarranted for this study effort.

Pertient geometry and design parameters for the optimum-sized vehicles (minimum cost systems) are shown in table 26-13. The resulting wing unit weights show a 20 percent increase over the baseline vehicle for the semimonocoque spanwise beaded concept.

The cost results for each vehicle are given in table 26-14. The airframe labor, material, and manufacturing costs are presented, in addition to avionics and propulsion costs. The individual flight vehicle costs, regardless of concept, do not vary appreciably ($31.4 million to $43.8 million), a trend also noted on the baseline vehicles. It is noted that the vehicle unit costs for the honeycomb concept and semimonocoque, spanwise beaded concepts are approximately the same ($43.8 x 10^6). However, the fleet size requirements due to the payload capability of each concept increases total cost over the minimum cost system by approximately 11 percent. Therefore, the primary factor influencing cost is the fleet size requirement, which is dictated by the wing-weight/payload-weight tradeoff. The operational costs for the sized vehicles are approximately 88 percent of the total system cost.

Constant Weight Vehicles
(Gross Takeoff Weight = 882 621 Pounds)

The vehicle weight corresponding to the vehicle sized for minimum total system cost (semimonocoque spanwise beaded-skin concept) was used for final comparison of the structure concepts. Figure 26-16 presents the total system cost (dollars) variation with vehicle size (in terms of gross takeoff weight) for each concept. Several approaches were taken in comparing concepts, including consideration of the following:

a. Baseline vehicle (gross takeoff weight = 550 000 lb)

b. Optimum-size vehicle, minimum total system cost vehicle (GTOW = variable)

c. Constant gross weight vehicle (GTOW = 882 621 lb)

d. Constant payload-fleet size vehicles (GTOW = variable)

Constant gross weight vehicles (GTOW = 882 621 lb) were selected for comparison of the concepts since the vehicles are of constant size (as in the case of the baseline 550 000-lb vehicle) but also since the total system costs are closer to the minimum for each concept. Cross plots of available data, such as shown in figure 26-17 of total system cost variation with fleet size, were used to obtain the fleet size required for each of the vehicles having a constant gross weight. The wing weight for each concept was obtained through use of the wing weight equation (ref. section 22). Table 26-15 presents the resulting wing total weights and wing unit weights, as well as fleet size requirements and total system costs. The total system cost variation with the nominal wing unit weights for the constant gross weight vehicle (GTOW = 882 621 lb) as well as the fleet size requirements, are presented in figure 26-18. The data indicate that a difference in cost between the minimum total system cost vehicle and the next least cost is $6.370 billion. Also noteworthy is the trend of increasing fleet size with the increase in wing unit weight. As previously noted, the increase in wing decreases the payload capability, requiring additional vehicles to perform the basic mission. Since the major portion of the total system cost is primarily due to the fleet size increase. An approximate cost-weight comparison can be made between the lowest weight (beaded) and the next lowest weight concept (tubular). Assuming an average fleet size (135 vehicles) and using the unit wing weights and corresponding total system costs shown in figures 26-18, the approximate cost-weight relationship can be determined from the following expression:

$$\$/\mathrm{lb} = \frac{\Delta \mathrm{TSC}}{(\Delta w)(S_{wing})(\mathrm{fleet})} = \$7000/\mathrm{lb}$$

where

ΔTSC = Total system cost differential = $\$6.37 \times 10^9$

w = Unit wing weight differential = $0.41\ lb/ft^2$

S = Wing planform area = $16\ 206\ ft^2$

Fleet = Average fleet size = 135

Thus the dollar per pound of saving by selection of the beaded-skin concept over the tubular concept is \$7000/lb of wing structure per vehicle.'

INTERACTION SUMMARY

A summary of wing unit weights and percentages for increase in wing weight and total system cost is presented in table 26-16 for the baseline vehicle (550 000 lb), minimum system cost vehicles (variable gross weight), and for the constant weight vehicles (882 621 lb). Since only the baseline and constant weight vehicles are for a constant vehicle size, the weight comparison data are meaningful. For the constant weight vehicles (882 621 lb), the tubular concept is approximately 5.5 percent heavier than the beaded-skin concept, but the total system cost is 8.5 percent greater. The third ranking primary structure is the honeycomb-core sandwich. This concept is 6.2 percent heavier and 10.8 percent more costly than the minimum weight concept. The statically determinate, chordwise-stiffened, and waffle are more costly than the first three concepts. It should be noted that small weight increases cause large cost increases. The weight order of concepts, which varies by as little as 6 percent, controls the total system cost in the same order, but to a greater degree.

REFERENCES

26-1 Jones, R.: Weight Synthesis and Sensitivity Programs, Lockheed-California Company; LR 21205, 1967.

26-2 Morris, R. E.: A Study of Advanced Airbreathing Launch Vehicles with Cruise Capability, Vol. V: Economics Model LR 21042, Lockheed-California Company, February 1968, NASA CR 73198.

26-3 Brewer, Glenn M.: The Learning Curve in the Airframe Industry, Air Force Institute of Technology, Wright-Patterson AFB, Ohio, August 1965.

26-4 Mentzer and Nourse: Some Economic Aspects of Transport Airplanes, United Airlines, Journal of Aeronautical Science, April-May 1940.

26-5 Federal Aviation Agency: Supersonic Transport Economic Model Ground Rules, Washington D.C., revised September 1965.

26-6 Wilcox, D. E.; and Smith, C. L.: Future Cost of Liquid Hydrogen For Use As An Aircraft Fuel, April 22, 1968. MA-68-3 Working Paper NASA OART, Mission Analysis Division, Moffett Field, California.

26-7 Indirect Operating Expense Constants for 1966, CMR 1010 Commercial Market Research, April 1968. Commercial Market Engineering and Research Division, Lockheed-California Company.

26-8 Method of Estimating Airline Indirect Expense Boeing/Lockheed Joint Report, August 30, 1964.

TABLE 26-1

SUMMARY OF INITIAL INVESTMENT COST ELEMENTS

Element	Description
1. Operational Vehicles — OV	Operational flight vehicles
2. Spares — OS	Replacement during operational period
3. Facilities — FAC	Complete launch facility and H_2 plant
4. Production Engineering — PE	Preliminary design conversion to production
5. Production Tooling — PT	Hard tooling
6. Sustaining Engineering — SE	Engineering support of operations
7. Sustaining Tooling — ST	Changes to tooling due to design
8. Aerospace Ground Equipment — AGEO	Additional equipment for operations
9. Technical Data — TDO	Production vehicle data
10. Miscellaneous Equipment — ME	Stock items, including trucks and office equipment
11. Initial Stocks — IST	30-day supply of fuel and misc items
12. Initial Training — IT	Operation, maintenance, and personnel training equipment
13. Initial Transportation — TRI	Personnel and hardware transportation
Initial Investment — IV = sum of items (1) through (13)	

TABLE 26-2

INDIRECT OPERATING EXPENSE CONSTANTS

Item No.	Description
1	Ground Property and Equipment Expense — System • Maintenance • Maintenance Burden • Depreciation
2	Ground Property and Equipment • Maintenance • Maintenance Burden • Depreciation Landing Fees Aircraft Servicing Service Administration
3	Aircraft Control and Communication
4	Cabin Attendant Expense
5	Food and Beverage Expense

TABLE 26-2. Concluded

INDIRECT OPERATING EXPENSE CONSTANTS

Item No.	Description
6	Passenger Handling Reservation and Sales
7	Baggage and Cargo Handling
8	Passenger Service – Other Expense Passenger Agency Commission Passenger Advertising and Publicity
9	Freight Commission Freight Advertising and Publicity
10	General and Administrative Expense

TABLE 26-3

COST MODEL COMPUTER PROGRAM

RESEARCH, DEVELOPMENT, TEST, AND EVALUATION – RDTE

AIRFRAME DESIGN AND DEVELOPMENT ENGINEERING – ADDE

CONCEPT FORMULATION – CF = 2080 * EHR * NEF * NYF * NCF * 10^{-6}

CONTRACT DEFINITION – CD = 2080 * EHR * NED * NYD * NCD * 10^{-6}

AIRFRAME DESIGN – AFD = (3.82 * (100 * AC) ** 0.91) * 10^{-2}

MISC SUBSYSTEM DESIGN – MSD = CPPD * WMSUB * 10^{-6}

SUPPORT EQUIPMENT DESIGN – SE = 0.047 * WEMPT * * 0.59

SYSTEM INTEGRATION – SI = 0.084 * WEMPT * * 0.48

FLIGHT TEST OPERATIONS – FTO = (985 * WG * * 0.8 * NP * * 1.1) * 10^{-6}

ADDE = CF + CD + AD + MSD + SE + SI + FTO

AVIONICS DEVELOPMENT – AD = 550 * (WGNAV + WGOMM) * * (-0.24)

PROPULSION DEVELOPMENT – PD = PCF * TSLE * * 0.744 * ME * * 0.17

DEVELOPMENT SUPPORT – DS

GROUND TEST VEHICLE – GTV = NG * AMFC

PROTOTYPE VEHICLE – PV = NP * FV

PROTOTYPE SPARES – PS = 0.25 PV

TOOLING AND SPECIAL TEST EQUIPMENT – TST = 0.10 * (WEMPT) * * .6

FLIGHT TEST FUEL – FTF = CH2(NFT) WFTOT * 10^{-6}

FLIGHT TEST MAINTENANCE – FTM = 1.5 * VM * NFT * 10^{-6}

GENERAL SUPPORT – GS = 0.3 (FTO + FTF + FTM)

MAINTENANCE TRAINERS – MT = MT (INPUT)

TABLE 26-3. Continued

COST MODEL COMPUTER PROGRAM

OPERATIONAL TRAINERS – OT = OT (INPUT)

AEROSPACE GROUND EQUIPMENT – AGEP = 0.15 * PV

TECHNICAL DATA – TDP = 0.02 * PV

DS = GTV + GTS + PV + PS + TST + FTF + FTM + GS + MT + OT + AGEP + TDP

RDTE = ADDE + AD + PD + DS

INITIAL INVESTMENT – IV

OPERATIONAL VEHICLES – OV

FLIGHT VEHICLES – FV

AIRFRAME MANUFACTURING – AMFC

LABOR LEARNING CURVE – LLC

LLC = (NV) * * -0.322

AIRFRAME LABOR – AL

FUSELAGE – FUSL = (WBODY + WDR) * CFUSL * LLC * 10^{-6}

FINS – FINL = (WTAIL) * CFINL * LLC * 10^{-6}

WING – WINGL

MAIN WING STRUCTURE – A – MWLA

MWLA = K5 * (WWING) * CMWLA * LLC * 10^{-6}

MAIN WING STRUCTURE – B – MWLB

MWLB = K6 * (WWING) * CMWLB * LLC * 10^{-6}

MAIN WING STRUCTURE – C – MWLC

MWLC = K7 * (WWING) * CMWLC * LLC * 10^{-6}

LEADING EDGES – LEL

LEL = K4 * (WWING) * CLEL * LLC * 10^{-6}

TABLE 26-3. Continued

COST MODEL COMPUTER PROGRAM

ELEVONS – EL

EL = K3 * (WWING) * CEL * LLC * 10^{-6}

WINGL = LEL + EL + MWLA + MWLB + MWLC

INLET INLL = WAIND * CINLL * LLC * 10^{-6}

NOSE CAP – NCL = KBSS * CNCL * LLC * 10^{-6}

INSULATION – INSLL = K2 * (WTPS) * CINSL * LLC * 10^{-6}

HEATSHIELDS – HTSL

HTSL = K1 * (WTPS) * CHTSL * LLC * 10^{-6}

AL = FUSL + FINL + WINGL + INLL + NCL + INSLL + HTSL

AIRFRAME MATERIAL – AM

MATERIALS LEARNING CURVE – MLC = (NV) * * -0.074

FUSELAGE – FUSM = (WBODY + WDR) * CFUSM * MLC * 10^{-6}

FINS – FINM = (WTAIL) * CFINM * MLC * 10^{-6}

WING – WINGM

MAIN WING STRUCTURE A – MWMA

MWMA = K5 * WWING * CMWMA * MLC * 10^{-6}

MAIN WING STRUCTURE B – MWMB

MWMB = K6 * WWING * CMWMB * MLC * 10^{-6}

MAIN WING STRUCTURE C – MWMC

MWMC = K7 * WWING * CMWMC * MLC * 10^{-6}

LEADING EDGES – LEM

LEM = K4 * WWING * CLEM * MLC * 10^{-6}

TABLE 26-3. *Continued*

COST MODEL COMPUTER PROGRAM

ELEVONS – EM

EM = K3 * WWING * CEM * MLC * 10^{-6}

WINGM = LEM + EM + MWMA + MWMB + MWMC

INLET – INLM = WAIND * CINLM * MLC * 10^{-6}

NOSE CAP – NCM = KBSS * CNCM * MLC * 10^{-6}

INSULATION – INSLM = K2 * WTPS * CINSM * MLC * 10^{-6}

HEATSHIELS – HTSM = K1 * WTPS * CHTSM * MLC * 10^{-6}

AM = FUSM + FINM + WINGM + INLM + NCM + INSLM + HTSM

LANDING GEAR – LG = WLRD * (CPLG * LLC + CPLGM * MLC) * 10^{-6}

MISCELLANEOUS SUBSYSTEMS – MS

FUEL SYSTEM – FS = (WPRT + WPPS + WPDS + WNPS + WPUS + WLUBE + WAUXFL) * (CFSL * LLC + CFSM * MLC) * 10^{-6}

FLIGHT CONTROLS – FCC = WFC * (CFCL * LLC + CFCM * MLC) * 10^{-6}

INSTRUMENTS – INSTC = WINST * (CINTL * LLC + CINTM * MLC) * 10^{-6}

HYDRAULIC – HYDRC = WHYD * (CHYDL * LLC + CHYDM * MLC) * 10^{-6}

ELECTRICAL – ELTRC = WELEC * (CELRL * LLC + CELRM * MLC) * 10^{-6}

ECS – ECSC = WECS * (CECSL * LLC + CESCM * MLC) * 10^{-6}

FURNISHINGS AND EQUIP – FUEQC = (WSORCE + WEQUIP – WCOMM) * (CFEQL * LLC + CFEQM * MLC) * 10^{-6}

MS = FS + FCC + INSTC + HYDRC + ELTRC + ECSC + FUEQC

QUALITY CONTROL – QC = 0.14 * (AL + AM + LG + MS)

STRUCTURE, FINAL ASSEMBLY – FA = 5.70 * WSTRUC * 10^{-6} * LLC

AMFG = AL + AM + LG + MS + QC + FA

TABLE 26-3. Continued

COST MODEL COMPUTER PROGRAM

AVIONICS – AV

WAV = WGNAV + WCOMM

AVIONCS PROCUREMENT – AVP = CPAV * WAV * 10^{-6} * MLC

AVIONICS INSTALLATION – AVI = ICPAV * WAV * 10^{-6} * (NP + NV) ** -.322

AV = AVP + AVI

PROPULSION – PROP

PROPULSION PROCUREMENT – PROPP = [2430 * TSLE * * .7 * [NTRJ * (NV + NP)] * * - .322] * NTRJ * 10^{-6}

PROPULSION INSTALLATION – PROPI = [5.6 * (WENG1 + WENG2 + WROC1) * [NE * (NP + NV)] * * - .322] * NE * 10^{-6}

PROP = PROPP + PROPI

FV = AMFG + AV + PROP

NUMBER OF OPERATIONAL VEHICLES – NV

NV = NV (INPUT)

OV = FV * NV

SPARES – OS

INITIAL SPARES – IOS = 0.25 * OV

REFURBISHMENT SPARES – ROS = 0.25 * IOS

OS = IOS + ROS

FACILITIES – FAC = FAC (INPUT)

PRODUCTION ENGINEERING – PE = 0.25 * (CF + CD + AFD)

PRODUCTION TOOLING – PT = 0.05 * WEMPT * * 0.75

SUSTAINING ENGINEERING – SEC = 0.0505 * (ADDE – CF – CD)

SUSTAINING TOOLING – ST = 0.15 * AL * NV * * 0.848

AEROSPACE GROUND EQUIPMENT – AGEO = 0.15 * OV

TABLE 26-3. Continued

COST MODEL COMPUTER PROGRAM

TECHNICAL DATA — TDO = 0.10 * TDP

MISCELLANEOUS EQUIPMENT — MEC = 500 * NPER * 10^{-6}

INITIAL STOCKS — IST = 0.083 * VM + 100 * NPER * 10^{-6}

INITIAL TRAINING — IT = 0.10 * OT * NPL

INITIAL TRANSPORTATION — TRI = 0.005 (OV + OS + AGEO + MEC + IST)

IV = OV + OS + FAC + PE + PT + SEC + ST + AGEO + TDO + MEC + IST + IT + TRI

DIRECT OPERATING COST — DOC

FLIGHT TIME — TF1 = DIST * TFU/(DIST + TFU * WIND)

TOTAL FLIGHT TIME — T7 = GRNDT + TF1

AMOUNT OF FUEL — FUEL = WFTOT

PCOST = [C1 * T7 + C2 (FUEL) + C3 * TF1 + C4] * (1. + PDOE)

PROT = C2 * FUEL * 10^{-6}

<u>INSURANCE</u> — QINS

PA = AMFG

AV = PAVO

QINS = (PA + PROP + PAVO + PROT) * RCON/(TVL/TF1) * (1. + PDOE) * 10^{+6}

TOTAL FLIGHT TIME PER DAY — TFTD = TF1 * NFD

NUMBER OF AVAILABLE FLIGHT DAYS — NAFD = TVL/TFTD

NUMBER OF FLIGHT YEARS — NFY = NAFD/365.0

NUMBER OF FLIGHTS PER YEAR — NFPY = NFD * 365.0

AIRFRAME DEPRECIATION PERIOD — TA = NFY

ENGINE DEPRECIATION PERIOD — TE = NFY

AVIONICS DEPRECIATION PERIOD — TAV = NFY

<u>DEPRECIATION</u> — QDEP

TABLE 26-3. Concluded

COST MODEL COMPUTER PROGRAM

$$QDEP = \left(\frac{PA * (1. -RA + CSF)}{TA} + \frac{PROP * (1. -RE + CSEFI)}{TE} + \frac{PAVO * (1. -RAV + CAVF)}{TAV} \right) * 10^{+6}$$

DOC = PCOST + BMAN * [C5 * T7 + C6 * (T7-GRNDT) + C7] + QINS + QDEP/NFPY

VM = BMAN * [C5 * T7 + C6 * (T7-GRNDT) + C7]

INDIRECT OPERATING COST — ENDOC

FCOST = E11 * [C5 * T7 + C6 * (T7 — GRNDT) + C7] + E12 + E13 * WG + E14 * TEND * T7 + DIST * [E20 * SEATS + E21 * PLMAX/TON] * (1. + PIOE)

NUMBER OF PASSENGER — PAS = SEATS * ALF

PASSENGER BLOCK HOUR — TPBH = PAS * T7

PASSENGER MILE — TPMI = PAS * DIST

WPART = PAS * CK1 * CK2

CARGO MILE — TCMI = WPART * DIST

ZYX = [E15 * C8 * TPBH + E 15A * C8 * PAS + E16 * PAS + (E17 * CK1 * CK2 * PAS + E17A * WPART)/TON + E18 * TPMI + E19 * C9 * TCMI/TON * (1. + PIOE)]

ENDOC = [(1. + E22) * (FCOST + ZYX) + E22A * (QINS + PCOST)] — BMAN * [C5 * T7 + C6 * (T7 — GRNDT) + C7]

TOTAL OPERATIONS COST — TOC = NFPY * NAY * (DOC + ENDOC)

TOTAL SYSTEM COST — TSC = TOC + RDTE + IV

TABLE 26-4

NOMENCLATURE FOR COST MODEL

AC	inlet capture area
AD	avionics development cost
AFD	airframe design cost
AGEO	aerospace ground equipment cost
AGEP	aerospace ground equipment cost
AL	airframe labor cost
ALF	average passenger load factor
AM	airframe material cost
AMAIL	minimum cargo weight
AMFG	airframe manufacturing cost
APAY	minimum payload weight
ASM	available seat mile
BLKF	total amount of fuel
BMAN	maintenance burden factor
C1	DOC block hour factor
C2	DOC fuel (lb) factor
C3	DOC flight hour factor
C4	DOC departure factor
C5	DML – block hour factor
C6	DML – flight time factor
C7	DML – departure factor
C8	passenger block hour weighting ratio
C9	ratio of freight to total cargo

TABLE 26-4. Continued

NOMENCLATURE FOR COST MODEL

CAVF	value for spare avionics factor
CD	contract definition cost
CF	concept formulation cost
CH2	cost of hydrogen ($/lb)
CK1	volume of baggage per passenger
CK2	density of baggage and cargo
CPAV	cost per pound of avionics
CPLG	cost per pound of landing gear (labor)
.PLGM	cost per pound of landing gear (material)
CPMS	cost per pound of miscellaneous subsystems
CPPD	cost per pound of development of miscellaneous subsystems
CPROF	value for spare propellants factor
CPT	cost per tire
CSEF1	value for spare engine factor
CSF	value for spare parts factor
DIST	flight distance
E11	IOD — direct maintenance labor
E12	IOD — aircraft departures
E13	IOD — departure times maximum landing weight
E14	IOC — cabin attendant block hours
E15	IOC — revenue passenger block hours (food)
E15A	IOC — revenue passenger carried (food)
E16	IOC — revenue passenger carried (servicing and sales)
E17	IOC — passenger baggage carried

TABLE 26-4. Continued

NOMENCLATURE FOR COST MODEL

E17A	IOC — cargo carried
E18	IOC — revenue passenger miles
E19	IOC — revenue freight ton miles
E20	IOC — available seat miles
E21	IOC — available ton miles
E22	IOC — general and administrative — indirect
E22A	IOC — general and administrative — direct
EHR	engineering hourly rate
ENDOC	indirect operating cost
FA	final assembly of structure cost
FAC	facilities cost
FHOLD	amount of fuel trapped in the vehicle
FTF	flight test fuel cost
FTM	flight test maintenance cost
FTO	flight test operations
FUEL	amount of fuel
FV	flight vehicle cost
GRNDT	ground taxi time (hr)
GS	general support cost
GTS	ground test spares cost
GTV	ground test vehicles cost
ICPAV	installation cost per pound of avionics
IOS	initial spares cost
IST	initial stocks cost

TABLE 26-4. Continued

NOMENCLATURE FOR COST MODEL

IT	initial training cost
LG	landing gear cost
ME	engine maximum operational Mach number
MEC	miscellaneous equipment cost
MS	miscellaneous subsystem cost
MSD	miscellaneous subsystem design cost
MT	maintenance trainers cost
NAFD	number of available flight days
NCD	number of contractors doing contract definitions
NCF	number of contractors doing concept formulation
NE	number of modules
NED	number of engineers on contract definition
NEF	number of engineers on concept formulation
NFD	number of flights per day
NFPY	number of flights per year
NFT	number of flight test
NFY	number of flight years
NG	number of ground test vehicles
NLGU	number of landing gear units
NMSU	number of miscellaneous subsystems units
NP	number of prototype vehicles
NPE	number of propulsion engines
NPER	number of total personnel
NPL	number of pilots

TABLE 26-4. Continued

NOMENCLATURE FOR COST MODEL

NT	number of tires per landing gear unit
NV	number of operational vehicles
NYD	number of years for engineering contract definition
NYF	number of years for engineering concept formulation
ODIST	flight distance
ONEP	fuel tankage fullness ratio
OT	operational trainers cost
OV	operational vehicle cost
OWE	operating weight empty
PA	airframe cost
PAS	number of passengers
PAVO	total avionics cost
PCF	propulsion development cost factor
PCOST	DOC less insurance and depreciation
PD	propulsion development cost
PDOE	percent change in DOE
PE	production engineering cost
PEC	total engine cost per aircraft
PIOE	percent change in IOE
PLBM	payload capacity weight
PLMAX	maximum payload
PROPI	propulsion installation cost
PROPP	propulsion procurement cost
PROT	total cost of propellant

TABLE 26-4. Continued

NOMENCLATURE FOR COST MODEL

PS	prototype spares cost
PT	production tooling cost
PV	prototype vehicles cost
QC	quality control cost
QINS	insurance cost
RA	airframe residual value
RAV	avionics residual value
RCON	insurance rate
RE	engine residual value
RPRO	propellant residual value
SE	support equipment design cost
SEATS	total number of seats
SEC	sustaining engineering cost
SI	systems integration cost
ST	sustaining tooling cost
T	sea-level static thrust
T7	total flight time (including taxis time)
TA	airframe depreciation period
TAV	avionics depreciation period
TAXI	rate of taxi fuel (lb/hr)
TCMI	cost per cargo mile
TD	number of operational hours per day
TDO	production vehicle data cost
TDP	supporting technical data cost

TABLE 26-4. Continued

NOMENCLATURE FOR COST MODEL

TE	engines depreciation period
TEND	number of cabin attendants
TF1	time to fly given distance with wind factor
TFTD	total flight time per day
TFU	time to fly given distance
TL	scheduling loss in hours
TOC	total operating cost
TOPER	total operating time in hours
TON	pounds per ton
TPBH	cost per passenger block hour
TPMI	cost per passenger mile
TPRO	propellant depreciation period
TSC	total system cost
TSLE	sea-level thrust per engine
TST	tooling and special test equipment cost
TT	minimum turnaround time
TVL	total vehicle life
TWOP	percentage of flight fuel for reserve
U	utilization factor
VM	vehicle maintenance cost
WAV	weight of avionics equipment
WE	vehicle empty weight
WEN	engine weight
WG	gross stage weight

TABLE 26-4. Concluded

NOMENCLATURE FOR COST MODEL

WGROSS	maximum gross take-off weight
WIND	wind factor
WLAND	aircraft weight for airport fees
WMSUB	weight of miscellaneous subsystems
WPART	weight of cargo
WPASS	passenger weight
WST	structure weight

TABLE 26-5

COST BREAKDOWN IN DOLLARS FOR EACH PRIMARY STRUCTURE AT EACH LEVEL OF RELIABILITY

Structure concept	Level of reliability	Vehicle weight, lb	Vehicle length, ft	Wing unit weight, lb/ft^2	Payload, lb	Fleet size, no. veh.	Cost per vehicle, millions
Semimonocoque spanwise beaded	Low	923 970	427	7.126	95 942	115	45.390
	Nominal	882 621	418	7.454	85 068	129	43.81[illegible]
	High	836 824	407	7.784	74 056	149	42.036
Semimonocoque spanwise tubular	Low	874 287	416	7.497	83 324	132	43.330
	Nominal	840 670	408	7.716	75 618	145	42.0[illegible]
	High	791 110	395	7.924	66 349	166	40.097
Monocoque honeycomb-core	Low	842 818	408	7.598	77.478	142	44.108
	Nominal	835 241	406	7.748	74.179	148	43.812
	High	799 753	398	7.841	68 388	161	42.368
Statically determinate spanwise beaded	Low	836 318	407	7.897[b]	71 933	153	43.603
	Nominal	797 493	397	8.186	62 906	175	41.997
	High	762 021	388	8.462	55 322	199	40.493
Semimonocoque chordwise tubular	Low	799 766	398	7.898	65 283	168	40.615
	Nominal	726 862	379	8.251	51 669	213	37.665
	High	709 737	375	8.596	45 085	244	36.827
Monocoque waffle	Low	599 236	344	9.809	20 903	526	34.475
	Nominal	562 904	334	10.432	10 748	1023	31.440
	High	529 254	323	10.888	3 323	3310	27.183

Structure concept	Cost oper vehicles, billions	Initial investment[a], billions	DOC, billions	IOC, billions	Total operational cost, billions	Total system-cost, billions	Relative total-system-cost
Semimonocoque spanwise beaded	5.204	8.689	43.327	16.625	59.952	68.641	
	5.666	9.354	46.821	18.567	65.388	74.742	1.00
	6.244	10.186	51.175	21.094	72.270	82.455	
Semimonocoque spanwise tubular	5.720	9.430	47.351	18.917	66.268	75.698	
	6.113	9.994	50.301	20.678	70.979	80.973	1.083
	6.648	10.757	54.028	23.435	77.463	88.219	
Monocoque honeycomb-core	6.262	10.214	49.606	20.194	69.800	80.015	
	6.497	10.558	51.381	21.053	72.434	82.993	1.110
	6.815	11.008	53.528	22.641	76.169	87.178	
Statically determinate spanwise beaded	6.668	10.816	53.004	21.717	74.721	85.538	
	7.344	11.796	57.984	24.600	82.584	94.380	1.263
	8.051	12.822	63.194	27.731	90.925	103.747	
Semimonocoque chordwise tubular	6.843	11.052	56.012	23.734	79.746	90.798	
	8.019	12.747	64.748	29.454	94.202	106.949	1.431
	8.985	14.167	72.536	33.612	106.148	120.315	
Monocoque waffle	18.142	27.599	134.453	70.450	204.903	232.501	
	32.177	48.247	245.120	135.739	380.859	429.106	5.741
	89.973	133.278	737.475	435.156	1,172.630	1,305.908	

[a]Includes spares.
[b]Includes weight of fuselage body penalty.

TABLE 26-6

COST BREAKDOW[illegible]NTS PER TON-MILE FOR EACH PRIMARY STRUCTURE
[illegible] EACH LEVEL OF REL[illegible]ABILITY

Structure concept	Level of reliability	Vehicle weight, lb	Vehicle length, ft.	Wing unit weight, lb/ft2	Payload, lb	Fleet size, no. veh.	Cost oper vehicles, cents/ton mi
Semimonocoque spanwise beaded	Low	923 970	427	7.126	95 942	115	2.533
	Nominal	882 621	418	7.454	85 068	129	2.75[illegible]
	High	836 824	407	7.784	74 056	149	3.039
Semimonocoque spanwise tubular	Low	874 287	416	7.497	83 324	132	2.784
	Nominal	840 670	408	7.716	75 618	145	2.975
	High	791 110	395	7.924	66 349	166	3.236
Monocoque honeycomb-core	Low	842 818	408	7.598	77 478	142	3.048
	Nominal	835 241	406	7.748	74 179	148	3.162
	High	799 753	398	7.841	68 388	161	3.317
Statically determinate spanwise beaded	Low	836 318	407	7.897[b]	71 933	153	3.245
	Nominal	797 493	397	8.186	62 906	175	3.574
	High	762 021	388	8.462	55 322	199	3.918
Semimonocoque chordwise tubular	Low	799 766	398	7.898	65 283	168	3.331
	Nominal	726 862	379	8.251	51 669	213	3.903
	High	709 737	375	8.596	45 085	244	4.373
Monocoque waffle	Low	599 236	344	9.809	20 903	526	8.830
	Nominal	562 904	334	10.432	10 748	1023	15.661
	High	529 2[illegible]	323	10.888	3 323	3310	43.791

Structure concept	Initial investment[a] cents/ton-mi	DOC, cents/ ton-mi	IOC, cents/ ton-mi	Total operational cost, cents/ton-mi	Total-system-cost cents/ton-mi	Relative total-system-cost
Semimonocoque spanwise beaded	4.229	21.09	8.09	29.18	33.41	
	4.55[illegible]	22.79	9.03	31.82	36.38	1.00
	4.957	24.91	10.26	35.17	40.13	
Semimonocoque spanwise tubular	4.589	23.04	9.21	32.25	36.84	
	4.864	24.48	10.07	34.55	39.41	1.083
	5.235	26.29	11.41	37.70	42.94	
Monocoque honeycomb-core	4.971	24.14	9.83	33.97	38.94	
	5.138	25.00	10.25	35.25	40.39	1.110
	5.356	26.05	11.02	37.07	42.43	
Statically determinate spanwise beaded	5.264	25.80	10.57	36.37	41.63	
	5.741	28.22	11.97	40.19	45.93	1.263
	6.240	30.75	13.50	44.25	50.49	
Semimonocoque chordwise tubular	5.379	27.26	11.55	38.81	44.19	
	6.204	31.51	14.34	45.85	52.05	1.431
	6.895	35.30	16.36	51.66	58.56	
Monocoque waffle	13.432	65.44	34.28	99.72	113.16	
	23.482	119.30	66.06	185.36	208.84	5.741
	62.866	358.92	211.79	570.71	635.58	

[a]Includes spares.
[b]Includes weight of fuselage body penalty.

TABLE 26-7

GROUP WEIGHT STATEMENT OF SIZED VEHICLES (550 000 LB)

Structure Concept	45° x 45° Waffle	Honeycomb	Tubular	Beaded	Tubular/ convex beaded	Statically determinate
Stiffening Direction	Monocoque	Monocoque	Spanwise	Spanwise	Chordwise	Spanwise
Aerodynamic surfaces	111 397	73 411	72 969	69 570	81 674	75 271
Wing	104 405	66 420	65 978	62 576	74 683	68 280
Body group	62 474	62 471	62 470	62 496	62 467	66 165
Pressurized compartments	2 000	2 000	2 000	2 000	2 000	2 000
Nonpressurized areas	60 474	60 471	60 470	60 496	60 467	64 165
Body thermal protection	18 558	18 557	18 557	18 563	18 556	18 557
Landing gears	16 501	16 500	16 500	16 506	16 499	16 501
Main Propulsion	82 494	82 492	82 491	82 507	82 490	82 493
Orientation control village	7 240	7 240	7 240	7 242	7 240	7 240
Power conversion and distrib.	6 350	6 350	6 350	6 352	6 350	6 350
Guidance and navigation	1 060	1 060	1 060	1 060	1 060	1 060
Instrumentation	1 100	1 100	1 100	1 100	1 100	1 100
Communication	240	240	240	240	240	240
Environmental Control System	1 730	1 730	1 730	1 730	1 730	1 730
Personnel provisions	2 450	2 450	2 450	2 450	2 450	2 450
Crew station controls & panels	200	200	200	200	200	200
Design reserve	6 236	5 476	5 467	5 400	5 641	5 587
Empty weight	318 030	279 278	278 824	275 417	287 696	284 944
Crew	660	660	660	660	660	660
Payload	10 571	49 064	49 689	53 208	39 081	43 379
Dry weight	329 261	329 002	329 173	329 285	327 437	328 984
Residuals, reserve, inflight losses, loiter, taxi, and run-up fuel	30 912	30 920	30 912	30 924	30 993	30 924
Performance propellant	189 869	190 085	189 913	189 989	191 548	190 115
Maximum Gross Weight	550 041	550 008	549 999	550 198	549 979	550 023

TABLE 26-8

BASELINE AIRPLANE MASS FRACTIONS
(GTOW = 550 000 LB)

Component	Initial Valves	Monocoque		Semimonocoque			Statically Determinate
		Waffle	Honeycomb	Tubular	Beaded	Chordwise	
Fuel[a]	0.40	0.40	0.40	0.40	0.40	0.40	0.40
Structure	0.27	0.35	0.28	0.28	0.27	0.30	0.31
Landing Gear	0.03	0.03	0.03	0.03	0.03	0.03	0.03
Propulsion	0.15	0.15	0.15	0.15	0.15	0.15	0.15
Equipment[b]	0.05	0.05	0.05	0.05	0.05	0.05	0.05
Payload	0.10	0.02	0.09	0.09	0.10	0.07	0.06

[a]Includes residuals, reserve, inflight losses, loiter, taxi, run-up, and performance propellant

[b]Includes equipment, crew, and design reserve

TABLE 26-9

GEOMETRY AND DESIGN PARAMETERS FOR BASELINE VEHICLES (550 000 LB)

Structure Concept	$45^\circ \times 45^\circ$ Waffle	Honeycomb	Tubular	Beaded	Tubular convex beaded	Statically Determinate
Stiffening Direction	Monocoque	Monocoque	Spanwise	Spanwise	Chordwise	Spanwise
Areas (sq ft)						
Wing reference	8 237.4	8 237.0	8 336.9	8 239.8	8 236.6	8 237.2
Wing actual	10 099	10 099	10 098	10 102	10 098	10 099
Body Wetted	16 437	16 437	16 436	16 442	16 436	16 437
Dimensions (ft)						
Wing span	102.8	102.8	102.8	102.8	102.8	102.8
Body length	329.8	329.8	329.8	329.9	329.9	329.9
Body width (max)	20.0	20.0	20.0	20.0	20.0	20.0
Volumes (cu ft)						
Fuel tank	52 069.1	52 122.3	52 079.8	52 100.4	52 484.6	52 130.1
Total body	72 158.9	72 154.1	72 152.3	72 191.4	72 148.4	72 157
Ratios						
Thrust to weight	0.510	0.510	0.510	0.510	0.510	0.510
Zero fuel wt over gross wt	0.6006	0.6002	0.6005	0.6005	0.5974	0.6001
CWING	0.012981	0.008236	0.008181	0.007752	0.009269	0.008468
RHOPAY	2.39092	11.253961	11.283883	12.047936	9.847397	9.962831
CMR	0.399398	0.399824	0.399504	0.399518	0.402624	0.399873
Nominal wing unit wt (psf)	10.338	6.577	6.534	6.194	7.396	6.761

[a]Fuselage penalty included

TABLE 26-10

COST RESULTS FOR BASELINE VEHICLE ($ MILLIONS)(550 000 LB)

Structure Concept	Cost Code	45° x 45° Waffle	Honeycomb	Tubular	Beaded	Tubular/ convex beaded	Statically Determinate
Stiffening Direction		Monocoque	Monocoque	Spanwise	Spanwise	Chordwise	Spanwise
No. of operational vehicles	NV	1 041	224	221	207	281	254
Fuselage	FUSL	0.6056	0.9841	0.9880	1.0096	0.9163	0.9875
Fins	FINL	0.1142	0.1872	0.1880	0.1922	0.1740	0.1799
Wing	WINGL	0.4775	0.6047	0.4739	0.4666	0.5886	0.6866
Inlet	INLL	1.0449	1.7129	1.7199	1.7582	1.5919	1.6463
Airframe labor	AL	2.2422	3.4890	3.3698	3.4267	3.2708	3.5003
Fuselage	FUSM	2.4007	2.6659	2.6681	2.6806	1.4224	2.7579
Fins	FINM	0.5268	0.5902	0.5907	0.5939	1.1400	0.5848
Wing	WINGM	6.9264	3.8973	3.0643	2.9964	3.4959	3.8191
Inlet	INLM	8.6856	9.7305	9.7396	9.7890	9.5680	9.6422
Airframe material	AM	18.5395	16.8839	16.0627	16.0599	16.2704	16.8040
Landing gear	LG	0.2897	0.3264	0.3267	0.3286	0.3206	0.3232
Miscellaneous subsystems	MS	3.4951	4.0156	4.0203	4.0474	3.9313	3.9698
Quality control	QC	3.4393	3.4601	3.3291	3.3408	3.3310	3.4436
Structure, final assy	FA	0.1316	0.1778	0.1780	0.1786	0.1729	0.1762
Airframe manufacturing	AMFG	28.1373	28.3526	27.2867	27.3818	27.2970	28.2172
Avionics	AV	1.2532	1.4129	1.4143	1.4219	1.3878	1.3992
Propulsion	PROP	1.5214	2.4885	2.4986	2.5538	2.3141	2.3926
Flight vehicles	FV	30.9119	32.2540	31.1995	31.3575	30.998	32.0089
Operational vehicles	OV	32 167	7 232	6 907	6 483	8 725	8 117
Initial investment	IV	48 223	11 451	10 971	10 341	13 665	12 766
Total operational cost		381 631	82 650	81 277	75 960	103 691	93 410
Total system cost		429 853	94 101	92 248	86 301	117 356	106 176

TABLE 26-11

GROUP WEIGHT STATEMENT OF OPTIMUM-SIZED VEHICLES (MINIMUM TOTAL SYSTEM COST)

Structure concept	45° x 45° Waffle	Honeycomb	Tubular	Beaded	Tubular/ convex beaded	Statically determinate
Stiffening Direction	Monocoque	Monocoque	Spanwise	Spanwise	Chordwise	Spanwise
Aerodynamic surfaces	14 97[illegible]	129 433	129 783	132 026	119 351	124 659
Wing	107 818	118 817	119 097	120 807	110 112	114 523
Body group	64 167	102 146	102 941	109 130	86 574	102 010
Pressurized compartments	2 000	2 000	2 000	2 000	2 000	2 000
Non-pressurized areas	62 167	100 146	100 941	107 130	84 574	100 010
Body thermal protection	18 991	28 181	28 364	29 780	24 524	26 907
Landing gears	16 886	25 057	25 220	26 479	21 805	23 925
Main propulsion	83 520	105 277	105 710	109 061	96 619	102 261
Orientation control village	7 394	10 663	10 728	11 231	9 362	10 210
Power conversion and distrib.	6 466	8 917	8 966	9 344	7 942	8 577
Guidance and navigation	1 060	1 060	1 060	1 060	1 060	1 060
Instrumentation	1 100	1 100	1 100	1 100	1 100	1 100
Communication	240	240	240	240	240	240
Environmental control system	1 730	1 730	1 730	1 730	1 730	1 730
Personnel provisions	2 450	2 450	2 450	2 450	2 450	2 450
Crew station controls & panels	200	200	200	200	200	200
Design reserve	6 383	8 329	8 370	8 677	7 459	8 107
Empty weight	325 560	424 783	426 862	442 508	380 418	413 437
Crew	660	660	660	660	660	660
Payload	10 748	74 179	75 618	85 068	51 669	62 906
Dry weight	336 968	499 622	503 140	528 236	432 746	477 003
Residuals, reserve, inflight losses, loiter, taxi, and run-up fuel	31 633	46 957	47 263	49 609	40 961	44 837
Performance propellant	194 304	288 661	290 280	304 777	253 153	275 653
Maximum gross weight	562 904	835 241	840 670	882 621	726 862	797 493

TABLE 26-12

OPTIMUM-SIZE AIRPLANE MASS FRACTIONS
(GTOW = VARIABLE)

Component	Initial Valves	Monocoque Waffle	Monocoque Honeycomb	Semimonocoque Tubular	Semimonocoque Beaded	Semimonocoque Chordwise	Statically Determinate
Fuel [a]	0.40	0.40	0.40	0.40	0.40	0.40	0.40
Structure	0.27	0.35	0.31	0.31	0.31	0.32	0.32
Landing Gear	0.03	0.03	0.03	0.03	0.03	0.03	0.03
Propulsion	0.15	0.15	0.13	0.13	0.12	0.13	0.13
Equipment [b]	0.05	0.05	0.04	0.04	0.04	0.05	0.04
Payload	0.10	0.02	0.09	0.09	0.10	0.07	0.08

[a] Includes residuals, reserve, inflight losses, loiter, taxi, run-up, and performance propellant

[b] Includes equipment, crew, and design reserve

TABLE 26-13

GEOMETRY AND DESIGN PARAMETERS FOR OPTIMUM-SIZED VEHICLES (MINIMUM TOTAL SYSTEM COST)

Structure Concept	$45^\circ \times 45^\circ$ Waffle	Honeycomb	Tubular	Beaded	Tubular convex beaded	Statically Determinate
Stiffening Direction	Monocoque	Monocoque	Spanwise	Spanwise	Chordwise	Spanwise
Areas (sq ft)						
Wing reference	8 429.7	12 508.9	12 590.2	13 218.6	10 885.7	11 943.6
Wing actual	10 334.8	15 335.9	15 435.6	16 206.0	13 345.9	14 642.8
Body wetted	16 821.1	24 961	25 123	26 377	21 722	23 833
Dimensions						
Wing span	104.0	126.7	127.1	130.3	118.2	123.8
Body Length	333.7	406.4	407.7	417.7	379.1	397.1
Body width (max)	20.2	24.7	24.7	25.3	23.0	24.1
Volumes (cu ft)						
Fuel tank	53 285	79 153	79 603	83 579	69 364	75 585
Total body	74 701	135 028	136 347	146 679	109 619	125 979
Ratios						
Thrust to weight	0.510	0.510	0.510	0.510	0.510	0.510
Zero fuel wt over gross wt.	0.6007	0.6002	0.6005	0.6005	0.5974	0.6001
CWING	0.012981	0.008236	0.008181	0.007752	0.009269	0.008468
RHOPAY	1.992578	2.292857	2.286263	2.222923	2.625112	2.253939
CMR	0.399398	0.399824	0.399504	0.399518	0.402624	0.399873
Nominal wing unit wt (psf)	10.432	7.748	7.716	7.454	8.251	7.821

[a]Fuselage penalty included

TABLE 26-14

COST RESULTS FOR OPTIMUM-SIZED VEHICLES ($ MILLION) (MINIMUM TOTAL SYSTEM COST)

Structure Concept	Cost Code	$45^\circ \times 45^\circ$ Waffle	Honeycomb	Tubular	Beaded	Tubular convex beaded	Statically Determinate
Stiffened Direction		Monocoque	Monocoque	Spanwise	Spanwise	Chordwise	Spanwise
No. of operational vehicles	NV	1023	148	145	129	213	175
Fuselage	FUSL	0.6297	1.8020	1.8263	2.0045	1.3714	1.6887
Fins	FINL	0.1175	0.3248	0.3289	0.3587	0.2516	0.2941
Wing	WINGL	0.4958	1.2358	0.9794	1.0477	0.9495	1.2980
Inlet	INLL	1.0505	1.9568	1.9689	2.0450	1.7417	1.8556
Airframe labor	AL	2.2885	5.3193	5.1037	5.4559	4.3141	5.1364
Fuselage	FUSM	2.4662	4.4059	4.4446	4.7374	3.6678	4.3012
Fins	FINM	0.5398	0.9241	0.9314	0.9864	0.7829	0.8716
Wing	WINGM	7.1616	7.1884	5.7059	5.9892	5.2619	6.5842
Inlet	INLM	8.6963	10.0327	10.0470	10.1349	9.7678	9.9111
Airframe material	AM	18.8640	22.5510	21.1289	21.8479	19.4804	21.6681
Landing gear	LG	0.2968	0.5120	0.5161	0.5469	0.4331	0.4825
Miscellaneous subsystems	MS	3.5664	5.9295	5.9739	6.3030	5.0862	5.6089
Quality control	QC	3.5022	4.8037	4.5811	4.7815	4.1039	4.6054
Structure, final assy	FA	0.1361	0.3367	0.3406	0.3676	0.2654	0.3109
Airframe manufacturing	AMFG	28.6539	39.4522	37.6943	39.3028	33.6831	37.8123
Avionics	AV	1.2548	1.4599	1.4621	1.4758	1.4186	1.4409
Propulsion	PROP	1.5311	2.8996	2.9186	3.0391	2.5636	2.7439
Flight vehicles	FV	31.4398	43.8117	42.0249	43.8177	37.6653	41.9971
Operational vehicles	OV	32 177	6 497	6 113	5 666	8 019	7 344
Initial investment	IV	48 247	10 558	9 994	9 384	12 747	11 796
Total operational cost	TOC	380 859	72 434	70 979	65 388	94 202	82 584
Total system cost	TSC	429 106	82 993	80 973	74 742	106 949	94 380

TABLE 26-15

NIO SUMMARY – STRUCTURE CONCEPT DESIGN AND COST DATA
GROSS WEIGHT: 882.621 LB, WING AREA: 16,206 SQ

Structure Concept	Cwing	Wing Weight (lb)	Wing Weight (psf)	Fleet Size	Total System Cost (Dollars)
Semimonocoque Spanwise Beaded	0.007752	120 807	7.454	129	74.742×10^9
Semimonocoque Spanwise Tubular	0.008181	127 492	7.867	140	81.112
Monocoque Honeycomb Sandwich	0.008236	128 350	7.920	143	82.853
Statically Determinate Spanwise-Beaded	0.008468	131 965	8.143[(a)]	164	95.020
Semimonocoque Chordwise Convex-beaded/tubular	0.009269	144 523	8.918	189	109.505
Monocoque Waffle $45^\circ \times 45^\circ$	0.012981	202 295	12.483	–	–

[a]Statically determinate concept body penalty = 0.2245 (26,300) = 5,900 lb
W′= (131, 965) + (5,900)/(16,206) = 8.507 psf

TABLE 26-16

SUMMARY-WING WEIGHTS AND PERCENTAGES FOR INCREASE IN WING WEIGHT AND TOTAL SYSTEM COST

Structure Concept	Baseline Vehicle (GTOW = 550 000 lb)			Minimum System Cost Vehicle (GTOW = Variable)			Constant Weight Vehicles (GTOW = 882 621 lb)		
	Wing[a] Weight (psf)	Wing Wt Increase (%)	Cost Increase (%)	Wing[b] Weight (psf)	Wing Wt Increase (%)	Cost Increase (%)	Wing[c] Weight (psf)	Wing Wt Increase (%)	Cost Increase (%)
Semimonocoque Spanwise Beaded	6.19	0	0	7.45	0	0	7.45	0	0
Semimonocoque Spanwise Tubular	6.53	5.4	6.9	7.72	3.5	8.3	7.87	5.5	8.5
Monocoque Honeycomb Sandwich	6.58	6.1	9.0	7.75	3.9	11.0	7.92	6.2	10.8
Statically Determinate Beaded	6.76	9.1	23.0	7.82	4.9	26.3	8.14	10.9	27.1
Semimonocoque Chordwise Convex Beaded/Tubular	7.40	19.3	36.0	8.25	10.7	43.1	8.92	19.6	46.5
Monocoque Unflanged Waffle	10.34	66.8	497.1	10.43	39.9	474.1	12.48	67.4	–

$^a S_{WING} = 10{,}099\ ft^2$ $^b S_{WING}$ = Variable $^c S_{WING} = 16{,}206\ ft^2$

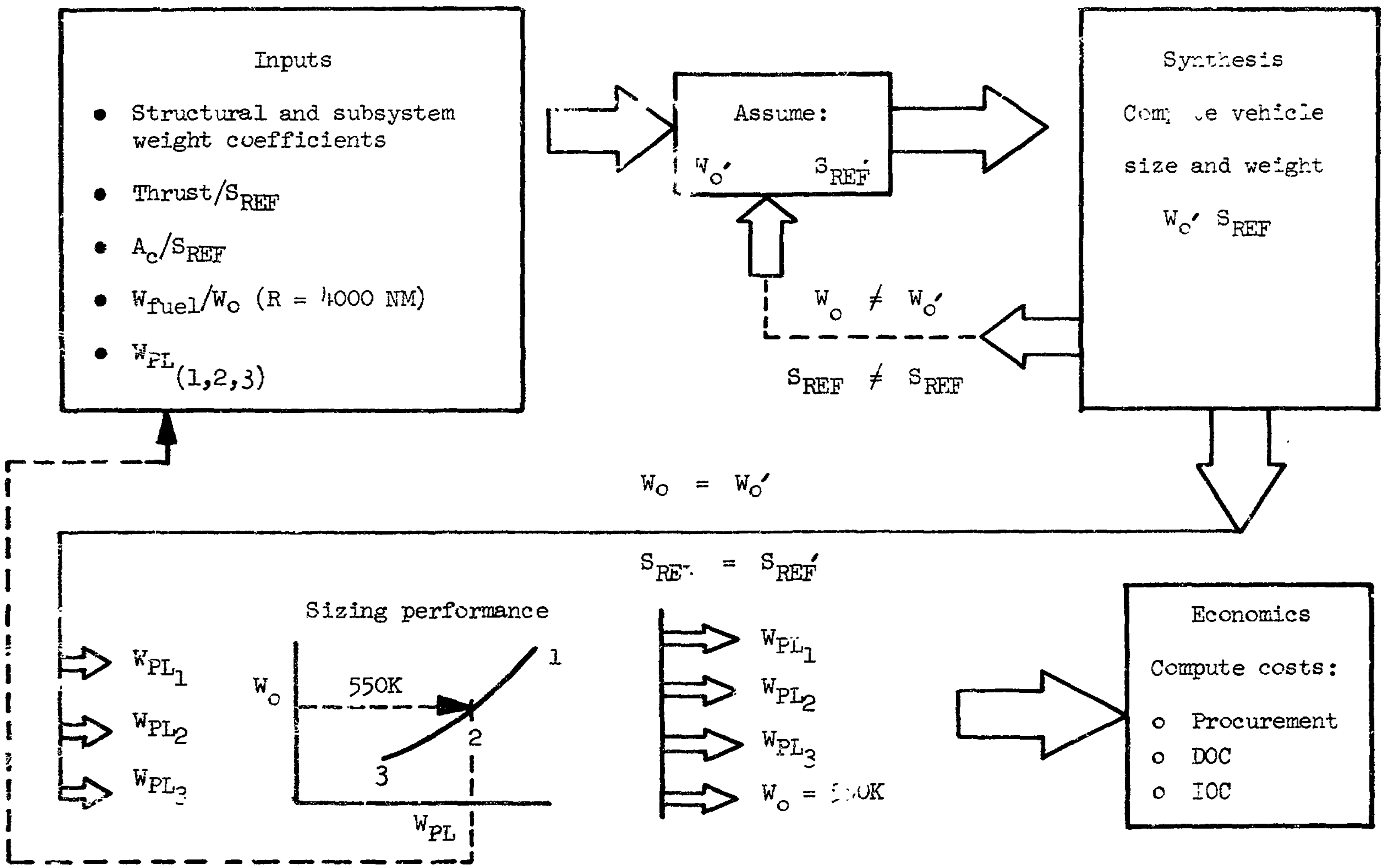

Figure 26-1. Interaction factor evaluation computer program

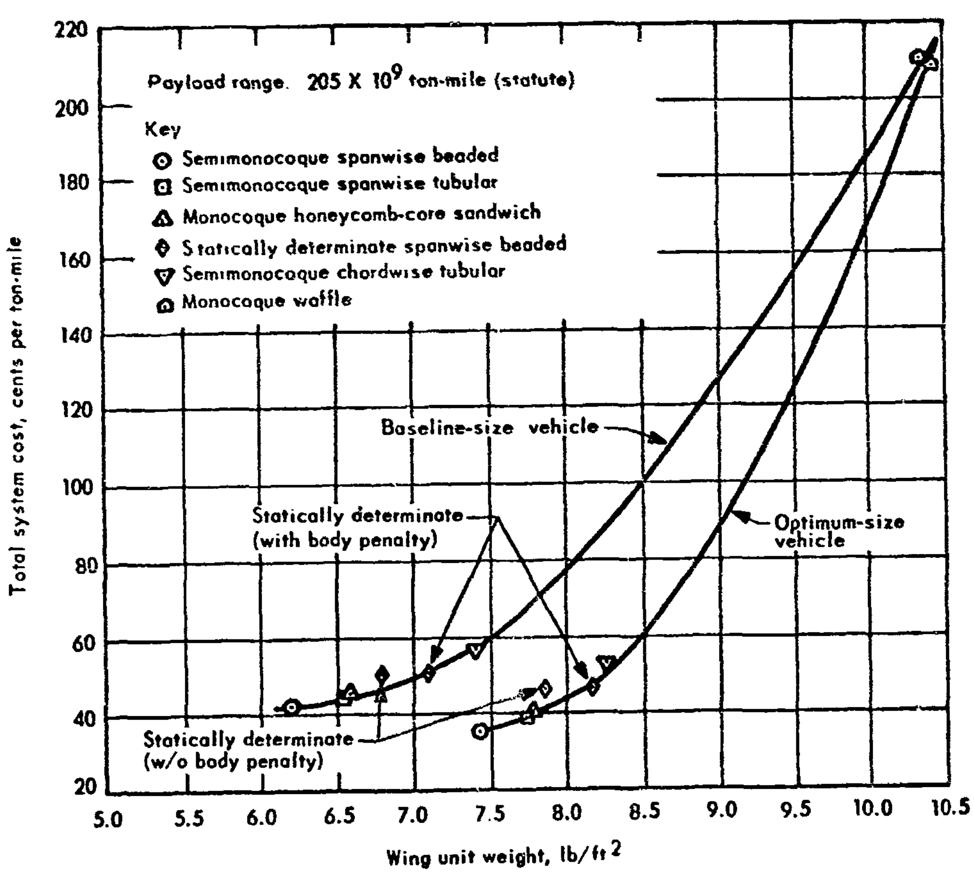

Figure 26-2. Total-system-cost for baseline and optimum-size vehicles of various wing constructions

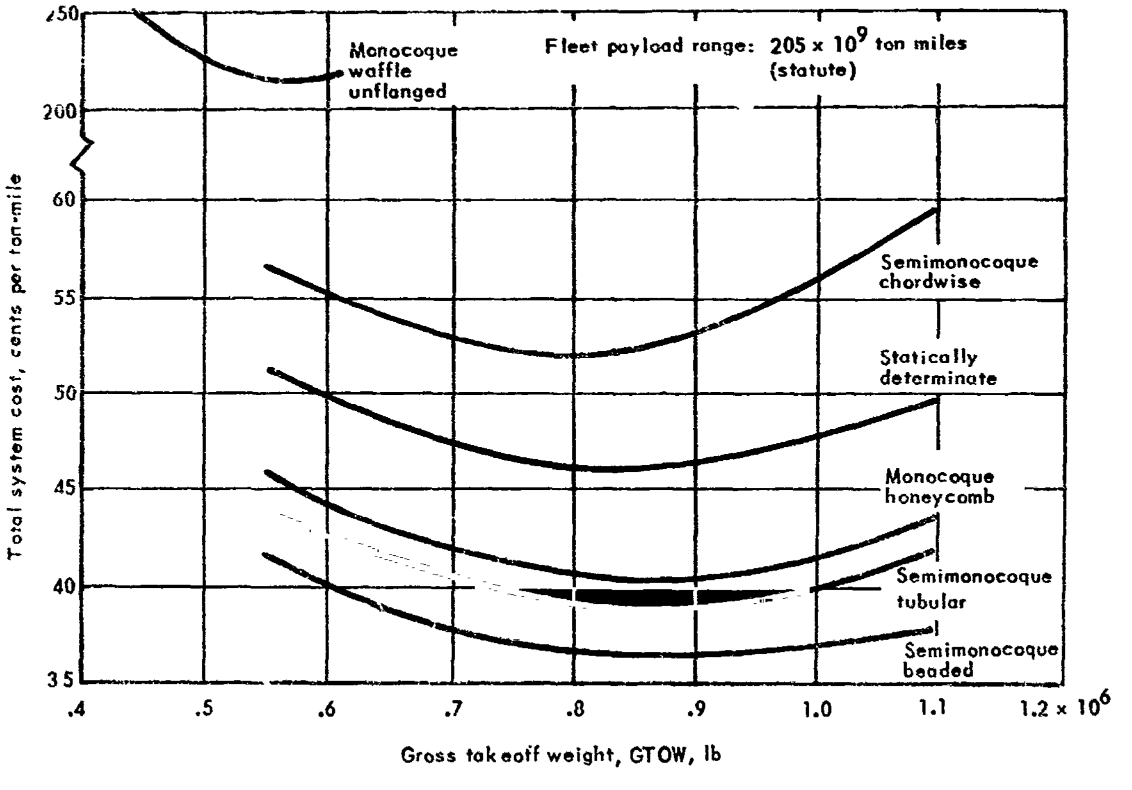

Figure 26-3. **Total system cost for various gross weight vehicles for the candidate wing constructions**

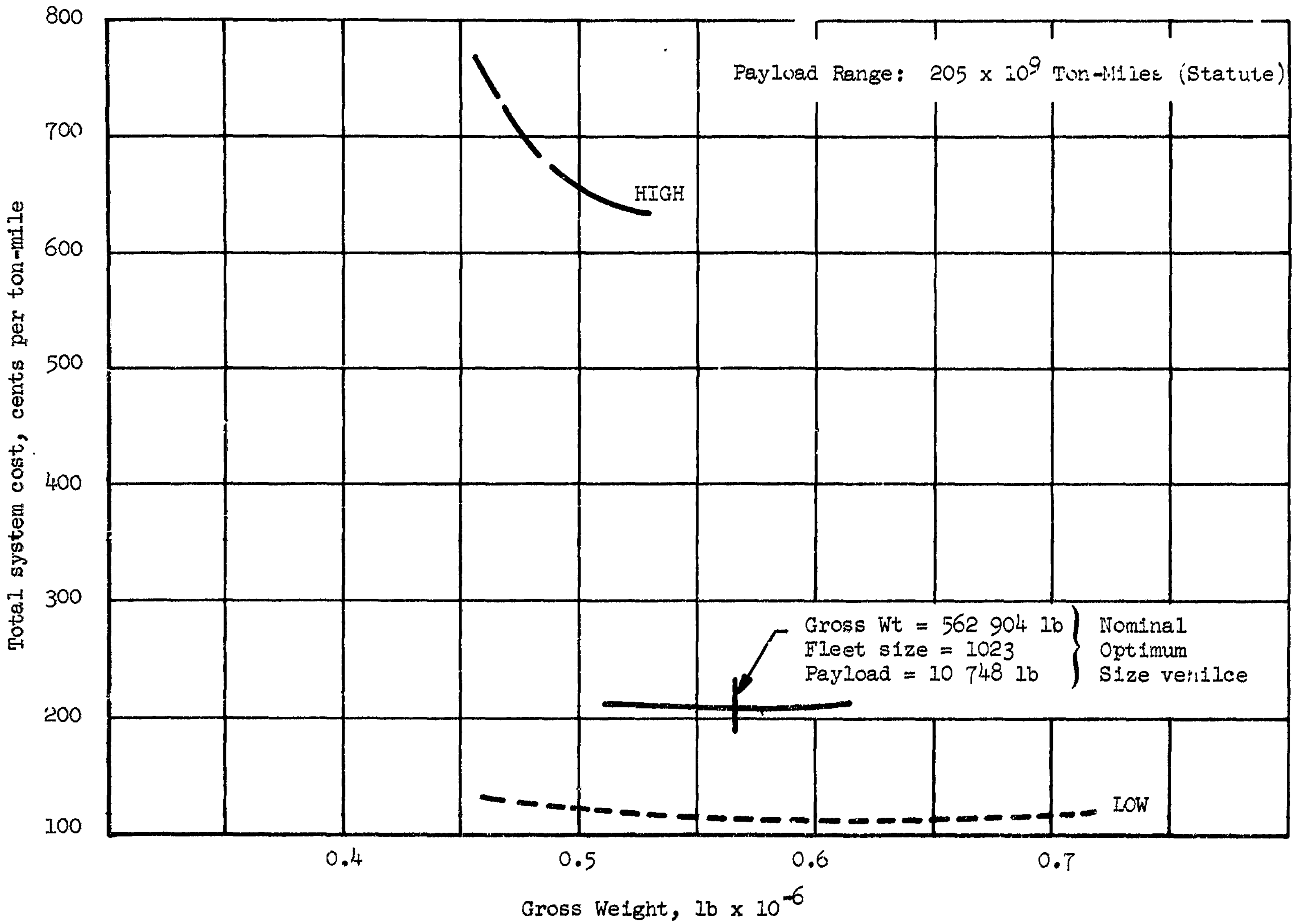

Figure 26-4. Total system cost variation with vehicle size - monocoque waffle concept

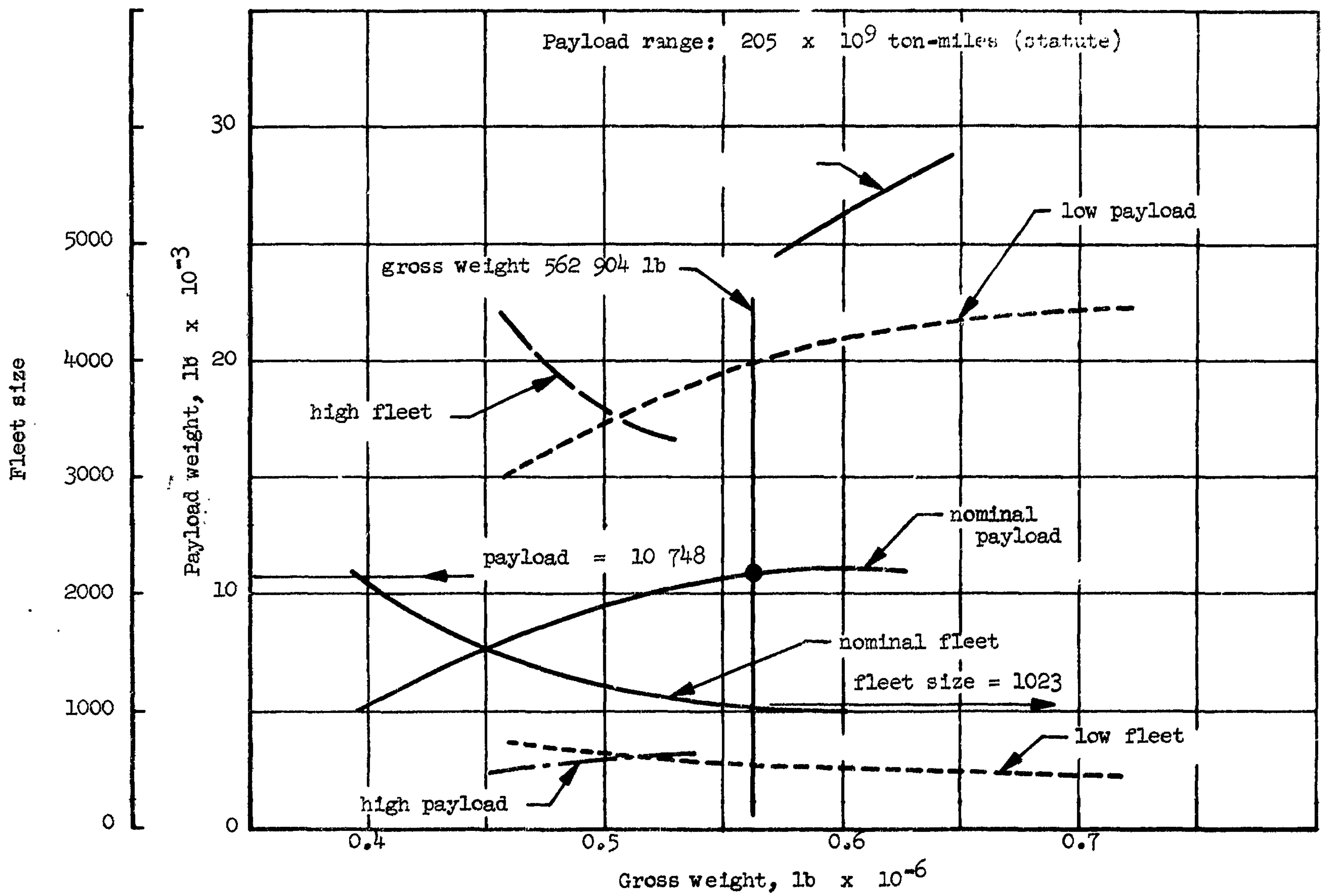

Figure 26-5. Payload and fleet size variation with vehicle size — monocoque waffle concept

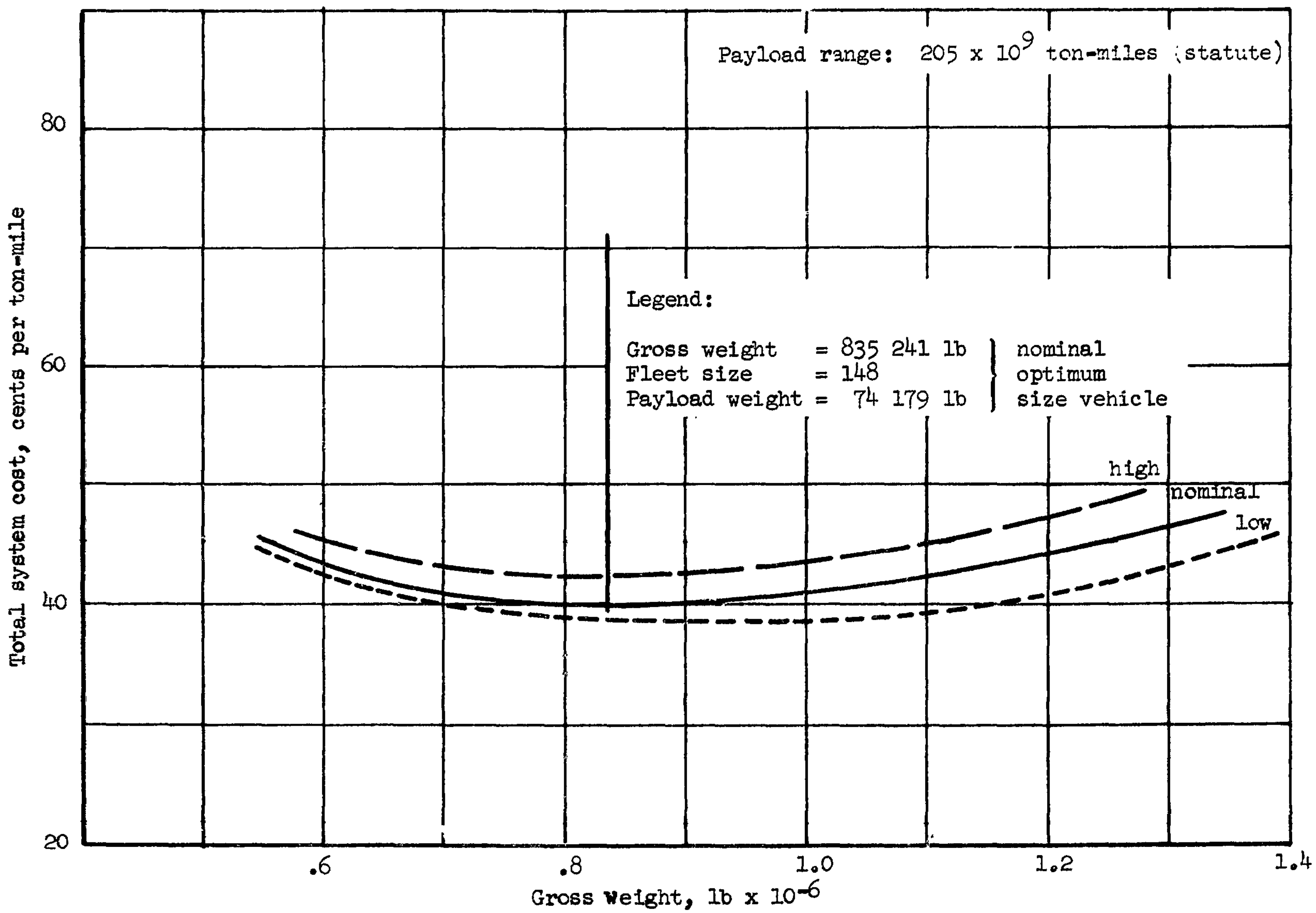

Figure 26-6. Total system cost variations with vehicle size - monocoque honeycomb sandwich concept

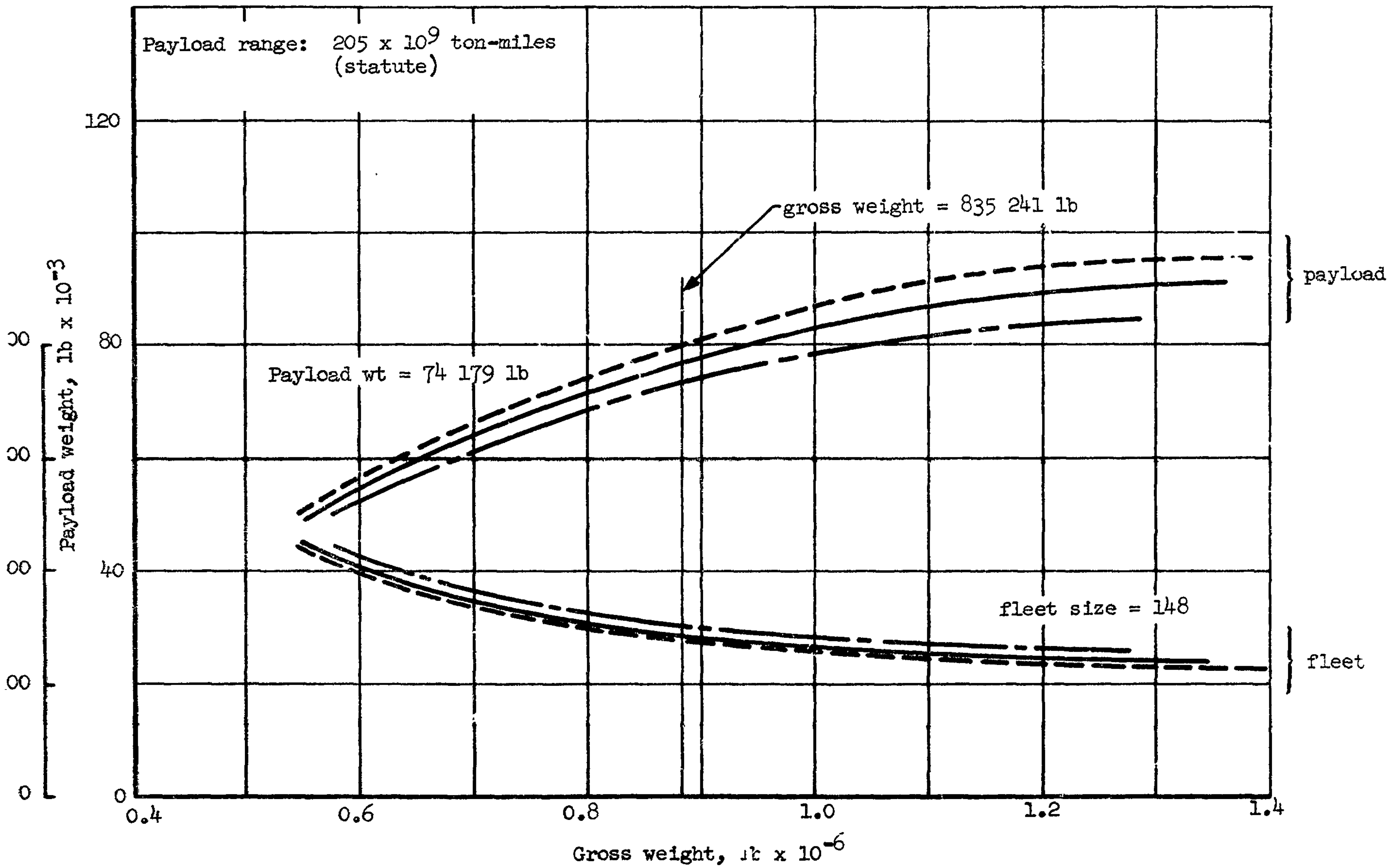

Figure 26-7. Payload and fleet size variation with vehicle size - monocoque honeycomb sandwich concept

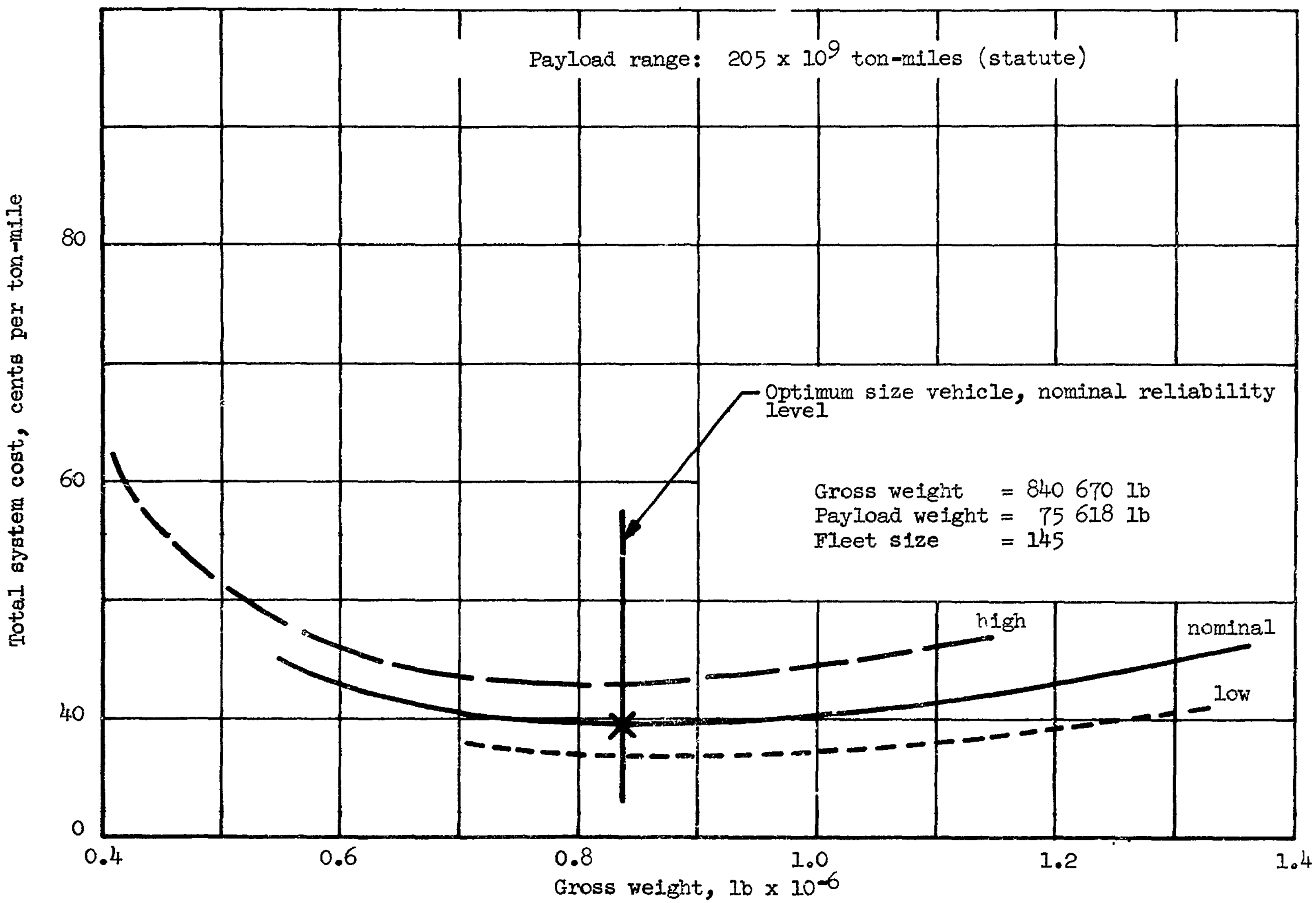

Figure 26-8. Total system cost variation with vehicle size - semimonocoque spanwise tubular concept

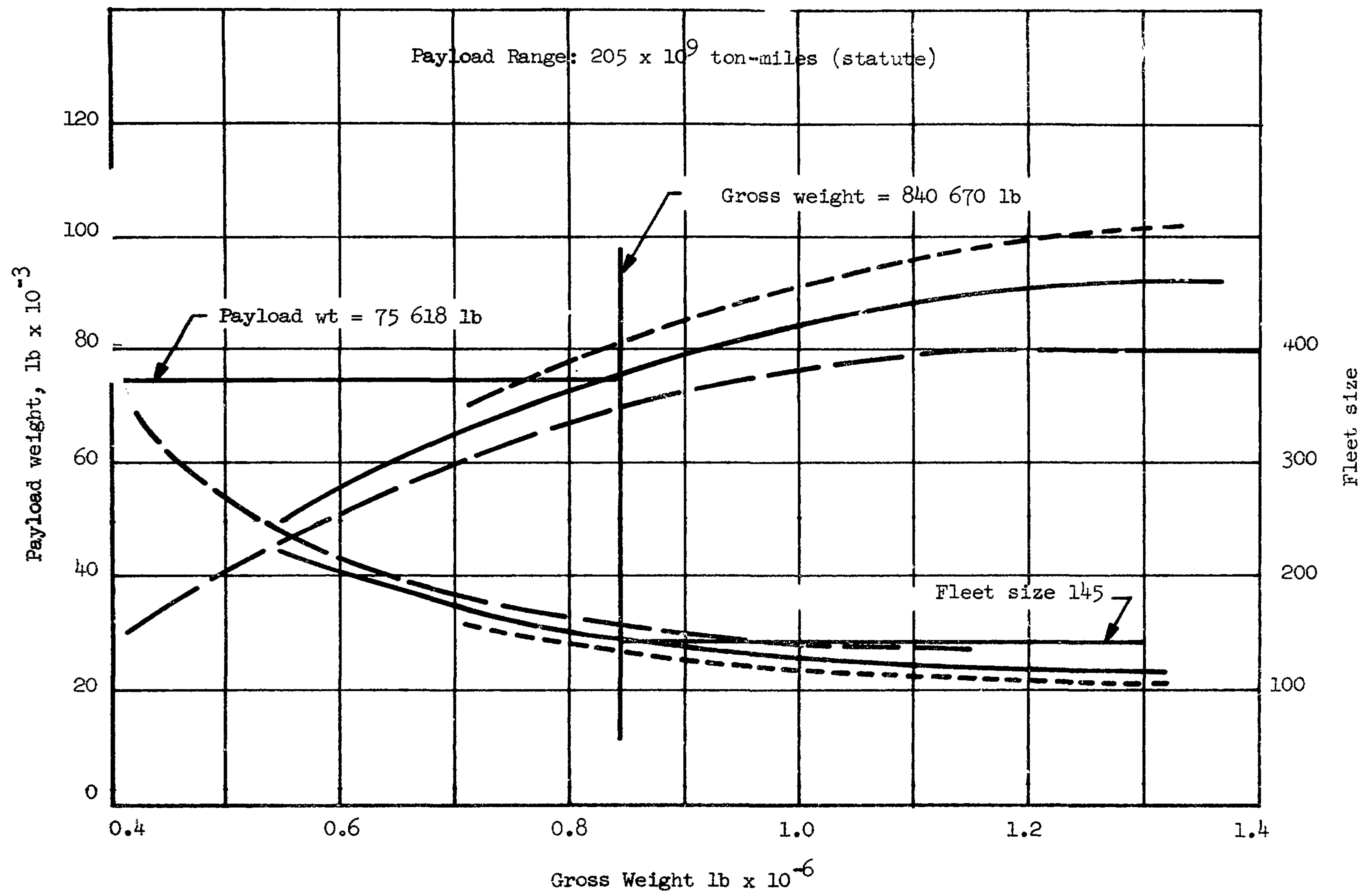

Figure 26-9. Payload and fleet size variation with vehicle size – semimonocoque spanwise tubular concept

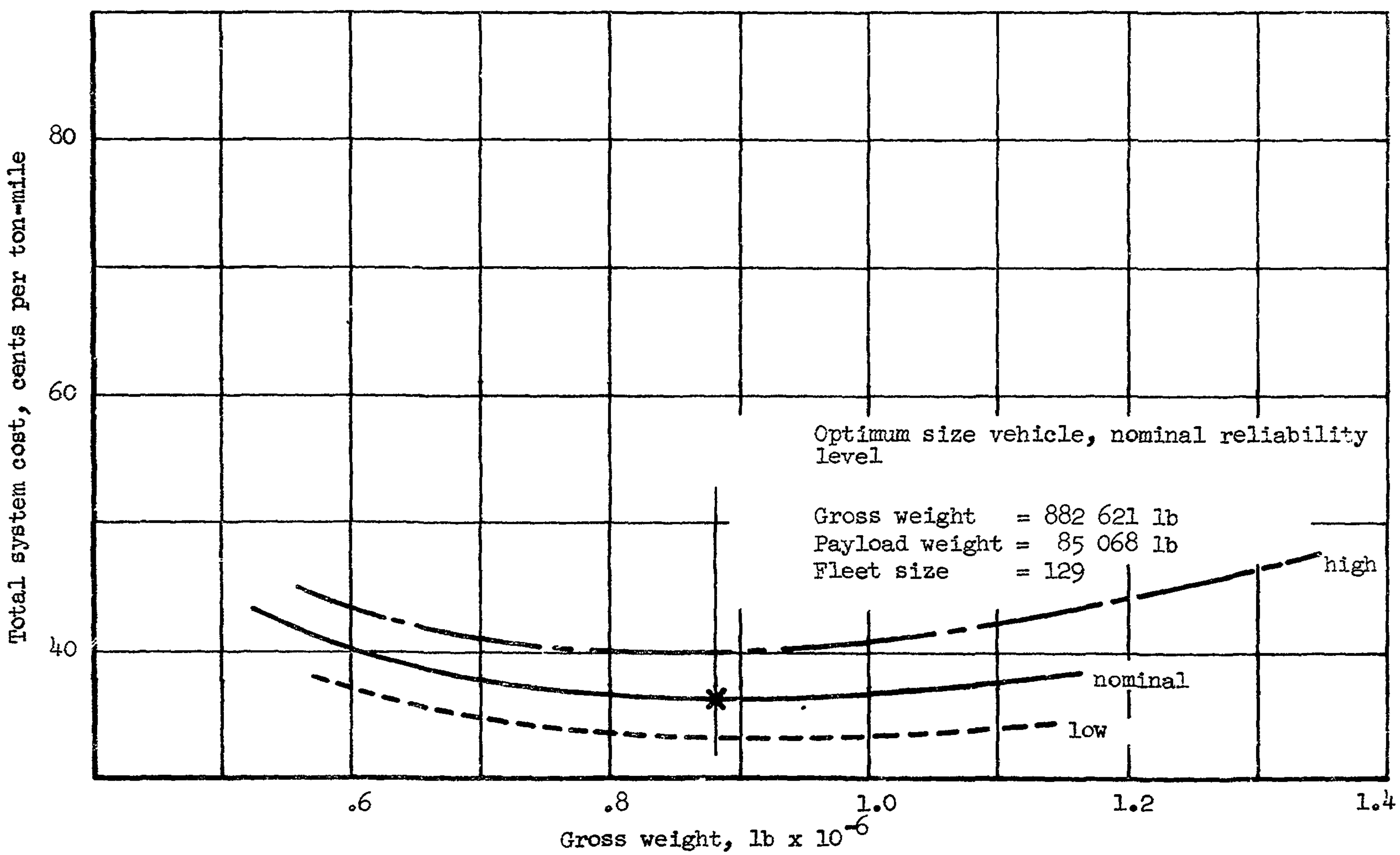

Figure 26-10. Total system cost variation with vehicle size - semimonocoque spanwise beaded concept

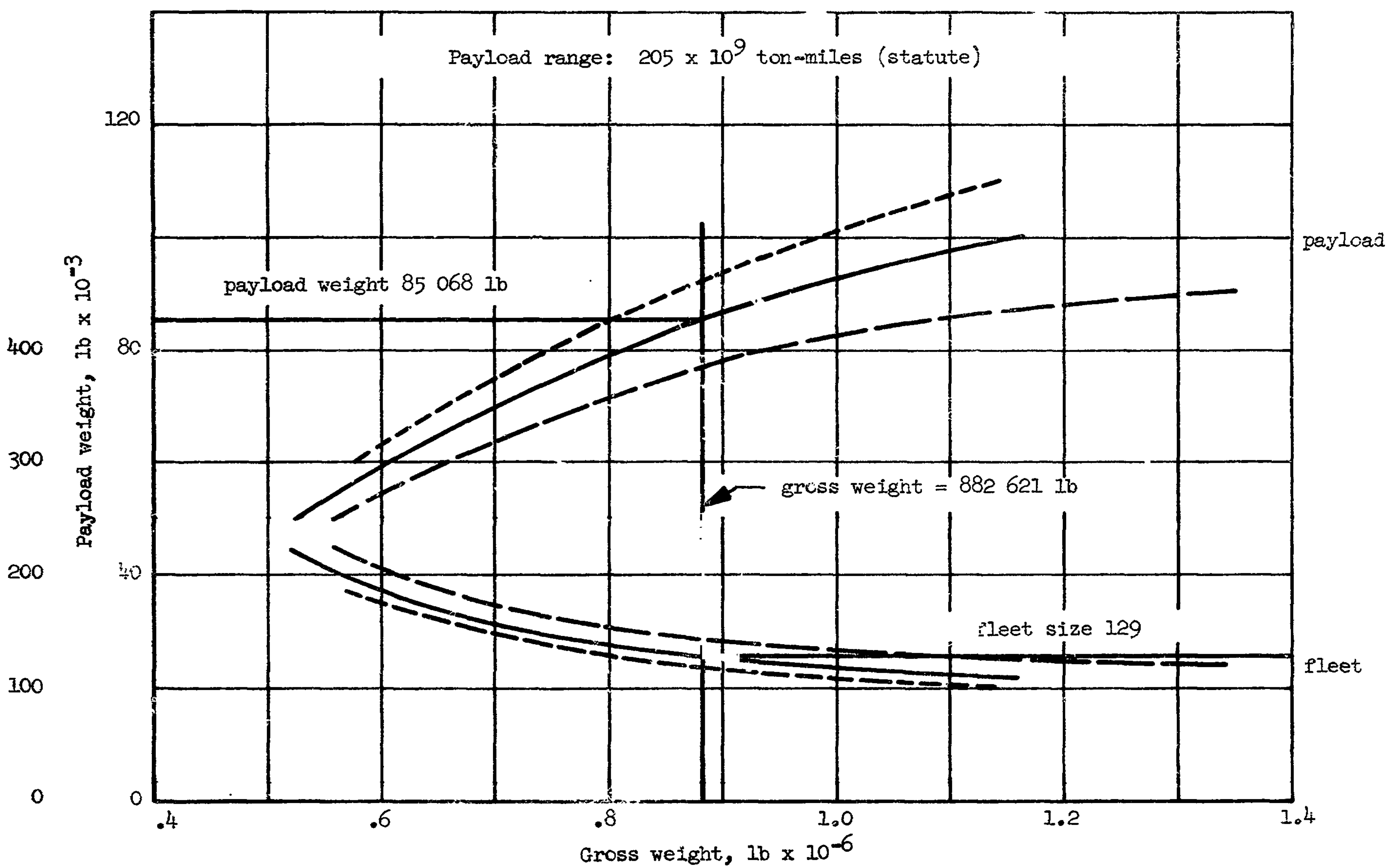

Figure 26-11. Payload and fleet size variation with vehicle size — semimonocoque spanwise beaded concept

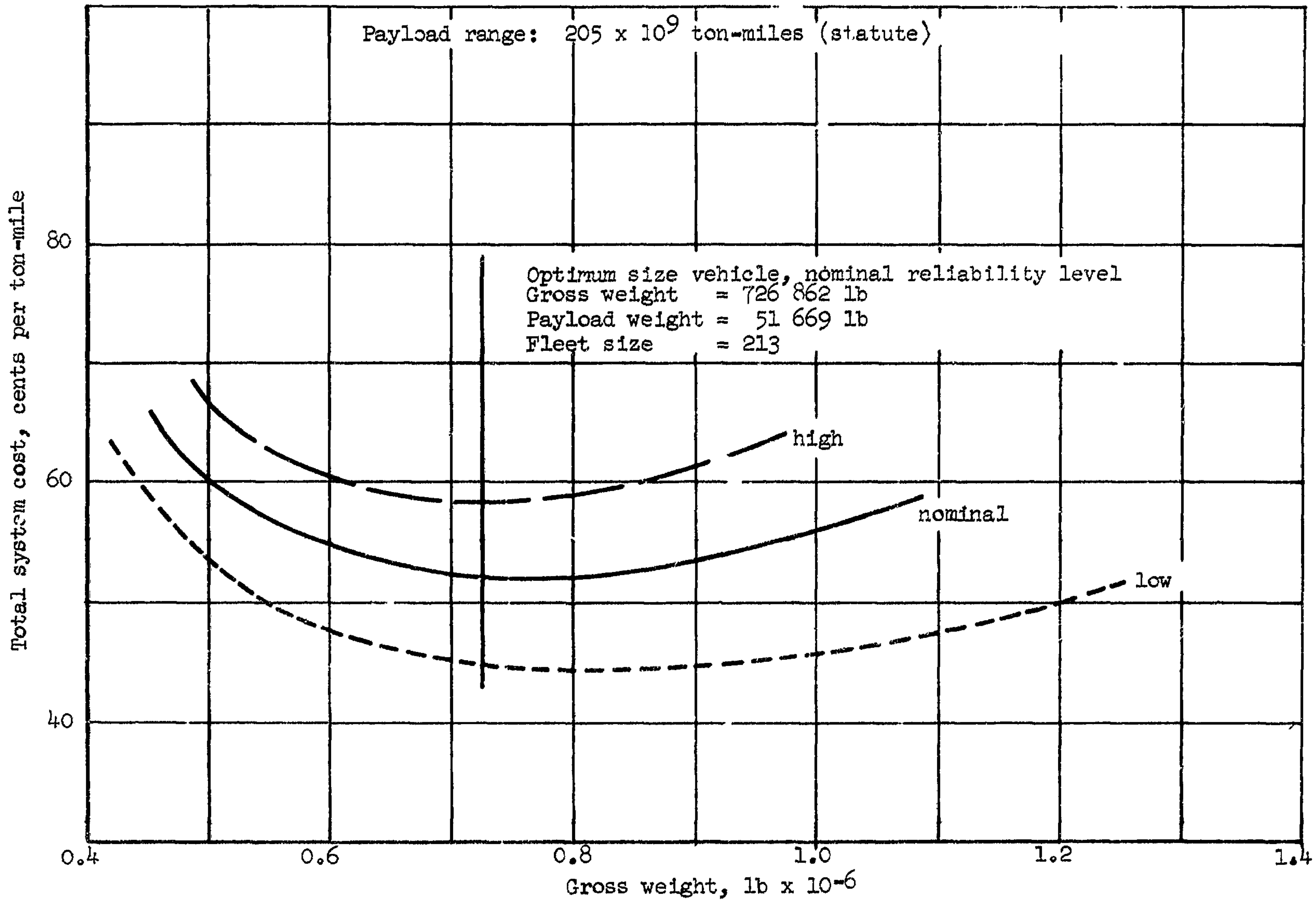

Figure 26-12. Total system cost variations with vehicle size — semimonocoque chordwise tubular concept

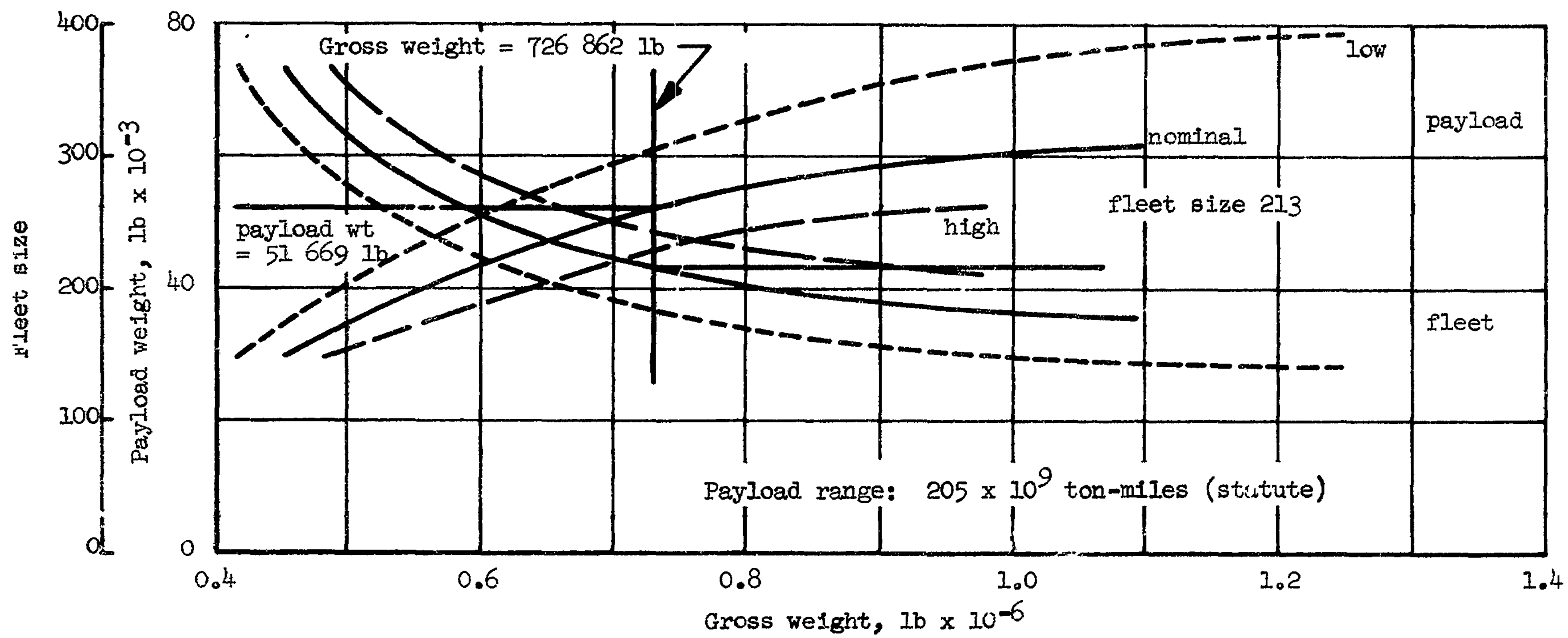

Figure 26-13. Payload and fleet size variations with vehicle size — semimonocoque chordwise tubular concept

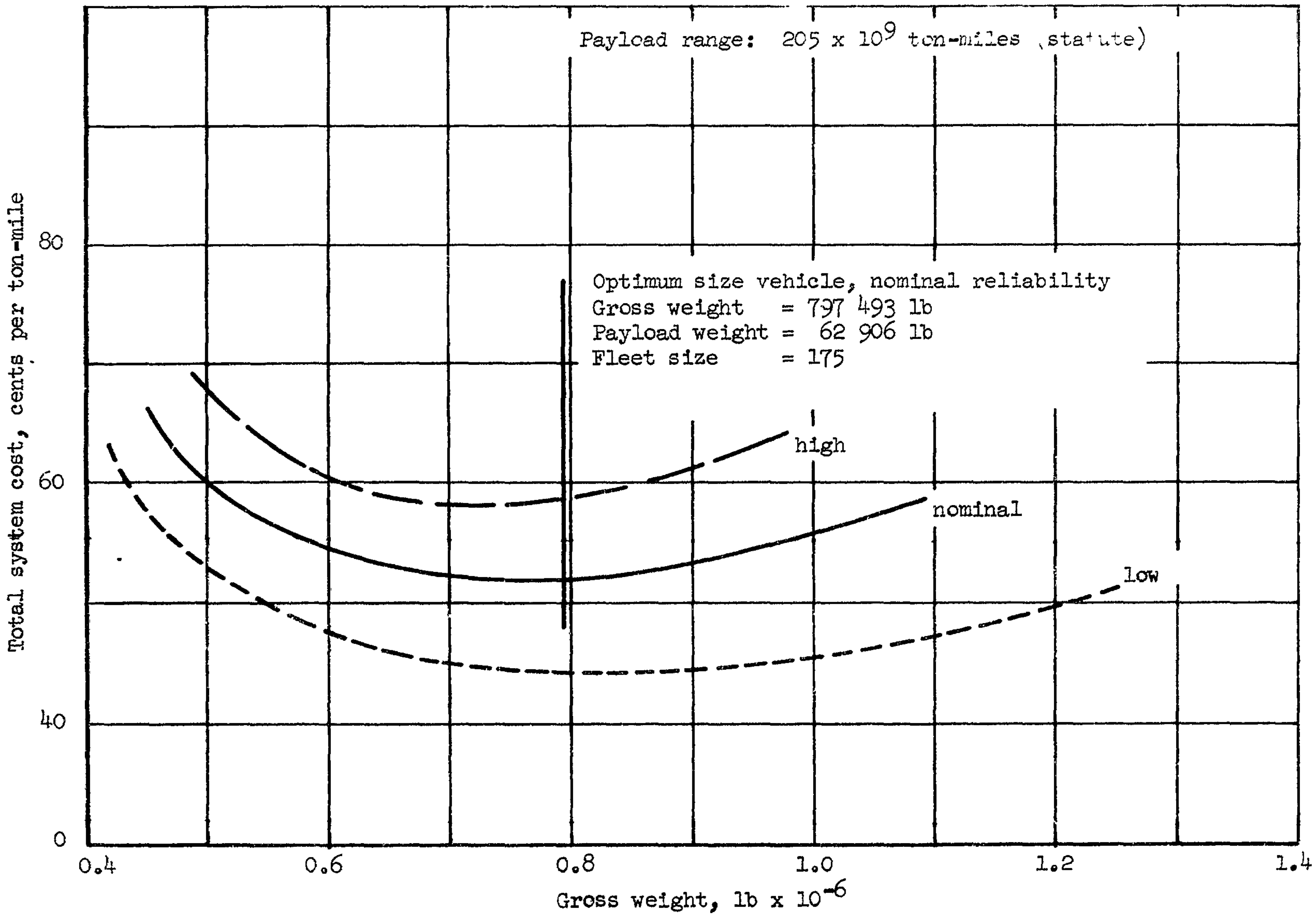

Figure 26-14. Total system cost variation with vehicle size – statically determinate beaded concept

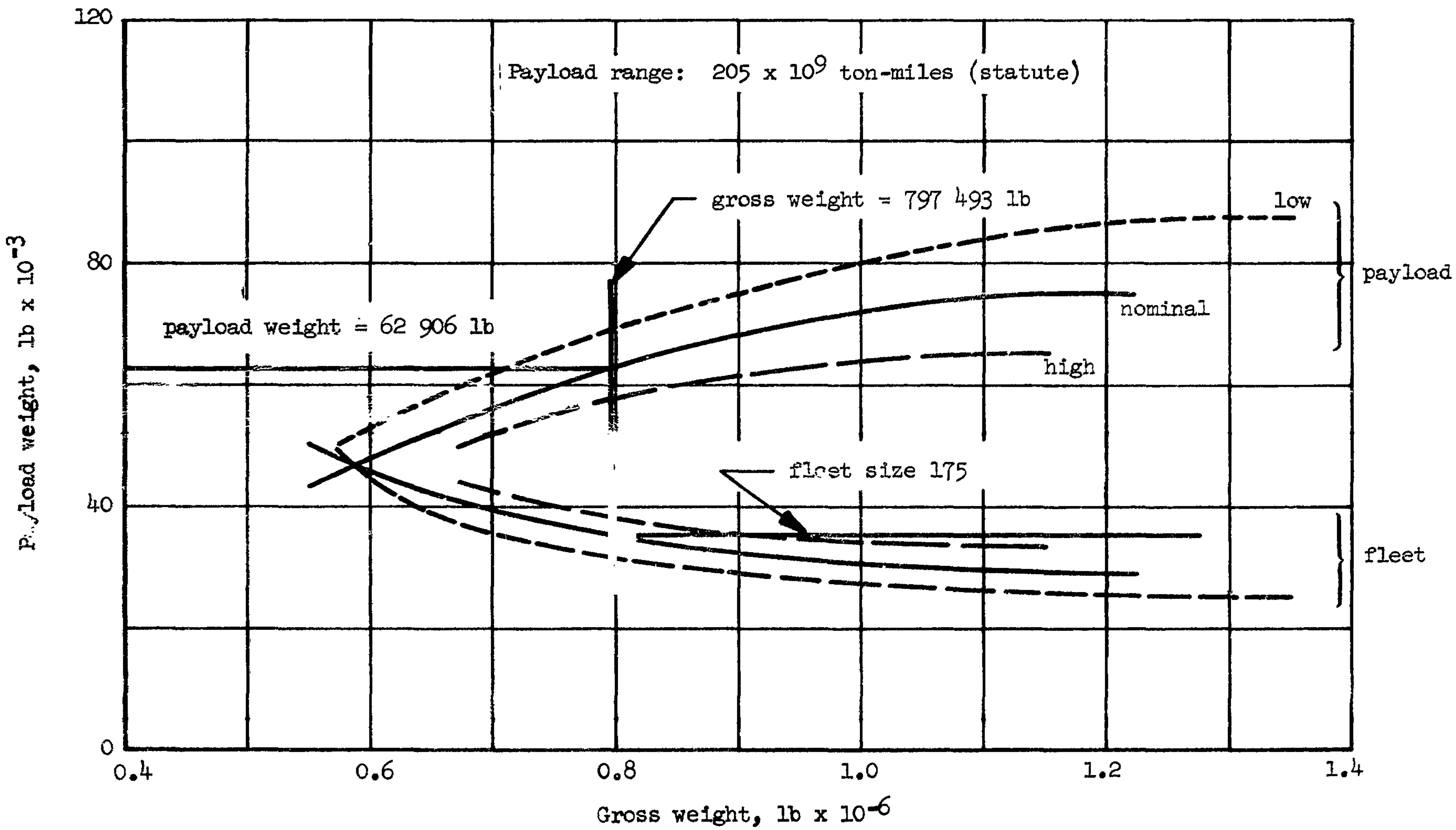

Figure 26-15. Payload and fleet size variation with vehicle size - statically determinate beaded concept

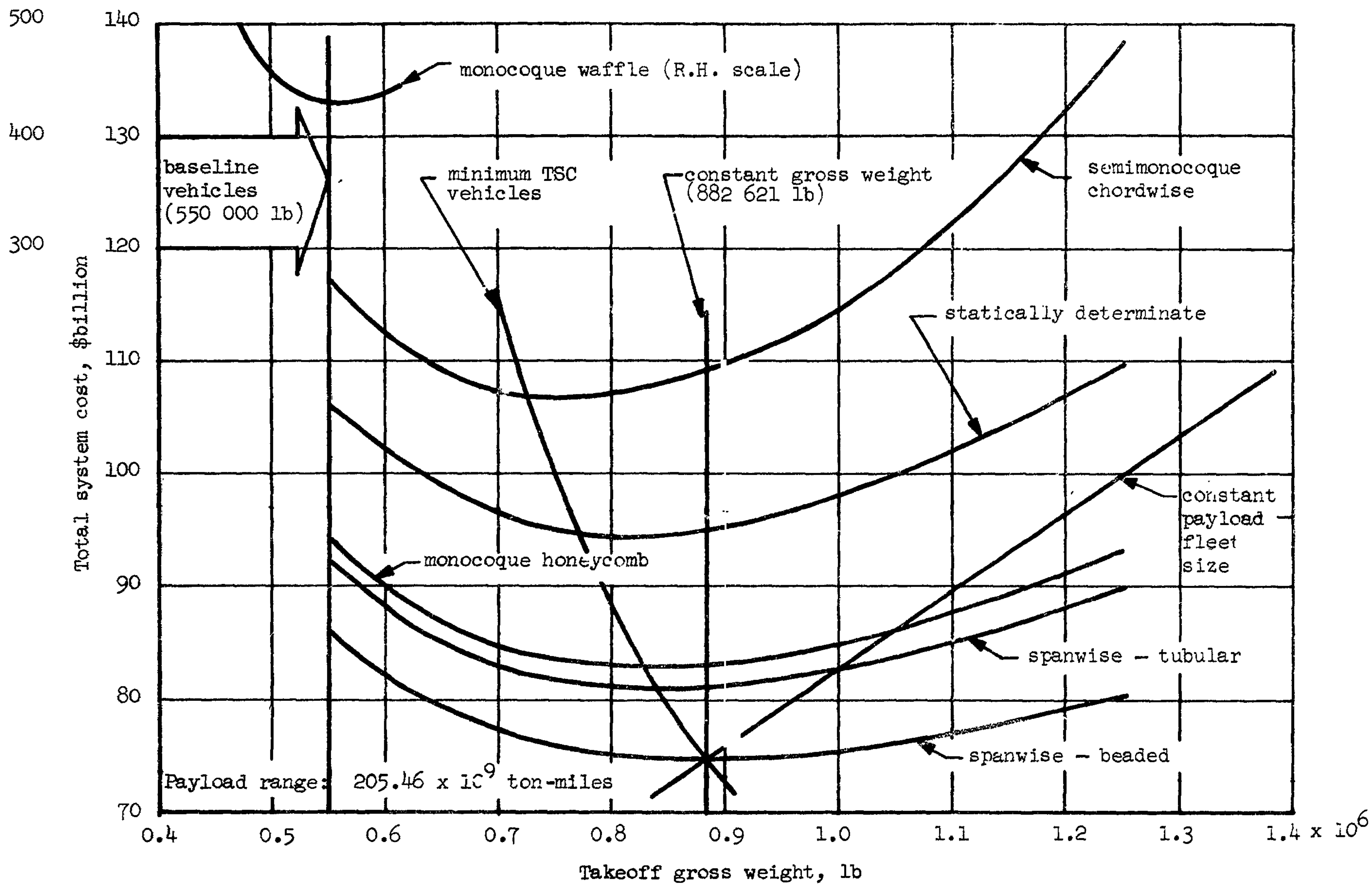

Figure 26-16. Total system cost variation with vehicle gross weight

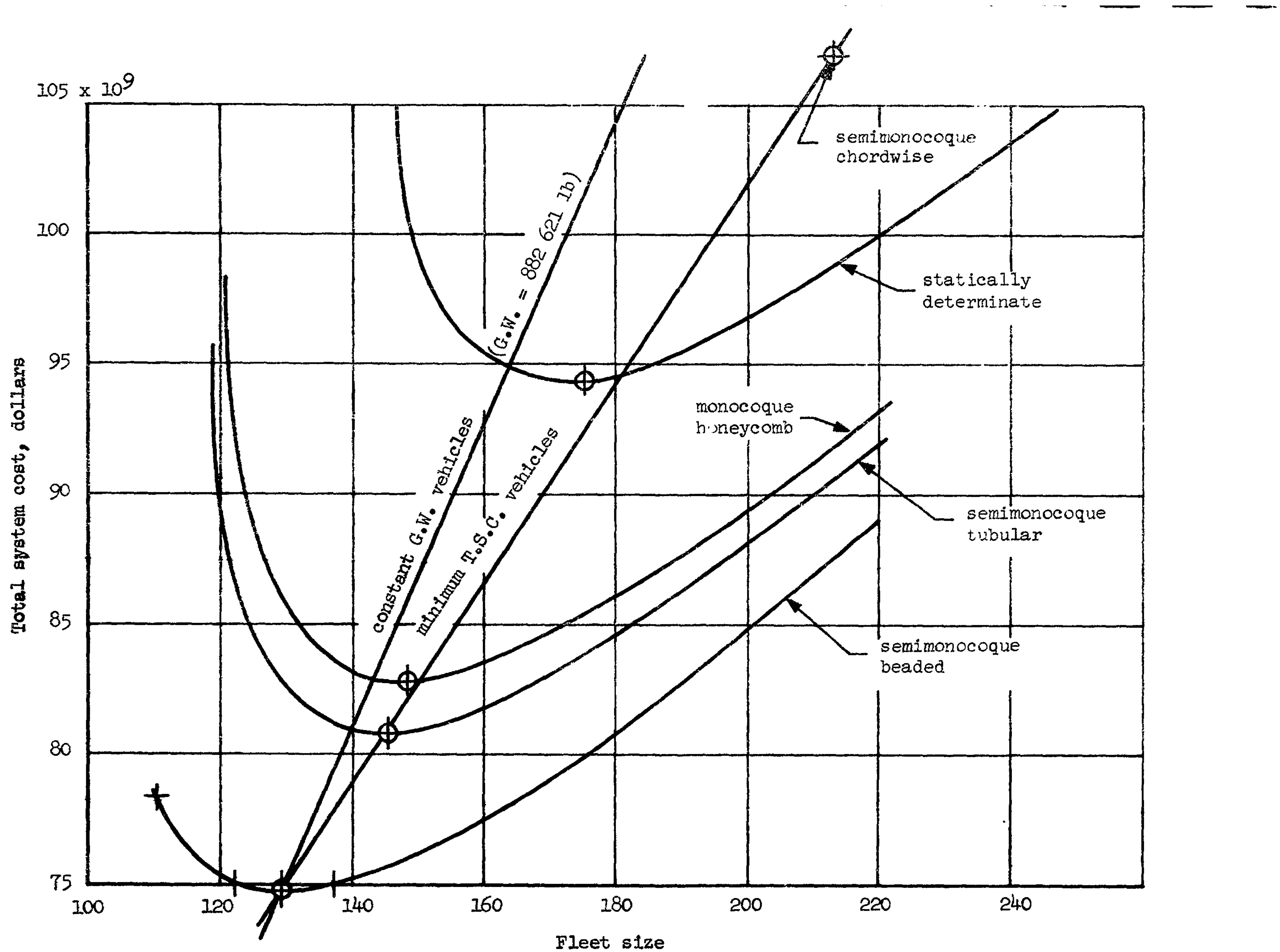

Figure 26-17. Total system cost variation with operational fleet size

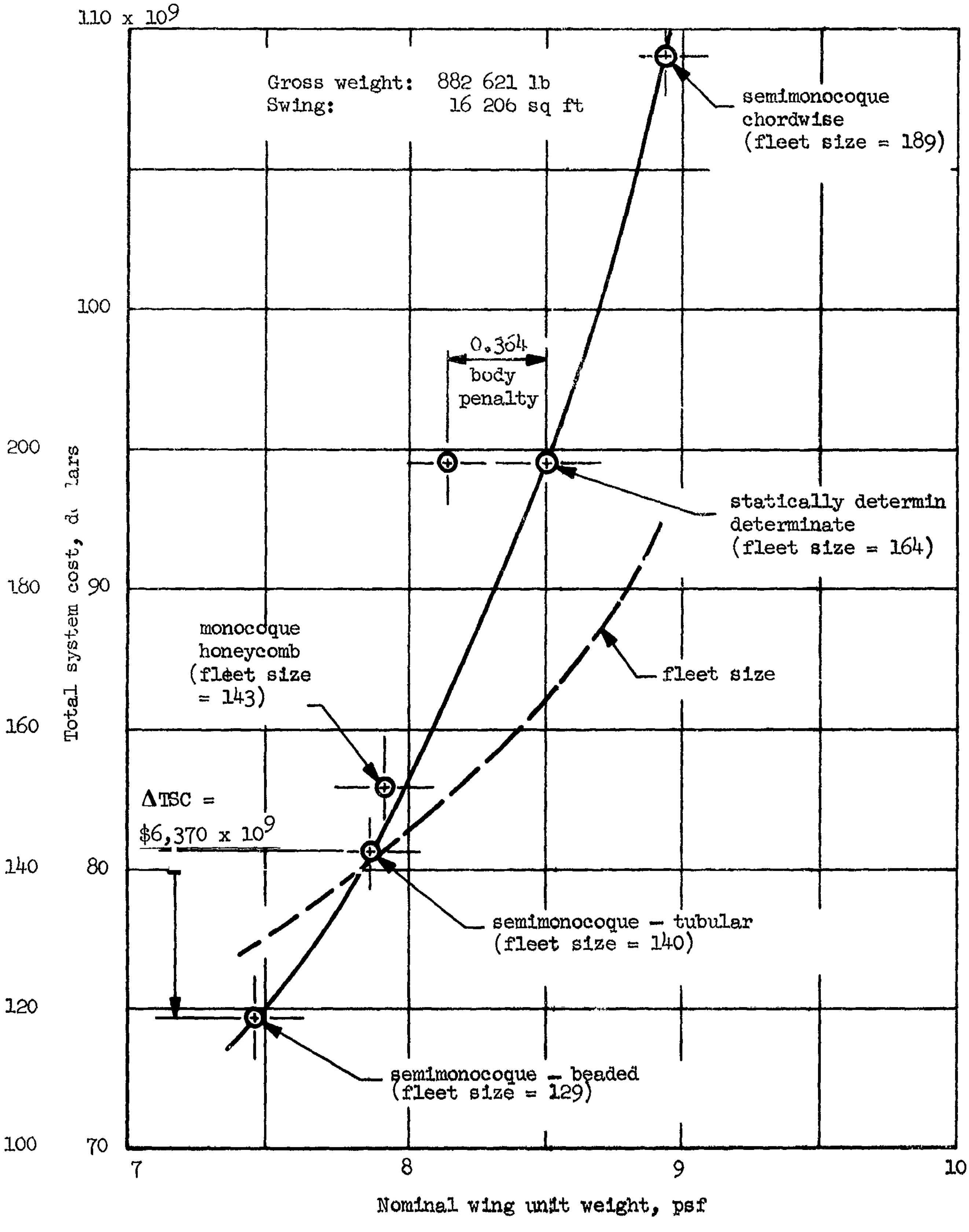

Figure 26-18. Total system cost variation with nominal wing unit weight for constant gross weight vehicle

Section 27

STRUCTURAL ELEMENT TESTING

by

R. S. Jusko, R. Swartz, C. E. Stuhlman, K. A. Wilhelm,
R. C. Dickason, J. J. Panik, L. D. Fogg, A. B. Burns,
G. W. Davis, I. F. Sakata, R. E. Hubka, F. T. Bevan

PRECEDING PAGE BLANK NOT FILMED.

CONTENTS

CONTENTS (Cont.)

TABLES

TABLES (Cont.)

ILLUSTRATIONS

Figure		Page

Figure		Page
27-44	Corrugation-stiffened end closeout panel after failure, room temperature	27-115
27-45	Strain gage locations for beaded end-closeout panel	27-116
27-46	Axial strains for beaded end-closeout panel, room temperature	27-117
27-47	Panel shortening curve $\Delta L/L$ for beaded end-closeout panel, room temperature	27-121
27-48	Beaded end-closeout panel after failure, room temperature	27-122
27-49	Strain gage locations for tubular end-closeout panel	27-123
27-50	Axial strains for tubular end-closeout panel, room temperature	27-124
27-51	Panel shortening curve $\Delta L/L$ for tubular end-closeout panel, room temperature	27-128
27-52	Tubular end-closeout panel after failure, room temperature test	27-129
27-53	Strain gage locations for corrugation-stiffened crippling panel	27-130
27-54	Axial strains for corrugation-stiffened skin crippling panel, room temperature	27-131
27-55	Panel shortening curve $\Delta L/L$ for corrugation-stiffened crippling panel, room temperature	27-135
27-56	Corrugation stiffened crippling panel after failure, room temperature test	27-136
27-57	Thermocouple locations for the corrugation-stiffened crippling panel	27-137
27-58	Panel shortening curve for corrugation-stiffened $\Delta L/L$ crippling panel, 1400° F	27-138
27-59	Corrugation-stiffened skin crippling panel after failure, 1400° F	27-139
27-60	Strain gage locations for trapezoidal corrugation crippling panel	27-140
27-61	Axial strains for trapezoidal corrugation crippling panel, room temperature	27-141
27-62	Panel shortening curve $\Delta L/L$ for trapezoidal corrugation crippling panel, room temperature	27-145
27-63	Trapezoidal corrugation crippling panel after failure, room temperature test	27-146

Figure		Page
27-86	Axial strains for corrugation stiffened skin compression panel, room temperature	27-173
27-87	Panel shortening curve $\Delta L/L$ for corrugation-stiffened skin compression panel, room temperature	27-181
27-88	Normal deflection curve for corrugation-stiffened skin compression panel, room temperature	27-181
27-89	Corrugation-stiffened skin compression panel after failure, room temperature test	27-182
27-90	Thermocouple locations for the corrugation-stiffened-skin compression panel	27-183
27-91	Panel shortening curve $\Delta L/L$ for corrugation-stiffened-skin compression panel, 1400°F test	27-184
27-92	Corrugation-stiffened skin compression panel after failure, 1400°F test	27-185
27-93	Strain gage locations for trapezoidal corrugation compression panel	27-186
27-94	Axial strains for trapezoidal corrugation compression panel, room temperature	27-187
27-95	Panel shortening curve $\Delta L/L$ for trapezoidal corrugation compression panel, room temperature	27-196
27-96	Normal deflections for trapezoidal corrugation compression panel, room temperature	27-196
27-97	Trapezoidal corrugation compression panel after failure, room temperature test	27-197
27-98	Thermocouple locations for the trapezoidal corrugation compression panel	27-198
27-99	Panel shortening curve $\Delta L/L$ for trapezoidal corrugation compression panel, 1400°F	27-199
27-100	Trapezoidal corrugation compression panel after failure, 1400° test	27-200
27-101	Strain gage locations for beaded compression panel	27-201
27-102	Axial strains for beaded compression panel, room temperature	27-202
27-103	Panel shortening curve $\Delta L/L$ for beaded compression panel, room temperature	27-211
27-104	Normal deflections for beaded compression panel, room temperature	27-211
27-105	Expansion of beaded compression panel due to axial compression loads, room temperature	27-212

Figure		Page
27-106	Beaded compression panel after failure, room temperature	27-213
27-107	Strain gage locations for tubular compression panel	27-214
27-108	Axial strains for tubular compression panel, room temperature	27-215
27-109	Panel shortening curve $\Delta L/L$ for tubular compression panel, room temperature	27-223
27-110	Tubular compression panel after failure, room temperature test	27-224
27-111	Thermocouple location for the tubular compression panel, 1400°F test	27-225
27-112	Panel shortening curve $\Delta L/L$ for tubular compression panel, 1400°F test	27-226
27-113	Tubular compression panel after failure, 1400°F test	27-227
27-114	Strain gage locations for the circular arc corrugation shear panel	27-228
27-115	Relationship of principal strains and applied vertical cantilever loading for circular arc corrugation shear panel (TIG weld with René 41 filler wire), room temperature	27-229
27-116	Relationship of shear strain and applied vertical cantilever loading for circular arc corrugation shear panel (TIG weld with René 41 filler wire), room temperature	27-229
27-117	Circular arc corrugation shear panel (TIG weld with René 41 filler wire) after failure, room temperature test	27-230
27-118	Relationship of principal strains and applied vertical cantilever loading for circular arc corrugation shear panel (TIG weld with Hastelloy W filler wire), room temperature	27-231
27-119	Relationship of shear strain and applied vertical cantilever loading for circular arc corrugation shear panel (TIG weld with Hastelloy W filler wire), room temperature	27-231
27-120	Circular arc corrugation shear panel (TIG weld with Hastelloy W filler wire) after failure, room temperature	27-232
27-121	Degree of conservatism in the wide-column analysis as applied to compression panels vs width-to-length ratio	27-233

Figure		Page
27-122	Comparison of tubular and beaded configuration initial buckling test results with predictions	27-234
27-123	Plasticity factors for 0.016-in. René 41 sheet at room temperature	27-235
27-124	Plasticity factors for 0.016-in. - 0.019-in. René 41 sheet at 1400°F	27-235
27-125	Plasticity factors for 0.060-in. René 41 sheet at room temperature	27-236

PRECEDING PAGE BLANK NOT FILMED.

LIST OF SYMBOLS

A	Area; mean of area enclosed by outer and inner boundary
A_n	Area of element n of cross section
a,b	X and Y distances between simply supported edges of plate
a/b	Aspect ratio
b	Width of flat plate for buckling analysis
b/d	Ratio of crest width to diagonal width for trapezoidal corrugation
c	End fixity
$D_I, D_{II}, D_1, D_2, D_3$	Stiffness coefficients of governing differential equation of plate
d	Width of diagonal element of trapezoidal corrugation
E_{el}	Elastic modulus
E_c	Compression modulus of elasticity
F_{cy}	Compression yield strength
F_{tu}	Ultimate tensile strength
F_{ty}	Tensile yield strength
$F_{0.7}$	Stress corresponding to modulus of 0.7 E_{el}
f_{cc}	Critical crippling stress
f_{cc_n}	Critical crippling stress of element n of cross section
$f_{c,d,cr}$	Critical compressive buckling stress for sides of trapezoidal corrugation
$f/_s$	Shear stress
$f_{s,cr}$	Critical shear buckling stress

G	Modulus of rigidity
I	Moment of inertia, $in.^4$
$\bar{I}$	Moment of inertia per unit length, $in.^3$
$\bar{J}$	Torsional stiffness per unit length
K'	Spring constant
K_n	Stress correction factor
k	Diagonal tension factor
k_c	Buckling coefficient in analysis of local compressive buckling
$k_{c,d}$	Buckling coefficient in analysis of local compressive buckling for diagonal element of trapezoidal corrugation
k_s	Buckling coefficient in analysis of shear buckling
L	Length
L'	$\frac{L}{\sqrt{c}}$ Effective panel length
MCF	Material correction factor
m	Number of half-waves in plate buckling equation
n	Shape parameter
p	Pitch
q	$\frac{K'L^3}{8EI}$
R	Radius
RT	Room temperature
t	Thickness
$\bar{t}$	Effective panel thickness
$\bar{t}_L$	Area per unit of diagonal width for beaded concept
U	Length of median boundary
x,y,z	Rectangular cartesian coordinates
X_T	Panel length in orthotropic panel buckling analysis

X_{II} Panel effective width in orthotropic panel buckling analysis

β_c $\frac{X_I}{X_{II}}\left(\frac{D_{II}}{D_I}\right)^{1/4}$

γ Correction factor

ΔL Change in length

$\Delta L/_L$ Panel shortening ratio

η $\sqrt{\eta_T}$, Plasticity reduction factor for calculating initial buckling stress of a flat plate simply supported

η_s $\frac{E_s}{E_{el}}$, Secant plasticity reduction factor

η_{ST} $\frac{E_{st}}{E_{el}}$, Stowell's plasticity reduction factor

η_T $\frac{E_t}{E_{el}}$, Tangent plasticity reduction factor

$\bar{\eta}$ $\sqrt{\eta_T \eta_s}$, Plasticity reduction factor for calculating the buckling stress for the circular arc sections

ν Poissons ratio

Σ Summation

Section 27

STRUCTURAL ELEMENT TESTING

TEST PLAN

Standard element tests were conducted concurrent with the theoretical analyses and the latter portion of the material screening test program (section 5) to evaluate primary structural concepts applicable to wing structure designs. The results of these tests and subelement tests (section 5) were used to refine the methods of analysis and concept design.

Twenty-two structural element panels were designed and fabricated for test and evaluation in accordance with the structural element test shcedule outlined in table 27-1.

End closeout, crippling, compression panel, and inplane shear tests were conducted at room temperature and at 1400°F for evaluation of the construction concepts. The information obtained from these tests included:

1. Evaluation of end-closure designs
2. Evaluation of joining methods
3. Combined effects of temperature and load
4. Substantiation of element and panel shear, crippling, and compression buckling stresses.

Details of the panel elements, fabrication and assembly schedules, test arrangements, instrumentation, test procedures, test results, and comparison of analyses with test results are presented in this section.

DESCRIPTION AND FABRICATION OF PANEL ELEMENTS

Twenty-two panels were constructed for test and evaluation. The panel types, sizes, and the number of each panel element fabricated are given in table 27-2.

A detailed description of each of these panel elements is given below and includes the fabrication and assembly schedules used in their construction.

Tubular Panels

The test panel design (fig. 27-1) consists of two beaded skins, four fingered end doublers, and two end bars for testing. Beaded face sheets were formed in a high-pressure Verson-Wheelon press; doublers were blanked using steel rule dies. End bars were installed using Hi-Lok, high-strength fasteners. Ends of the panel assembly were machine-ground to a close tolerance (±0.001 inch) across the panel width. Crippling and end closeout panels were saw cut from full-length panels; ends of crippling panels and one end of an end closeout panel were cast in Densite or Pyroform for testing, depending on the test environment.

Fabrication and assembly plan for 30.0-in. panel:

1. Formed skins – two required per panel assembly

   Shear 24.0-in. by 34.0-in. blanks, 0.016-in. gage René 41

   Deburr

   Process clean – degrease, alkaline wash, pickle rinse, and dry

   Encase in preoxidized Type 321 Cres steel envelope (26.0-in. by 36.0-in.), evacuated and seam-welded

   First stage forming at 3500 psi (17-20% elongation) on form block FB-CL 1125-1-9 (fig. 27-2)

   Anneal package – air furnace 1950° to 2000°F for 15 min; air cool to 1000°F within 3 sec

   Pickle – nitric-hydrofluoric (vapor blast to remove residual scale)

   Second stage forming at 3500 psi (8-10% elongation) on FB-CL 1125-1-9

   Anneal package – air furnace 1950° to 2000°F for 15 min; air cool to 1000°F within 3 sec

   Pickle – nitric-hydrofluoric (vapor blast to remove residual scale)

   Third stage forming at 3500 psi (4-5% elongation) on FB-CL 1125-1-9

   Anneal package – air furnace 1950° to 2000°F for 15 min; air cool to 1000°F within 3 sec

   Remove package from part; hand shear

   Final stage forming at 8000 psi (2-3% elongation) on FB-CL 1125-1-9

   Lay out finish panel dimensions and shear

   Drill No. 30 vent holes in one end of beads, one panel only (fig. 27-3)

   Deburr

   Clean for welding (chromic-sulfuric per ref. 27-1)

   Prepare coupons from trim material, 8 required

2. Finger doublers – four required per panel

   Shear 5.45-in. by 17.37-in. blanks, 0.030-in. gage René 41

   Blank – steel rule die in 200-ton punch press

   Deburr

   Final clean prior to assembly (chromic-sulfuric per ref. 27-1)

3. End bars – four required per panel

   Saw .38-in. by 1.00-in. Inconel bar to 17.38-in. length

   Normalize at 1800°F for 30 min; air cool

   Check and straighten

   Mill one face and one edge square

   Clean prior to assembly

4. Assembly – record weight of each detail part

   Locate panels and doublers in universal weld fixture (fig. 27-[illegible]); resistance weld (figs. 27-5 and 27-6); (ref. 27-2)

   Remove electrode deposit – hand swab using chromic acid followed with alcohol rinse

   Age and heat oxidize at 1400°F for 16 hr in air furnace using ceramic fixtures for heating and air cooling

   Drill and ream panel and end bars in drill fixture (no coolant or lubricant)

   Deburr holes

   Record weight of assembly, less end bars

   Install Hi-Lok fasteners

   Mill panel end bars normal to axis of beads within ±0° 15', flat and parallel within ±0.001 in. (ref. 27-1).

Modified tubular panels. – The end closeout designs were modified by the addition of tapered doublers (0.016 in. thick by 5.00 in. long) to each side of each flat of the finished panel assembly (figs. 27-1 and 27-7). The area to be covered by these doublers was hand-sanded, scraped, and wire-brushed to remove oxide. Doublers were sheared to size (0.40 in. wide at one end; 0.26 in. wide at the other end), cleaned (alkaline wash, chromic/sulfuric pickle, hot water and deionized water rinse, air dry), and located in position by probe tack welding. Structural welds followed schedule previously established for four thicknesses of 0.016 in. René 41. Due to inability to remove all surface contamination from the heat-oxidized surfaces, spot-weld strength per spot was reduced; average values obtained from test strips indicated loss of approximately 30 lb per spot. Average shear strength of spots was 517 lb (547 lb per spot on clean material), which exceeds MIL W-6858C specification requirements.

Fabrication of crippling and end closeout panels. – One panel assembly was completed in accordance with the above plan except that end bars were omitted from one end of panel. The remaining panel was then sawed into required end closeout and crippling sections (figs. 27-8 and 27-9).

1. Crippling panel end casting for test – one crippling panel after being sawed to 8.0-in. length, was fixtured in 1.0-in. deep mold and cast with Densite. After drying, panel was reversed and opposite end cast in Densite. Ends were then ground flat, parallel, and normal to bead axis.

   A second crippling panel was cast in Pyroform (a high-temperature ceramic) in a similar manner, except that shims were placed to provide space for panel elongation during high-temperature testing.

2. End closeout panel was sawed to 9.0-in. length with sawed edge cast in Densite, then ground parallel to end bars.

Beaded Panels

The test panel assembly (fig. 27-10) consists of one beaded skin, four fingered end doublers, and four end bars. Beaded panels were formed by hydraulic forming in a Clearing 1500-ton press, using auxiliary pump for fluid movements.

Fabrication and assembly plan for 30.0-in. panel

1. Formed skins – one required per panel assembly

   Shear 32.0-in. by 38.0-in. blank, 0.020-in. gage René 41

   Deburr

   Clean – alkaline wash, pickle, rinse dry

First stage forming at 2000 psi using HFB (hydraulic forming block) (fig. 27-11)

Degrease

Anneal – air furnace 1950° to 2000°F for 10 min; air blast cool to 1000°F within 3 sec

Descale – deoxidizer, nitric-hydrofluoric pickle, rinse, oven dry

Final stage forming at 3000 psi using HFB – CL 1125-1-10

Lay out finish panel dimensions and shear (fig. 27-12)

Final clean prior to assembly (ref. 27-1).

Prepare coupons from trim material, 8 required

2. Finger doublers, 4 required – same as for tubular panel

3. End bars, 4 required – same as for tubular panel

4. Assembly – same procedure as for tubular panel (figs. 27-13 and 27-14); record weight of each detail and final assembly, less end bars

Modified beaded panel. – The end closeout designs were modified by extension of the finger doublers. This was achieved by use of 0.016-inch and 0.020-inch by 2.0-inch doublers laminated on each side of the original fingers and extending a total of 3.0 inches toward the panel center. Twenty 0.020-inch by 0.35-inch by 2.0-inch; twenty 0.016-inch by 0.35-inch by 2.0-inch; and twenty 0.016-inch by 0.35-inch by 3.0-inch René 41 doublers were resistance spot-welded (fig. 27-15). New weld schedules were developed for the laminated sections modified by the finger doublers. The locations and thicknesses for the laminated section are as follows:

	Location			
	At end of finger doubler	1.0 in. beyond end of finger doubler	2.0 in. beyond end of finger doubler	3.0 in. beyond end of finger doubler
Added (.016 x 2.0)		0.016	0.016	
Added (.016 x 3.0)		0.016	0.016	0.016
Added (.020 x 2.0)	0.020	0.020		
Finger doubler	0.030			
Corrugation	0.018	0.018	0.018	0.018
Finger doubler	0.030			
Added (.020 x 2.0)	0.020	0.020		
Added (.016 x 3.0)		0.016	0.016	0.016
Added (.016 x 2.0)		0.016	0.016	
Total thickness	0.118	0.122	0.082	0.050
No. sheets	5	7	5	3

Fabrication of crippling and end closeout panels:

End closeout – similar to tubular panel.

Crippling – similar to tubular panel (fig. 27-16).

Trapezoidal Corrugation Panels

The test panel assembly (fig. 27-17) consists of a trapezoidal corrugation center, two trapezoidal corrugation ends, four finger splices, and two zee sections. The corrugations were formed on a corrugating die as a one-piece panel, then cut into center and end sections. Doublers were blanked from sheet using steel rule die in a punch press; zee sections were power-brake formed on standard tooling.

Fabrication and Assembly Plan for 30.0-in. panel:

1. Trapezoidal corrugations – one 22.0-in. and two 4.0-in. sections required per panel assembly.

   Shear 32.0-in. by 36.0-in. blank from 0.016-in. gage René 41

Deburr

Form in corrugation die CD-CL 1125-1-12 (fig. 27-18)

Size to 0.578-in. height, standard tools, power brake

Lay out for saw

Saw parts (center corrugation and end corrugations)

Prepare coupons from trim material, 8 required

Deburr

Joggle – cerrobend cast tooling, arbor press

Clean for welding

2. Finger splices – 4 required per panel assembly

Shear 3.71-in. by 20.0-in. blank from 0.040-in. gage René 41

Deburr

Blank – steel rule die BD CL 1125-1-11-6 and -7.

Cut to length – shear per -6 and -7 details

Deburr

Clean for welding.

3. Zee section – 2 required per panel assembly

Shear 2.58-in. by 19.46-in. blanks from 0.020-in. gage René 41

Deburr

Power brake form, standard tooling.

Clean for welding

4. Assembly

Record weights of each detail part (fig. 27-19)

Locate corrugation sections and zee sections in weld fixture; resistance weld

Install splice plates; resistance weld (fig. 27-20)

Remove electrode pickup, swab with chromic acid

Alcohol rinse

Age and heat-oxidize, 1400°F, air furnace, for 16 hr (fig. 27-21)

Mill ends of panel square, parallel, and normal to corrugated axis

End cast in Densite and Pyroform (one panel each material)

Fabrication of crippling panels. – One center corrugation was saw-cut into two 8.0-in. lengths, aged and heat-oxidized, 1400°F for 16 hr. Ends were cast (one panel in Densite, the other in Pyroform) then ground flat, parallel and normal to corrugation axis. (fig. 27-22).

Corrugation-Stiffened Panels

The panel assembly (fig. 27-23) consists of one corrugated sheet with formed closeouts, one flat skin, two tapered fingered end doublers, two end spacer doublers, and two Tee end bars. Corrugation, skin, and doublers are resistance spotwelded together; end Tees are attached with high-temperature shear fasteners. Two full length panels (30.0 in.), two crippling panels (8.0 in.) and one end closeout panel (9.0 in.) were fabricated.

Fabrication and assembly plane for 30.0-in. panel:

1. Corrugation with formed closeouts – one required per panel assembly

   Shear 24.0-in. by 34.0-in. blank from 0.016-in. gage René 41

   Encase in preoxidized type 321 Cres steel envelope

   First stage forming in Verson-Wheelon at 6000 psi (17% elongation) on CL 1125-1-13 form block (fig. 27-24)

   Anneal at 1950° to 2000°F for 15 min; air quench

   Remove scale – pickle and vapor blast

   Second stage forming at 6000 psi using filler strips in CL 1125-1-13 form block (12% elongation)

   Anneal

   Pickle

   Third stage forming at 6000 psi using filler strips in CL 1125-1-13 form block (10% elongation)

Anneal

Remove envelope; hand shear

Final stage forming at 10 000 psi using filler strips in 1125-1-13 form blcok (2% elongation)

Lay out and trim to 19.00 in. by 30.75 in.

Prepare coupons from trim material, 8 required

Drill No. 30 holes in one end of each bead

Deburr

Clean for welding

2. Skin — one required per panel assembly

   Shear 19.00-in. by 30.75-in. finish skin from 0.026-in. gage René 41

   Deburr

   Clean for welding

3. Tapered fingered doublers — two required per panel

   Shear 4.00-in. by 19.00-in. blanks from 0.060-in. gage René 41

   Deburr

   Blank fingers — BD CL 1125-1-13 steel rule die in 200-ton punch press

   Deburr

   Mill taper fingers — mill fixture

   Deburr

   Clean for welding

4. End spacers — two required per panel

   Shear 0.75-in. by 19.00-in. blanks from 0.040-in. gage René 41

   Deburr

   Clean for welding

5. Tee bars

   Saw 19.00-in. blanks from 0.38-in. by 1.00-in. Inconel 600 alloy bar

   Stress relieve at 2000°F for 30 min

   Check and straighten — hand arbor press

   Mill Tee configuration

   Clean for assembly

6. Assembly

   Record weight of each detail part (fig. 27-25)

   Resistance weld skin, corrugation, and doublers in universal weld fixture (ref. 27-2)

   Remove electrode pickup; chromic acid swab

   Alcohol rinse

   Age and heat-oxidize at 1400°F for 16 hr (fig. 27-26)

   Drill for Tee end attachment

   Deburr

   Install end tees with Hi-Lok fasteners

   Grind ends of Tee members flat, parallel, and normal to bead axis.

7. Fabrication of end closeout and crippling specimens. One full length panel was cut into smaller specimens which, in turn, were end cast either in Densite or in Pyroform similar to the circular-arc stiffened end closeout and crippling specimens (fig. 27-27).

Circular-Arc Corrugation Shear Panels

The panel assembly (fig. 27-28) consists of circular-arc corrugated web design, with channel caps and edge doublers. The cap is TIG welded to the corrugation using René 41 and Hastelloy W filler wires and doublers are resistance spot-welded to the corrugation.

Fabrication and Assembly Plan:

1. Corrugation – one required per panel assembly

   Shear 20.0-in. by 26.0-in. blank from 0.016-in. gage René 41

   Deburr

   Form on FB/CL 1125-1-12 – Verson-Wheelon at 5000 psi (fig. 27-29)

   Lay out and saw/shear to 15.50 in. by 17.00 in.

   Prepare tensile coupons from trim material, 4 required

   Grind ends flat, parallel, and normal to axis of corrugation using CL 1125-1-12 TIG weld fixture

   Deburr

   Clean for welding

2. Side doublers – four required per panel assembly

   Shear 1.42-in. by 15.26-in. blanks from 0.016-in. gage René 41

   Deburr

   Clean for welding

3. Cap Channel – two required per panel assembly

   Shear 3.25-in. by 17.00-in. blanks from 0.060-in. gage René 41

   Deburr

   Drill 10 V-size holes (0.376-0.383-in. diam) using drill jig

   Deburr

   Form flanges – power brake using end holes for location of bends

   Clean for welding

4. Assembly

   Record weight of all detail parts (fig. 27-30)

   Locate corrugation in weld fixture

   Trace contour and ink template

Locate cap in position and seal

Weld cap to corrugation, tracing from template (fig. 27-31)

Reposition and repeat sequence for other cap

Weld schedule:

Vicers DC arc welder Model MT 4K40, 400 amp

Weld amperage – 85

Voltage – 10

Travel speed – 9 in. per min

Electrode – thoriated tungsten (2% ThO_2), 0.093-in. diameter

Torch nozzle – 0.31-in. diameter

Torch shield gas – Argon at 12 ft^3/min

Backup gas – Argon at 25 ft^3/min

Trailing shield – 3.0-in. by 6.0-in. glass cloth attached to torch

Filler wire – 0.045-in. diam Hastelloy W for one other panel, 0.060-in. diam René 41 for other panel; both automatic feed

Install edge doublers, hand clamp and resistance spot weld

Lay out and drill ten 6.4 mm holes (0.251 - 0.258-in. diam) each edge of panel

Deburr

Age and heat-oxidize – 1400°F for 16 hr (fig. 27-32)

Record weight of finished assembly

Spar Cap Crippling Panel

The panel assembly (fig. 27-33) consists of a circular-arc corrugation web and two channel caps. The caps are TIG welded (melt through) to corrugation.

Fabrication and assembly plan: Detailed fabrication and assembly plan for the beam cap crippling panels is identical to the circular-arc corrugation shear panel, except for the following:

1. Hastelloy W filler wire was used to join the cap to arc (welding schedule same as for the in-plane shear panel test)

2. The height of the cap flanges is 3/8 in.

3. The ends of the panel were milled flat, square, and parallel

TEST SETUP

Room Temperature Compression Tests

The test setup for the room temperature compression tests of the end-closeout, crippling, compression panels, and the beam cap crippling specimens was essentially the same. Typical test arrangements are shown in figure 27-34 for the crippling and compression panels. The compression panels are shown positioned in the compression bay of a suitable capacity testing machine and are located between a base plate and a compression head test fixture. All bearing surfaces of these fixtures were Blanchard ground flat and parallel. Two cylindrical plates are shown sandwiched between the compression head and the positioning (or movable) head of the test machine. These plates are tapered in thickness (0.001 in./in.) to allow for initial parallel alignment of the ground surfaces of the base plate and compression head test fixture prior to installation of the test panel. The initial alignment of the compression surfaces was held to within 0.0005 inches across the total bearing surfaces of the loading fixture.

Prior to installation of the test panel, slit tubes were attached to the free edges of the panel to provide simple edge support. Sufficient clearance (0.050 in. at each end of the tube) was provided at the tube ends to avoid the introduction of axial tube loading due to specimen contraction when test loads were applied.

Elevated Temperature Compression Tests

The test setup for the elevated temperature compression tests of the crippling and column panels was essentially the same. A typical test arrangement is shown in figure 27-35. In addition to the room temperature test fixtures previously described (including the tubular edge supports), figure 27-35 shows two Pyroform (cast ceramic) blocks, 1/2 in. thick by 6 in. wide by 24 in. long, and a 3/16-in. thick Inconel bearing plate attached to the loading and reaction heads of the test machine. The Pyroform blocks adjacent to the Inconel plates contained nichrome heating elements which were threaded through pre-cast holes in the blocks. This arrangement reduced heat losses from the ends of the test panel and provided insulation at the test machine loading and reaction heads.

The Pyroform block heaters were electrically connected in parallel and were energized by an Inductrol type 60-cycle power supply. The Inductrol unit is essentially a two-winding power transformer that incorporates a movable secondary coil permitting a variable electrical output from the transformer. This unit was used to provide electrical isolation between the block heaters and the 490-volt, 60-cycle power supply used for the radiant heat lamps.

An overall view of the elevated temperature test setups for the crippling and column panels is shown in figure 27-36. Two radiant heat lamp assemblies were used, one assembly on either side of the test panel. Refrasil batting (a high-temperature spun glass insulation blanket) was used to encapsulate the panel test setup. The lamp assemblies consisted of 1000T3/CL/HT quartz lamps and the Research Incorporated AU8-612 lampholders. Two Thermac power units were used to energize the heat lamp assemblies. Chromel-alumel thermocouples spotwelded centrally on each side of the panels provided the feedback signals to regulate the power controllers.

Shear Panel Tests

The general arrangement for the in-plane shear test is shown in figure 27-37. The test panel is mounted in a cantilever type loading test fixture. Flexure pivots are incorporated in the test fixture design at each of the four corners to eliminate the friction associated with pin connections. A hydraulic jack was used to apply vertical loading to the cantilevered test fixture. Hydraulic pressure was supplied to the jack by means of an Edison load maintainer. Test loads were monitored by means of a load transducer mounted in series with the hydraulic jack. Lateral supports were pin-connected to the cantilever fixture to prevent racking during load application.

INSTRUMENTATION

The instrumentation schedule for the structural element tests is outlined in table 27-3 and indicates the number of strain gages and thermocouples used for each panel test. The strain gages used included Baldwin Lima Hamilton (BLH) foil gages, type FAE-25-12 S6, and Budd foil gages, type C6-122A. An epoxy adhesive system was used to bond the BLH gages to the specimens using accepted standard strain gage bonding techniques. The Budd gages were bonded using the water-activated epoxy adhesive incorporated with each gage. Specimen axial deformations (panel shortening) were measured by means of electrical deflection transducers mounted at the four corners of the compression head fixture previously described. The deflection transducers, normally designed as LVDTs (linear variable differential transducers) are Model SS-105 (6-volt excitation), G. L. Collins Corporation.

Specimen temperatures were measured using 30-gage chromel-alumel thermocouples having glass-over-glass type insulation. The thermocouples were attached to the test specimens by means of the capacitance discharge spotweld method. A 150°F Pace reference junction was used for the thermocouple data reference point. The strain gage and thermocouple locations and identification numbers for each panel specimen are presented in the paragraphs describing test results.

DATA ACQUISITION

A modified Sadic, 200-channel medium speed data acquisition system was used for the panel tests. The system has an inherent maximum speed of approximately 250 msec per data point with five digit resolution to ±30 000 counts and 0.03 percent linearity. This represents a system accuracy of ±10 microinches/in. strain for all strain levels up to ±30 000 microinches/in. strain, or ±0.2°F when using chromel-alumel thermocouples from -300°F to +700°F. The system converts the millivolt signals from strain gages, deflection transducers, and thermocouples into digital data and stores them on perforated tape. This information is then transferred to IBM cards for further processing. For this program, tab runs were the end product for data display. The strain gage and deflection transducer data have been plotted in curvilinear form; the thermocouple data are presented in tabular form. All of these data are included in the test results paragraphs of this section.

TEST PROCEDURES

Preliminary Tests

Prior to conducting the compression failure tests at either room or elevated temperature, a preliminary test run was conducted to assure proper specimen alignment in the test machine so that a uniform loading would be achieved across the entire specimen width. Test loading during this aligning procedure was held below 50 percent of the predicted initial buckling load for the particular specimen configuration tested. Uniformity of load distribution was determined by the LVDT readings that measured test head displacement and by panel strain gage readings. After satisfactory alignment of the test panel was achieved, the failure test was conducted.

Failure Tests, Room Temperature Compression Panels

The failure test consisted of the application of compression loads in suitable steps while panel deformations and strains were recorded at each loading step. Test loading in this manner was continued to failure. The maximum load sustained by the panel was obtained from the reading of the load indicating follower located on the face of the test machine console.

Failure Tests, Elevated Temperature Compression Panels

After satisfactory alignment of the test panel, the test specimen was then heated to the 1400°F test temperature. This was accomplished by first energizing the heating elements in the Pyroform blocks which in turn heated the Inconel bearing plates located between the specimen ends and the Pyroform heating blocks. The radiant heat lamps were then energized by means of the Thermac power regulators.

In the actual operation of the Thermac units, the set-point control was adjusted for the desired temperature as determined from the calibration curves provided. The limiter control was then advanced slowly to limit the rate of panel temperature rise. The advantages accrued from this procedure were.

1. Limitation of the temperature rise rate

2. Limitation of maximum power to the lamp assemblies, which is a safety feature in the event of a circuit failure

3. Minimum fluctuation of lamp intensity, which provides for a better steady-state temperature condition

4. Increased life of the radiant heat lamps.

Throughout the entire heating phase of the test panel to the 1400°F test temperature, a 2000-lb compression load was maintained on the specimen by the test machine operator. The test panel was soaked at the test temperature for a minimum of one-half hour before loading was commenced to failure. The procedure used for the failure test at the elevated temperature was identical to the procedure previously described for the room temperature failure test.

Failure Tests, Shear Panels

The procedure used to conduct the shear panel failure tests consisted of applying cantilever loads at a rate of approximately 100 lb per minute by means of the Edison load maintainer. Test loading was interrupted to permit strain gage data recording from both the back-to-back rosette gages on the test panel and the load transducer mounted in series with the hydraulic jack. A readout time of approximately three seconds was required. The load levels at which data were recorded are indicated by the test points of the strain gage plots for each panel. An electrically operated dump valve was energized by hand to dump the test load at panel failure.

TEST RESULTS

Panel Material Tests

The manufacturing processes used for the fabrication of the test panels included interstage annealing for several of the panel configurations. Mechanical property tests were conducted to establish the material characteristics resulting from these processes, and are summarized in table 27-4. Stress-strain curves for each of the material conditions are presented in figures 27-38, 27-39, and 27-40.

Panel Tests

A summary of the panel element tests conducted in this program is presented in table 27-5 and includes panel descriptions, test temperatures, panel areas (computed from the panel weight measurements), panel ultimate loads, and ultimate stresses for each of the end closeout, crippling, compression, and shear panel configurations tested. A detailed description of the test results for each of these configurations is given below.

End closeout tests. — The end closeout panel configurations were tested at room temperature and included the following panels:

Corrugation-stiffened panel — The strain gage locations for this panel configuration are given in figure 27-41. Curve plots of the strain gage data are presented in figure 27-42. A curve plot of the panel shortening due to the applied compression loads is given in figure 27-43. Photographs of the panel after failure are shown in figure 27-44. Thickness measurements of the panel cross-section are given in table 27-6.

Beaded panel — The strain gage locations for this panel configuration are given in figure 27-45. Curve plots of the strain gage data are presented in figure 27-46. A curve plot of the panel shortening due to compression loads is given in figure 27-47. Photographs of the panel after failure are shown in figure 27-48. Thickness measurements of the panel cross-section are given in table 27-7.

Tubular panel — The strain gage locations for this panel configuration are given in figure 27-49. Curve plots of the strain gage data are presented in figure 27-50. A curve plot of the panel shortening due to compression loads is given in figure 27-51. Photographs of the panel after failure are shown in figure 27-52. Thickness measurements of the panel cross section are given in table 27-8.

Crippling tests. — Crippling panel tests were conducted at room temperature and at 1400°F for each of the following panels.

Corrugation-stiffened skin panel

Trapezoidal corrugation panel

Beaded panel

Tubular panel

The spar cap crippling specimen was tested at room temperature.

1. Corrugation-stiffened skin crippling panel room temperature test — The strain gage locations for this panel configuration are given in figure 27-53. Curve plots of the strain gage data are presented in figure 27-54. A curve plot of the panel shortening due to compression loads is given in figure 27-55. Photographs of the panel after failure are shown in figure 27-56. Thickness measurements of the panel cross section are given in table 27-9.

2. Corrugation-stiffened skin crippling panel elevated temperature test – The thermocouple locations for this panel are given in figure 27-57. Tab runs of the thermocouple data showing the temperature distribution are presented in table 27-10. A curve plot of the panel shortening due to the applied compression loads is given in figure 27-58. Photographs of the panel after failure are shown in figure 27-59. Thickness measurements of the panel cross section are given in table 27-11.

3. Trapezoidal corrugation crippling panel room temperature test – The strain gage locations for this panel configuration are given in figure 27-60. Curve plots of the strain gage data are presented in figure 27-61. A curve plot of the panel shortening due to compression loads is given in figure 27-62. Photographs of the panel after failure are shown in figure 27-63. Thickness measurements of the panel cross section are given in table 27-12.

4. Trapezoidal corrugation crippling panel elevated temperature test – The thermocouple locations for this panel are given in figure 27-64. Tab runs of the thermocouple data showing the temperature distribution are presented in table 27-13. A curve plot of the panel shortening due to the applied compression loads is given in figure 27-65. Photographs of the panel after failure are shown in figure 27-66. Thickness measurements of the panel cross section are given in table 27-14.

5. Beaded crippling panel room temperature test – The strain gage locations for this panel configuration are given in figure 27-67. Curve plots of the strain gage data are presented in figure 27-68. A curve plot of the panel shortening due to the applied compression loads is given in figure 27-69. Photographs of the panel after failure are shown in figure 27-70. Thickness measurements of the panel cross section are given in table 27-15.

6. Beaded crippling panel elevated temperature test – The thermocouple locations for this panel are given in figure 27-27. Tab runs of the thermocouple data showing the temperature distribution are presented in table 27-16. A curve plot of the panel shortening due to the applied compression loads is given in figure 27-72. Photographs of the panel after failure are shown in figure 27-73. Thickness measurements of the panel cross section are given in table 27-17.

7. Tubular crippling panel room temperature test – The strain gage locations for this panel are given in figure 27-74. Curve plots of the strain gage data are presented in figure 27-75. A curve plot of the panel shortening due to the applied compression load is given in figure 27-76. Photographs of the panel after failure are shown in figure 27-77. Thickness measurements of the panel cross section are given in table 27-18.

8. Tubular crippling panel elevated temperature test – The thermocouple locations for this panel are given in figure 27-78. Tab runs of the thermocouple data showing the temperature distribution are presented in table 27-19. A curve plot of the panel shortening due to the applied compression loads is given in figure 27-79. Photographs of the panel after failure are shown in figure 27-80. Thickness measurements of the panel cross section are given in table 27-20.

9. Spar cap crippling specimen room temperature test – The spar cap crippling specimen configuration presented in figure 27-81 was tested at room temperature. The upturned flanges of the cap specimen were 3/8-in. The strain gage locations for this specimen are given in figure 27-81. Curve plots of the strain gage data are presented in figure 27-82. A curve plot of the specimen shortening due to the applied compression loads is given in figure 27-83. Photographs of the cap specimen after failure are shown in figure 27-84. Thickness measurements of the cap specimen are given in table 27-21.

Compression panel tests. – Compression panel tests are scheduled at room temperature and at 1400°F for each of the following panel configurations:

Corrugation-stiffened skin panel

Trapezoidal corrugation panel

Beaded panel

Tubular panel

Modifications to the finger doubler design were incorporated in the beaded panel and the tubular panel as described in the panel fabrication discussion. After reviewing the room temperature test data for the beaded compression panel, the elevated temperature test for this panel configuration was deleted from the test schedule. The results of the room and elevated temperature compression panel tests are given below.

1. Corrugation-stiffened skin compression panel room temperature test – The strain gage locations for the corrugation-stiffened skin compression panel are given in figure 27-85. Curve plots of the strain gage data are presented in figure 27-86. A curve plot of the panel shortening due to the applied compression loads is given in figure 27-87. Panel deflections, perpendicular to the plane of the skin, were obtained from three dial gages mounted across the width of the panel. These gages were symmetrically positioned about the center of the panel, with the two outboard gages located approximately 5 inches from the center gage. The normal deflections obtained from these gages are presented in figure 27-88. Photographs of the panel after failure are shown in figure 27-89. Thickness measurements of the panel cross section are given in table 27-22.

2. Corrugation-stiffened skin compression panel elevated temperatu ›st — The thermocouple location for this panel are given in figure 27-90. Tab runs of the thermocouple data showing the temperature distribution for this panel are presented in table 27-23. A curve plot of the panel shortening due to the applied compression loads is given in figure 27-91. Photographs of the failed panel are shown in figure 27-92. Thickness measurements of the panel cross section are given in table 27-24.

3. Trapezoidal corrugation compression panel room temperature test — The strain gage locations for this panel are given in figure 27-93. Curve plots of the strain gage data are presented in figure 27-94. A curve plot of the panel shortening due to the applied compression loads is given in figure 27-95. Panel deflections perpendicular to the corrugations were obtained from three dial gages mounted across the width of the panel. These gages were symmetrically positioned about the center of the panel, with the two outboard gages located approximately 5 inches from the center page. The normal deflections obtained from these gages are presented in figure 27-96. Photographs of the panel after failure are shown in figure 27-97. Thickness measurements of the panel cross section are given in table 27-25.

4. Trapezoidal corrugation compression panel elevated temperature test — The thermocouple locations for this panel are given in figure 27-98. Tab runs of the thermocouple data showing the temperature distributions for this panel are presented in table 27-26. A curve plot of the panel shortening due to the applied compression loads is given in figure 27-99. Photographs of the failed panel are shown in figure 27-100. Thickness measurements of the panel cross section are given in table 27-27.

5. Beaded compression panel room temperature test — The strain gage locations for this panel are given in figure 27-101. Curve plots of the strain gage data are presented in figure 27-102. A curve plot of the panel shortening due to the applied compression loads is given in figure 27-103. Panel deflection normal to the corrugation was measured using a dial gage located at the centerline of the panel length and width. These data are presented in figure 27-104. Panel expansion (or widening) resulting from the applied compression loads was measured by attaching a scale to the panel and recording the change in position of fiducial lines. The expansion over two corrugation pitches and four corrugation pitches is shown in figure 27-105. Photographs of the panel after failure are shown in figure 27-106. Thickness measurements of the panel cross section are given in table 27-28.

6. Tubular compression panel room temperature test — The strain gage locations for this panel are given in figure 27-107. Curve plots of the strain gage data are presented in figure 27-108. A curve plot of the panel shortening due to the applied compression loads is given in

figure 27-109. Photographs of the panel after failure are shown in figure 27-110. Thickness measurements of the panel cross section are given in table 27-29.

7. Tubular compression panel elevated temperature test – The thermocouple locations for this panel are given in figure 27-111. Tab runs of the thermocouple data showing the temperature distribution for this panel are presented in table 27-30. A curve plot of the panel shortening due to the applied compression loads is given in figure 27-112. Photographs of the failed panel are shown in figure 27-113. Thickness measurements of the panel cross section are given in table 27-31.

Shear tests. – In-plane shear tests were conducted at room temperature to evaluate the actual and predicted strength of the corrugated web design. Two specimens were prepared: one TIG welded with René 41 filler wire, the other TIG welded with Hastelloy W filler wire. The results of the shear tests are given below.

1. Shear specimen TIG welded with René 41 filler wire – The strain gage locations for this shear panel are given in figure 27-114 which included back-to-back rectangular rosette gages. The rosette gage data were reduced by means of a computer and curve plots of the principal strains and maximum shear strain versus applied cantilever loading are presented in figures 27-115 and 27-116. Photographs of the failed panel are shown in figure 27-117. No cracks were evidenced in the weld. Thickness measurements of the web cross section for this panel are given in table 27-32.

2. Shear specimen TIG welded with Hastelloy W filler wire – The strain gage locations for this panel are shown in figure 27-114. Curve plots of the principal strains and maximum shear strain versus applied cantilever loading are presented in figures 27-118 and 27-119. Photographs of the failed panel are shown in figure 27-120. No cracks were evidenced in the weld. Thickness measurements of the web cross section for this panel are given in table 27-33.

COMPARISON OF ANALYSIS AND TEST RESULTS

A summary of the correlation between the analysis and test results of the structural element test specimens is presented in table 27-34. The following observations are pertinent:

1. The initial compression buckling stress test results correlated reasonably well with initial buckling stress predictions whenever it was possible to positively identify initial buckling in either the room- or elevated-temperature tests. This correlation was noted for about half the tests. The correlation with theory for the remaining tests indicated variations of approximately 50 percent. Table 52 gives reasons for the disagreements when possible. Tests in which the variation is not explainable indicate a need for further tests.

2. The tubular and beaded-skin configurations exhibit the same sensitivity to initial imperfections and other disturbances as found in axially compressed large thin cylindrical shells. Consequently, a conservative method of predicting compression buckling was employed. Even with this conservative m ethod, large variations between test and theory were noted, as described above.

3. All of the configurations exhibit about a ±10 percent variation in thicknesses across their widths, resulting from the forming process. This is within the normal tolerance of the sheet material. The analytical methods show significant fluctuations with these thickness variations; however, fair agreement exists between test and theory when the thickness used in calculations is based on the lower limit of the tolerance.

4. The corrugation-stiffened concept demonstrated substantial post-buckling strength. Therefore, this configuration has a higher potential than the initial buckling analysis allows, providing permanent set due to inelastic deformation after initial buckling is acceptable. The test results indicated a variation of more than 20 percent over the predicted values for four of the tests performed. Of these tests, three were comparisons of the failure stresses.

5. Panel instability was obxerved in several of the tests of 30-in. specimens, and the test loads agreed favorably with the analysis based on orthotropic theory for plates simply supported on all four sides. It is shown that the wide-column analysis used in the optimization of these configurations is a simplified form of the orthotropic plate theory ($n = 0$). This theory is valid for panel width-to-length ratios of 2 or more when the unloaded edges are supported but it is conservative for ratios less than 2. However, the wide-column analysis is valid for any width-to-length ratio when tested with unsupported edges. It is concluded that the test panels demonstrated in part the validity of the

theory. However, no tests were performed for unsupported edges, for buckling due to inplane shear, or for bending due to lateral pressure. Since the optimum ratio for the hypersonic-vehicle wing structure is greater than 2, the use of wide-column analysis in the optimization program is also valid.

6. The configuration composed of a single beaded skin is susceptible to a local instability mode with a very short transverse half-wavelength, which can be predicted with reasonable accuracy. This mode of failure was accounted for in the analysis.

7. The shear-panel test specimens correlated with 7 percent of the calculated initial buckling stresses.

8. The measured initial buckling stress on the spar cap was within 5 percent of the calculated initial buckling stress.

A comparison is presented in this section between analyses and test results for the four semimonocoque wing-cover configurations, and for the circular-arc corrugated web and beam cap configurations for spars or ribs. Because of the nonconventional nature of the wing-cover configurations, three types of tests were performed: namely, (1) end closeout, (2), crippling, and (3) compression panel tests. The lengths of these test panels were nominally 9, 8, and 30 in., respectively; the end closeout panels and the crippling panels were expected to yield similar test loads for a given configuration provided no premature failure developed in the closeout area. Although the crippling panel tests were conducted to failure, primary interest centered on the test load at which local buckling developed, since local buckling rather than crippling was the mode considered in the optimization analyses for sizing hypersonic cruise vehicle structures. Crippling (failure) results are also shown to supplement the initial buckling data.

All of the compression panels were supported along their unloaded edges with slotted tubes. Because of the panel dimensions, the wide column analysis yields conservative predictions, and for this reason the general instability analysis of equation 10-34, section 10, was employed. It should be noted, however, that the wide column analysis, as used in the optimization analyses for sizing hypersonic cruise vehicle structures is an appropriate means for analyzing compression panels, when the width-to-length ratio is equal to or greater than about 2. This is shown in figure 27-12, which has been developed from the geometry for the tubular compression panel, discussed in the following paragraphs. A curve representing an unstiffened plate is also shown for comparison. The latter, of course, could represent a plate equally stiffened in the x and y directions, and shows that a predominance of stiffening in the x direction, as in the tubular configuration, causes the difference in analytical methods to decrease much more rapidly with increasing b/a. The optimum b/a developed by the optimization analyses for the semimonocoque wing-cover configurations is 2.25. Of further interest is the fact that the wide column analysis, and the general instability analysis for compression panels as represented by equation 10-34, section 10, may both be derived from the same set of equations, where m, the number of half-waves in the y-direction, is taken to zero for the wide column, and to unity for the compression panel. Thus, the theory may be tested for any panel dimensions, but for $b/a > 2$ the simpler wide column analysis may be utilized with small conservatism.

Tubular Configuration

Analysis. – The test panel drawing is shown in figure 27-1. After forming, the nominal sheet thickness of 0.010 in. varied across the panel width. Traverses of the test specimens are given in tables 27-8, 27-18, 27-20, 27-29, and 27-31 for the end closeout, room and elevated crippling, and room and elevated temperature compression panels, respectively. The cross-sectional areas presented in table 27-34 are based on the actual weights of the specimens.

A correlation between the test results for critical buckling of the circular-arcs in compression and predictions based on equation 12-14 of section 12 are presented in figure 27-122 and table 27-35. From figure 27-122, it is evident that the average stresses in the test panels at buckling for the beaded configuration were well below the predicted stresses. The tubular elevated panel test failed at an average stress greater than the predicted based on least measured thickness. With this exception, all of the panels buckled at an elastic average stress and thus plasticity reduction factors based on the average stress do not come into play.

The critical buckling stress in the arc of the tubular configuration is, therefore:

$$f_{c,cr} = 1.75\ \eta E_{el}\left(\frac{t}{R}\right)^{1.35}$$

where, $E = 29 \times 10^6$ psi at 75°F

$= 21.2 \times 10^6$ at 1400°F

$\bar{\eta} = \sqrt{\eta_T \eta_s}$ (from figs. 27-123 and 27-124)

$R = 1.05$ in.

$t = 0.011$ in.

then, $f_{c,cr} = 105\ 300$ psi at RT

$= 78\ 500$ psi at 1400°F

The initial buckling stress of the flat is based on a simple supported flat plate:

$$f_{c,cr} = 3.62\, \eta E_{el} \left(\frac{t}{b}\right)^2$$

where t = 2 x single flat thickness, in. = 0.030 in.

b = 0.556 in.

$\eta = \sqrt{\eta_T}$ (figures 27-123 and 27-124)

then $f_{c,cr}$ = 130 000 psi at RT

= 111 000 psi at 1400°F

Note that the supports along the unloaded edges of the panel are arranged to simulate the next tube; that is, the visible flat at each edge is 0.556 in. However, since the total edge width is 1.10 inches, a width of flat equal to 0.544 in. is hidden from view inside the edge support. Because this flat has a free unloaded edge, the buckling coefficient for this flat is 0.5, rather than 4.0, and the buckling stresses are 39 900 psi at room temperature and 29 200 psi at 1400°F. These are the lowest local buckling stresses in the panels and they may have precipitated buckling of the panel. Perturbations in the tubes closest to the unloaded edges of the panels due to buckling of the panel edges inside the support tubes may have occurred, indicating that a smaller flat with a small flange may be required at the panel edges. Local compression buckling in the field of the end closeout and crippling test specimens is expected to occur initially in the circular arcs at the stresses shown. Because the circular arcs are not expected to have any post-buckling strength, and they represent over 80 percent of the panel cross section, the onset of buckling also constitutes failure.

Referring to equation 10-34 of section 10, panel instability for a 30-inch panel length may be calculated when J, D_3, D_1 and k_c are formulated as follows:

1. $$\bar{J} = \frac{\alpha 4A^2 t}{pU} = 0.00922 \text{ in}^3$$

where $\bar{J}$ = effective torsional stiffness

A = enclosed area of tube = 2.488 in^2

t = thickness = 0.011 in.

p = pitch between tubes = 2.614 in.

U = circumferential length = 5.648 in.

α = correction factor = 0.50

2. $$D_3 = \frac{\overline{GJ}}{2} = \frac{\bar{J}\eta_s E}{5.2} = 0.00177\ \eta_s E$$

3. $$D_1 = \overline{EI} = 0.00824\ \eta_T E$$

4. $$k_c = \left[2\left(\frac{a}{b}\right)^2\left(\frac{D_3}{D_1}\right) + 1\right]\left(\frac{b}{a}\right)^2$$

$$= \left[2\left(\frac{30}{16.37}\right)^2\left(\frac{0.00177\eta_s E}{0.00824\eta_T E}\right) + 1\right]\left(\frac{16.37}{30}\right)^2$$

$$= 0.4296\,\frac{\eta_s}{\eta_T} + 0.2977$$

Note that the correction factor (refs. 27-5 and 27-6) is based on limited tests of corrugation-stiffened panels performed at Lockheed. In effect, it accounts for distortions of the tubes as a torsional moment varying with the amplitude of the axial wave pattern is applied to the tube. The critical stress for panel instability is now:

$$f_{c,cr} = \frac{k_c\,\pi^2 D_1}{\bar{t}b^2}$$

$$= \left(0.4296\,\frac{\eta_s}{\eta_T} + 0.2977\right)\frac{\pi^2\left(0.00824\ \eta_T E\right)}{0.0281\ (16.37)^2}$$

$$= 134\ 600\ \eta_s + 93\ 400\ \eta_T,\ \text{at } 75^\circ F$$

$$= 98\ 400\ \eta_s + 68\ 300\ \eta_T,\ \text{at } 1400^\circ F$$

$$= 146\ 500 \text{ psi at RT}$$

$$= 108\ 500 \text{ psi at } 1400^\circ F$$

A comparison of these stresses with the local buckling stresses calculated earlier shows the local buckling stresses to be critical. The proportions for the panel configuration were not necessarily optimum since the forming dies were fabricated for panels of a different material.

Test Results. — The room temperature end closeout test specimen failed at 44 000 lb, at an average stress of 85 000 psi. Because this test load was below that for the crippling test specimen, additional doublers were added to the compression panel test specimen. Examination of the strain gage data (see figs. 27-49 through 27-52) indicates some local buckling along the unloaded edges of [illegible] panel at loads below failure, as expected from the panel buckling test results. Buckling of a tube arc occurred at 43 000 lb, at an average stress of 83 000 psi. Failure followed quickly. The ratio of test-to-predicted initial buckling stress is 0.79.

The room temperature crippling test specimen failed at 47 850 lb, at an average stress of 90 400 psi. The specimen behaved very much like the end closeout specimen. The strain gage data are presented in figures 27-74 through 27-77. Buckling of a tube arc occurred between 46 000 and 47 000 lb (approximately 88 000 psi). The ratio of test-to-predicted initial buckling stress is 0.84.

The elevated temperature crippling test specimen failed without prior local buckling at 34 100 lb, at an average stress of 66 700 psi. The test data are presented in figures 27-78 through 27-80 and table 27-19. The thermocouples on the specimen indicated a small thermal gradient, which when accounted for would reduce the predicted stress by a small amount. In addition, some detached spotwelds between tubes were observed after the test. It may be shown that the buckling stress of the flat between tubes, based on one sheet thickness, is 56 000 psi at 1400°F. This stress is essentially the same as the local buckling stress for the arc of the tube (53 500 psi). Thus, the presence of some detached spotwelds was probably not a significant influence on the strength of the test specimen. The ratio of test-to-predicted initial buckling stress is 0.85, neglecting any thermal stress effects.

The room-temperature compression panel test failed without prior local buckling at 40 000 lb, at an average stress of 73 800 psi. The strain gage data are presented in figures 27-107 through 27-109. A photograph of the failed panel is shown in figure 27-110. Failure was due to local buckling of the tube walls; the failure was not significantly different from the failures in the previous tests. (See, for example, the room-temperature crippling specimen after test, fig. 27-77.) The ratio of test-to-predicted initial buckling stress is 0.70. This ratio is below those for the previous tests and probably reflects the fact that this test panel had a somewhat poorer quality than the other test panels. Note that the end closeout specimen, and the two crippling specimens were all cut from the same 30-in. long panel. Thus, the quality of these three specimens is reasonably consistent, and one would expect their ratios of test-to-predicted initial buckling stress to be rather close, which is seen to be the case.

The elevated-temperature compression panel test specimen failed without prior local buckling at 42 800 lb, at an average stress of 80 200 psi. The test data are presented in figures 27-111 through 27-113 and table 27-30. Failure was due to local buckling of the tube walls. The ratio of test-to-predicted initial buckling stress is 1.02. The relatively large amount of conservatism in the predicted stress in this case may be due to the quality of the specimen, as discussed earlier, or it may be due to some variance in the compressive elastic modulus at the test temperature. The tendency of the material to thin out in highly formed areas such as the tub arc requires use of the least material thickness in the analysis, which is quite sensitive to small changes in sheet thickness. Although panel instability was not experienced in the compression panel tests, the elevated temperature specimen reached 74 percent of the predicted panel instability stress before failing in a local buckling mode. Calculations show that in order for the present cross section to become critical in the panel instability mode, the length of the panel would have to exceed 40 inches.

Beaded Configuration

Analysis. – The test panel drawing is shown in figure 27-10. Again, the test panel cross-sectional areas presented in table 27-34 are based on the actual weights of the specimens. Traverses of the specimens are presented in table 27-7, 27-15, 27-17, and 27-28 for the end closeout, room and elevated temperature crippling and room-temperature compression panel test specimens, respectively. The arcs of the beads for analysis purposes are 0.013 in. (least measured value) in thickness; the flats between beads are 0.017 in. in thickness for all panels.

Referring to the discussion of the tubular configuration, the initial buckling stress of the crippling specimen of the beaded configuration is:

$$f_{c,cr} = 1.75 \ \eta E_{el}\left(\frac{t}{R}\right)^{1.35}$$

where $E_{el} = 29 \times 10^6$ psi at RT

$= 21.2 \times 10^6$ psi at 1400°F

$\bar{\eta} = \sqrt{\eta_T \eta_S}$ (from figs. 27-123 and 27-124)

$R = 1.05$ in.

$t = 0.013$ in. (least measure value)

then $f_{c,cr} = 130\ 000$ psi at RT

$= 92\ 500$ psi at 1400°F

The initial buckling stress of the flat is based on a simply supported flat plate:

$$f_{c,cr} = 3.62 \ \eta E_{el}\left(\frac{t^2}{b}\right)$$

where t = flat thickness = 0.017 in. (least measured value)

$b = 0.556$ in.

$\eta = \sqrt{\eta_T}$ (figs. 27-123 and 27-124)

then $f_{c,cr} = 97\ 500$ psi at 75°F

$= 71\ 200$ psi at 1400°F

As discussed for the tubular configuration, the unloaded edges of the panel are supported by tubes which grip the specimens in about the center of the available edge width. Therefore, an element with one edge free lies inside the tube. This element buckles at room and elevated temperatures at stresses substantially below the stresses noted above, and this will very likely influence the strain gage data on the nearest beads. Local compression buckling in the field of the end closeout and crippling test specimens, therefore, is expected to occur initially in the arcs of the beads at the stresses shown. The arcs are not expected to have any post-buckling strength, and buckling will also constitute failure.

If equation 10-34 of section 10 is utilized to predict local buckling which occurred during panel instability test for the beaded configuration, predictions for a 30-in. panel length and a 16.37-in. panel width are obtained, which exceed the calculated local buckling stresses reported for the crippling specimens. These predictions, however, are based on the assumption of isotropic cylinder type buckling in the panel, and the beaded panel does buckle in this manner when specimens are longer than the crippling specimens. Instead, the beads tend to behave under axial load like plates, with elastic support provided along their unloaded edges at the crests of adjacent beads. It is apparent that local buckling occurs between adjacent beads like small individual panels, and that these small panels may be analyzed by the proper application of equation 10-34. This is, indeed, the development leading to equation 12-13. Utilizing 12-13, the following prediction for panel instability is obtained (where the term "panel" refers to a single repeatable element of the beaded configuration):

$$f_{c,cr} = \frac{\pi^2 k_c D_I}{X_{II}^2 \bar{t}_L}$$

where the buckling coefficient is defined by the following equation:

$$k_c = \left(\left(\frac{2X_I}{X_{II}^2}\right)^2 \frac{D_3}{D_I} + m^2 + \frac{\beta_c^4}{m^2} \right) \left(\frac{X_{II}}{X_I^2} \right)^2$$

where the bending stiffnesses D_I, D_{II}, and D_{37}, which are defined in section 12 by equation 12-35, have the following elastic room temperature values:

D_I = 5666 lb/in.

D_{II} = 8.13 lb/in.

D_3 = 6.59 lb/in.

and the effective panel dimensions are:

X_I = 30.0 in., panel length

X_{II} = 3.085 in. effective panel width measured diagonally from crest to crest

The term β_c is defined by:

$$\beta_c = \frac{X_I}{X_{II}} \left(\frac{D_{II}}{D_I}\right)^{1/4}$$

$$\beta_c = \left(\frac{30.0}{3.085}\right) \left(\frac{8.13}{5666}\right)^{1/4} = 1.8926$$

Therefore, the minumum buckling coefficient (k_c) is attained for a half wave length of 15 inches $(m = 2)$

$$k_c = \left[\frac{2 \times \overline{30.0}^2}{3.\overline{085}^2} \left(\frac{6.59}{5666}\right) + 2^2 + \frac{1.8926^4}{2^2}\right] \left(\frac{3.085}{30.0}\right)^2$$

$$k_c = 0.0785$$

The area per unit of diagonal width, X_{II}, of the effective panel between crests is

$$\bar{t}_2 = 0.01653 \text{ in.}$$

The critical panel instability stress is then:

$$f_{c,cr} = \frac{\pi^2 k_c D_I}{X_{II}^2 \bar{t}_L}$$

$$= \frac{\pi^2 (0.0785)(5666)}{(3.085)^2 (0.01653)}$$

$$= 27{,}900 \text{ psi at room temperature}$$

The values shown above were computed by a computer program for an arc thickness of 0.015 in. and a column length of 30 in. A comparison of the above stress with the local buckling stresses calculated earlier shows the panel instability stress to be considerably lower. The room-temperature compression panel test specimen, therefore, is expected to fail in the panel instability mode with a half-wave length of about 15 in. Further computations were performed to determine if this mode might also be critical for the other, shorter test panels. For these calculations, the length of the crippling panels, which were examined first, was taken as 7 in. in order to allow for the cast material at both ends of the specimens. The panel instability stresses obtained were 72 800 psi at room temperature and 53 300 psi at 1400°F, with the panels buckling into a single half-wave in the axial direction. These stresses are based on the assumption of simply supported edges which is obviously conservative for a panel buckling into this particular pattern; a more reasonable approach would be to set the length of the panels equal to the effective column length. Thus for the crippling test specimens, assuming clamped edges, $\ell = 3.5$ in. For the end closeout specimen, $\ell = 0.7\ (8.5) = 5.95$ in., taking the cast edge clamped and the other edge simply supported. The room-temperature panel instability stress obtained for the end closeout panel is 100 000 psi. The prediction for the room-temperature crippling test specimen obviously will be higher, and by examination one may see that panel instability for the elevated-temperature crippling test specimen will not be critical. The end closeout and crippling test panels, therefore, may be expected to buckle locally and not in the panel instability mode.

Test results. - The room temperature end closeout test specimen failed at 24 950 lb, at an average stress of 84 600 psi. Because this test load was below that of the room temperature crippling specimen, additional doublers were added to the compression panel test specimen. The strain gage data (see figs. 27-45 through 27-47) indicate that buckling occurred at about 22 000 lb at an average stress of 74 500 psi. Examination of the failed specimen, figure 27-48, shows failure by crippling at the end of the edge doubler. The back-to-back strain gages 5 and 6 show a fair amount of local bending across the sheet thickness, probably because of the proximity of an imperfection. A comparison of the data for these two gages with data from gages 15 and 16 shows significantly greater strains for the former pair. It would appear that this is caused by stress concentrations at the end of the doubler between the locations for these two pairs of gages. The ratio of test-to-predicted initial buckling stress is 0.58. This low value is probably due chiefly to the stress pileup at the end of the doubler.

The room temperature crippling test specimen failed at 32 500 lb, at an average stress of 105 000 psi. The test data are presented in figures 27-67 through 27-69. Initial buckling occurred at 30 000 lb, at an average stress of 96 700 psi. The failed specimen, figure 27-70, exhibits a crippling mode of failure. The ratio of test-to-predicted initial buckling stress is 0.75, which would imply the panel was of reasonably good quality.

The elevated-temperature crippling test speciment failed at 22 100 lb, at an average stress of 72 200 psi. The test data for this panel are given in figures 27-71 and 27-72, and table 72-16. Initial buckling occurred at about 20 000 lb, at an average stress of 65 400 psi. The thermocouples indicated a small thermal gradient which would induce some thermal stress in the specimen. The photograph of the failed specimen, figure 27-73, shows a crippling mode of failure. The ratio of test-to-predicted initial buckling stress, neglecting any thermal stress, is 0.71. If the estimated thermal stress of 4300 psi is included, the ratio increases to 0.75.

The room-temperature compression-panel test specimen failed at 13 000 lb, at an average stress of 42 600 psi. The test data are given in figures 27-101 through 27-105. The failed specimen, figure 27-106, shows an obvious panel instability mode of failure, with an axial half-wave of about 10 in. Buckling occurred at about 10 000 lb, which corresponds to an average stress of 32 600 psi. The ratio of test-to-predicted panel instability stress is 1.17. It is probable that the actual edge conditions for the test were somewhat better than simply support, which, of course would add slightly to the capability of a panel buckling into two to three axial half-waves.

The same summary comments presented for the tubular configuration also apply to the beaded configuration, with the exception that panel instability is much more critical for the beaded configuration than for the tubular configuration. This of course is to be expected on the basis of the relative stiffnesses of open versus closed sections.

Corrugation-Stiffened Panel Configuration

Analysis. – The test panel drawing is shown in figure 27-73. The test panel cross-sectional areas shown in table 27-34 are based on the actual weights of the specimens. As in the previous configurations, forming caused thickness variations across the width of the panels. These variations are shown in the transverses presented in tables 27-6, 27-9, 27-11, 27-22, and 27-24 for the end closeout, room and elevated temperature crippling, and room and elevated temperature compression panel tests specimens, respectively. In the following analyses, the sides of the corrugations are 0.011 in. thick, the crests of the corrugations are 0.010-in. thick, the attach widths for the corrugations are 0.015-in. thick, and the skin to which the corrugation is attached is 0.027-in. thick. The panels are 19.00 in. wide and have 1.0-in. wide flats at either unloaded edge. The lengths of the panels are the same as in the previous configurations.

It is well known that flat sheet develops varying amounts of postbuckling strength depending upon the configuration in which it is used. Although the determination of initial buckling stresses was the primary purpose of the tests, the panels were taken to failure, which occurred in all the specimens at significantly higher loads. Predictions for crippling and panel instability are provided here as supplemental information to correlate with these failure stresses.

The initial buckling stress for the sides of the corrugations may be obtained from:

$$f_{c,d,cr} = \frac{k_{c,d}\,\pi^2\,\eta^*_{ST}\,E_{el}}{12(1-\nu^2)}\left(\frac{t}{d}\right)^2$$

where

$b/d = 0.65/0.82 = 0.793$

$k_{c,d} = 4.7$ (refer to section 12)

$\eta^*_{ST} = 1.0$ Stowell's plasticity correction factor

$d/t = 0.82/0.011 = 74.5$

then

$f_{c,d,cr} = 22\,200$ psi at RT

$= 16\,200$ psi at 1400°F

The initial buckling stress for the crests of the corrugations is based on:

$$f_{c,cr} = 3.62\ E_{el} \left(\frac{t}{b}\right)^2$$

where

$b = 0.656$ in.

$t = 0.010$ in.

then

$f_{c,cr} = 24\ 400$ psi at RT

$= 17\ 800$ psi at 1400°F

The initial buckling strength of the skin is based on the equation above:

where

$b = 2.125 - 0.38 = 1.745$ in. (between spotwelds)

$t = 0.027$ in.

then

$f_{c,cr} = 25\ 000$ psi at RT

$= 18\ 300$ psi at 1400°F

Thus local buckling in the corrugation-stiffened configuration may be expected to occur initially in the sides of the corrugation. However, the buckling stresses for all of the elements of the cross section, except the flats between corrugations, are close enough together that buckling may well occur initially in any one of them.

Panel instability for a 30-in. panel length may be calculated with equation 10-34. The quantities J, D_3, D_1 and k_c are defined as follows:

$$\bar{J} = \frac{\alpha\, 4A^2}{p \sum \left(\frac{U_1}{t_1} + \frac{U_2}{t_2} + \ldots\right)} = 0.001986$$

where

A = the enclosed area of the corrugation = 0.7906 in.^{2}

p = the pitch = 2.125 in.

$$\sum\left(\frac{U_1}{t_1} + \frac{U_2}{t_2} + \ . \ . \ .\right) = 296.146$$

α = correction factor = 0.50

$$D_3 = \frac{\bar{G}\ \bar{J}}{2} = 0.000382\ \eta_s\ E$$

$$D_1 = \bar{E}\ \bar{I} = 0.002521\ \eta_T\ E$$

$$k_c = \left[2\left(\frac{a}{b}\right)^2\left(\frac{D_3}{D_1}\right) + 1\right]\left(\frac{b}{a}\right)^2$$

$$= \left[2\left(\frac{30}{17.65}\right)^2\left(\frac{0.000382\quad \eta_s E}{0.002521\quad \eta_T E}\right) + 1\right]\left(\frac{17.65}{30}\right)^2$$

$$= 0.649$$

The basis for taking $\alpha = 0.50$ is the same as discussed for the tubular configuration. The critical stress for panel instability is now:

$$f_{c,cr} = \frac{k_c\ \pi^2\ D_1}{\bar{t}\ b^2}$$

$$= 0.649\ \frac{\pi^2\ (0.002521\ E)}{(0.809/17.65)\ 17.65^2}$$

$f_{c,cr}$ = 32 900 psi at RT

$f_{c,cr}$ = 24 000 psi at 1400°F

A comparison of these stresses with the local buckling stresses calculated earlier shows that local buckling should precede panel instability in the compression panel tests. However, since local buckling does not constitute failure in this configuration, the panels are expected to sustain additional load and fail in the panel instability mode. The effect of local buckling on panel instability is to decrease the effective stiffness of the cross section. Studies conducted at Lockheed (ref. 27-8) on this configuration in aluminum indicate, however, that the effect has slight influence on panel ultimate capability, even when local buckling occurs at one-half of the expected ultimate load.

Crippling of the composite cross section may be predicted using the method presented in LAC Stress Memo 80C (see also ref. 27-7 for a description of this method). Because of the thinness of the corrugated sheet at the attachment joint, and the width of flat required in order to place two rows of spots between corrugations, the joint was checked for wrinkling instability (using the methods of ref. 27-9) and found to be not critical. Therefore, one may expect the configuration to carry the average crippling stress computed from the above reference. Using the material properties from figure 27-122 and 27-123, and the thicknesses cited previously, the following average crippling stresses are obtained:

$$f_{cc} = 55\,000 \text{ psi at RT}$$

$$f_{cc} = 41\,500 \text{ psi at } 1400°\text{F}$$

Note that panel instability is expected to occur in the compression panel tests prior to the onset of crippling.

Test results. - The room-temperature end closeout test specimen failed at 35 950 lb, at an average stress of 47 300 psi. The test data are presented in figures 27-41 through 27-43. Failure occurred at the top edge of the panel as pictured in figure 27-44. Bending due to the eccentricity of the end load is apparent in the strain gage data at an early stage of the test. The gages show nonuniformities at about 20 000 lb which presumably signaled the onset of local buckling. The average stress at this load level is 26 300 psi. The ratio of test-to-predicted initial buckling stress is 1.19.

The room-temperature crippling test specimen failed at 53 700 lb, at an average stress of 69 200 psi. The test data are presented in figures 27-53 through 27-55. From this data, it may be determined that initial buckling occurred at about 26 000 psi. The ratio of test-to-predicted initial buckling stress, therefore, is 1.17. The specimen after failure is shown in figure 27-56. A crippling mode of failure is apparent. The ratio of test-to-predicted failure stress is 1.26. Note that the specimen at failure carried twice the initial buckling stress because of the post-buckling capability of the corners in the cross section of the specimen.

The elevated-temperature crippling test specimen failed at 35 000 lb, at an average stress of 43 700 psi. The test data for this specimen are given in figures 27-57 and 27-58, and table 27-10. These data indicate initial buckling took place at about 30 000 psi, which is rather high compared to the predicted initial buckling stress of 16 200 psi. This disparity is due to the absence of strain gages in the elevated temperature tests and difficulties in making visual observations in these same tests. There can be little doubt that some initial buckling did take place at a stress level which is more compatible with the predicted stress. Figure 27-59 shows the specimen after test; a crippling failure is apparent. The ratio of test-to-predicted failure stress is 1.05. Again, the specimen supported a large load increment above the initial buckling load before failure occurred. A small thermal gradient in the panel can be noted from the test data, but it has been neglected in the above comparisons.

The room-temperature compression panel test specimen failed at 32 000 lb, at an average stress of 39 600 psi. The test data are presented in figures 27-85 through 27-88. The failed specimen is shown in figure 27-89. This specimen had a blow after fabrication measuring approximately 0.1 in. at the center of the panel. This, combined with the fact that the end load is attached eccentric to the centroid of the cross section of the panel, resulted in substantial bending in the panel as indicated by the strain gage data. Because none of the gages were back-to-back pairs, the onset of initial buckling under these conditions was not clearly defined. It is estimated that initial buckling occurred at 20 000 lb, or at an average stress of 24 700 psi. The ratio of te[illegible]-to-predicted initial buckling stress, therefore, is 1.11. As indicated i[illegible] figure 27-89, the specimen failed in the panel instability mode. The ratio of test-to-predicted failure stress is 1.20.

The elevated-temperature compression panel test speciment failed at 25 900 lb, at an average stress of 32 000 psi. The test data are given in figures 27-90 and 27-91, and table 27-23. The specimen after test is pictured in figure 27-92. Again, the onset of initial buckling was difficult to determine exactly; from the load shortening curve, figure 27-91, it was estimated to have occurred at 14 000 lb, or at an average stress of 17 300 psi. The ratio of test-to-predicted initial buckling stress is then 1.07. The test data indicate a small thermal gradient in the panel, but this was considered insignificant in view of the approximate nature of the test initial buckling stress. The long axial half-wave buckle pattern associated with panel instability results in a specimen after test which does not show definite indications of the mode of failure as one would find, for example, in a crippling failure. The ratio of test-to-predicted failure stress is 1.33.

In summary, the trapezoidal corrugation-stiffened configuration tests and analytical predictions correlate reasonally well, both for initial buckling and failure. Conservatism in the predicted initial buckling stresses is due in some degree to the fact that the widths of the corrugation elements ignore the presence of bend radii. The importance of a capability for predicting initial buckling is here somewhat reduced, compared to the two previous configurations, because of the post buckling strength of the flat elements in the cross section of the configuration.

Trapezoidal Corrugation Panel Configuration

Analysis. – The test panel drawing is shown in figure 27-17. As in previous configurations, the panel cross-sectional areas presented in table 27-34 are based on the actual weights of the panels because of nonuniformities across the panel widths due [illegible] forming. Traverses of the specimens are presented in tables 27-12, 27-1[illegible] 27-25, and 27-27 for the room and elevated crippling, and room and eleva[illegible]ed temperature compression panel test specimens, respectively. The panels we[illegible] 19.46 in. wide with a 0.715-in. flat along each vertical edge. End closeout [illegible]plices were simulated in the compression panel test specimens by cutting the 30-in. long panel at a distance of 3.90 in. from each end, inserting a zee section of 0.020-in. sheet with 0.95-in. flanges, and spotwelding an 0.040-in. sheet finger doubler to each side. Each end of all of the specimens was embedded in Densite or Pyroform (for elevated temperature tests) to a depth of one inch.

This configuration, like the previous configuration, is expected to develop some post-buckling strength because the cross section of the configuration consists of a number of corners. Therefore, both initial buckling and failure stresses will be calculated.

The initial buckling stress of the corrugation is:

$$f_{c,d,cr} = \frac{k_{c,d}\, \pi^2\, \eta_{ST}^{**}\, E_{el}}{12(1-\nu^2)} \left(\frac{t}{d}\right)^2$$

where

$k_{c,d}$ = 4.4, the buckling coefficient for b/d = 0.9 (refer to section 12)

η^{*}_{ST} = 1.0, Stowell's plasticity correction factor (refer to section 12)

E_{el} = 29×10^6 psi at room temperature

= 21.2×10^6 psi at 1400°F

t = 0.016 in.

d = 0.65 in. = the widest element in the cross section

then

$f_{c,d,cr}$ = 69 600 psi at RT

= 50 800 psi at 1400°F

Crippling of the trapezoidal corrugation may be calculated using the methods of LAC Stress Memo 80C. Based on the stress strain data of figures 27-121 and 27-122, the average crippling stress at room temperature is 86 600 psi; at 1400°F, the average crippling stress is 64 300 psi. Note that the differences here between initial buckling and crippling (failure) are much smaller than in the corrugation-stiffened skin configuration.

Panel instability was calculated both for the full panel width, and for a single corrugation (the same as for the circular beaded configuration). Because of the close spacing of the trapezoidal corrugations and the lack of a flat link for hinge between corrugations, the calculated panel instability stress for buckling of a single corrugation is in excess of 100 000 psi at room temperature. This stress is substantially larger than the calculated crippling stress at room temperature; thus, this mode is not critical and details are not presented here. The panel instability stress for the full panel width may be calculated from equation 10-34. In performing these calculations, it is necessary to note that the edge conditions along the loaded edges of the compression panels for all of the previous configurations conformed closely with the assumption of simply supported edge conditions, which is inherent in equation 10-34. The edge conditions in the present compression panels are significantly different; the ends of the panels are cast to a depth of one inch in a matrix, and, in addition, a transverse splice is built into the panel at a distance of 3.90 in. from each end. It will be assumed that the transverse members provide the panel with an elastic support. From an analysis of the stiffness of this support, an effective panel length L' may be determined. Thus, examining the splice geometry:

$$K' = \frac{384}{5} \frac{E\,I}{L_1^3} = 0.0001004E \quad (\text{lb/in.})$$

where

$I = 0.00765$ in.^{4} (approximately) for the zee and splice plates

$L_1 = 18.03$ in., length of the zee

and

$$q = \frac{K'\,L^3}{8EI} = 126$$

and

$$x/L = 0.733$$

where

$I = 0.0215$ in.^{4} for the panel

$L = 30$ in. for the panel

$x = 22$ in., the distance between the zees

then

$c = 4.3$ from figure C2.26 of reference 27-3 (for $q = 126$ and $x/L = 0.733$)

and

$$L' = a = \frac{L}{\sqrt{c}} = \frac{30}{2.075} = 14.45$$

Now, referring to equations 10-34:

$$\sigma = \frac{K_c \pi^2 D_1}{\bar{\bar{t}}\, b^2}$$

where

$$k_{c_{min}} = 1.805 \quad (m = 1)$$

$$b = 19.46 \text{ in.}$$

$$t = 0.390/19.46 = 0.020 \text{ in.}$$

$$D_1 = 0.0215 \; E/19.46 = 0.001105E$$

then

$$f_{c,cr} = 75\,200 \text{ psi at RT}$$

$$= 55\,100 \text{ psi at } 1400^{\circ}\text{F}$$

The panel instability stresses are lower than the crippling stresses calculated earlier; thus, the compression parel test specimens are expected to fail in the panel instability mode. Calculations for panel instability in the 8-in. long crippling panels yield predictions much higher than the predicted crippling stresses. These panels, therefore, are expected to fail in crippling.

Test results. — The room-temperature crippling test specimen failed at 37 600 lb, at an average stress of 92 400 psi. The test data are presented in figures 27-60 through 27-62. The failed panel, shown in figure 27-63, shows a crippling mode of failure. Initial buckling occurred at an average stress of approximately 69 600 psi. The ratio of test-to-predicted initial buckling stress, therefore, is 1.0. The ratio of test-to-predicted failure stress is 1.07.

The elevated temperature crippling test specimen failed at 26 900 lb, at an average stress of 66 800 psi. The test data are given as figures 27-64 and 27-65, and table 27-13. The specimen after test, shown in figure 27-66, exhibits a crippling mode of failure. From the load-shortening curve, it appears that initial buckling occurred at about 22 000 lb, at an average stress of 54 500 psi. A small thermal gradient was observed in the panel, but its affect was neglected because of the approximate manner in which initial buckling was determined. The ratio of test-to-predicted initial buckling stress is 1.07. The ratio of test-to-predicted failure stress is 1.04.

The room-temperature compression panel test specimen failed at 29 500 lb, at an average stress of 75 600 psi. The test data are presented in figures 27-93 through 27-96. The strain gage data indicate initial buckling occurred at an average stress of about 69 300 psi. The ratio of test-to-predicted initial buckling stress is 1.0. The specimen, shown after test in figure 27-97, failed in panel instability mode with one half-wave in the axial direction. The onset of initial buckling prior to failure by panel instability may be expected to reduce the stiffness of the panel to some degree, which has not been taken into account in the prediction for panel instability. In this test, the ratio of test-to-predicted failure stress is 1.01. This ratio is somewhat less than the ratios obtained in other tests failing in panel instability, and is probably due to the interaction of the initial buckling and panel instability modes.

The elevated-temperature compression panel test specimen failed at 19 950 lb, at an average stress of 49 800 psi. The test data are given in figures 27-98 and 27-99, and table 27-26. The load shortening curve is reasonably linear up to the failure load, and on this basis, initial buckling and failure are considered coincident. The maximum thermal gradient in the panel is 26°F, which does not appear to be large enough to be a significant factor in the behavior of the panel. The specimen after failure is pictured in figure 27-100; numerous local (initial) buckles can be seen. On the basis of the crippling test results, and the room-temperature compression panel test result, it is apparent that the configuration has some post buckling strength which may be limited by panel instability. Since this test specimen did not develop any post buckling strength, it is concluded that loss of stiffness caused by initial buckling (and/or the geometric abnormalities) triggered premature failure of the specimen in the panel instability mode. This interaction between modes results in a ratio of test-to-predicted failure stress of 0.90; the ratio of test-to-predicted initial buckling stress is 0.98.

The same summary remarks can be made here as were made previously for the corrugation-stiffened skin configuration. It is apparent in comparing the two configurations that the corrugation has less post buckling strength. In addition, the corrugation compression panels are nearer to being optimum than their corrugation-stiffened skin counterparts, since initial buckling and panel instability occurred nearly simultaneously in the corrugation compression panels. It is important to note that there is apparently some interaction between these modes when they are close to each other. This interaction results in a somewhat lower panel capability than when either of these modes is critical alone.

Circular-Arc Corrugation Shear Panel Configuration

Analysis. - The test panel drawing is shown in figure 27-28. Traverses of the two room-temperature test specimens are presented in tables 27-32 and 27-33, which indicate that the specimens may be considered to be of uniform thickness, namely, 0.0151 and 0.0145 in., respectively. The analysis for these specimens also covers both initial buckling and failure. Initial buckling, which may be expected to occur in the circular arcs, does not necessarily mean that the panel cannot carry additional load. Therefore, analyses for panel instability and web rupture are also presented.

The shear stress for initial buckling may be calculated from equation 11-6 of section 11.

$$f_{s,cr} = 1.55\sqrt{\eta_T}\, E_{el}\left(\frac{t}{2R}\right)^{3/2}$$

where

E_{el} = 29 x 10^6 psi

t = 0.0151 in. and 0.0145 in. for test specimens 1 and 2, respectively

R = 0.80 in.

then

$$f_{s,cr} = 41\,200 \text{ psi for } t = 0.0151 \text{ in.}$$

$$= 38\,700 \text{ psi for } t = 0.0145 \text{ in.}$$

Note that equation 11-6 is based on extensive tests and is applicable for corrugation half-angles between 20 and 90 deg. It is assumed that this equation a applies both to initial buckling of the arcs of the corrugation and to buckling of the corrugation between adjacent arc crests, should this latter mode occur within the range of corrugation half-angles cited.

The shear stress for panel instability may be calculated from equations 10-36 through 10-37b:

$$f_{s,cr} = \frac{k_s \pi^2 \left(D_1 D_2^3\right)^{1/4}}{b^2 t}$$

where

K_s = 3.3 (from fig. 10-8)

a = 17.00 in.

b = 15.62 in.

$$\left.\begin{aligned} D_1 &= 6.86 \text{ lb/in.} \\ D_2 &= 46\,000 \text{ lb/in.} \\ D_3 &= 12.14 \text{ lb/in.} \end{aligned}\right\} \text{ for } t = 0.0151 \text{ in.}$$

$$\left.\begin{aligned} D_1 &= 6.08 \text{ lb/in.} \\ D_2 &= 44\,200 \text{ lb/in.} \\ D_3 &= 10.73 \text{ lb/in.} \end{aligned}\right\} \text{ for } t = 0.0145 \text{ in.}$$

then $$f_{s,cr} = 44\,200 \text{ psi for } t = 0.0151 \text{ in.}$$

$$= 43\,300 \text{ psi for } t = 0.0145 \text{ in.}$$

Data are presented in NACA TN-2661 (ref. 27-10) for the allowable web gross area shear stress for two aluminum alloys as a function of the diagonal tension factor k. It may be shown that approximate values for other materials may be obtained by multiplying $f_{s,max}$ for 2024-Tw aluminum by the ratio of the ultimate tensile stress of the new material to the ultimate tensile stress of 2024-T3 (62 000 psi). Taking F_{tu} = 165 000 psi for René 41 and k = 0.1, $f_{s,max}$ for the shear panels is 68 000 psi.

The analysis shows initial buckling and panel instability occurring rather close together; one might expect, therefore, some interaction between these modes modes.

Test results. – The room-temperature shear panel test specimens failed at 9500 lb (t = 0.0151 in.) and 8700 lb (t = 0.0145 in.). These loads represent average shear stresses of 40 500 psi and 38 400 psi, respectively. The test data are presented in figures 27-114 through 27-120. From these data, it appears that the thicker specimen buckled locally at an average shear stress of about 38 500 psi. The specimen carried only a small additional increment of load before failure. The thinner specimen showed no signs of initial buckling prior to failure. Both specimens developed the panel instability mode of failure, followed by rupture of the web (see figs. 27-117 and 27-120). The ratio of test-to-predicted initial buckling stress for the two specimens are 0.93 (t = 0.0151 in.) and 0.99 (t = 0.0145 in.). The ratios of test-to-predicted failure stress are likewise 0.92 and 0.89. It is apparent that the nearness of the initial buckling and panel instability modes in these specimens resulted in some interaction between the modes, which lowered the capability of the panels. The rupture of the webs is considered to be an aftereffect of primary failure in the panel instability mode.

Spar Cap Configuration

Analysis. – The test specimen drawing is presented in figure 27-33; thickness measurements are recorded in table 27-21. These measurements indicate a cap thickness of 0.058 in. in the region of failure. Analyses for initial buckling and crippling of the cap follow.

Initial buckling in compression of the cap may be calculated from the equation:

$$f_{c,cr} = 3.62\sqrt{\eta_T}\, E_{el} \left(\frac{t}{b}\right)^2$$

where

η_T = 0.99 (see fig. 27-125)

E_{el} = 29×10^6 psi

t = 0.058 in.

b = 1.79 in. = the maximum unsupported distance in the cap between the corrugated web and the edge bend radius

then

$$f_{c,cr} = 110\ 000 \text{ psi}$$

The crippling stress as determined from LAC Stress Memo 126* is:

Element	A_n, in.^{2}	b/t or (R/t)	f_{cc_n}, psi	$f_{cc_n} A_n$, lb
(0.192 x 0.058)2	0.02227	3.31	56 000**	1247
(0.125R x 0.058)2	0.02806	(2.65)	55 200	1549
(1.607 x 0.058)	0.09321	27.7	29 100	2712
(0.777 x 0.058)	0.04507	13.4	57 000	2569
Σ	0.1886			8077

* The LAC Stress Memo Manual recommends Stress Memo 120 for the crippling analysis of single sections, and Stress Memo 80C for the crippling analysis of stiffeners attached to panels. The use of Stress Memo 80C here would yield a lower average stress, namely, 114 000 psi. Stress Memo 126 utilizes the unit material approach; MCF is the material correction factor.

** One edge free; other flat elements have no edge free.

Assume

$$F_{cy}/E_c = F_{ty}/E$$

$$= 146\ 000/29\ 000\ 000 = 0.00503$$

$$k_m = 0.0214 \text{ (fig. 15 of LAC Stress Memo 126)}$$

$$MCF = 0.0214 \times 146 = 3.12$$

then

$$f_{cc} = \frac{\Sigma\left(f_{cc_n} A_n\right)}{\Sigma A_n} (MCF)$$

$$= \frac{8077 \times 3.12}{0.1886} = 133\ 500 \text{ psi}$$

Test results. – The spar cap crippling specimen failed at 48 000 lb, at an average stress (for two beam caps) of 127 200 psi. The test data are given in figures 27-81 through 27-84. These data show initial buckling occurring at an average stress of about 104 000 psi. The ratio of test-to-predicted initial buckling stress is 0.95; the ratio of test-to-predicted failure stress is also 0.95. Using the more conservative crippling analysis of Stress Memo 80C, rather than that of Stress Memo 126*, results in a test-to-predicted failure stress ratio of 1.12. In this analysis, the crippling stress for the element for which initial buckling is calculated above is 83 500 psi. This value is probably conservative; on the other hand it may be optimistic to consider this element to be simply supported along both unloaded edges. In summary, the predicted stresses are somewhat high and consideration should be given to the use of more conservative methods.

REFERENCES

27-1 Wilhelm, K. A.: Preparation of Sub-Elements for Materials and Process Development Tests. CMRI-1465, Lockheed-California Co., 1968.

27-2 Panik, J. J.: Spot Welding of Structural Elements for Hypersonic Cruise Vehicle Wing Structure. CMRI-1465-2, Lockheed California Co., 25 July 1968.

27-3 Bruhn, E. F.: Analysis and Design of Flight Vehicle Structures. Tristate Offset Co., 1965.

27-4 Donnell, L. H.; and Wan, C. C.: Effect of Imperfections on Buckling of Thin Cylinders and Columns Under Axial Compression. Journal of Applied Mechanics, March 1950, pp. 73-83.

27-5 Dooley, J. F.: On the Torsional Stiffness of Closed-Section Web Stiffners. Int. J. Mech. Sci., 1965, Vol. 7, pp 183-196.

27-6 Bushnell, D.; Almroth, B. O.; and Sobel, L. H.: Buckling of Shells of Revolution with Various Wall Constructions. Volume II, Basic Equations and Method of Solution, NASA-CR-1050, May 1968.

27-7 Cozzone, F. P.; and Melcon, M. A.: Nondimensional Buckling Curves – Their Development and Applications. Journal of Aeronautical Sciences, October 1946, pp. 511-517.

27-8 Holmes, A. M. C.: Compression Tests on Large Panels Having Corrugated Reinforcement. LMSC F-70-69-2, June 1969.

27-9 Semonian, J. W.; and Peterson, J. P.: An Analysis of the Stability and Ultimate Compressive Strength of Short Sheet Stringer Panels with Special Reference to the Influence of Riveted Connection Between Sheet and Stringer. NASA TN-3431, March 1955

27-10 Kuhn, Paul; Peterson, J. P.; and Levin, L. R.: A Summary of Diagonal Tension. Part I – Methods of Analysis, NASA TN-2661, May 1952.

TABLE 27-1

STRUCTURAL-ELEMENT TEST SCHEDULE

Test-panel configuration	Type of test	Number of panels tested: End closeout	Crippling		Compress. panel		Inplane shear
	Temp, ^{o}F	RT	RT	1400	RT	1400	RT
Tubular 		1	1	1	1	1	–
Beaded 		1	1	1	1	–	–
Corrugation-stiffened 		1	1	1	1	1	–
Trapezoidal-corrugation 		–	1	1	1	1	–
Shear web 		–	–	–	–	–	2
Channel cap 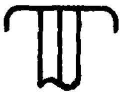		–	1	–	–	–	–
Total number of panels		3	5	4	4	3	2
Grand total							21

TABLE 27-2

SUMMARY OF PANEL ELEMENT FABRICATION

Panel description	Panel type	Panel size, in.	No. of panels fabricated
Tubular	End closeout Crippling Compression panel	9.0 x 17.37 8.0 x 17.37 30.0 x 17.37	1 2 2
Beaded	End closeout Crippling Compression panel	9.0 x 17.37 8.0 x 17.37 30.0 x 17.37	1 2 2
Corrugation stiffened skin	End closeout Crippling Compression panel	9.0 x 19.00 8.0 x 19.00 30.0 x 19.00	1 2 2
Trapezoidal corrugation	Crippling Compression panel	8.0 x 19.46 30.0 x 19.46	2 2
Circular arc corrugation	Shear	15.62x 17.00	2
Channel cap	Crippling	5.50x 2.75 x .38	1
Total No. of panels			22

TABLE 27-3

INSTRUMENTATION SCHEDULE FOR STRUCTURAL ELEMENT TESTS

Panel configuration	Type of test	End closeout	Crippling		Compression Panel		In-plane shear
	Panel size,[a] in.	9 x (W)	8 x (W)		30 x (W)		15 x 15
	Test temperature, °F	RT	RT	1400	RT	1400	RT
Tubular	No. panels	1	1	1	1	1	0
	No. strain gages	22	18	0	33	0	0
	No. thermocouples	0	0	15	0	20	0
Beaded	No. panels	1	1	1	1	1	0
	No. strain gages	22	16	0	44	0	0
	No. thermocouples	0	0	15	0	15	0
Corrugation-stiffened	No. panels	1	1	1	1	1	0
	No. strain gages	25	14	0	37	0	0
	No. thermocouples	0	0	15	0	20	0
Trapezoidal corrugation	No. panels	0	1	1	[illegible]	1	0
	No. strain gages	0	16	0	42	0	0
	No. thermocouples	0	0	15	0	20	0
Shear web	No. panels	0	0	0	0	0	2
	No. strain gages	0	0	0	0	0	6
	No. thermocouples	0	0	0	0	0	0
Channel cap	No. panels	1	0	0	0	0	0
	No. strain gages	2	0	0	0	0	0
	No. thermocouples	0	0	0	0	0	0

[a] W = panel width

TABLE 27-4

MECHANICAL PROPERTIES DATA FOR SOME RENÉ 41 COMPRESSION PANEL MATERIALS SUBJECTED TO VARIOUS THERMAL CYCLES

Test panel configuration	Tubular and corrugation-stiffened skin panels		Beaded panel		Beam cap crippling and shear panels
Element of panel	Corrugations for both configurations		Bead		Caps
Material gage, in.	.016		.019		.060
Grain direction	Longitudinal		Longitudinal		Longitudinal
Heat No.	HT-2490-7-8513		HT-2490-7-8248		E96091
Thermal cycle[a]	Exposed to three anneal cycles and aged		Exposed to 2 anneal cycles and aged		Aged
Coupon test temperature	RT	1400°F	RT	1400°F	RT
Properties Mechanical					
F_{tu}, ksi	165	129	160	127	195
F_{ty}, ksi	135	115	153	118	146
% elong (1 inch gage)	7	5	3	4	21
E, psi x 10^{-6}	29	22.6	29	18.4	29
Ramberg Osgood parameters					
$F_{0.7}$, ksi	135	109	154	120	147
Shape parameter, n	21	18	36	18	25

[a] Anneal cycle: Heated to 1950°F for 15 minutes, air cooled; then aged 1400°F for 16 hours and air cooled

Aging cycle: Heated to 1400°F for 16 hours and air cooled

TABLE 27-5

SUMMARY OF PANEL ELEMENT TEST RESULTS

Panel figure number	Panel description	Test temperature, °F	Panel area by weight, in^2	Ultimate load, kips	Average ultimate stress, ksi
27-23	Corrugation-stiffened end-closeout panel	RT	.760	35.95	47.30
27-10	Beaded end-closeout panel	RT	.295	24.95	84.58
27-1	Tubular end-closeout panel	RT	.517	44.00	85.11
27-23	Corrugation-stiffened crippling panel	RT 1400	.776 .801	53.70 35.0	69.20 43.70
27-17	Trapezoidal corrugation crippling panel	RT 1400	.407 .403	37.6 26.9	92.38 66.75
27-10	Beaded crippling panel	RT 1400	.310 .306	32.5 22.1	104.84 72.22
27-1	Tubular crippling panel	RT 1400	.528 .512	47.85 34.10	95.51 66.60
27-23	Corrugation-stiffened compression panel	RT 1400	.809 .809	32.0 25.9	39.56 32.01
27-17	Trapezoidal corrugation compression panel	RT 1400	.390 .401	29.5 19.95	75.64 49.75
27-10	Beaded compression panel	RT	.307	13.1	42.67
27-1	Tubular compression panel	RT 1400	.542 .534	40.0 42.8	73.80 80.15
27-33	Beam cap crippling (3/8 in. LIP)	RT	[a].406	48.0	118.2
27-28	Shear panel (Rene 41 filler)	RT	15.5-in. length	9.5	[b]613 lb/in.
27-28	Shear panel (Hastelloy filler)	RT	15.5-in. length	8.7	[b]561 lb/in.

[a]Area of two caps

[b]Ultimate shear flow

TABLE 27-6

THICKNESS MEASUREMENTS OF CORRUGATION-STIFFENED END-CLOSEOUT PANEL

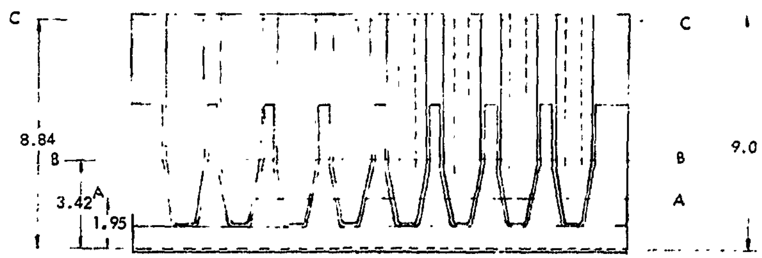

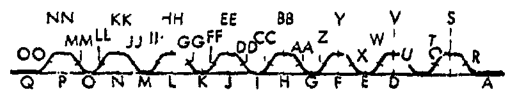

SECTION	A	B	C	D	E	F	G	H	I	J	K	L	M	N	O	P	Q	R	S	T	U
AA	.1012	.0246	.0995	.0248	.1002	.0249	.0972	.0248	.1004	.0246	.0987	.0246	.0974	.0248	.0998	.0247	.0967	.0130	.0128	.0128	.0130
BB	.0764	.0254	.0746	.1253	.0749	.0253	.0746	.0256	.0745	.0253	.0758	.0252	.0756	.0251	.0752	.0257	.0758	.0125	.0114	.0114	.0110
CC	.0444	.0255	.0424	.0250	.0433	.0250	.0431	.0251	.0430	.0251	.0423	.0252	.0422	.0252	.0422	.0252	.0429	.0115	.0110	.0117	.0115

SECTION	V	W	X	Y	Z	AA	BB	CC	DD	EE	FF	GG	HH	II	JJ	KK	LL	MM	NN	CO	-
AA	.0121	.0124	.0128	.0120	.0119	.0126	.0121	.0125	.0124	.0115	.0125	.0120	.0117	.0122	.0125	.0115	.0114	.0118	.0116	[illegible]	-
BB	.0114	.0121	.0130	.0110	.0118	.0115	.0117	.0113	.0114	.0116	.0119	.0118	.0112	.0112	.0118	.0115	.0116	.0120	.0117	.0117	-
CC	.0107	.0113	.0113	.0108	.0110	.0116	.0109	.0112	.0115	.0108	.0109	.0115	.0109	.0111	.0114	.0107	.0112	.0114	.0107	.0112	-

TABLE 27-7

THICKNESS MEASUREMENTS OF BEADED END-CLOSEOUT PANEL

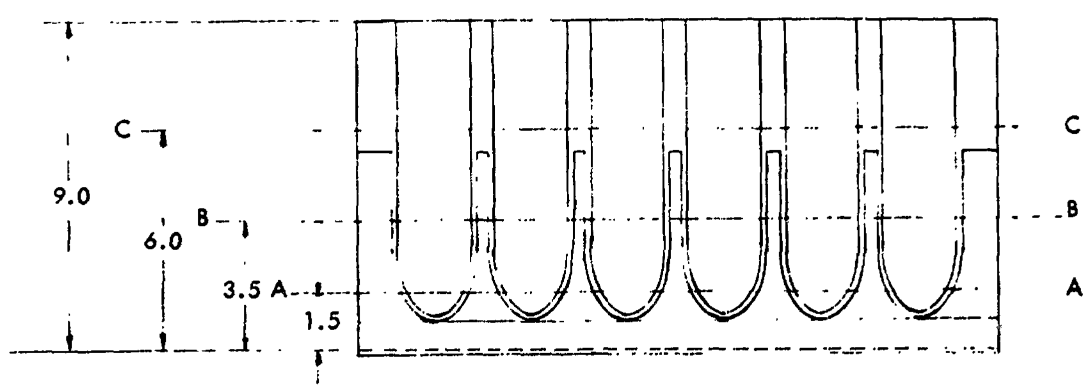

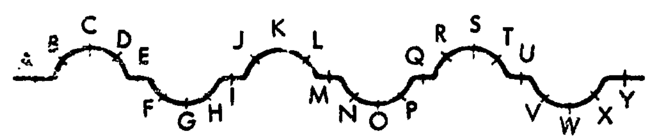

SECTION	A	B	C	D	E	F	G	H	I	J	K	L	M
AA	.0832	.0162	.0152	.0160	.0863	.0158	.0152	.0159	.0832	.0158	.0152	.0160	.0837
BB	.0846	.0138	.0133	.0135	.0834	.0135	.0133	.0132	.0862	.0134	.0138	.0129	.0863
CC	.0184	.0151	.0152	.0158	.0187	.0137	.0148	.0140	.0192	.0170	.0152	.0180	.0175
SECTION	N	O	P	Q	R	S	T	U	V	W	X	Y	-
AA	.0159	.0155	.0159	.0836	.0159	.0152	.0156	.0834	.0158	.0149	.0158	.0842	-
BB	.0132	.0129	.0133	.0856	.0134	.0131	.0135	.0882	.0132	.0132	.0135	.0836	-
CC	.0164	.0167	.0135	.0196	.0148	.0144	.0141	.0207	.0160	.0170	.0140	.0190	-

TABLE 27-8

THICKNESS MEASUREMENTS OF TUBULAR END-CLOSEOUT PANEL

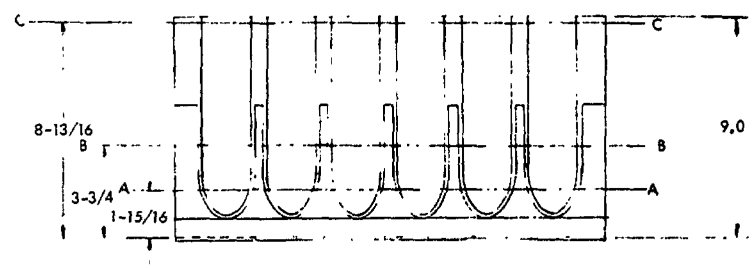

SECTION	A	B	C	D	E	F	G	H	I	J	K	L	M	N	O	P	Q	R	S	T	U	V
AA	.0950	.0136	.0131	.0136	.0950	.0133	.0132	.0133	.0952	.0138	.0133	.0138	.0945	.0138	.0134	.0138	.0950	.0134	.0132	.0138	.0940	.0133
BB	.0960	.0113	.0115	.0118	.0950	.0112	.0115	.0114	.0952	.0114	.0113	.0115	0950	.0116	.0119	.0115	.0950	.0116	.0118	0115	0962	.0114
CC	.0485	.0127	.0130	.0115	.0434	.0115	.0115	.0117	.0328	.0121	.0122	.0115	.0327	.0115	.0118	.011[illegible]	.0416	.0116	.0120	.0118	.0495	.0120
SECTION	W	X	Y	Z	AA	BB	CC	DD	EE	FF	GG	HH	II	JJ	KK	LL	MM	NN	OO	PP	QQ	-
AA	.0132	.0134	.0940	.0132	.0128	.0132	.0131	.0130	.0132	.0132	.0128	.0132	.0132	.0130	.0132	.0132	.0130	.0132	.0130	0130	0130	-
BB	.0115	.0[illegible]16	.0945	.0113	.0112	.0113	.0112	.0109	.0112	.0111	.0112	.0113	.0112	.0112	.0112	.0112	.0112	.0114	0112	.0112	.0113	-
CC	.0116	.0113	.0313	.0125	.0125	.0116	.0113	.0116	.0115	.0118	.0118	.0118	.0114	.0116	.0112	.0116	.0120	0116	.0123	.0117	0113	-

TABLE 27-9

THICKNESS MEASUREMENTS OF CORRUGATION-STIFFENED CRIPPLING PANEL
(ROOM TEMPERATURE)

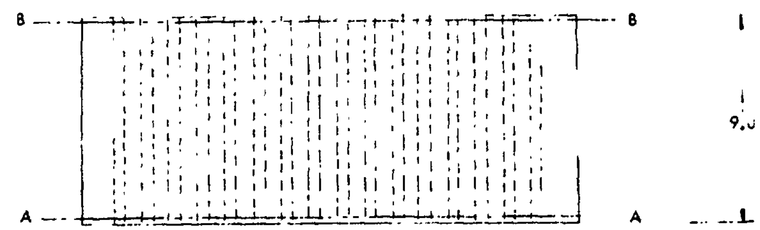

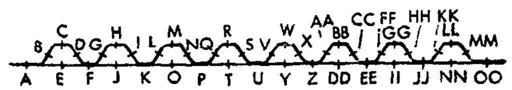

SECTION	A	B	C	D	E	F	G	H	I	J	K	L	M	N	O	P	Q	R	S	T	U
AA	.0449	.0115	.0113	.0114	.0249	.0435	.0120	.0118	.0112	.0259	.0448	.0115	.0115	.0109	.0235	.0458	.0112	.0105	.0118	.0254	.0425
BB	.0435	.0125	.0111	.0125	.0255	.0438	.0117	.0122	.0129	.0260	.0425	.0122	.0119	.0113	.0268	.0438	.0113	.0104	.0115	.0255	.0422
SECTION	V	W	X	Y	Z	AA	BB	CC	DD	EE	FF	GG	HH	II	JJ	KK	LL	MM	NN	OO	-
AA	.0114	.0107	.0115	.0274	.0432	.0115	.0112	.0110	.0257	.0468	.0118	.0108	.0110	.0256	.0435	.0120	.0101	.0115	.0254	.0443	-
BB	.0117	.0113	.0114	.0259	.0422	.0114	.0105	.0125	.0268	.0412	.0154	.0114	.0119	.0257	.0419	.0119	.0122	.0120	.0260	.0429	-

TABLE 27-10

TEMPERATURE DISTRIBUTIONS FOR CORRUGATION-STIFFENED CRIPPLING PANEL

LOAD	TIME	CH 151	CH 152	CH .54	CH 155	CH 156	CH 157
		T-1 DEG F	T-2 DEG F	T-4 DEG F	T-5 DEG F	T-6 DEG F	T-7 DEG F
002	1325.6	1455.9F	1416.0F	1368.2F	1416.5F	1371.3F	1348.7F
004	1326.4	1455.4F	1415.6F	1366.5F	1407.3F	1365.2F	1347.5F
006	1327.2	1458.1F	1417.3F	1371.3F	1412.6F	1370.0F	1346.6F
008	1328.1	1459.5F	1420.4F	1370.0F	1418.2F	1370.8F	1349.1F
010	1329.3	1463.0F	1423.4F	1373.9F	1417.8F	1377.3F	1356.0F
012	1330.1	1462.6F	1423.0F	1370.0F	1413.9F	1367.3F	1353.9F
014	1330.9	1460.8F	1421.7F	1368.6F	1413.4F	1369.5F	1349.5F
016	1331.7	1461.3F	1421.7F	1368.6F	1415.2F	1367.8F	1351.3F
018	1332.6	1466.5F	1425.6F	1369.5F	1418.6F	1371.3F	1356.0F
020	1333.5	1467.3F	1428.2F	1375.6F	1421.3F	1378.6F	1355.6F
020	1333.9	1462.6F	1423.4F	1371.7F	1414.7F	1370.4F	1352.6F
022	1334.5	1469.1F	1427.3F	1376.9F	1421.3F	1372.1F	1348.7F
024	1335.3	1469.1F	1427.3F	1377.3F	1418.6F	1374.7F	1356.9F
026	1336.0	1466.0F	1426.5F	1373.0F	1416.9F	1373.4F	1354.7F
028	1336.9	1465.6F	1426.0F	1370.0F	1412.6F	1371.7F	1351.3F
030	1337.9	1466.9F	1426.9F	1373.0F	1415.6F	1375.2F	1348.3F
032	1338.7	1468.6F	1429.1F	1376.0F	1416.9F	1371.7F	1349.5F
034	1339.7	1470.8F	1431.3F	1375.6F	1412.1F	1374.3F	1352.1F
035	1340.7	1471.3F	1431.3F	1379.1F	1412.1F	1376.5F	1352.1F

LOAD	TIME	CH 158	CH 159	CH 160	CH 161	CH 162	CH 163
		T-8 DEG F	T-9 DEG F	T-10 DEG F	T-11 DEG F	T-12 DEG F	T-13 DEG F
002	1325.6	1370.0F	1357.3F	1358.2F	1404.3F	1376.0F	1347.5F
004	1326.4	1370.8F	1354.7F	1355.6F	1403.9F	1371.7F	1353.9F
006	1327.2	1370.0F	1356.0F	1354.3F	1407.3F	1378.2F	1340.8F
008	1328.1	1372.1F	1357.8F	1361.7F	1408.2F	1377.8F	1352.6F
010	1329.3	1376.0F	1361.7F	1360.8F	1408.6F	1383.7F	1350.4F
012	1330.1	1373.4F	1356.0F	1357.8F	1406.0F	1376.0F	1353.4F
014	1330.9	1372.6F	1355.6F	1359.1F	1403.9F	1376.5F	1349.5F
016	1331.7	1372.1F	1356.0F	1357.8F	1402.6F	1374.3F	1351.7F
018	1332.6	1375.6F	1360.0F	1362.6F	1407.3F	1378.2F	1360.8F
020	1333.5	1375.6F	1362.6F	1363.0F	1405.2F	1377.8F	1358.2F
020	1333.9	1371.3F	1360.0F	1360.4F	1406.0F	1379.5F	1356.9F
022	1334.5	1372.6F	1357.3F	1356.0F	1410.0F	1385.4F	1342.9F
024	1335.3	1373.0F	1361.7F	1364.3F	1406.5F	1383.3F	1359.1F
026	1336.0	1374.7F	1360.4F	1361.7F	1406.5F	1385.4F	1353.9F
028	1336.9	1373.9F	1359.1F	1357.8F	1406.0F	1381.2F	1343.7F
030	1337.9	1374.3F	1362.1F	1356.5F	1404.7F	1384.5F	1339.5F
032	1338.7	1371.3F	1359.1F	1360.0F	1403.0F	1378.6F	1350.4F
034	1339.7	1374.7F	1360.0F	1360.8F	1406.0F	1379.1F	1354.3F
035	1340.7	1374.7F	1360.0F	1365.6F	1409.1F	1380.4F	1355.6F

LOAD	TIME	CH 164	CH 165	CH 179	CH 180	CH 181	CH 182
		T-14 DEG F	T-15 DEG F	LVDT-1 INCHES	LVDT-2 INCHES	LVDT-3 INCHES	LVDT-4 INCHES
002	1325.6	1410.4F	1393.0F	0.000J	0.000J	0.000J	0.000J
004	1326.4	1411.7F	1393.4F	0.004	0.002	0.002	0.002
006	1327.2	1408.2F	1401.7F	0.004	0.004	0.006	0.005
008	1328.1	1400.8F	1399.1F	0.007	0.007	0.007	0.007
010	1329.3	1419.1F	1408.6F	0.006	0.007	0.005	0.008
012	1330.1	1410.4F	1399.5F	0.009	0.009	0.006	0.009
014	1330.9	1418.2F	1400.8F	0.009	0.011	0.008	0.011
016	1331.7	1416.0F	1401.3F	0.012	0.011	0.009	0.010
018	1332.6	1418.6F	1406.9F	0.011	0.011	0.011	0.010
020	1333.5	1427.8F	1406.5F	0.010	0.012	0.010	0.013
020	1333.9	1420.0F	1408.2F	0.009	0.012	0.010	0.011
022	1334.5	1412.6F	1413.0F	0.011	0.013	0.012	0.011
024	1335.3	1427.3F	1410.0F	0.013	0.013	0.010	0.013
026	1336.0	1422.6F	1409.5F	0.013	0.015	0.015	0.013
028	1336.9	1425.6F	1411.3F	0.016	0.017	0.015	0.015
030	1337.9	1413.4F	1415.2F	0.013	0.019	0.018	0.017
032	1338.7	1426.5F	1409.1F	0.018	0.020	0.024	0.018
034	1339.7	1426.5F	1410.8F	0.020	0.023	0.025	0.023
035	1340.7	1421.7F	1412.6F	0.037	0.039	0.037	0.038

TABLE 27-11

THICKNESS MEASUREMENTS OF CORRUGATION-STIFFENED CRIPPLING PANEL
(ELEVATED TEMPERATURE)

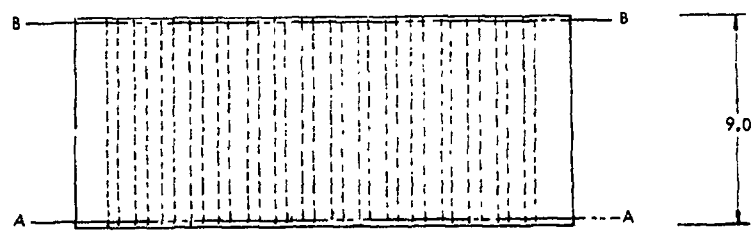

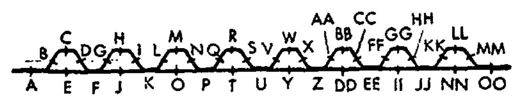

SECTION	A	B	C	D	E	F	G	H	I	J	K	L	M	N	O	P	Q	R	S	T	U
AA	.0455	.0121	.0112	.0127	.0257	.0435	.0119	.0110	.0116	.0257	.0450	.0121	.0111	.0118	.0253	.0459	.0118	.0125	.0121	.0255	.0500
BB	.0435	.0119	.0109	.0118	.0257	.0433	.0118	.0112	.0117	.0255	.0433	.0118	.0109	.0113	.0257	.0432	.0114	.0108	.0114	.0258	.0435
SECTION	V	W	X	Y	Z	AA	BB	CC	DD	EE	FF	GG	HH	II	JJ	KK	LL	MM	NN	OO	-
AA	.0125	.0110	.0122	.0257	.0488	.0120	.0115	.0117	.0254	.0451	.0118	.0110	.0113	.0257	.0453	.0116	.0113	.0115	.0255	.0462	-
BB	.0118	.0108	.0115	.0260	.0445	.0114	.0105	.0113	.0258	.0440	.0111	.0104	.0117	.0258	.0450	.0118	.0113	.0115	.0259	.0452	-

TABLE 27-12

THICKNESS MEASUREMENTS OF TRAPEZOIDAL CORRUGATION CRIPPLING PANEL
(ROOM TEMPERATURE)

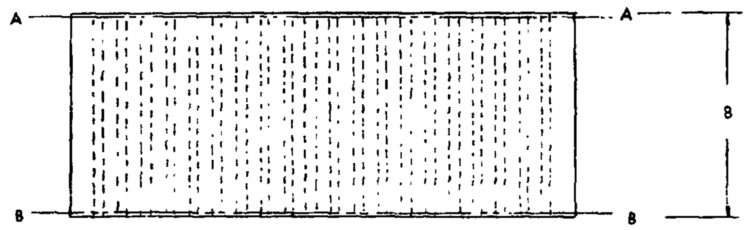

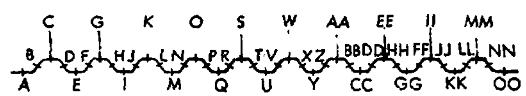

SECTION	A	B	C	D	E	F	G	H	I	J	K	L	M	N	O	P	Q	R	S	T	U
AA	.0169	.0194	.0185	.0172	.0172	.0170	.0187	.0172	.0170	.0169	.0185	.0168	.0169	.0172	.0176	.0175	.0168	.0187	.0186	.0169	.0169
BB	.0170	.0199	.0174	.0167	.0169	.0165	.0174	.0171	.0168	.0165	.0175	.0167	.0167	.0164	.0178	.0171	.0168	.0167	.0180	.0168	0166
SECTION	V	W	X	Y	Z	AA	BB	CC	DD	EE	FF	GG	HH	II	JJ	KK	LL	MM	NN	OO	-
AA	.0169	.0186	.0170	.0173	.0169	.0187	.0170	.0170	.0172	.0180	.0168	.0173	.0168	.0182	.0170	.0170	.0168	.0168	.0178	.0169	-
BB	.0168	.0172	.0165	.0168	.0167	.0174	.0168	.0186	.0168	.0183	.0168	.0168	.0171	.0178	.0168	.0169	.0169	.0171	.0168	.0167	-

TABLE 27-13

TEMPERATURE DISTRIBUTIONS FOR TRAPEZOIDAL CORRUGATION CRIPPLING PANEL

LOAD	TIME	CH 151	CH 152	CH 153	CH 154	CH 155	CH 156
		TC-1 DEG F	TC-2 DEG F	TC-3 DEG F	TC-4 DEG F	TC-5 DEG F	TC-6 DEG F
002	1430.3	1420.4F	1382.5F	1389.5F	1357.3F	1400.8F	1402.6F
004	1431.2	1421.7F	1385.4F	1386.6F	1353.9F	1396.9F	1399.5F
006	1431.8	1431.7F	1376.0F	1384.1F	1347.9F	1392.6F	1395.6F
008	1432.5	1436.9F	1399.5F	1388.7F	1356.5F	1403.0F	1397.3F
010	1433.3	1439.5F	1388.3F	1388.7F	1351.7F	1395.2F	1400.0F
012	1434.0	1441.3F	1391.3F	1387.5F	1351.3F	1401.3F	1400.8F
014	1435.1	1418.2F	1393.0F	1388.7F	1336.0F	1398.2F	1400.4F
016	1436.0	1431.3F	1402.6F	1392.1F	1357.8F	1398.2F	1403.0F
018	1437.0	1433.4F	1403.4F	1393.0F	1355.2F	1403.4F	1401.3F
020	1437.8	1429.5F	1399.1F	1392.1F	1355.6F	1400.8F	1400.0F
021	1438.5	1430.4F	1404.3F	1396.0F	1362.6F	1407.8F	1401.7F
022	1439.3	1433.4F	1408.6F	1395.2F	1359.1F	1408.2F	1400.8F
023	1440.9	1427.8F	1401.3F	1392.6F	1358.2F	1405.6F	1404.7F
024	1441.6	1433.9F	1401.7F	1390.0F	1353.4F	1400.4F	1400.0F
025	1442.7	1433.9F	1397.3F	1391.7F	1359.5F	1403.0F	1403.0F
026	1443.4	1436.9F	1410.0F	1393.9F	1362.6F	1406.9F	1408.2F

LOAD	TIME	CH 157	CH 158	CH 159	CH 160	CH 161	CH 162
		TC-7 DEG F	TC-8 DEG F	TC-9 DEG F	TC-10 DEG F	TC-11 DEG F	TC-12 DEG F
002	1430.3	1370.8F	1394.7F	1389.1F	1401.7F	1415.2F	1350.8F
004	1431.2	1363.9F	1394.7F	1392.1F	1403.0F	1416.0F	1357.8F
006	1431.8	1369.5F	1392.1F	1387.5F	1400.4F	1419.1F	1353.4F
008	1432.5	1368.6F	1393.0F	1393.9F	1400.8F	1425.2F	1365.2F
010	1433.3	1375.2F	1395.6F	1382.9F	1402.1F	1426.5F	1361.7F
012	1434.0	1370.4F	1395.6F	1391.7F	1406.5F	1419.5F	1356.9F
014	1435.1	1366.9F	1393.0F	1392.6F	1402.1F	1410.8F	1354.3F
016	1436.0	1367.3F	1395.2F	1396.0F	1402.1F	1413.4F	1353.9F
018	1437.0	1370.0F	1393.9F	1389.5F	1403.9F	1419.5F	1359.1F
020	1437.8	1369.5F	1393.0F	1393.4F	1400.4F	1412.6F	1350.4F
021	1438.5	1370.8F	1394.7F	1390.8F	1400.4F	1417.8F	1356.0F
022	1439.3	1366.5F	1392.6F	1393.9F	1407.3F	1423.9F	1365.2F
023	1440.9	1373.4F	1395.2F	1396.9F	1404.7F	1423.0F	1356.9F
024	1441.6	1371.7F	1394.7F	1390.8F	1401.7F	1413.4F	1356.5F
025	1442.7	1373.4F	1396.0F	1391.3F	1402.6F	1411.7F	1353.0F
026	1443.4	1373.9F	1395.6F	1397.8F	1407.3F	1416.9F	1362.6F

LOAD	TIME	CH 163	CH 164	CH 165	CH 179	CH 180	CH 181
		TC-13 DEG F	TC-14 DEG F	TC-15 DEG F	LVDT. PT-1 INCHES	LVDT. PT-2 INCHES	LVDT. PT-3 INCHES
002	1430.3	1395.6F	1460.8F	1461.7F	0.000√	0.000√	0.000√
004	1431.2	1400.8F	1460.8F	1461.3F	0.007	0.008	0.006
006	1431.8	1402.1F	1458.1F	1463.4F	0.014	0.012	0.010
008	1432.5	1413.9F	1467.8F	1470.4F	0.013	0.014	0.012
010	1433.3	1408.6F	1464.3F	1470.4F	0.016	0.016	0.013
012	1434.0	1402.1F	1463.0F	1467.3F	0.019	0.018	0.016
014	1435.1	1396.9F	1460.8F	1463.9F	0.021	0.022	0.017
016	1436.0	1396.9F	1463.4F	1466.0F	0.022	0.023	0.019
018	1437.0	1401.7F	1465.2F	1471.3F	0.024	0.027	0.023
020	1437.8	1397.3F	1464.7F	1467.3F	0.026	0.026	0.025
021	1438.5	1399.5F	1468.2F	1469.1F	0.028	0.028	0.026
022	1439.3	1408.6F	1472.1F	1476.5F	0.028	0.029	0.027
023	1440.9	1406.0F	1469.5F	1473.4F	0.029	0.031	0.028
024	1441.6	1399.1F	1460.0F	1464.7F	0.031	0.031	0.029
025	1442.7	1395.6F	1463.4F	1465.2F	0.033	0.033	0.032
026	1443.4	1402.1F	1469.1F	1469.1F	0.035	0.039	0.035

TABLE 27-14

THICKNESS MEASUREMENTS OF TRAPEZOIDAL CORRUGATION CRIPPLING PANEL
(ELEVATED TEMPERATURE)

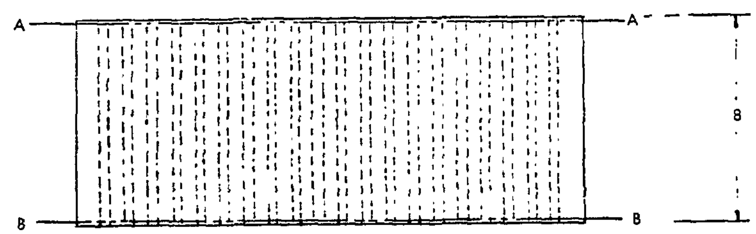

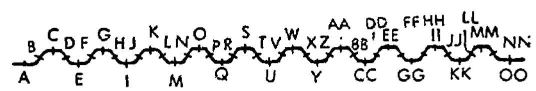

SECTION	A	B	C	D	E	F	G	H	I	J	K	L	M	N	O	P	Q	R	S	T	U
AA	.0175	.0203	.0189	.0170	.0175	.0164	.0170	.0166	.0165	.0165	.0173	.0168	.0165	.0168	.0172	0175	0169	0167	.0183	.0167	.0168
BB	.0170	.0210	.0181	.0165	.0164	.0182	.0171	.0165	.0168	.0176	.0172	.0162	.0165	.0182	.0172	.0164	.0165	.0178	.0174	.0163	.0163
SECTION	V	W	X	Y	Z	AA	BB	CC	DD	EE	FF	GG	HH	II	JJ	KK	LL	MM	NN	OO	-
AA	.0165	.0172	0169	[illegible]	.0168	.0171	.0170	.0170	.0166	.0179	0172	.0169	.0169	.0188	.0171	.0169	0169	.0172	0171	0167	-
BB	.0178	.0185	.0165	-	0178	.0179	.0163	.0165	.0180	0174	.0165	.0168	.0181	.0183	.0162	.0167	.0170	.0172	0168	0170	-

TABLE 27-15

THICKNESS MEASUREMENTS OF BEADED CRIPPLING PANEL
(ROOM TEMPERATURE)

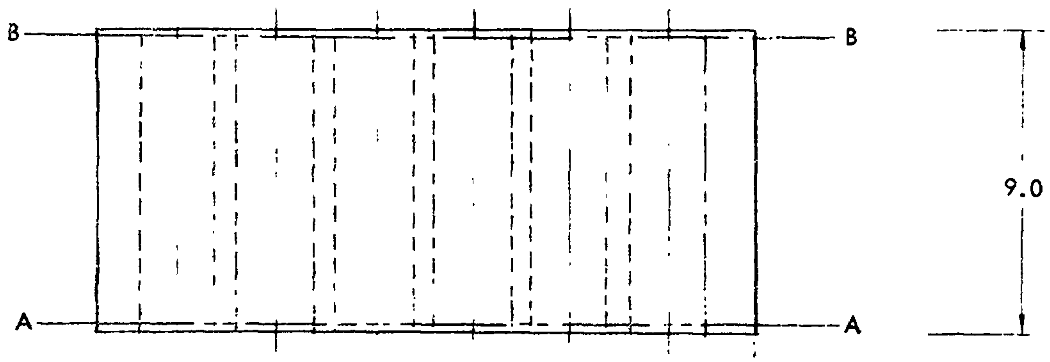

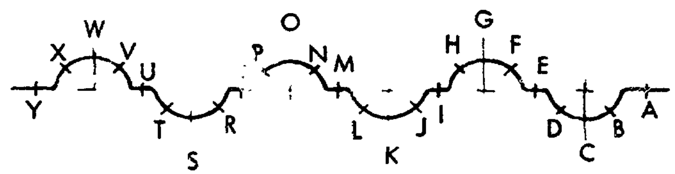

SECTION	A	B	C	D	E	F	G	H	I	J	K	L	M
AA	.0182	.0144	.0138	.0151	.0180	.0137	.0135	.0138	.0173	.0136	.0132	.0139	.0179
BB	.0186	.0145	.0142	.0142	.0184	.0142	.0136	.0140	.0179	.0139	.0135	.0138	.0188
SECTION	N	O	P	Q	R	S	T	U	V	W	X	Y	-
AA	.0139	.0132	.0135	.0174	.0140	.0137	.0132	.0175	.0137	.0131	.0133	.0183	-
BB	.0137	.0136	.0140	.0179	.0138	.0136	.0137	.0181	.0139	.0137	.0143	.0186	-

TABLE 27-16

TEMPERATURE DISTRIBUTIONS FOR BEADED CRIPPLING PANEL

LOAD	TIME	CH 151	CH 152	CH 154	CH 155	CH 156	CH 157
		T-1 DEG F	T-2 DEG F	T-4 DEG F	T-5 DEG F	T-6 DEG F	T-7 DEG F
002	1116.8	1378.2F	1387.0F	1375.2F	1412.6F	1407.3F	1392.6F
004	1117.9	1387.5F	1396.5F	1376.0F	1414.7F	1408.6F	1390.4F
006	1118.7	1380.4F	1381.6F	1373.4F	1411.7F	1406.5F	1394.3F
008	1119.6	1391.7F	1400.4F	1369.5F	1414.7F	1406.0F	1392.6F
008	1121.6	1394.7F	1401.7F	1372.6F	1406.5F	1403.9F	1385.0F
010	1122.8	1386.2F	1400.0F	1376.5F	1412.6F	1410.0F	1390.8F
012	1123.9	1390.0F	1386.2F	1381.2F	1412.1F	1406.5F	1394.3F
014	1124.7	1402.6F	1385.4F	1378.2F	1411.3F	1406.0F	1390.8F
016	1125.5	1386.2F	1390.4F	1366.0F	1409.5F	1403.9F	1388.7F
018	1126.2	1389.5F	1388.7F	1368.6F	1421.3F	1411.7F	1394.7F
020	1127.0	1398.6F	1390.4F	1371.3F	1410.0F	1401.7F	1390.4F
021	1127.7	1393.9F	1389.1F	1378.2F	1410.4F	1403.0F	1394.3F
022	1128.4	1413.0F	1399.1F	1356.5F	1406.5F	1390.4F	1382.9F

LOAD	TIME	CH 158	CH 159	CH 160	CH 161	CH 162	CH 163
		T-8 DEG F	T-9 DEG F	T-10 DEG F	T-11 DEG F	T-12 DEG F	T-13 DEG F
002	1116.8	1400.4F	1394.7F	1401.3F	1403.4F	1408.6F	1403.0F
004	1117.9	1392.1F	1393.9F	1403.9F	1407.8F	1421.3F	1403.0F
006	1118.7	1397.8F	1397.8F	1406.5F	1410.8F	1412.1F	1396.9F
008	1119.6	1399.1F	1398.6F	1407.3F	1412.1F	1423.0F	1406.0F
008	1121.6	1395.2F	1398.6F	1400.8F	1410.4F	1423.0F	1403.9F
010	1122.8	1399.1F	1395.6F	1399.1F	1406.0F	1414.7F	1406.5F
012	1123.9	1397.3F	1400.0F	1407.8F	1407.8F	1410.4F	1402.1F
014	1124.7	1402.6F	1395.2F	1397.3F	1406.5F	1412.6F	1399.1F
016	1125.5	1393.0F	1393.4F	1401.7F	1405.6F	1416.0F	1406.0F
018	1126.2	1396.5F	1392.6F	1409.5F	1404.7F	1404.3F	1406.0F
020	1127.0	1395.6F	1401.3F	1407.8F	1410.4F	1412.1F	1396.0F
021	1127.7	1404.7F	1400.4F	1403.4F	1410.4F	1416.5F	1402.1F
022	1128.4	1392.1F	1399.1F	1402.6F	1402.1F	1414.7F	1402.1F

LOAD	TIME	CH 164	CH 165	CH 179	CH 180	CH 181	CH 182
		T-14 DEG F	T-15 DEG F	LVDT-1 INCHES	LVDT-2 INCHES	LVDT-3 INCHES	LVDT-4 INCHES
002	1116.8	1445.6F	1428.2F	0.000√	0.000√	0.000√	0.000√
004	1117.9	1448.6F	1433.4F	0.004	0.004	0.004	0.004
006	1118.7	1447.8F	1427.8F	0.009	0.010	0.009	0.008
008	1119.6	1451.3F	1441.7F	0.010	0.013	0.012	0.010
008	1121.6	1450.9F	1432.1F	0.011	0.014	0.013	0.011
010	1122.8	1445.2F	1434.3F	0.015	0.017	0.015	0.014
012	1123.9	1447.8F	1427.3F	0.019	0.022	0.020	0.018
014	1124.7	1452.7F	1430.4F	0.022	0.025	0.024	0.021
016	1125.5	1449.5F	1432.1F	0.026	0.030	0.026	0.025
018	1126.2	1455.0F	1433.9F	0.027	0.034	0.032	0.029
020	1127.0	1453.1F	1432.6F	0.034	0.040	0.038	0.034
021	1127.7	1457.2F	1435.2F	0.036	0.042	0.040	0.036
022	1128.4	1451.3F	1430.0F	0.041	0.049	0.044	0.042

TABLE 27-17

THICKNESS MEASUREMENTS OF BEADED CRIPPLING PANEL
(ELEVATED TEMPERATURE)

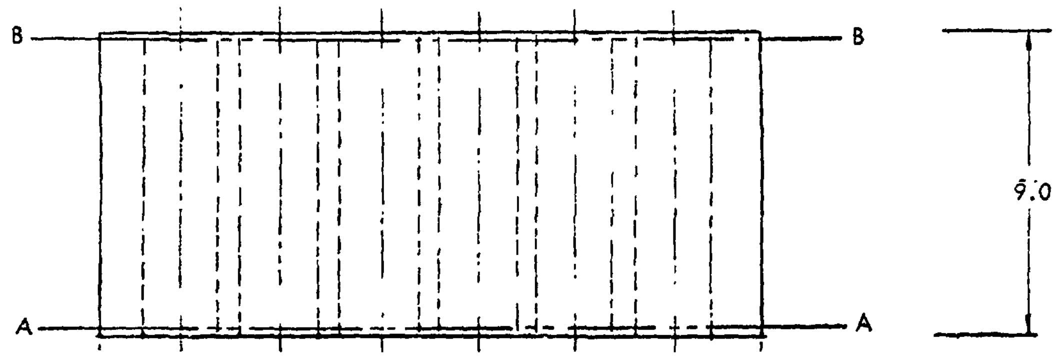

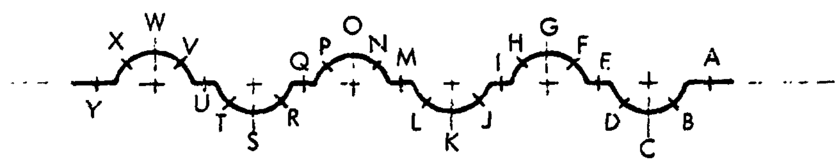

SECTION	A	B	C	D	E	F	G	H	I	J	K	L	M
AA	.0184	.0137	.0140	.0137	.0175	.0131	.0135	.0137	.0170	.0134	.0135	.0135	.0175
BB	.0189	.0146	.0139	.0139	.0180	.0138	.0136	.0136	.0175	.0135	.0135	.0139	.0180
SECTION	N	O	P	Q	R	S	T	U	V	W	X	Y	-
AA	.0132	.0134	.0130	.0172	.0134	.0137	.0135	.0178	.0131	.0134	.0132	.0189	-
BB	.0137	.0134	.013[illegible]	.0179	.0138	.0136	.0136	.0175	.0133	.0134	.0135	.0188	-

TABLE 27-18

THICKNESS MEASUREMENTS OF TUBULAR CRIPPLING PANEL
(ROOM TEMPERATURE)

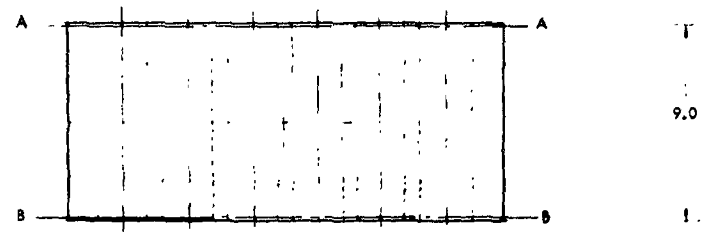

SECTION	A	B	C	D	E	F	G	H	I	J	K	L	M	N	O	P	Q	R	S	T	U	V
AA	.031	.0115	.0115	.0116	.0327	.0112	.0114	.0112	.0322	.0114	.0118	.0115	.0338	.0112	.0119	.0112	.0362	.0111	.0118	.0111	.0360	.0115
BB		.0117	.0120	.0122		.0114	.0119	.0116		.0115	.0117	.0115		.0115	.0115	.0118		.0122	.0120	.0117		.0120
SECTION	W	X	Y	Z	AA	BB	CC	DD	EE	FF	GG	HH	II	JJ	KK	LL	MM	NN	OO	PP	QQ	-
AA	.0119	.0115	.0395	.0112	.0120	.0118	.0118	.0117	.0117	.0115	.0118	.0115	.0118	.0118	.0119	.0114	.0117	.0115	.0119	.0119	.0116	-
BB	.0120	.0119		.0112	.0118	.0120	.0117	.0115	.0113	.0117	.0120	.0114	.0118	.0118	.0118	.0111	.0115	.0116	.0118	.0118	.0117	-

TABLE 27-19

TEMPERATURE DISTRIBUTIONS FOR TUBULAR CRIPPLING PANEL

LOAD	TIME	CH 151	CH 152	CH 154	CH 155	CH 156	CH 157
		T-1 DEG F	T-2 DEG F	T-4 DEG F	T-5 DEG F	T-6 DEG F	T-7 DFG F
002	1452.8	1480.4F	1427.8F	1350.4F	1362.6F	1413.9F	1414.7F
004	1454.3	1483.0F	1435.2F	1353.4F	1364.3F	1417.3F	1421.7F
006	1455.0	1476.5F	1426.5F	1350.8F	1360.0F	1406.5F	1412.1F
008	1455.7	1479.5F	1431.7F	1345.0F	1361.3F	1405.6F	1406.0F
010	1456.3	1482.6F	1434.7F	1345.0F	1360.8F	1410.4F	1410.4F
012	1457.0	1479.5F	1430.0F	1351.3F	1363.9F	1408.6F	1412.6F
014	1457.6	1481.3F	1433.0F	1352.6F	1370.8F	1415.6F	1409.1F
016	1458.4	1476.9F	1431.7F	1348.7F	1357.3F	1407.8F	1410.4F
018	1459.2	1480.8F	1433.0F	1346.6F	1354.7F	1403.0F	1406.9F
020	1459.7	1485.2F	1436.5F	1353.4F	1362.1F	1417.8F	1425.2F
022	1500.5	1480.4F	1431.3F	1350.4F	1358.6F	1410.4F	1415.2F
024	1501.1	1480.0F	1433.4F	1345.4F	1360.8F	1409.1F	1414.3F
026	1501.9	1479.5F	1433.4F	1349.5F	1364.3F	1409.5F	1412.6F
028	1502.6	1477.3F	1433.9F	1338.6F	1364.3F	1402.6F	1403.4F
030	1503.7	1481.3F	1435.2F	1340.8F	1362.1F	1406.5F	1406.5F
031	1504.2	1484.3F	1438.2F	1355.2F	1360.8F	1415.2F	1416.0F
032	1504.9	1482.1F	1438.2F	1346.6F	1356.5F	1411.7F	1417.3F
033	1505.7	1481.3F	1432.1F	1340.4F	1358.6F	1399.1F	1405.6F
034	1506.2	1487.3F	1432.1F	1352.1F	1365.2F	1419.5F	1423.9F

LOAD	TIME	CH 158	CH 159	CH 160	CH 161	CH 162	CH 163
		T-8 DEG F	T-9 DEG F	T-10 DEG F	T-11 DEG F	T-12 DEG F	T-13 DFG F
002	1452.8	1386.2F	1373.4F	1403.9F	1363.9F	1349.5F	1394.3F
004	1454.3	1383.7F	1378.6F	1405.6F	1372.6F	1366.9F	1395.6F
006	1455.0	1372.1F	1370.0F	1400.8F	1358.2F	1344.1F	1388.7F
008	1455.7	1366.0F	1368.6F	1396.9F	1364.3F	1344.5F	1390.4F
010	1456.3	1375.6F	1379.1F	1403.0F	1366.0F	1356.5F	1389.1F
012	1457.0	1373.4F	1370.4F	1400.0F	1365.6F	1354.3F	1386.6F
014	1457.6	1373.9F	1374.3F	1399.1F	1364.7F	1356.5F	1390.4F
016	1458.4	1376.9F	1376.5F	1402.1F	1368.2F	1353.4F	1388.3F
018	1459.2	1368.6F	1374.7F	1398.6F	1366.0F	1354.7F	1390.0F
020	1459.7	1394.3F	1385.0F	1407.3F	1373.4F	1361.3F	1393.9F
022	1500.5	1377.3F	1380.0F	1403.4F	. 66.5F	1360.4F	1388.7F
024	1501.1	1373.4F	1377.3F	1401.7F	1363.4F	1347.5F	1388.3F
026	1501.9	1370.8F	1377.8F	1401.7F	1366.5F	1354.7F	1390.0F
028	1502.6	1358.6F	1370.4F	1394.3F	1360.4F	1343.3F	1390.4F
030	1503.7	1370.8F	1375.2F	1400.5F	1365.6F	1353.9F	1390.8F
031	1504.2	1384.1F	1384.5F	1405.2F	1369.5F	1360.4F	1391.3F
032	1504.9	1385.4F	1380.4F	1406.5F	1374.3F	1355.2F	1389.1F
033	1505.7	1367.3F	1374.7F	1402.6F	1368.6F	1356.5F	1387.9F
034	1506.2	1397.8F	1388.3F	1405.6F	1370.8F	1360.4F	1392.1F

LOAD	TIME	CH 164	CH 165	CH 179	CH 180	CH 181	CH 182
		T-14 DEG F	T-15 DEG F	LVDT-1 INCHES	LVDT-2 INCHES	LVDT-3 INCHES	LVDT-4 INCHES
002	1452.8	1435.6F	1409.5F	0.000J	0.000J	0.000J	0.000J
004	1454.3	1438.6F	1417.8F	0.001	0.002	0.000	0.001
006	1455.0	1426.0F	1410.0F	0.005	0.007	0.005	0.006
008	1455.7	1433.4F	1409.5F	0.007	0.010	0.006	0.008
010	1456.3	1438.6F	1419.1F	0.008	0.011	0.008	0.009
012	1457.0	1436.9F	1413.9F	0.009	0.013	0.011	0.010
014	1457.6	1435.2F	1418.6F	0.011	0.015	0.012	0.012
016	1458.4	1435.6F	1411.7F	0.012	0.017	0.013	0.014
018	1459.2	1434.7F	1417.3F	0.013	0.018	0.015	0.016
020	1459.7	1441.7F	1415.2F	0.014	0.019	0.017	0.017
022	1500.5	1433.0F	1417.3F	0.019	0.022	0.019	0.018
024	1501.1	1439.1F	1416.5F	0.018	0.023	0.022	0.020
026	1501.9	1436.5F	1422.6F	0.020	0.026	0.024	0.021
028	1502.6	1442.6F	1419.1F	0.021	0.028	0.025	0.023
030	1503.7	1442.1F	1421.3F	0.023	0.030	0.027	0.024
031	1504.2	1435.6F	1422.1F	0.024	0.031	0.027	0.025
032	1504.9	1440.8F	1420.0F	0.024	0.032	0.029	0.026
033	1505.7	1435.2F	1417.8F	0.025	0.034	0.031	0.028
034	1506.2	1442.6F	1425.6F	0.027	0.035	0.034	0.031

TABLE 27-20

THICKNESS MEASUREMENTS OF TUBULAR CRIPPLING PANEL

(ELEVATED TEMPERATURE)

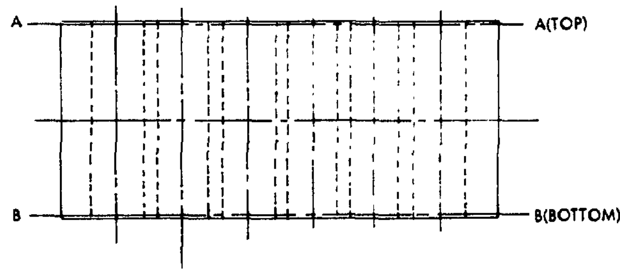

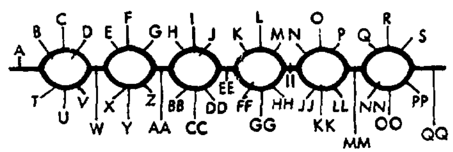

SECTION	A	B	C	D	E	F	G	H	I	J	K	L	M	N	O	P	Q	R	S	T	U	V
AA	.0338	.0115	.0113	.0111	.0110	.0112	.0111	.0110	.0112	.0108	.0112	.0113	.0108	.0112	.0112	.0109	.0110	0112	.0108	.0110	.0108	0108
BB	.0354	.0110	.0113	.0109	.0110	.0112	.0111	.0110	.0112	.0113	.0112	.0112	.0110	.0109	.0109	.0109	.0108	.0112	.0114	.0106	.0113	.0108

SECTION	W	X	Y	Z	AA	BB	CC	DD	EE	FF	GG	HH	II	JJ	KK	LL	MM	NN	OO	PP	QQ	-
AA	.0327	.0109	.0109	.0108	.0394	.0110	.0109	.0107	.0334	.0110	.0110	.0109	.0311	.0109	.0108	.0108	.0316	.0109	.0111	.0105	.0300	-
BB	.0383	.0110	.0114	.0108	.0448	.0109	.0110	.0108	.0408	.0110	.0113	.0108	.0323	.0109	.0108	.0108	.0314	.0107	.0110	.0114	0303	-

TABLE 27-21

THICKNESS MEASUREMENTS OF SPAR CAP CRIPPLING SPECIMEN (3/8-INCH FLANGE)
(ROOM TEMPERATURE)

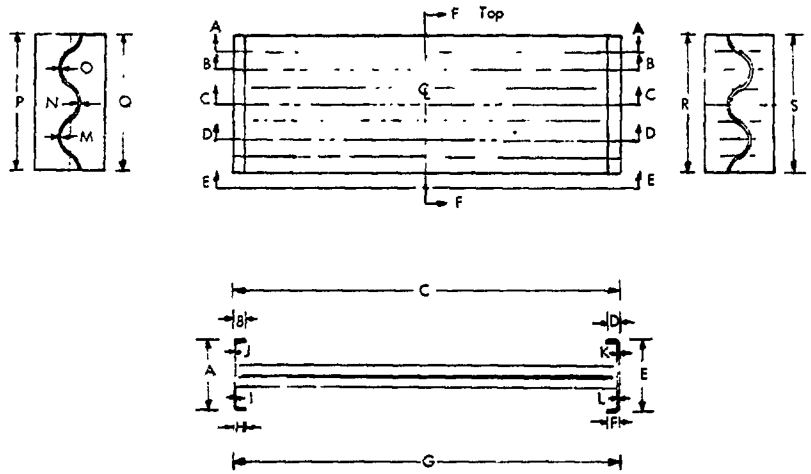

Typical Section View

SECTION	A	B	C	D	E	F	G	H	I	J	K	L	M	N	O	P	Q	R	S
AA	2.738	.361	15.566	.387	2.703	.374	15.552	.365	.0582	.0588	.0585	.0605	-	-	-	5.572	5.563	5.565	5.571
BB	-	-	-	-	-	-	-	-	.058	.059	.059	.058	-	-	-	-	-	-	-
CC	-	-	-	-	-	-	-	-	.058	.058	.058	.058	-	-	-	-	-	-	-
DD	-	-	-	-	-	-	-	-	.058	.060	.059	.058	-	-	-	-	-	-	-
EE	2.718	.349	15.568	.393	2.711	.378	15.560	.371	.0591	.0590	.0573	.0565	-	-	-	-	-	-	-
FF	-	-	-	-	-	-	-	-	-	-	-	-	.0140	.0130	.0150	-	-	-	-

TABLE 27-22

THICKNESS MEASUREMENTS FOR CORRUGATION-STIFFENED SKIN COMPRESSION PANEL
(ROOM TEMPERATURE)

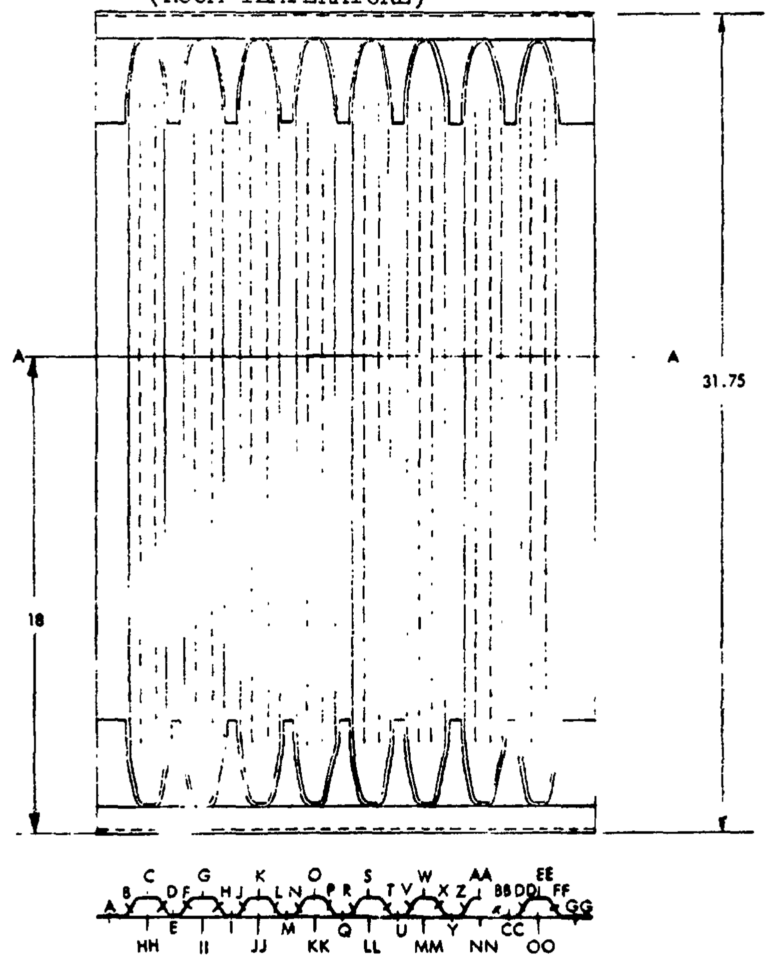

SECTION	A	B	C	D	E	F	G	H	I	J	K	L	M	N	O	P	Q	R	S	T	U
AA	.0440	.0104	.0100	.0102	.0440	.0103	.0100	.0103	.0430	.0103	.0100	.0103	.0440	.0104	.0103	.0104	.0430	.0103	.0100	.0102	.0430
SECTION	V	W	X	Y	Z	AA	BB	CC	DD	EE	FF	GG	HH	II	JJ	KK	LL	MM	NN	OO	-
AA	.0100	.0100	.0102	.0430	.0102	.0100	.0100	.0430	.0102	.0103	.0110	.0430	.027	.027	.0273	.0266	.0268	.0266	.0265	.0263	-

TABLE 27-23

TEMPERATURE DISTRIBUTIONS FOR CORRUGATION-STIFFENED SKIN COMPRESSION PANEL

LOAD	TIME	CH 47 LVDT. PT-1 INCHES	CH 48 LVDT. PT-2 INCHES	CH 49 LVDT. PT-3 INCHES	CH 50 LVDT. PT-4 INCHES	CH 51 TC-1 DEG F	CH 52 TC-2 DEG F
002	1032.9	0.000J	0.000J	0.000J	0.000J	1316.5F	1267.3F
004	1033.9	0.007	0.006	0.007	0.008	1314.7F	1275.4F
006	1034.8	0.013	0.013	0.014	0.015	1322.1F	1277.9F
008	1035.6	0.018	0.018	0.020	0.020	1318.2F	1284.3F
010	1036.3	0.025	0.026	0.026	0.026	1317.8F	1287.3F
012	1037.0	0.031	0.033	0.032	0.032	1324.7F	1286.5F
014	1037.8	0.038	0.041	0.039	0.039	1329.5F	1294.7F
016	1038.7	0.046	0.051	0.046	0.047	1337.8F	1299.5F
018	1039.7	0.055	0.061	0.055	0.055	1347.0F	1304.5F
020	1040.5	0.065	0.071	0.066	0.066	1349.5F	1310.0F
021	1041.2	0.071	0.077	0.073	0.073	1352.1F	1307.5F
022	1041.8	0.077	0.084	0.080	0.079	1359.1F	1311.7F
023	1042.4	0.083	0.092	0.086	0.086	1357.8F	1312.6F
024	1043.1	0.091	0.101	0.094	0.093	1364.3F	1318.2F
025	1043.8	0.101	0.113	0.104	0.103	1361.7F	1318.2F
026	1044.7	0.140	0.154	0.134	0.134	1373.4F	1320.8F

LOAD	TIME	CH 59 TC-9 DEG F	CH 60 TC-10 DEG F	CH 61 TC-11 DEG F	CH 62 TC-12 DEG F	CH 63 TC-13 DEG F	CH 64 TC-14 DEG F
002	1032.9	1393.4F	1403.9F	1406.5F	1419.5F	1404.3F	1415.2F
004	1033.9	1381.2F	1413.0F	1412.6F	1427.8F	1405.6F	1404.7F
006	1034.8	1384.1F	1404.3F	1408.6F	1412.6F	1402.6F	1410.8F
008	1035.6	1385.0F	1401.3F	1414.3F	1411.7F	1399.1F	1414.3F
010	1036.3	1378.6F	1391.7F	1407.8F	1418.2F	1396.0F	1407.3F
012	1037.0	1375.2F	1401.7F	1435.6F	1409.1F	1399.5F	1407.3F
014	1037.8	1382.9F	1400.8F	1416.5F	1414.3F	1399.5F	1411.3F
016	1038.7	1385.8F	1393.4F	1404.3F	1413.0F	1403.0F	1410.8F
018	1039.7	1383.3F	1410.4F	1423.4F	1414.7F	1400.0F	1424.3F
020	1040.5	1396.0F	1403.9F	1421.7F	1423.9F	1413.4F	1418.2F
021	1041.2	1391.3F	1413.9F	1432.6F	1423.9F	1410.4F	1443.0F
022	1041.8	1408.2F	1417.3F	1434.7F	1430.4F	1411.3F	1422.1F
023	1042.4	1400.0F	1413.9F	1426.9F	1433.0F	1420.4F	1428.6F
024	1043.1	1406.0F	1423.0F	1433.0F	1435.2F	1419.5F	1436.9F
025	1043.8	1399.5F	1406.0F	1425.6F	1423.0F	1414.3F	1429.1F
026	1044.7	1413.9F	1410.4F	1433.0F	1444.7F	1430.0F	1446.0F

LOAD	TIME	CH 53 TC-3 DEG F	CH 54 TC-4 DEG F	CH 55 TC-5 DEG F	CH 56 TC-6 DEG F	CH 57 TC-7 DEG F	CH 58 TC-8 DEG F
002	1032.9	1370.4F	1415.2F	1387.5F	1391.7F	1388.7F	1366.9F
004	1033.9	1363.4F	1413.0F	1385.8F	1391.3F	1370.8F	1381.6F
006	1034.8	1364.3F	1412.6F	1388.7F	1387.9F	1379.5F	1374.7F
008	1035.6	1368.2F	1413.9F	1385.0F	1390.8F	1412.6F	1387.9F
010	1036.3	1377.3F	1413.9F	1388.3F	1392.1F	1441.7F	1372.1F
012	1037.0	1365.6F	1416.9F	1391.3F	1392.1F	1451.3F	1380.8F
014	1037.8	1373.9F	1415.6F	1386.2F	1394.7F	1449.5F	1376.9F
016	1038.7	1373.9F	1413.0F	1390.4F	1395.6F	1481.3F	1385.0F
018	1039.7	1374.3F	1409.1F	1389.5F	1393.9F	1455.9F	1381.2F
020	1040.5	1373.0F	1424.3F	1405.6F	1400.8F	1427.3F	1385.8F
021	1041.2	1378.2F	1425.6F	1399.1F	1395.2F	1438.6F	1406.5F
022	1041.8	1384.1F	1434.3F	1406.5F	1396.0F	1417.3F	1397.3F
023	1042.4	1383.7F	1427.3F	1404.3F	1393.4F	1387.5F	1400.4F
024	1043.1	1373.4F	1433.9F	1403.0F	1397.3F	1412.6F	1405.2F
025	1043.8	1394.3F	1433.4F	1403.9F	1399.1F	1424.3F	1405.2F
026	1044.7	1392.6F	1437.8F	1412.1F	1412.6F	1353.0F	1404.7F

LOAD	TIME	CH 65 TC-15 DEG F	CH 66 TC-16 DEG F	CH 67 TC-17 DEG F	CH 68 TC-18 DEG F	CH 69 TC-19 DEG F	CH 70 TC-20 DEG F
002	1032.9	1371.3F	1359.1F	1366.9F	1296.9F	1166.9F	1207.0F
004	1033.9	1356.5F	1352.1F	1367.8F	1302.0F	1173.3F	1210.0F
006	1034.8	1367.3F	1352.6F	1367.8F	1295.2F	1170.8F	1214.7F
008	1035.6	1368.2F	1373.4F	1373.9F	1300.0F	1178.7F	1216.0F
010	1036.3	1360.8F	1365.2F	1373.0F	1299.1F	1174.1F	1229.1F
012	1037.0	1372.1F	1363.4F	1369.1F	1297.8F	1173.7F	1230.8F
014	1037.8	1364.3F	1366.9F	1363.9F	1295.2F	1180.4F	1241.3F
016	1038.7	1362.1F	1366.0F	1364.7F	1292.6F	1186.5F	1246.9F
018	1039.7	1363.9F	1369.1F	1367.3F	1293.9F	1194.3F	1254.1F
020	1040.5	1370.8F	1367.8F	1373.4F	1312.1F	1204.1F	1257.9F
021	1041.2	1374.7F	1380.8F	1400.4F	1317.3F	1210.0F	1262.1F
022	1041.8	1375.6F	1363.4F	1378.6F	1315.6F	1207.0F	1261.7F
023	1042.4	1383.7F	1370.4F	1371.3F	1316.5F	1211.3F	1269.5F
024	1043.1	1382.0F	1369.1F	1382.0F	1319.5F	1207.5F	1269.1F
025	1043.8	1392.1F	1382.5F	1382.9F	1305.4F	1212.1F	1274.5F
026	1044.7	1379.5F	1391.3F	1376.0F	1304.5F	1219.5F	1293.4F

TABLE 27-24

THICKNESS MEASUREMENTS OF CORRUGATION-STIFFENED SKIN COMPRESSION PANEL
(ELEVATED TEMPERATURE)

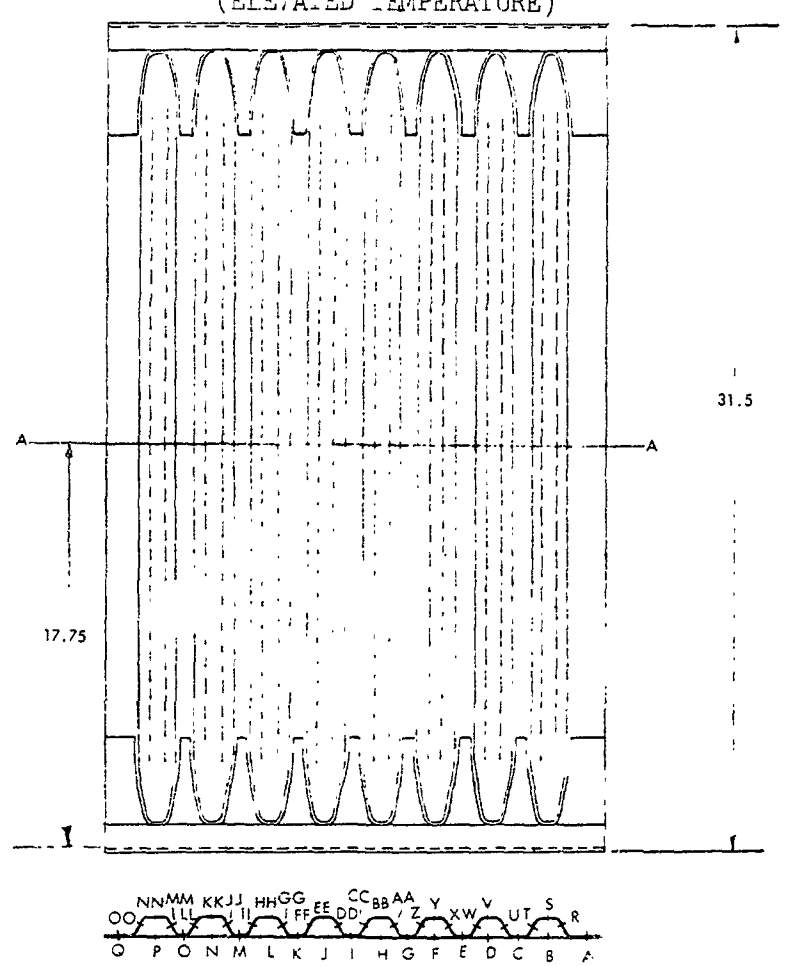

SECTION	A	B	C	D	E	F	G	H	I	J	K	L	M	N	O	P	Q	R	S	T	U
AA	.0485	.0268	.0464	.0265	.0478	.0267	.0486	.0263	.0475	0264	0468	.0263	.0469	0268	0486	0264	.0452	.0106	.0104	0112	.0108
SECTION	V	W	X	Y	Z	AA	BB	CC	DD	EE	FF	GG	HH	II	JJ	KK	LL	MM	NN	OO	-
AA	.0102	.0107	.0107	.0101	.0108	.0115	.0103	.0108	0115	0102	.0109	.0108	.0102	.0112	.0106	.0103	.0108	.0107	0102	.0109	-

TABLE 27-25

THICKNESS MEASUREMENTS OF TRAPEZOIDAL CORRUGATION COMPRESSION PANEL
(ROOM TEMPERATURE)

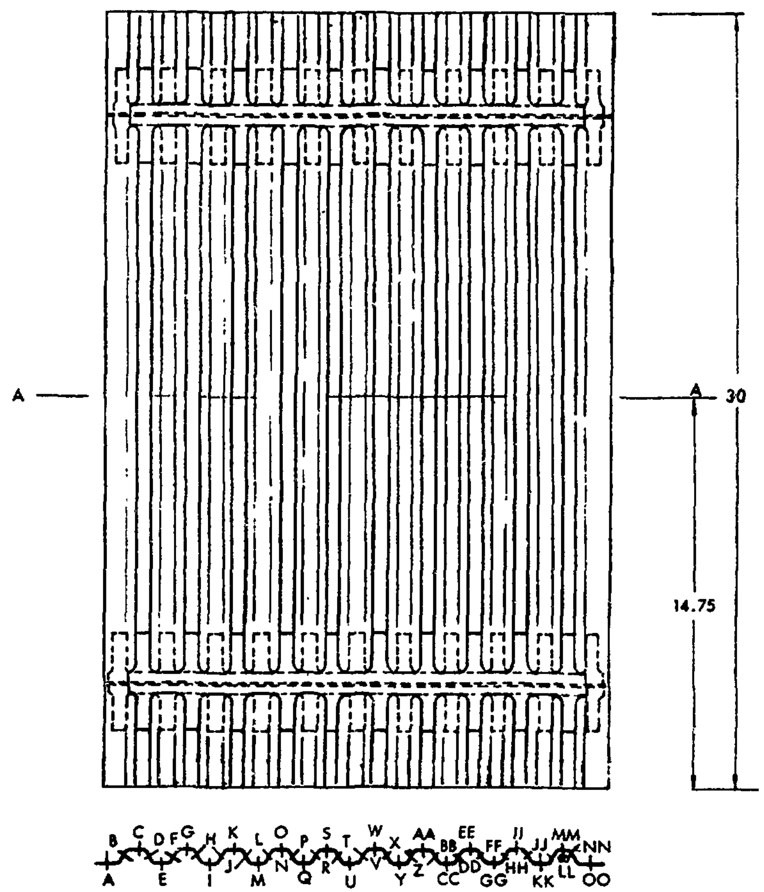

SECTION	A	B	C	D	E	F	G	H	I	J	K	L	M	N	O	P	Q	R	S	T	U
AA	.0162	.0175	.0174	.0177	.0162	.0160	.0175	.0162	.0161	.0162	.0169	.0163	.0162	.0159	.0178	.0167	.0163	.0161	.0175	.0167	.0161
SECTION	V	W	X	Y	Z	AA	BB	CC	DD	EE	FF	GG	HH	II	JJ	KK	LL	MM	NN	OO	-
AA	.0162	.0176	.0167	.0166	.0162	.0165	.0164	.0162	.0161	.0166	.0163	.0161	.0161	.0166	.0165	.0161	.0161	.0164	.0169	.0162	-

TABLE 27-26

TEMPERATURE DISTRIBUTIONS FOR TRAPEZOIDAL CORRUGATION COMPRESSION PANEL

LOAD	TIME	CH 47 LVDT. PT-1 INCHES	CH 48 LVDT. PT-2 INCHES	CH 49 LVDT. PT-3 INCHES	CH 50 LVDT. PT-4 INCHES	CH 51 TC-1 DEG F	CH 52 TC-2 DEG F
002	2231.3	0.000J	0.000J	0.000J	0.000J	1337.3F	1340.0F
004	2232.1	0.010	0.012	0.010	0.010	1337.3F	1339.5F
006	2232.8	0.018	0.020	0.018	0.018	1338.6F	1339.1F
008	2233.5	0.024	0.026	0.026	0.026	1337.3F	1340.0F
010	2234.2	0.030	0.033	0.033	0.033	1338.2F	1339.5F
012	2234.9	0.037	0.039	0.041	0.040	1337.8F	1339.1F
014	2235.6	0.043	0.047	0.047	0.047	1339.5F	1341.6F
016	2236.3	0.049	0.053	0.054	0.054	1339.1F	1341.2F
018	2236.8	0.056	0.060	0.061	0.061	1338.6F	1341.2F
019	2237.2	0.060	0.064	0.065	0.064	1340.4F	1342.0F

LOAD	TIME	CH 53 TC-3 DEG F	CH 54 TC-4 DEG F	CH 55 TC-5 DEG F	CH 56 TC-6 DEG F	CH 57 TC-7 DEG F	CH 58 TC-8 DEG F
002	2231.3	1366.5F	1405.2F	1347.9F	1405.2F	1344.5F	1329.1F
004	2232.1	1366.0F	1406.5F	1347.5F	1405.6F	1347.0F	1330.8F
006	2232.8	1366.9F	1405.6F	1350.8F	1406.5F	1347.5F	1330.0F
008	2233.5	1367.8F	1404.7F	1353.0F	1404.7F	1344.1F	1329.1F
010	2234.2	1366.0F	1405.6F	1351.7F	1402.1F	1345.8F	1328.6F
012	2234.9	1369.5F	1406.0F	1350.8F	1407.3F	1345.8F	1326.0F
014	2235.6	1365.2F	1405.2F	1348.7F	1402.6F	1344.5F	1329.1F
016	2236.3	1366.9F	1406.5F	1350.0F	1405.2F	1345.4F	1328.2F
018	2236.8	1367.8F	1405.2F	1351.7F	1406.5F	1341.6F	1325.6F
019	2237.2	1367.8F	1407.8F	1350.8F	1407.8F	1346.6F	1332.6F

LOAD	TIME	CH 59 TC-9 DEG F	CH 60 TC-10 DEG F	CH 61 TC-11 DEG F	CH 62 TC-12 DEG F	CH 63 TC-13 DEG F	CH 64 TC-14 DEG F
002	2231.3	1346.2F	1393.9F	1392.6F	1403.9F	1379.5F	1408.6F
004	2232.1	1347.5F	1392.6F	1393.4F	1404.7F	1377.8F	1406.5F
006	2232.8	1351.7F	1394.7F	1392.6F	1403.4F	1378.6F	1407.3F
008	2233.5	1351.3F	1394.3F	1391.3F	1403.0F	1376.9F	1408.2F
010	2234.2	1350.8F	1393.4F	1390.4F	1401.7F	1376.5F	1405.6F
012	2234.9	1347.9F	1394.3F	1389.5F	1400.8F	1377.8F	1406.0F
014	2235.6	1349.1F	1395.2F	1391.7F	1401.7F	1376.0F	1404.3F
016	2236.3	1346.2F	1392.1F	1392.1F	1403.0F	1378.6F	1406.5F
018	2236.8	1346.2F	1390.8F	1387.9F	1401.3F	1379.1F	1408.2F
019	2237.2	1347.0F	1392.1F	1393.9F	1404.3F	1380.0F	1406.5F

LOAD	TIME	CH 65 TC-15 DEG F	CH 66 TC-16 DEG F	CH 67 TC-17 DEG F	CH 68 TC-18 DEG F	CH 69 TC-19 DEG F	CH 70 TC-20 DEG F
002	2231.3	1326.0F	1321.3F	1327.3F	1204.1F	1125.4F	1231.7F
004	2232.1	1328.2F	1320.8F	1329.5F	1207.0F	1124.5F	1230.0F
006	2232.8	1326.9F	1320.0F	1327.3F	1206.6F	1123.7F	1230.0F
008	2233.5	1329.5F	1320.0F	1328.6F	1206.6F	1123.7F	1228.3F
010	2234.2	1328.2F	1316.9F	1325.6F	1207.0F	1124.5F	1226.6F
012	2234.9	1324.7F	1319.1F	1326.0F	1206.6F	1126.2F	1227.5F
014	2235.6	1326.9F	1319.5F	1324.3F	1204.1F	1123.3F	1228.7F
016	2236.3	1326.0F	1320.4F	1327.3F	1209.1F	1125.8F	1227.0F
018	2236.8	1325.6F	1320.4F	1326.9F	1209.1F	1127.5F	1228.7F
019	2237.2	1325.2F	1321.7F	1329.1F	1205.0F	1125.8F	1230.0F

TABLE 27-27

THICKNESS MEASUREMENTS OF TRAPEZOIDAL CORRUGATION COMPRESSION PANEL

(ELEVATED TEMPERATURE)

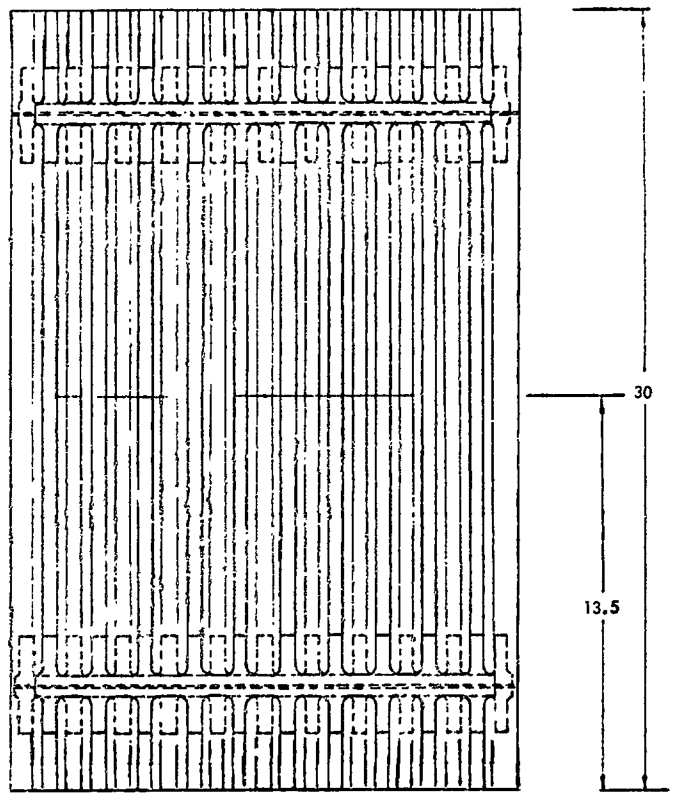

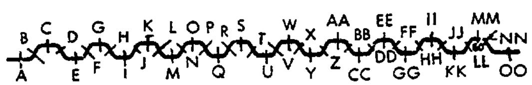

SECTION	A	B	C	D	E	F	G	H	I	J	K	L	M	N	O	P	Q	R	S	T	U
AA	.0165	.0200	.0190	.0165	.0164	.0175	.0175	.0170	.0162	.0168	.0180	.0160	.0160	.0180	.0180	.0160	.0160	.0165	.0175	.0164	.0160
SECTION	V	W	X	Y	Z	AA	BB	CC	DD	EE	FF	GG	HH	II	JJ	KK	LL	MM	NN	OO	-
AA	.0170	.0185	.0170	.0160	.0130	.0182	.0168	.0162	.0170	.0185	.0158	.0160	.0175	.0180	.0165	.0160	.0175	.0175	.0165	.0160	-

TABLE 27-28

THICKNESS MEASUREMENTS FOR BEADED COMPRESSION PANEL
(ROOM TEMPERATURE)

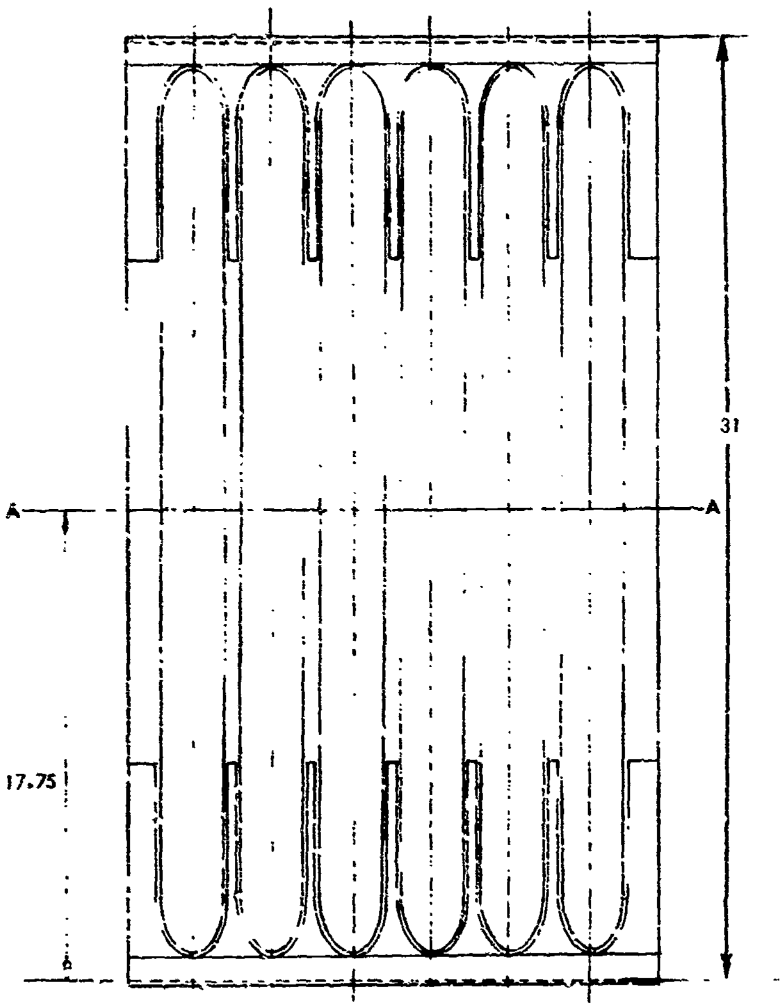

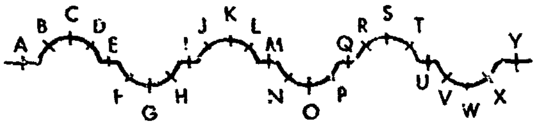

SECTION	A	B	C	D	E	F	G	H	I	J	K	L	M
AA	.0125	.0140	.0130	.0135	.0180	.0140	.0130	.0135	.0180	.0130	.0130	.0130	.0170
SECTION	N	O	P	Q	R	S	T	U	V	W	X	Y	-
AA	.0135	.0130	.0134	.0170	.0130	.0125	.0135	.0170	.0128	.0130	.0130	.0180	-

TABLE 27-29

THICKNESS MEASUREMENTS OF TUBULAR COMPRESSION PANEL
(ROOM TEMPERATURE)

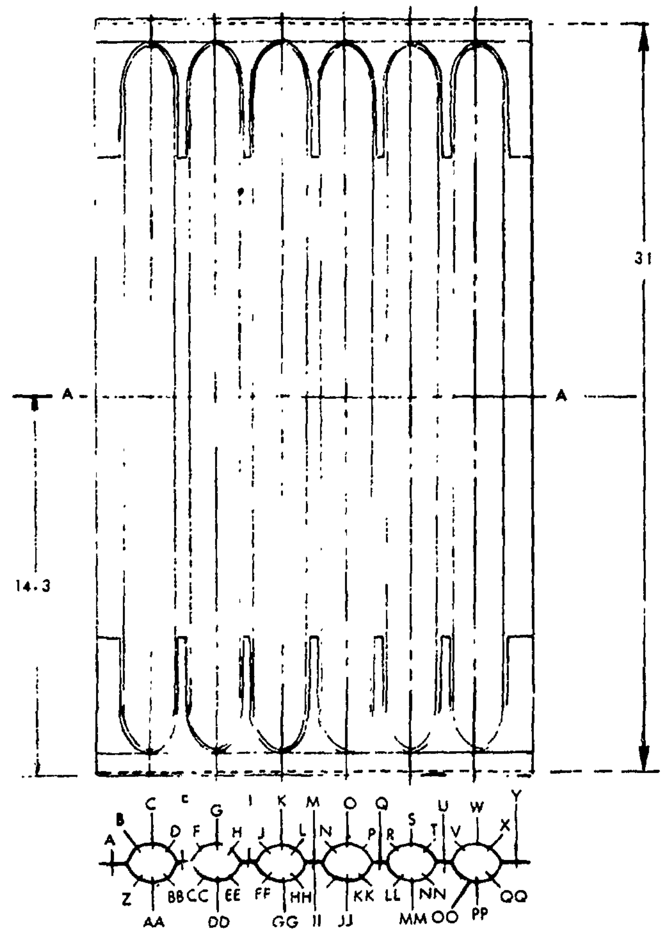

SECTION	A	B	C	D	E	F	G	H	I	J	K	L	M	N	O	P	Q	R	S	T	U	V
AA	.0362	.0121	.0122	.0122	.0348	.0126	.0135	.0125	.0367	.0118	.0124	.0122	.0352	.0118	.0125	.0121	.0348	.0118	.0134	.0123	.0382	0123
SECTION	W	X	Y	Z	AA	BB	CC	DD	EE	FF	GG	HH	II	JJ	KK	LL	MM	NN	OO	PP	QQ	-
AA	.0147	.0135	0352	.0113	.0114	.0112	.0109	.0109	.0108	.0109	.0110	.0109	.0109	.0108	.0110	.0109	.0109	.0110	.0110	0110	0110	-

TABLE 27-30

TEMPERATURE DISTRIBUTIONS FOR TUBULAR COMPRESSION PANEL

LOAD	TIME	CH 47 LVDT. PT-1 INCHES	CH 48 LVDT. PT-2 INCHES	CH 49 LVDT. PT-3 INCHES	CH 50 LVDT. PT-4 INCHES	CH 51 TC-1 DEG F	CH 52 TC-2 DEG F
002	1447.5	0.000J	0.000J	0.000J	0.000J	1406.5F	1380.8F
004	1448.1	0.008	0.008	0.007	0.006	1383.3F	1415.6F
006	1448.9	0.013	0.014	0.013	0.012	1393.0F	1413.9F
008	1449.5	0.019	0.021	0.020	0.019	1393.0F	1419.1F
010	1450.1	0.024	0.027	0.026	0.025	1375.2F	1412.6F
012	1450.8	0.029	0.032	0.032	0.030	1407.3F	1420.0F
013	1451.3	0.031	0.035	0.033	0.032	1409.1F	1421.3F
014	1452.0	0.034	0.037	0.036	0.036	1407.3F	1423.9F
015	1452.7	0.036	0.040	0.039	0.039	1400.0F	1426.0F
016	1453.3	0.039	0.043	0.042	0.042	1402.6F	1418.6F
017	1453.8	0.041	0.046	0.046	0.045	1368.2F	1421.3F
018	1454.4	0.044	0.048	0.047	0.047	1418.2F	1428.2F
019	1455.0	0.045	0.050	0.049	0.048	1417.3F	1418.6F
020	1455.7	0.047	0.053	0.051	0.050	1416.9F	1431.7F
021	1456.2	0.050	0.055	0.054	0.053	1417.8F	1423.4F
022	1456.8	0.052	0.057	0.056	0.055	1417.8F	1441.3F
023	1457.3	0.054	0.059	0.059	0.058	1420.0F	1418.2F
024	1457.9	0.056	0.061	0.061	0.060	1422.1F	1433.0F
026	1458.8	0.060	0.067	0.066	0.065	1416.5F	1420.8F
027	1459.3	0.063	0.069	0.069	0.067	1424.3F	1438.6F
028	1459.7	0.065	0.071	0.070	0.069	1422.1F	1437.8F
029	1500.2	0.066	0.073	0.074	0.071	1423.4F	1419.5F
030	1500.8	0.069	0.076	0.075	0.073	1410.0F	1432.1F
031	1501.3	0.072	0.079	0.078	0.076	1424.3F	1437.3F
032	1501.7	0.074	0.081	0.080	0.079	1418.2F	1426.5F
033	1502.1	0.076	0.085	0.083	0.081	1423.0F	1436.5F
034	1502.5	0.078	0.086	0.086	0.084	1410.0F	1408.6F
035	1503.0	0.081	0.090	0.087	0.086	1425.6F	1433.9F
036	1503.5	0.083	0.092	0.091	0.089	1416.9F	1431.7F
037	1503.9	0.086	0.095	0.094	0.092	1419.1F	1428.6F
038	1504.2	0.088	0.097	0.096	0.094	1421.3F	1430.8F
039	1504.7	0.091	0.099	0.099	0.096	1422.1F	1434.3F
041	1505.4	0.095	0.105	0.104	0.102	1424.3F	1424.3F
042	1505.9	0.098	0.108	0.108	0.104	1421.3F	1434.7F

LOAD	TIME	CH 53 TC-3 DEG F	CH 54 TC-4 DEG F	CH 55 TC-5 DEG F	CH 56 TC-6 DEG F	CH 57 TC-7 DEG F	CH 58 TC-8 DEG F
002	1447.5	1413.9F	1432.6F	1470.0F	1431.7F	1253.7F	1372.1F
004	1448.1	1397.3F	1450.4F	1466.9F	1417.3F	1252.5F	1376.9F
006	1448.9	1422.1F	1461.7F	1473.4F	1442.1F	1262.6F	1384.5F
008	1449.5	1423.0F	1443.4F	1474.7F	1435.2F	1254.1F	1385.8F
010	1450.1	1419.5F	1460.4F	1475.6F	1443.0F	1264.7F	1341.6F
012	1450.8	1424.7F	1445.6F	1464.3F	1446.0F	1254.1F	1383.7F
013	1451.3	1425.6F	1465.2F	1474.7F	1447.8F	1266.9F	1390.4F
014	1452.0	1423.4F	1470.8F	1470.4F	1443.9F	1242.1F	1367.8F
015	1452.7	1409.5F	1444.7F	1475.6F	1450.0F	1269.1F	1380.8F
016	1453.3	1426.9F	1464.7F	1473.4F	1398.2F	1272.9F	1385.0F
017	1453.8	1426.0F	1465.6F	1476.9F	1443.4F	1274.1F	1393.4F
018	1454.4	1423.0F	1472.6F	1471.7F	1442.6F	1275.0F	1393.0F
019	1455.0	1426.9F	1461.3F	1479.5F	1444.7F	1265.6F	1393.4F
020	1455.7	1417.8F	1468.6F	1476.9F	1446.9F	1276.2F	1390.8F
021	1456.2	1413.9F	1466.0F	1472.6F	1432.1F	1273.7F	1389.1F
022	1456.8	1425.2F	1463.9F	1479.5F	1448.6F	1280.0F	1388.7F
023	1457.3	1432.1F	1462.1F	1468.2F	1443.0F	1277.9F	1391.3F
024	1457.9	1422.1F	1469.5F	1483.0F	1446.9F	1278.3F	1395.2F
026	1458.8	1426.0F	1470.8F	1470.8F	1442.1F	1283.9F	1387.5F
027	1459.3	1430.4F	1470.4F	1465.6F	1435.6F	1280.4F	1379.1F
028	1459.7	1428.6F	1476.5F	1477.8F	1443.4F	1281.7F	1391.3F
029	1500.2	1430.0F	1469.5F	1477.8F	1449.1F	1278.3F	1396.0F
030	1500.8	1430.4F	1471.3F	1486.5F	1444.3F	1278.7F	1394.3F
031	1501.3	1432.1F	1471.3F	1481.7F	1437.3F	1282.1F	1396.0F
032	1501.7	1414.7F	1466.5F	1471.7F	1437.8F	1267.3F	1383.3F
033	1502.1	1421.3F	1468.2F	1478.6F	1440.0F	1286.0F	1381.6F
034	1502.5	1427.3F	1470.4F	1466.0F	1442.6F	1284.7F	1387.5F
035	1503.0	1410.4F	1455.0F	147[illegible].7F	1450.4F	1276.2F	1393.4F
036	1503.5	1429.1F	1466.0F	1466.5F	1446.5F	1264.7F	1374.7F
037	1503.9	1423.9F	1460.8F	1474.3F	1440.8F	1279.1F	1385.4F
038	1504.2	1425.6F	1458.6F	1472.6F	1439.1F	1281.7F	1389.5F
039	1504.7	1420.4F	1463.0F	1475.6F	1440.4F	1280.4F	1391.3F
041	1505.4	1418.2F	1450.9F	1483.4F	1443.0F	1276.6F	1390.0F
042	1505.9	1430.4F	1464.7F	1476.0F	1436.0F	1279.5F	1383.3F

TABLE 27-30

(Concluded)

LOAD	TIME	CH 59	CH 60	CH 61	CH 62	CH 63	CH 64
		TC-9 DEG F	TC-10 DEG F	TC-11 DEG F	TC-12 DEG F	TC-13 DEG F	TC-14 DEG F
002	1447.5	1368.6F	1389.1F	1425.2F	1431.3F	1433.9F	1408.6F
004	1448.1	1361.3F	1345.4F	1454.0F	1435.6F	1413.0F	1419.1F
006	1448.9	1361.3F	1387.0F	1453.6F	1425.2F	1421.3F	1413.0F
008	1449.5	1375.2F	1389.5F	1431.3F	1449.5F	1420.8F	1413.9F
010	1450.1	1350.0F	1389.5F	1434.7F	1439.1F	1433.9F	1402.6F
012	1450.8	1371.7F	1367.3F	1454.5F	1442.1F	1439.5F	1423.0F
013	1451.3	1356.9F	1393.4F	1456.3F	1450.0F	1435.2F	1399.5F
014	1452.0	1362.1F	1390.8F	1448.6F	1422.1F	1433.0F	1408.6F
015	1452.7	1370.0F	1376.0F	1456.8F	1451.3F	1426.0F	1423.0F
016	1453.3	1350.0F	1391.7F	1451.8F	1432.6F	1426.0F	1409.1F
017	1453.8	1373.4F	1397.3F	1449.1F	1451.8F	1436.9F	1413.0F
018	1454.4	1378.6F	1396.9F	1423.9F	1442.6F	1423.4F	1414.7F
019	1455.0	1379.5F	1390.8F	1453.1F	1450.4F	1435.2F	1418.6F
020	1455.7	1382.0F	1400.0F	1452.7F	1448.2F	1440.0F	1420.8F
021	1456.2	1378.2F	1395.6F	1457.2F	1453.6F	1427.3F	1413.4F
022	1456.8	1376.5F	1395.2F	1458.1F	1447.3F	1440.4F	1423.0F
023	1457.3	1372.1F	1384.5F	1458.6F	1454.5F	1440.8F	1425.2F
024	1457.9	1375.6F	1392.1F	1456.8F	1442.1F	1433.0F	1416.9F
026	1458.8	1382.5F	1400.4F	1458.6F	1455.9F	1436.5F	1420.4F
027	1459.3	1384.5F	1368.2F	1465.6F	1442.1F	1438.6F	1417.3F
028	1459.7	1358.2F	1402.1F	1462.6F	1453.1F	1432.6F	1420.4F
029	1500.2	1370.8F	1398.6F	1460.4F	1451.3F	1434.7F	1416.0F
030	1500.8	1389.5F	1400.8F	1465.6F	1455.0F	1437.8F	1408.2F
031	1501.3	1378.6F	1393.4F	1461.3F	1450.0F	1435.2F	1413.4F
032	1501.7	1350.8F	1385.4F	1409.5F	1410.0F	1425.6F	1413.9F
033	1502.1	1381.2F	1396.0F	1437.3F	1443.9F	1439.5F	1400.4F
034	1502.5	1348.3F	1396.9F	1461.7F	1449.5F	1420.0F	1413.4F
035	1503.0	1379.1F	1400.4F	1458.1F	1432.1F	1434.3F	1413.4F
036	1503.5	1370.8F	1391.3F	1439.1F	1442.6F	1427.3F	1430.4F
037	1503.9	1356.9F	1392.1F	1452.2F	1442.1F	1433.0F	1411.7F
038	1504.2	1374.3F	1377.8F	1454.5F	1446.0F	1429.1F	1408.6F
039	1504.7	1364.7F	1391.3F	1446.0F	1438.2F	1432.1F	1415.2F
041	1505.4	1376.9F	1393.9F	1452.7F	1444.3F	1427.8F	1396.9F
042	1505.9	1360.4F	1385.0F	1434.3F	1442.1F	1428.6F	1423.9F

LOAD	TIME	CH 65	CH 66	CH 67	CH 68	CH 69	CH 70
		TC-15 DEG F	TC-16 DEG F	TC-17 DEG F	TC-18 DEG F	TC-19 DEG F	TC-20 DEG F
002	1447.5	1427.8F	1378.6F	1365.6F	1331.7F	1346.2F	1292.1F
004	1448.1	1396.9F	1397.3F	1389.1F	1350.8F	1350.8F	1300.0F
006	1448.9	1413.4F	1385.4F	1380.4F	1348.3F	1347.5F	1300.0F
008	1449.5	1420.8F	1386.2F	1392.6F	1346.6F	1357.8F	1313.0F
010	1450.1	1390.4F	1395.2F	1382.0F	1331.3F	1356.5F	1291.3F
012	1450.8	1405.6F	1382.0F	1396.9F	1349.1F	1360.4F	1307.0F
013	1451.3	1415.6F	1405.2F	1394.7F	1346.2F	1341.2F	1305.4F
014	1452.0	1397.8F	1398.6F	1373.0F	1305.4F	1353.9F	1294.3F
015	1452.7	1426.0F	1405.2F	1399.1F	1341.6F	1314.3F	1309.1F
016	1453.3	1420.0F	1381.6F	1385.4F	1333.4F	1358.6F	1318.2F
017	1453.8	1430.8F	1401.3F	1393.4F	1340.4F	1357.3F	1321.3F
018	1454.4	1424.7F	1360.8F	1379.1F	1346.2F	1360.0F	1319.5F
019	1455.0	1424.7F	1401.7F	1397.8F	1338.2F	1364.7F	1323.4F
020	1455.7	1428.6F	1396.5F	1390.0F	1352.6F	1366.0F	1324.3F
021	1456.2	1429.1F	1404.7F	1398.2F	1344.1F	1366.0F	1321.7F
022	1456.8	1435.2F	1402.6F	1395.2F	1351.3F	1366.5F	1321.3F
023	1457.3	1431.3F	1407.8F	1401.3F	1366.0F	1368.6F	1324.3F
024	1457.9	1431.3F	1404.7F	1388.7F	1356.9F	1368.2F	1321.7F
026	1458.8	1427.8F	1403.9F	1396.0F	1354.3F	1369.1F	1325.2F
027	1459.3	1400.8F	1399.1F	1399.1F	1363.9F	1370.8F	1313.4F
028	1459.7	1428.6F	1405.2F	1403.0F	1348.7F	1366.0F	1326.5F
029	1500.2	1434.3F	1403.9F	1404.7F	1360.0F	1368.2F	1327.3F
030	1500.8	1431.7F	1393.9F	1395.2F	1354.7F	1371.3F	1329.5F
031	1501.3	1428.6F	1406.9F	1400.4F	1345.8F	1345.8F	1327.3F
032	1501.7	1415.2F	1395.6F	1385.8F	1350.8F	1310.8F	1320.8F
033	1502.1	1426.5F	1404.3F	1396.0F	1334.7F	1364.3F	1315.6F
034	1502.5	1418.2F	1395.2F	1393.0F	1336.9F	1372.1F	1308.4F
035	1503.0	1433.0F	1382.5F	1396.9F	[illegible]	1371.3F	1327.3F
036	1503.5	1414.3F	1386.6F	1392.6F	1345.0F	1359.5F	1324.3F
037	1503.9	1426.0F	1396.5F	1392.1F	[illegible]	1366.9F	1321.7F
038	1504.2	1426.0F	1378.2F	[illegible]	[illegible]	1366.9F	1323.4F
039	1504.7	1419.5F	1396.9F	1381.6F	[illegible]	[illegible]	1320.8F
041	1505.4	1420.4F	1396.0F	1386.6F	1344.5F	[illegible]	1383.0F
042	1505.9	1392.1F	1397.3F	1388.8F	1337.3F	[illegible]	1308.8F

TABLE 27-31

THICKNESS MEASUREMENTS OF TUBULAR COMPRESSION PANEL

(ELEVATED TEMPERATURE)

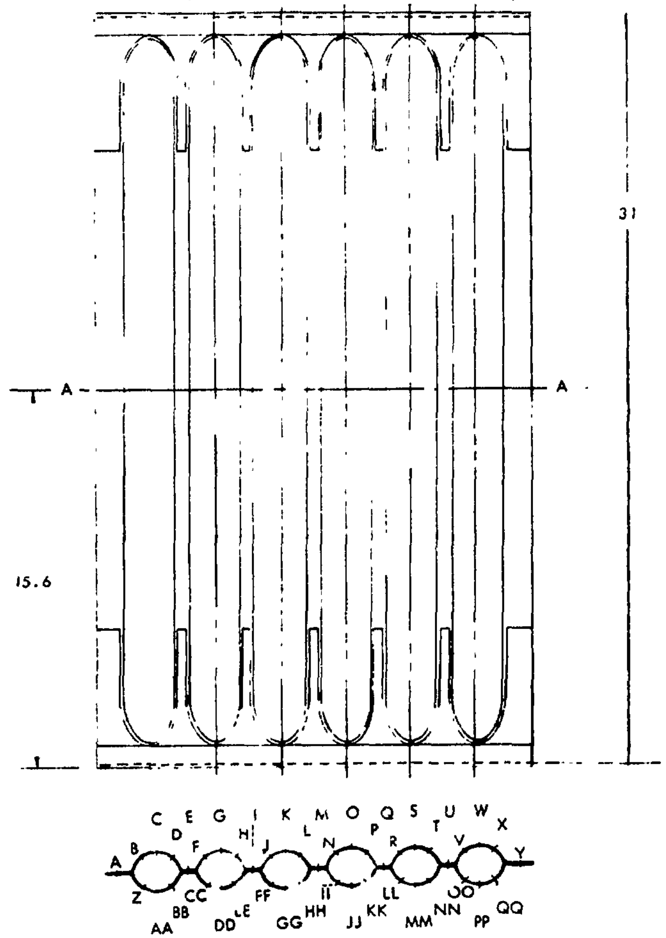

SECTION	A	B	C	D	E	F	G	H	I	J	K	L	M	N	O	P	Q	R	S	T	U	V
AA	.0310	.0130	.0130	.0130	.0310	.0120	.0130	.0120	.0310	.0120	.0120	.0120	.0310	.0120	.0120	.0130	.0310	.0120	.0120	.0120	.0310	.0120
SECTION	W	X	Y	Z	AA	BB	CC	DD	EE	FF	GG	HH	II	JJ	KK	LL	MM	NN	OO	PP	QQ	-
AA	.0130	.0140	.0320	.0120	.0120	.0120	.0110	.0110	.0110	.0110	.0110	.0110	.0110	.0110	.0110	.0110	.0120	.0110	.0120	.0130	.0120	-

TABLE 27-32

THICKNESS MEASUREMENTS OF CIRCULAR ARC CORRUGATION SHEAR PANEL (RENE 41, FILLER WIRE)

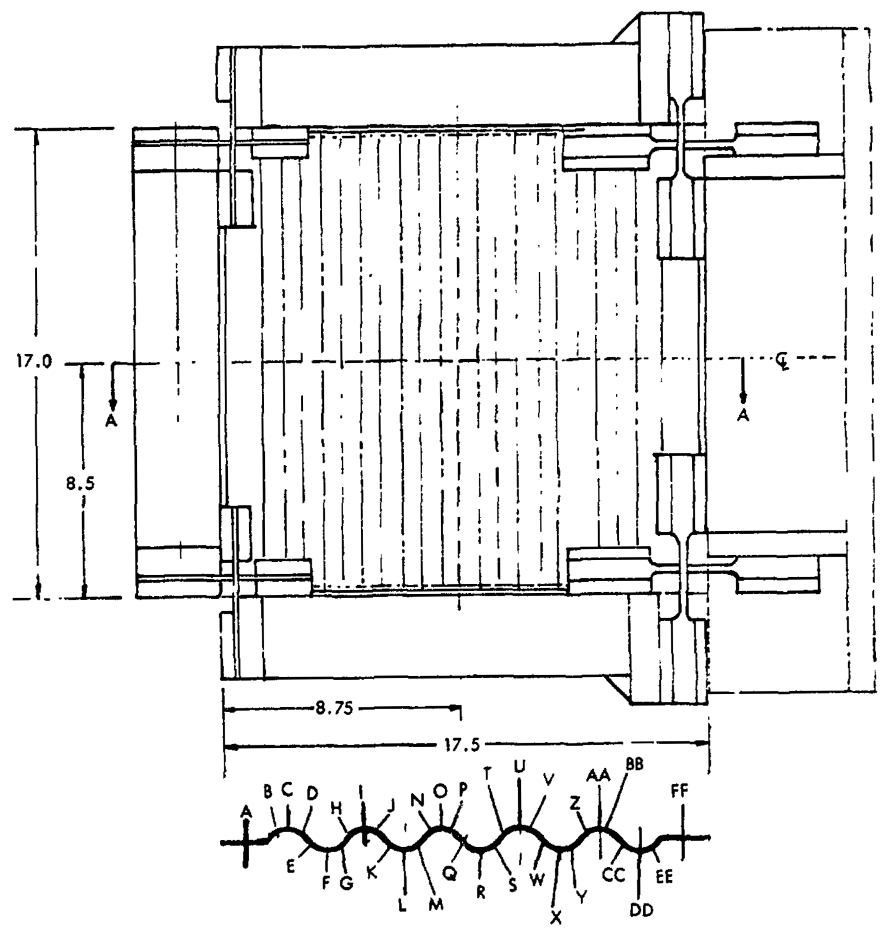

SECTION	A	B	C	D	E	F	G	H	I	J	K	L	M	N	O	P
AA	.0636	.0147	.0138	.0149	.0149	.0159	.0137	.0128	.0148	.0139	.0129	.0131	.0129	.0134	.0149	.0136
SECTION	Q	R	S	T	U	V	W	X	X	Z	AA	BB	CC	DD	EE	FF
AA	.0134	.0153	.0135	.0128	.0132	.0147	.0129	.0148	.0132	.0128	.0129	.0128	.0135	.0147	.0148	.0680

TABLE 27-33

THICKNESS MEASUREMENTS OF CIRCULAR ARC CORRUGATION VERTICAL WEB (HASTELLOY W FILLER WIRE)

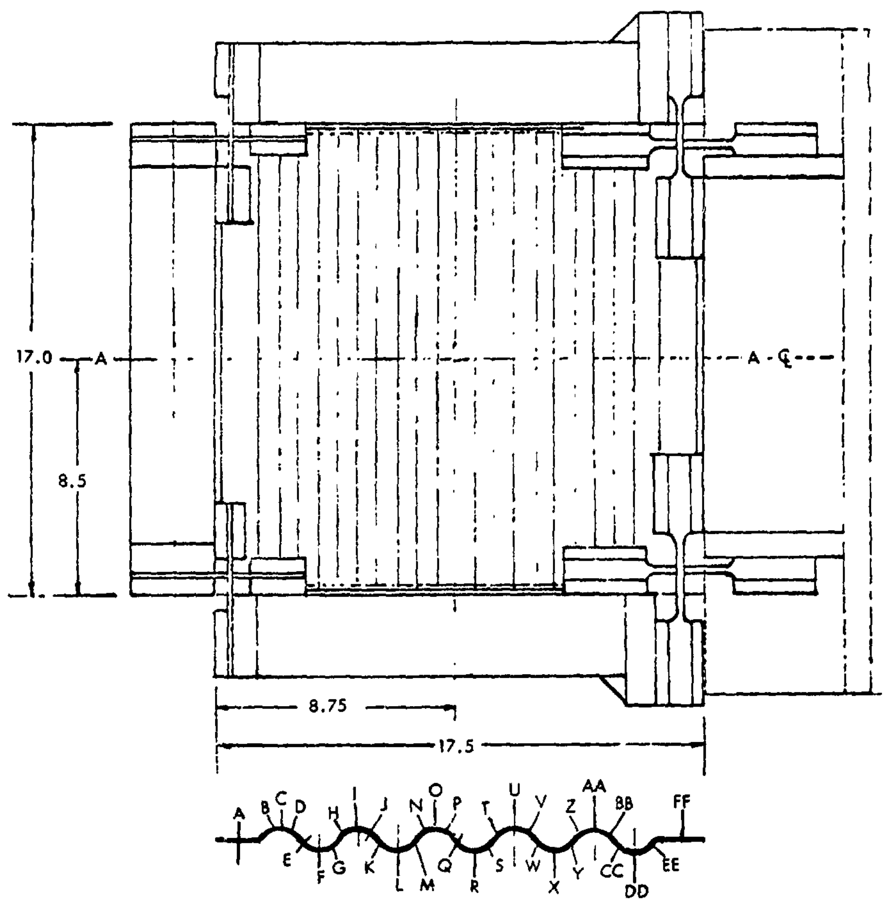

SECTION	A	B	C	D	E	F	G	H	I	J	K	L	M	N	O	P
AA	.0640	.0148	.0162	.0132	.0131	.0131	.0130	.0133	.0155	.0132	.0128	.0129	.0128	.0132	.0158	.0129
SECTION	Q	R	S	T	U	V	W	X	Y	Z	AA	BB	CC	DD	EE	FF
AA	.0131	.0132	.0129	.0138	.0163	.0132	.0129	.0128	.0129	.0138	.0158	0142	.0135	.0138	.0138	.0890

TABLE 27-34

SUMMARY CORRELATION OF STRUCTURAL ELEMENT TESTS

Panel concept	Test type	Test temp., °F	Calculated Stresses		Avg. test stresses		Remarks
			Initial buckling,[a] psi	Failure, psi	Initial buckling, psi	Failure, psi	
Tubular	Closeout	RT	105 300 L	105 300 C	83 000	85 000	End doublers were too short
	Crippling	RT	105 300 L	105 300 C	88 000	90 400	Uneven load distribution
	Crippling	1400	78 500 L	78 500 C	66 700	66 700	Some detached spotwelds
	Panel[c]	RT	105 300 L	105 300 C	73 800	73 800	Some detached spotwelds; and unknown amount of bending load was applied in test
	Panel[c]	1400	78 500 L	78 500 C	80 200	80 200	None
Beaded	Closeout	RT	130 000 L	130 000 C	74 500	84 600	End doublers were too short
	Crippling	RT	130 000 L	130 000 C	96 700	105 000	Proportional limit being approached and actual values for the tested sheet unknown
	Crippling	1400	92 500 L	92 500 C	65 400	72 200	
	Panel	RT	27 900 L	27 900 L	32 600	42 600	Some postbuckling behavior
Corrugation-stiffened	Closeout	RT	22 200 L	55 000 C	26 300	47 300	Failure in edge support due to eccentric loading
	Crippling	RT	22 200 L	55 000 C	26 000	69 200	Substantial postbuckling strength indicated in test
	Crippling	1400	16 200 L	41 500 C	30 000	43 700	Unknown
	Panel[c]	RT	22 200 L	32 900 P	24 700	39 600	Eccentric end loading and a panel bowing imperfection of 0.10 measured at midpanel
	Panel[c]	1400	16 200 L	24 000 P	17 300	32 000	Some postbuckling behavior
Trapezoidal corrugation	Crippling	RT	69 600 L	86 600 C	69 600	92 400	None
	Crippling	1400	50 800 L	64 300 C	54 500	66 800	None
	Panel[b,c]	RT	69 600 L	75 200 P	69 300	75 600	None
	Panel[b,c]	1400	50 800 L	55 100 P	49 800	49 800	Panel instability with possible interaction with initial buckling
Circular arc Corrugation Shear panel	Shear	RT	41 200 L	44 200 P	38 500	40 500	None
		RT	38 700 L	43 300 P	38 400	38 400	
Spar cap	Crippling	RT	110 000 L	133 500 C	104 000	127 200	Slight eccentric cap loading

[a]Code for type of buckling: L local, P panel, C crippling.
[b]Tested with clamped loaded edges; all other types of panels tested with simple support-loaded edges.
[c]All panels tested for panel buckling were 30 in. long.

TABLE 27-35

COMPARISON OF TUBULAR AND BEADED CONFIGURATION INITIAL BUCKLING TEST RESULTS WITH PREDICTIONS

Panel concept	Tubular				Beaded	
Test type	Crippling		Panel		Crippling	
Test temperature	RT	1400°F	RT	1400°F	RT	1400°F
• Avg test initial Buckling stress (psi)	88 000	66 700	73 800[c]	80 200	96 700	65 400
• Calculated initial Buckling stresses (psi)						
12-14, arc-buckling (local)	105 300	78 500	105 300	78 500	130 000	92 500
Test/Pred.	0.84	0.85	0.70	1.02	0.75	0.71
• Interrivet buckling[a]	82 500	60 500	82 500	60 500	–	–
Test/Pred.	1.07	1.10	0.90	1.33	–	–
• Buckling of flat[b]	76 600	56 000	76 000	56 000	97 500	71 200
Text/Pred.	1.15	1.19	0.97	1.43	0.99	0.92
• Comments	–	detached spots	–	–	–	–

[a]Based on one loose spotweld in each row of double row, located side-by-side; S = 0.5 in., K = 3.5.

[b]Based on treating one sheet in the flat as a place with no spotwelds.

[c]Unknown amount of bending was applied

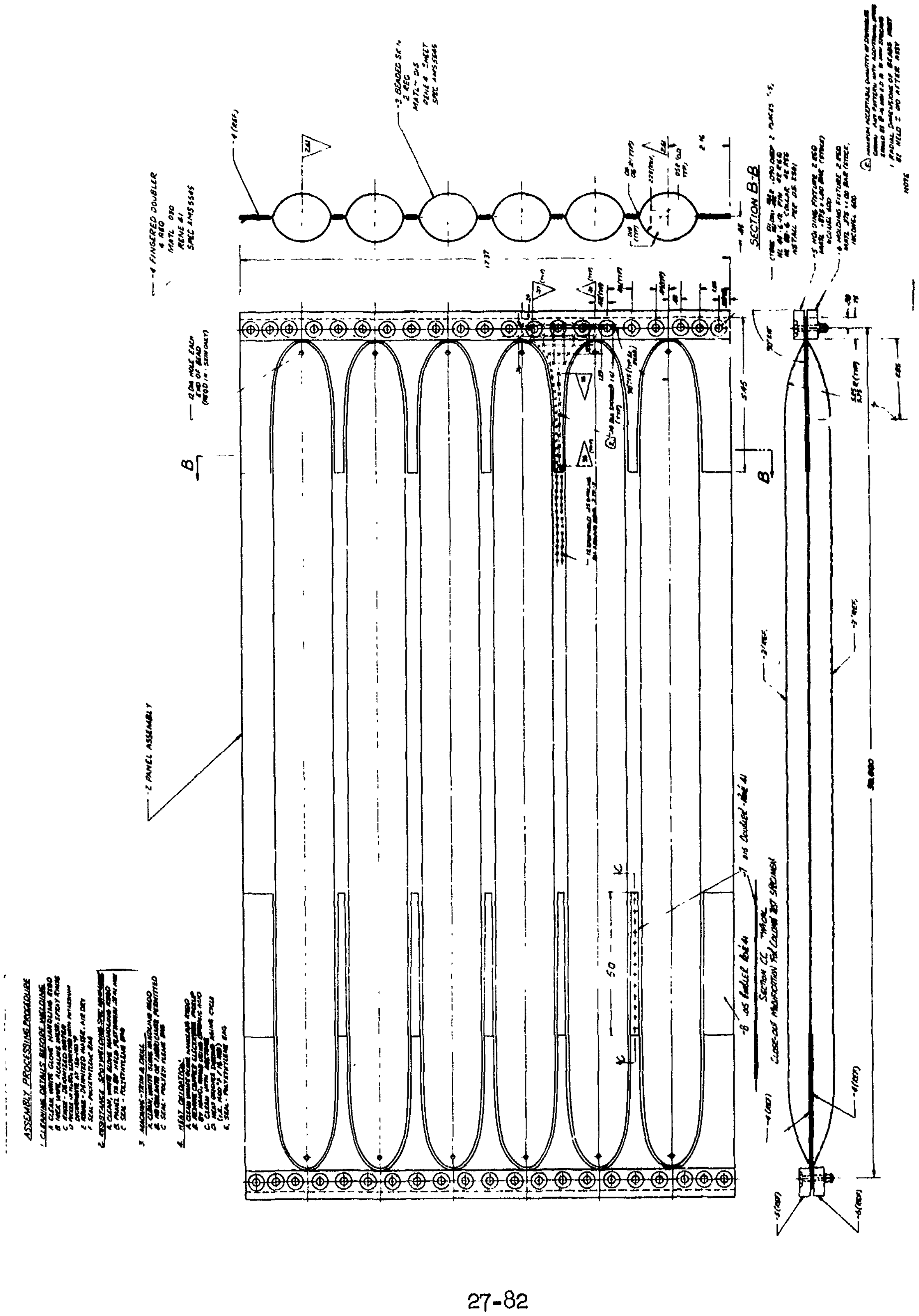

Figure 27-1. Test panel assembly - tubular concept

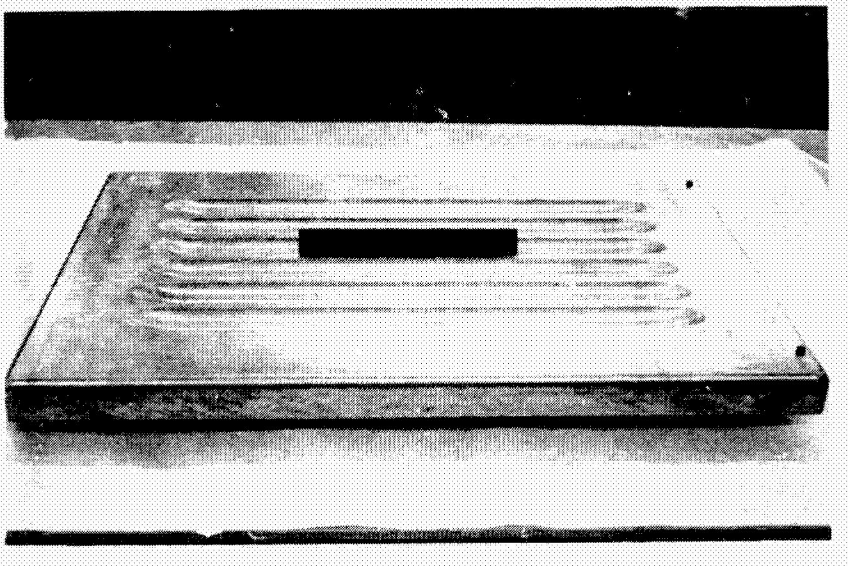

For use in Verson-Wheelon high
pressure rubber forming press

Figure 27-2. Formblock for tubular panels

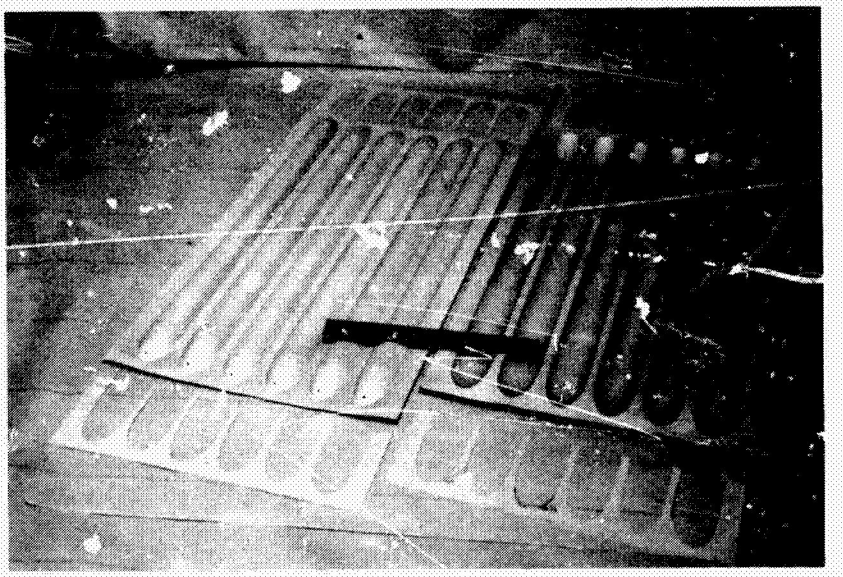

Note vent holes drilled
in ends of formed beads

Figure 27-3. Tubular panel details prior to assembly

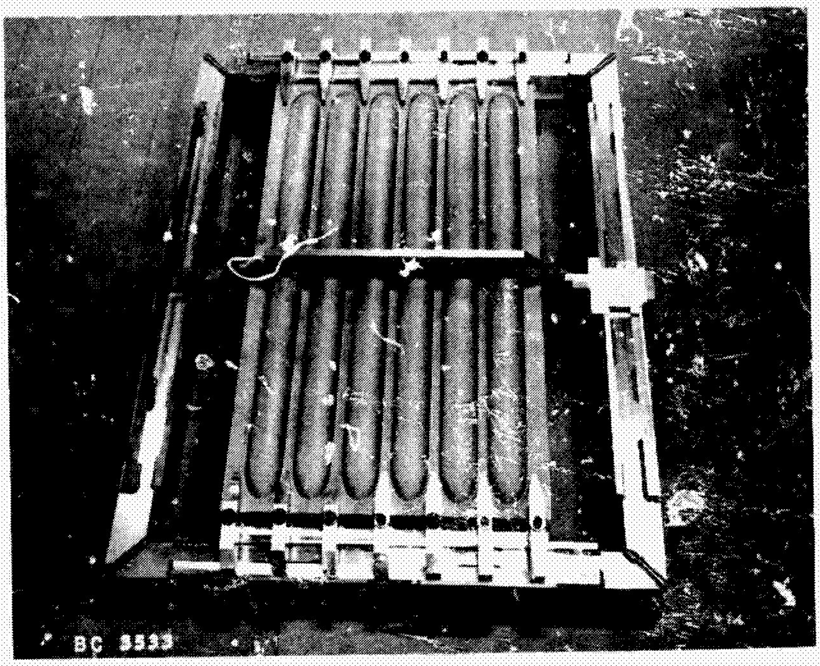

Figure 27-4. Tubular panel in weld fixture ready for resistance spot weld assembly

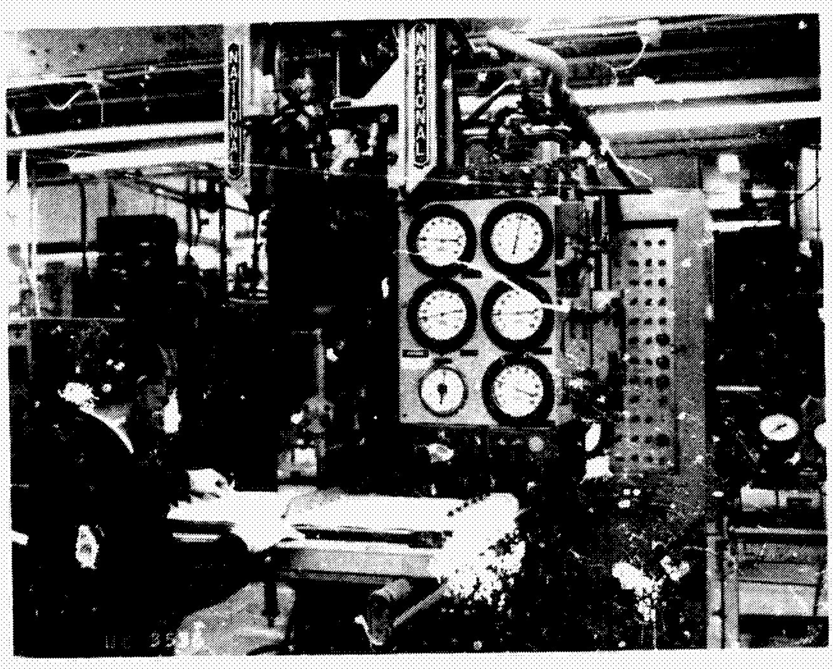

100 kva, three phase, silicon
diode rectified dc welder

Figure 27-5. Panel details being resistance spot welded

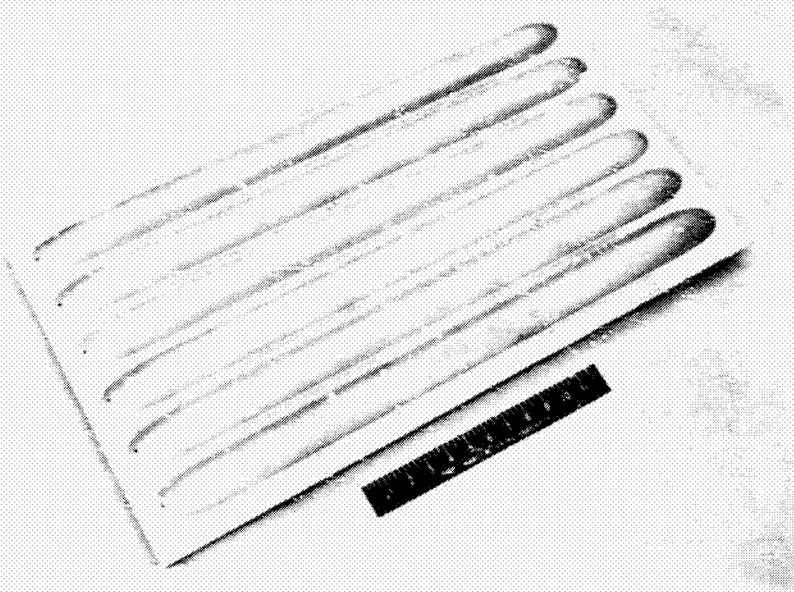

Figure 27-6. Tubular panel after resistance spot welding.

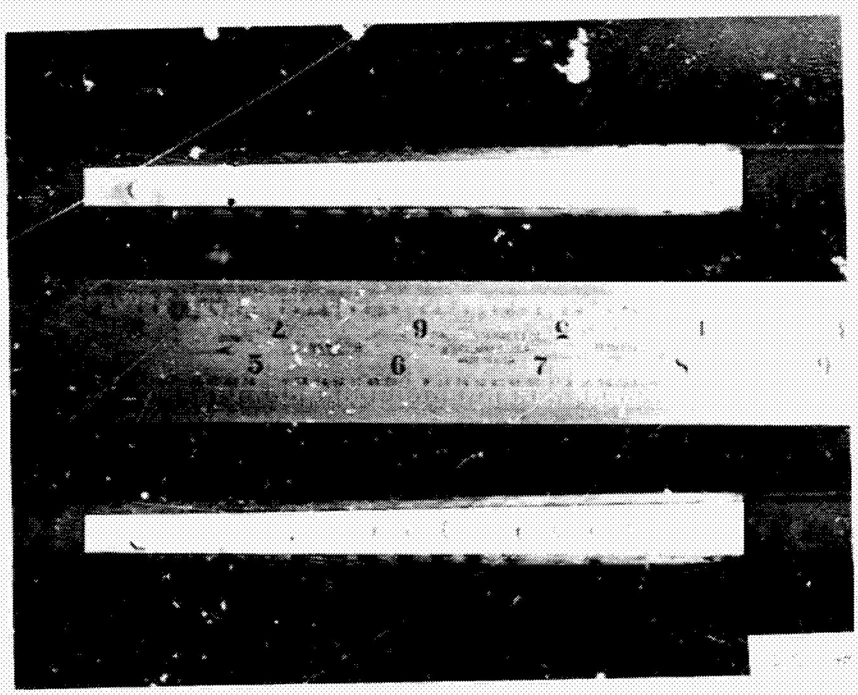

Figure 27-7. Finger doubler extensions for tubular panel

Figure 27-8. Circular arc stiffened tubular end closeout specimen prior to end casting and grinding

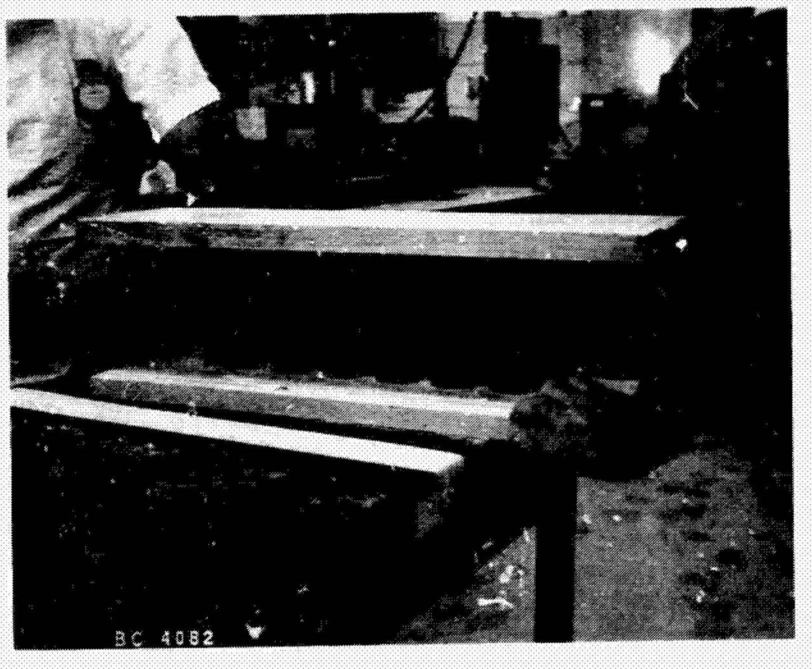

Figure 27-9. Tubular crippling panel shown with ends cast in densite

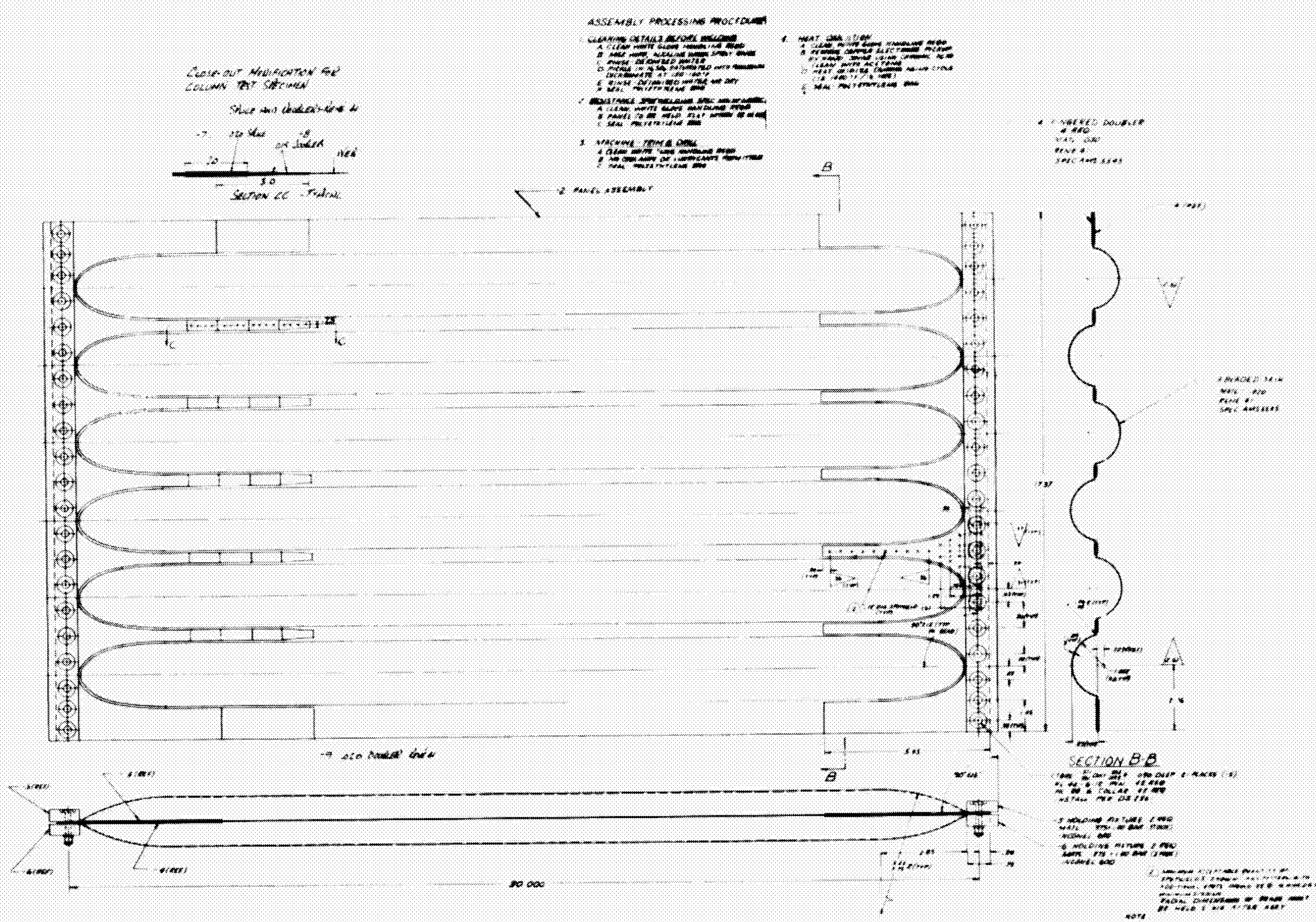

Figure 27-10. Test panel assembly — beaded panel

Figure 27-11. Beaded panel hydraulic forming dieblock

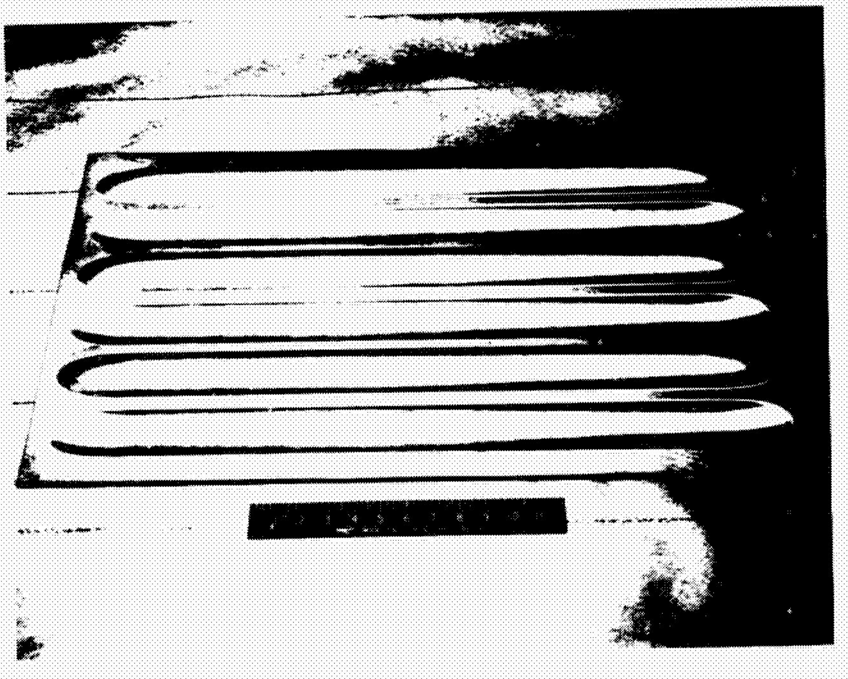

Figure 27-12. Beaded panel trimmed prior to assembly

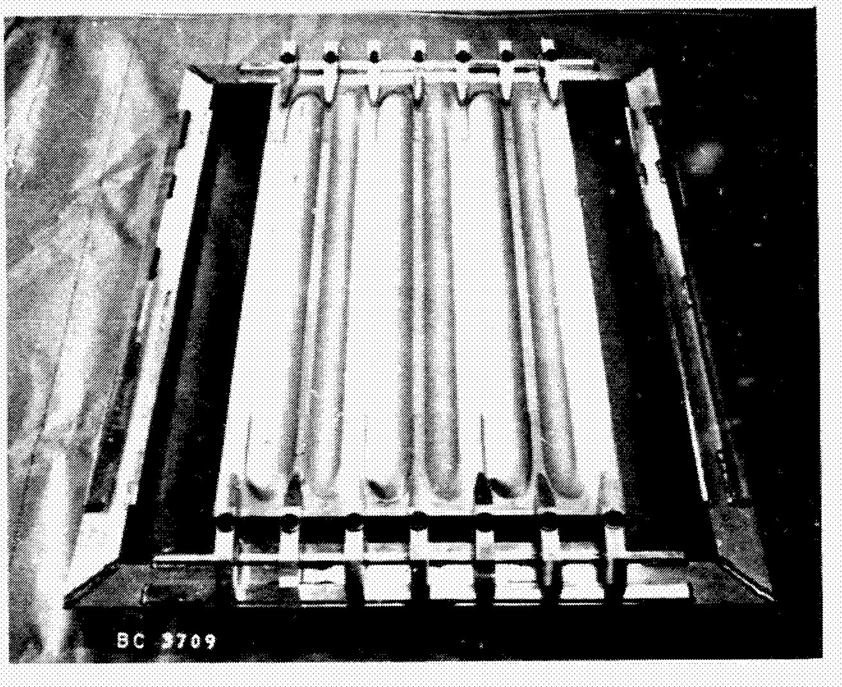

Figure 27-13 Beaded panel details in weld fixture prior to resistance spot weld assembly

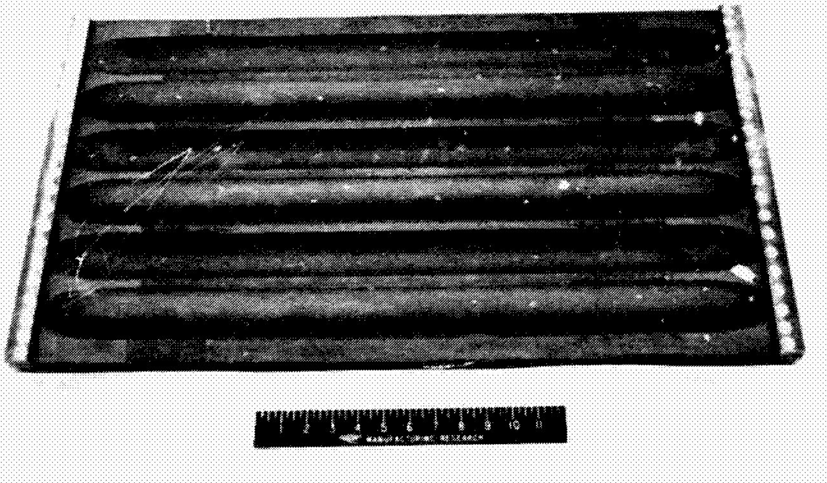

Figure 27-14 Beaded panel after aging, heat oxidation and installation of end bars

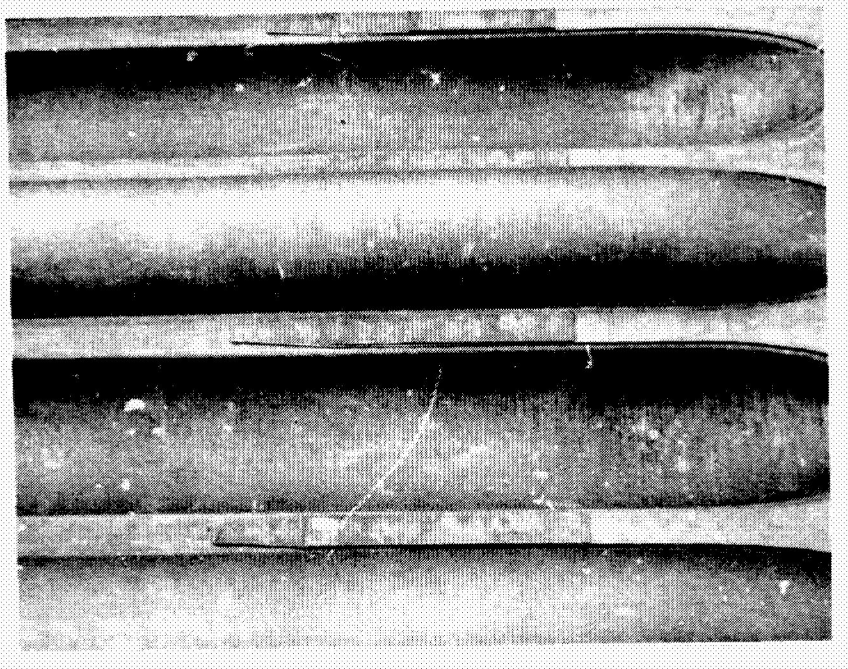

Figure 27-15. Beaded panel showing finger doubler extensions

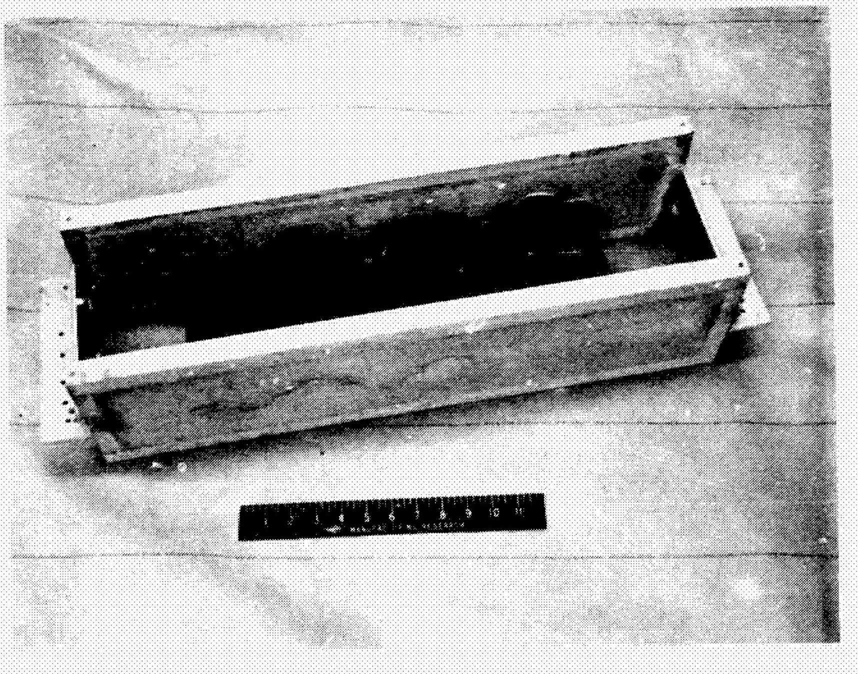

Figure 27-16. Beaded crippling specimen with ends cast in densite

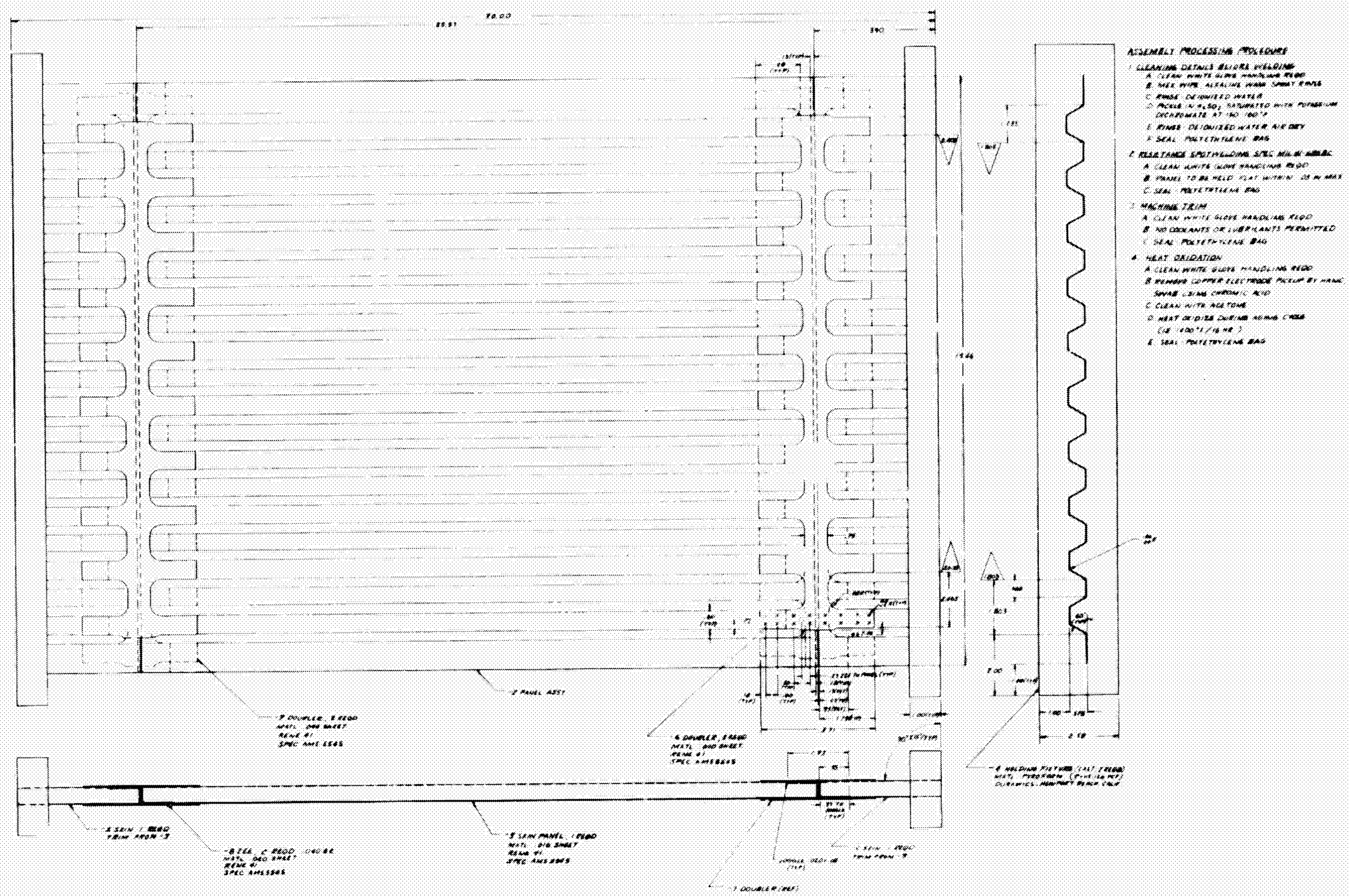

Figure 27-17. Test panel assembly — trapezoidal corrugation

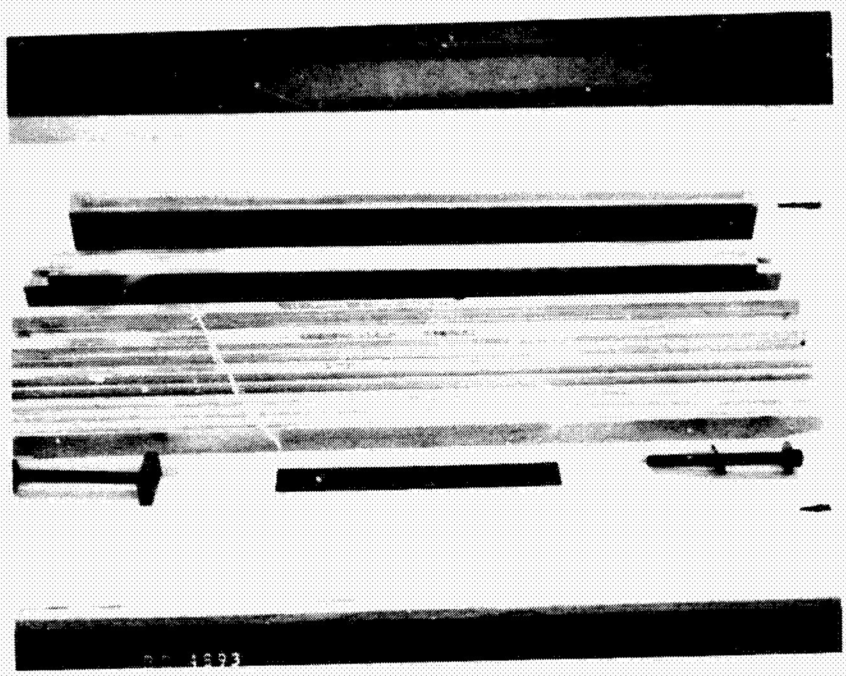

Figure 27-18. Trapezoidal corrugation panel forming die

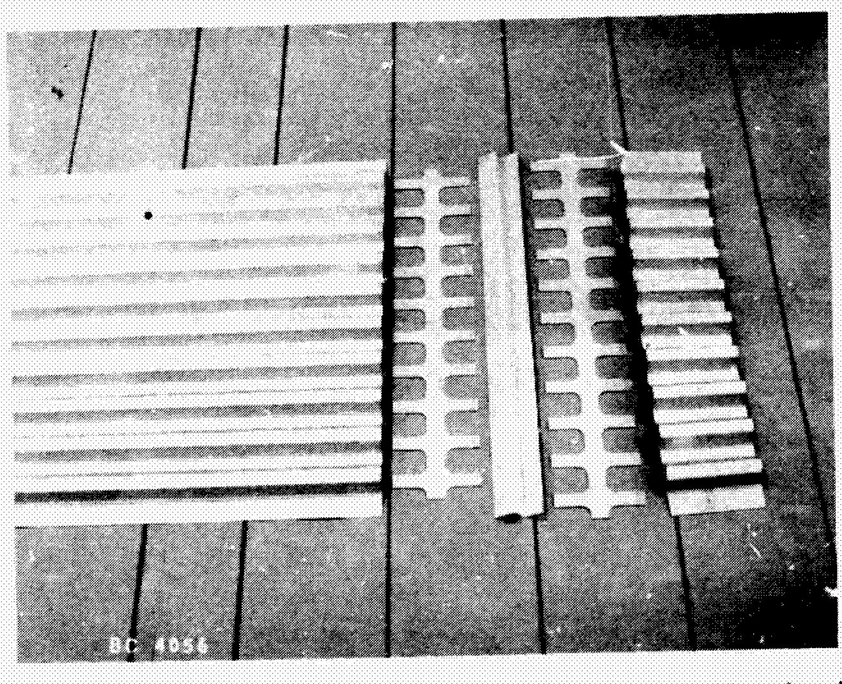

Figure 27-19. Trapezoidal corrugation panel details showing central section corrugation, end corrugation, zee section and fingered splices

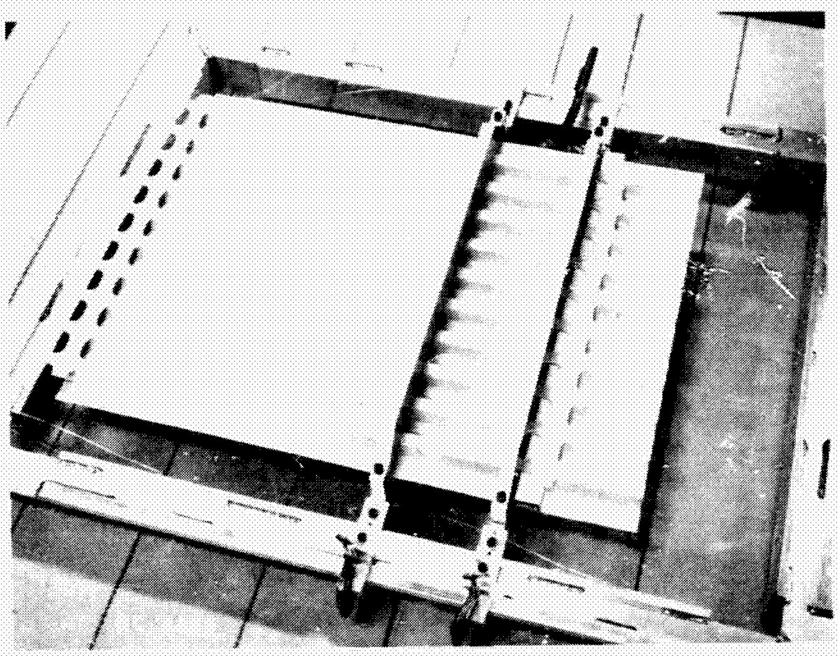

Figure 27-20. Trapezoidal corrugation panel details in weld fixture ready for resistance spot weld assembly

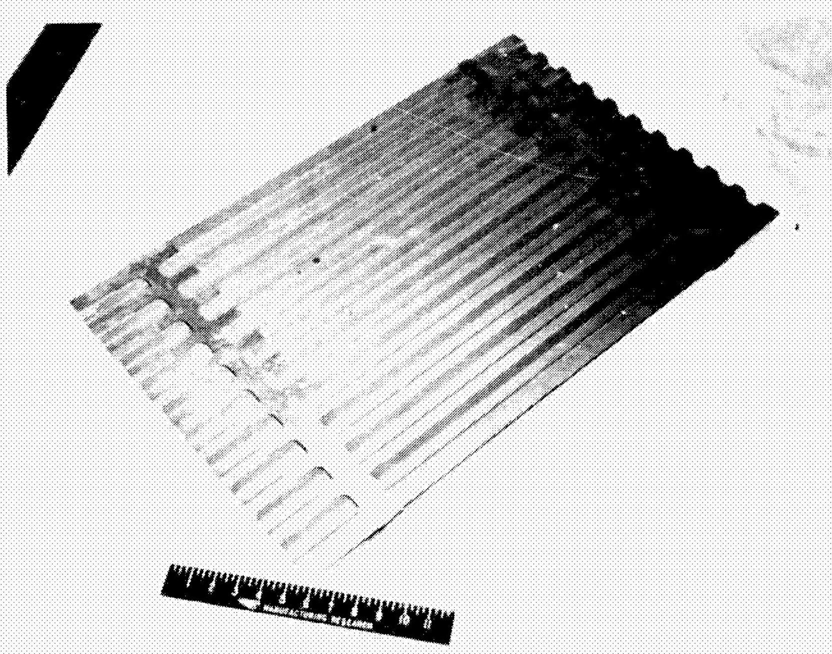

Figure 27-21. Trapezoidal corrugation panel assembly after aging and heat oxidation

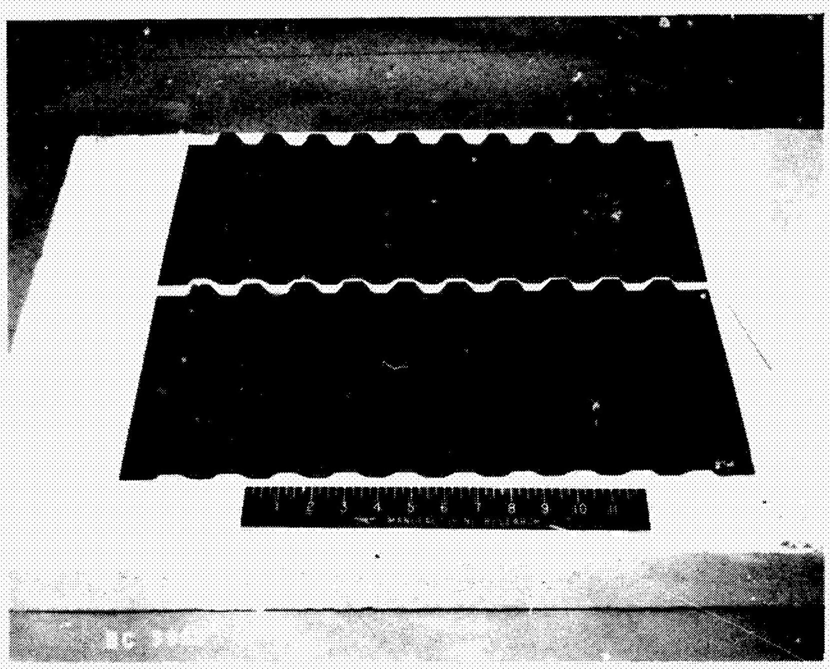

Figure 27-22. Trapezoidal corrugation panel cut to two 8-inch lengths for crippling panel tests

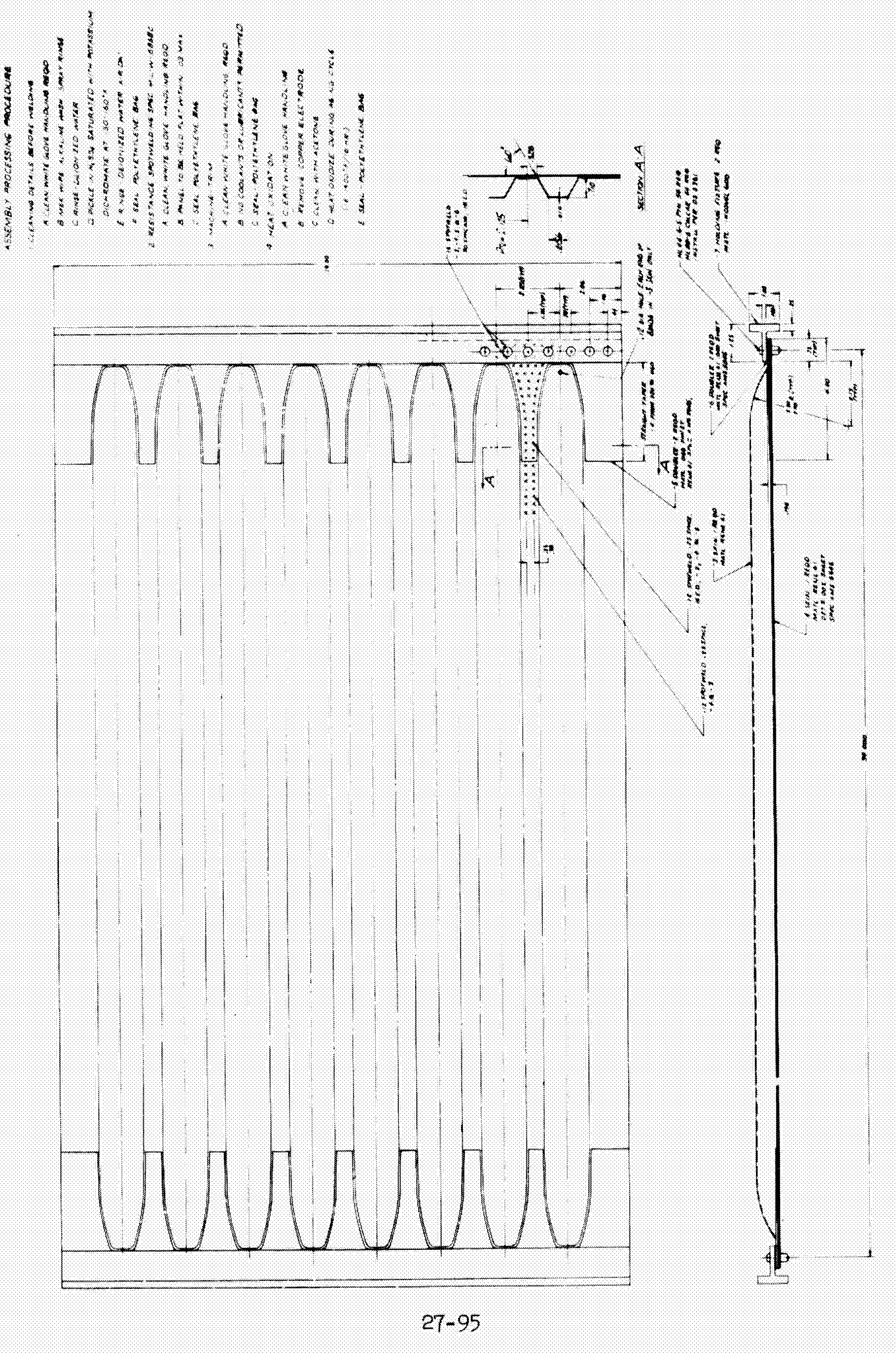

Figure 27-23. Test panel assembly - corrugation stiffened

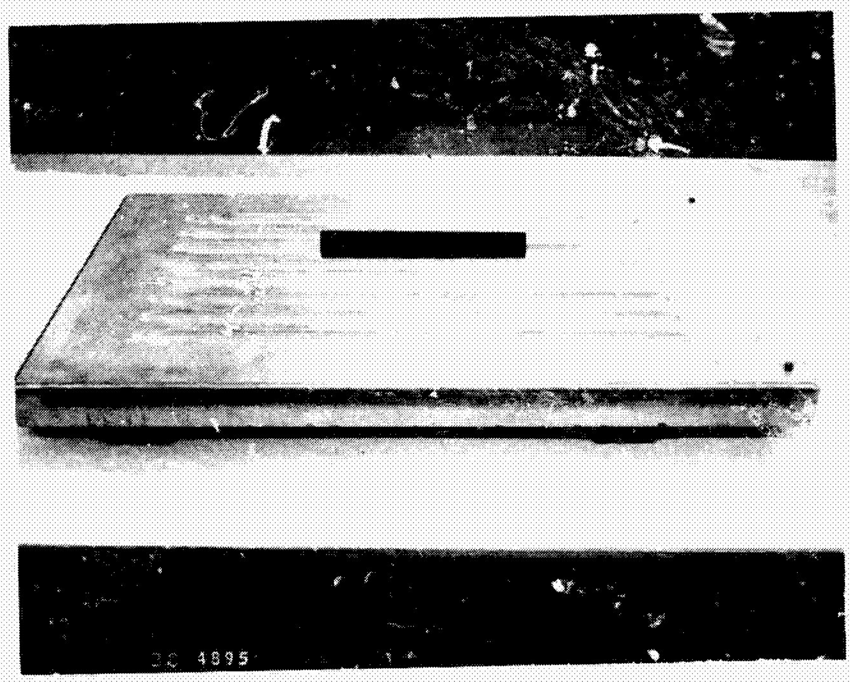

Figure 27-24. Forming die for closed end corrugation-stiffened panel

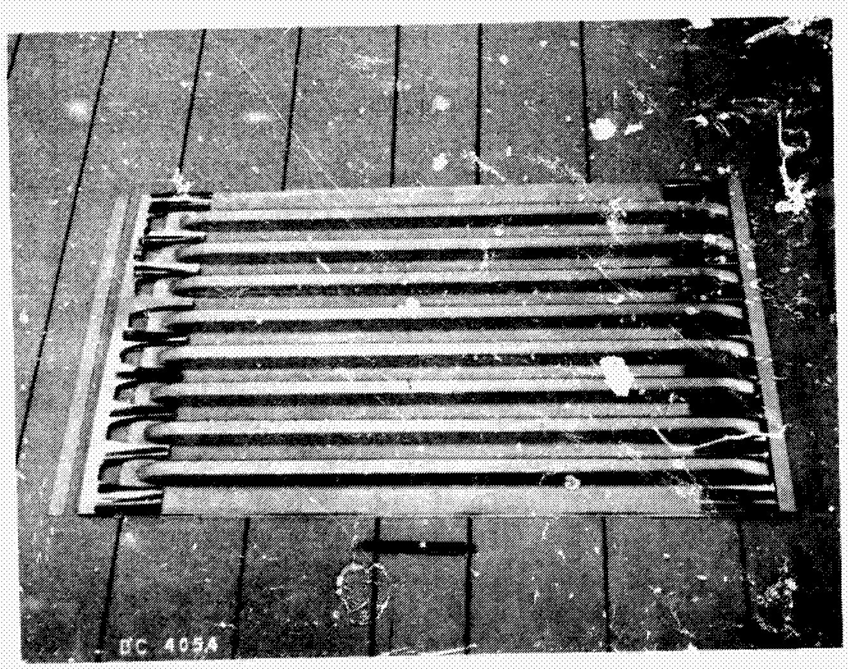

Figure 27-25. Corrugation-stiffened panel details including corrugation, skin, fingered doublers, and end doubler

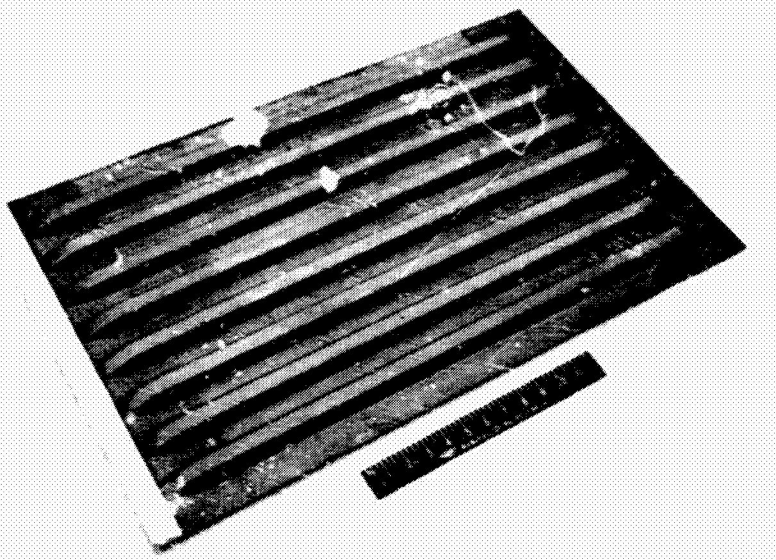

End T-bar installed prior to sawing
for end closure and crippling specimens

Figure 27-26. Corrugation-stiffened panel after aging and heat oxidation

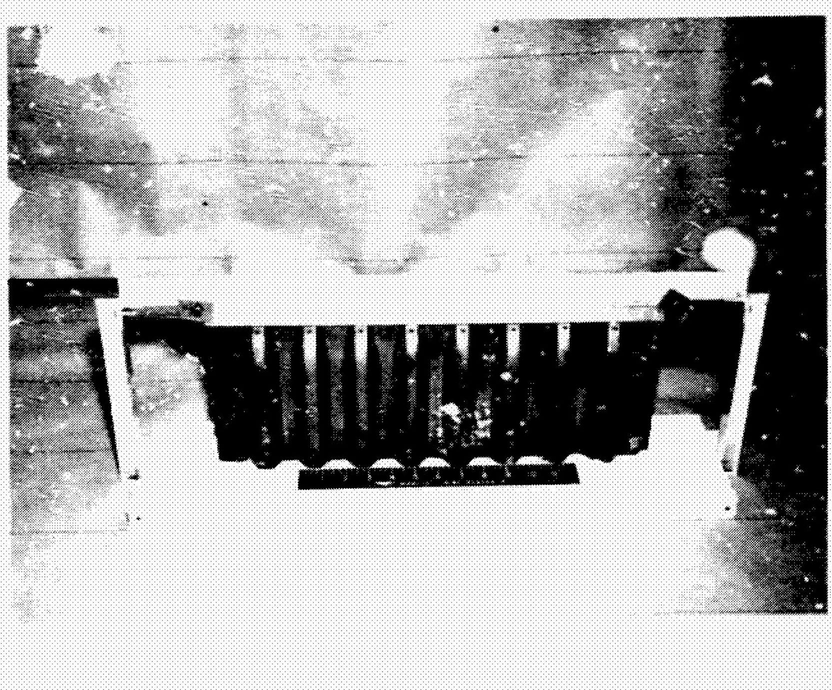

Figure 27-27. Corrugation-stiffened end closure specimen cast in densite

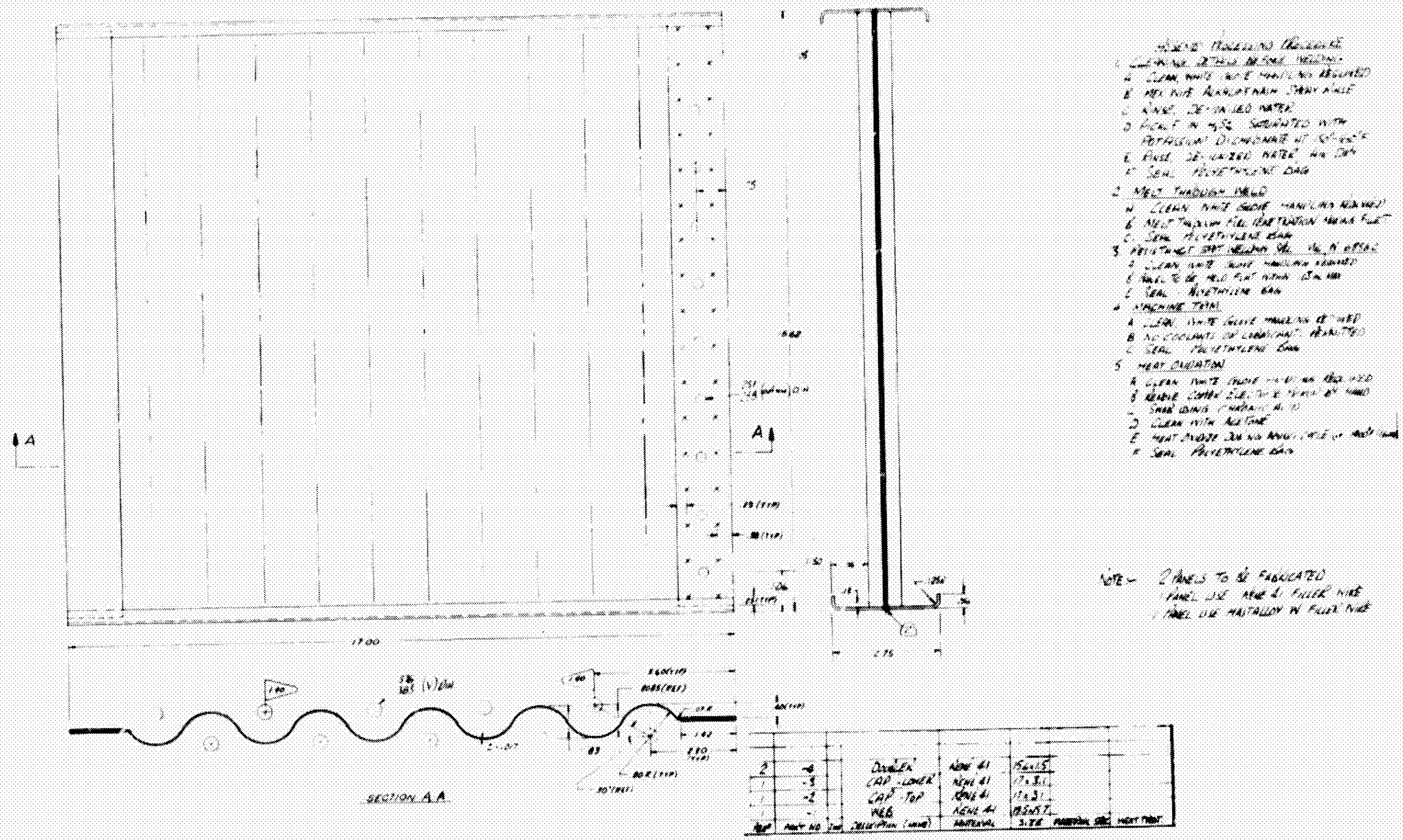

Figure 27-28. Shear panel assembly – circular arc corrugation

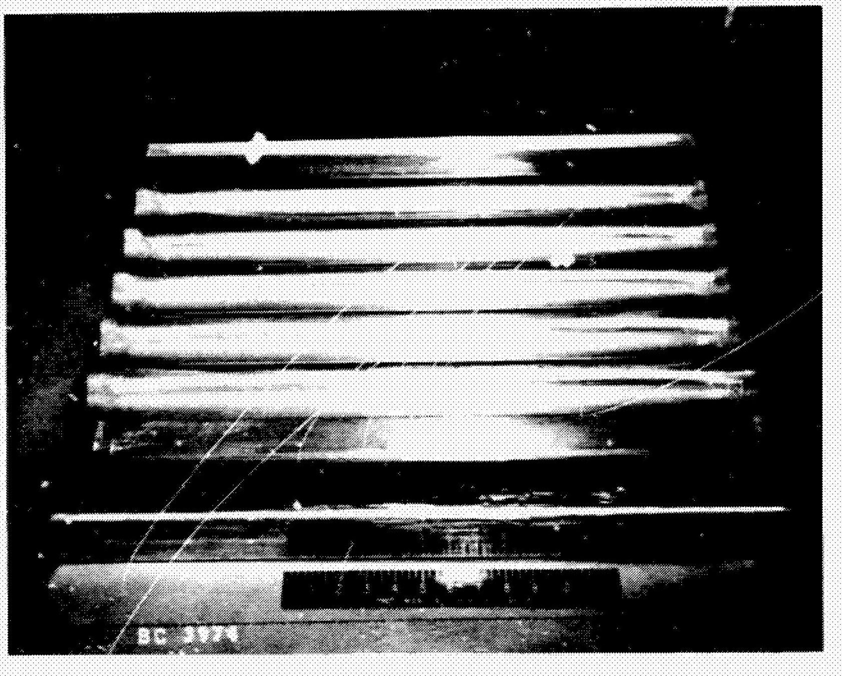

Figure 27-29. Corrugated shear web forming block

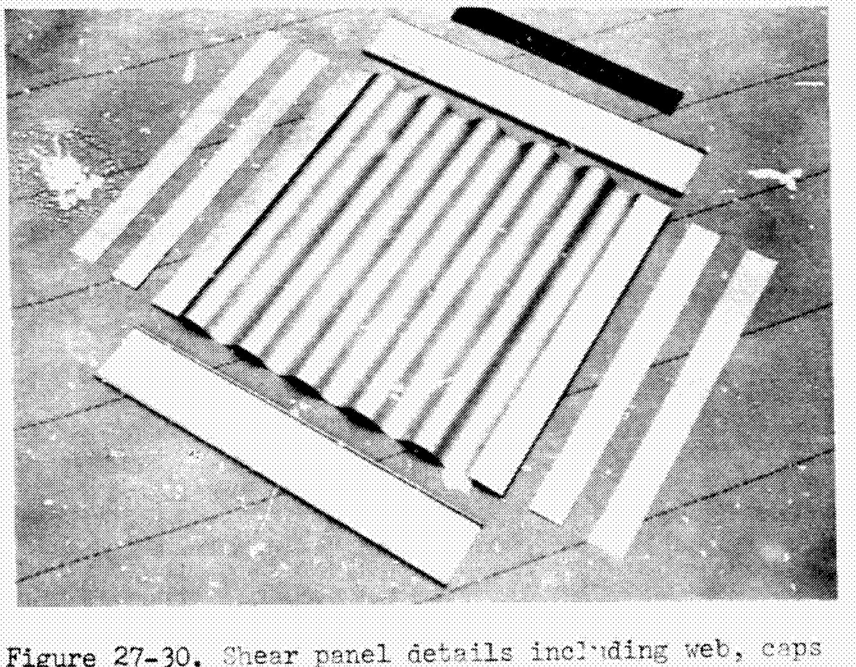

Figure 27-30. Shear panel details including web, caps and edge doublers prior to assembly

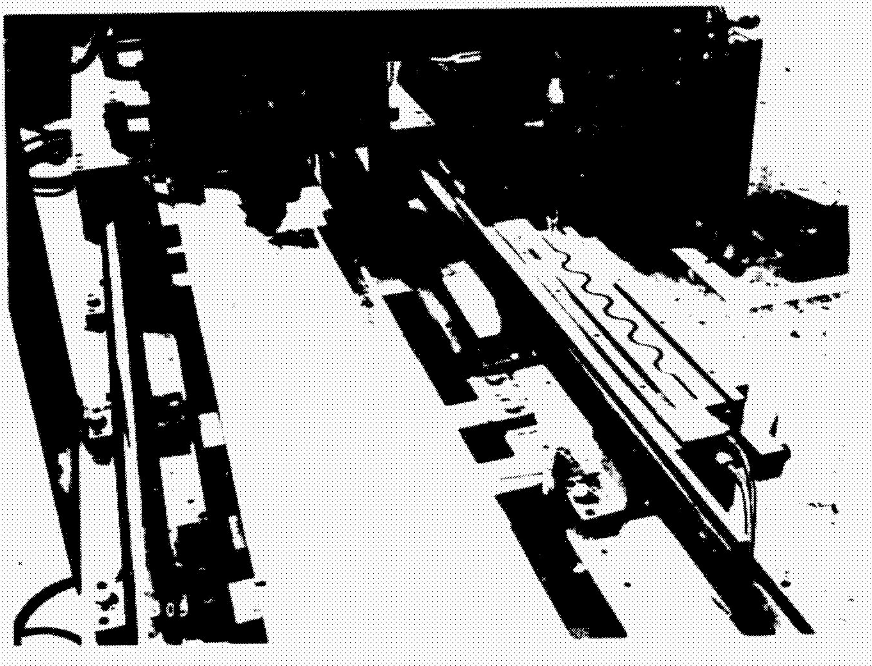

Figure 27-31 Overall view of tracer template ready for fixturing parts for shear panel TIG welding

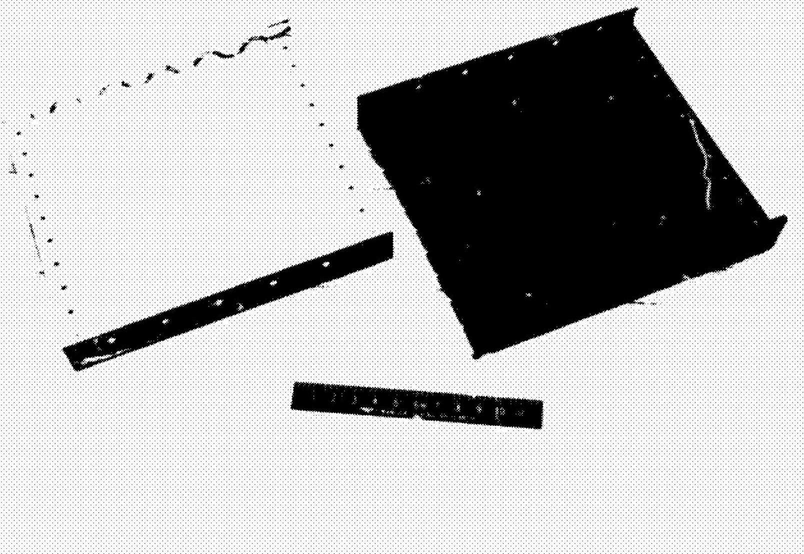

Figure 27-32 Two-shear web panel assemblies, one before and one after aging and heat oxidation

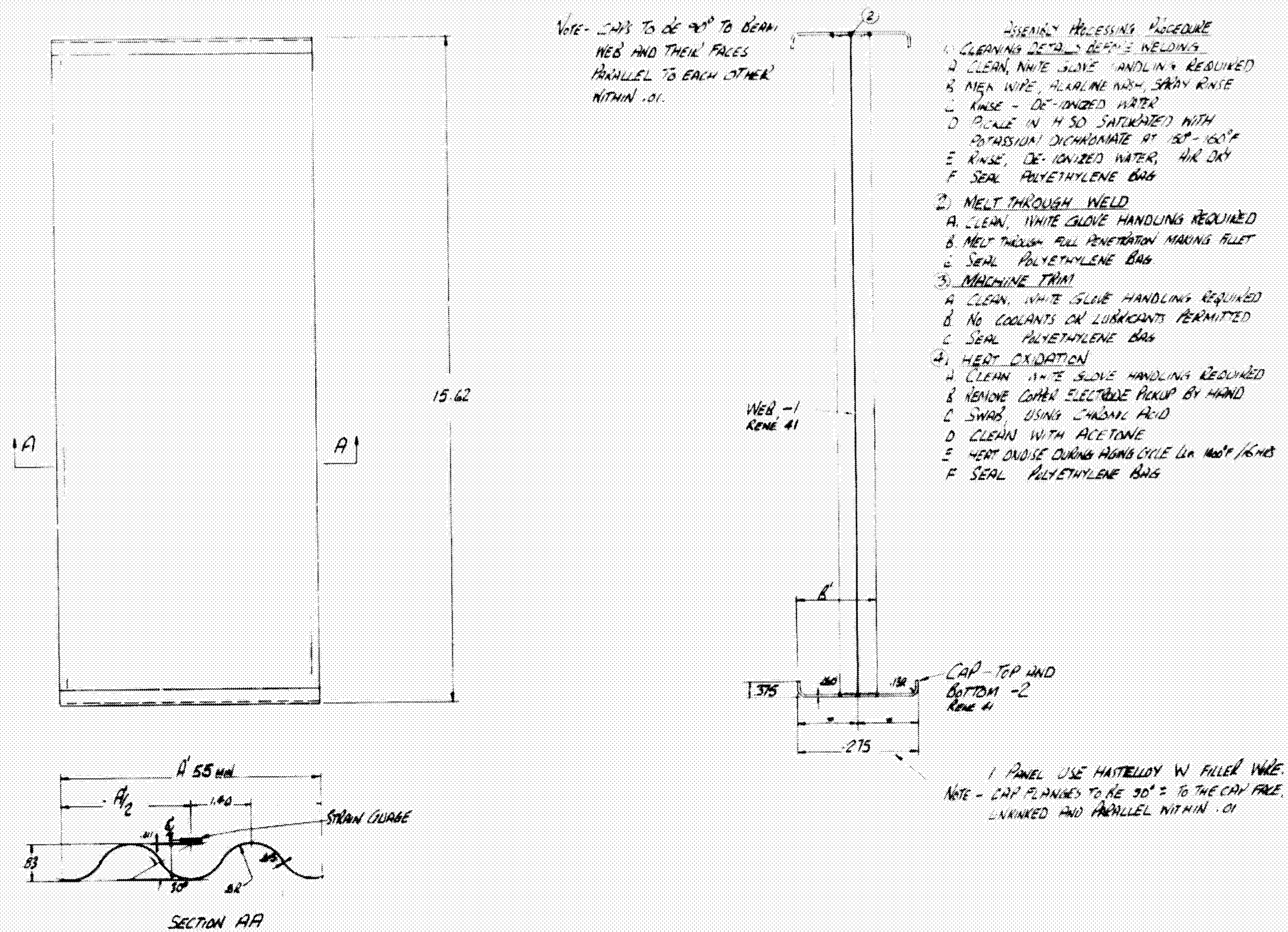

Figure 27-33. Beam cap crippling specimen

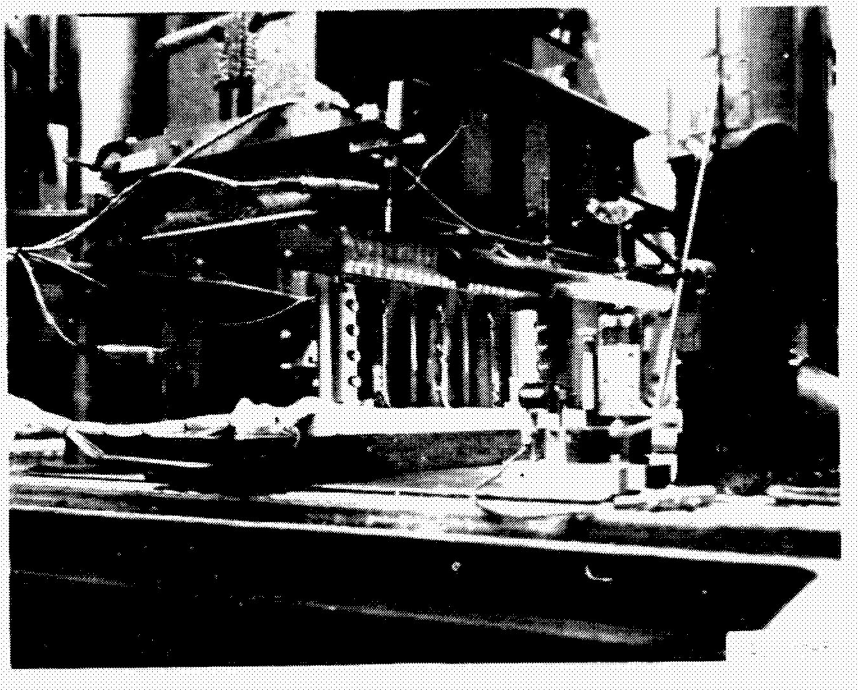

Typical crippling panel test

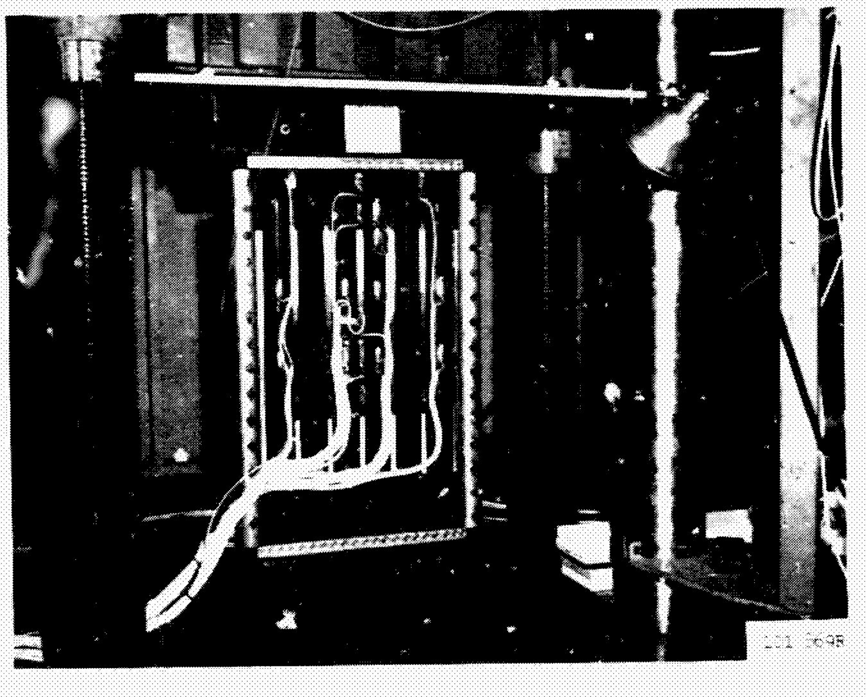

Typical compression panel test

...e 27-34 Typical room temperature compression test set-ups

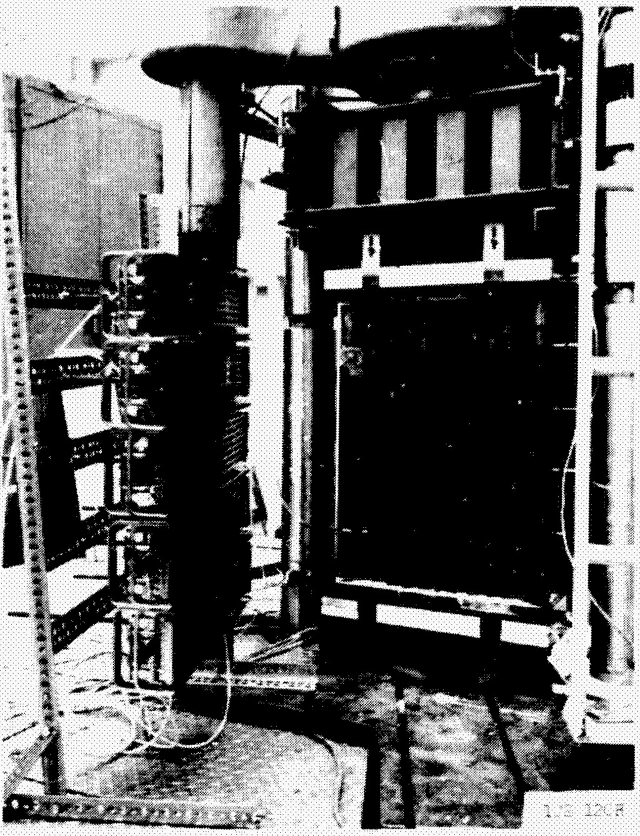

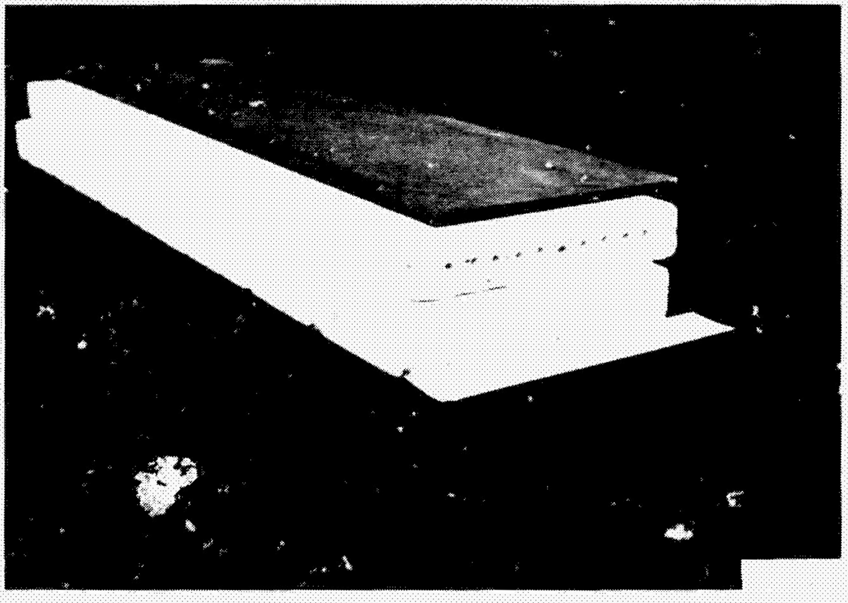

Inconel bearing plate and pyroform blocks used for elevated temperature test setup. Nichrome heating elements are inserted into precast holes.

Figure 27-35. Typical elevated temperature test set up for 30-inch compression panel

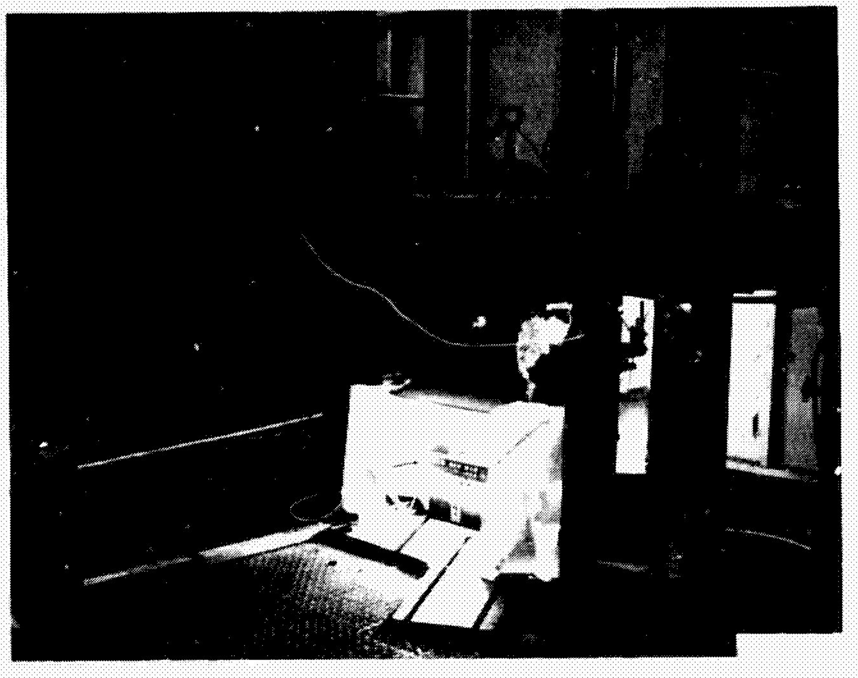

Crippling tests

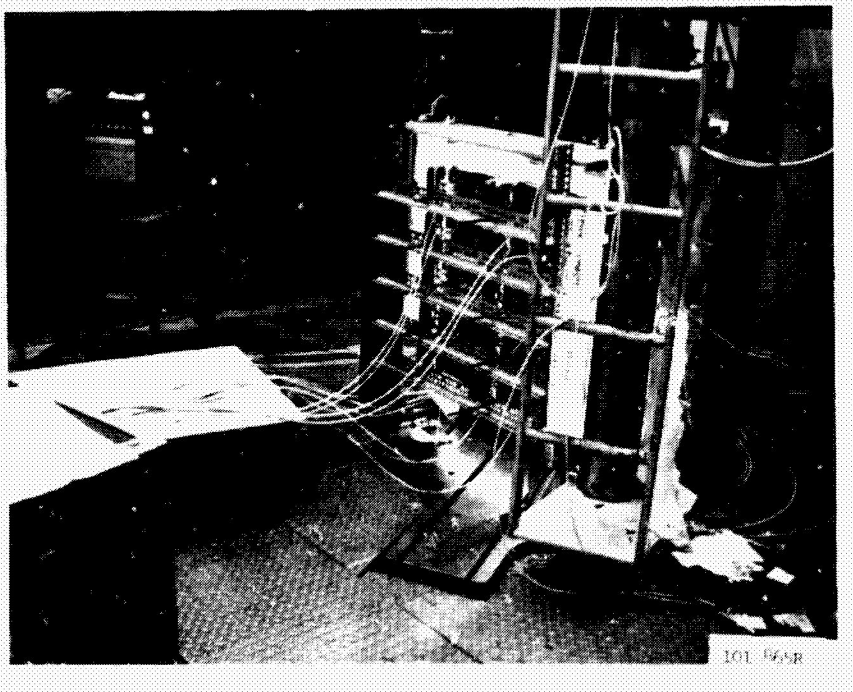

Compression panel tests

Figure 27-36 Typical elevated temperature compression test s .-ups

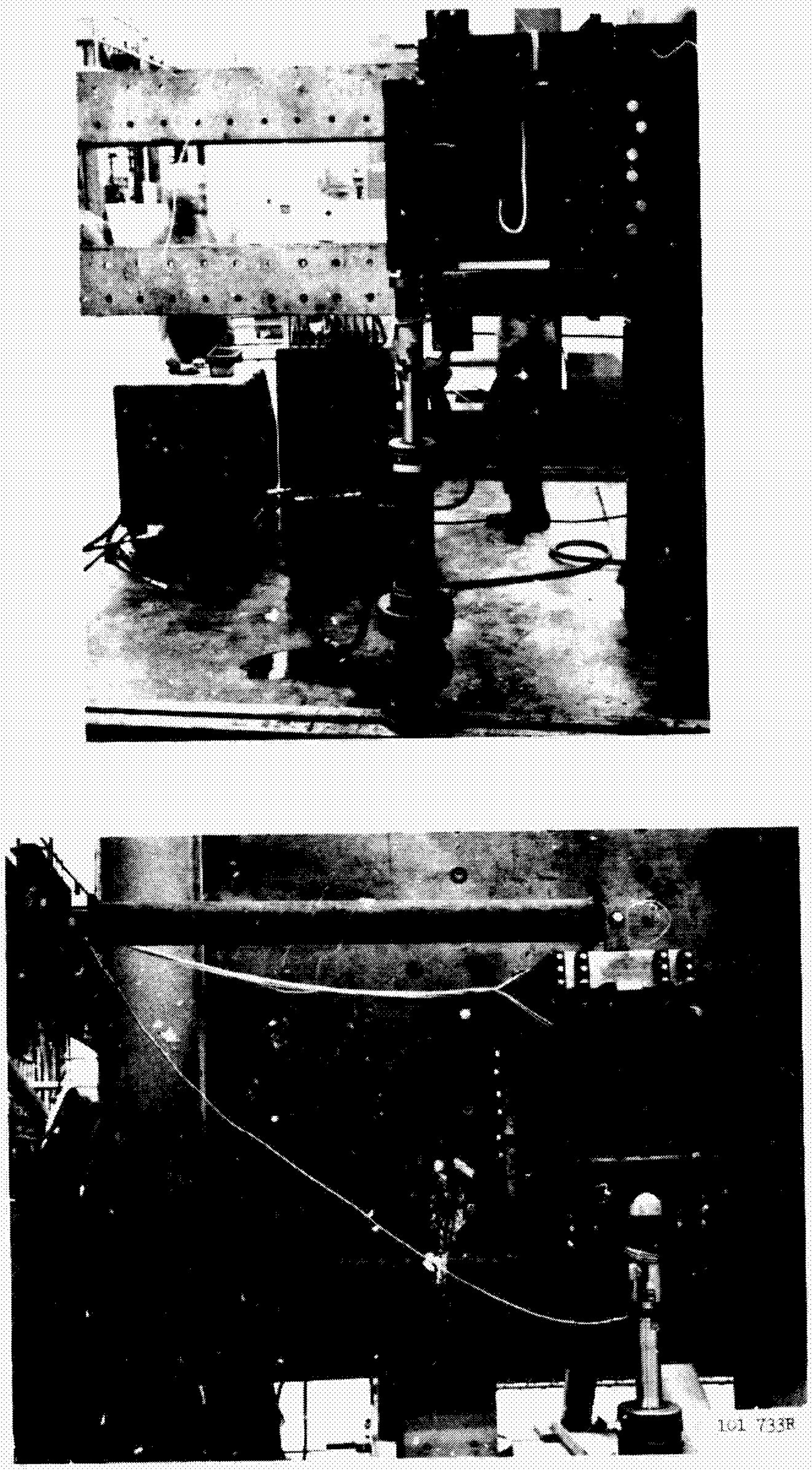

Figure 27-37. Test set-up for in-plane shear panel tests

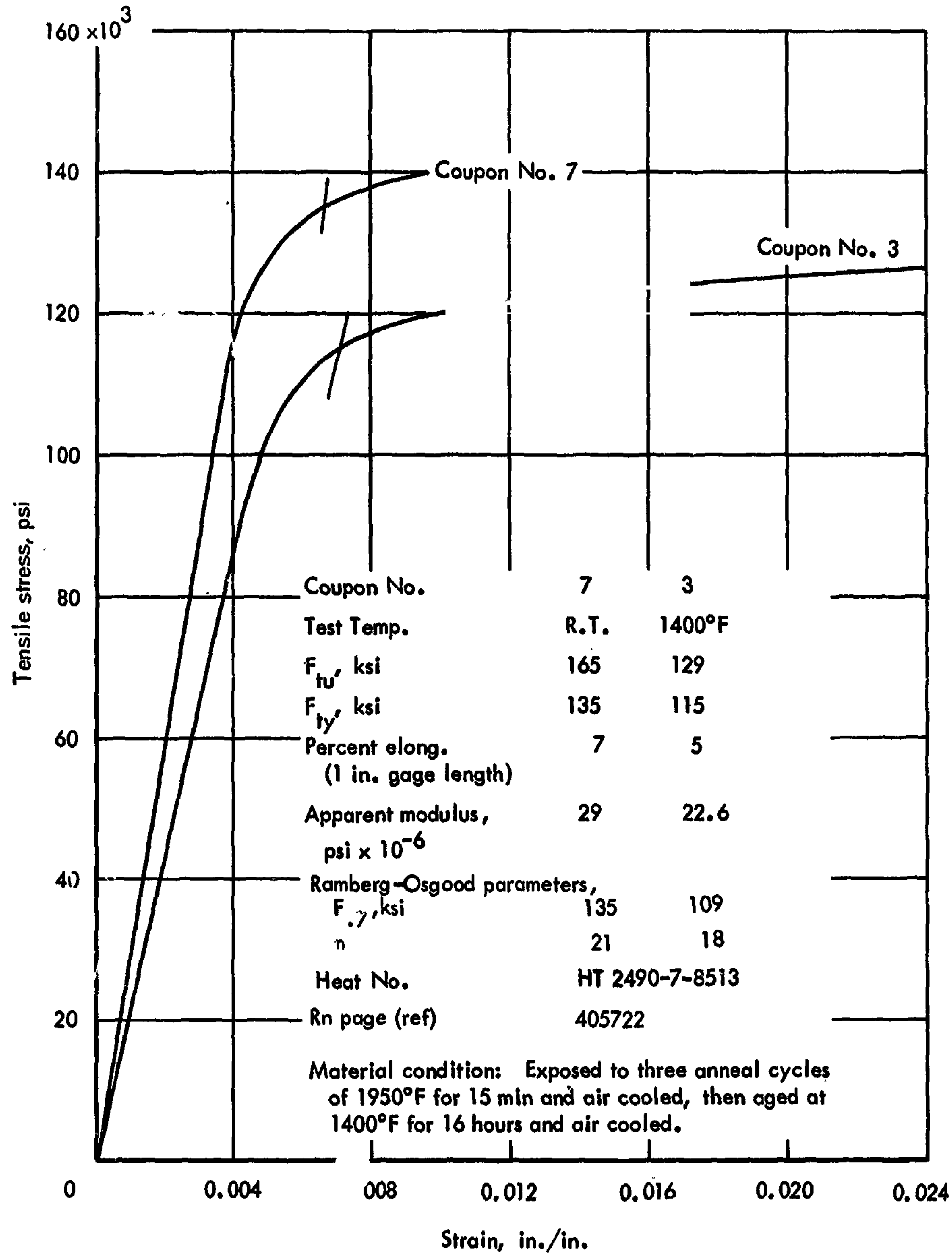

Figure 27-38. Tensile stress-strain curves for .016 gage René 41 compression panel sheet material, longitudinal grain direction

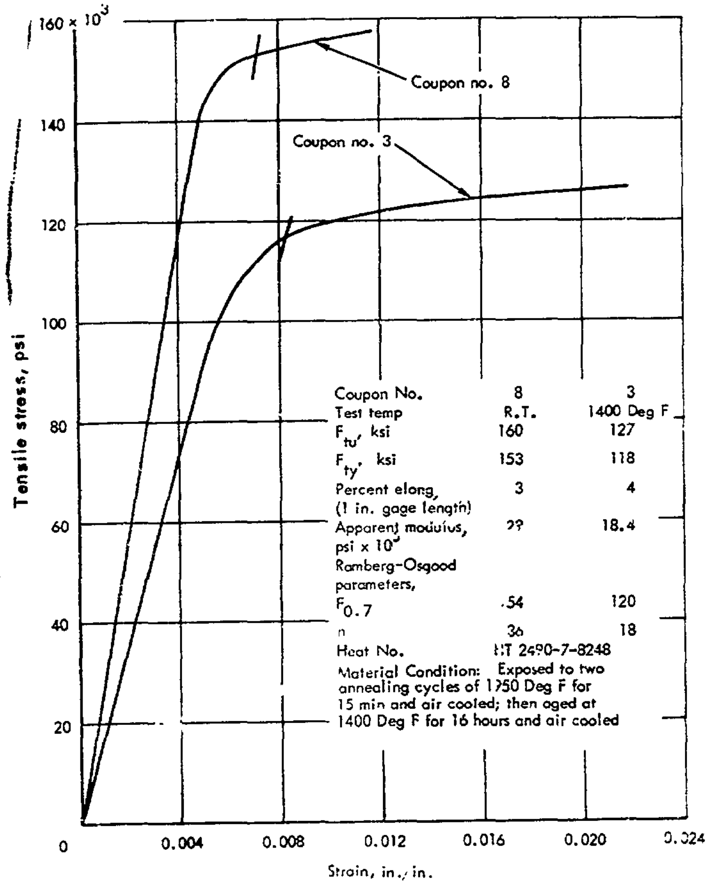

Figure 27-39. Tensile stress-strain curves for .019 gage René 41 compression panel sheet material, longitudinal grain direction

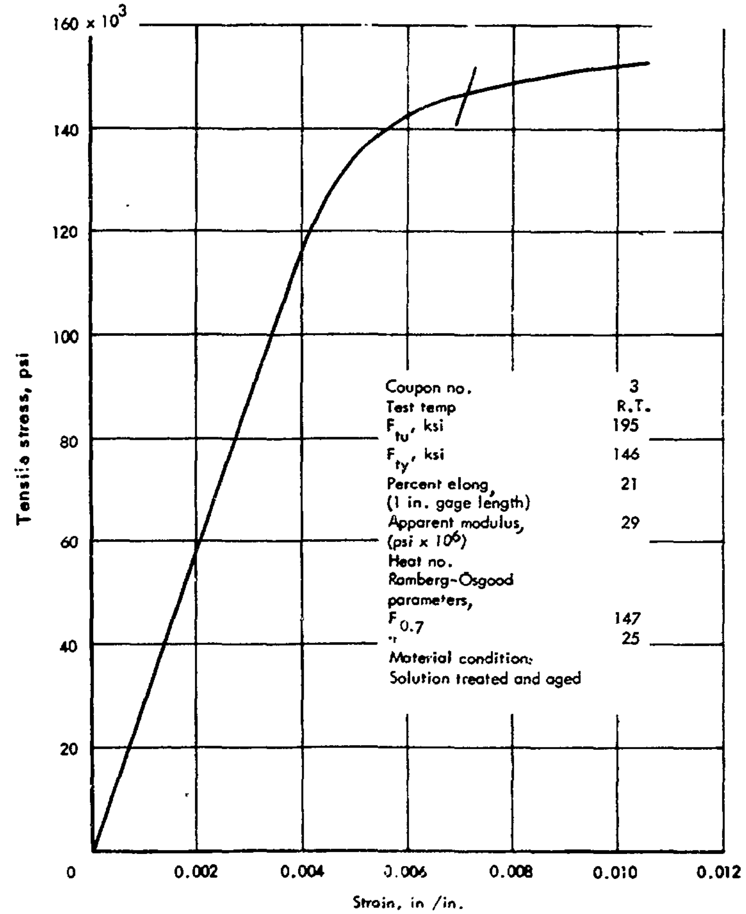

Figure 27-40. Tensile stress-strain curve for .060 gage René 41 beam cap shear and crippling specimen material, longitudinal grain direction

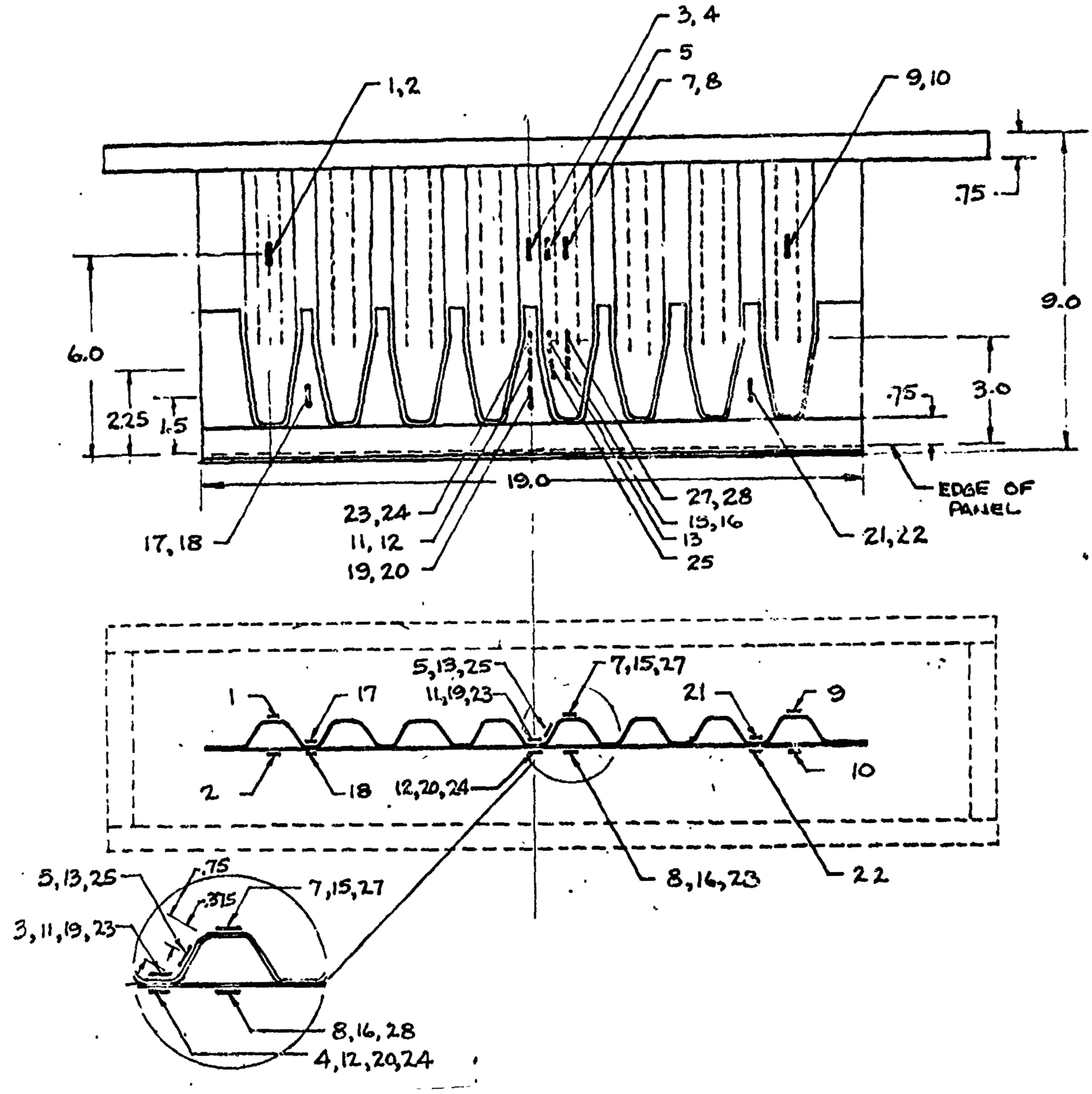

Figure 27-41. Strain gage locations for corrugation stiffened skin end-closeout panel

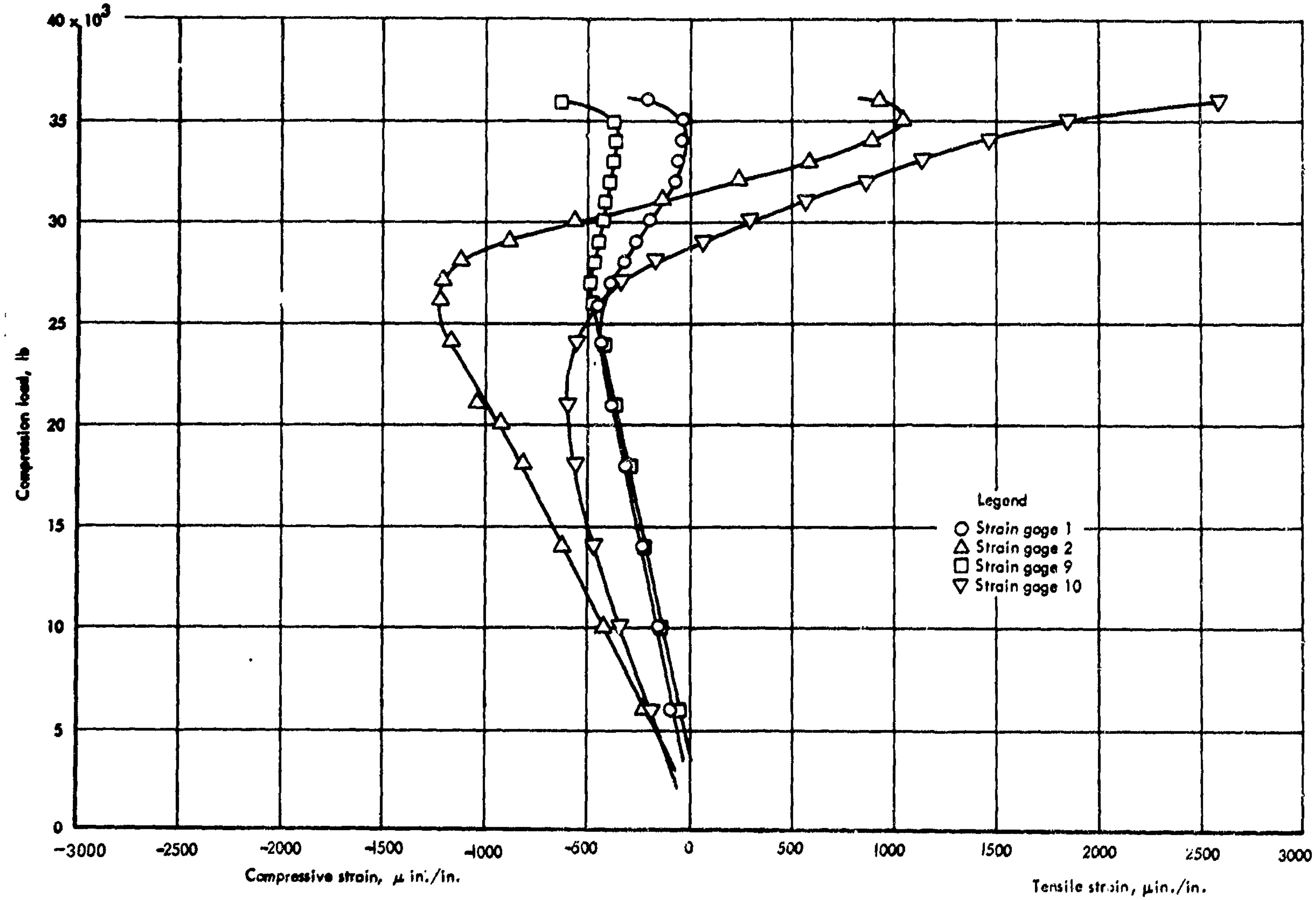

Figure 27-42. Axial strains for corrugation-stiffened skin end closeout panel, room temperature

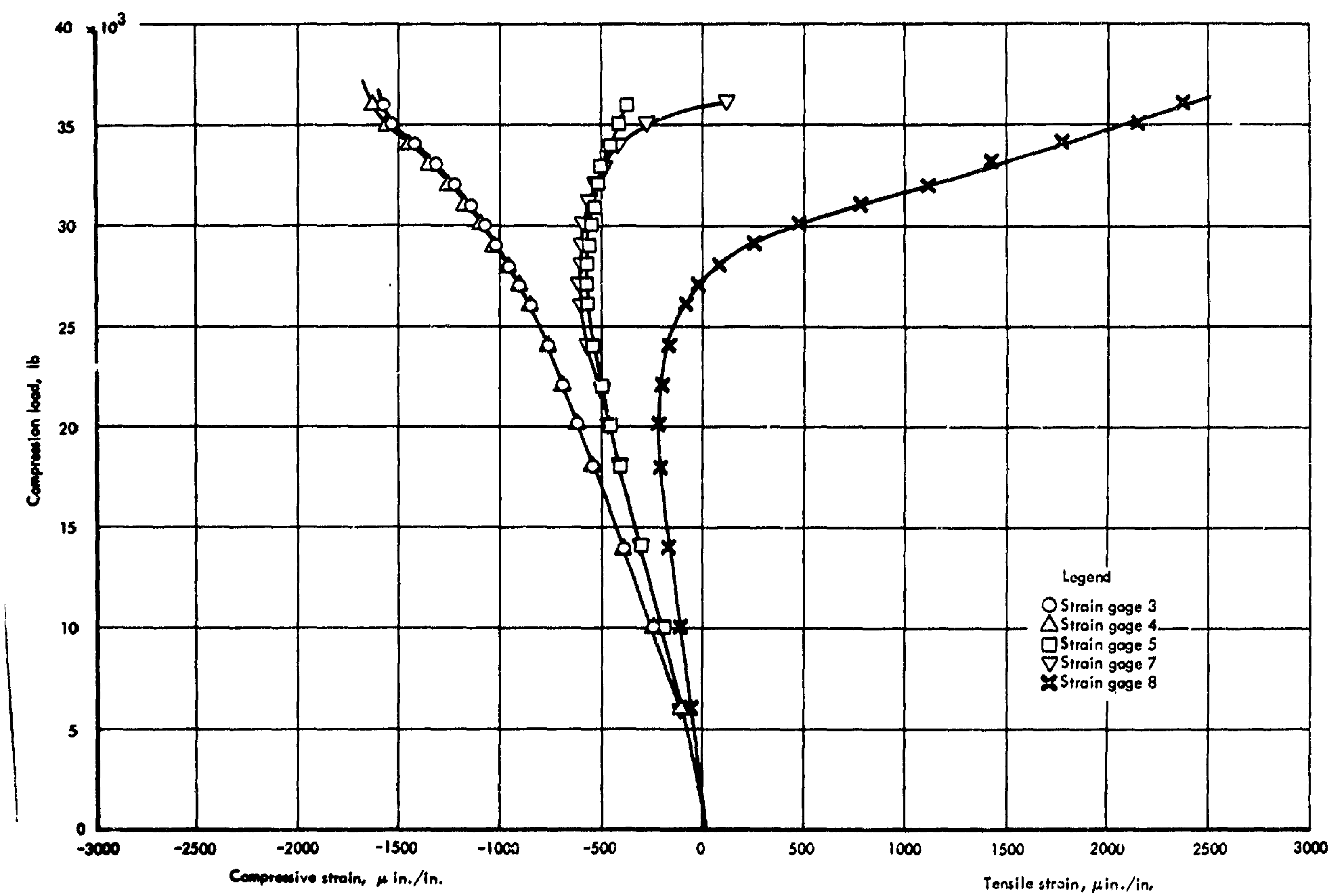

Figure 27-42. (Continued)

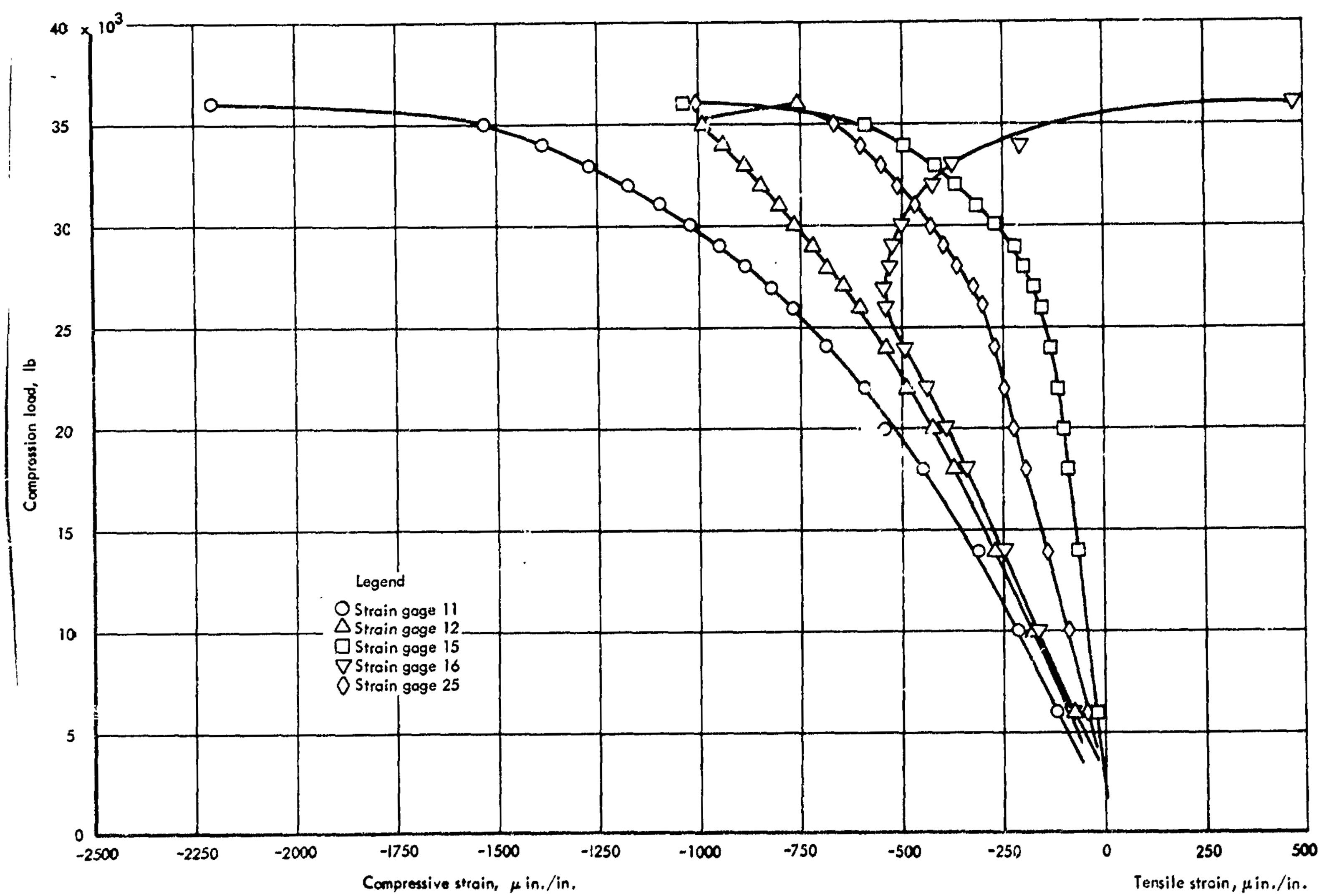

Figure 27-42. (Continued)

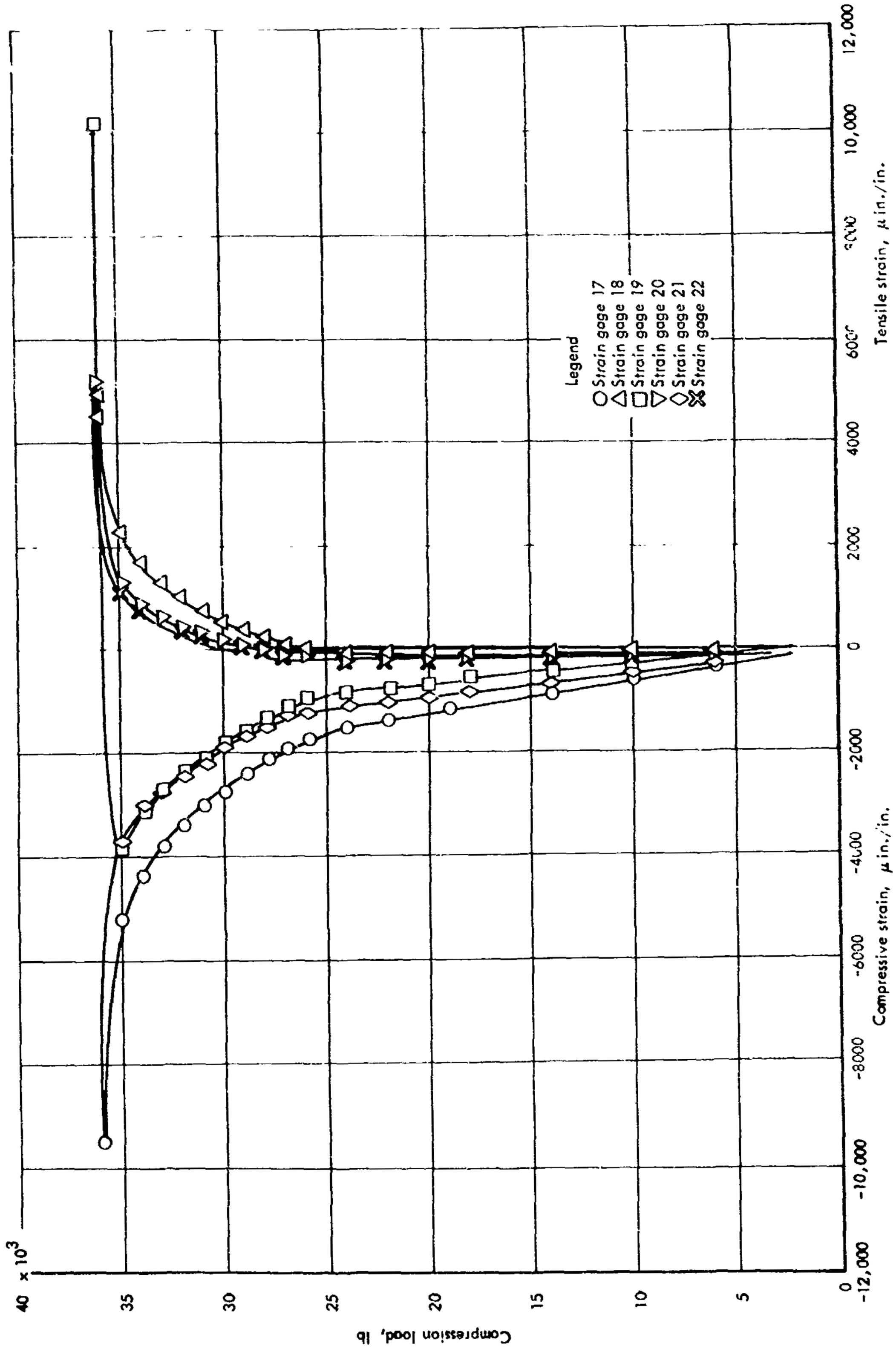

Figure 27-42. (Continued)

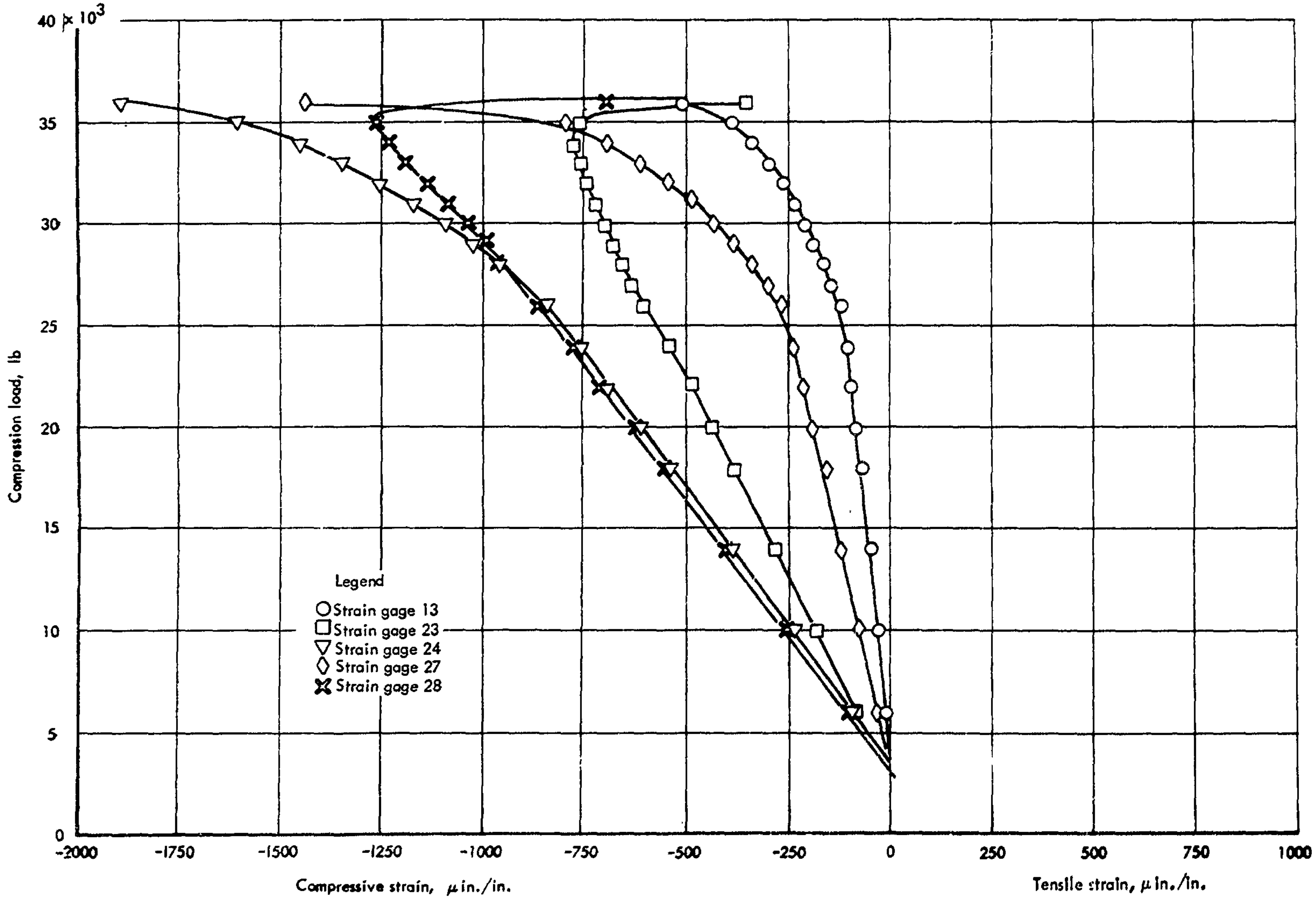

Figure 27-42. (Concluded)

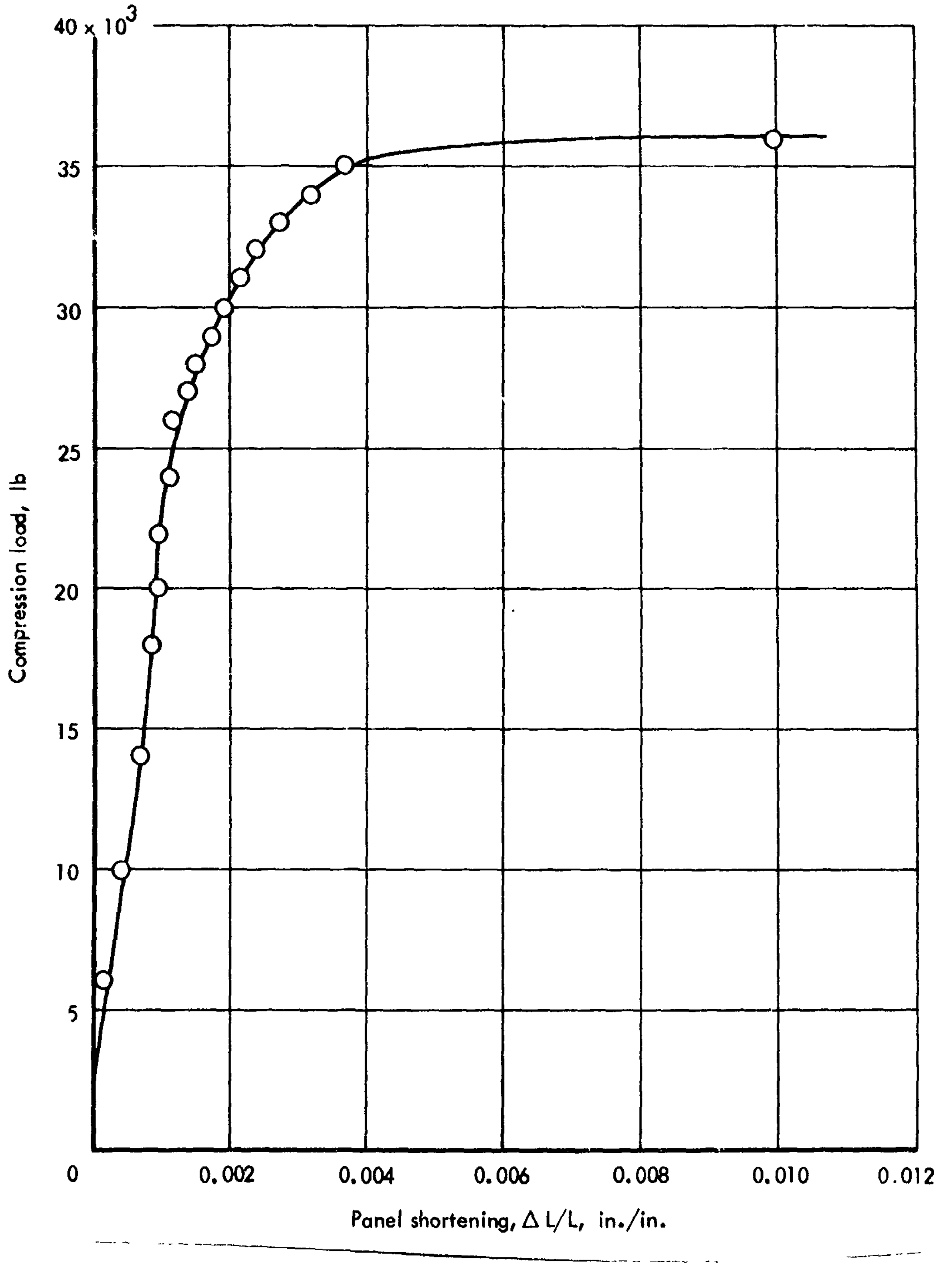

Figure 27-43. Panel shortening curve $\Delta L/L$ for corrugation-stiffened end closeout panel, room temperature

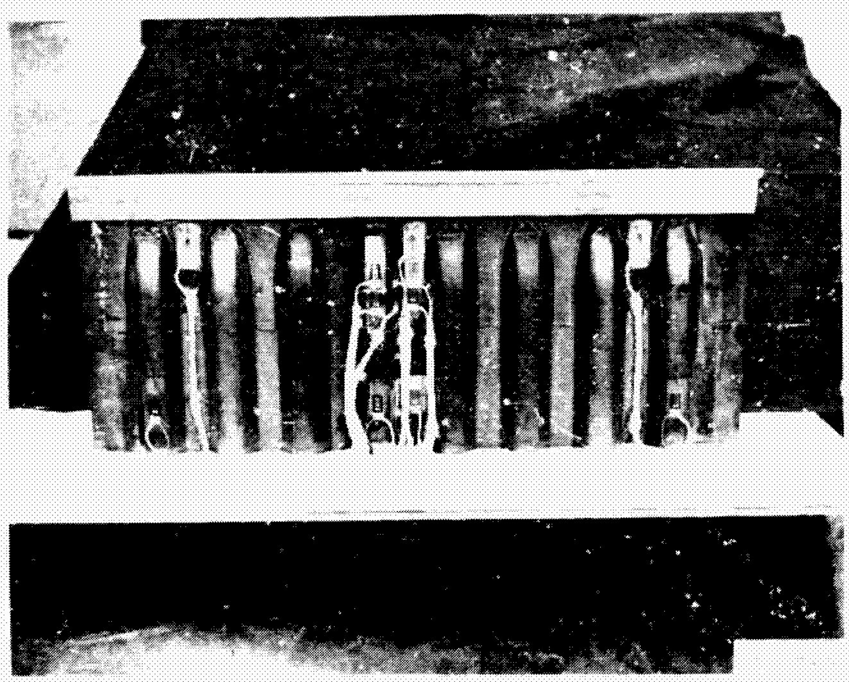

Front

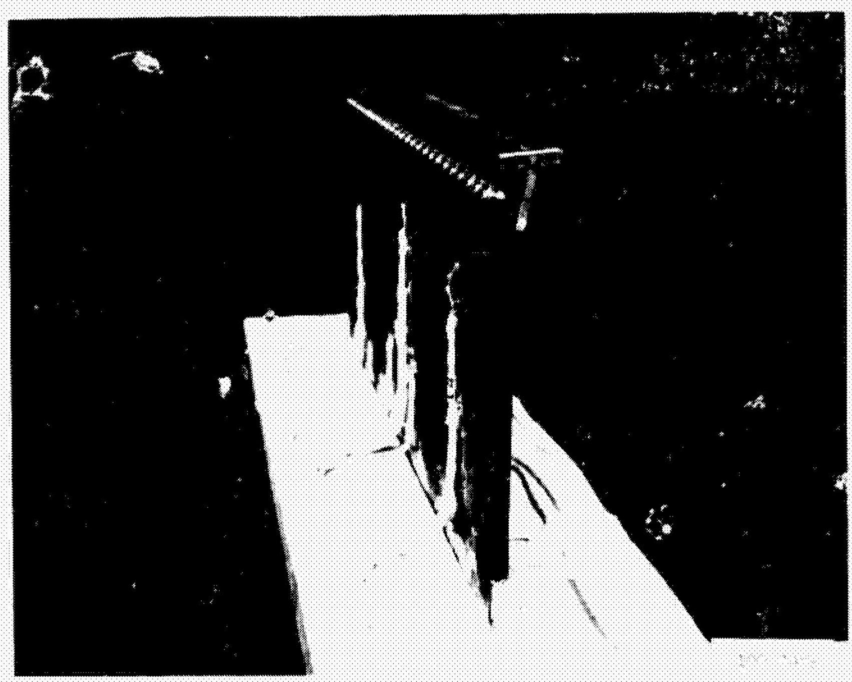

Edge

Figure 27-44. Corrugation-stiffened end closeout panel after failure, room temperature

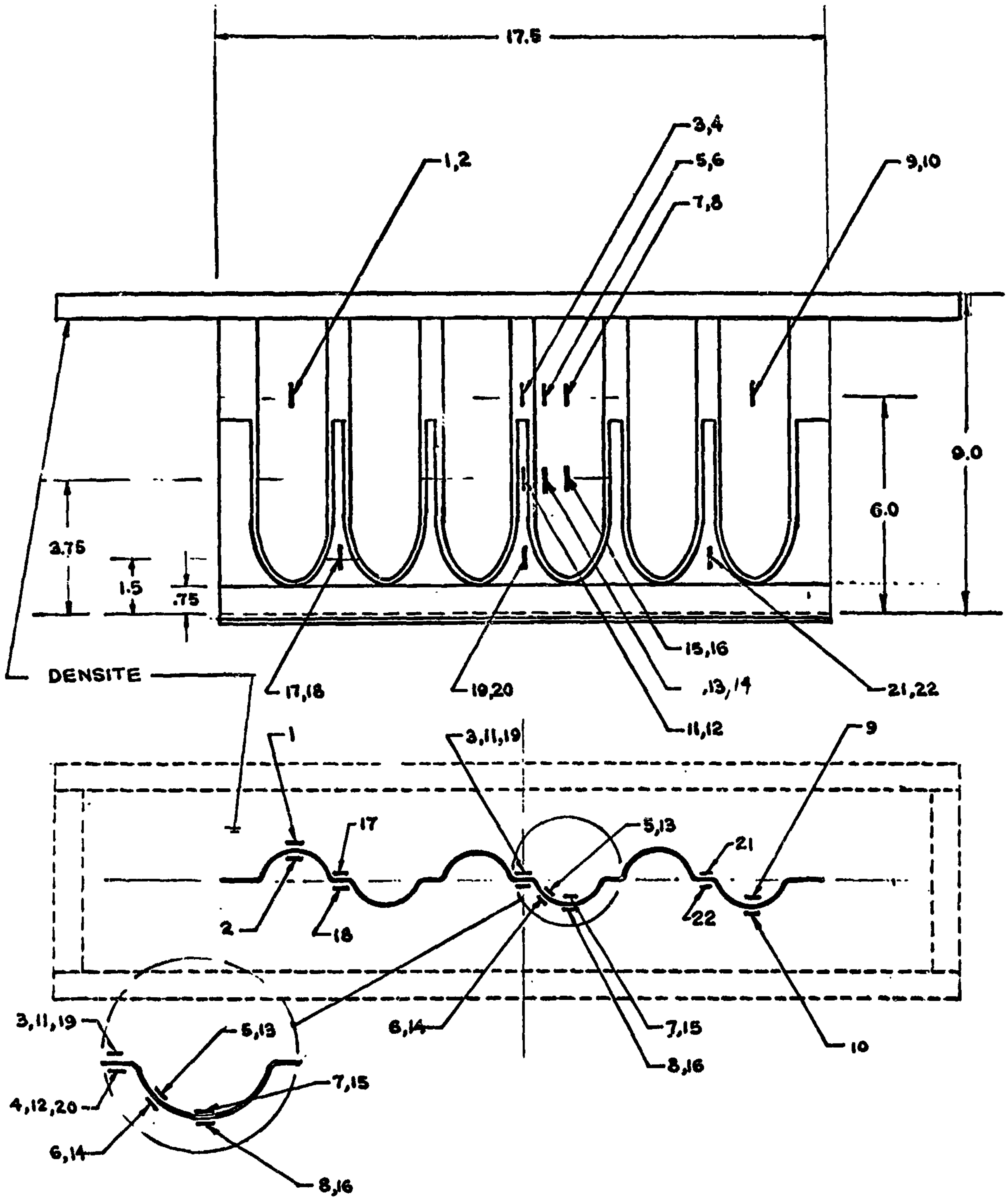

Figure 27-45. Strain gage locations for beaded end-closeout panel

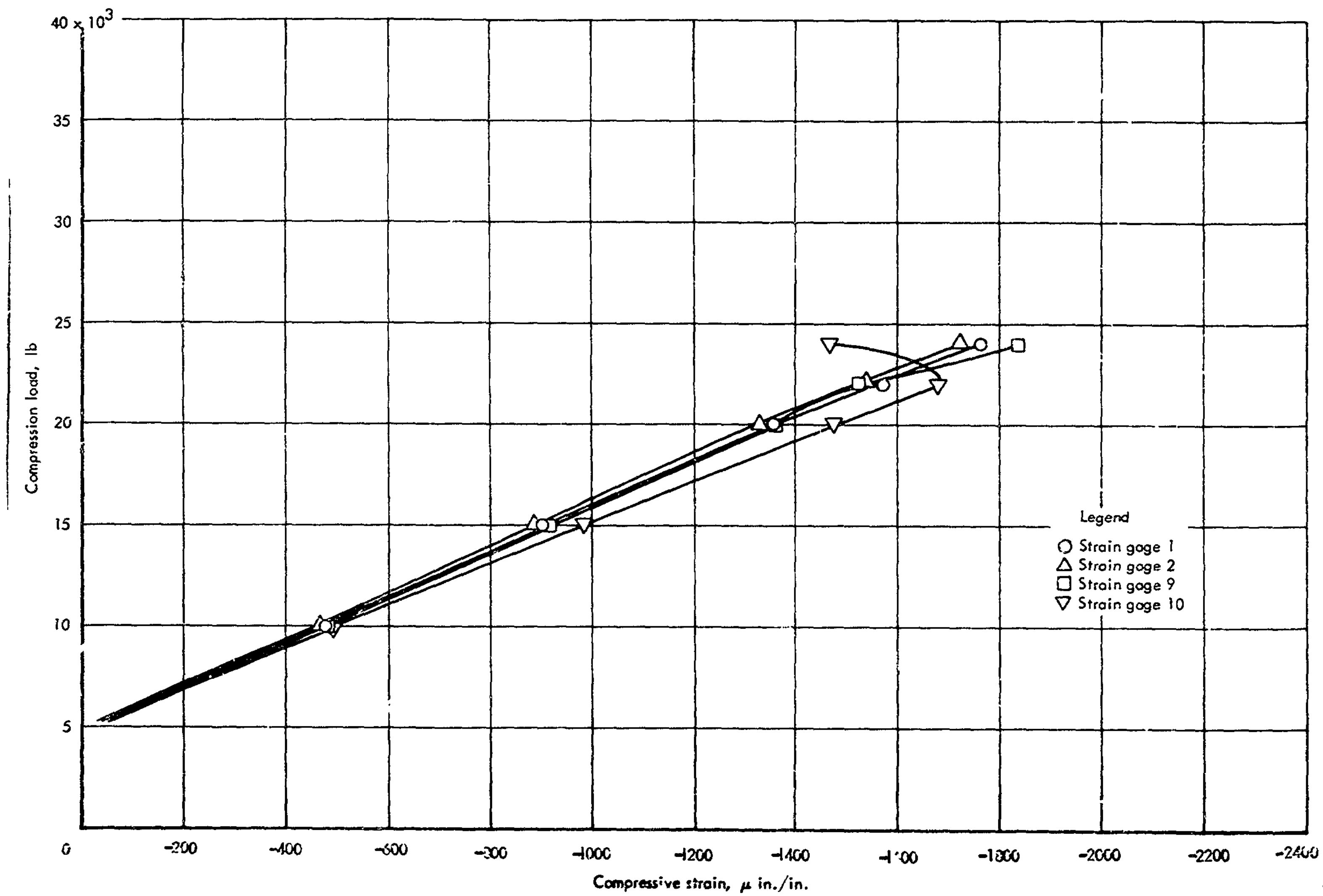

Figure 27-46. Axial strains for beaded end-closeout panel, room temperature

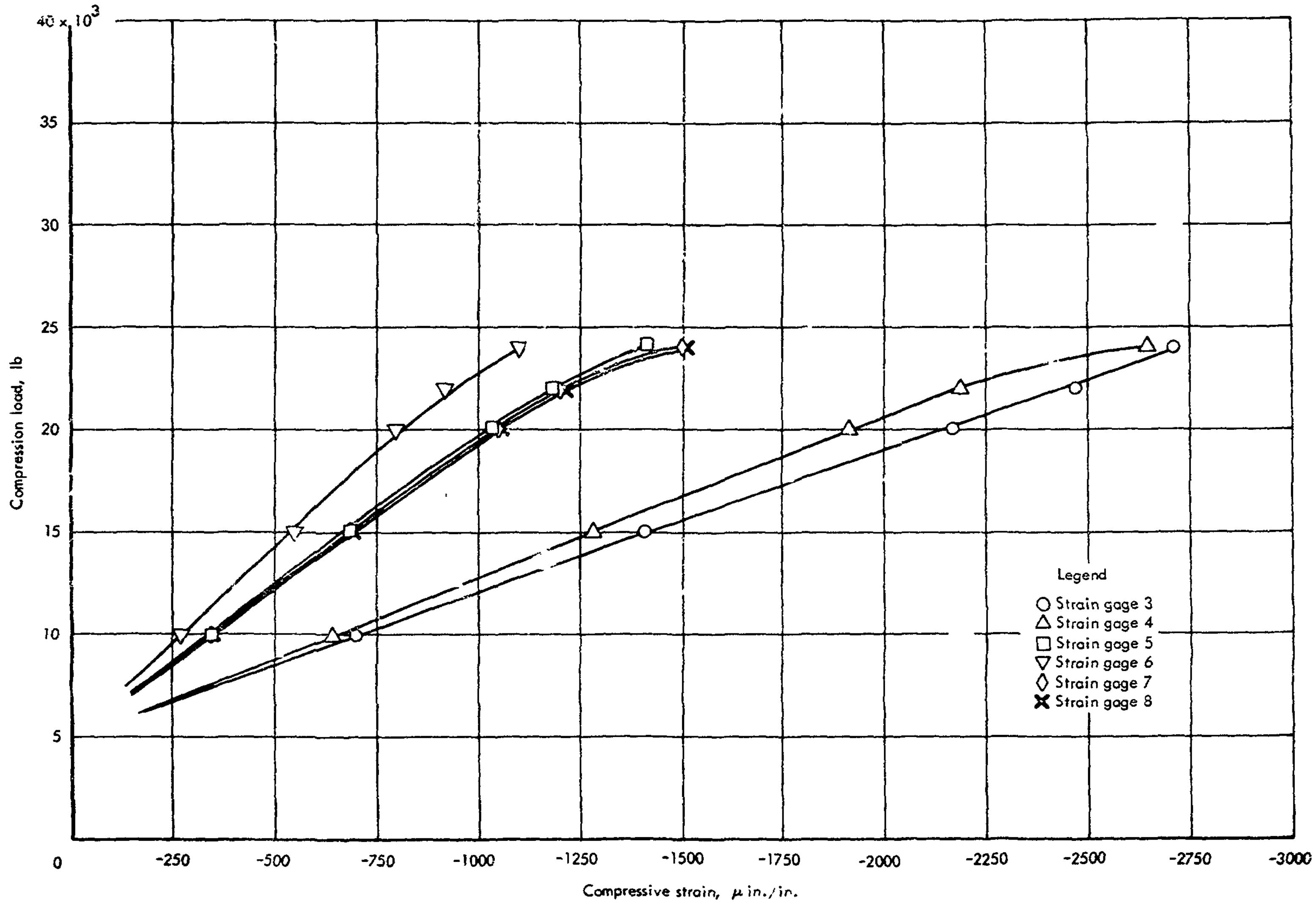

Figure 27-46. (Continued)

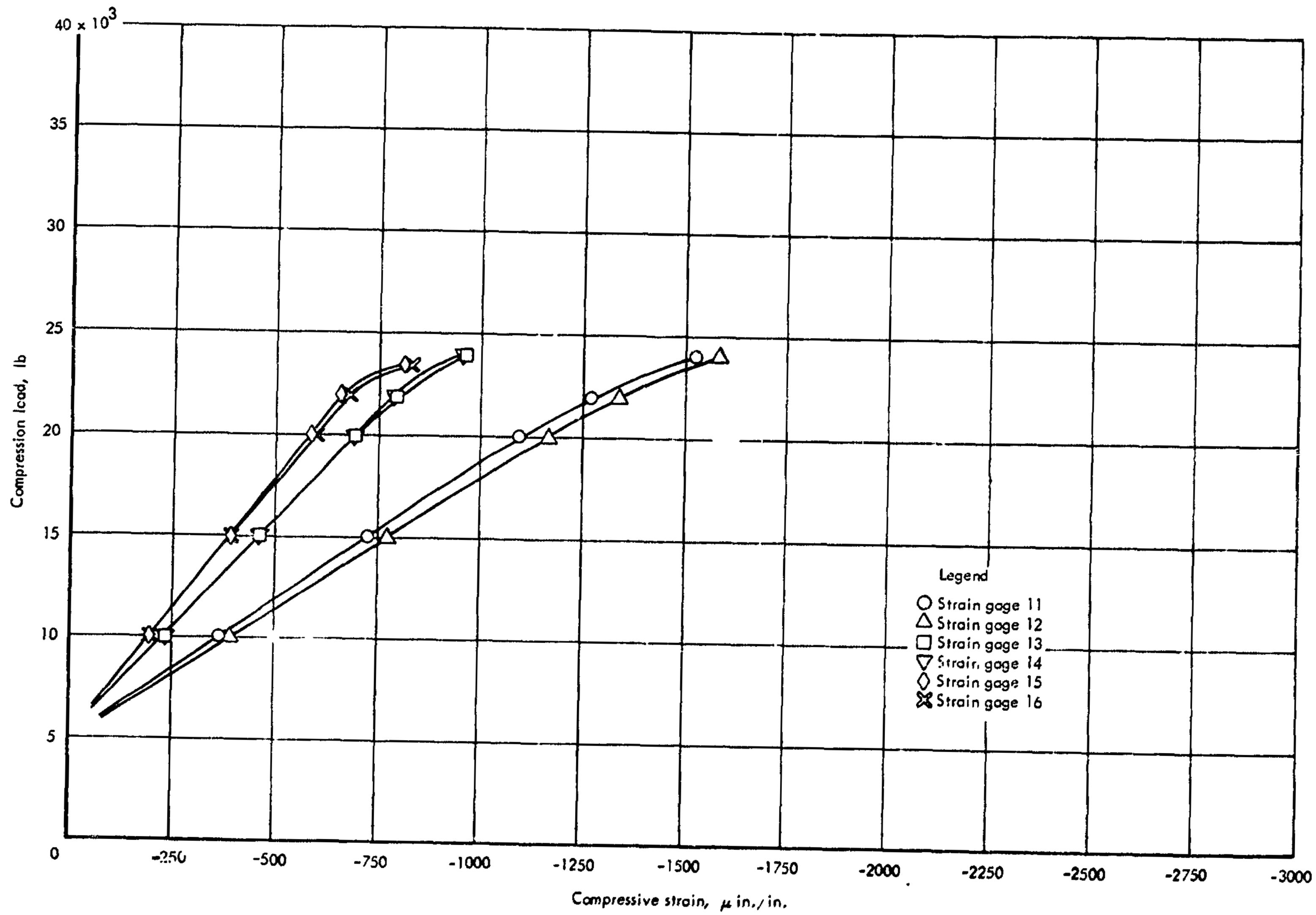

Figure 27-46. (Continued)

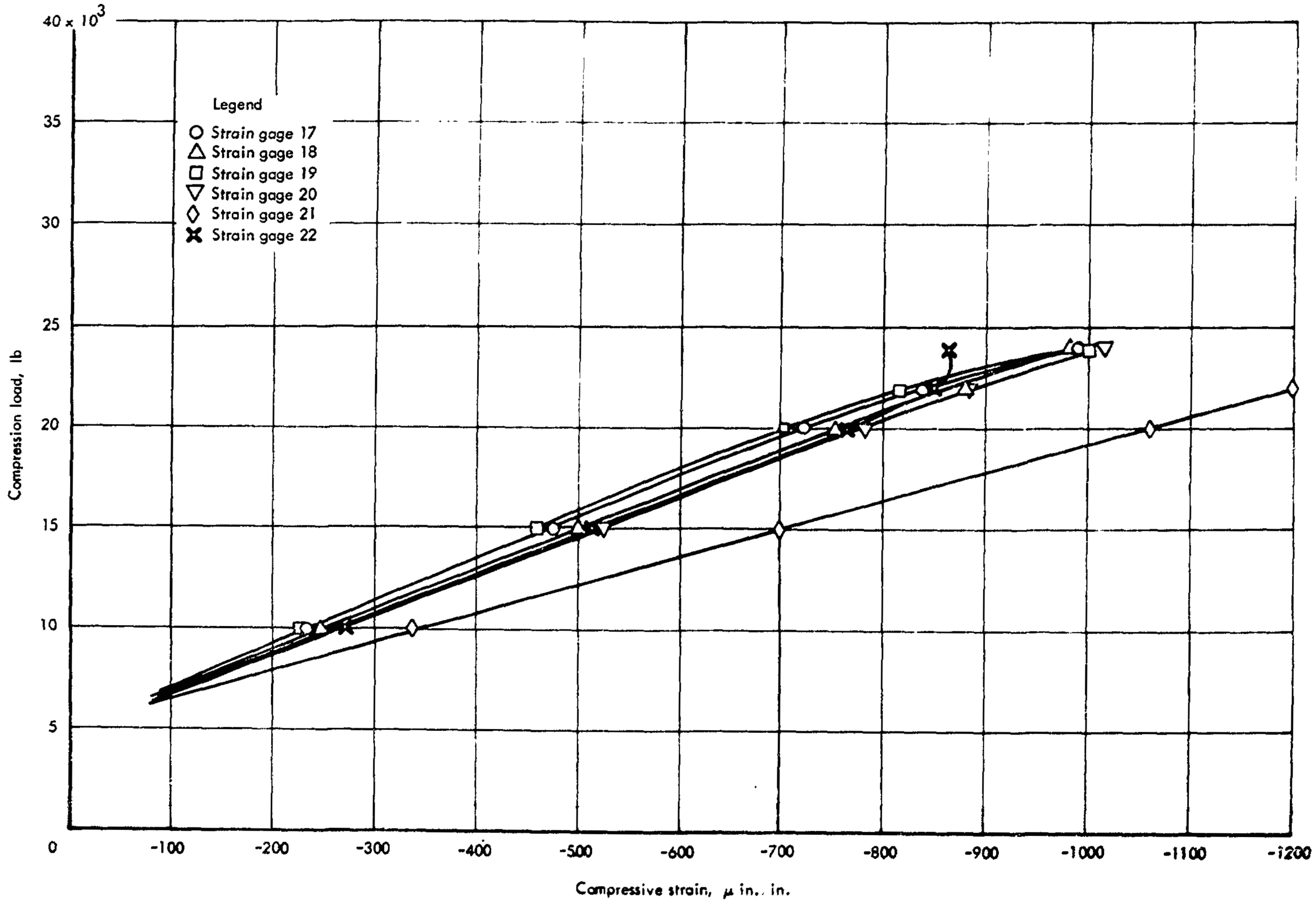

Figure 27-46. (Concluded)

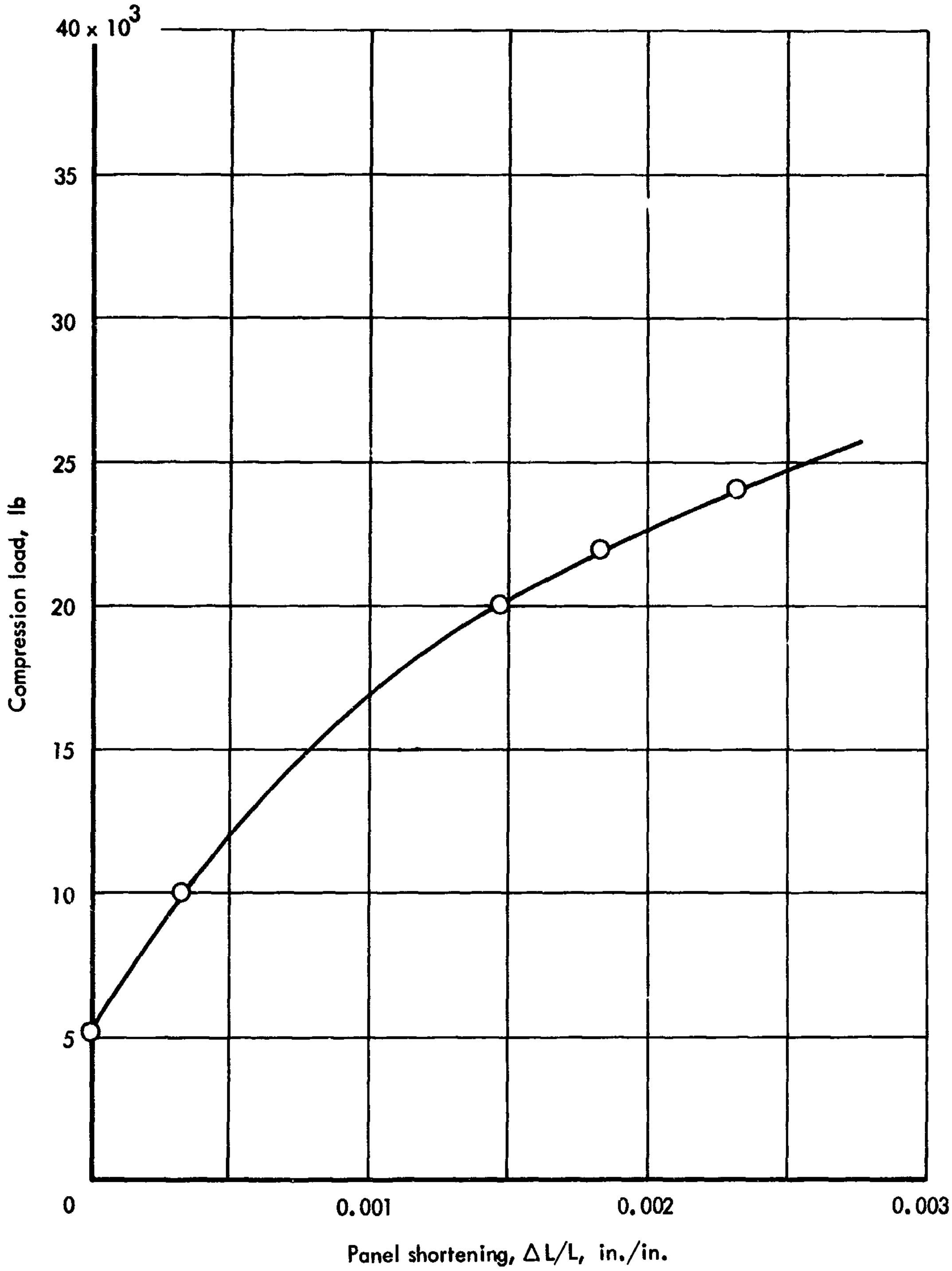

Figure 27-47. Panel shortening curve $\Delta L/L$ for beaded end-closeout panel, room temperature

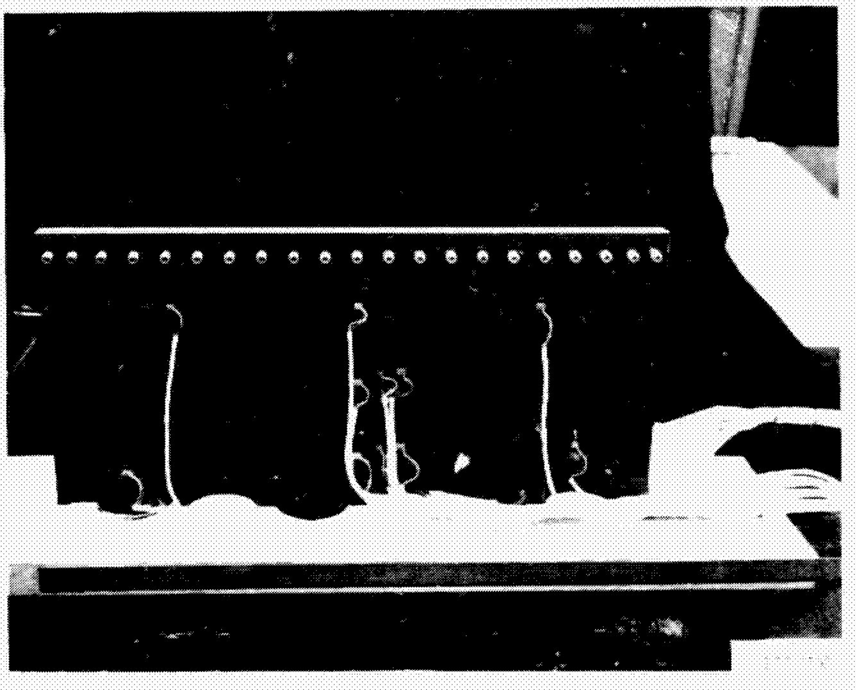

Front

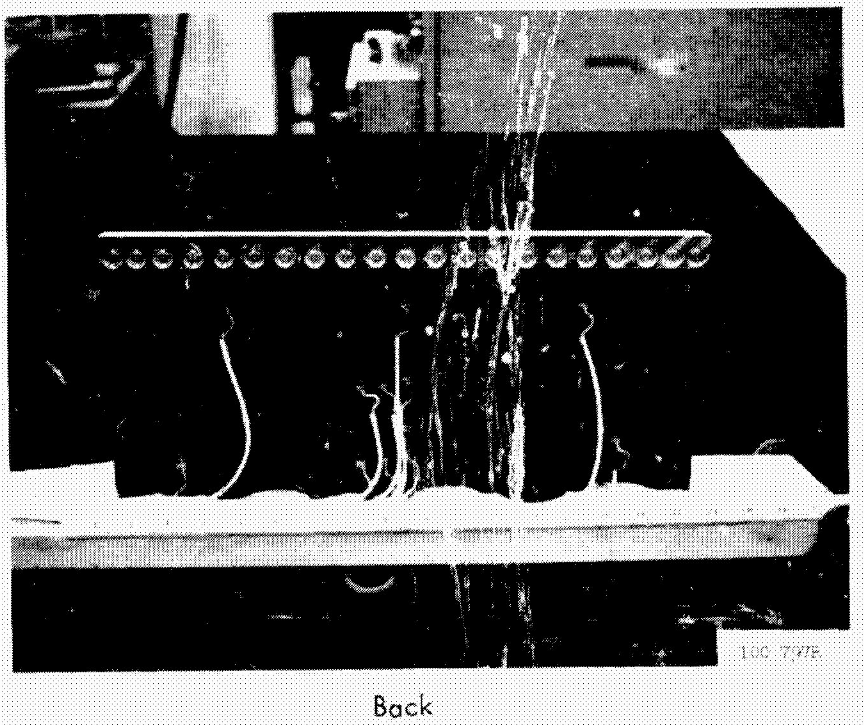

Back

Figure 27-48. Beaded end-closeout panel after failure, room temperature

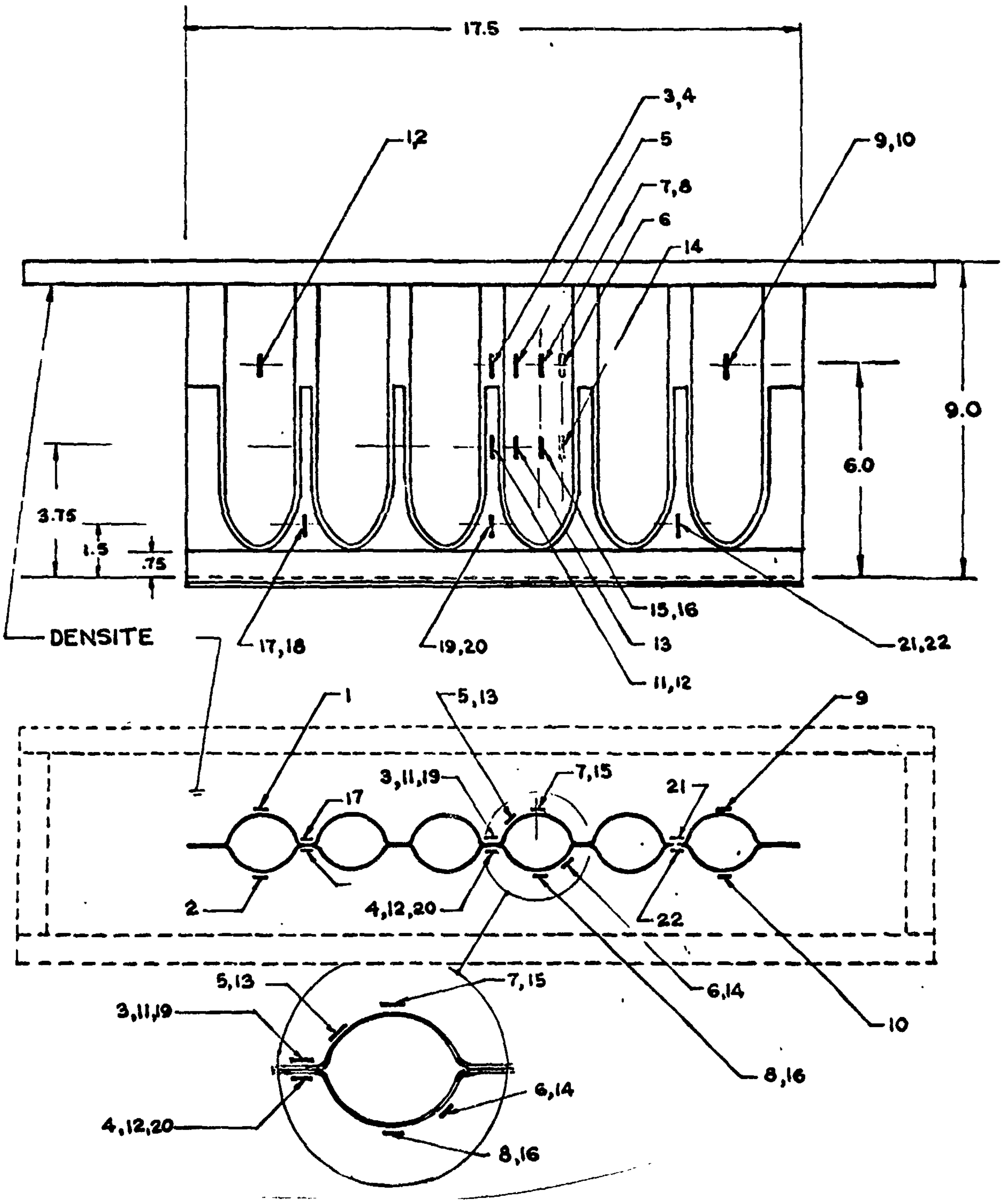

Figure 27-49. Strain gage locations for tubular end-closeout panel

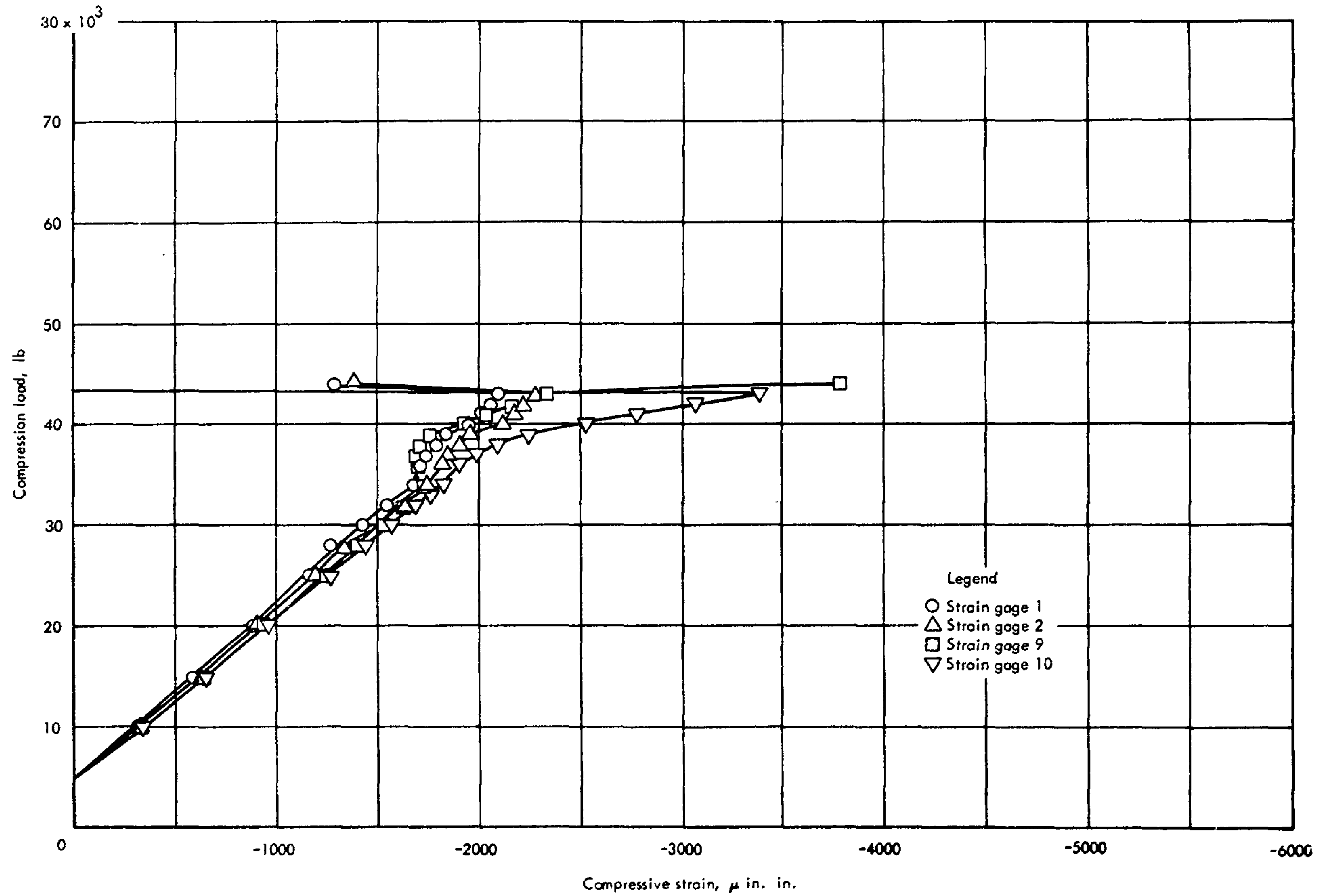

Figure 27-50. Axial strains for tubular end-closeout panel, room temperature

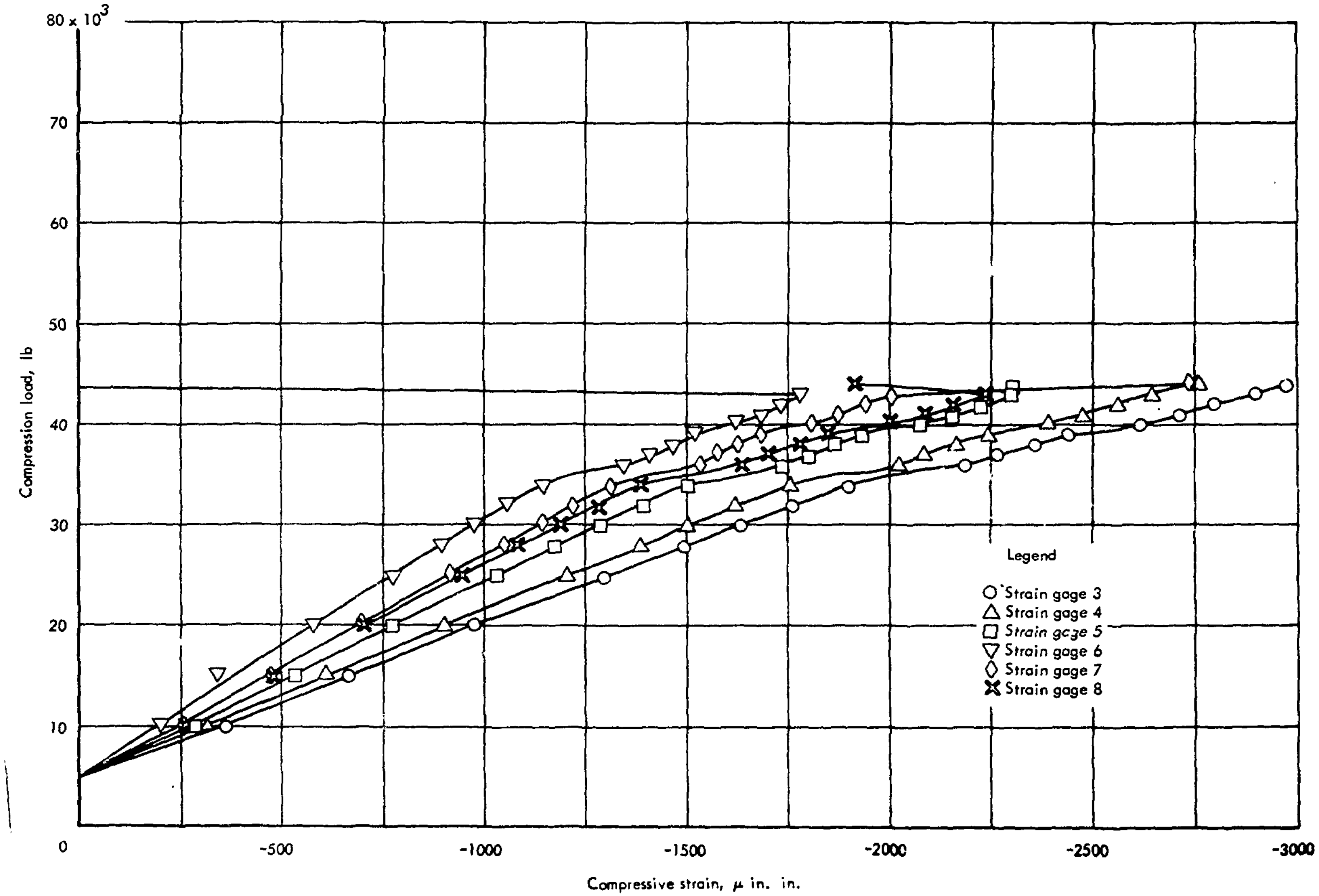

Figure 27-50. (Continued'

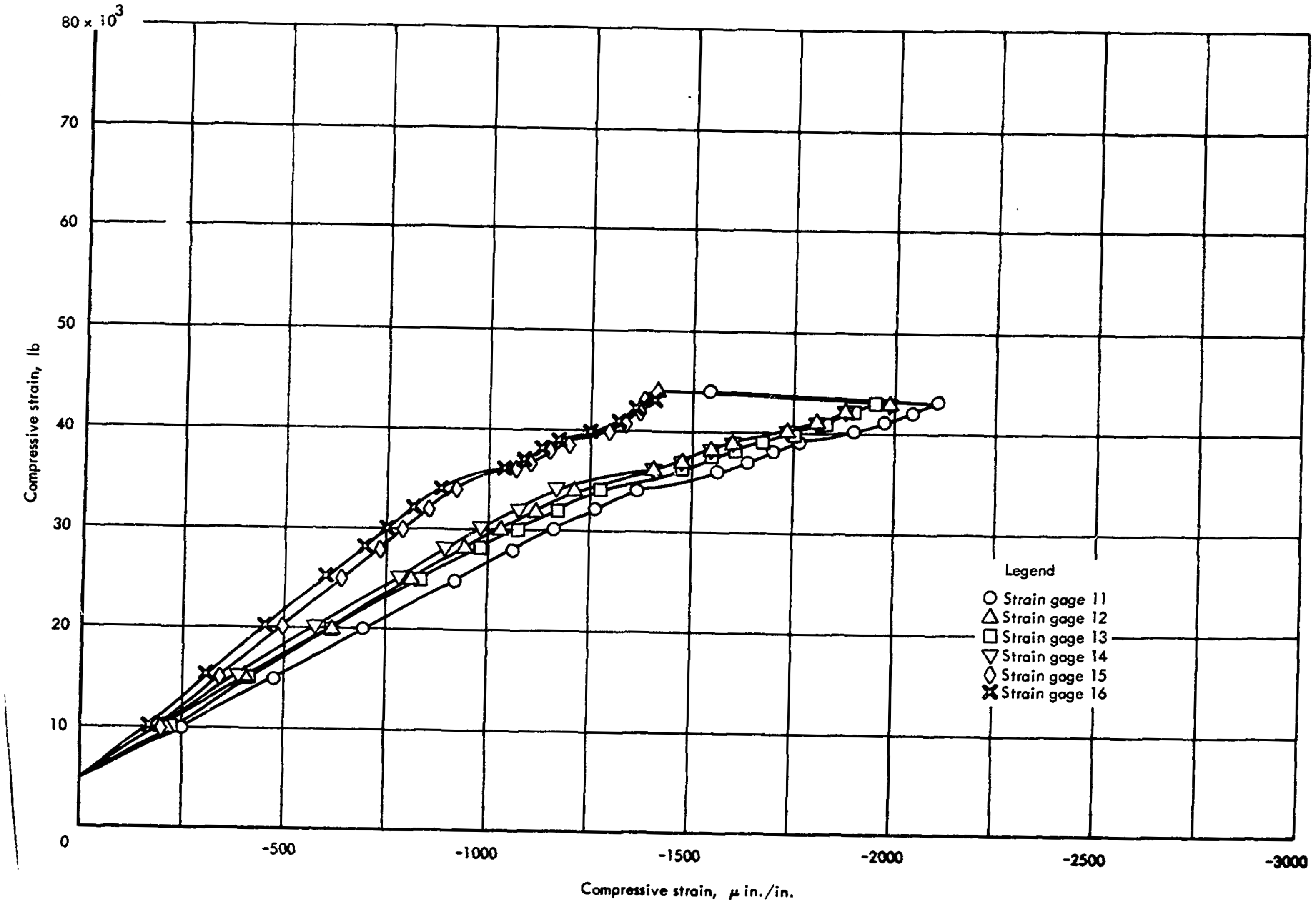

Figure 27-50. (Continued)

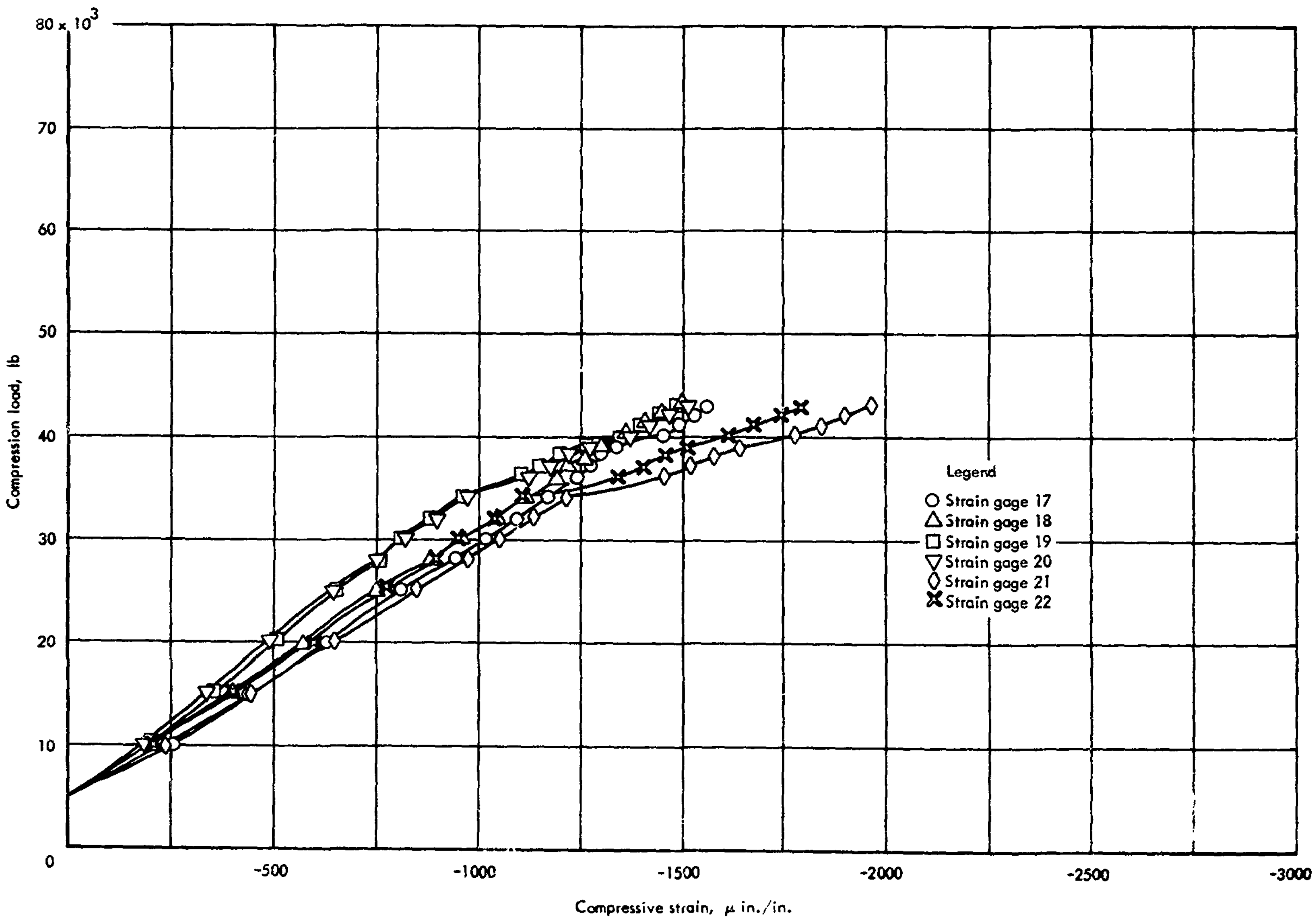

Figure 27-50. (Concluded)

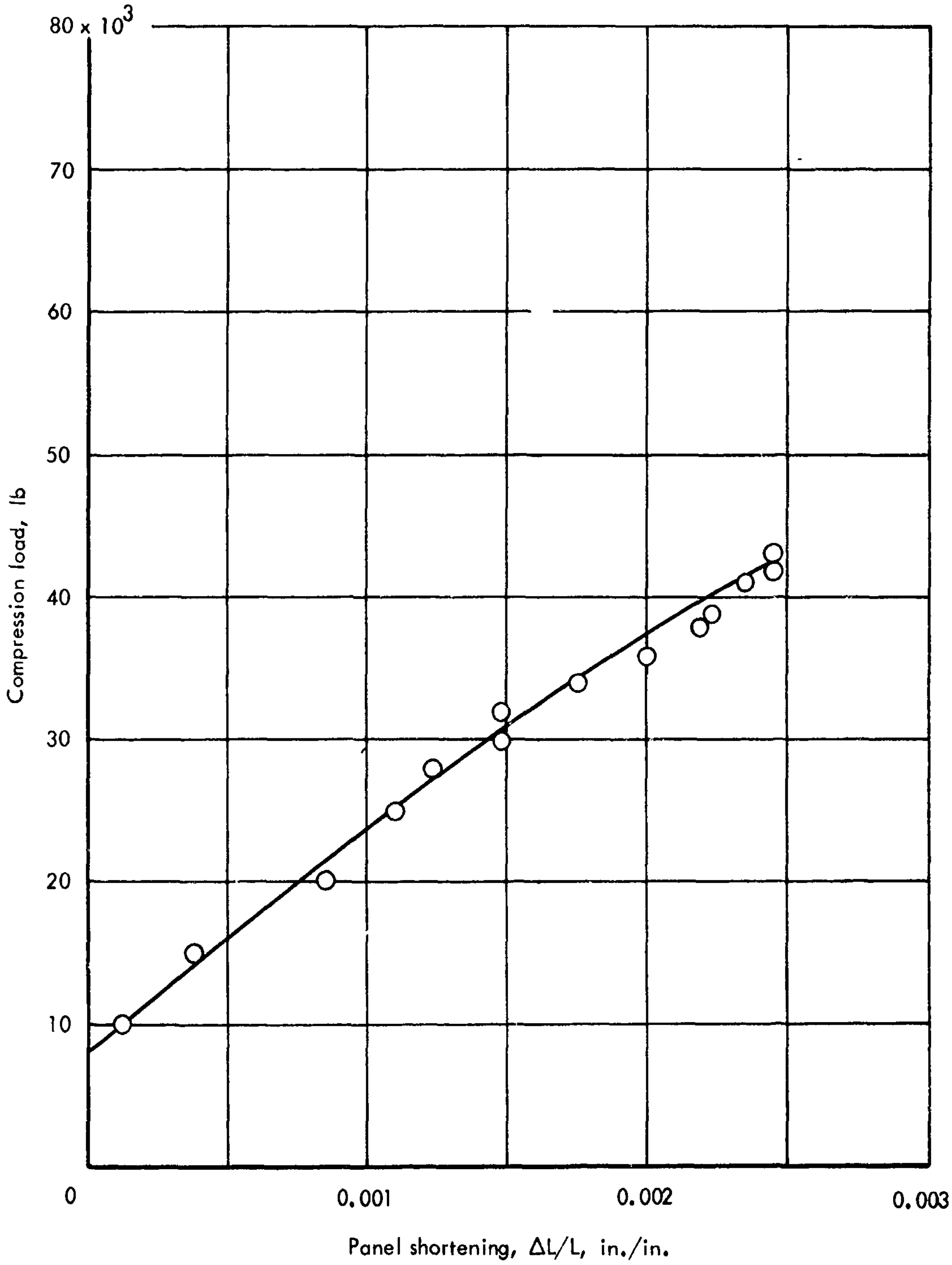

Figure 27-51. Panel shortening curve $\Delta L/L$ for tubular end-closeout panel, room temperature

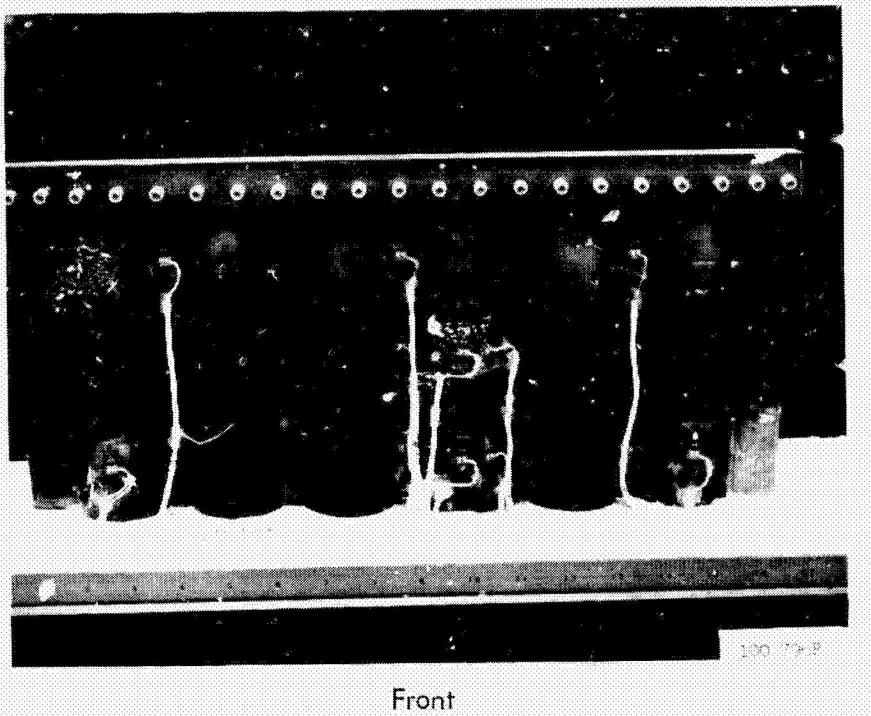

Front

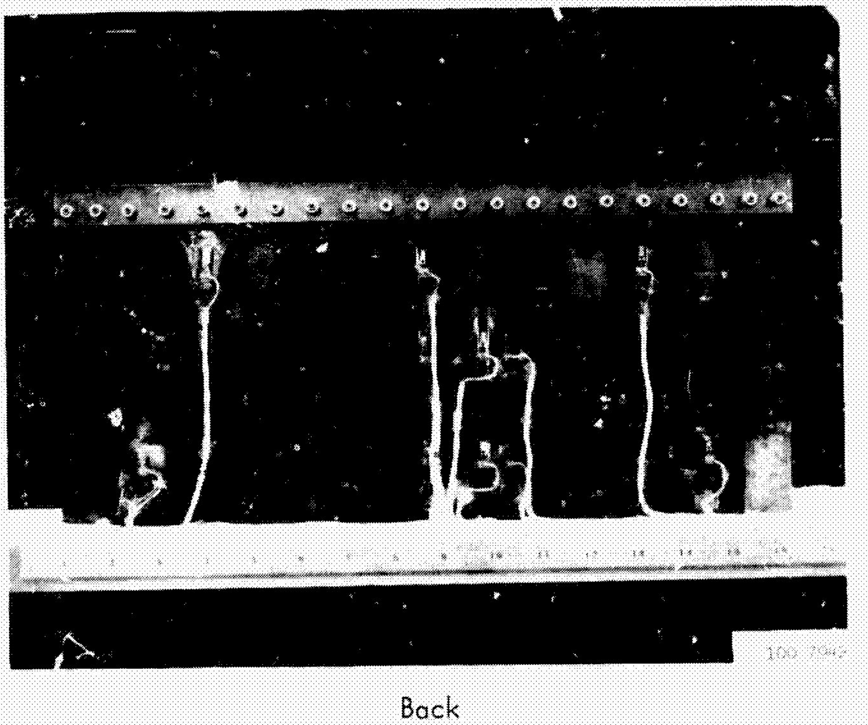

Back

Figure 27-52. Tubular end-closeout panel after failure, room temperature test

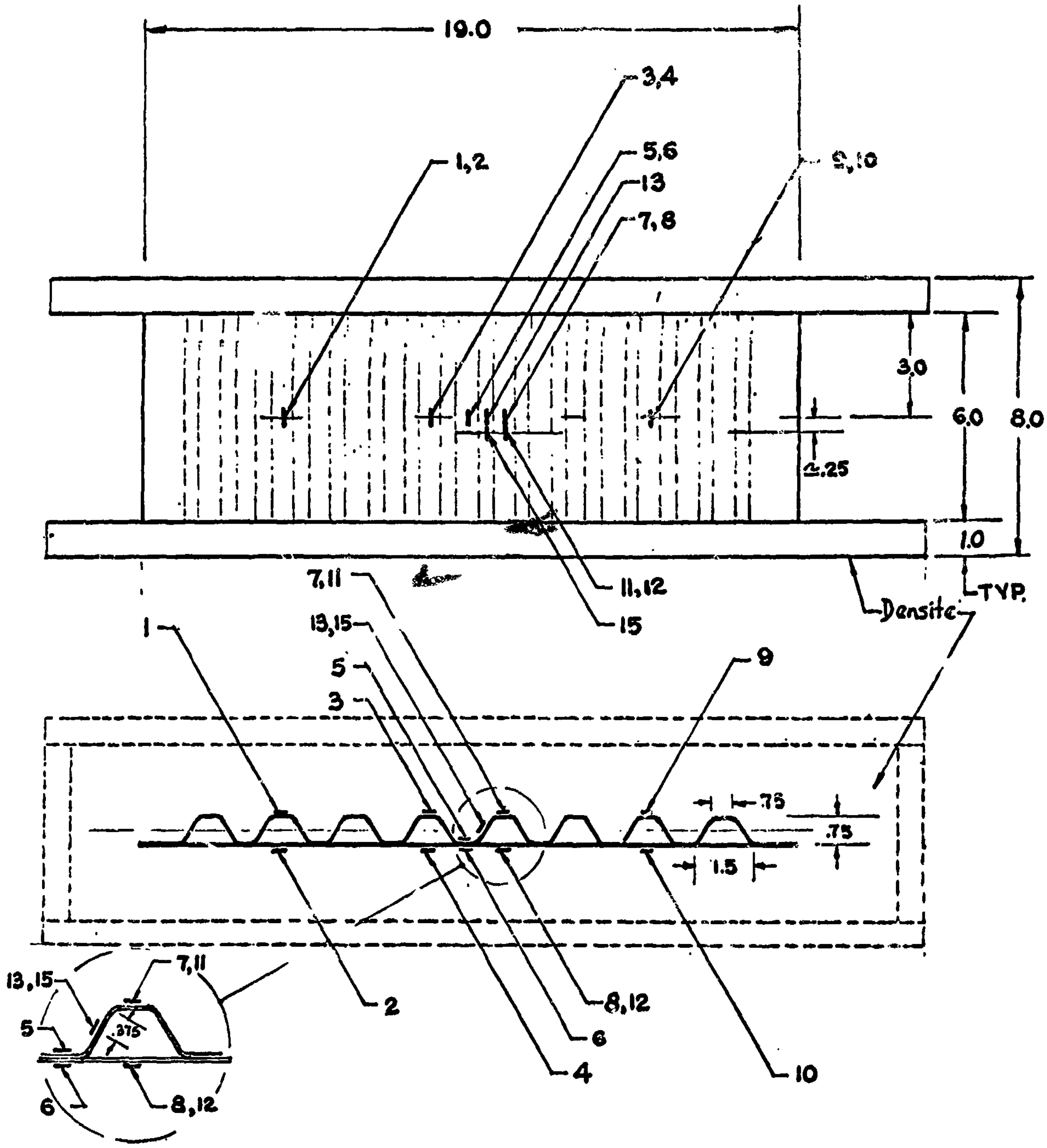

Note:

- Total no. of gages = 14.
- Gages 11, 12, and 15 located directly below gages 7, 8, and 13.

Figure 27-53. Strain gage locations for corrugation-stiffened crippling panel

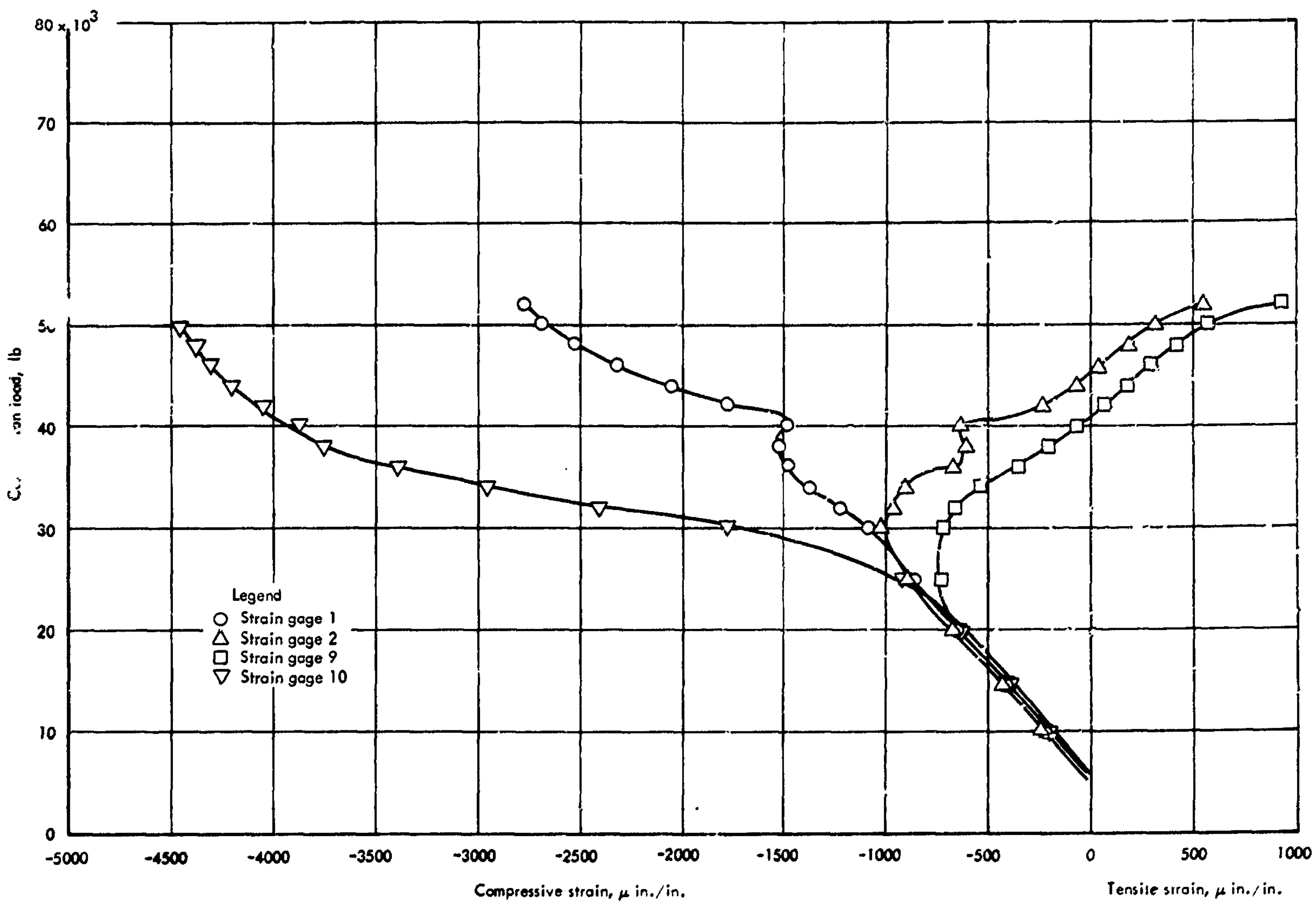

Figure 27-54. Axial strains for corrugation-stiffened skin crippling panel, room temperature

ıel

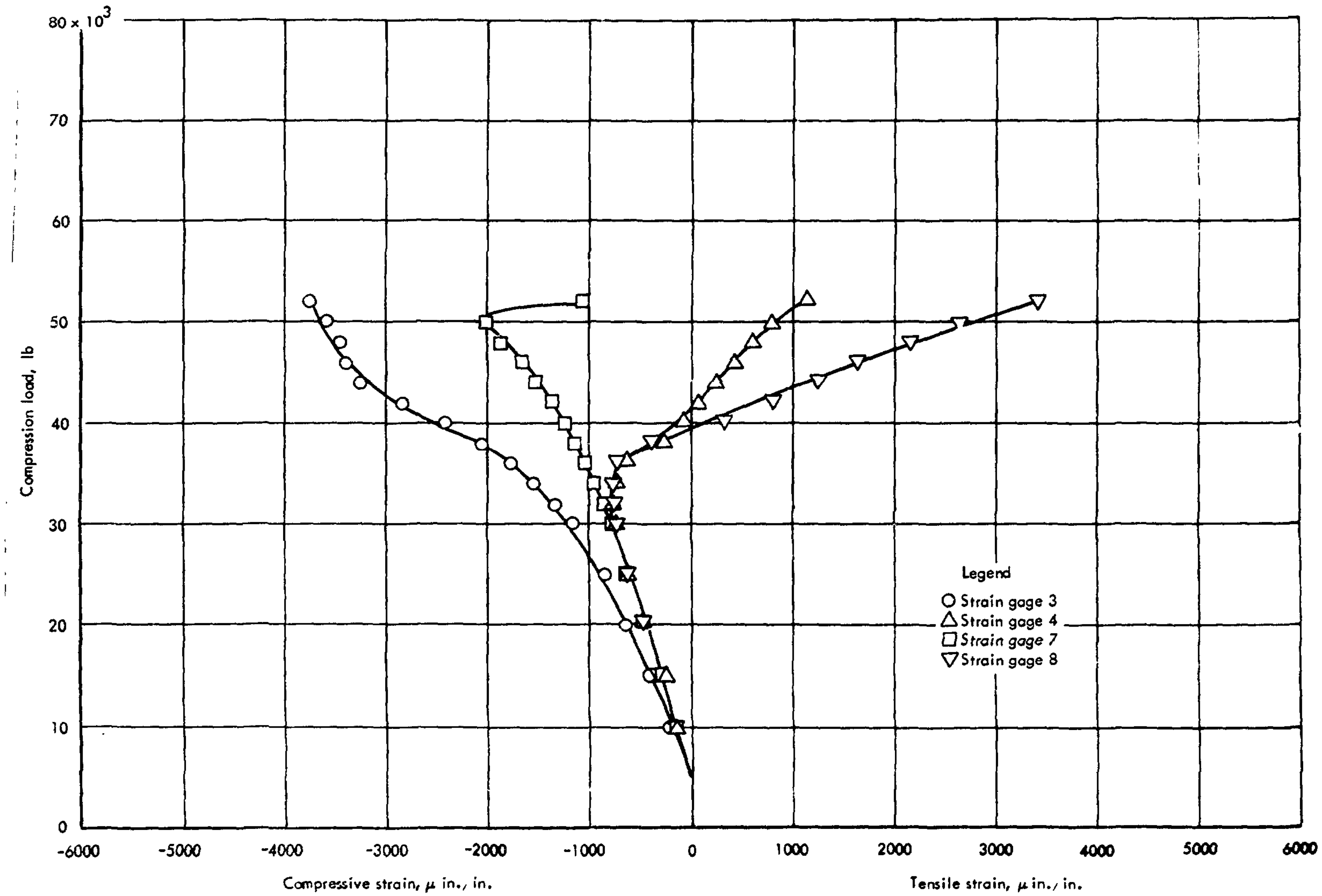

Figure 27-54. (Continued)

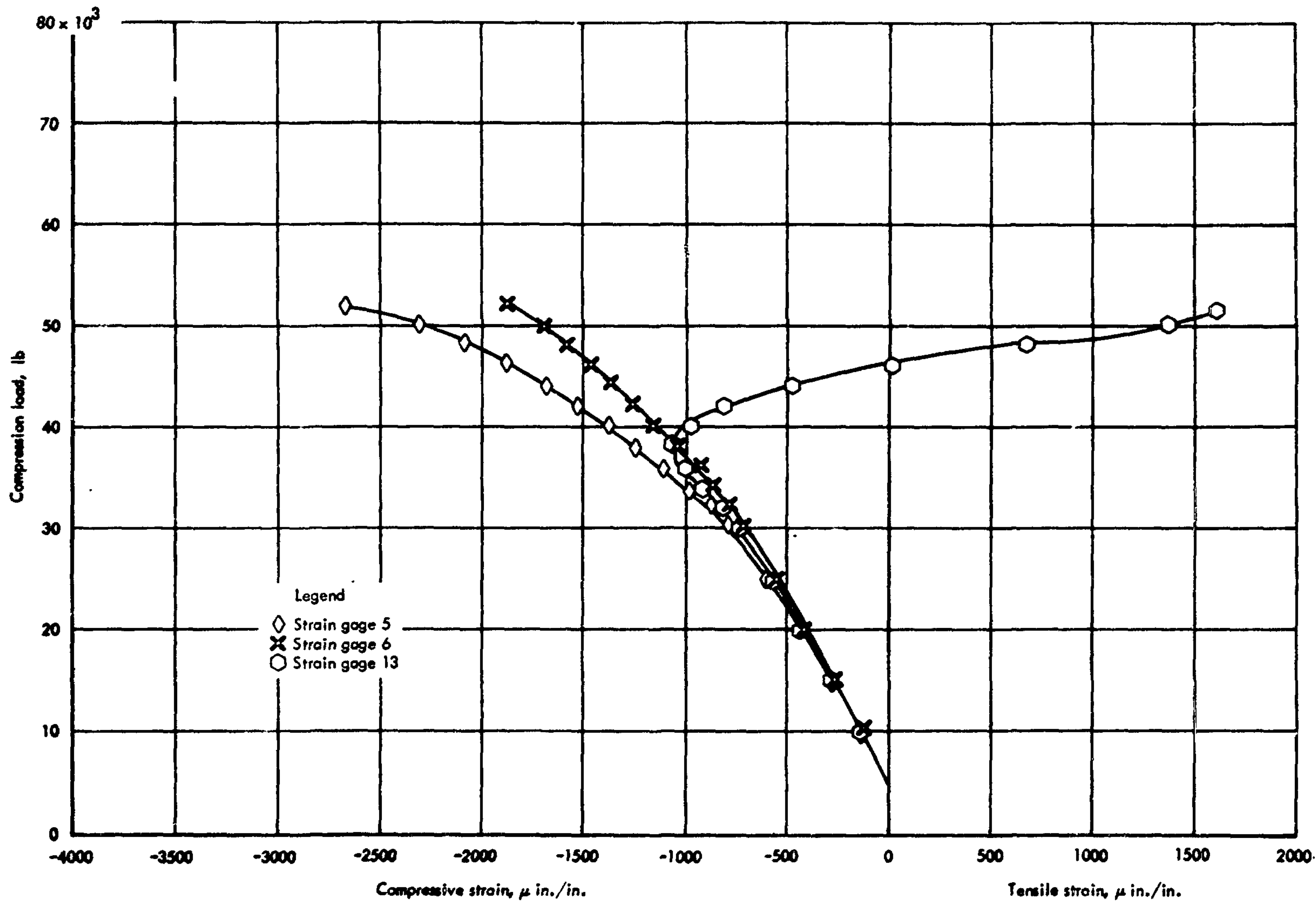

Figure 27-54. (Continued)

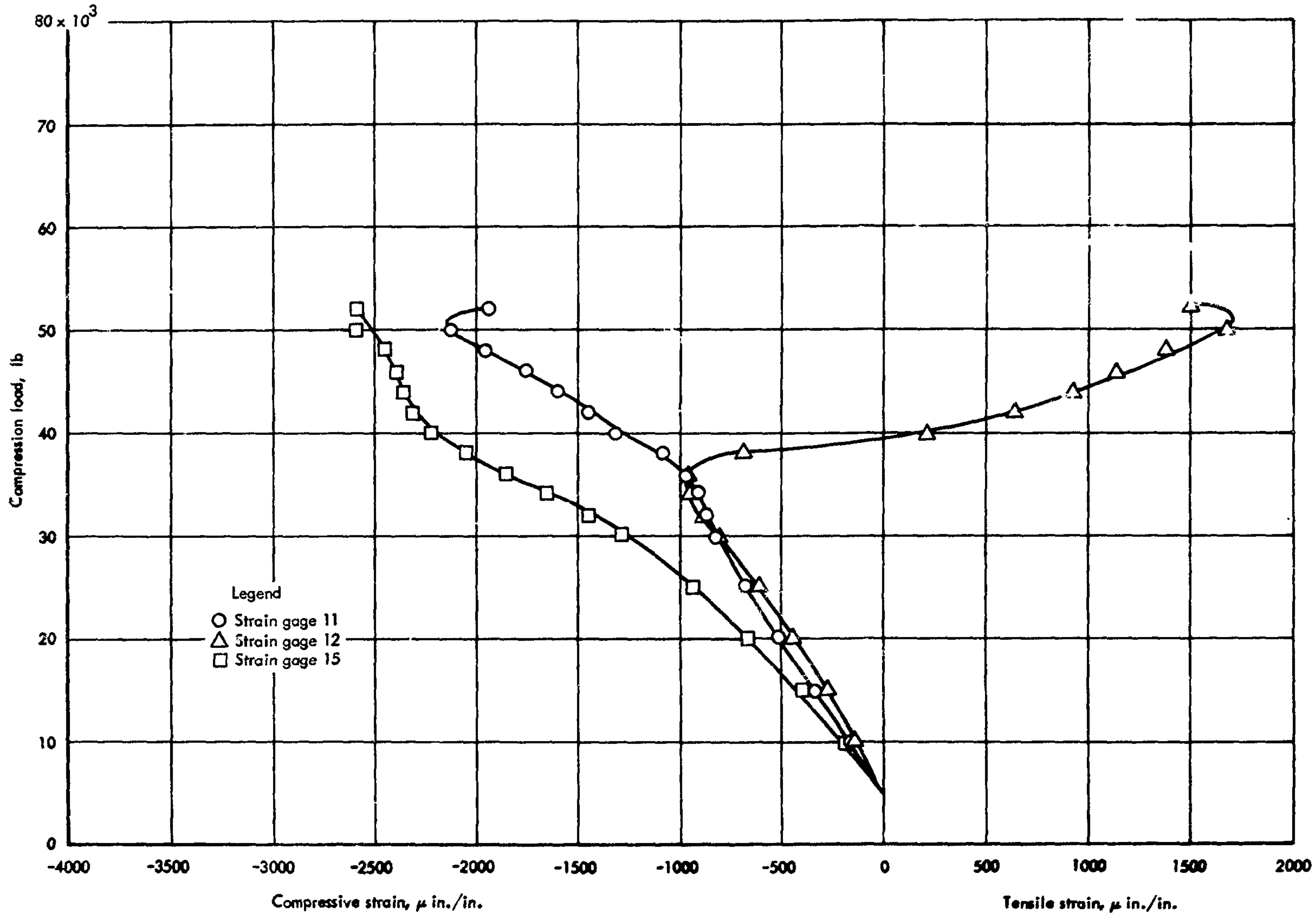

Figure 27-54. (Concluded)

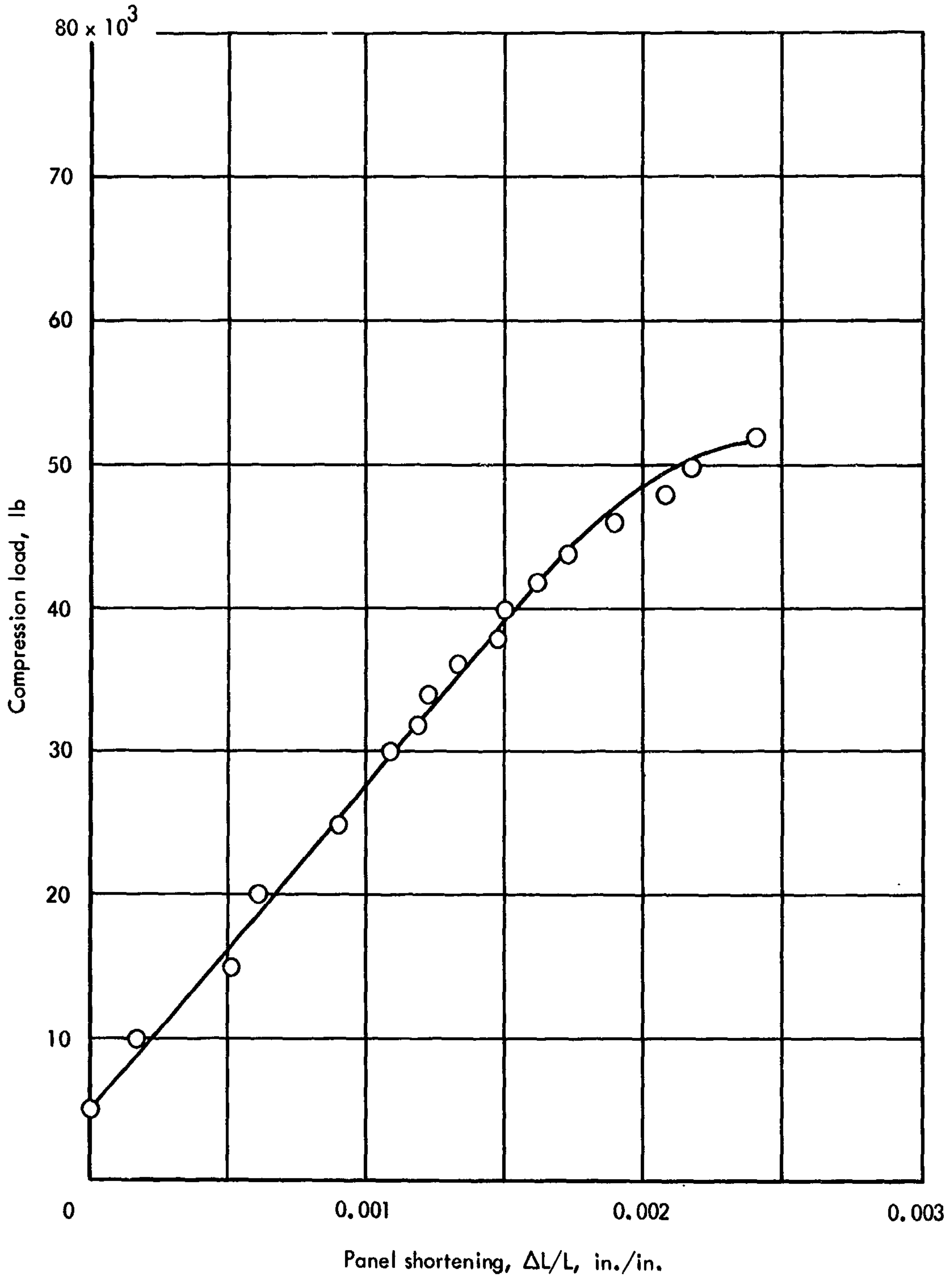

Figure 27-55. Panel shortening curve $\Delta L/L$ for corrugation-stiffened crippling panel, room temperature

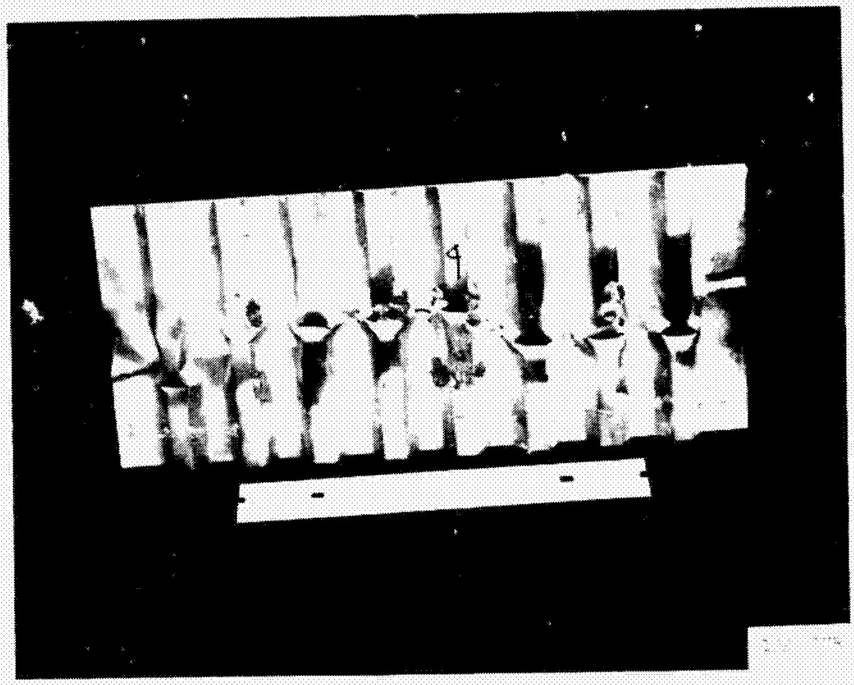

Corrugation side

Skin side

Figure 27-56. Corrugation stiffened crippling panel after failure, room temperature test

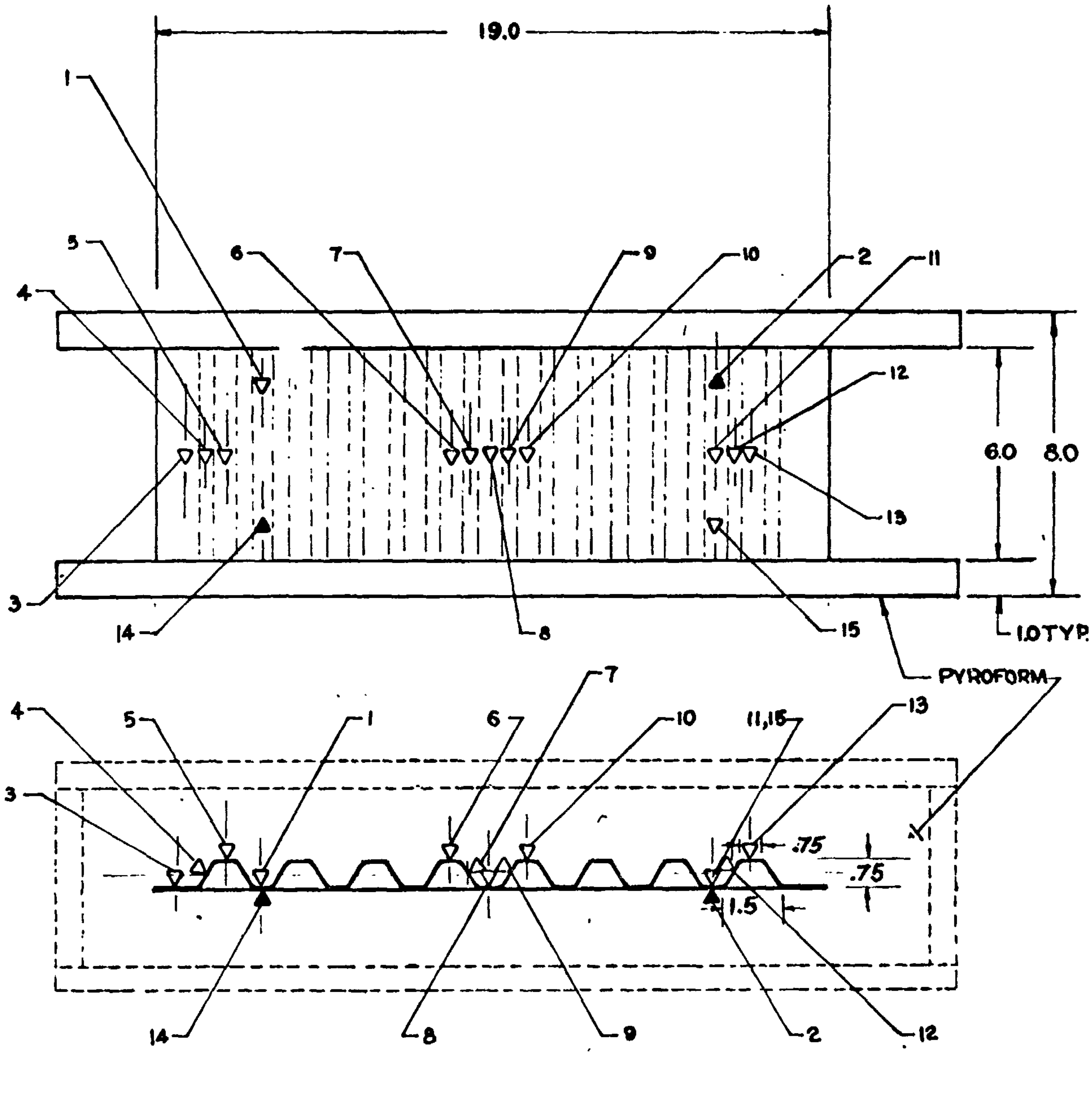

Figure 27-57. Thermocouple locations for the corrugation-stiffened crippling panel

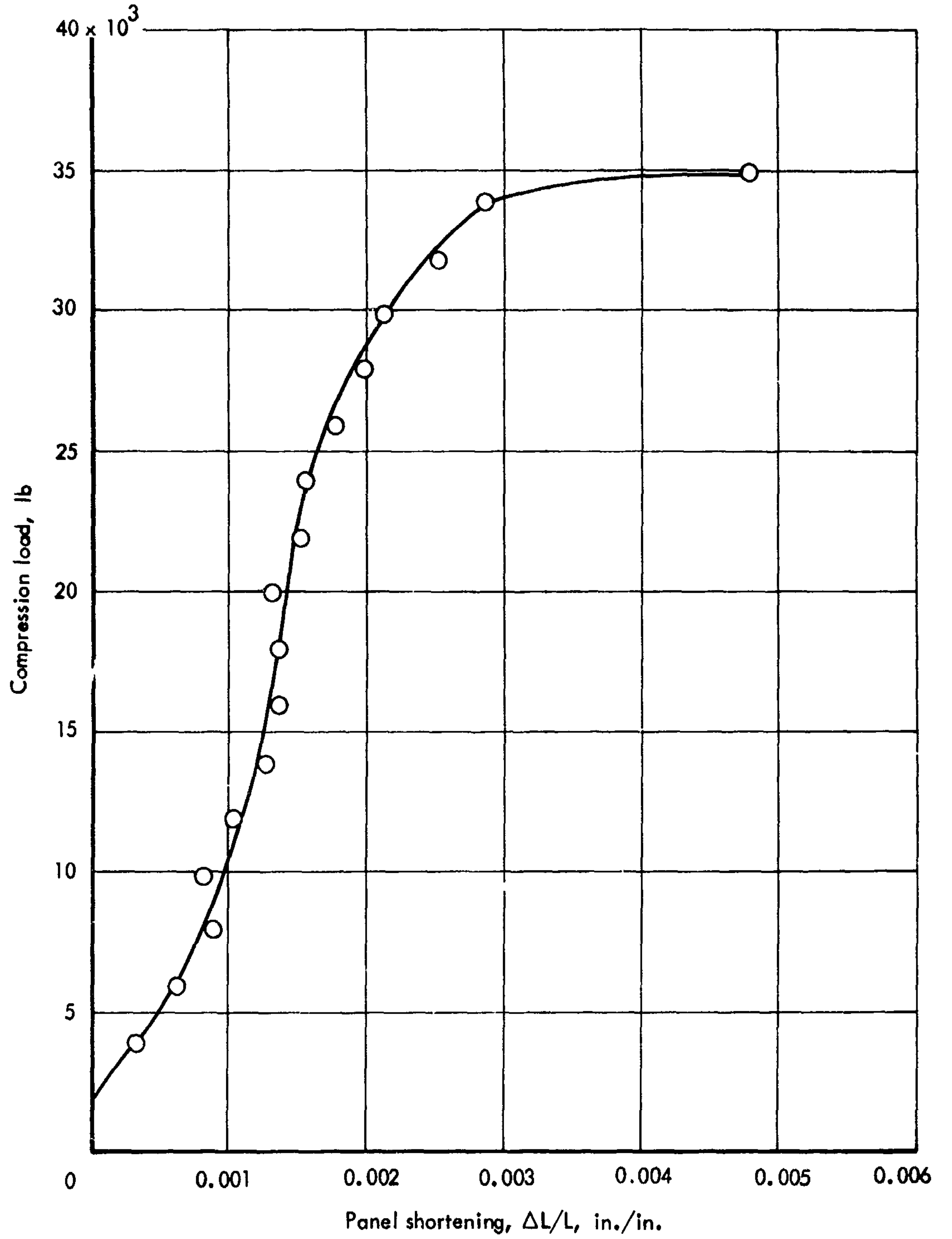

Figure 27-58. Panel shortening curve for corrugation-stiffened ΔL/L crippling panel, 1400° F

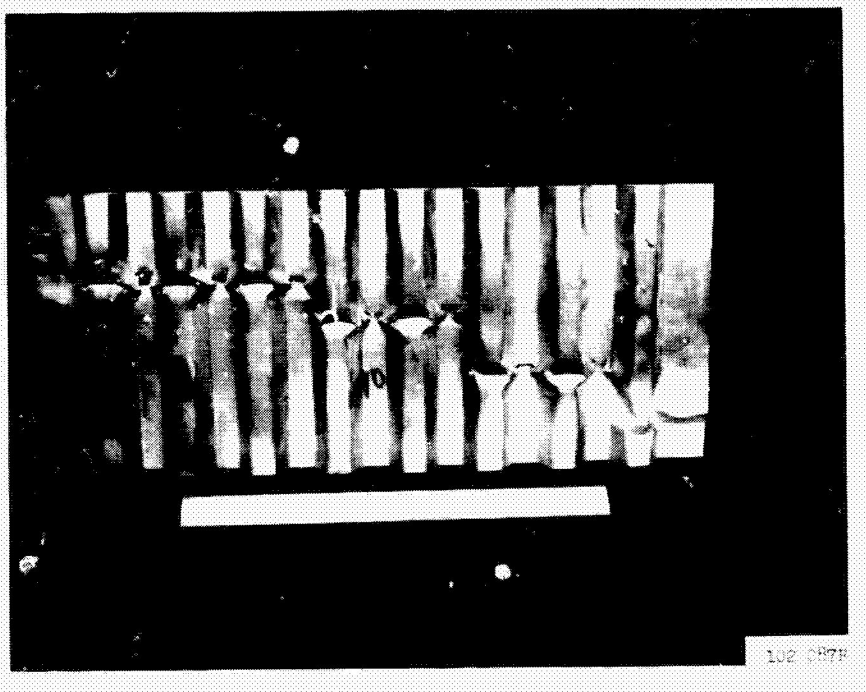

Corrugation side

Skin side

Figure 27-59. Corrugation-stiffened skin crippling panel after failure, 1400° F

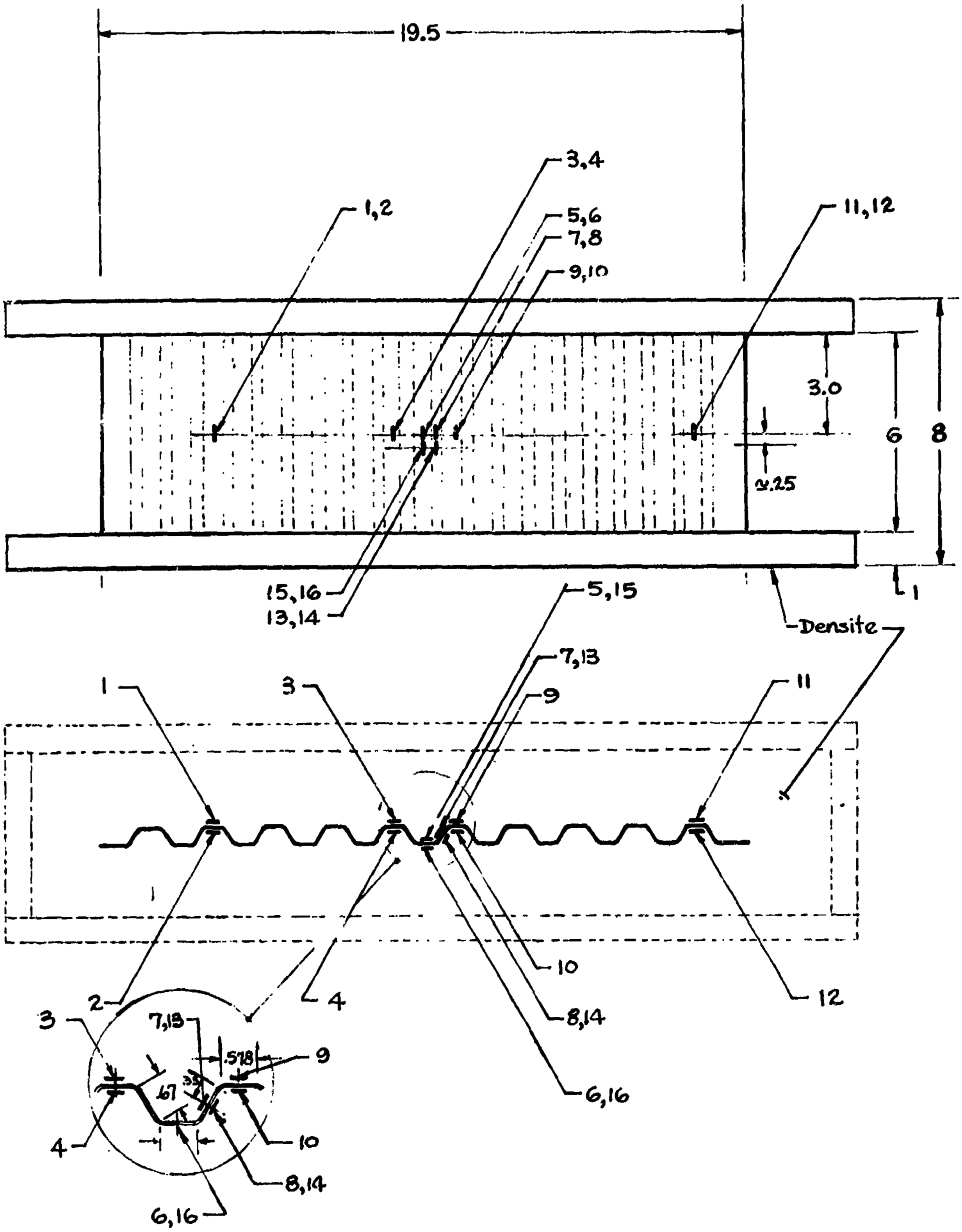

Figure 27-60. Strain gage locations for trapezoidal corrugation crippling panel

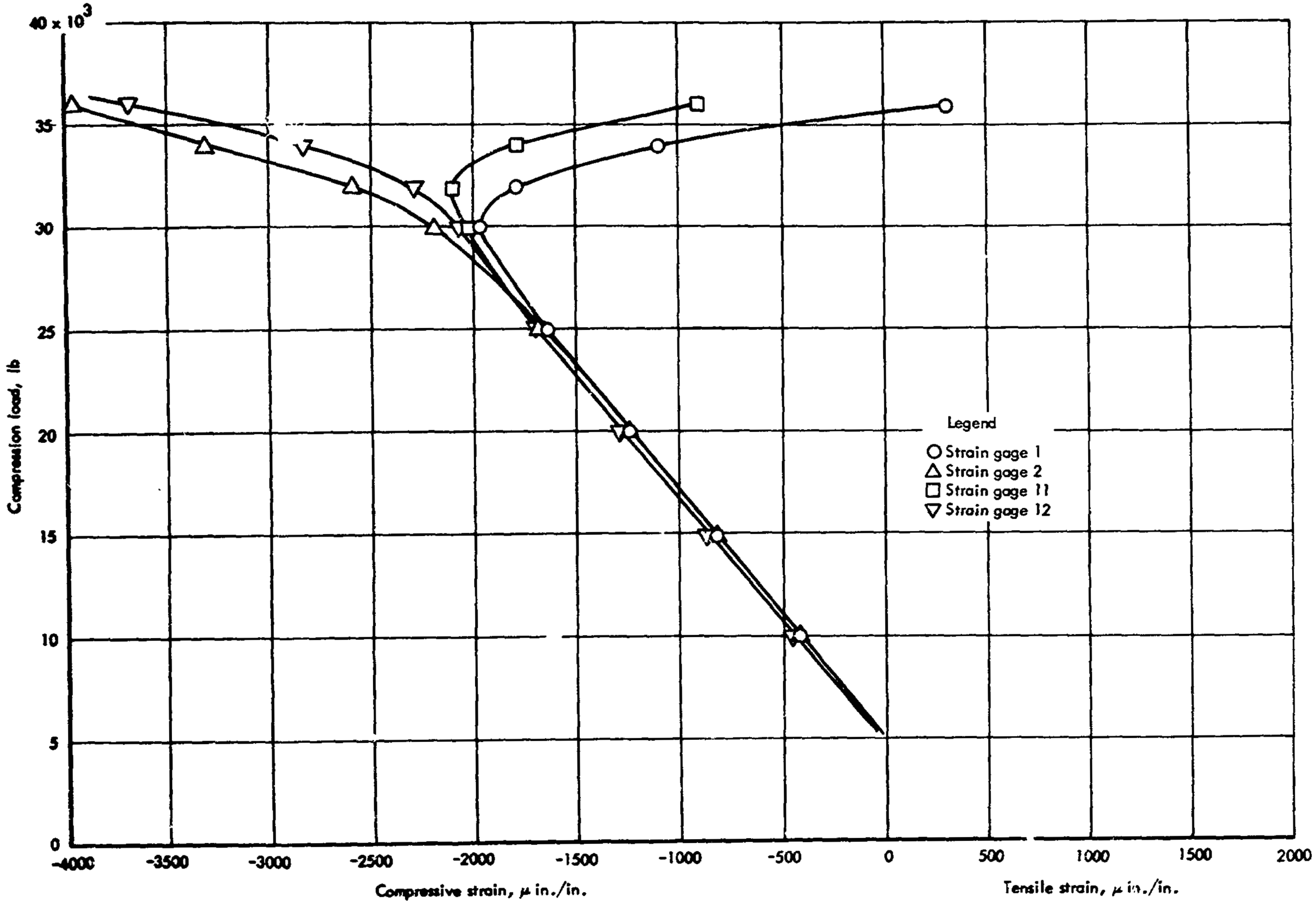

Figure 27-61. Axial strains for trapezoidal corrugation crippling panel, room temperature

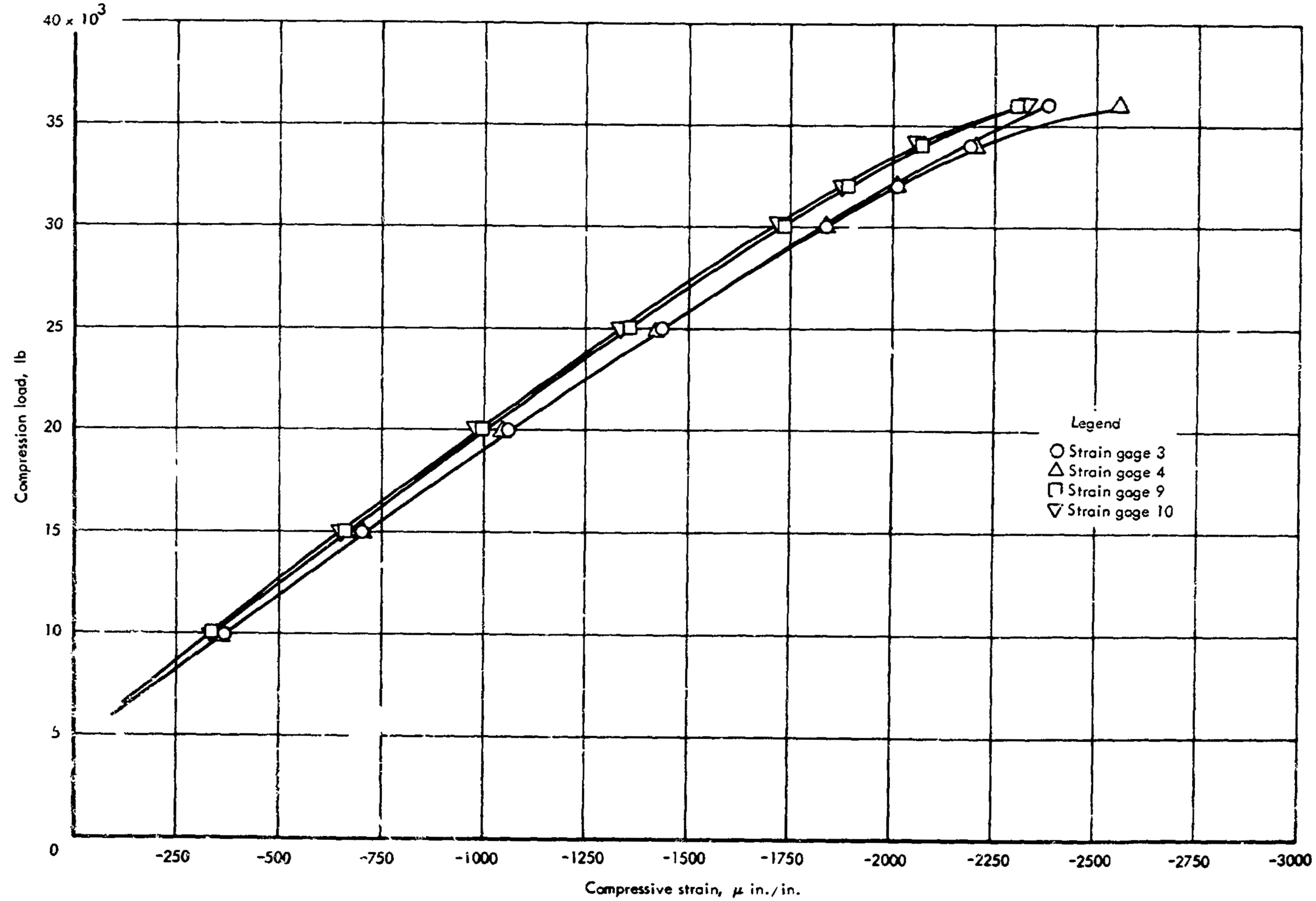

Figure 27-61. (Continued)

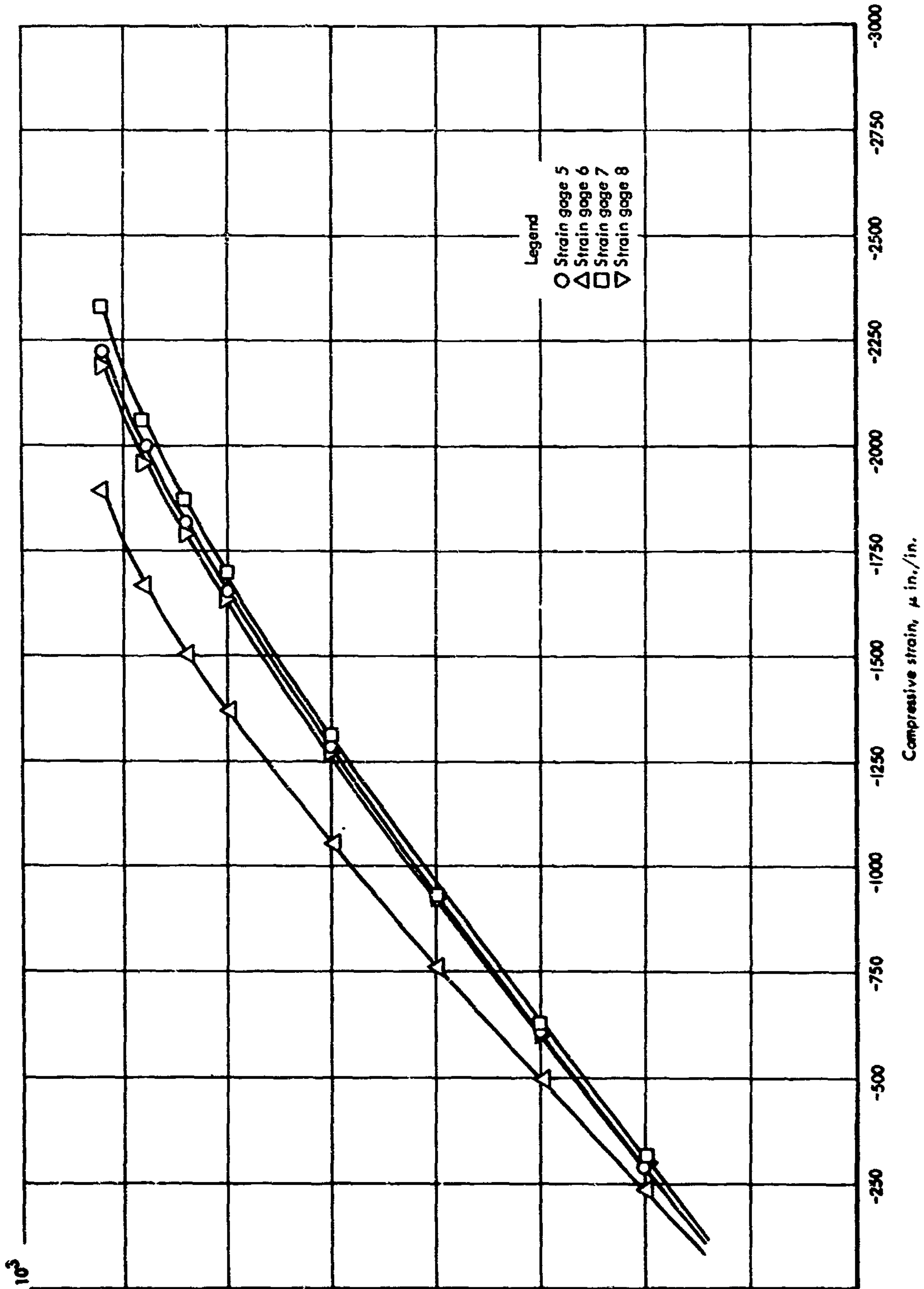

Figure 27-61 (continued)

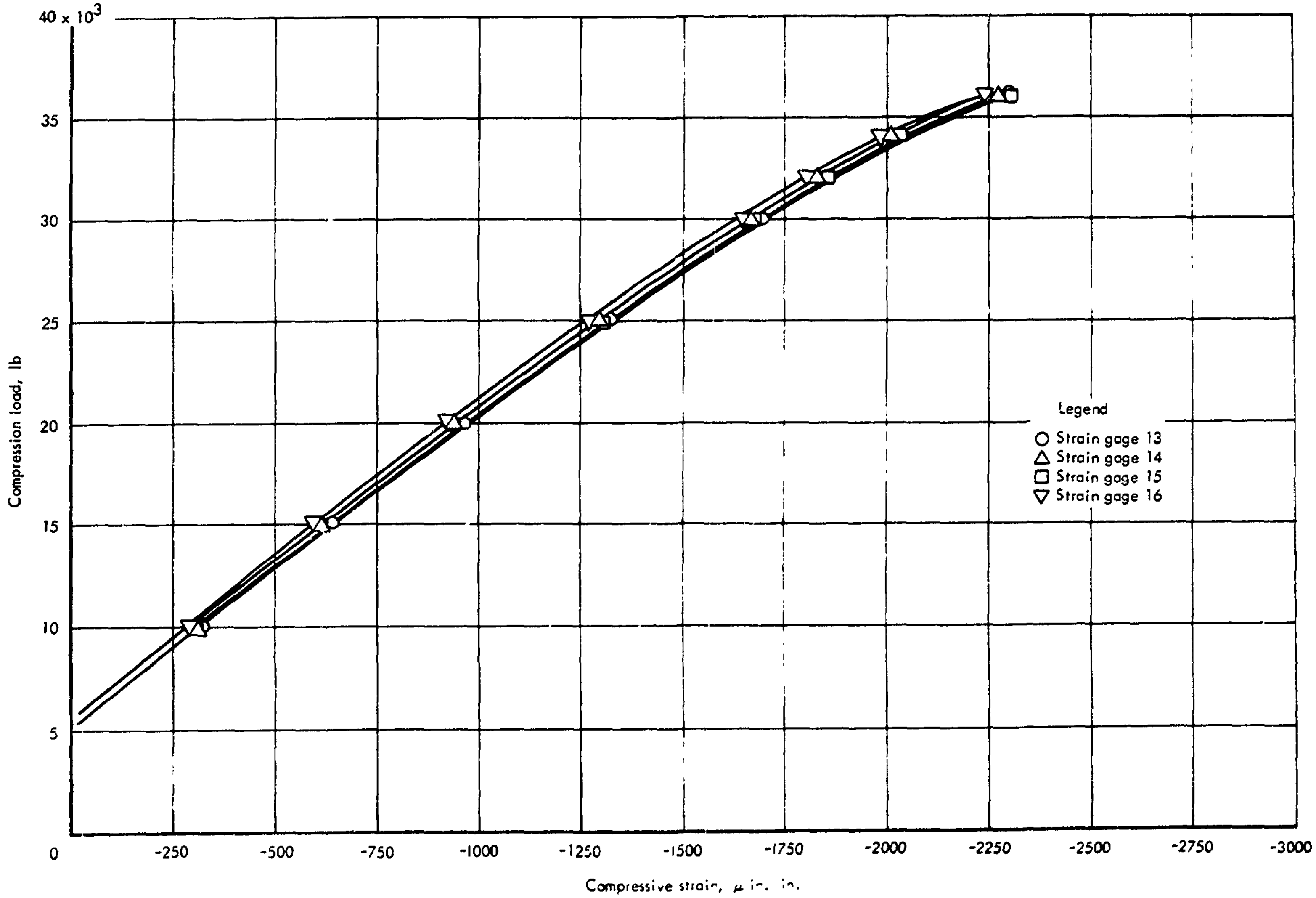

Figure 27-61 (Concluded)

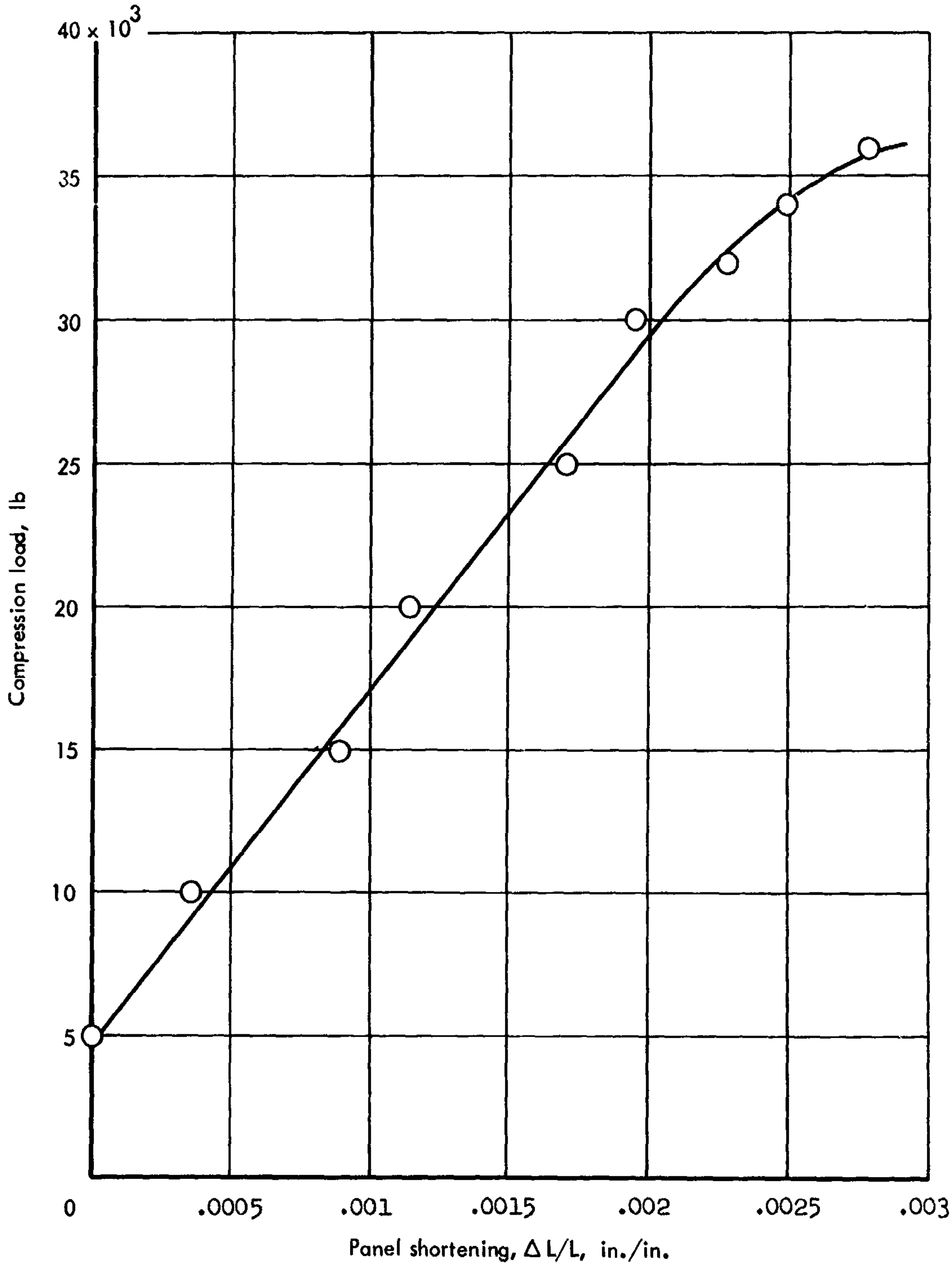

Figure 27-62 Panel shortening curve ΔI 'L for trapezoidal corrugation crippling panel, room temperature

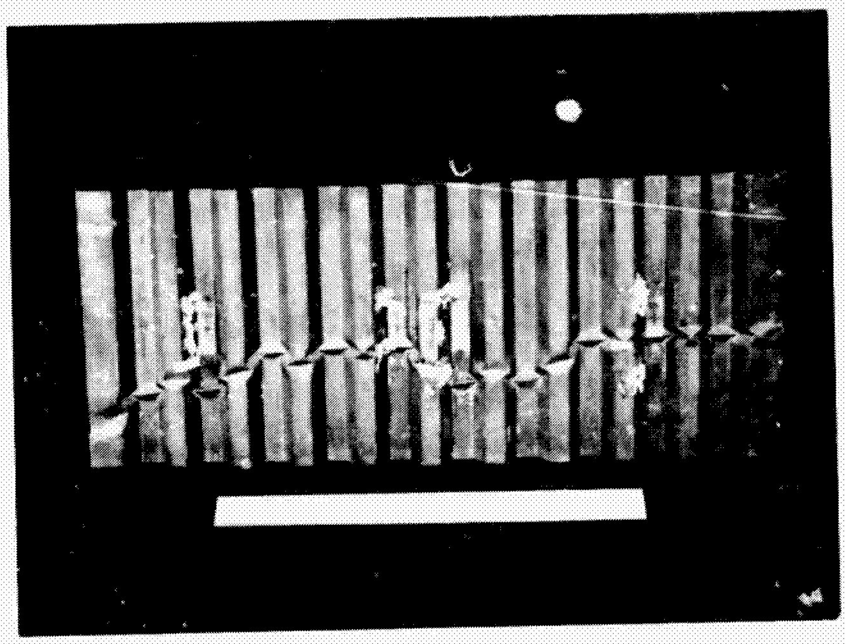

Front

Back

Figure 27-63 Trapezoidal corrugation crippling panel after failure, room temperature test

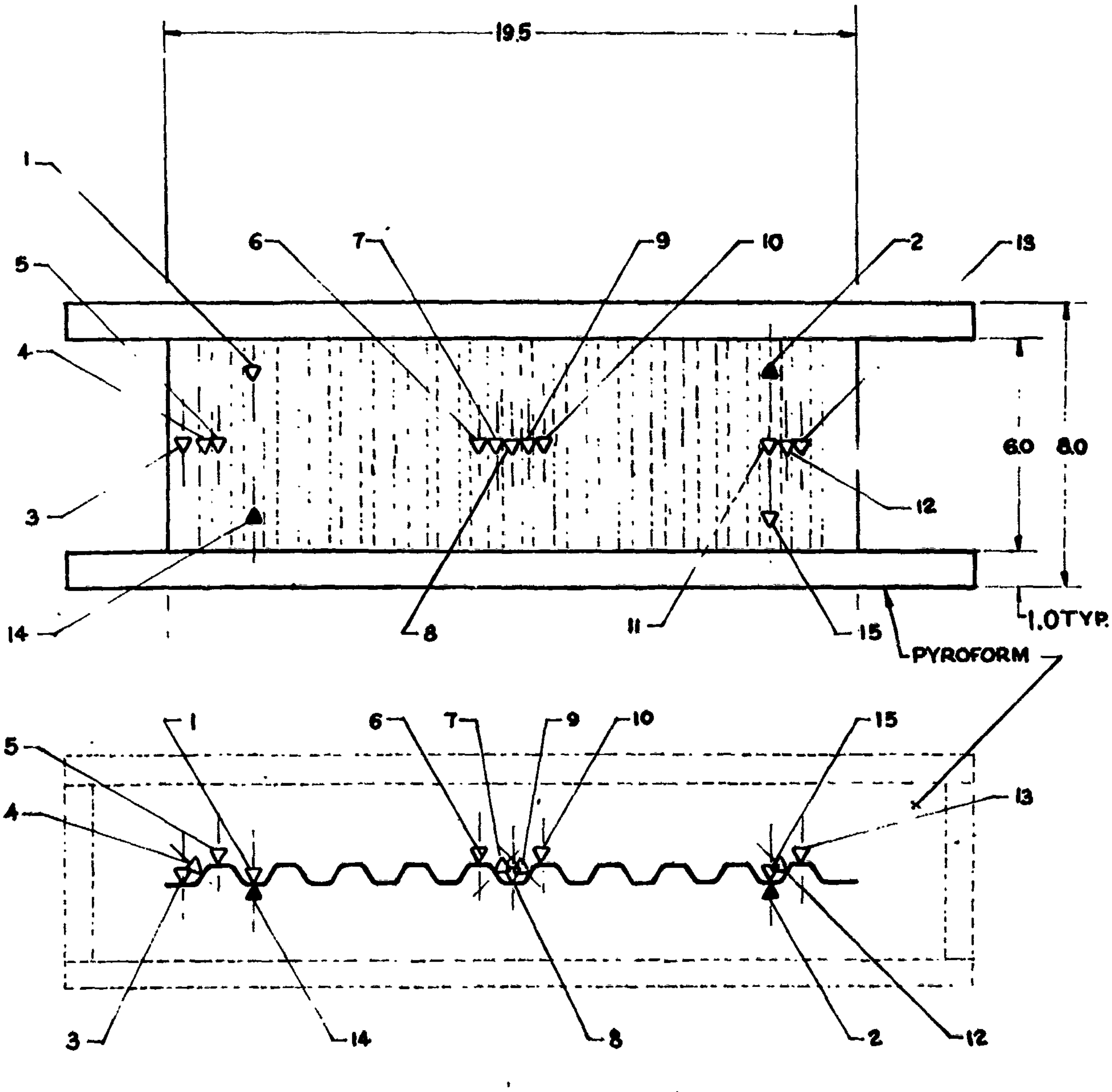

Figure 27-64 Thermocouple locations for the trapezoidal corrugation crippling panel

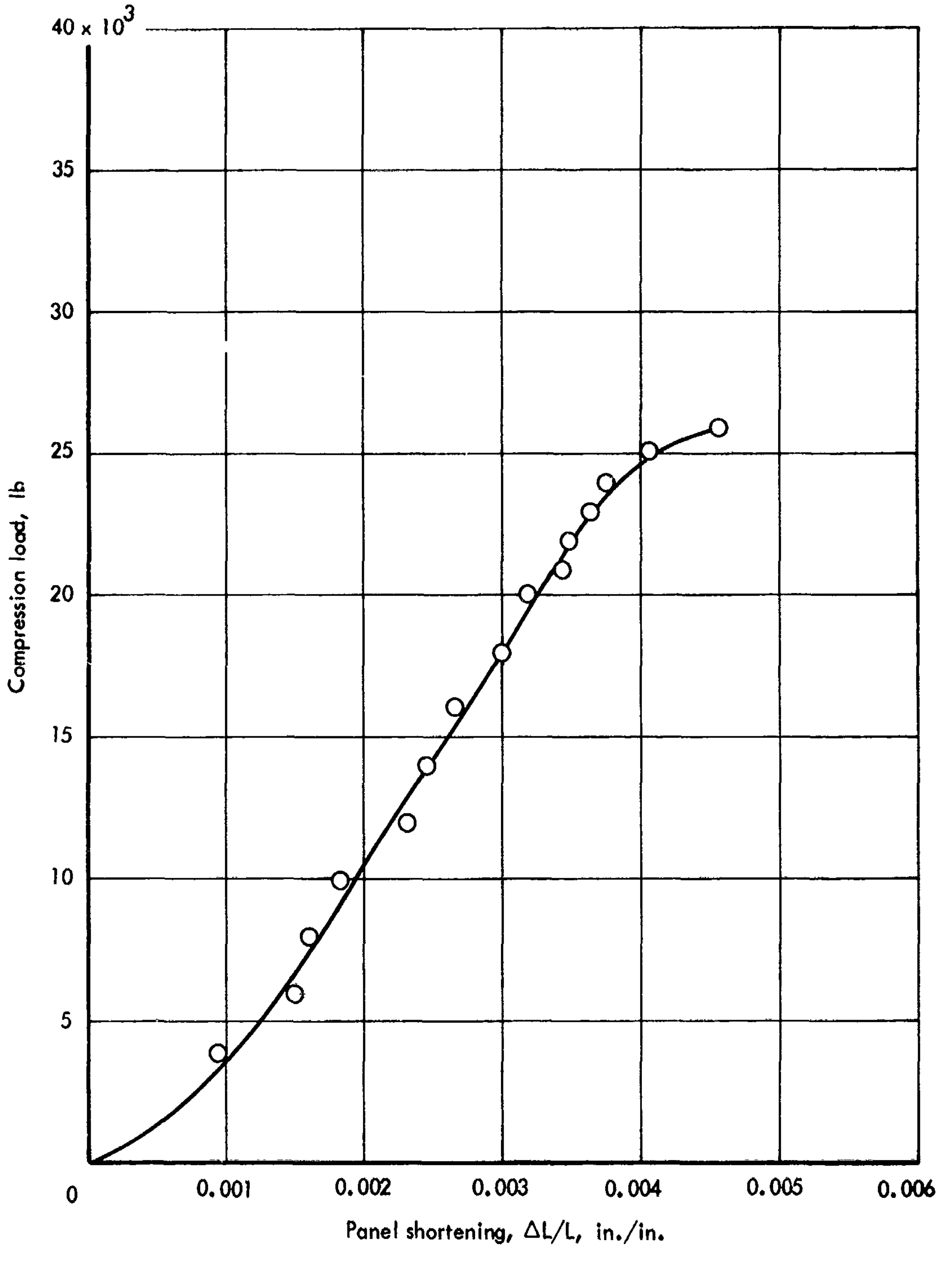

Figure 27-65 Panel shortening curve $\Delta L/L$ for trapezoidal corrugation crippling panel

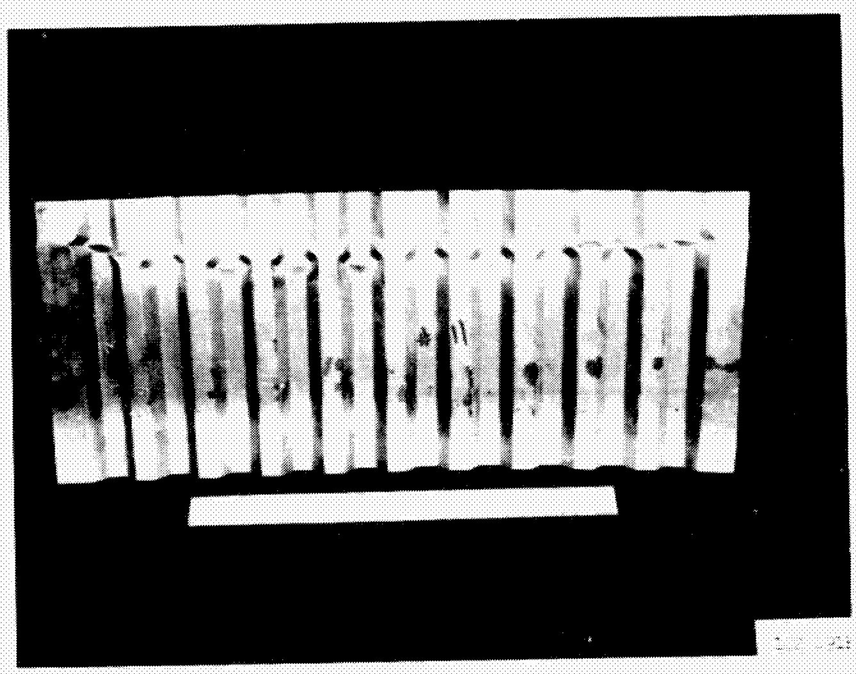

Front

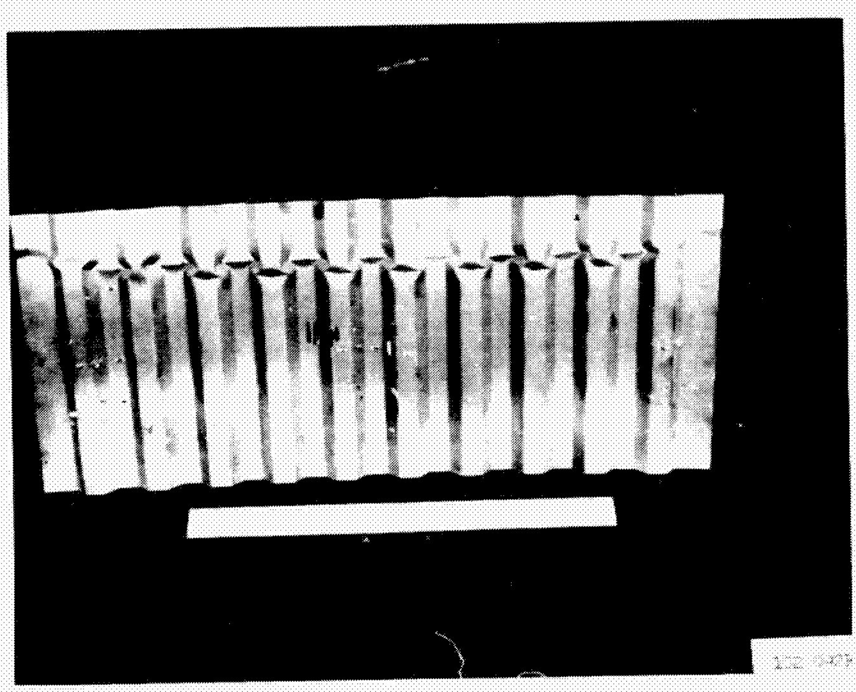

Back

Figure 27-66 Trapezoidal corrugation crippling panel after failure, $1400^{\circ}F$ test

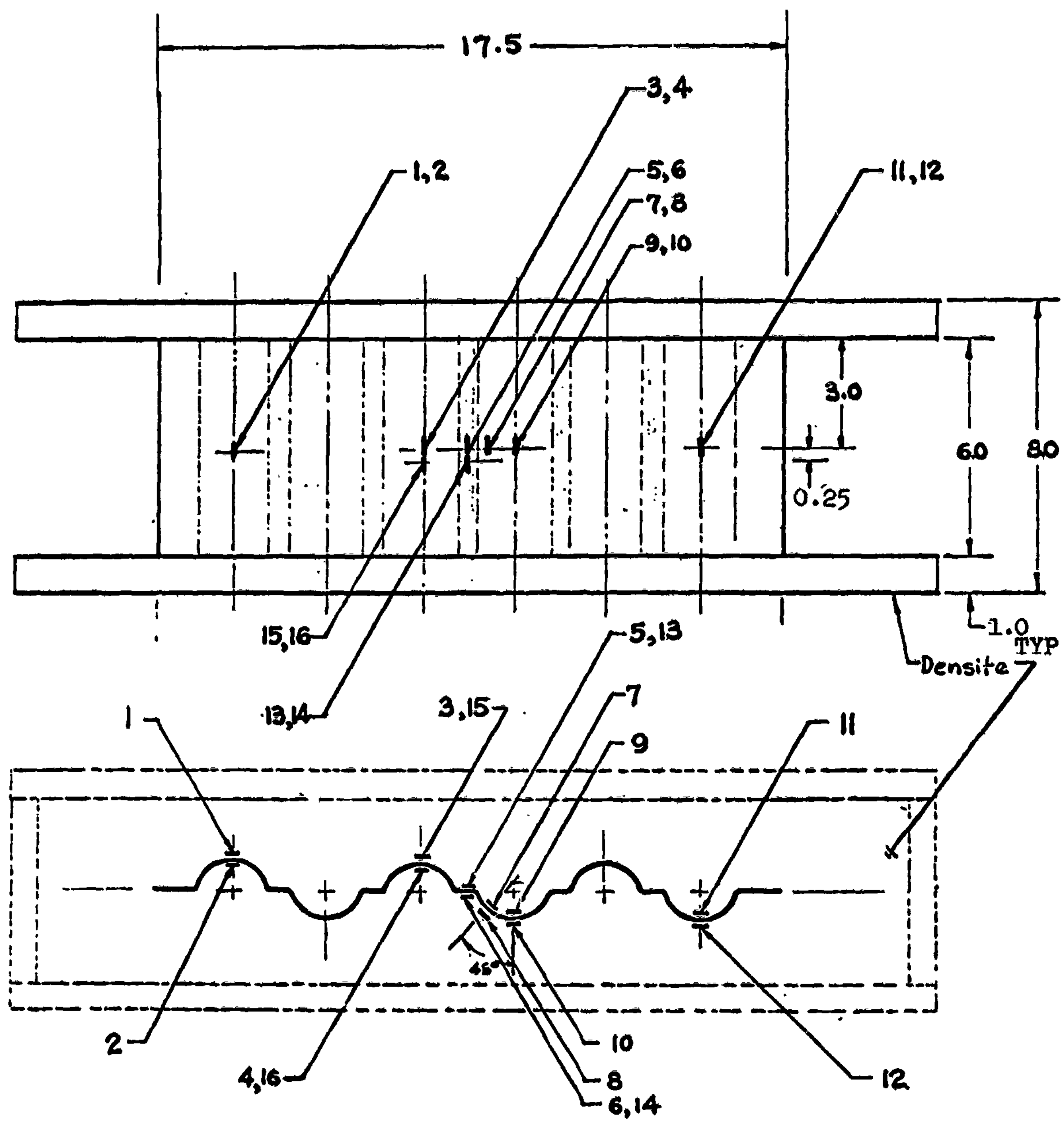

Note:

- Total no. gages = 16.
- Gages 13, 14, and 15, 16 located directly below gages 3, 4 and 5, 6.

Figure 27-67 Strain gage locations for beaded crippling panel

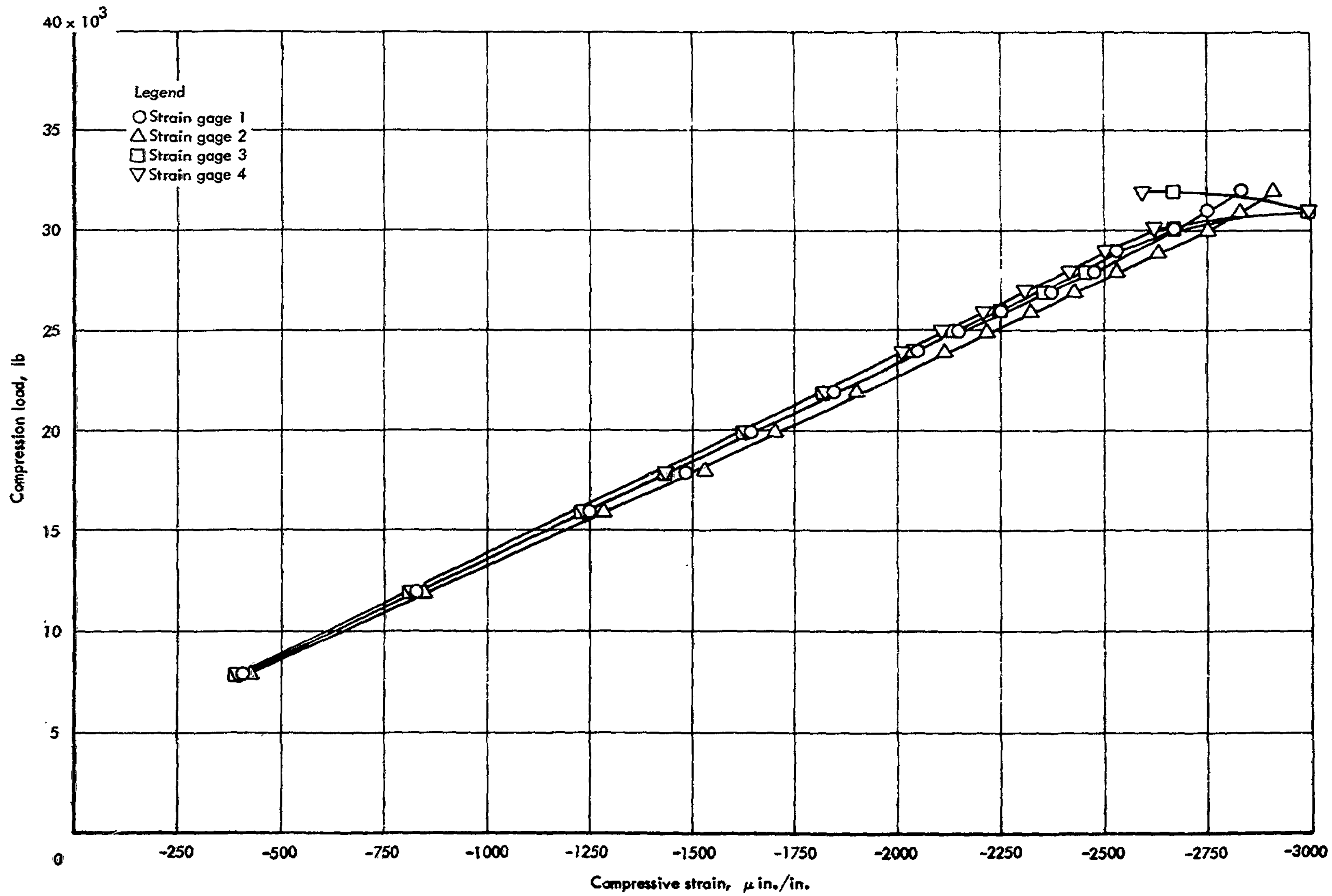

Figure 27-68 Axial strains for beaded crippling panel, room temperature

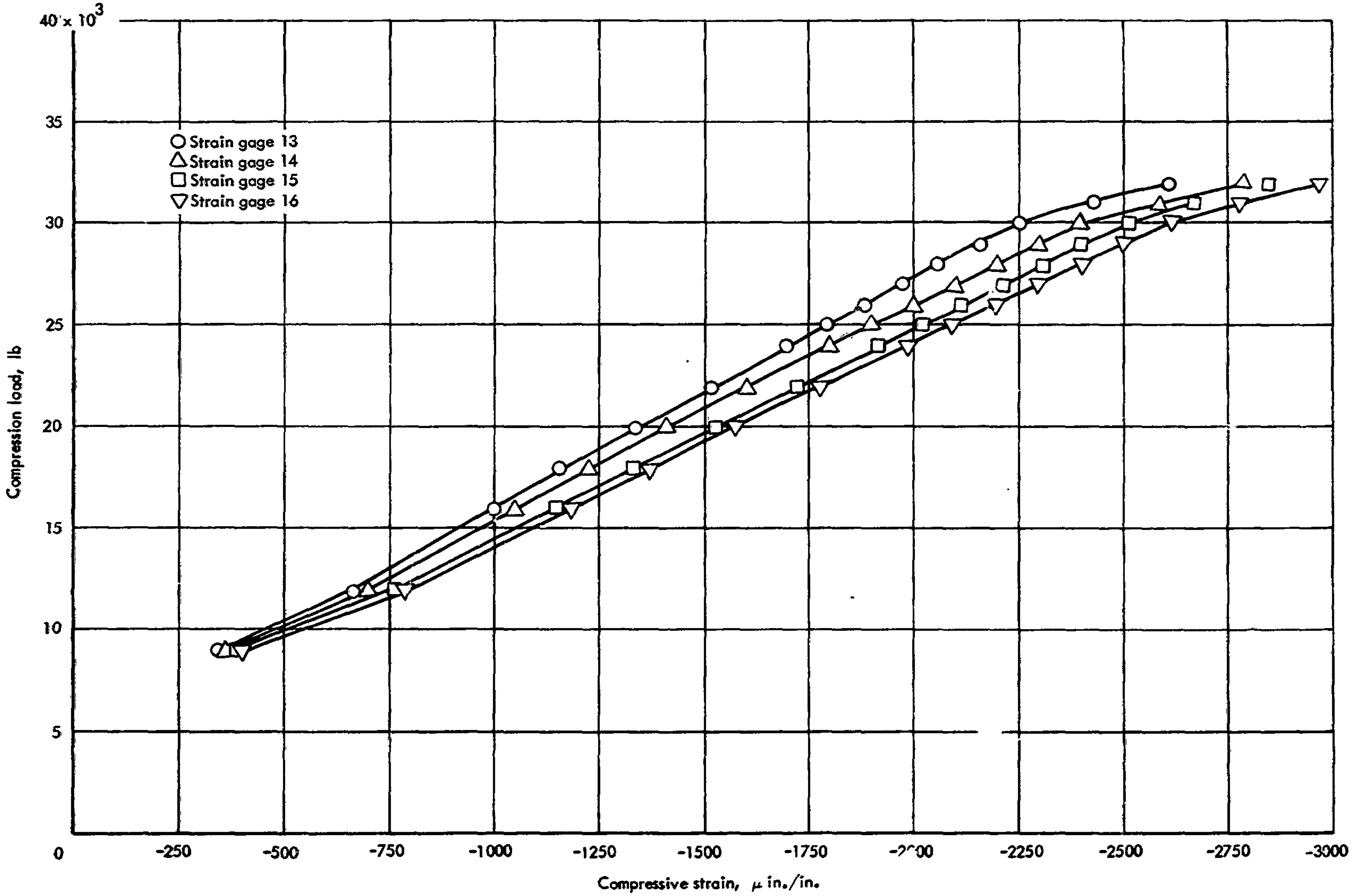

Figure 27-68 (Continued)

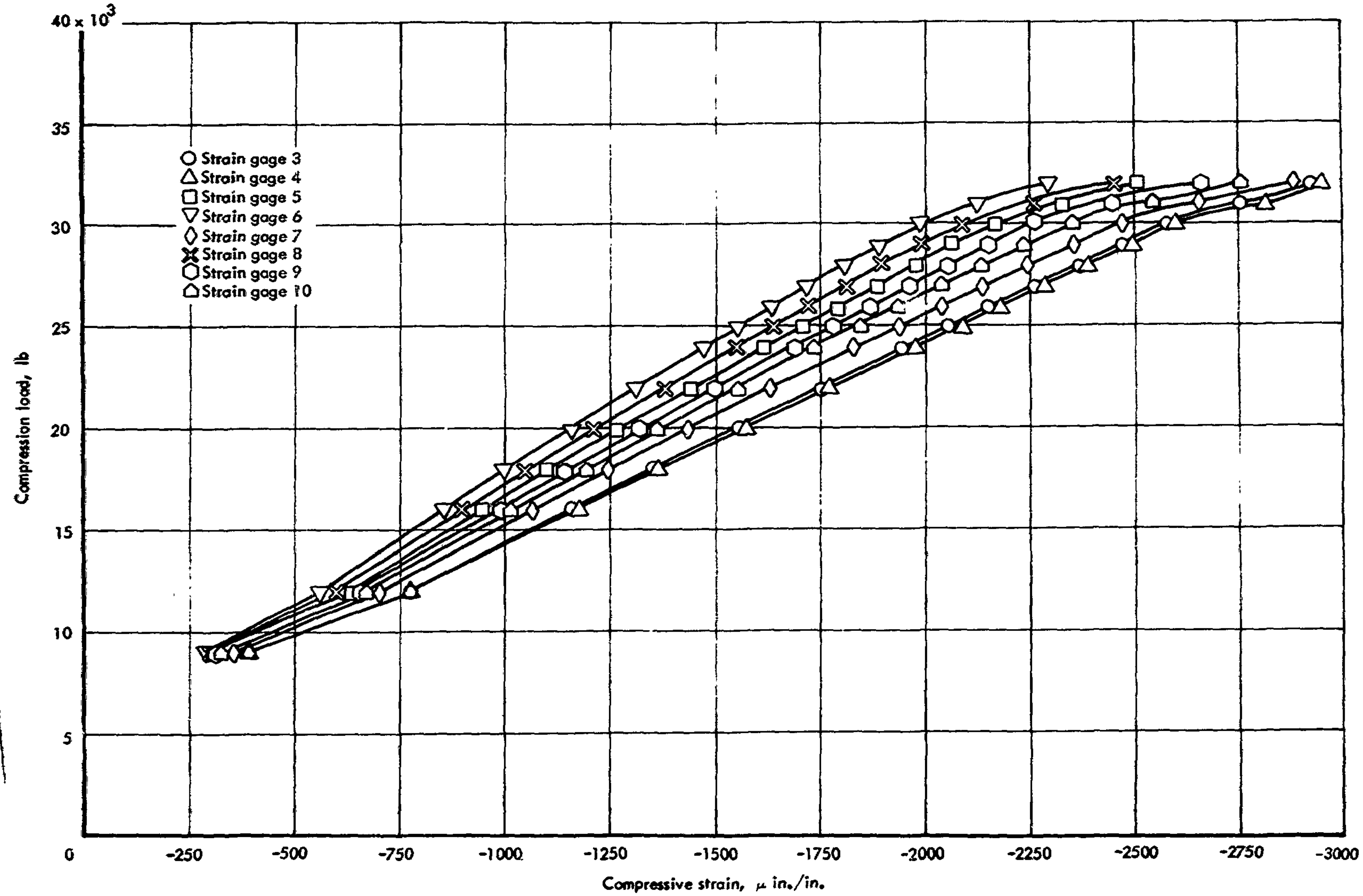

Figure 27-68 (Concluded)

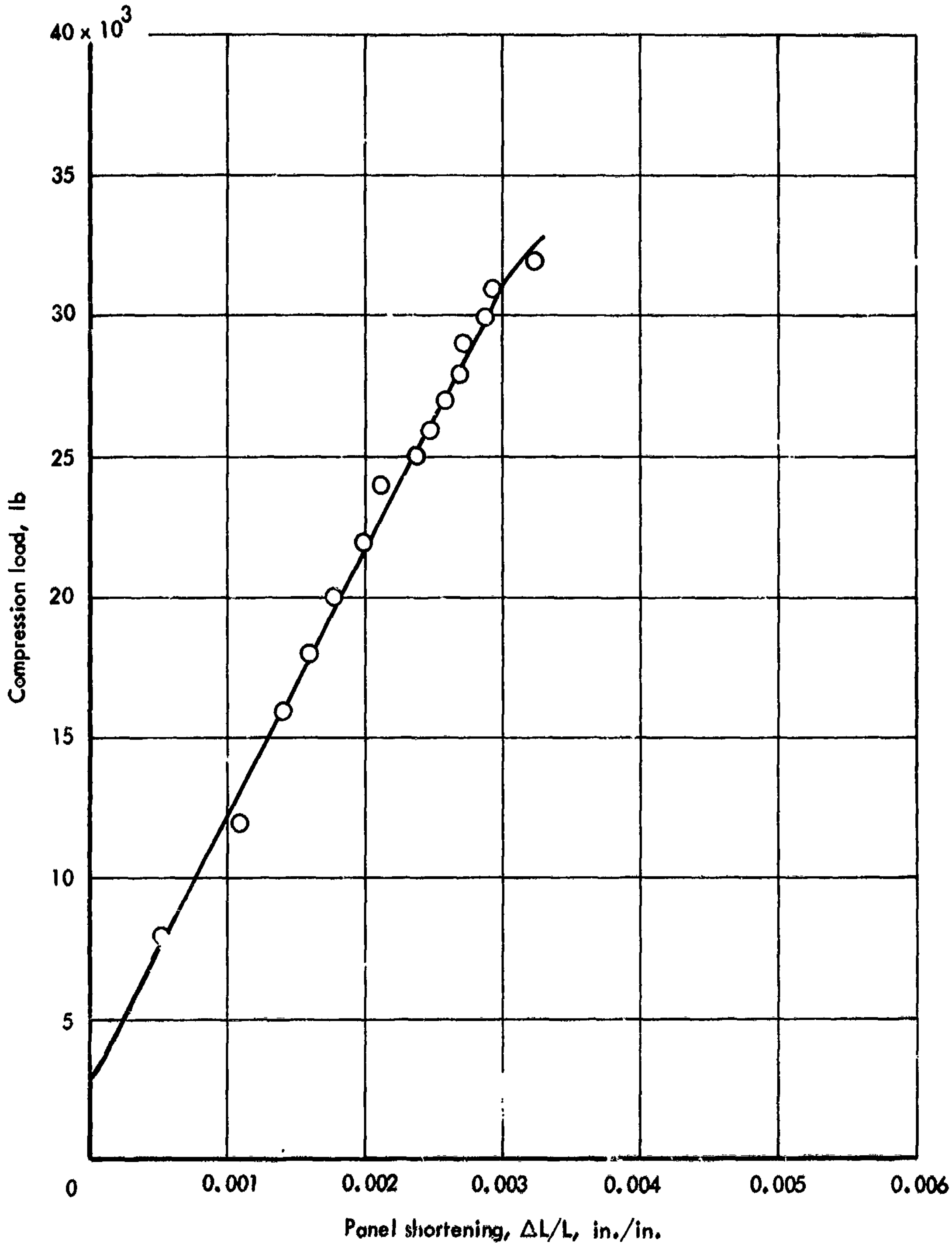

Figure 27-69 Panel shortening curve $\Delta L/L$ for beaded crippling panel, room temperature

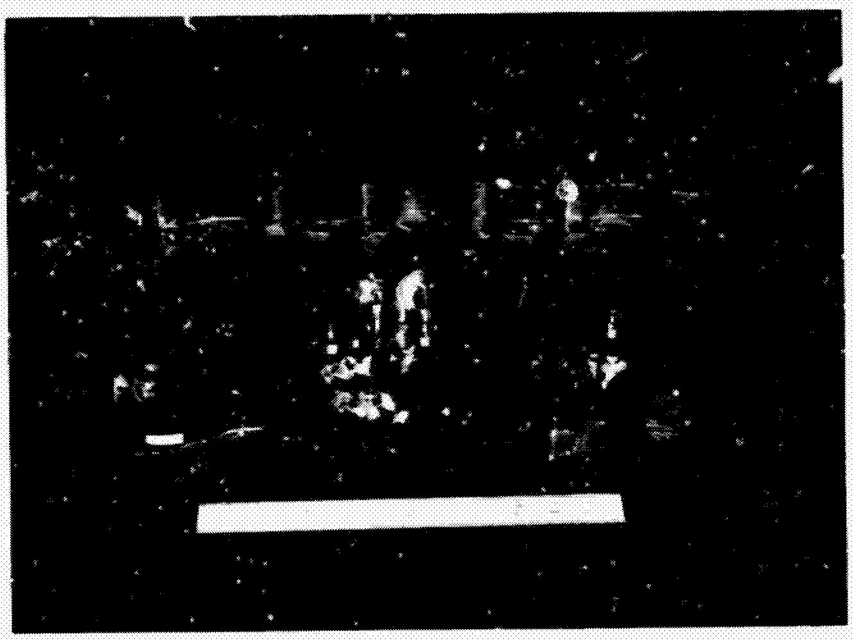

Front

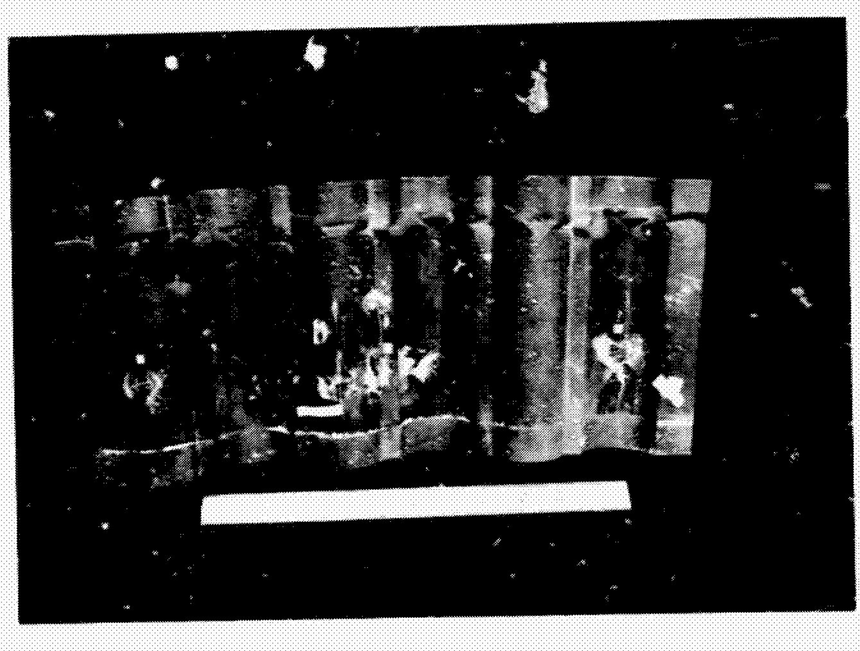

Back

Figure 27-70 Beaded crippling panel after failure. Room temperature test

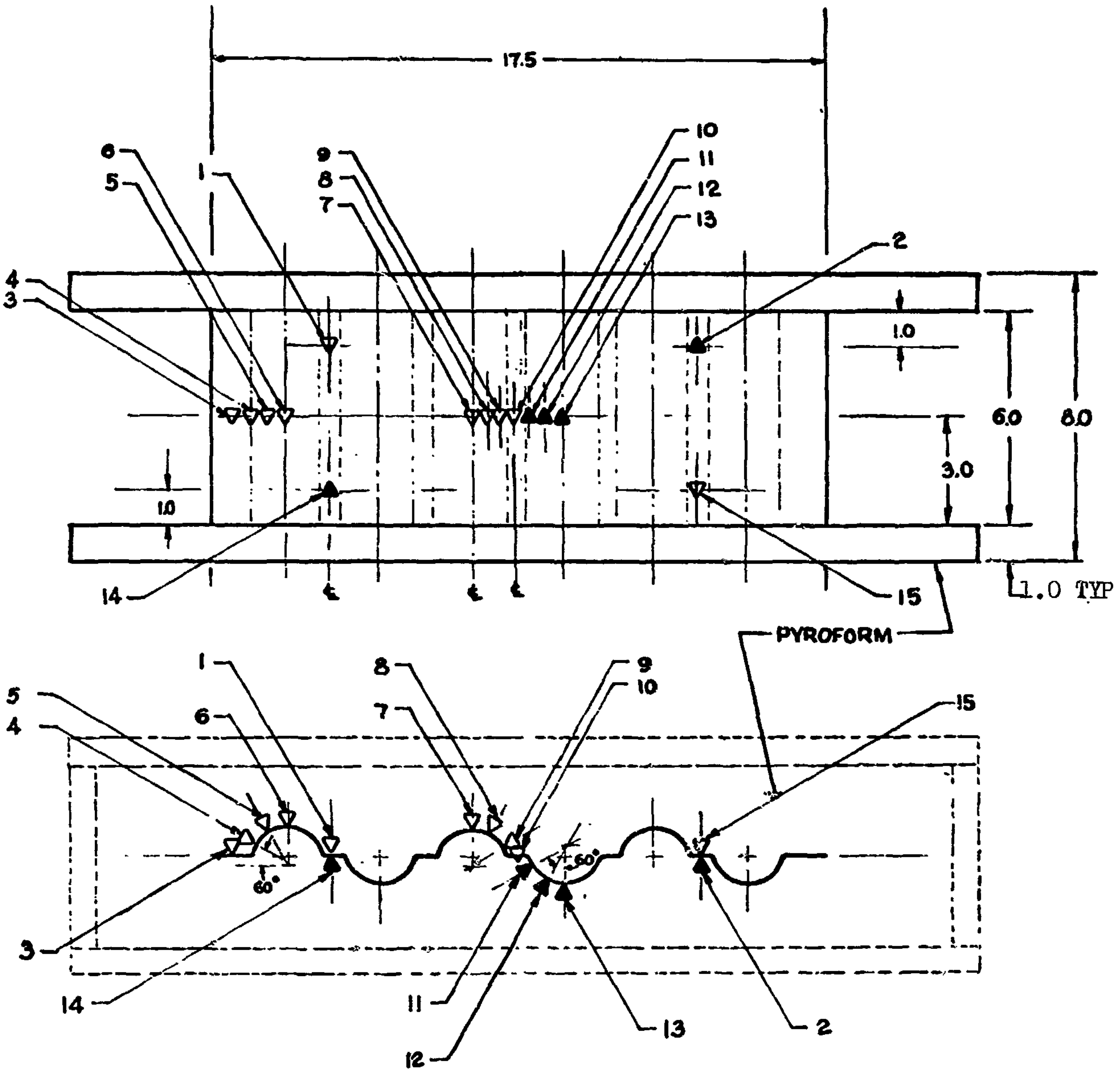

Figure 27-71 Thermocouple locations for the beaded crippling panel

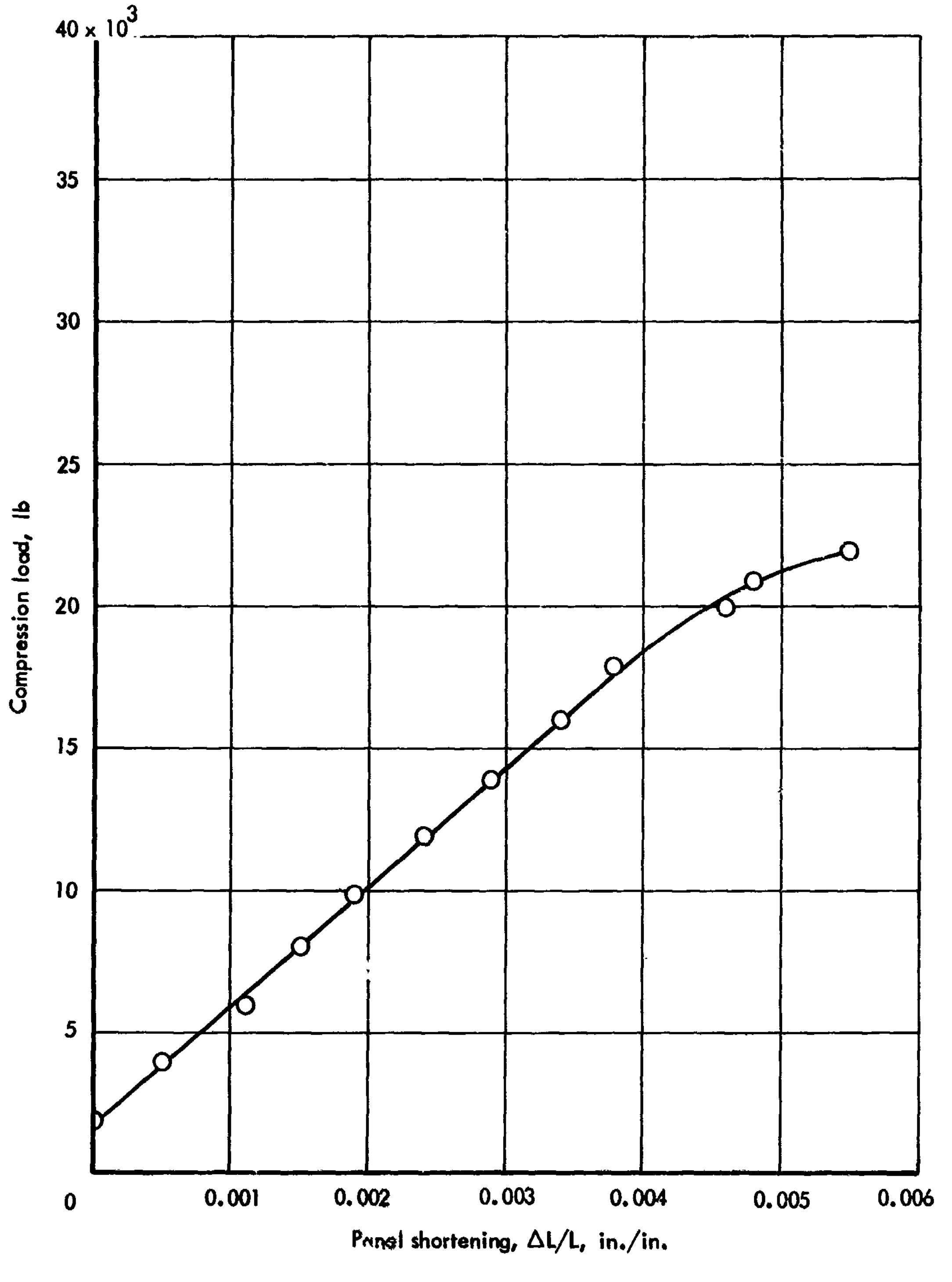

Figure 27-72 Panel shortening curve $\Delta L/L$ for beaded crippling panel, 1400°F

Front

Back

Figure 27-73 Beaded crippling panel after failure, 1400°F test

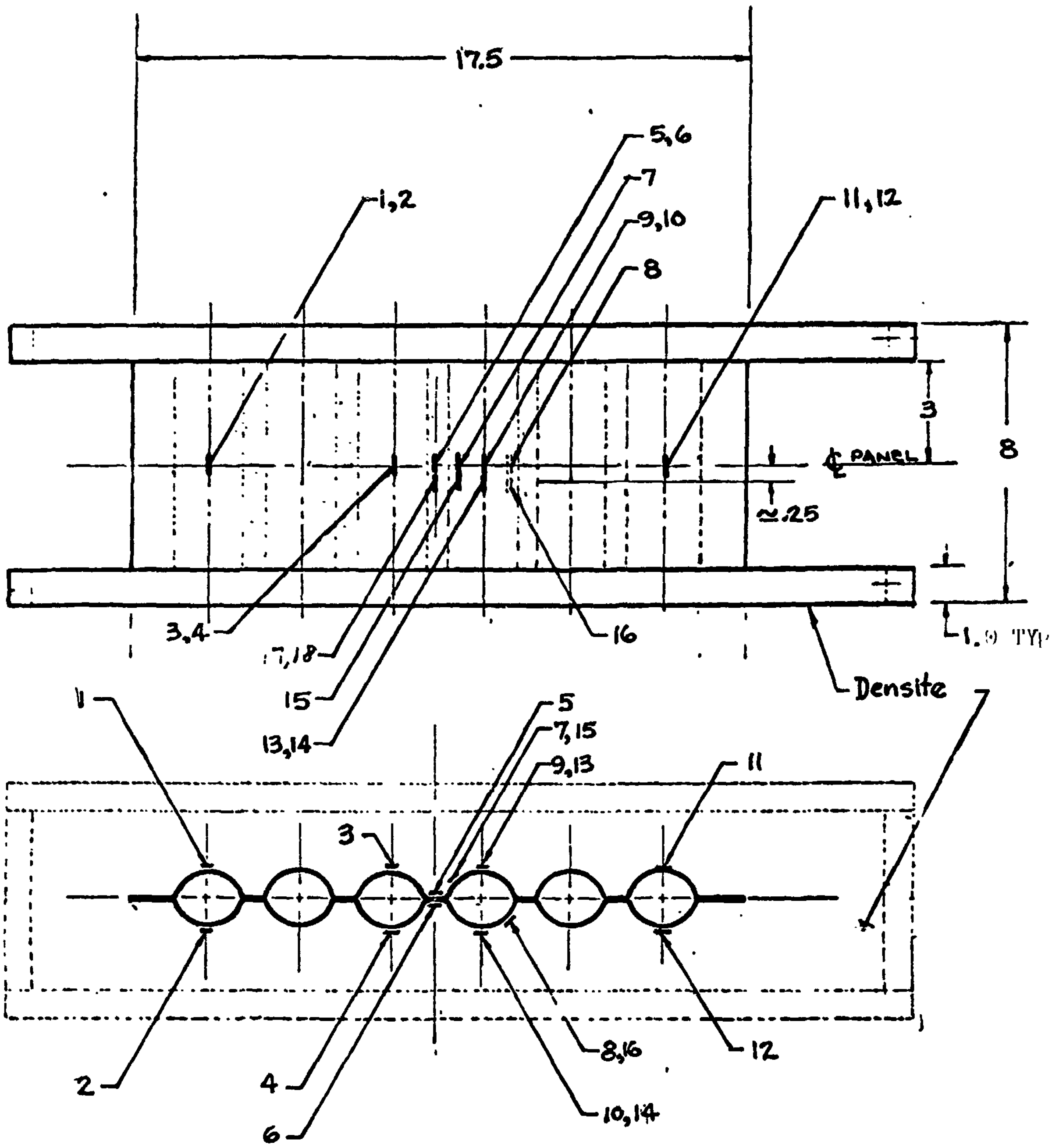

Note:

- Total no. of S.G. = 16.
- Gages 7 and 8 located 1/2 distance from ℄ tube to flange.
- Gages 13, 14, 15, 16 located directly below 9, 10, 7 and 8.

Figure 27-74 Strain gage locations for tubular crippling panel

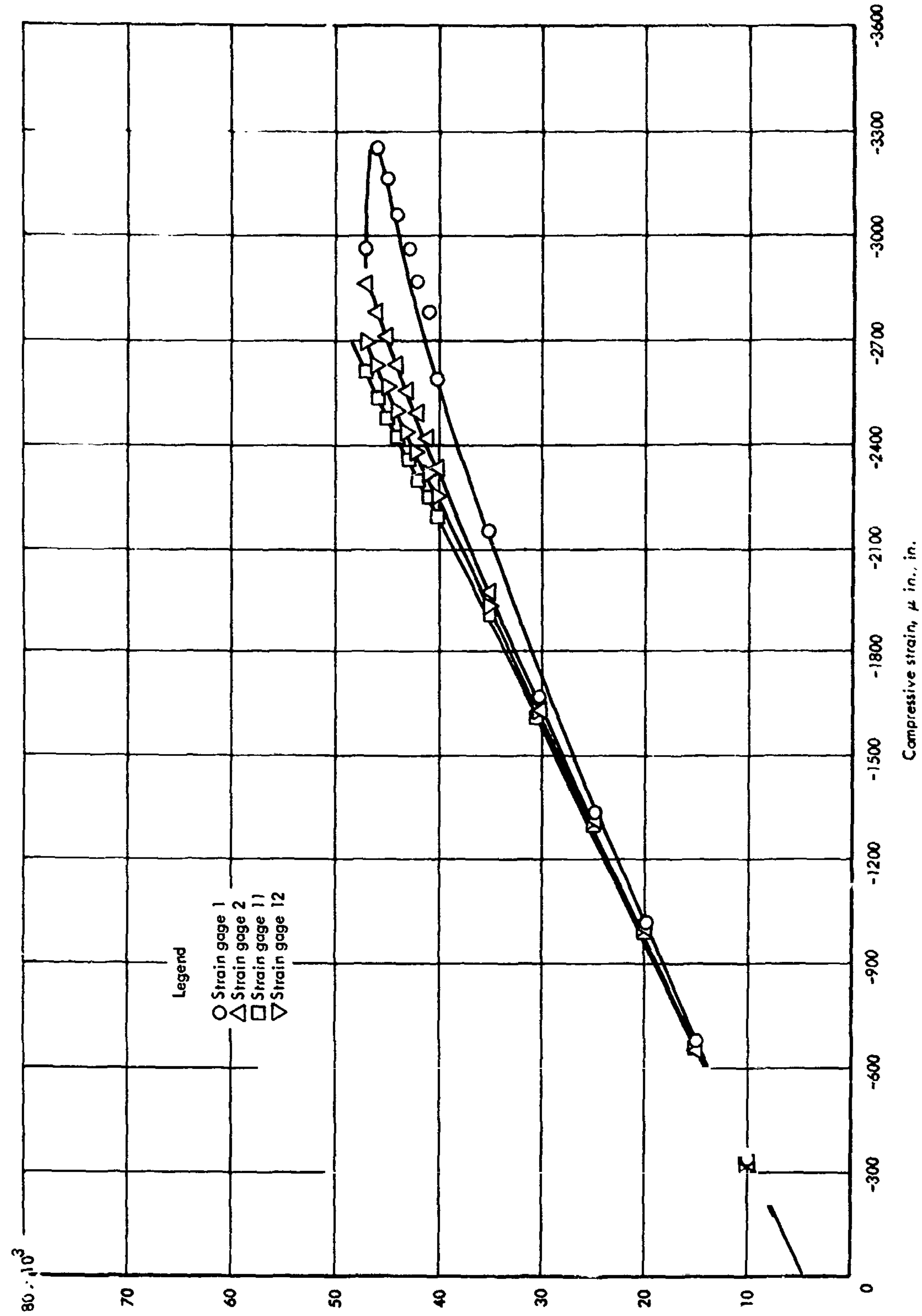

Figure 27-75 Axial strains for tubular crippling panel, room temperature

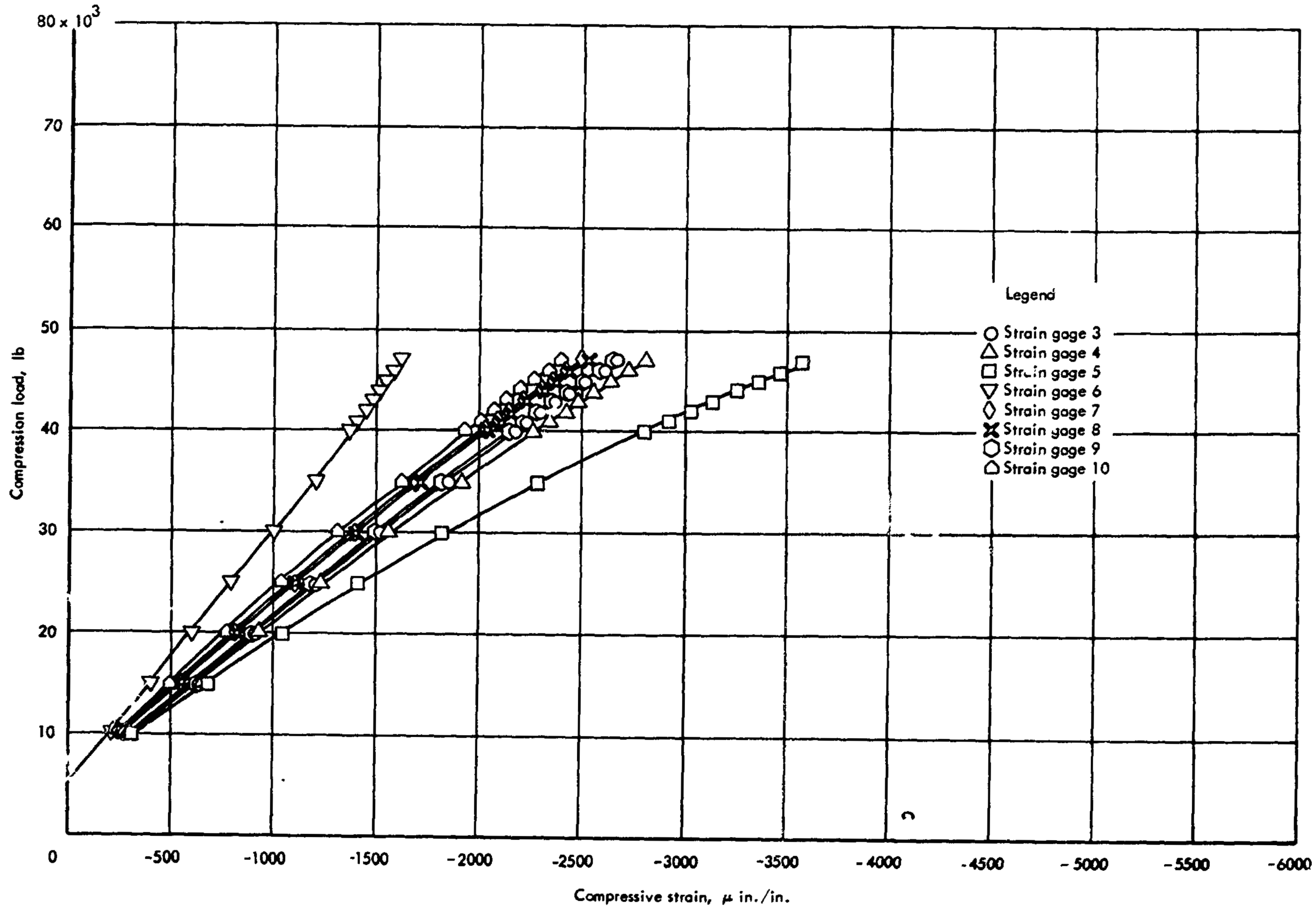

Figure 27-75 (Continued)

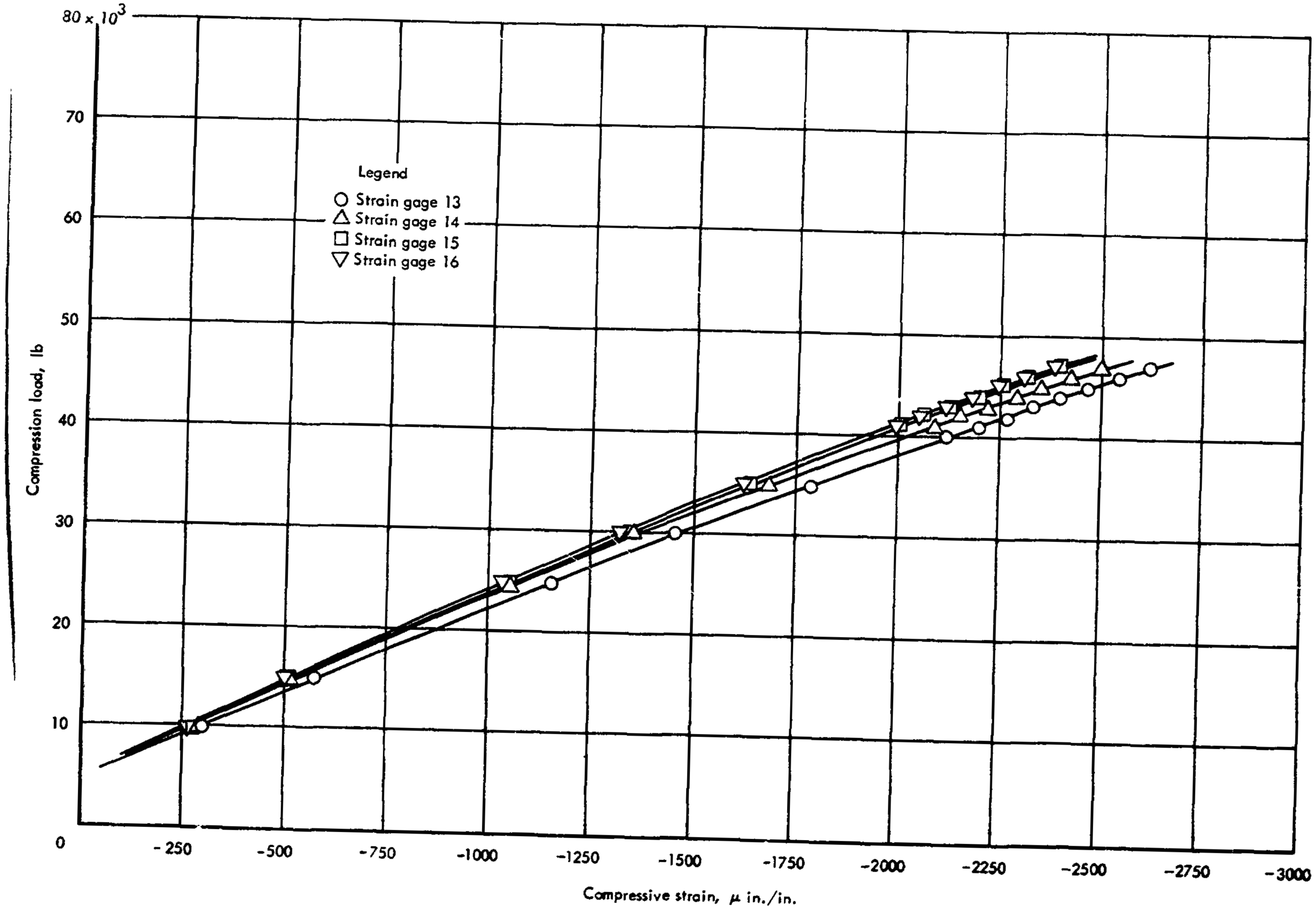

Figure 27-75 (Continued)

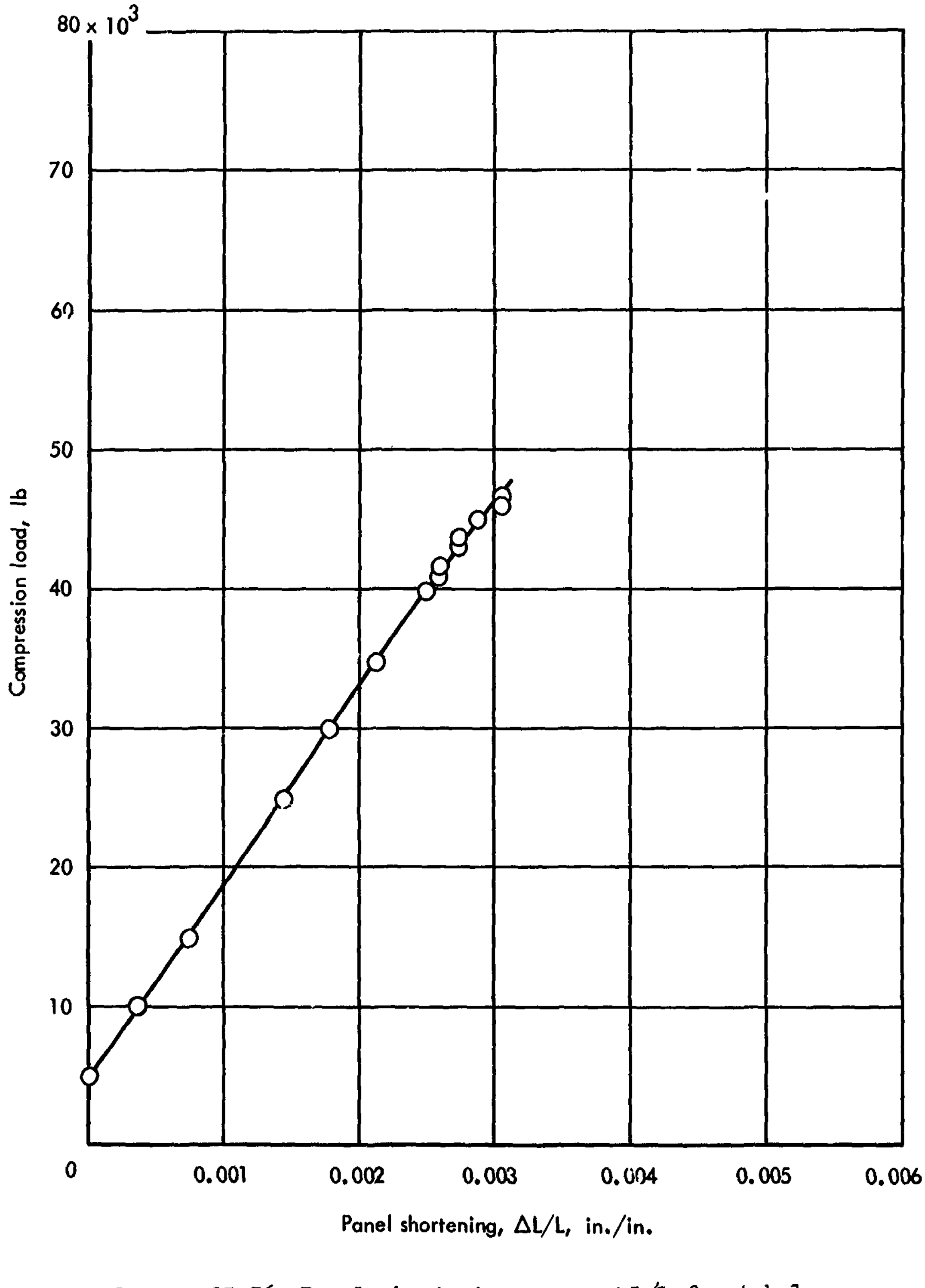

Figure 27-76 Panel shortening curve $\Delta L/L$ for tubular crippling panel, room temperature

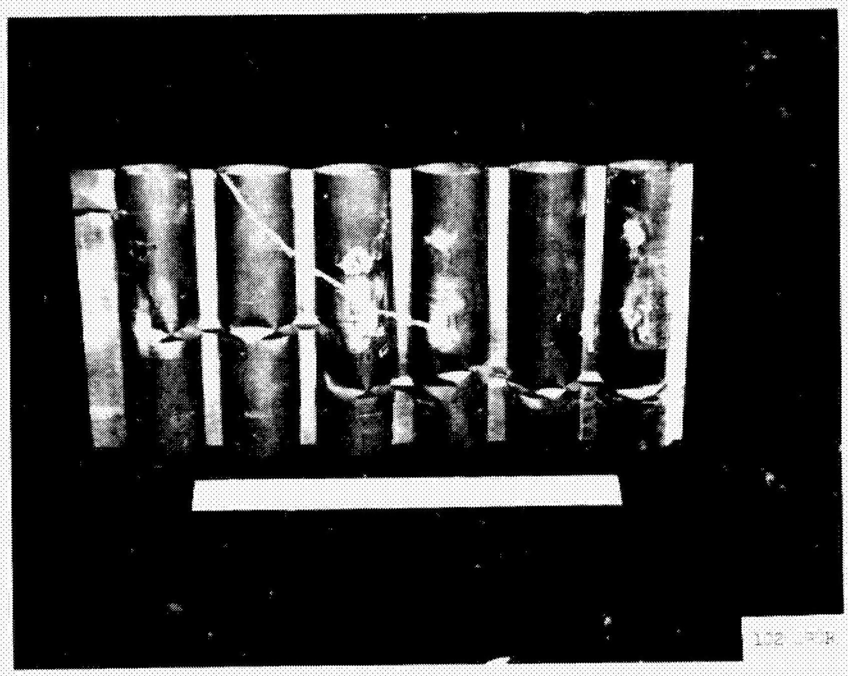

Front

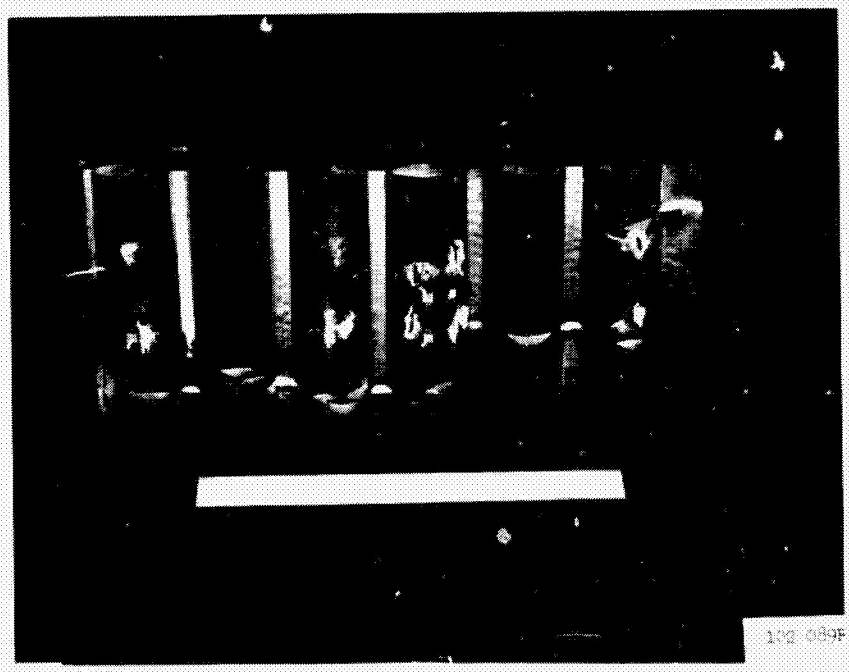

Back

Figure 27-77 Tubular crippling panel after failure, room temperature test

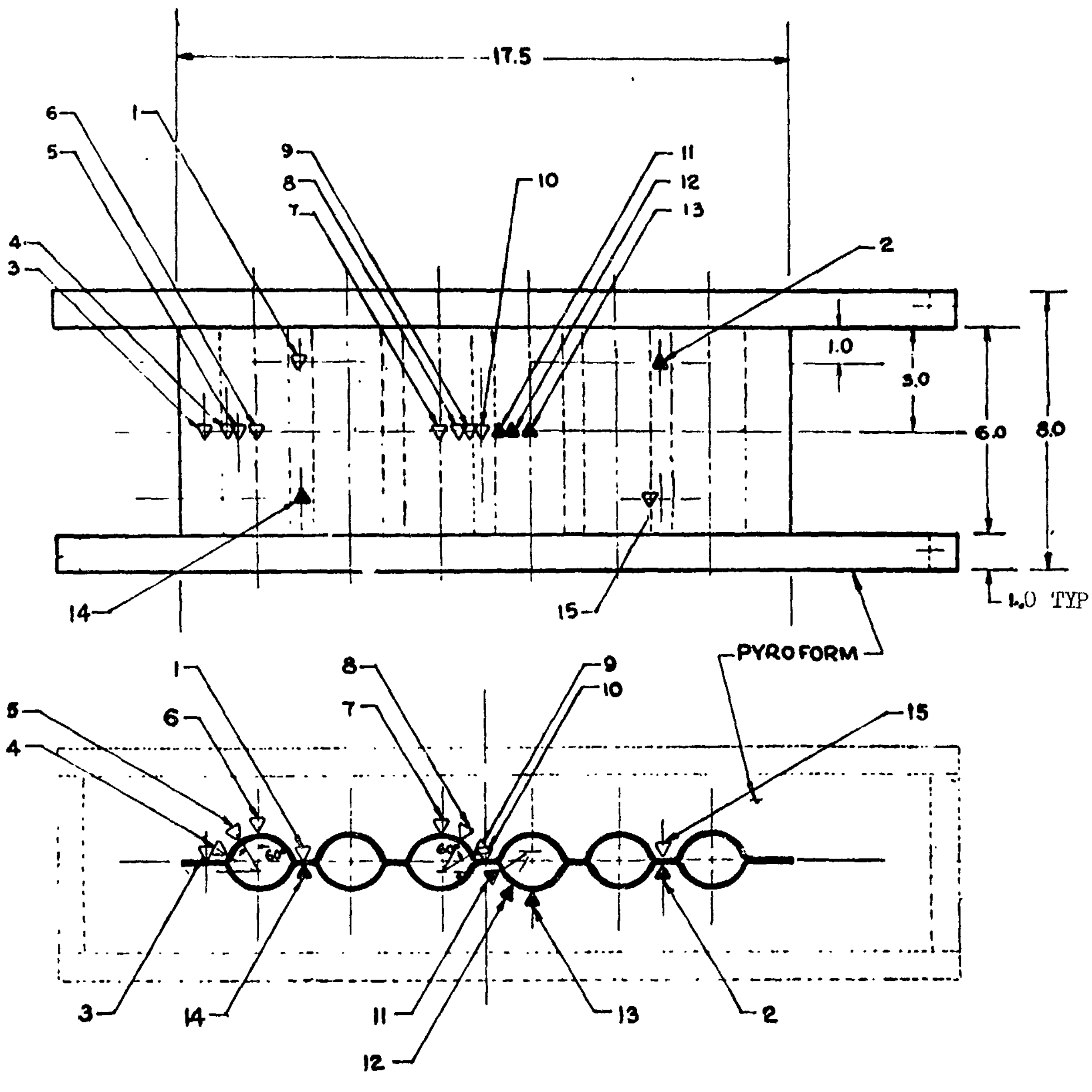

Figure 27-78 Thermocoupling locations for the tubular crippling panel

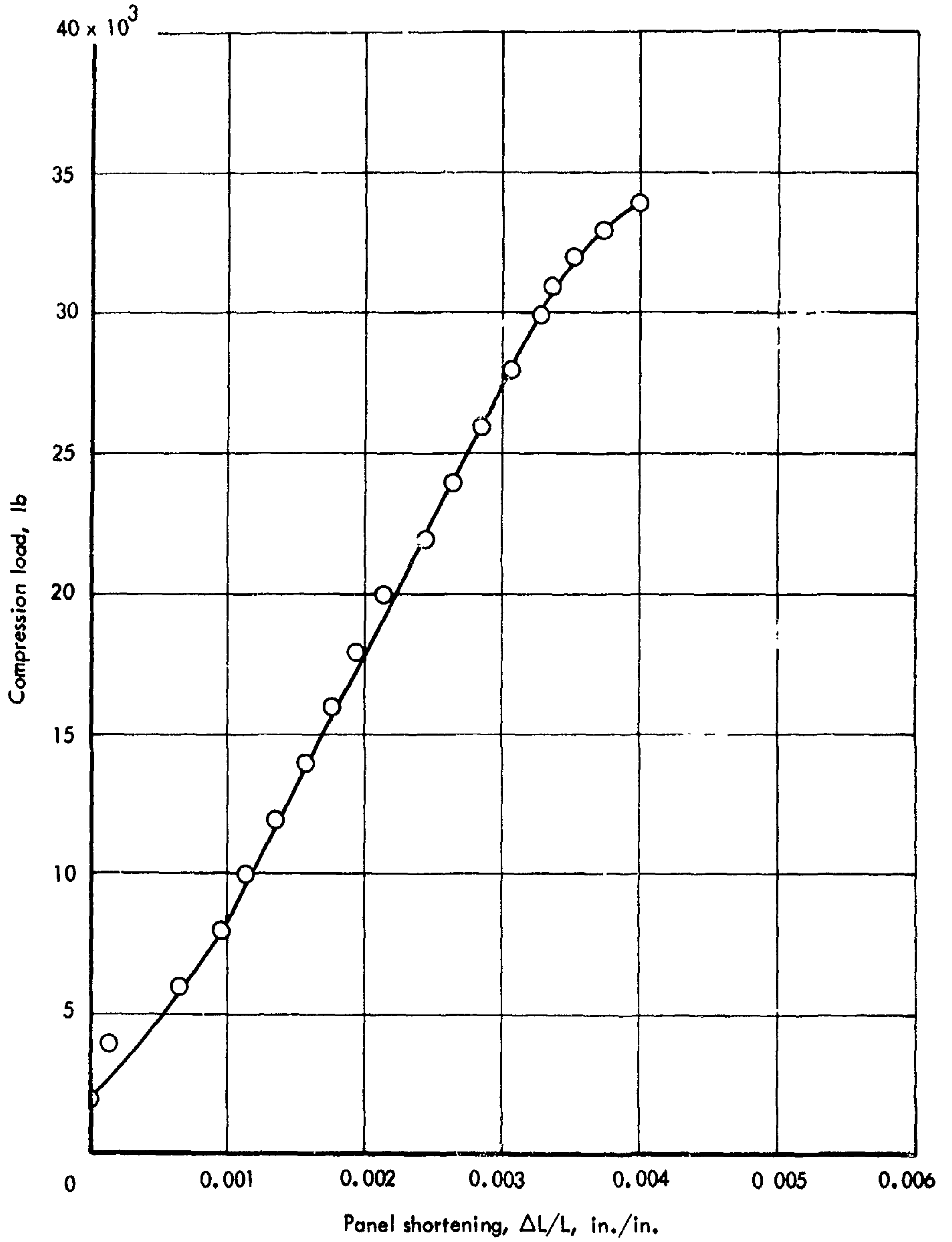

Figure 27-79 Panel shortening curve $\Delta L/L$ for tubular crippling panel, 1400°F

Front

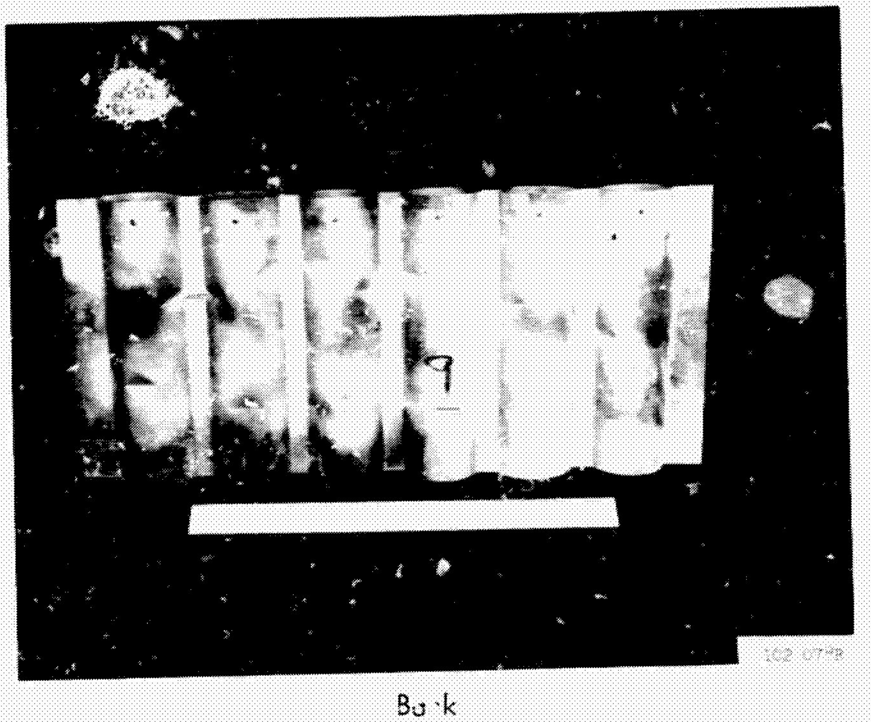

Back

Figure 27-80 Tubular crippling panel after failure, 1400°F test

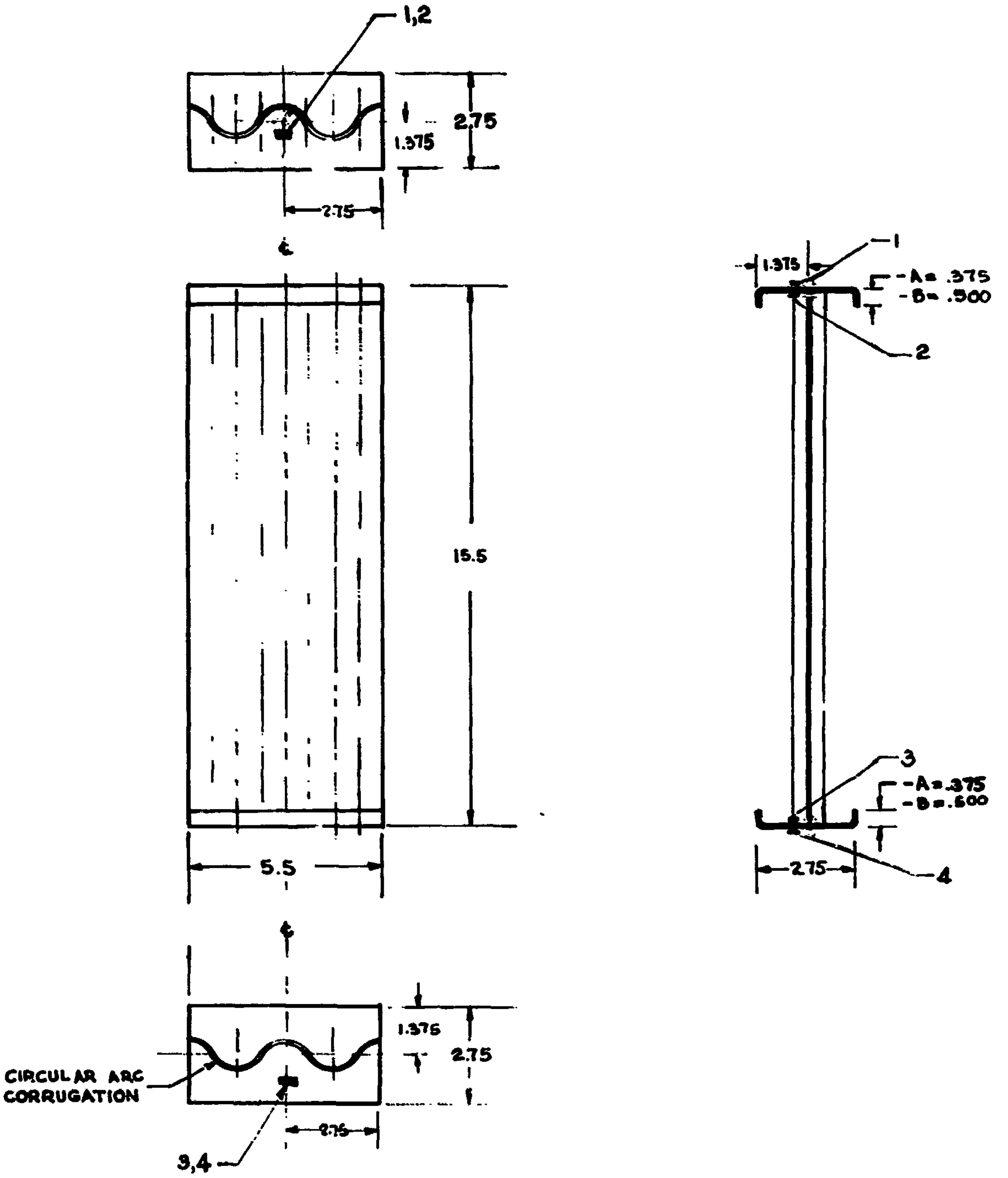

Figure 27-81 Strain gage locations for the spar cap crippling specimens

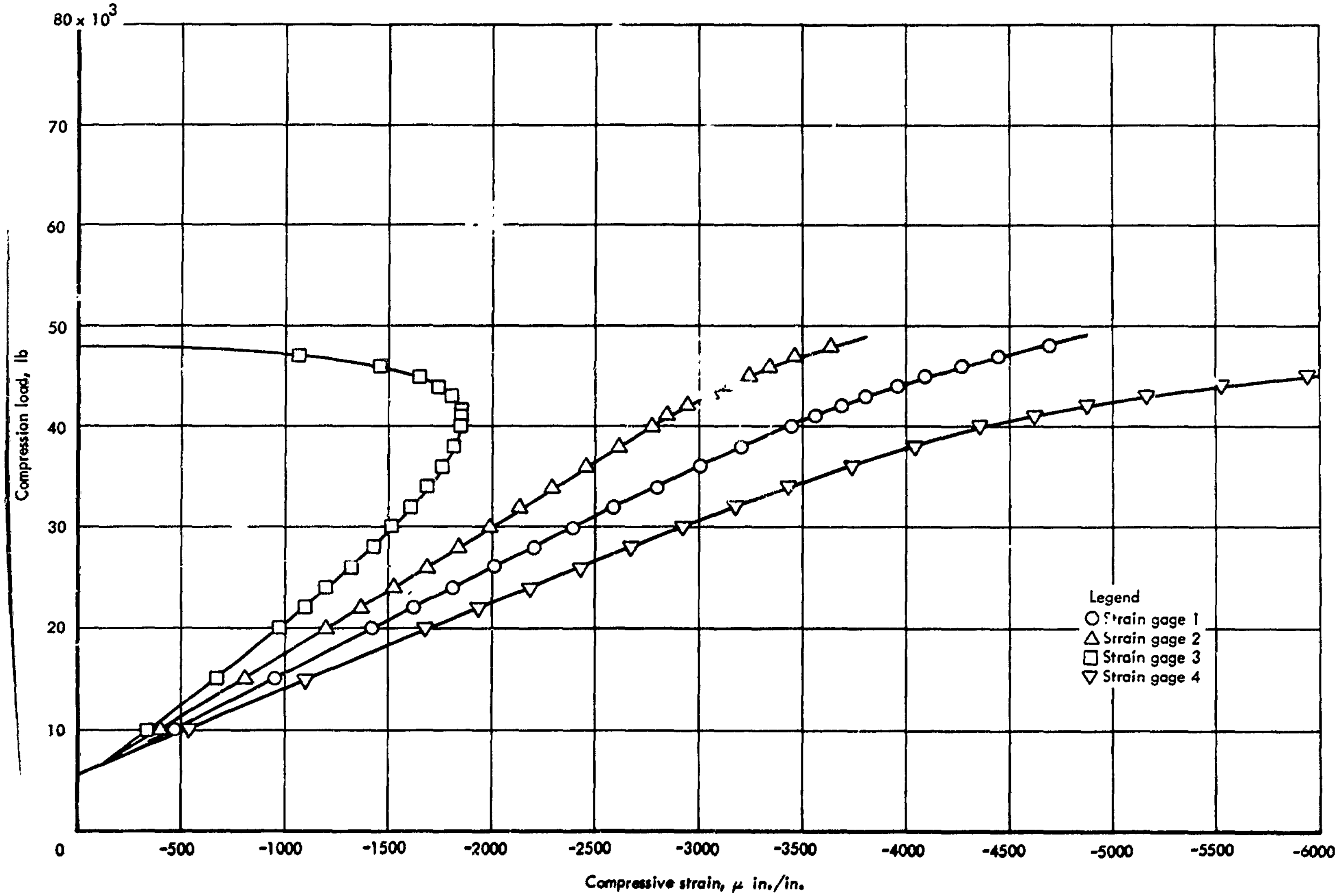

Figure 27-82 Axial strains for spar cap crippling specimen - 3/8 inch flange, room temperature

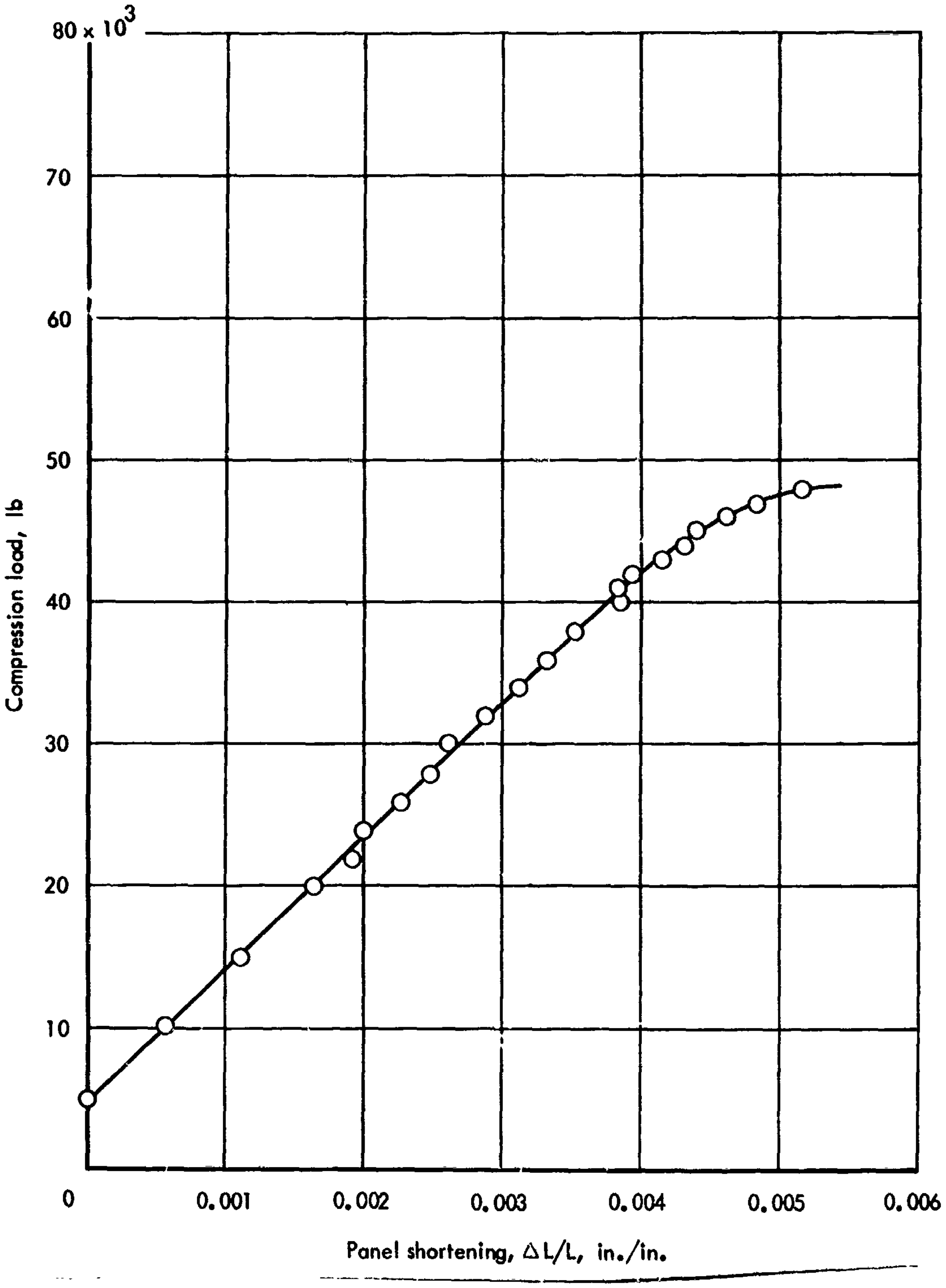

Figure 27-83 Spar cap shortening curve $\Delta L/L$ for 3/8 inch flange specimen, room temperature

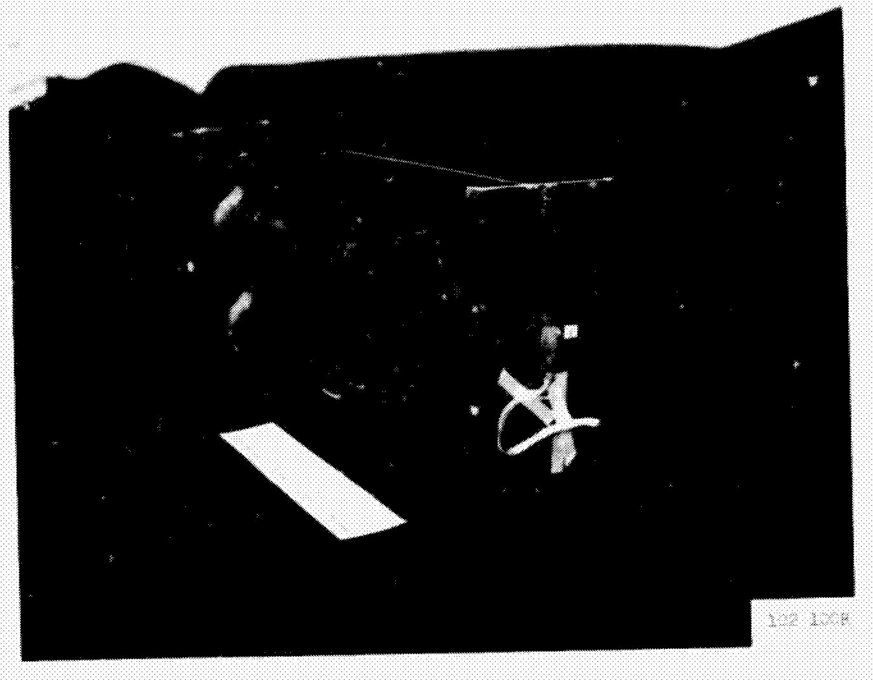

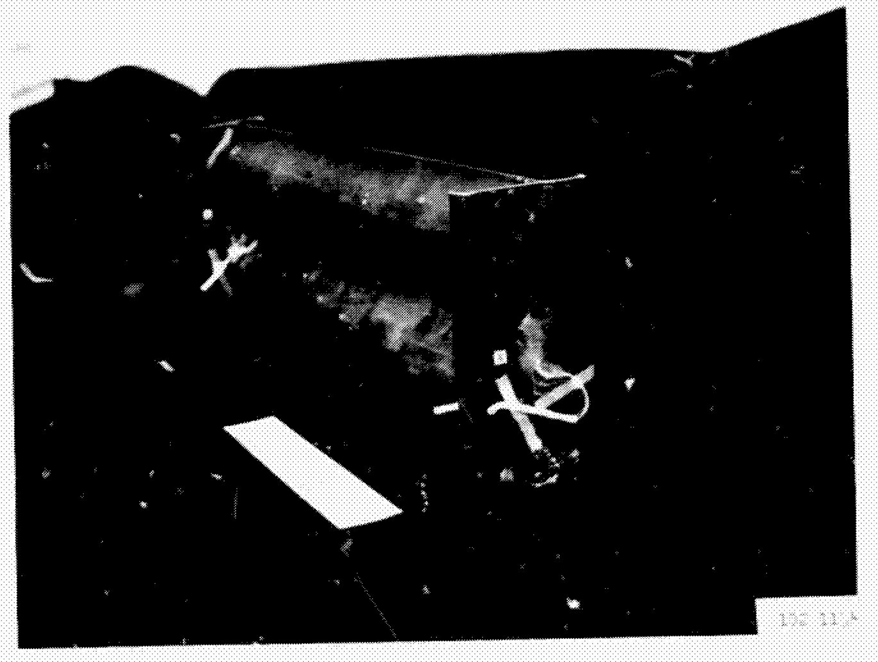

Figure 27-84 Spar cap crippling specimen (3/8 inch flange) after failure, room temperature test

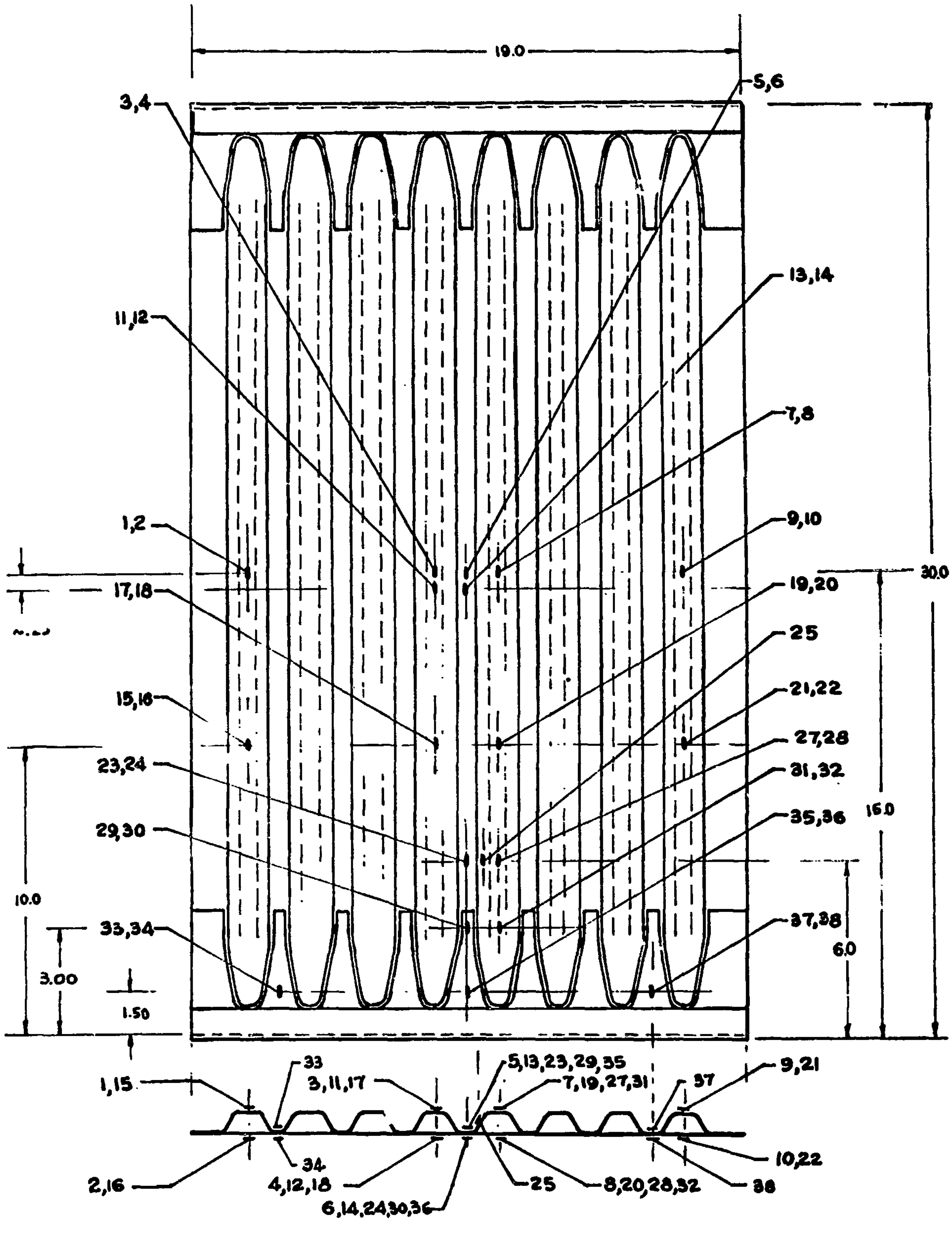

Figure 2,-85 Strain gage locations for corrugation - stiffened skin compression panel

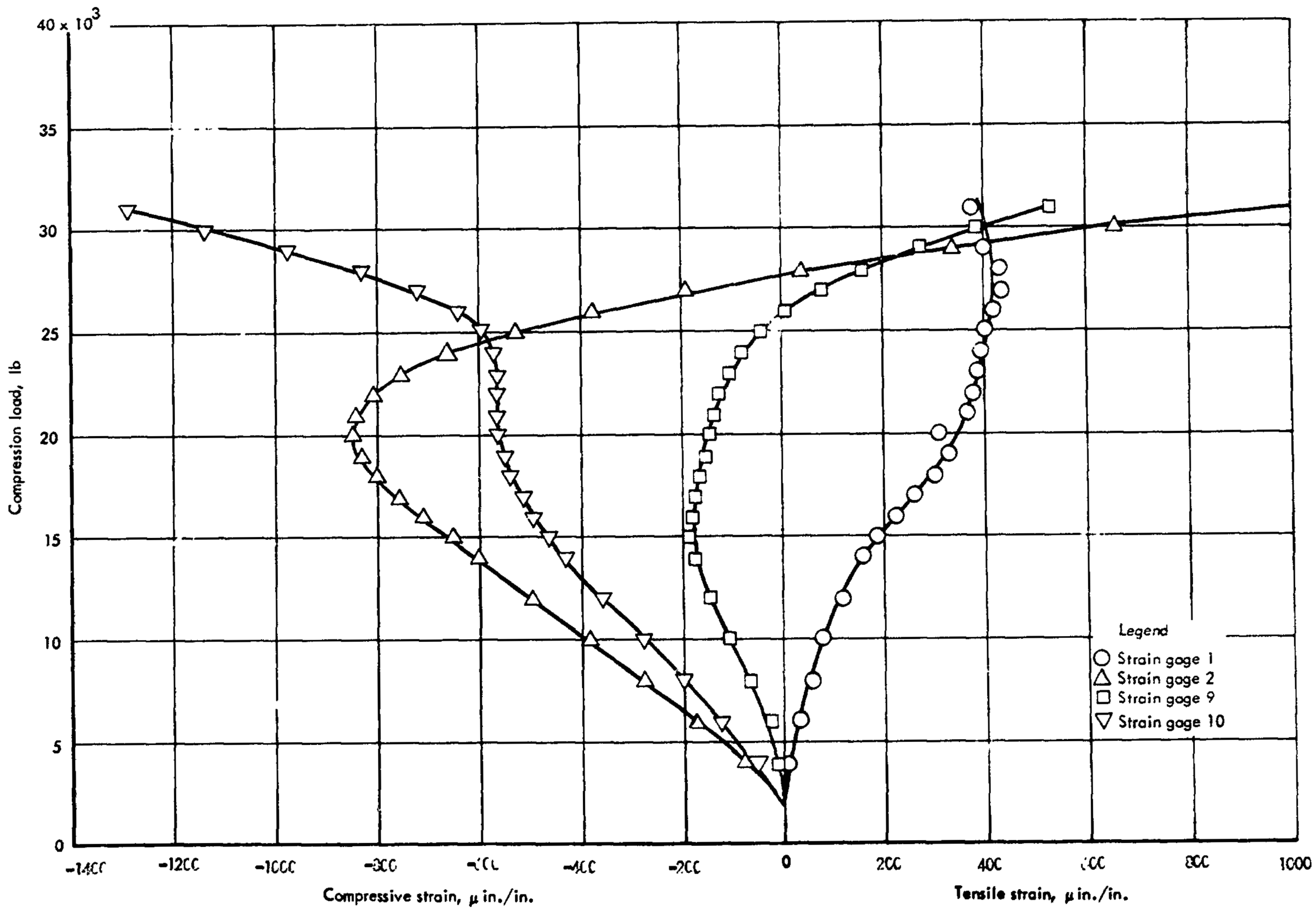

Figure 27-86 Axial strains for corrugation stiffened skin compression panel, room temperature

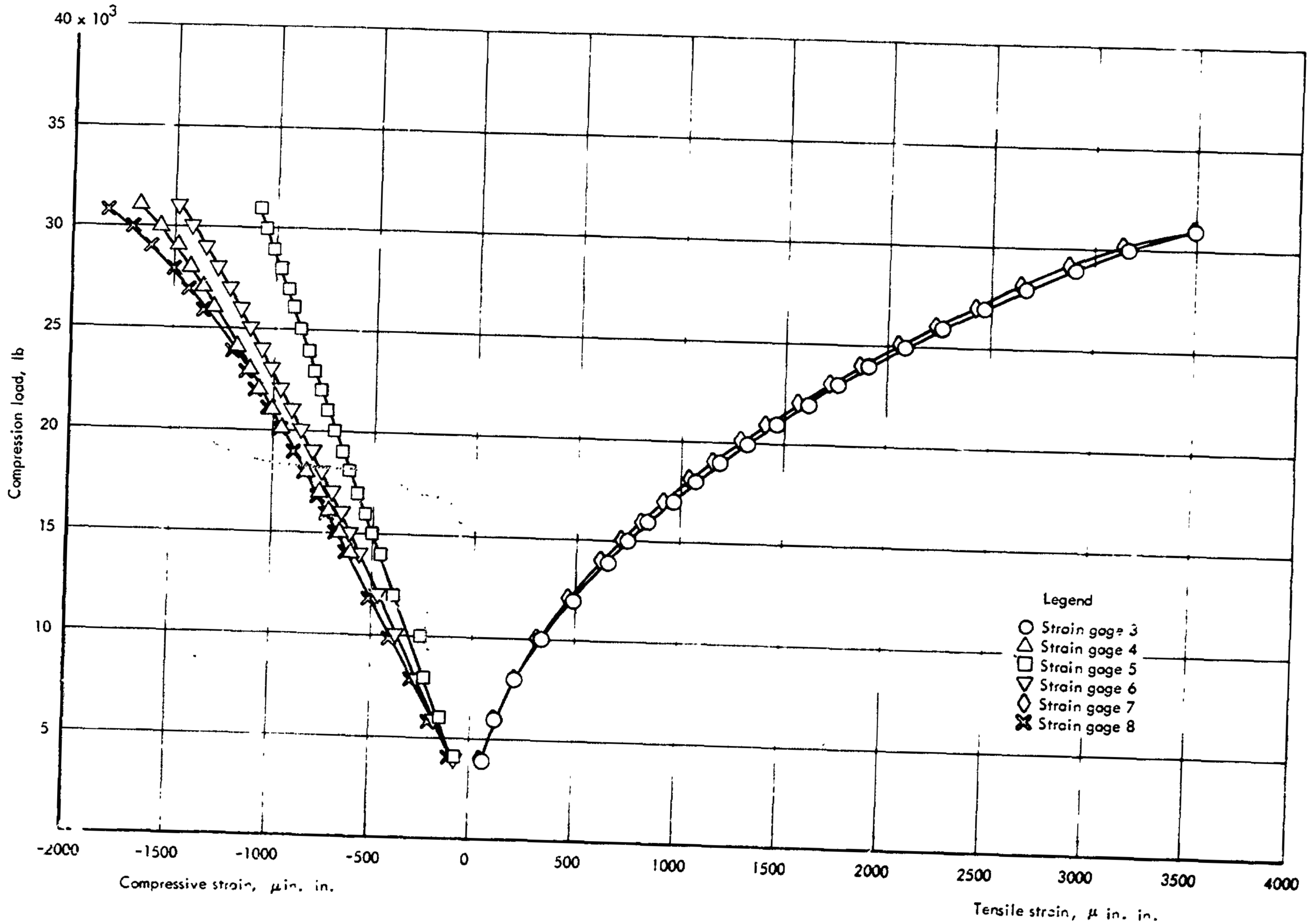

Figure 27-86 (continued)

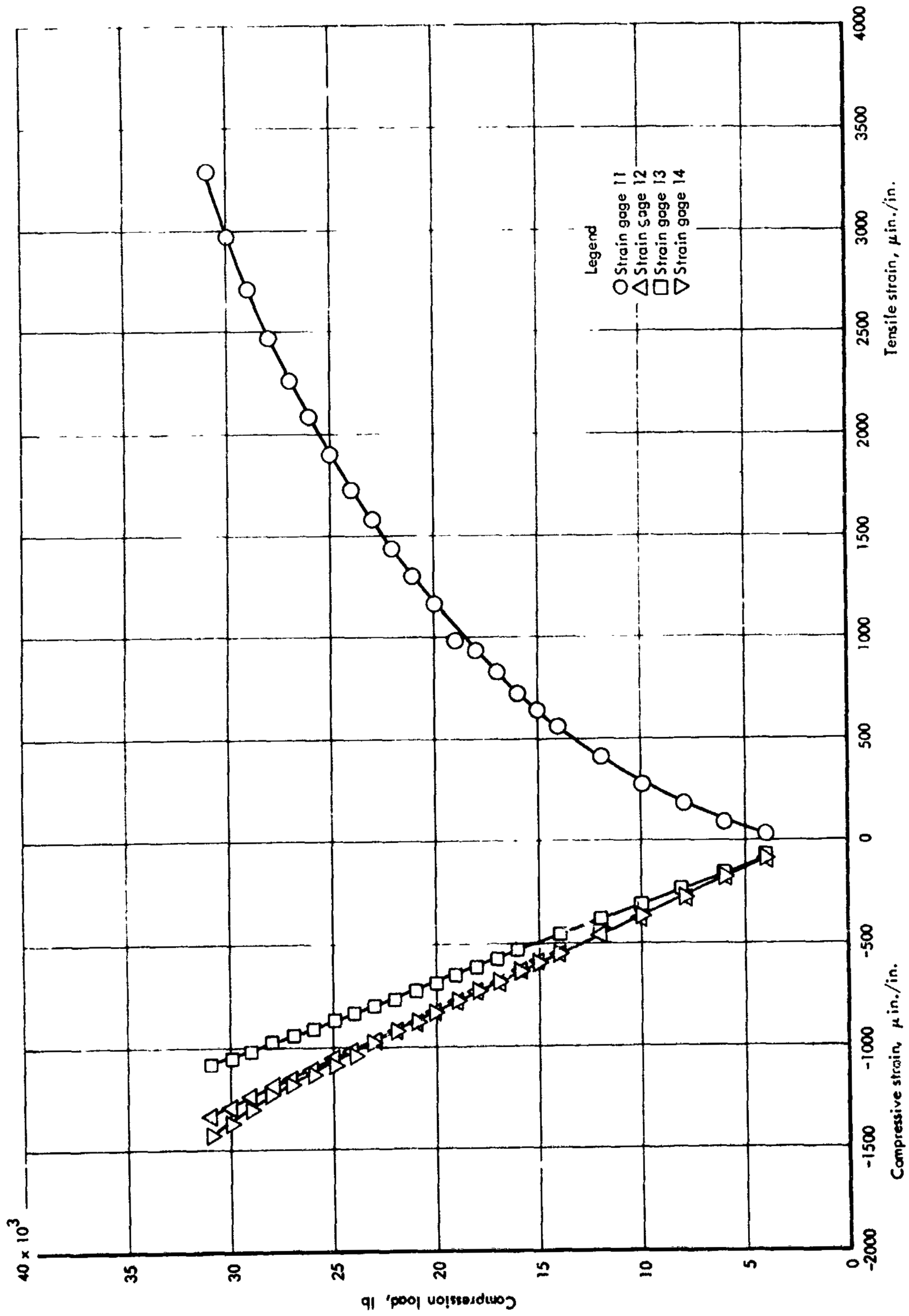

Figure 27-86 (continued)

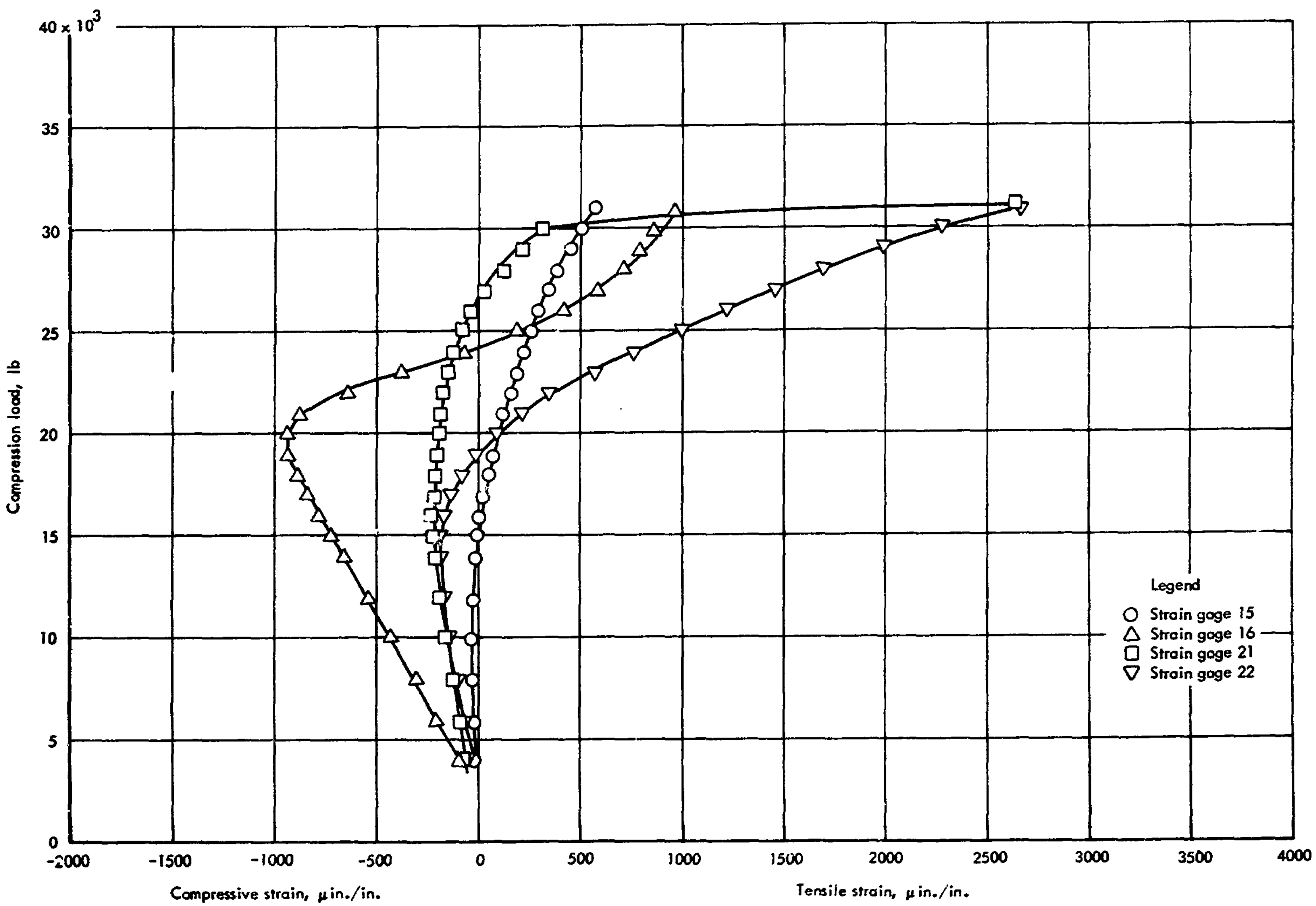

Figure 27-86 (continued)

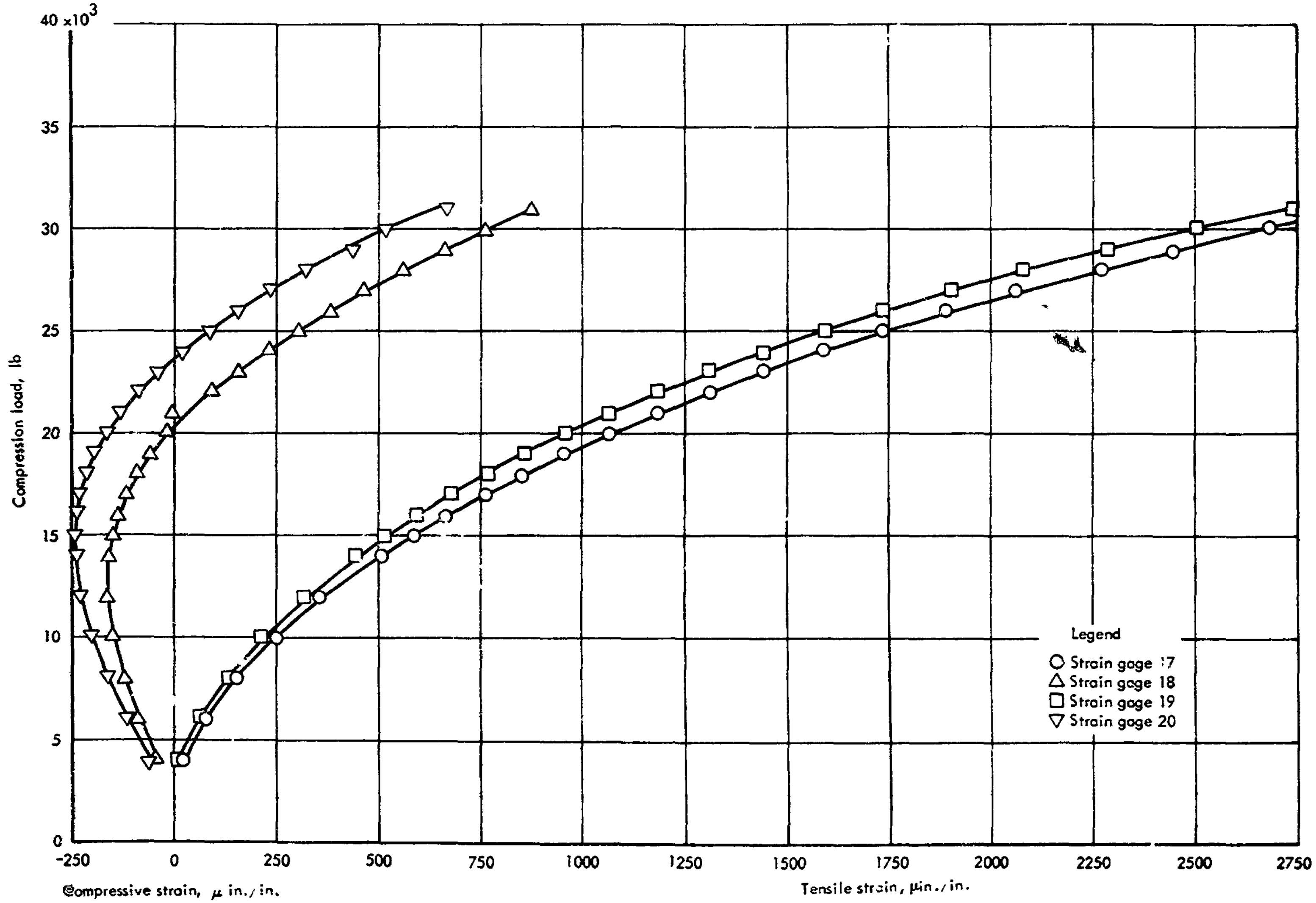

Figure 27-86 (continued)

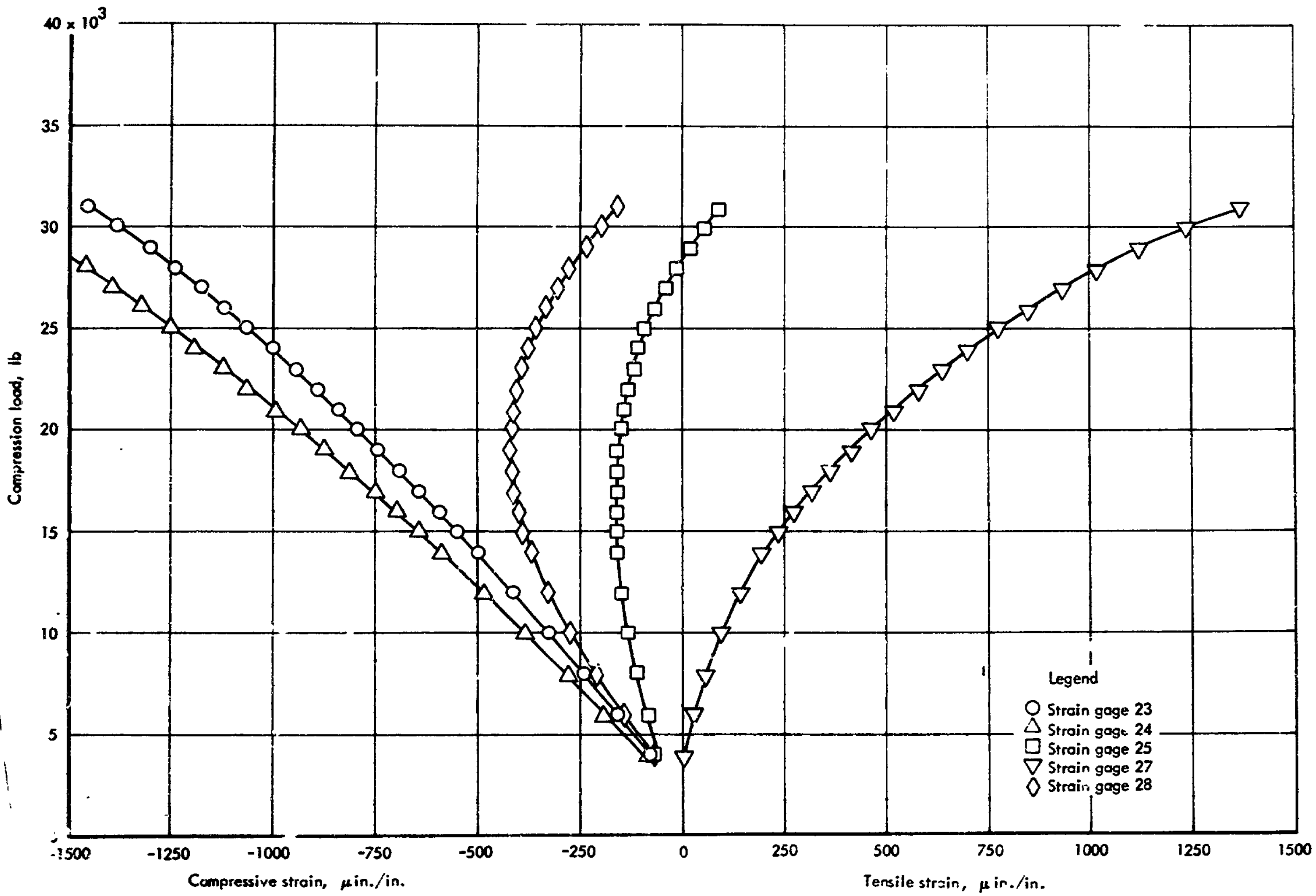

Figure 27-86 (continued)

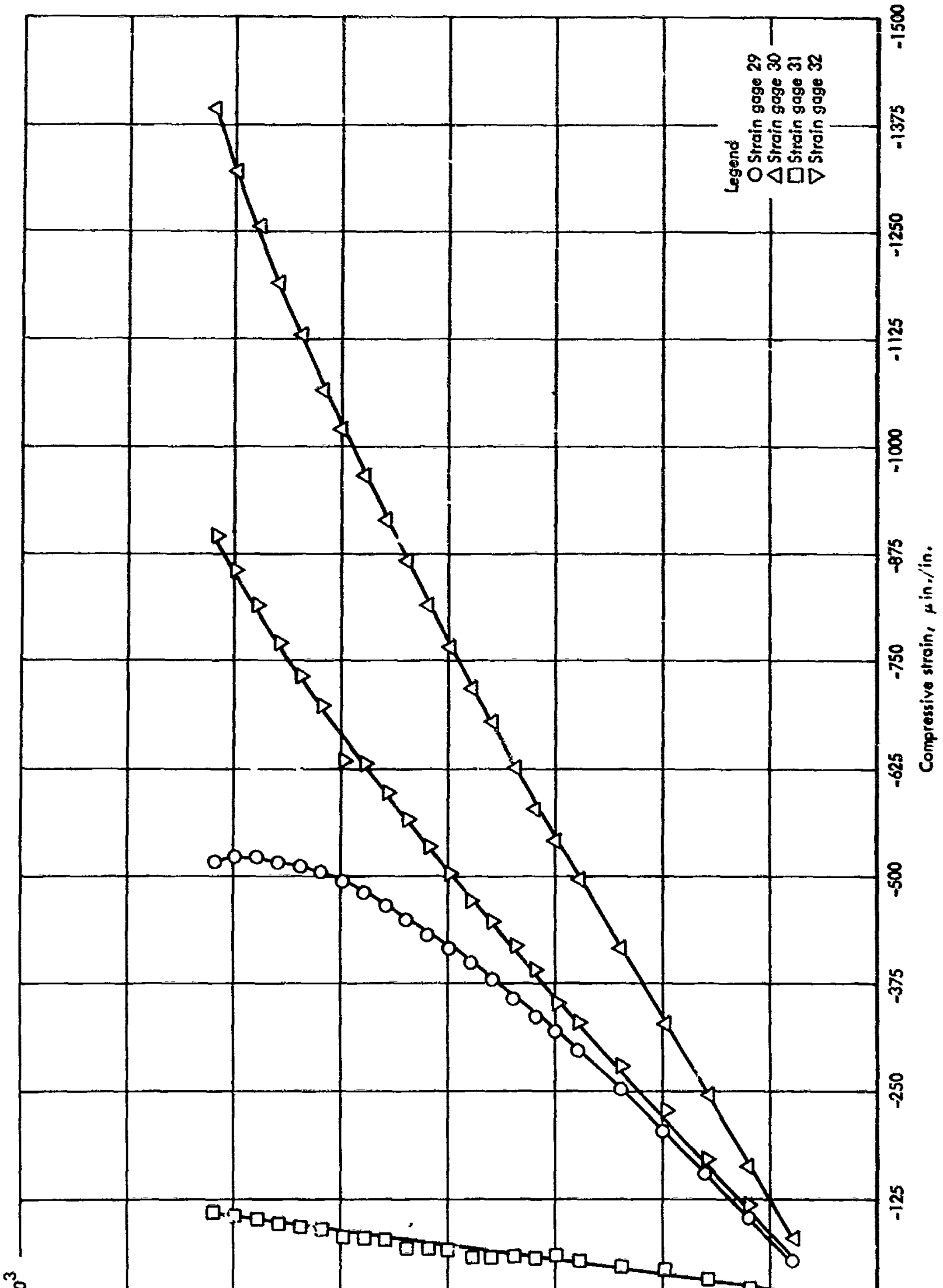

Figure 27-86 (continued)

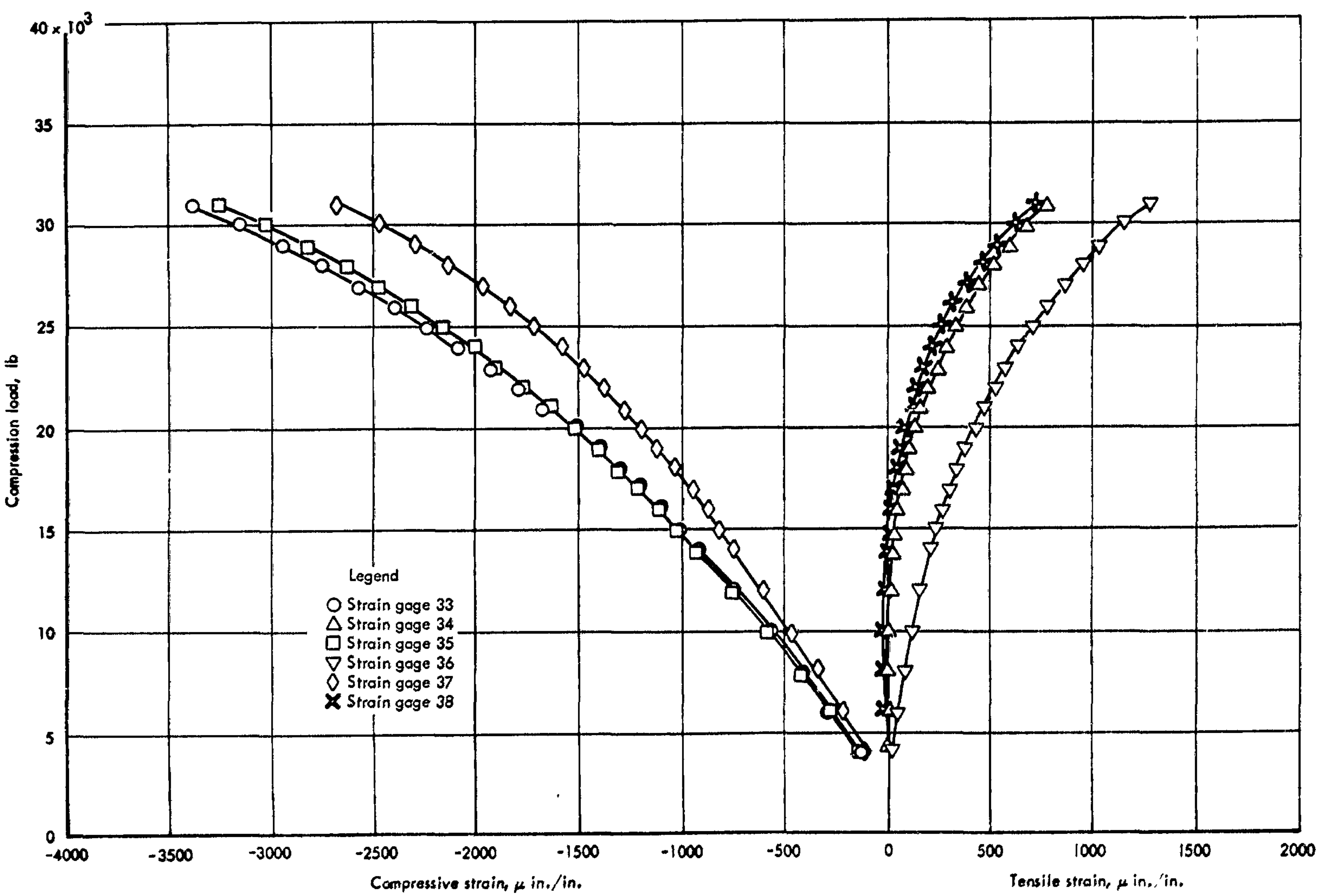

Figure 27-86 (continued)

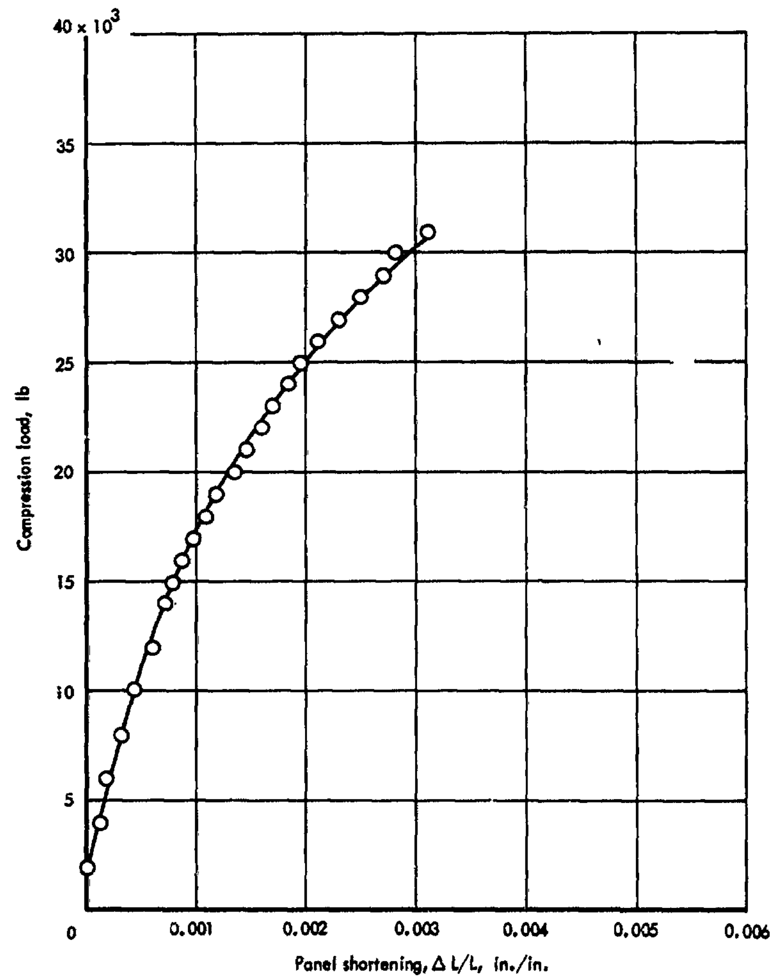

Figure 27-87 Panel shortening curve $\Delta L/L$ for corrugation-stiffened skin compression panel, room temperature

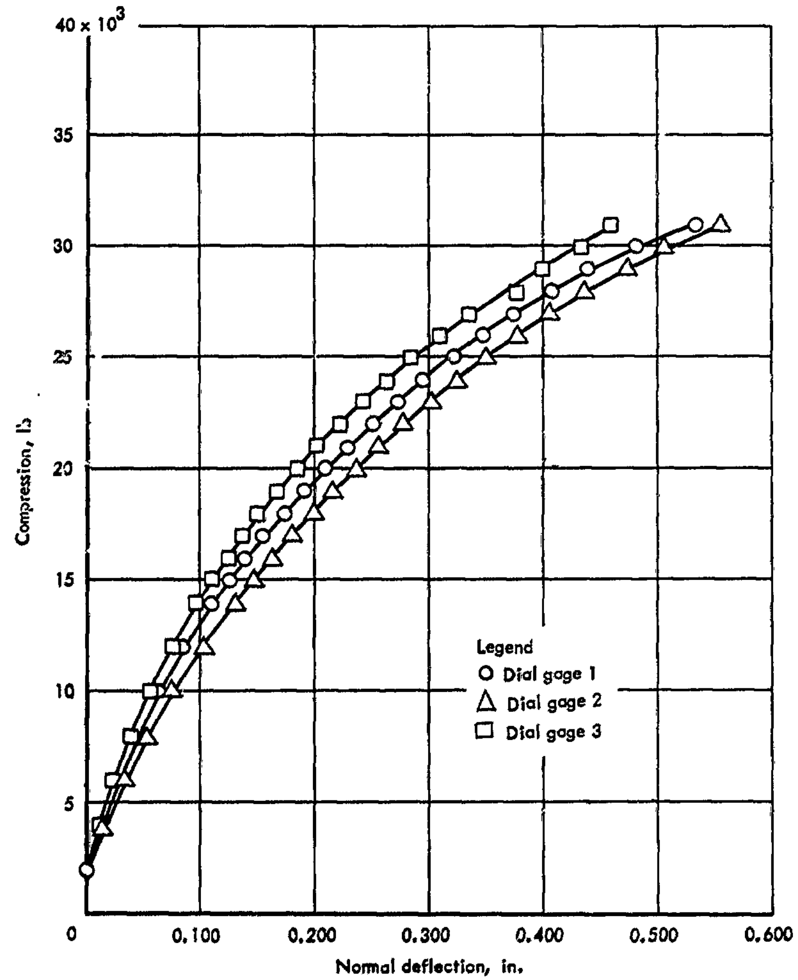

Figure 27-88 Normal deflection curve for corrugation-stiffened skin compression panel, room temperature

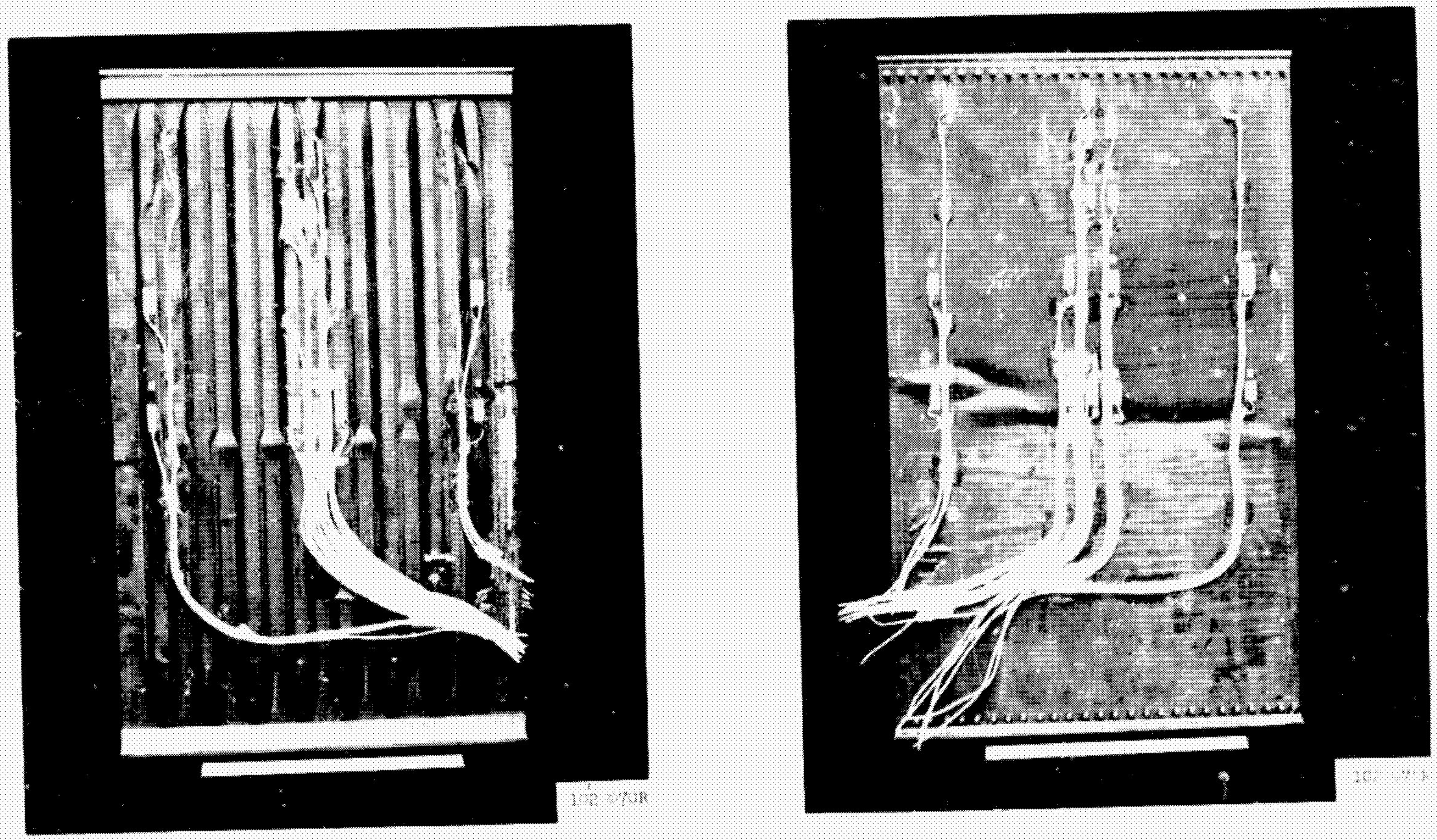

Corrugation side

Skin side

Figure 27-89 Corrugation-stiffened skin compression panel after failure, room temperature test

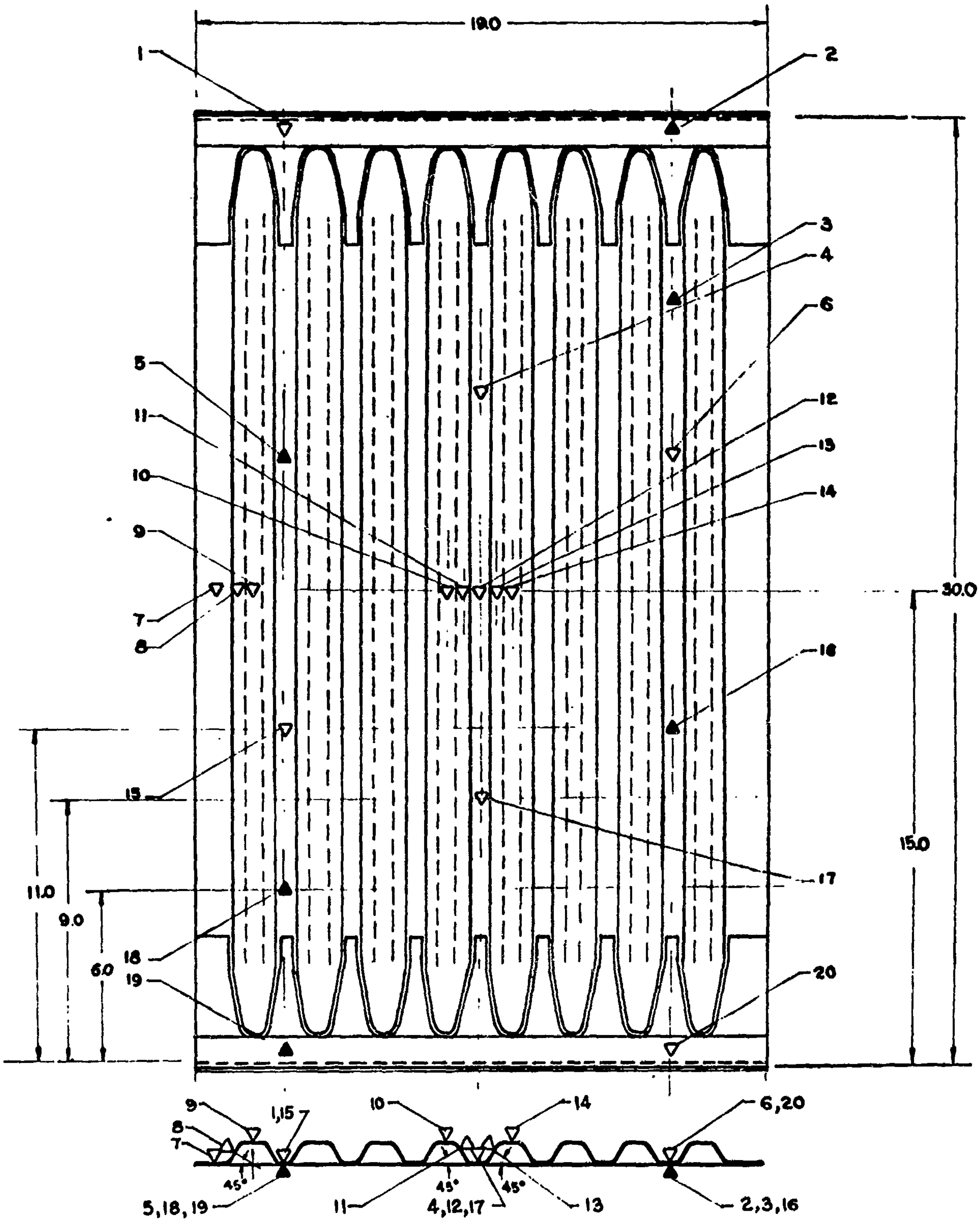

Figure 27-90 Thermocouple locations for the corrugation-stiffened-skin compression panel

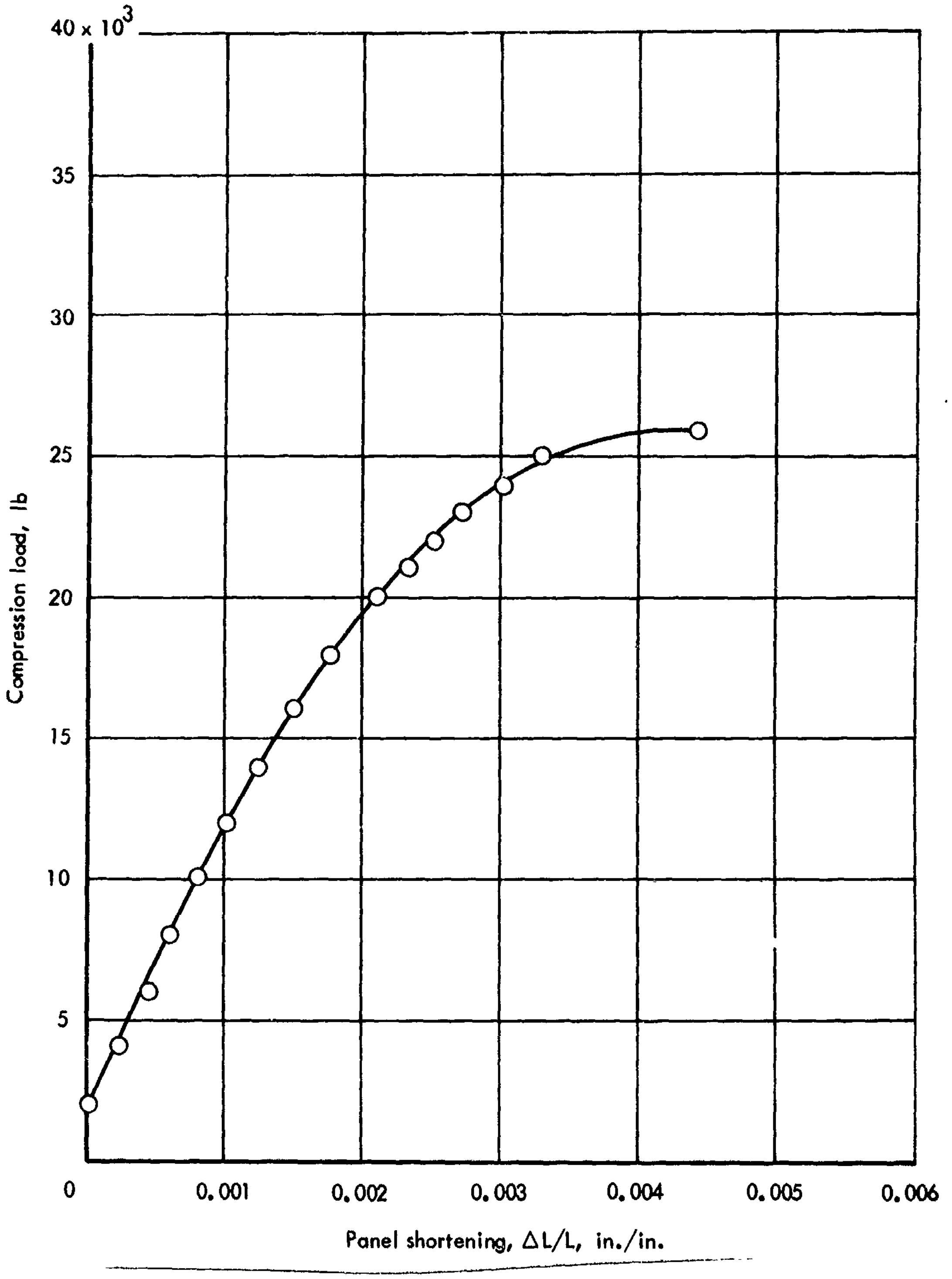

Figure 27-91 Panel shortening curve ΛL/L for corrugation-stiffened-skin compression panel, 1400°F test

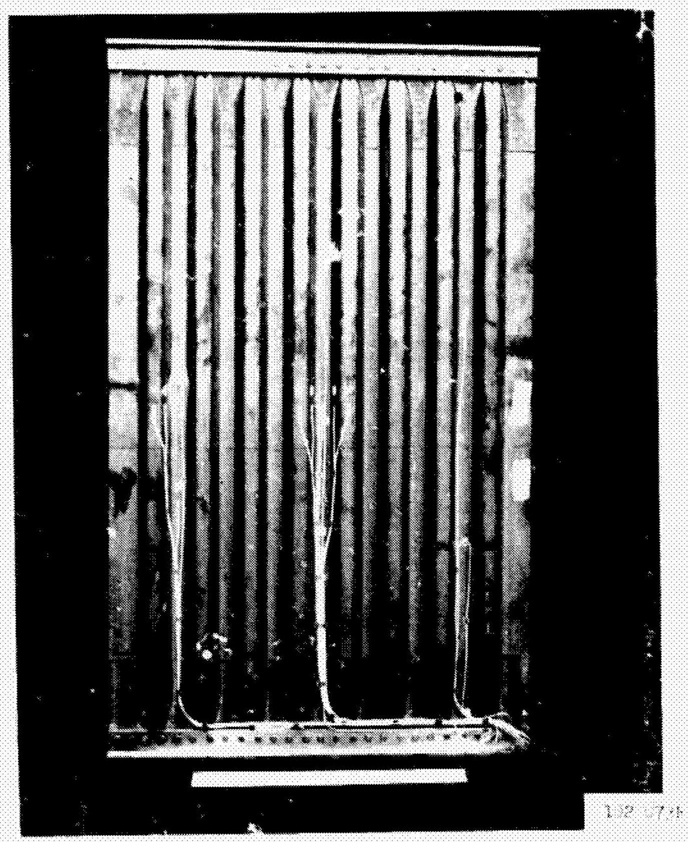

Corrugation side

Skin side

Figure 27-92 Corrugation-stiffened skin compression panel after failure, 1400° F test

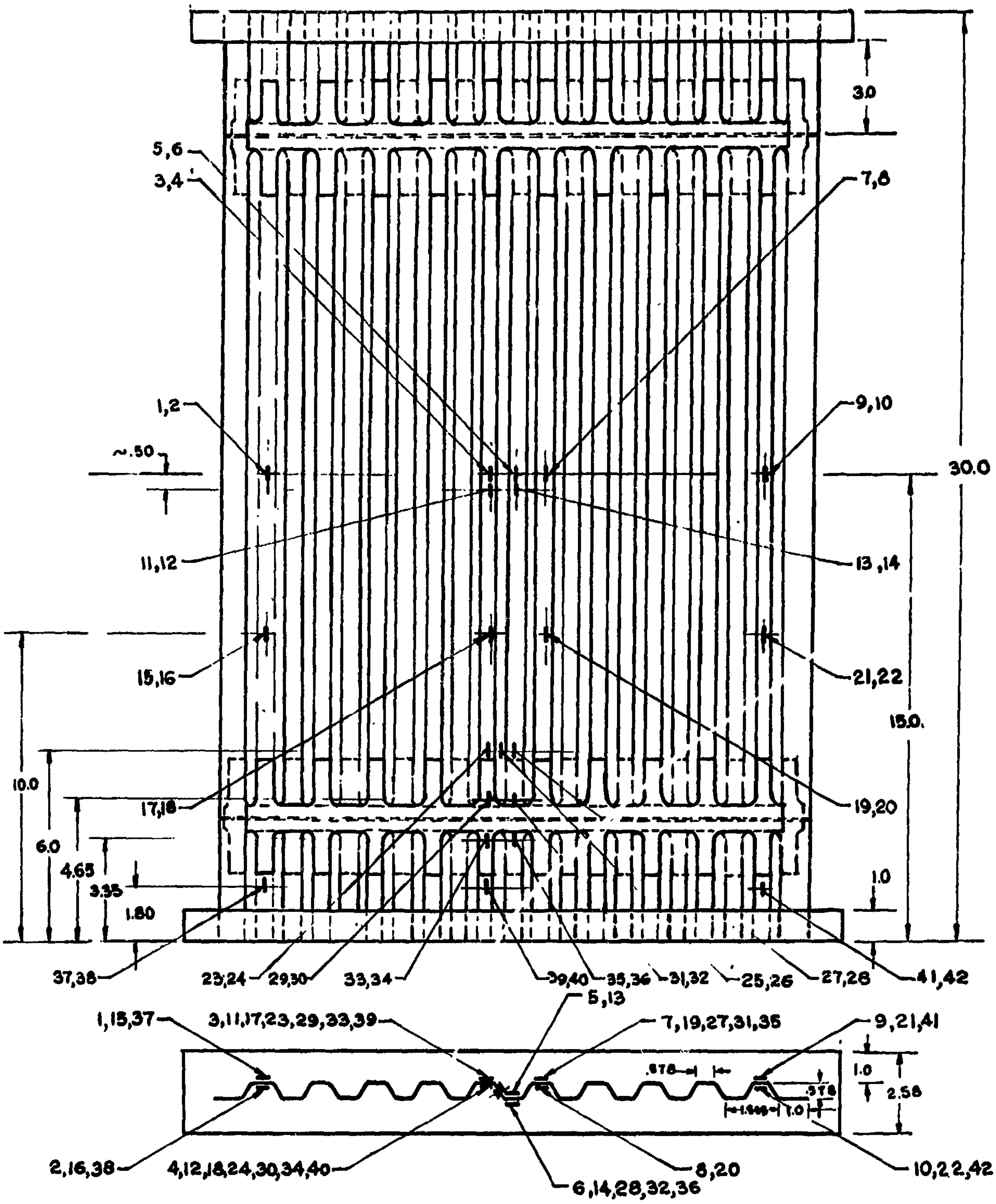

Figure 27-93 Strain gage locations for trapezoidal corrugation compression panel

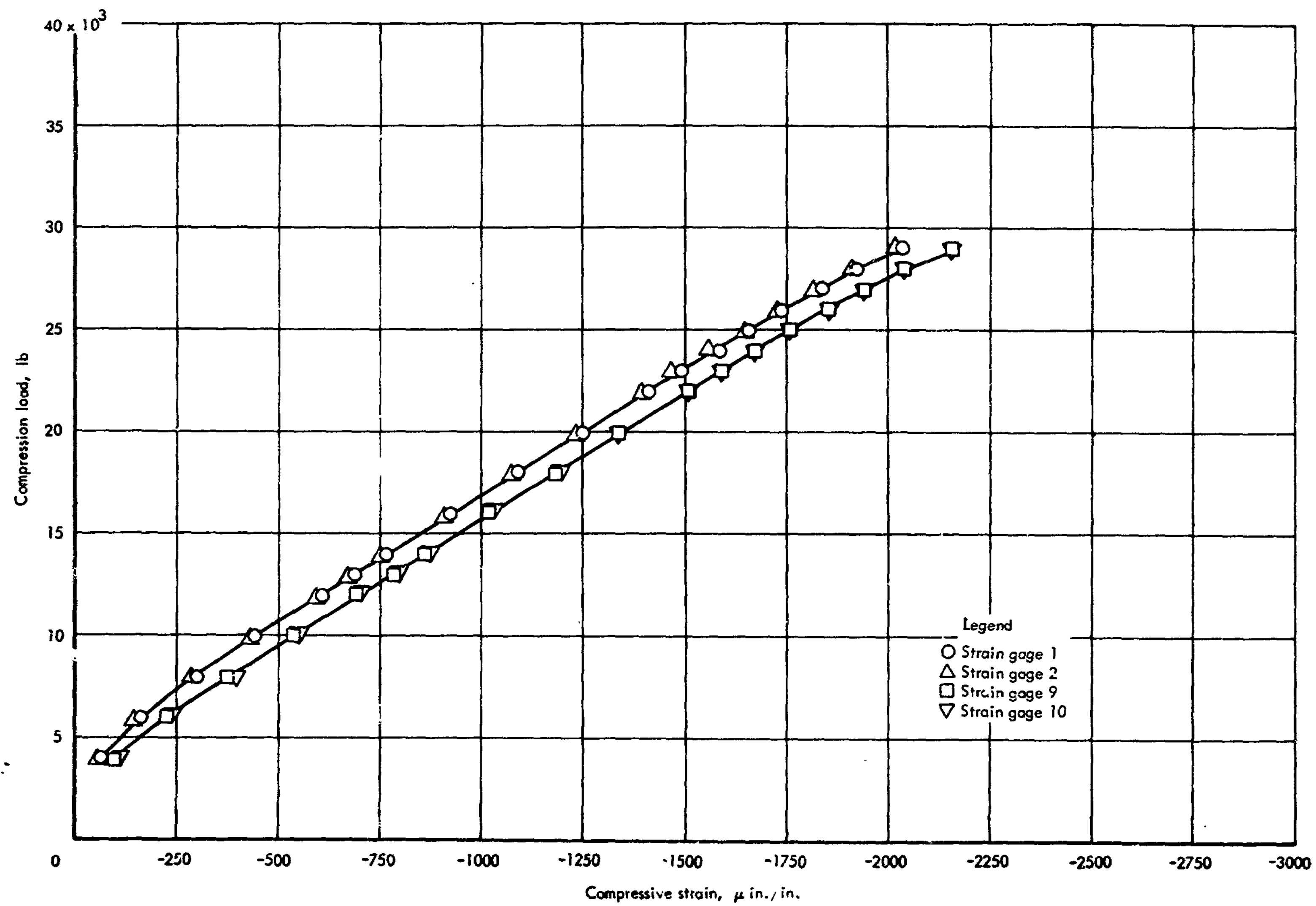

Figure 27-94 Axial strains for trapezoidal corrugation compression panel, room temperature

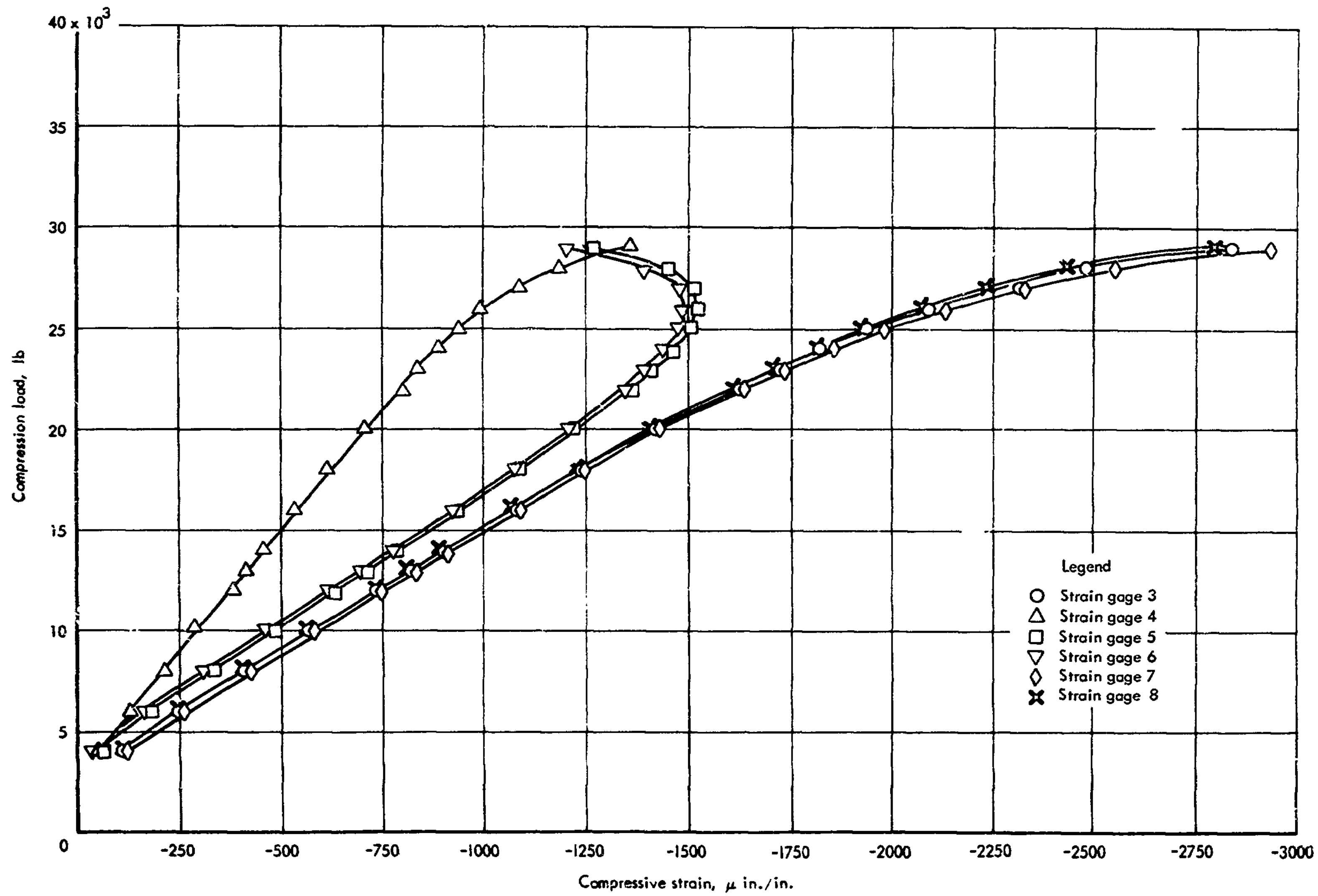

Figure 27-94 (continued)

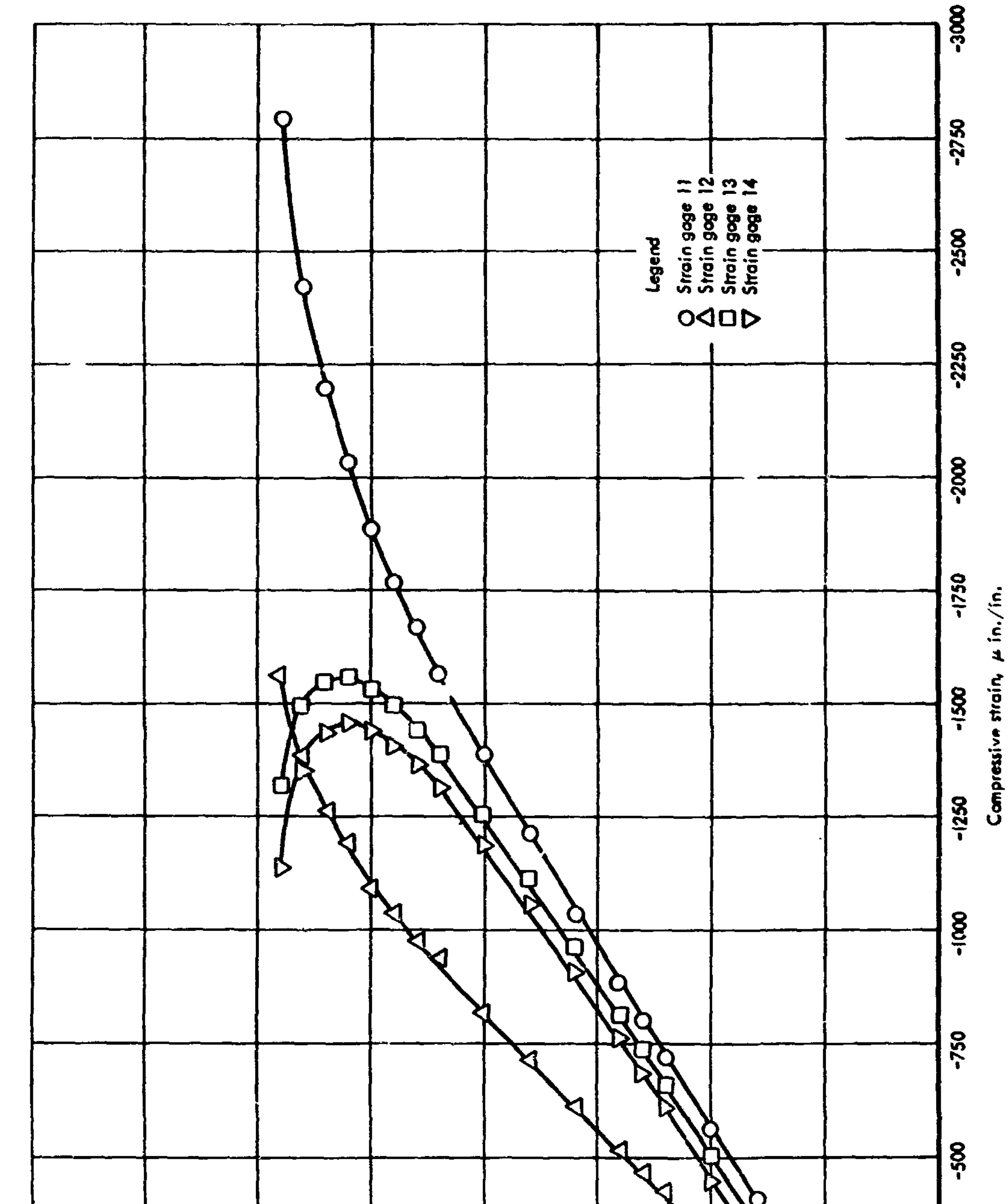

Figure 27-94 (continued)

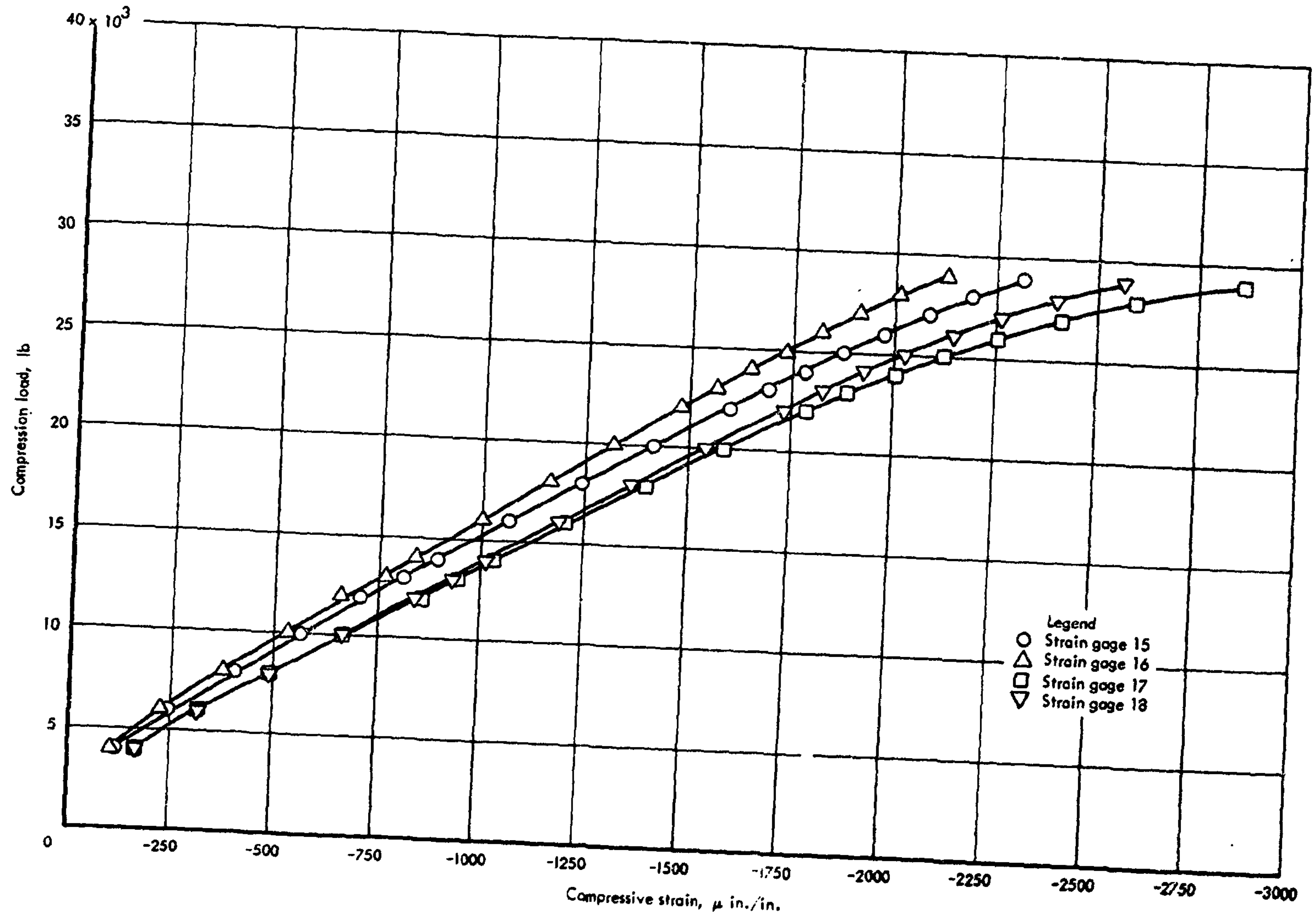

Figure 27-94 (continued)

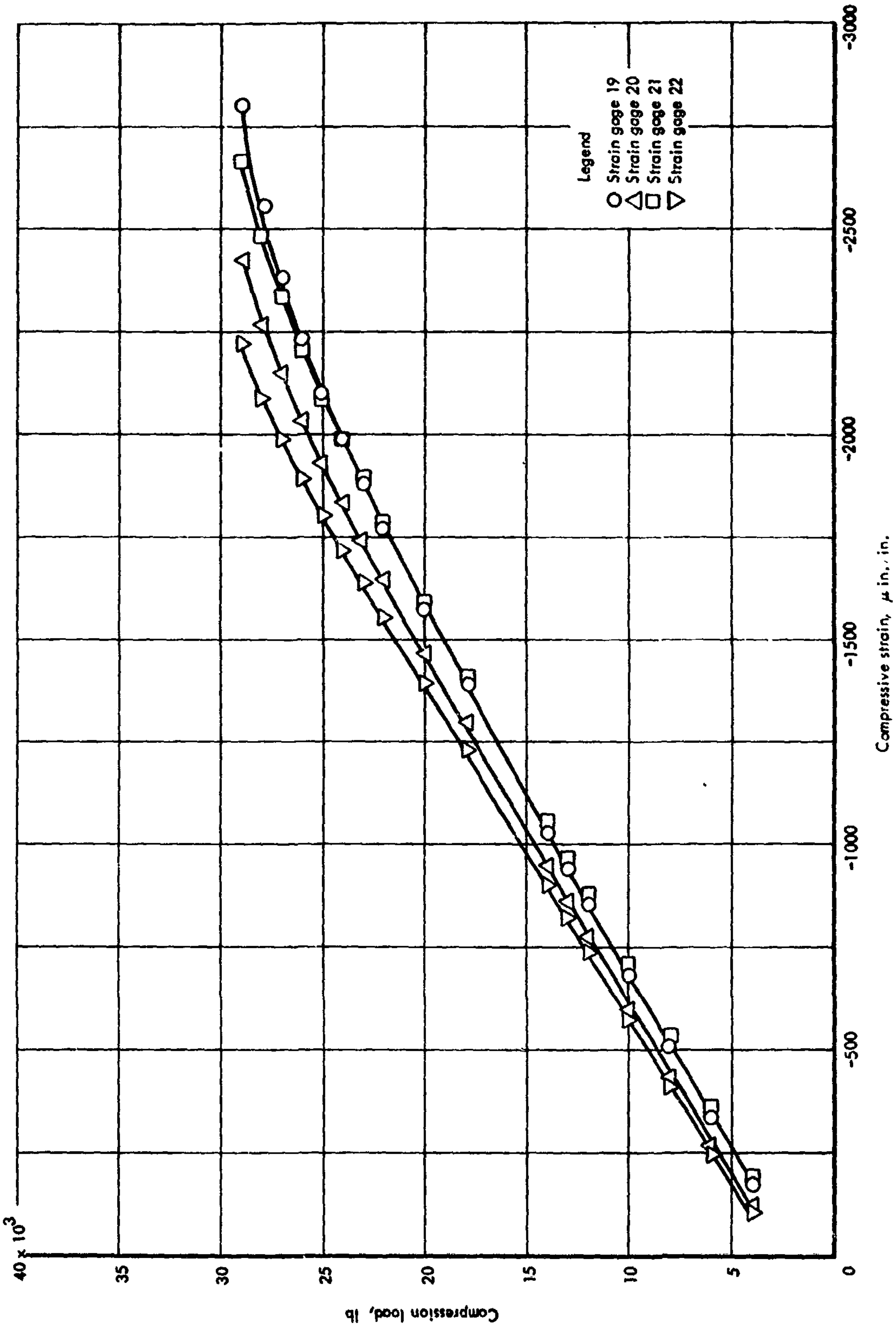

Figure 27-94 (continued)

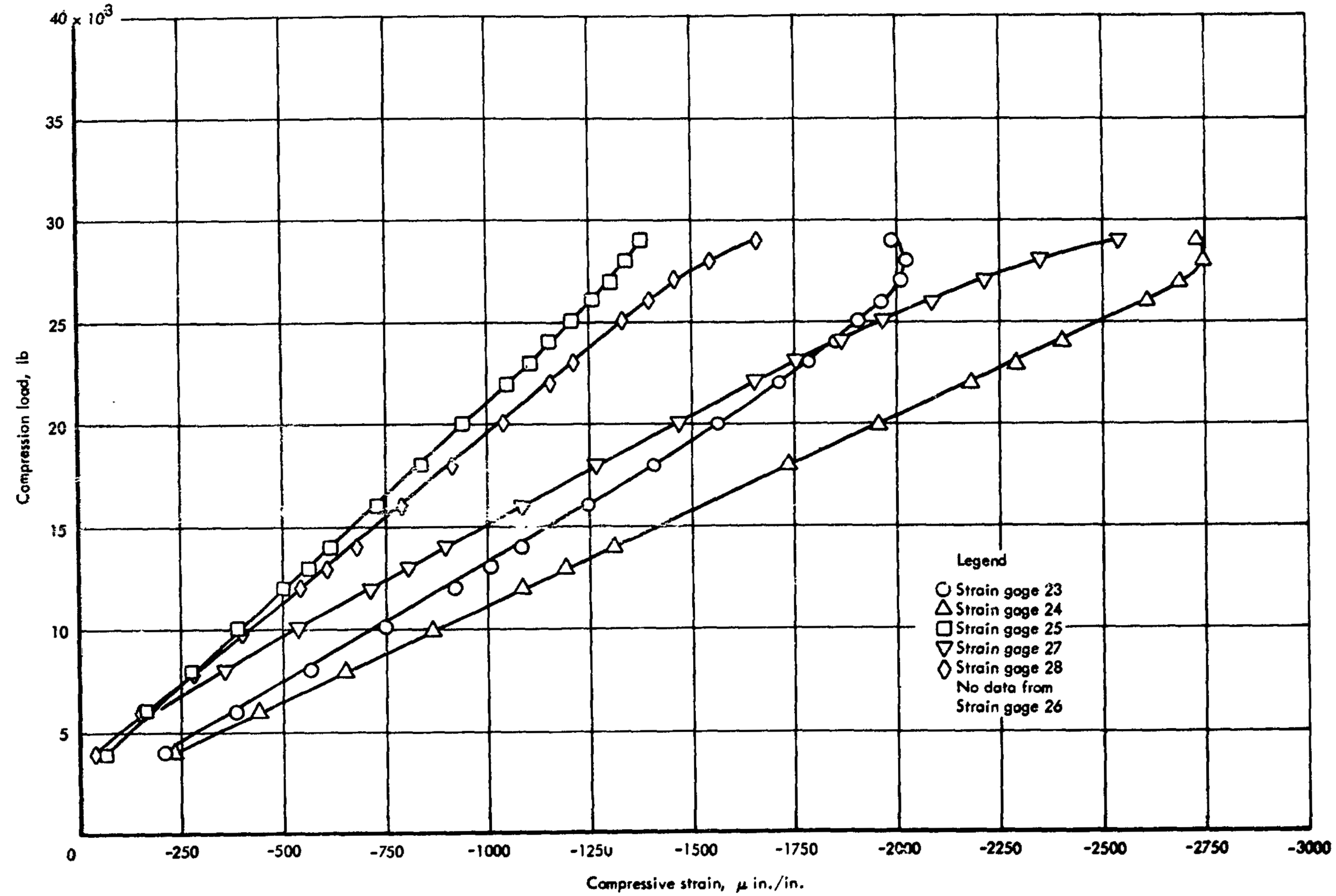

Figure 27-94 (continued)

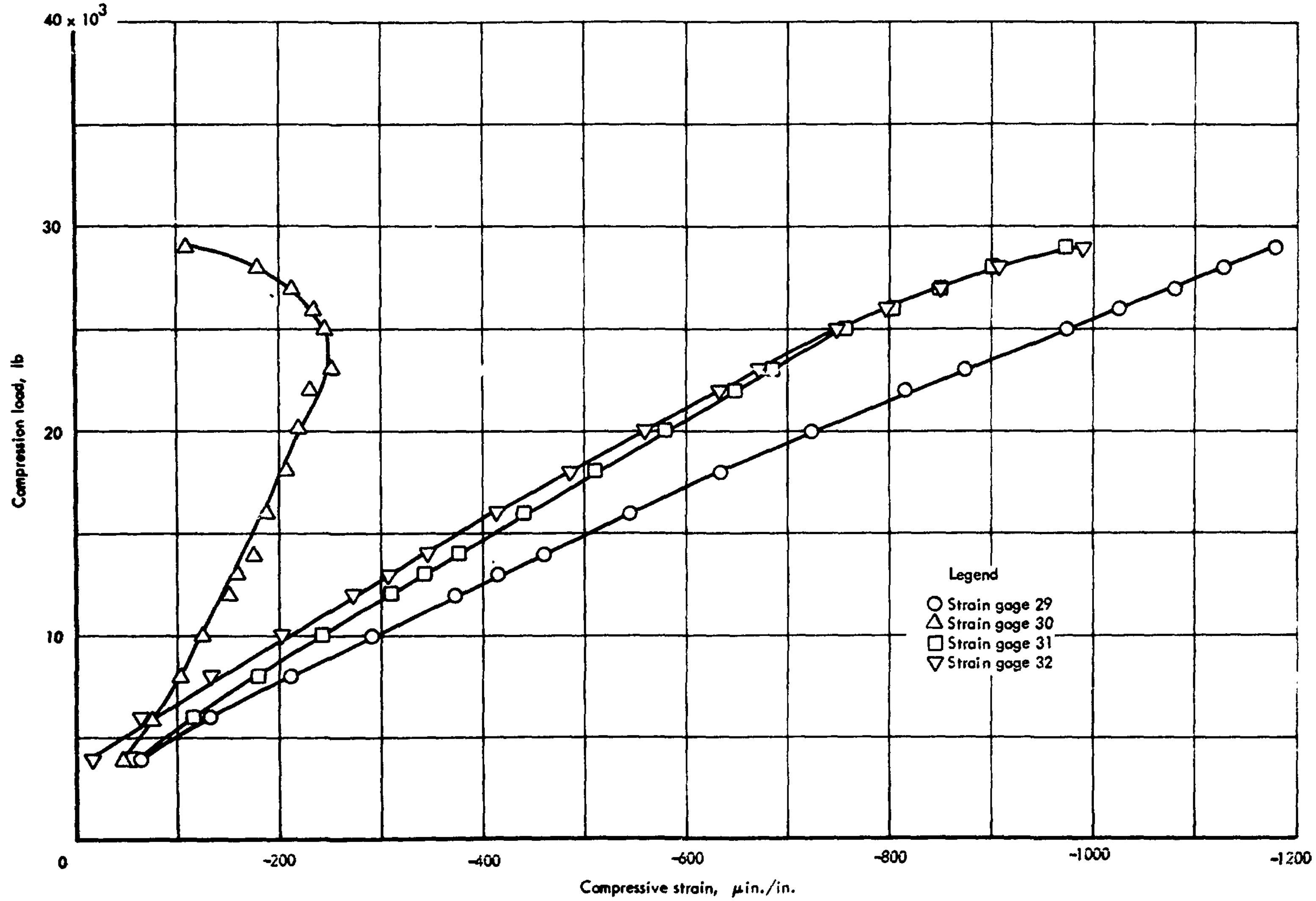

Figure 27-94 (continued)

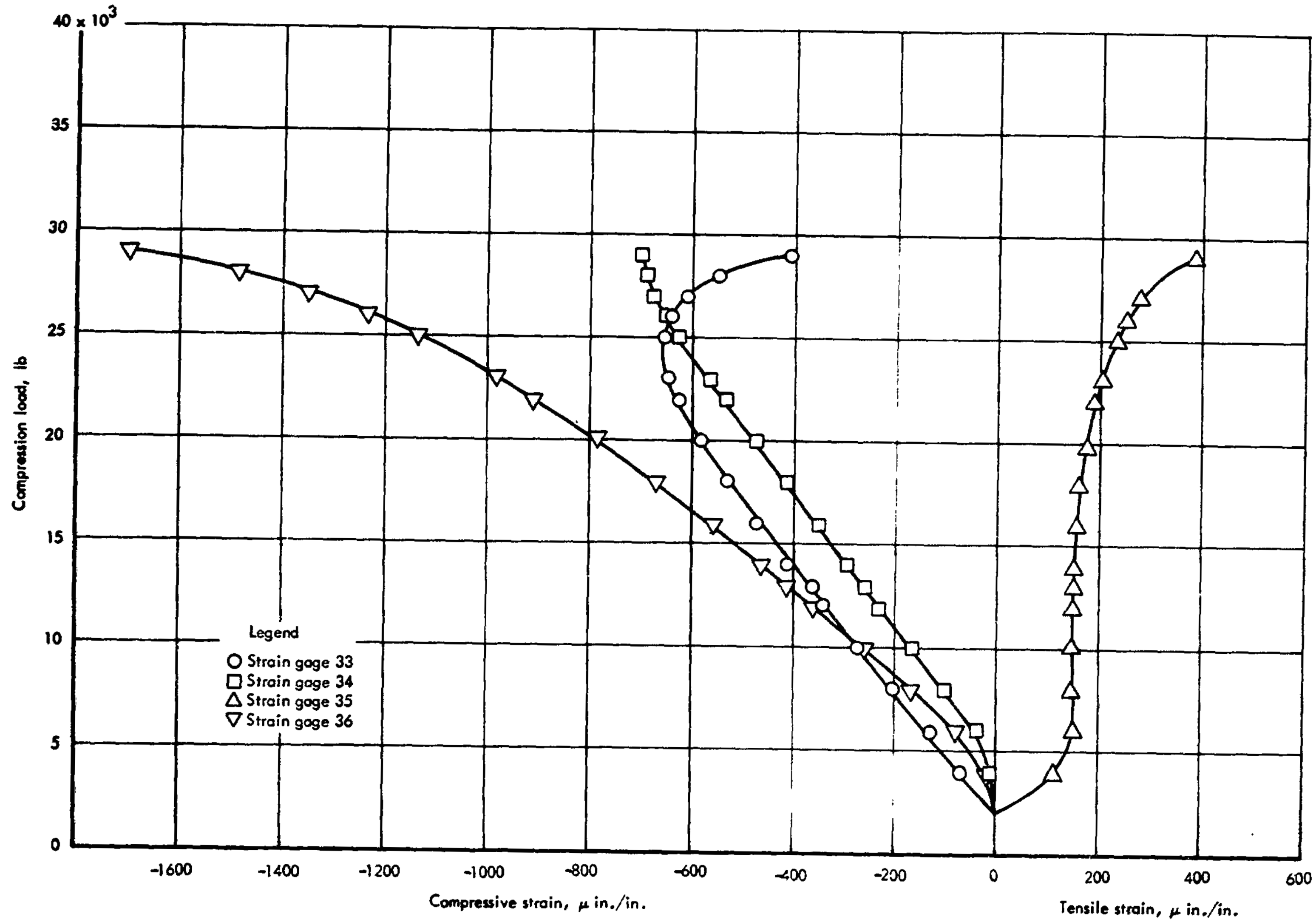

Figure 27-94 (continued)

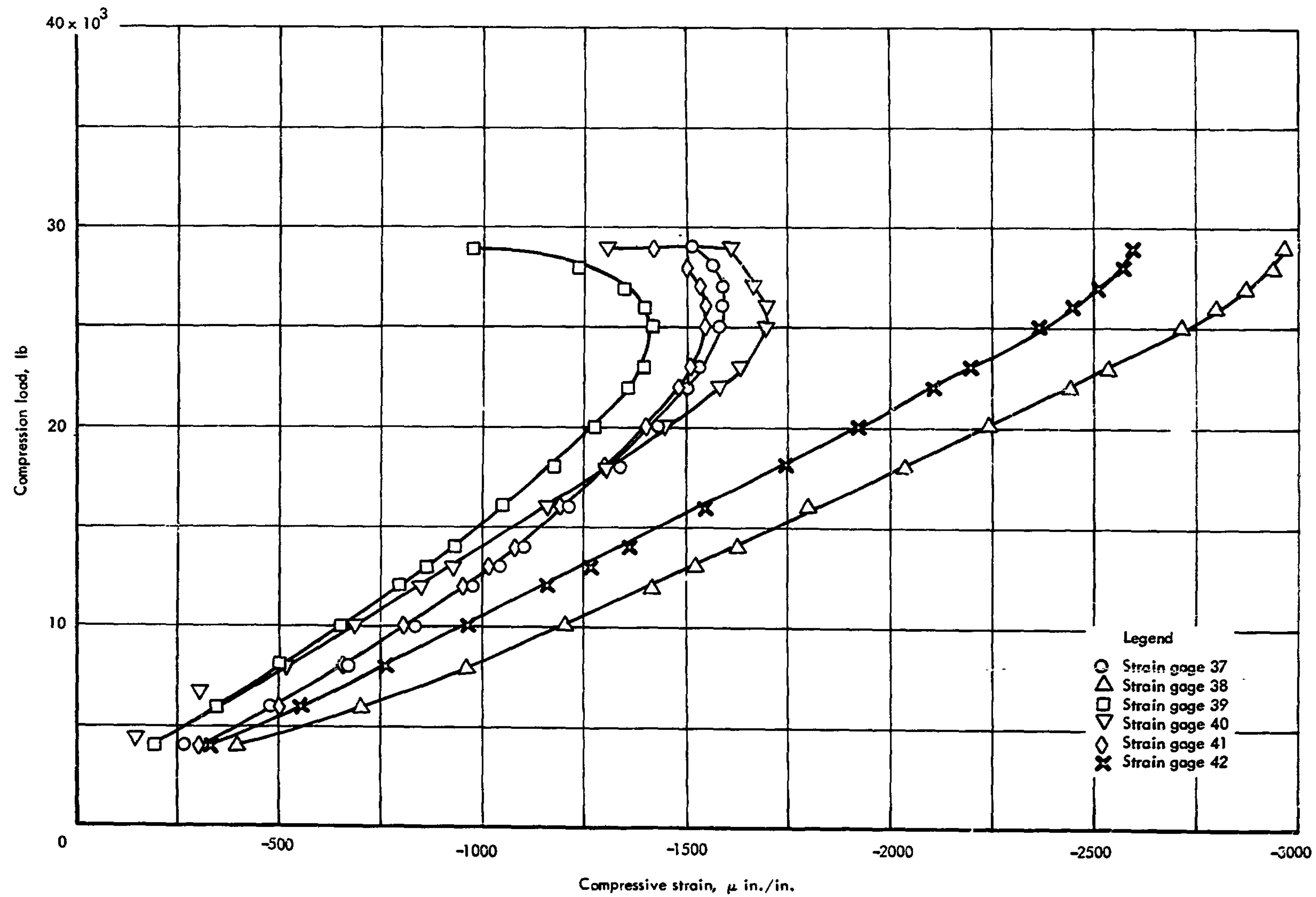

Figure 27-94 (Concluded)

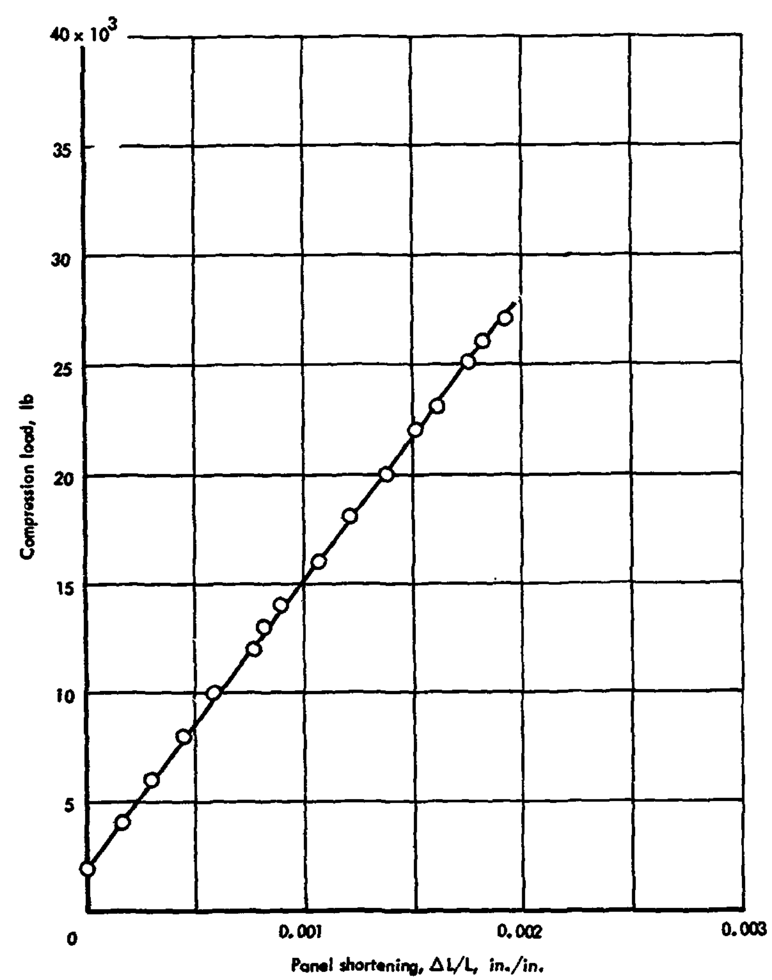

Figure 27-95 Panel shortening curve $\Delta L/L$ for trapezoidal corrugation compression panel, room temperature

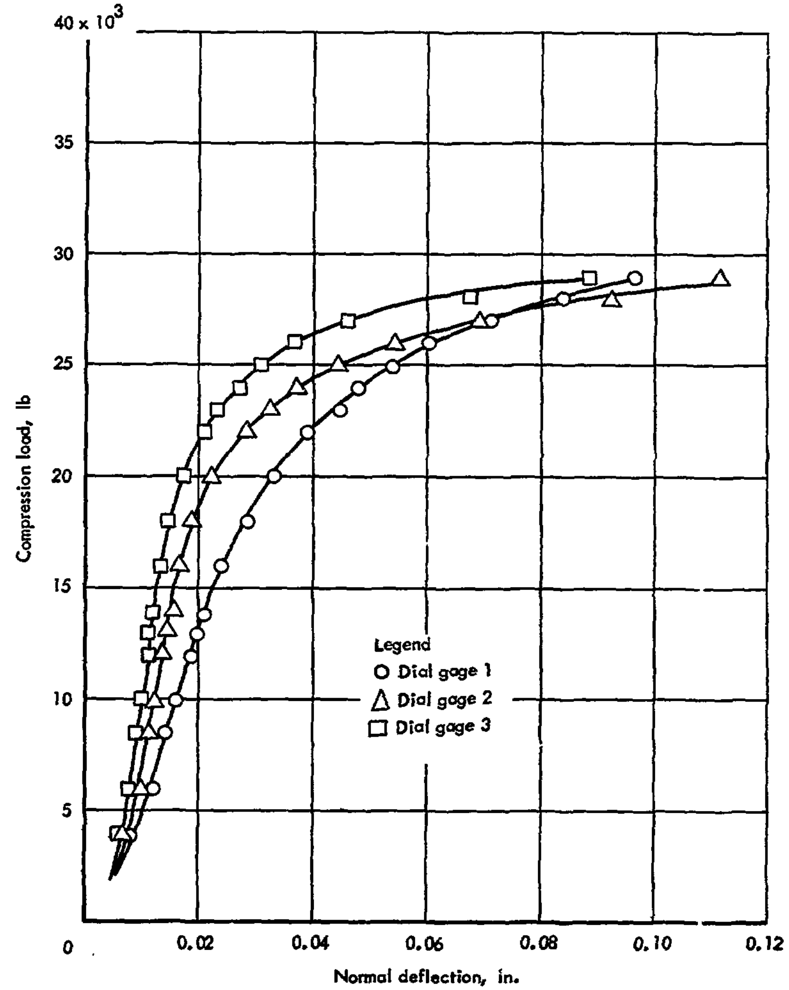

Figure 27-96 Normal deflections for trapezoidal corrugation compression panel, room temperature

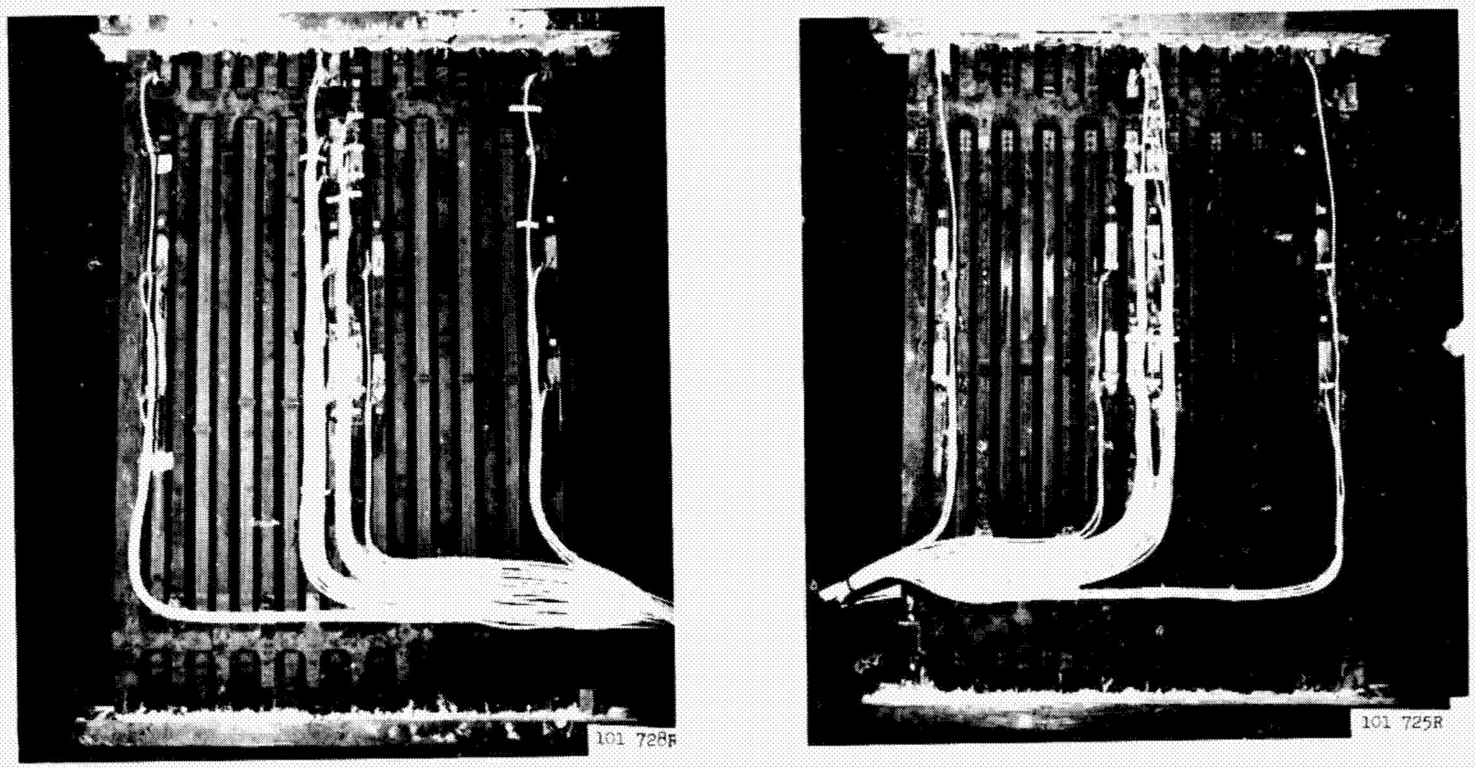

Front

Back

Figure 27-97 Trapezoidal corrugation compression panel after failure, room temperature test

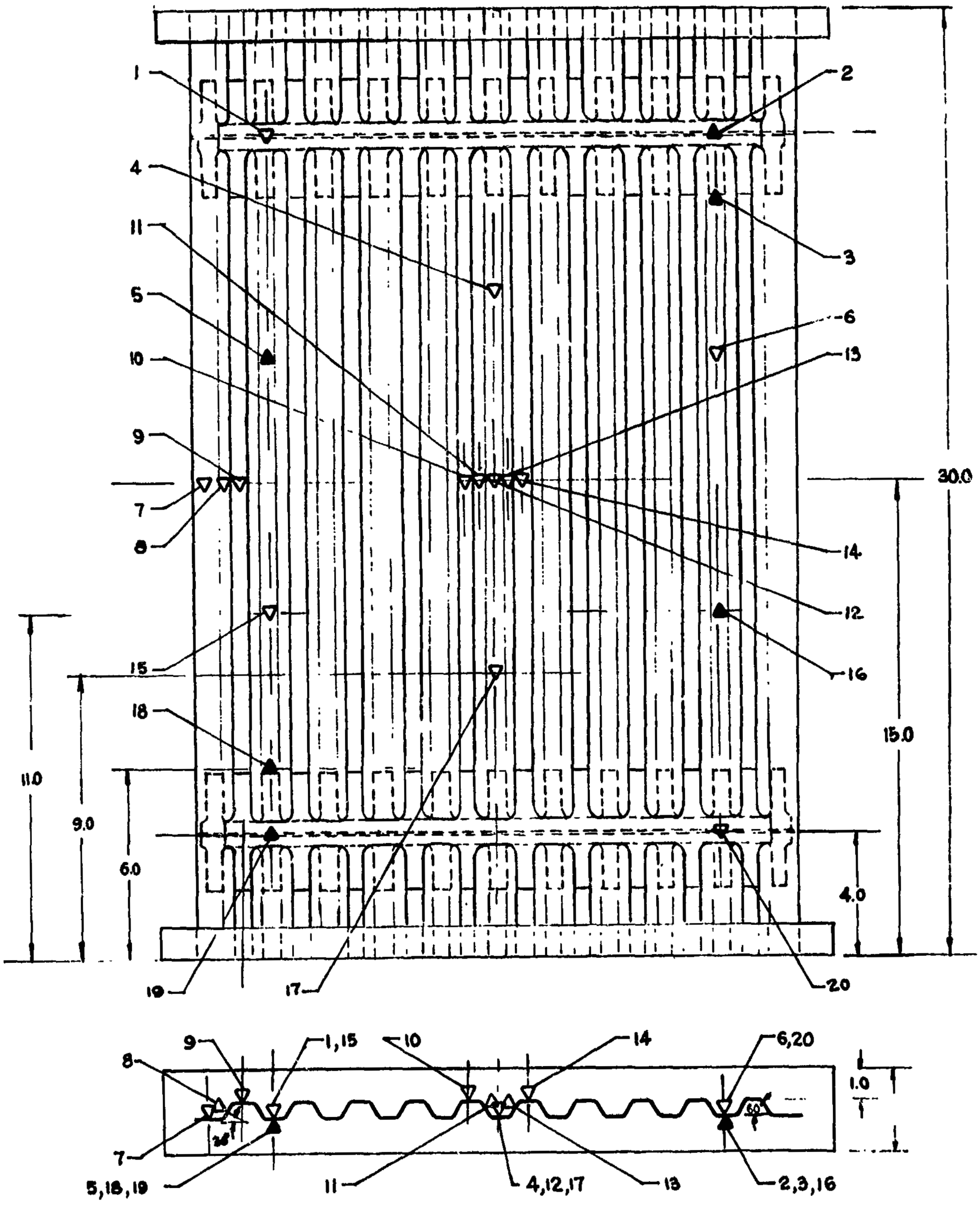

Figure 27-98 Thermocouple locations for the trapezoidal corrugation compression panel

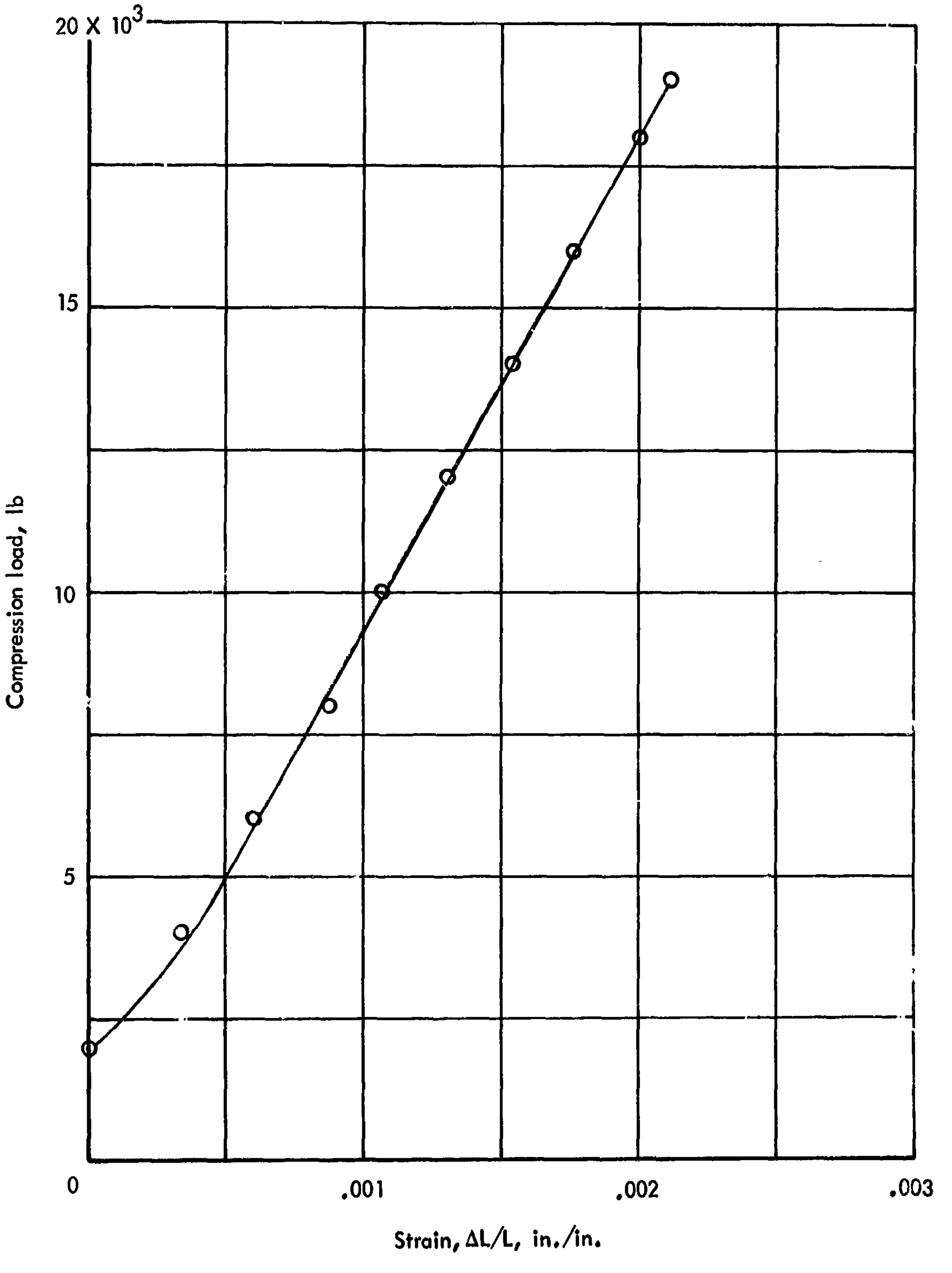

Figure 27-99 Panel shortening curve $\Delta L/L$ for trapezoidal corrugation compression panel, 1400°F

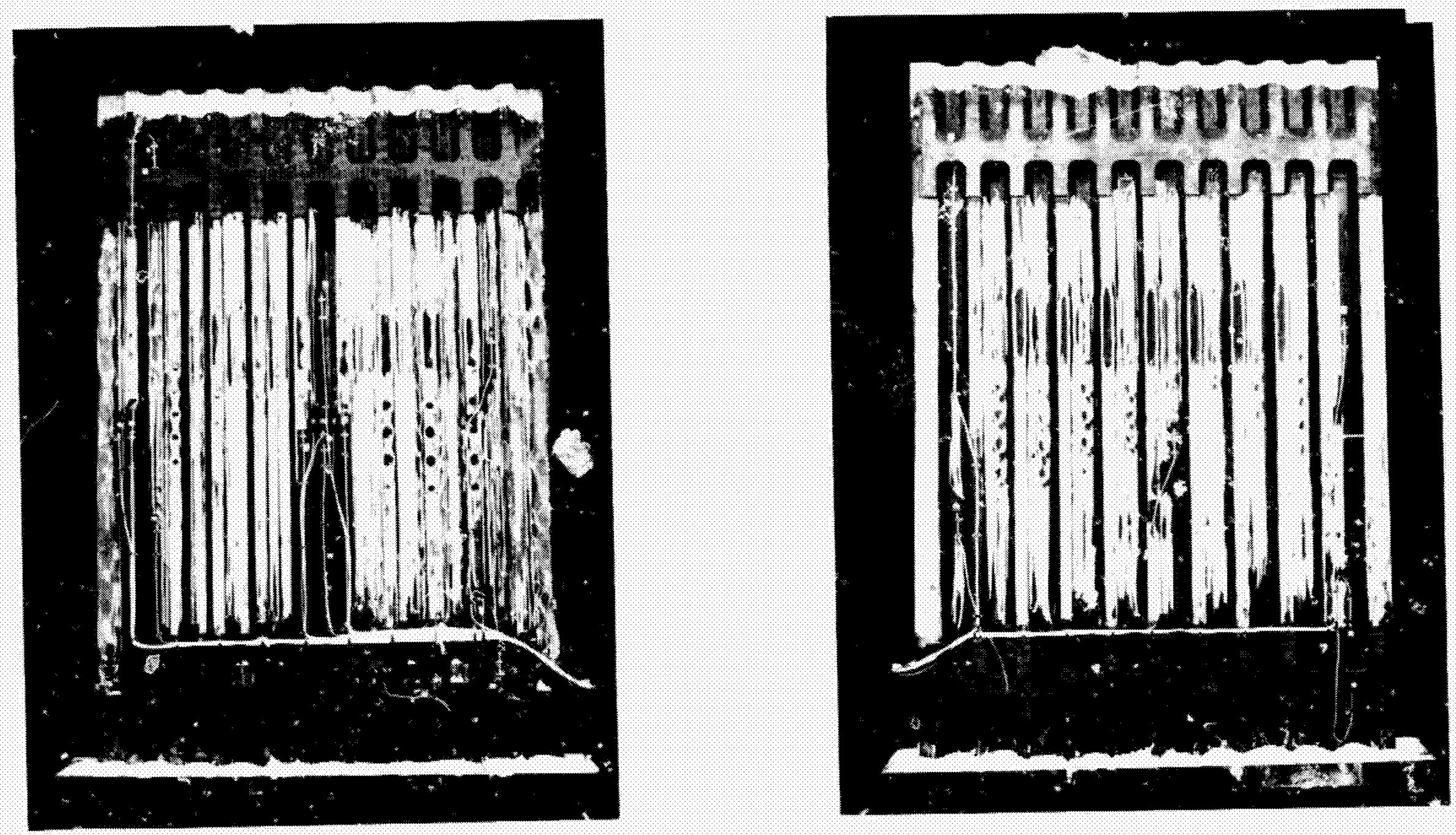

Front

Back

Figure 27-100 Trapezoidal corrugation compression panel after failure, 1400° F test

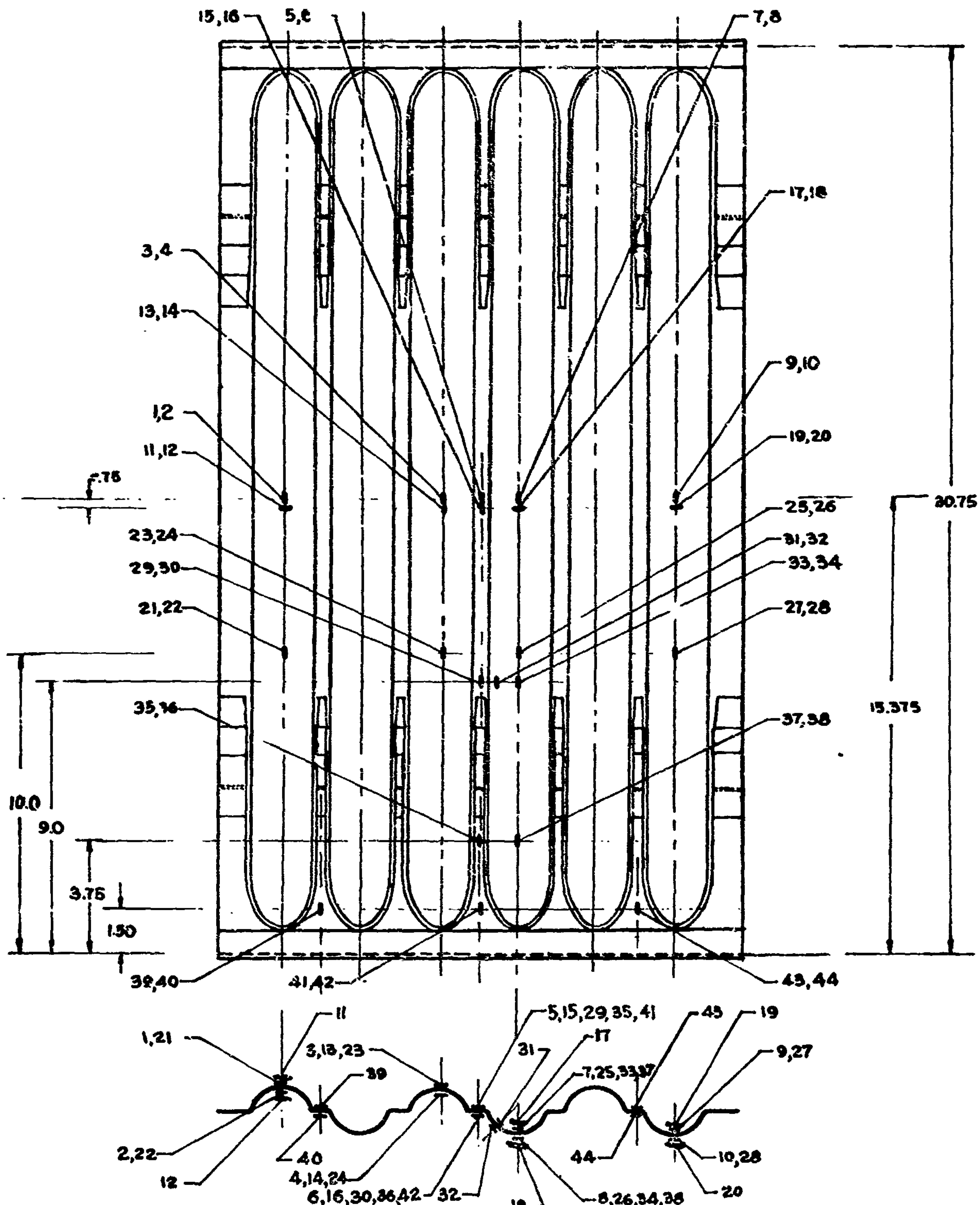

Figure 27-101 St[illegible] gag[illegible] locations for beaded [illegible]ation panel

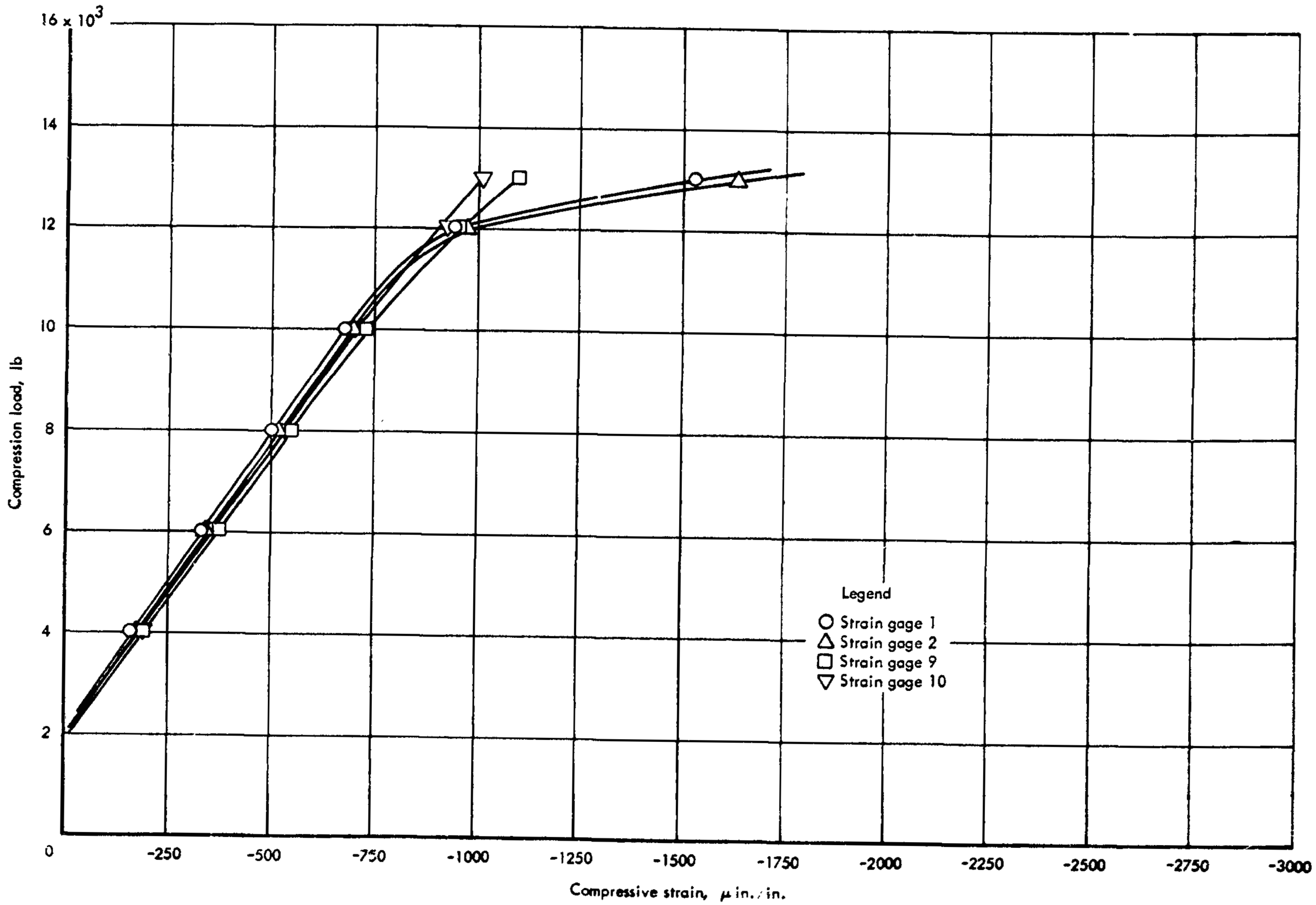

Figure 27-102 Axial strains for beaded compression panel, room temperature

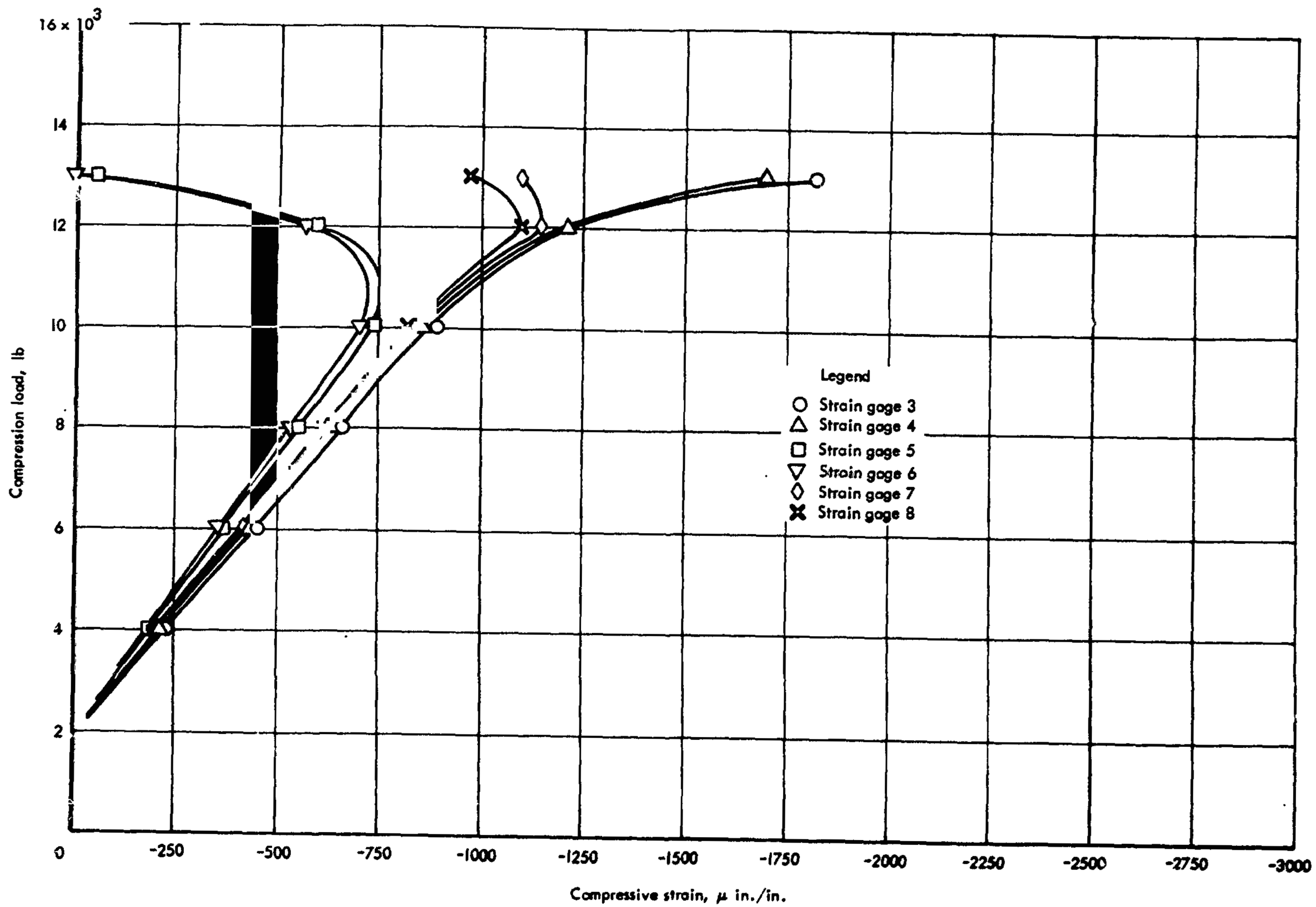

Figure 27-102 (continued)

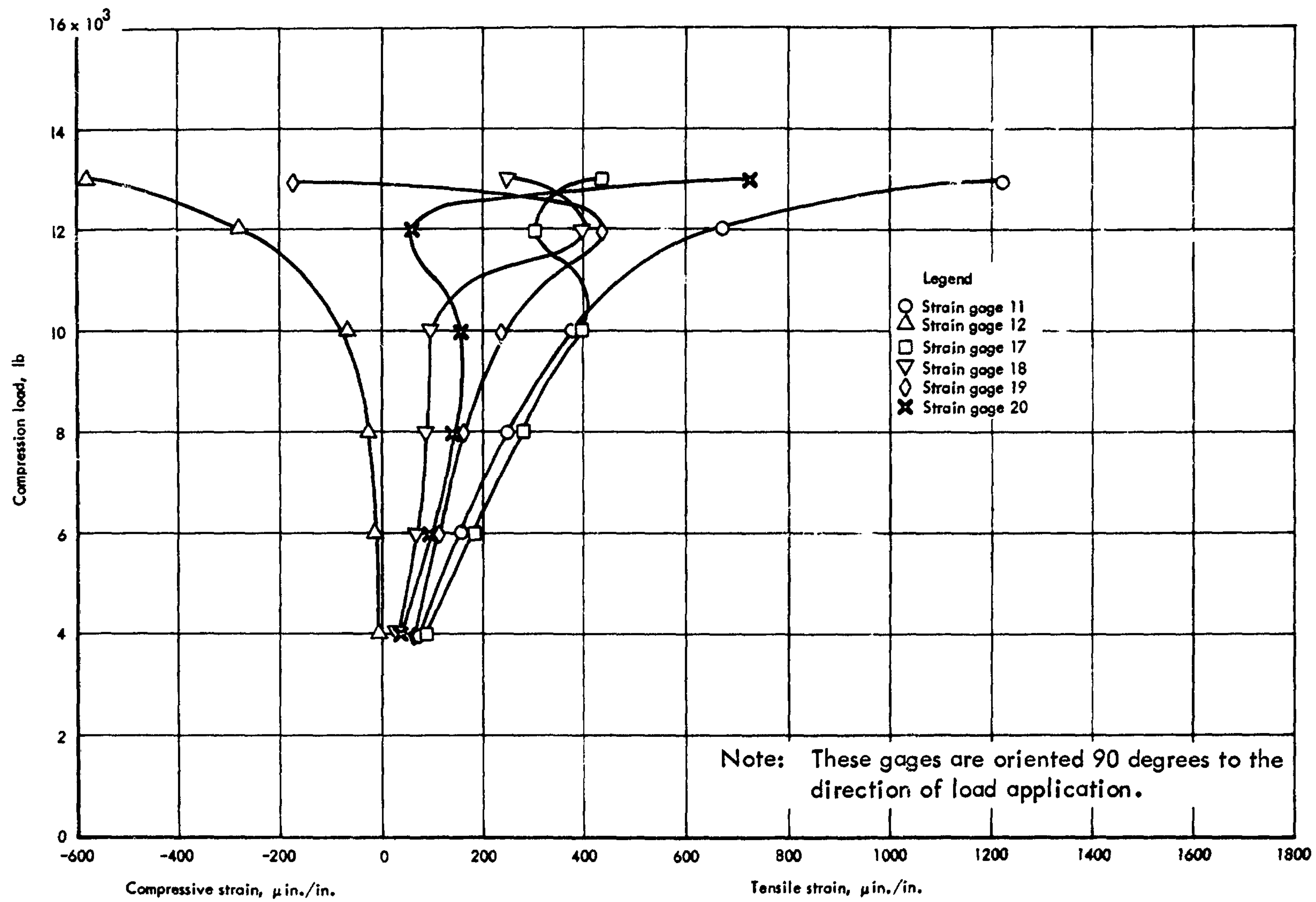

Figure 27-102 (continued)

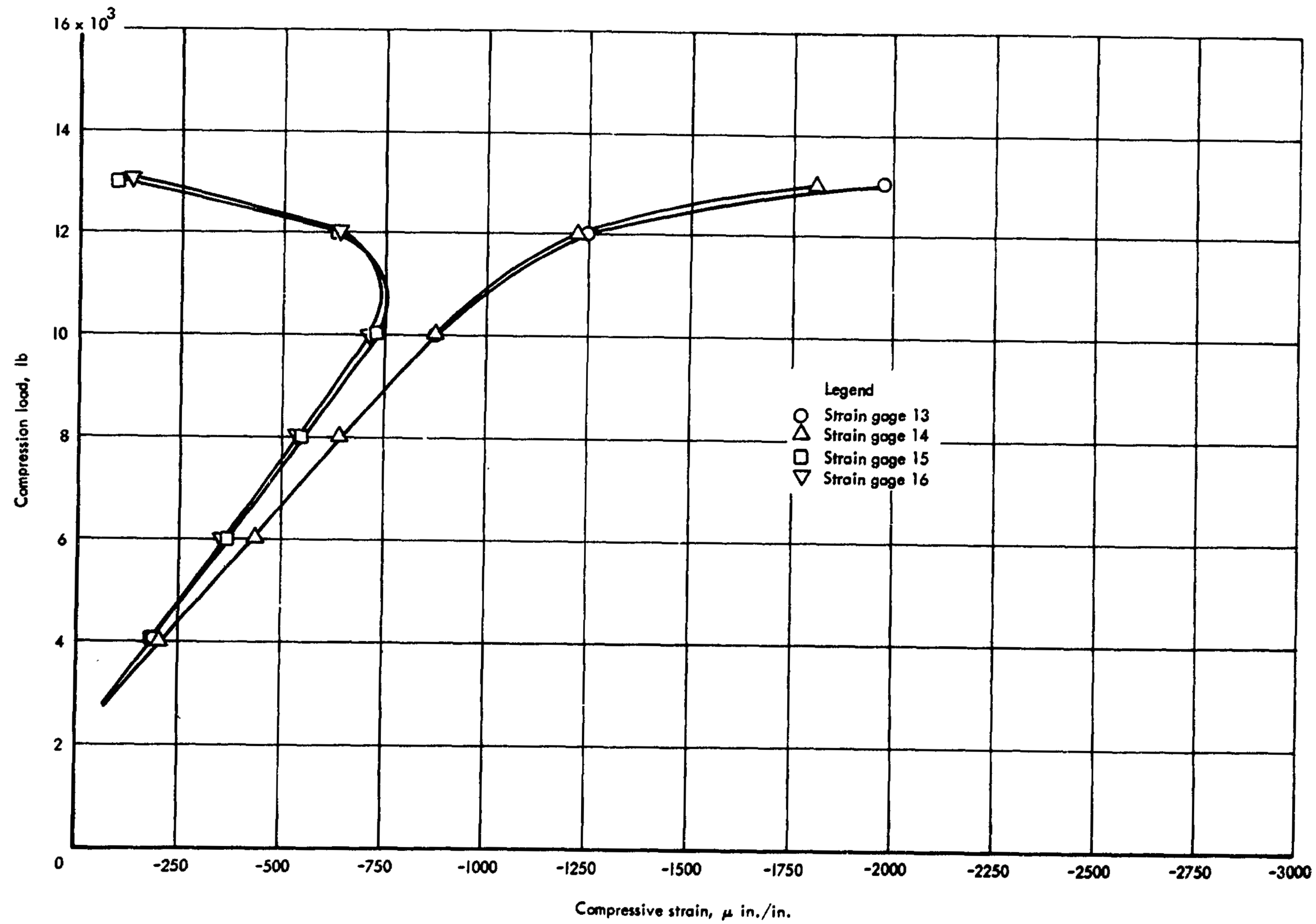

Figure 27-102 (continued)

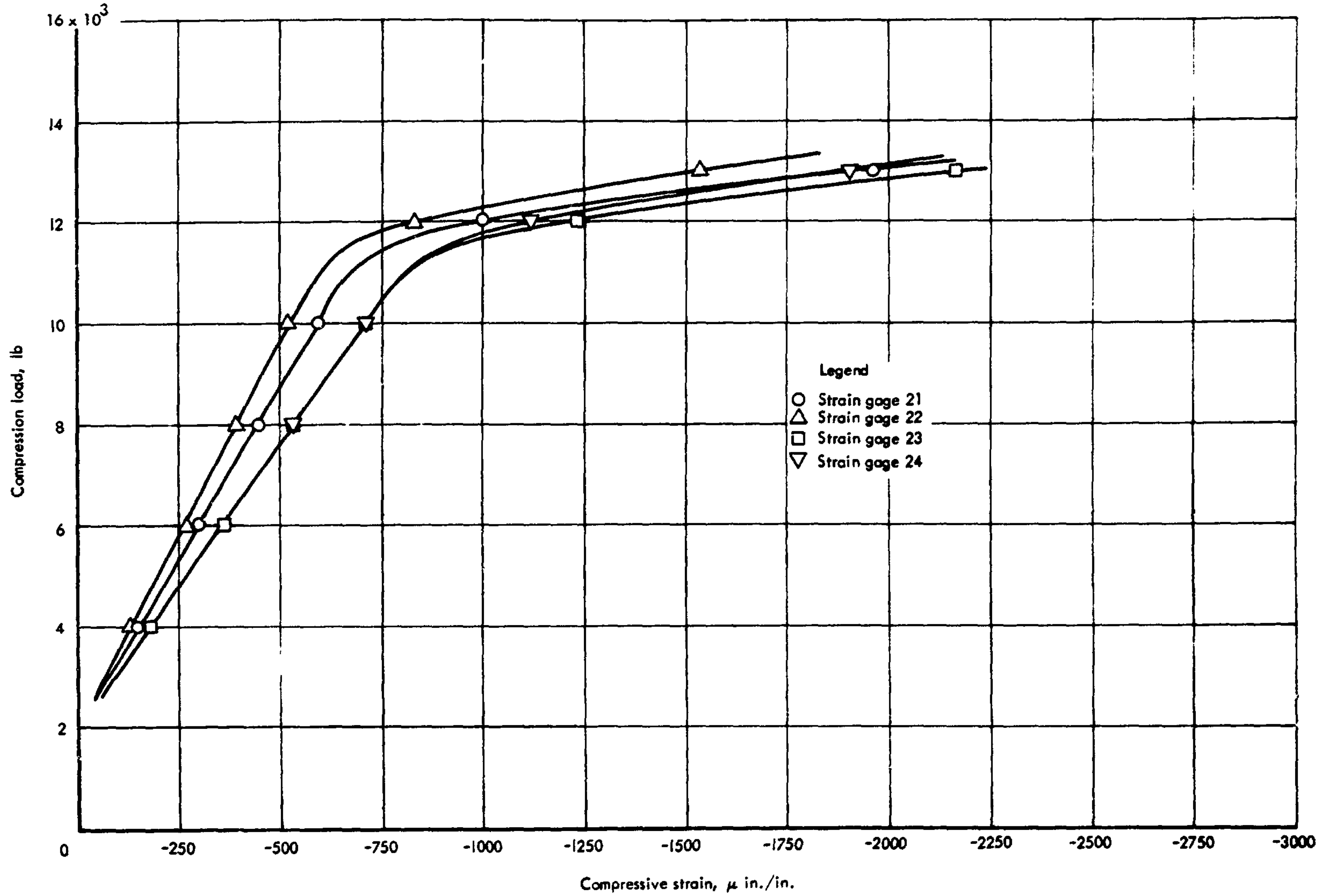

Figure 27-102 (continued

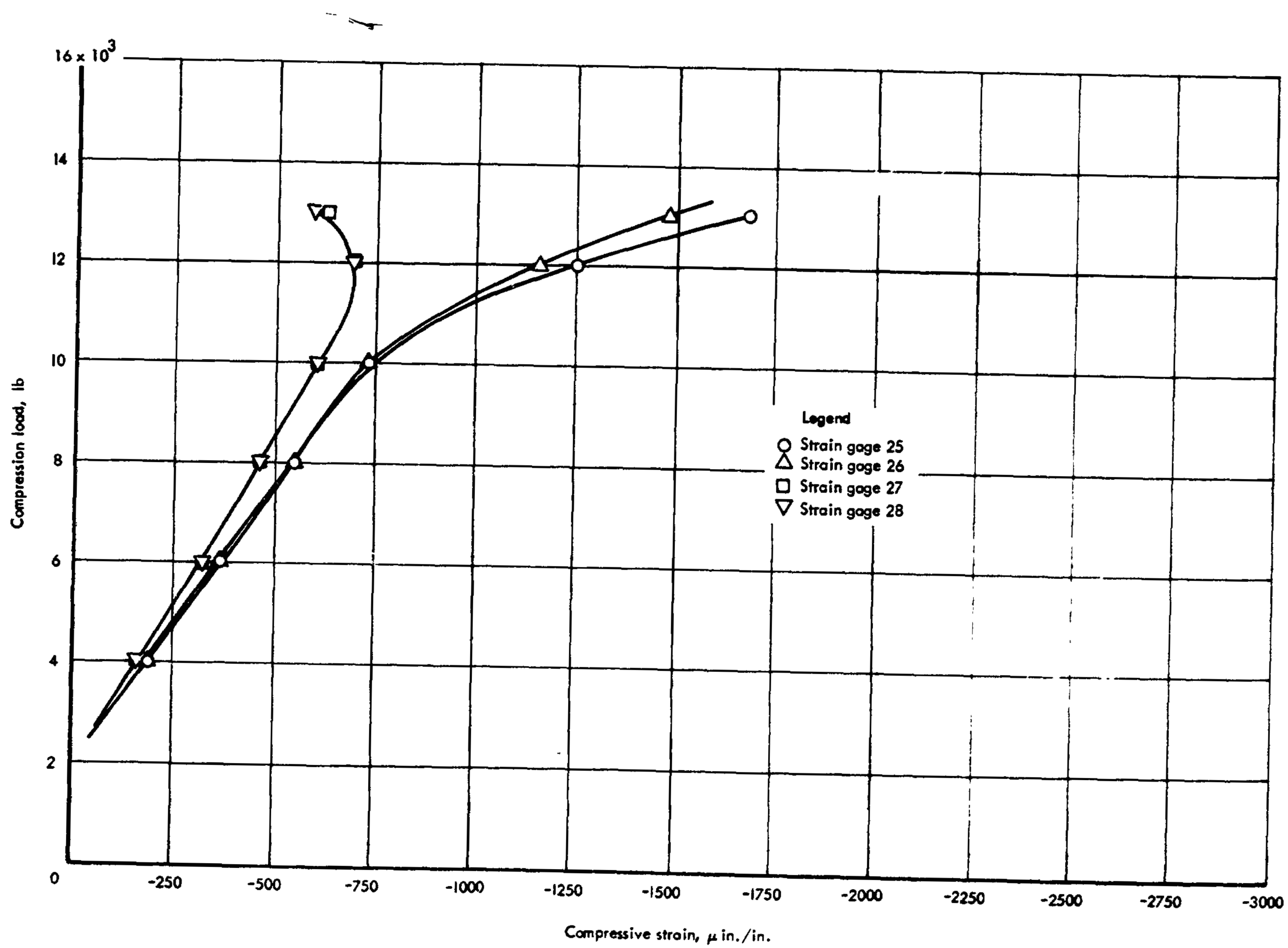

Figure 27-102 (continued)

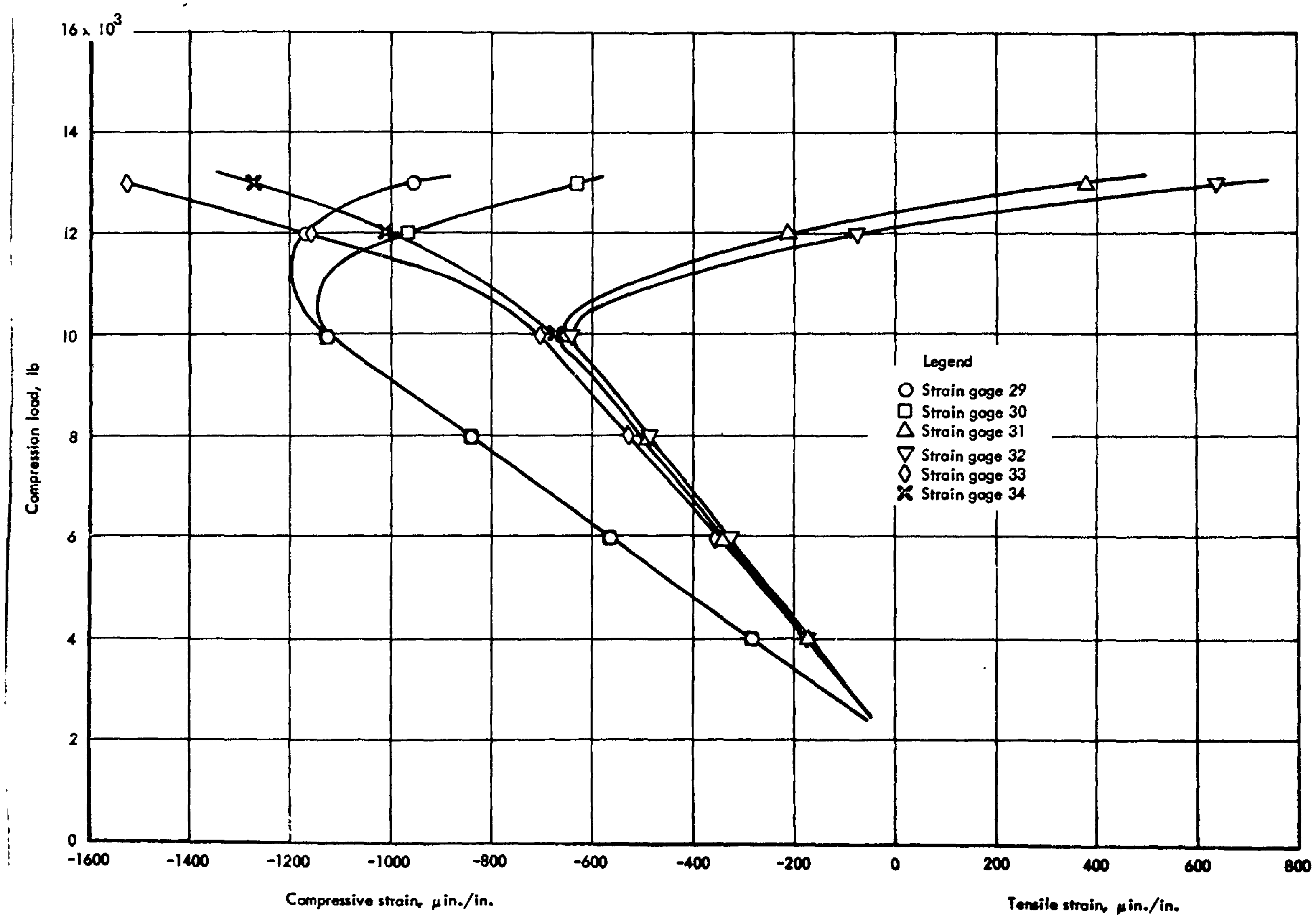

Figure 27-102 (continued)

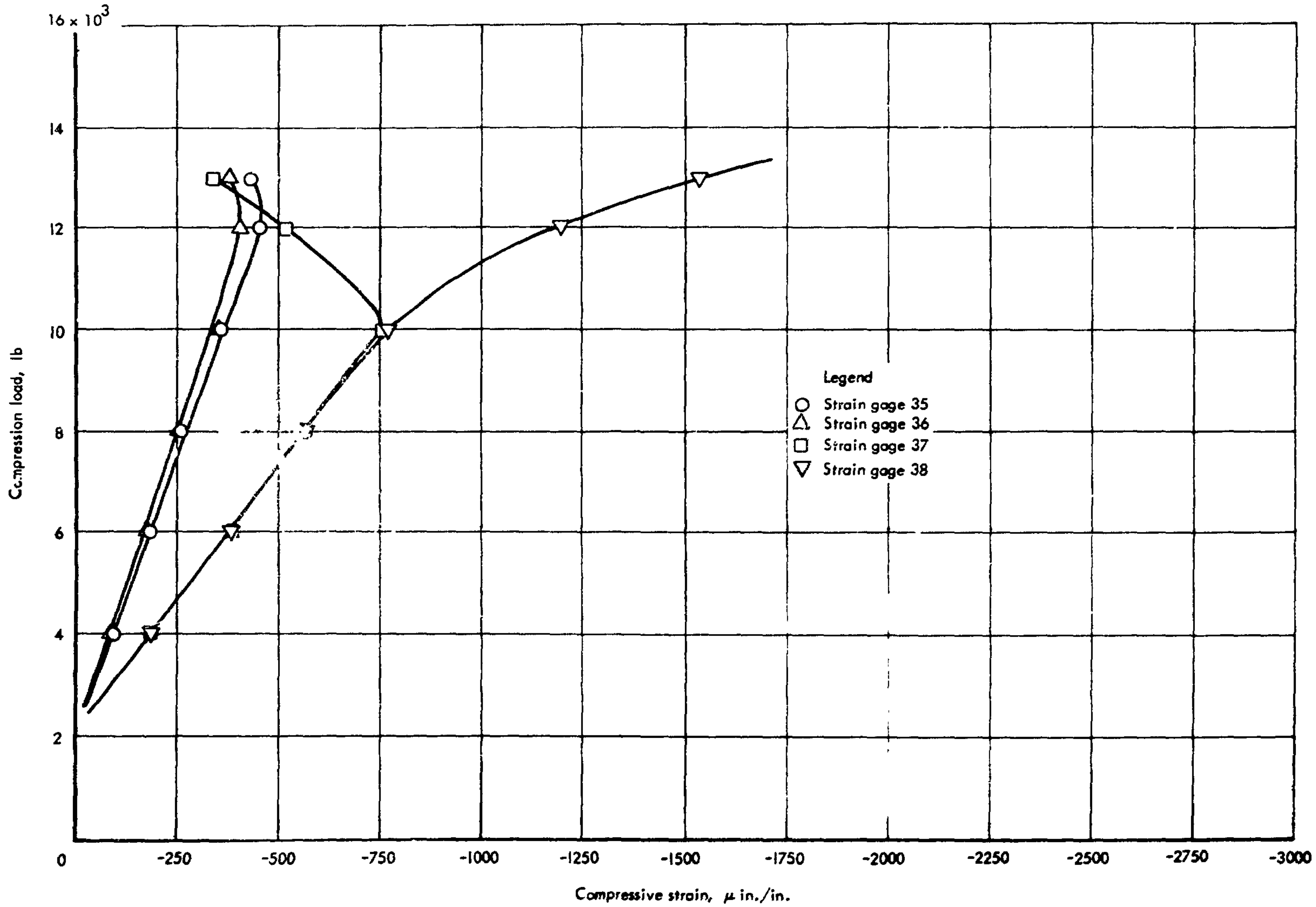

Figure 27-102 (continued)

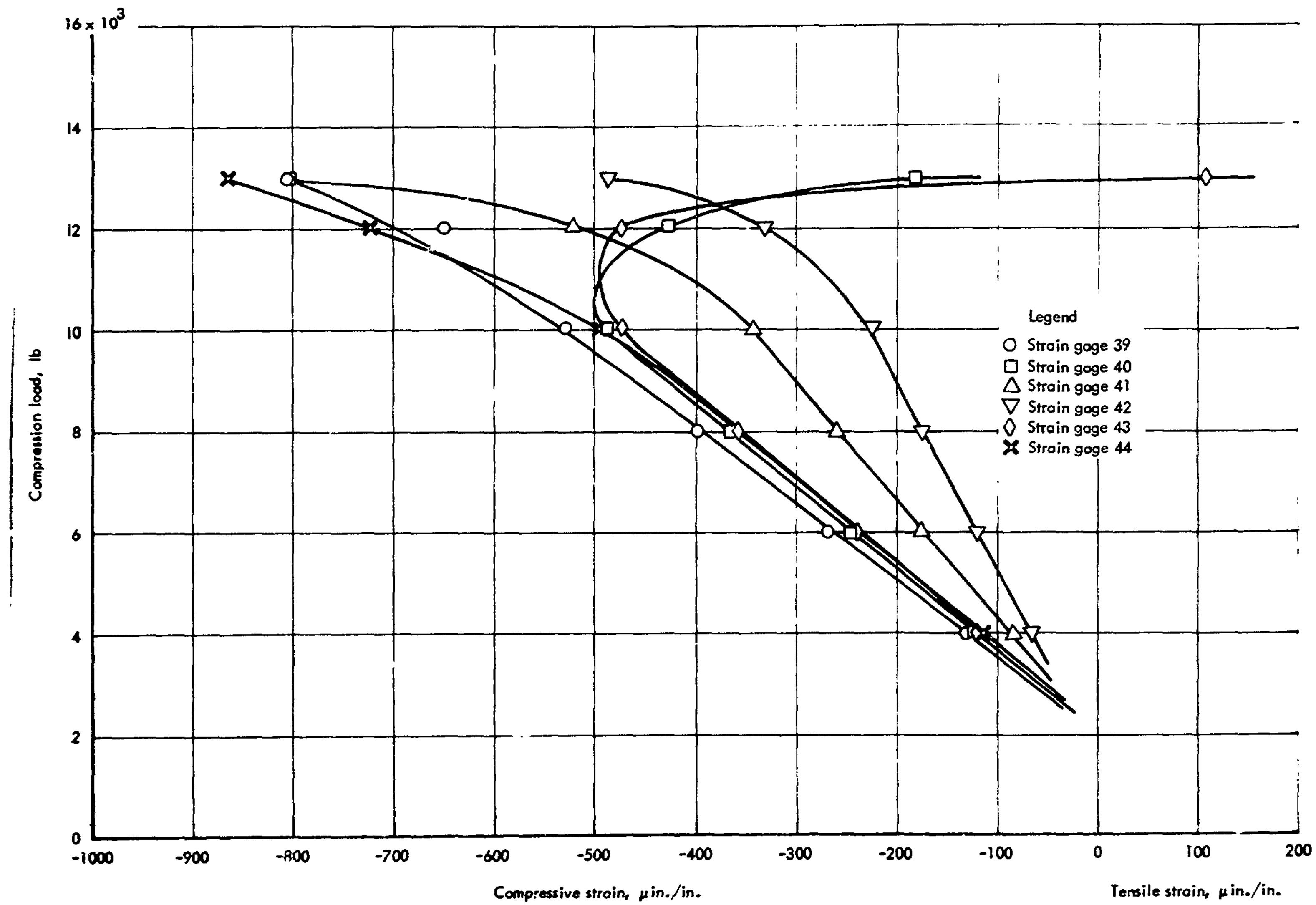

Figure 27-102 (continued)

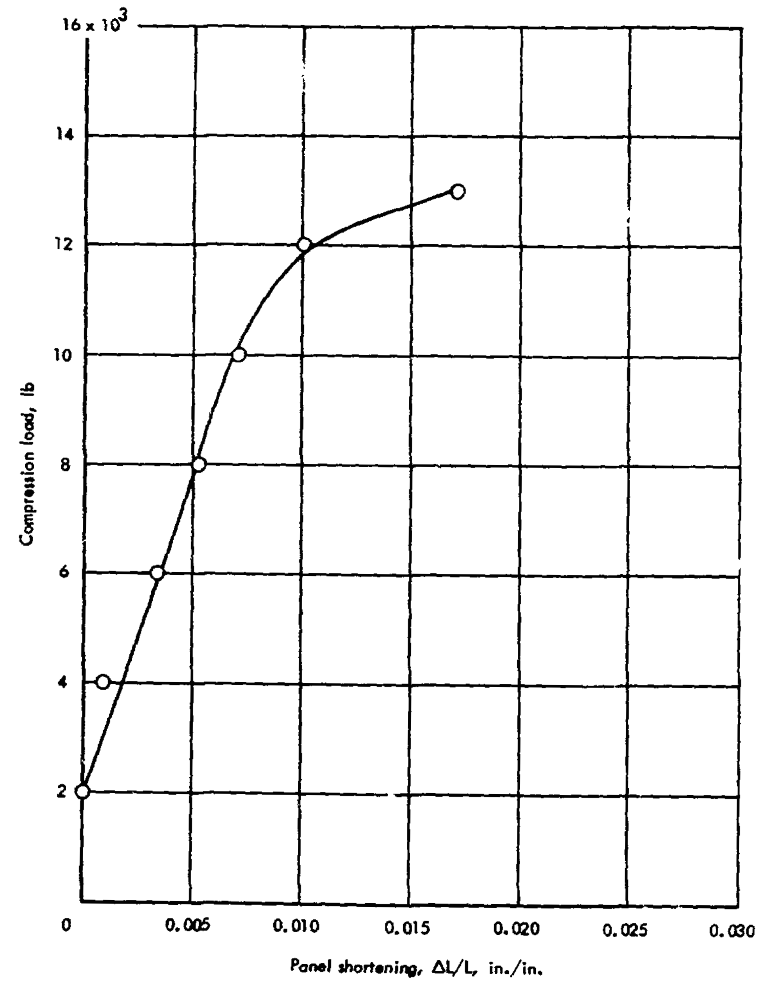

Figure 27-103 Panel shortening curve $\Delta L/L$ for beaded compression panel, room temperature

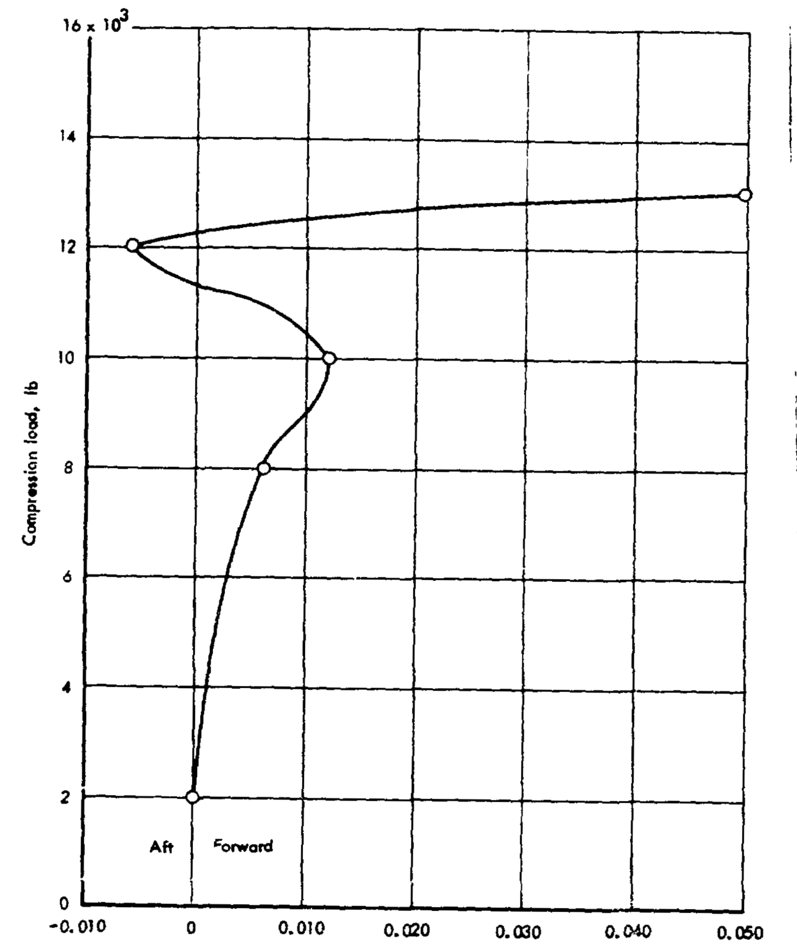

Figure 27-104 Normal deflections for beaded compression panel, room temperature

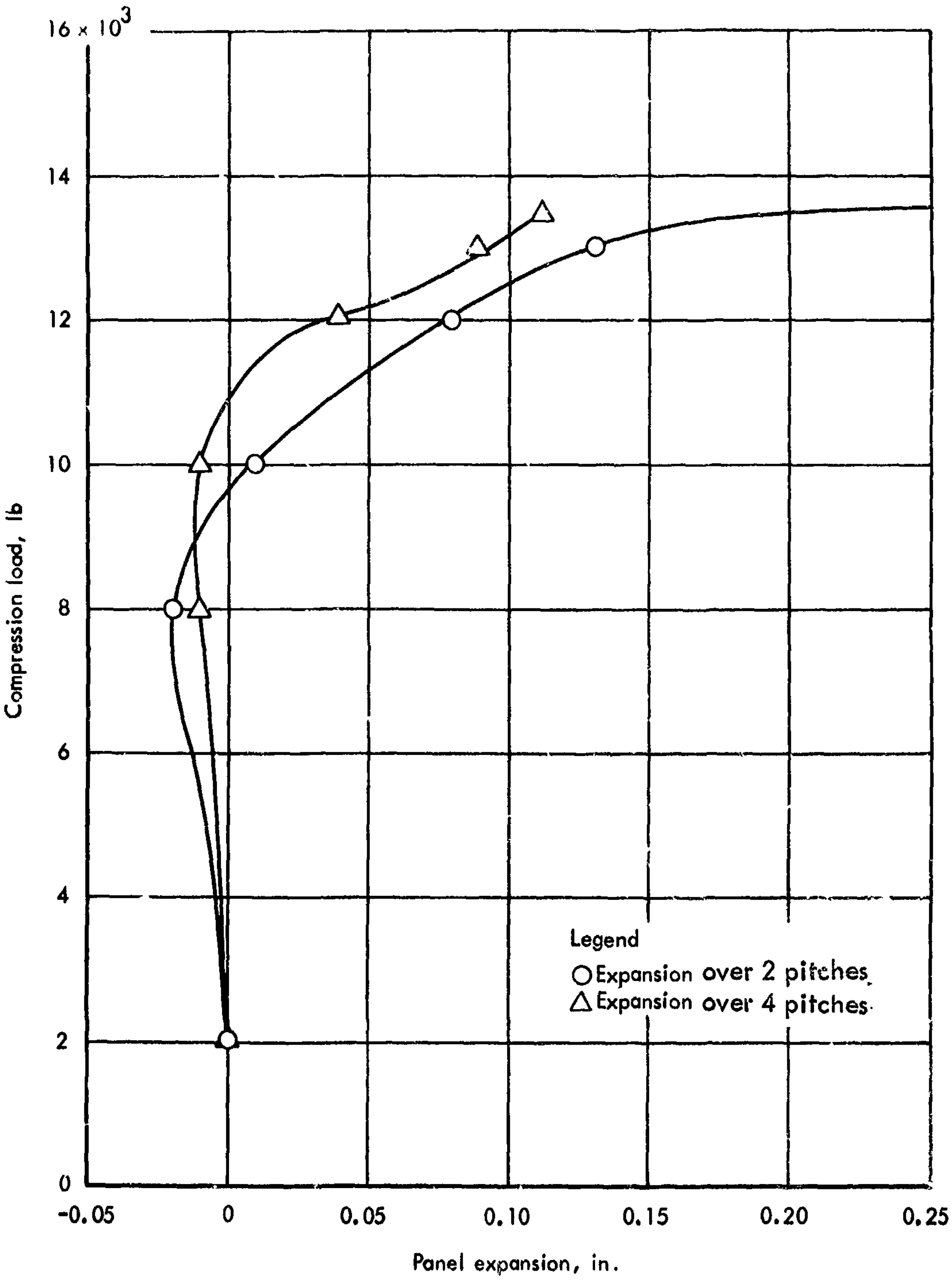

Figure 27-105 Expansion of beaded compression panel due to axial compression loads, room temperature

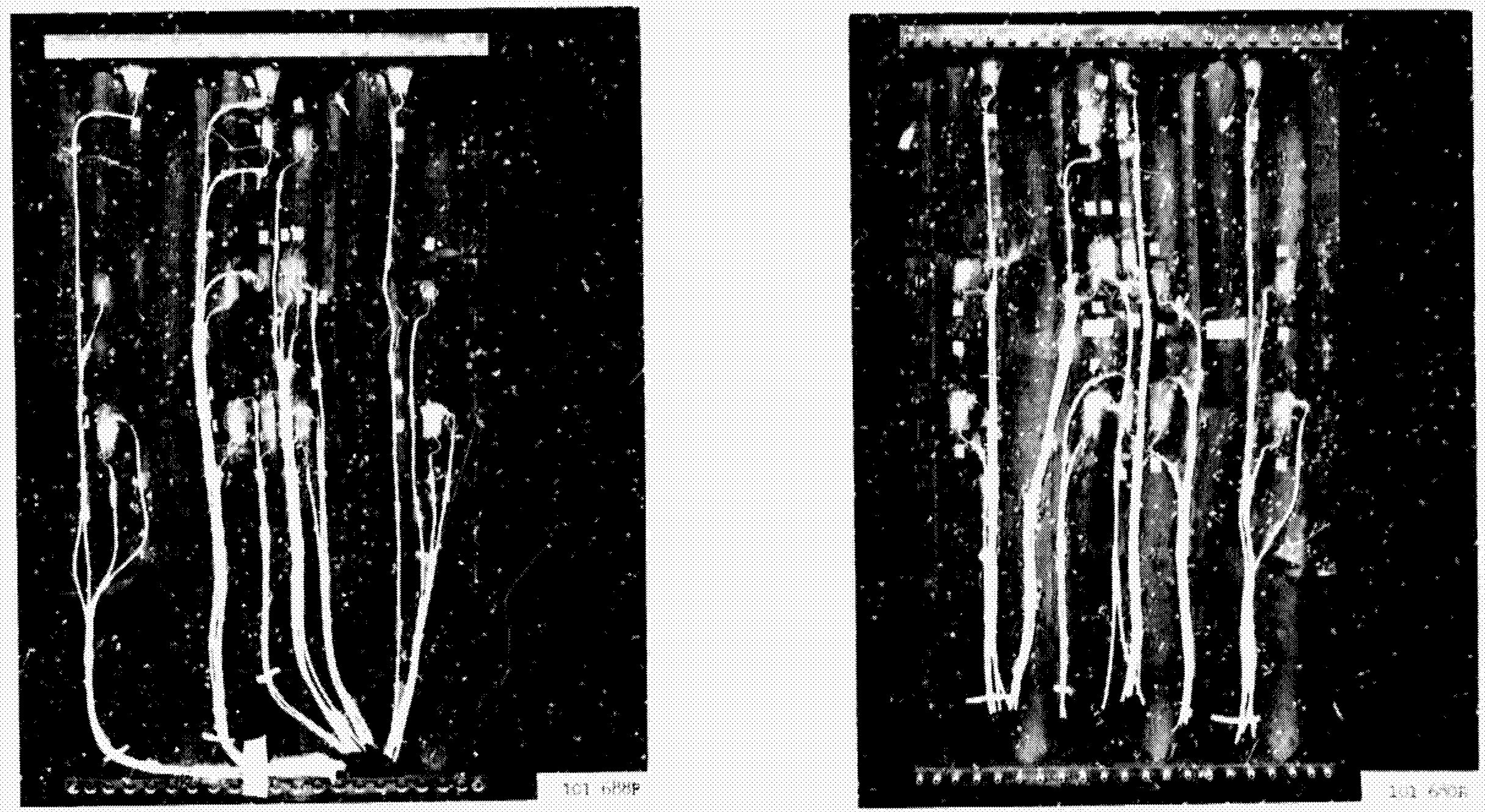

Front

Back

Figure 27-106 Beaded compression panel after failure, room temperature

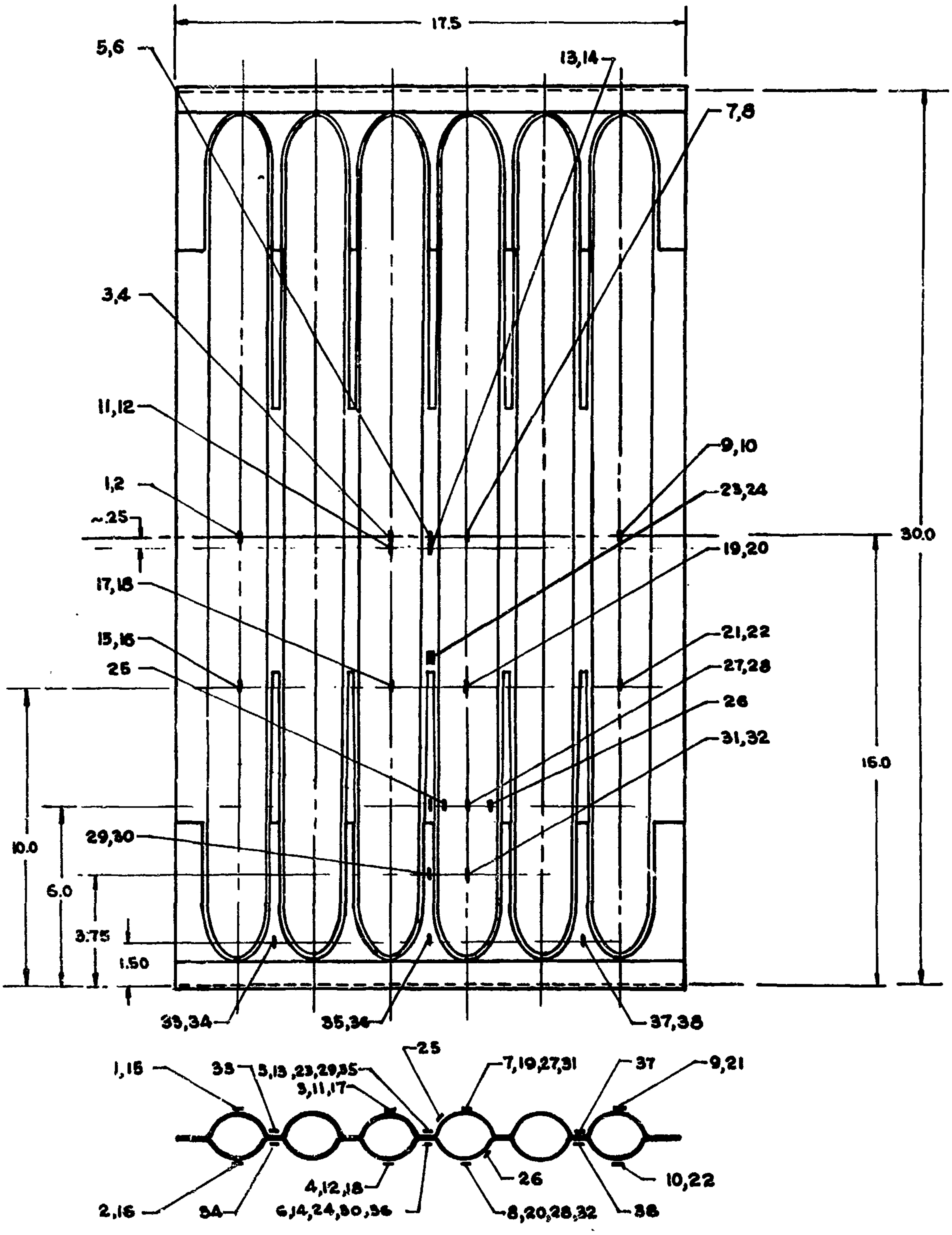

Figure 27-107 Strain gage locations for tubular compression panel

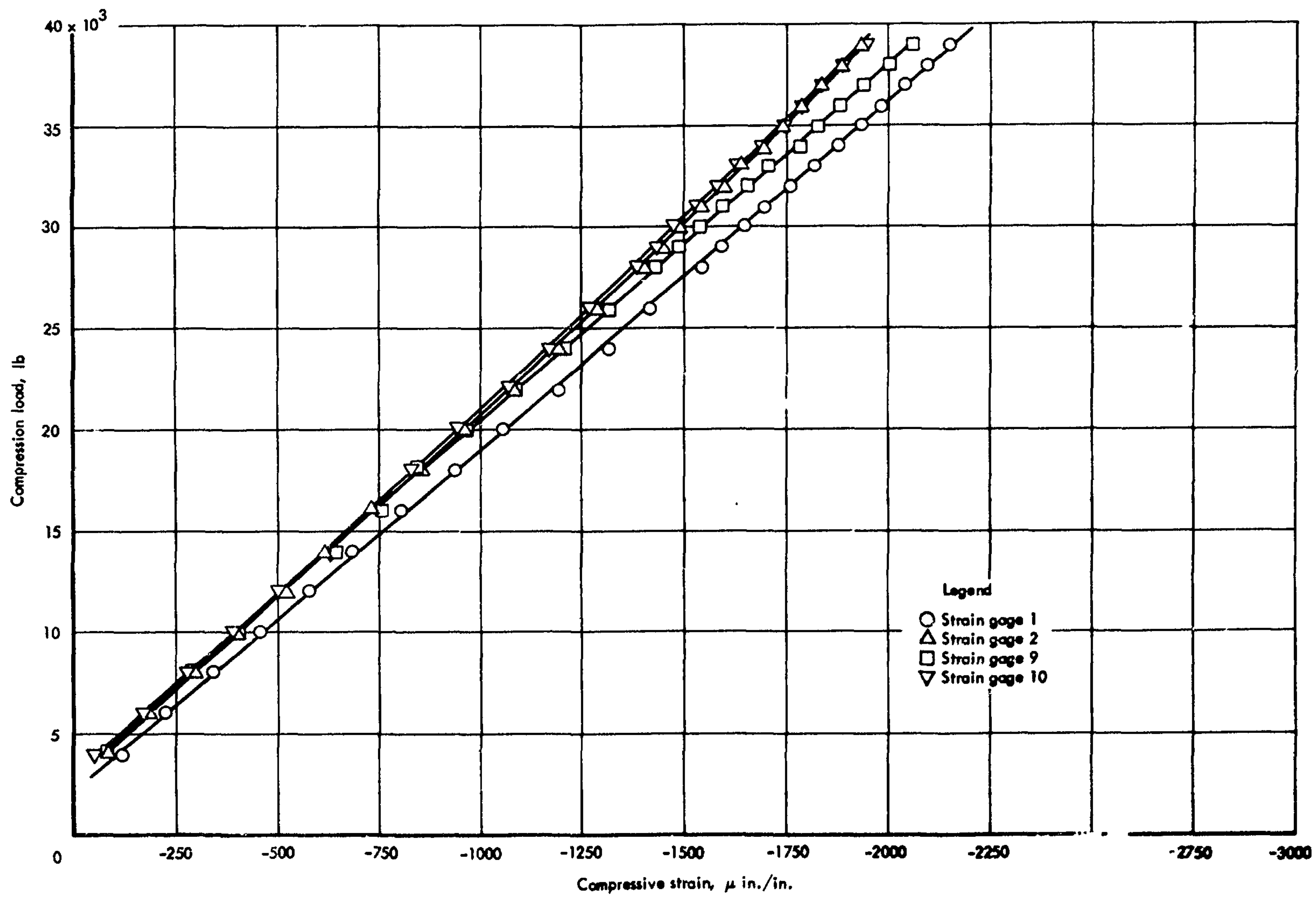

Figure 27-108 Axial strains for tubular compression panel, room temperature

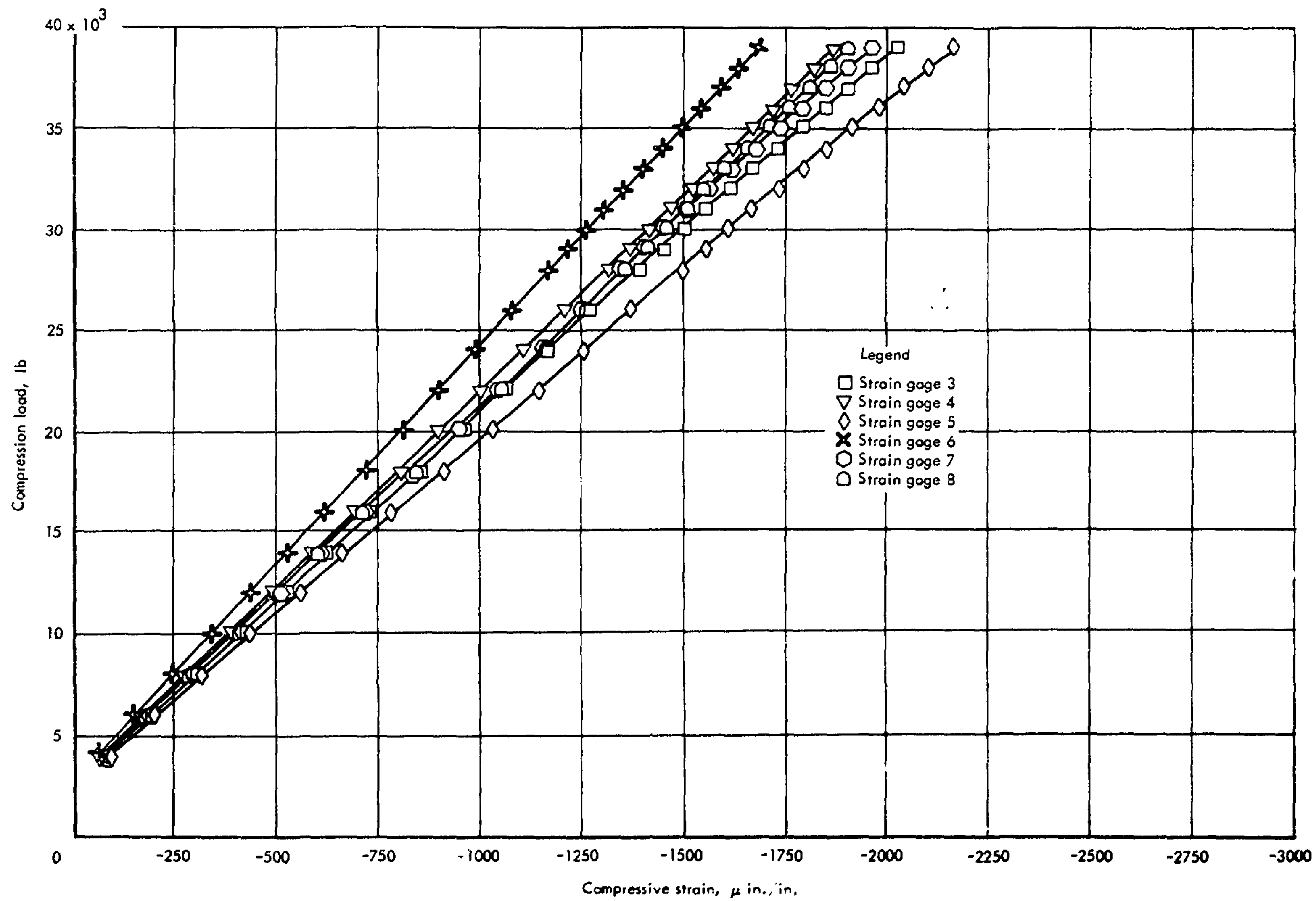

Figure 27-108 (continued)

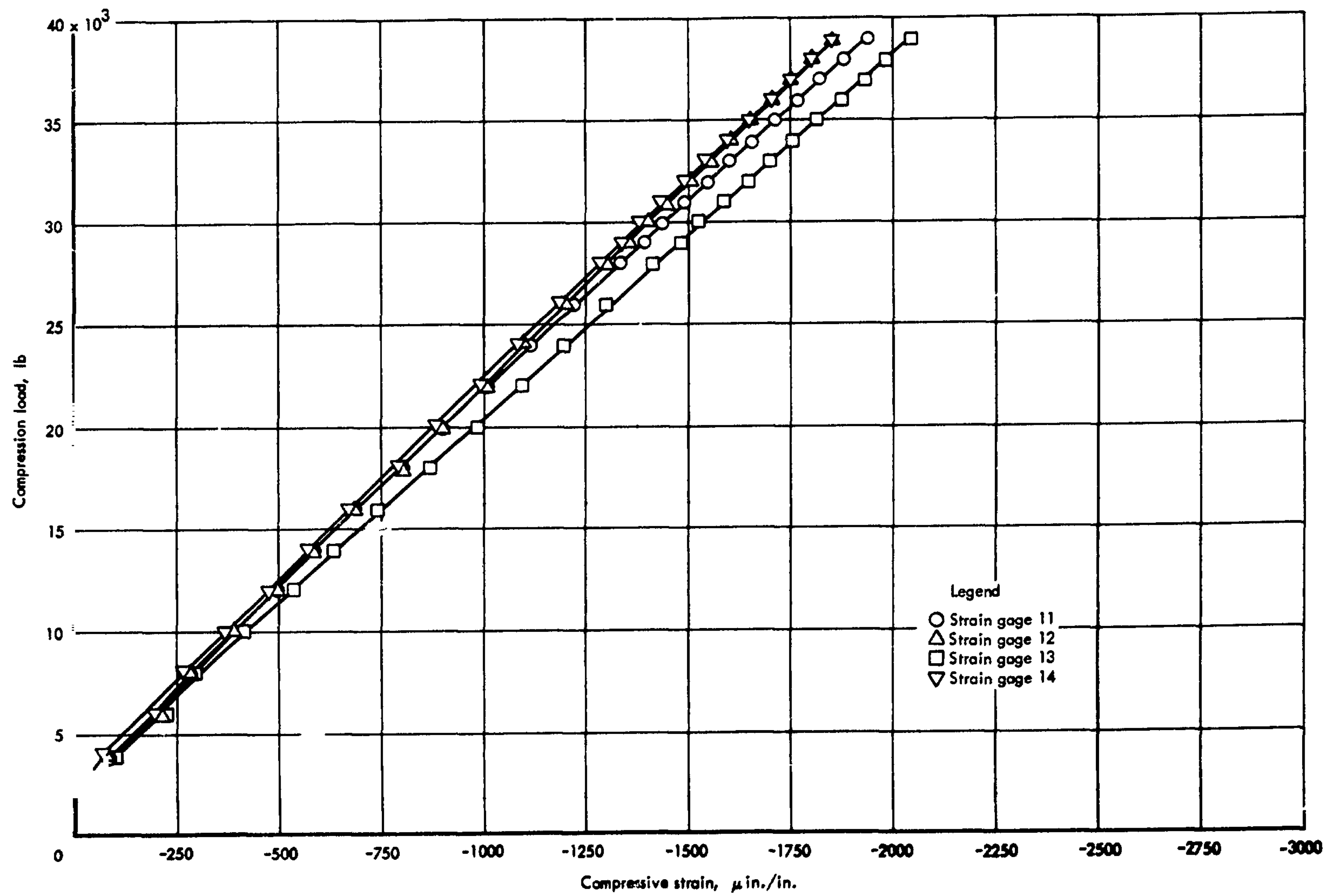

Figure 27-108 (continued)

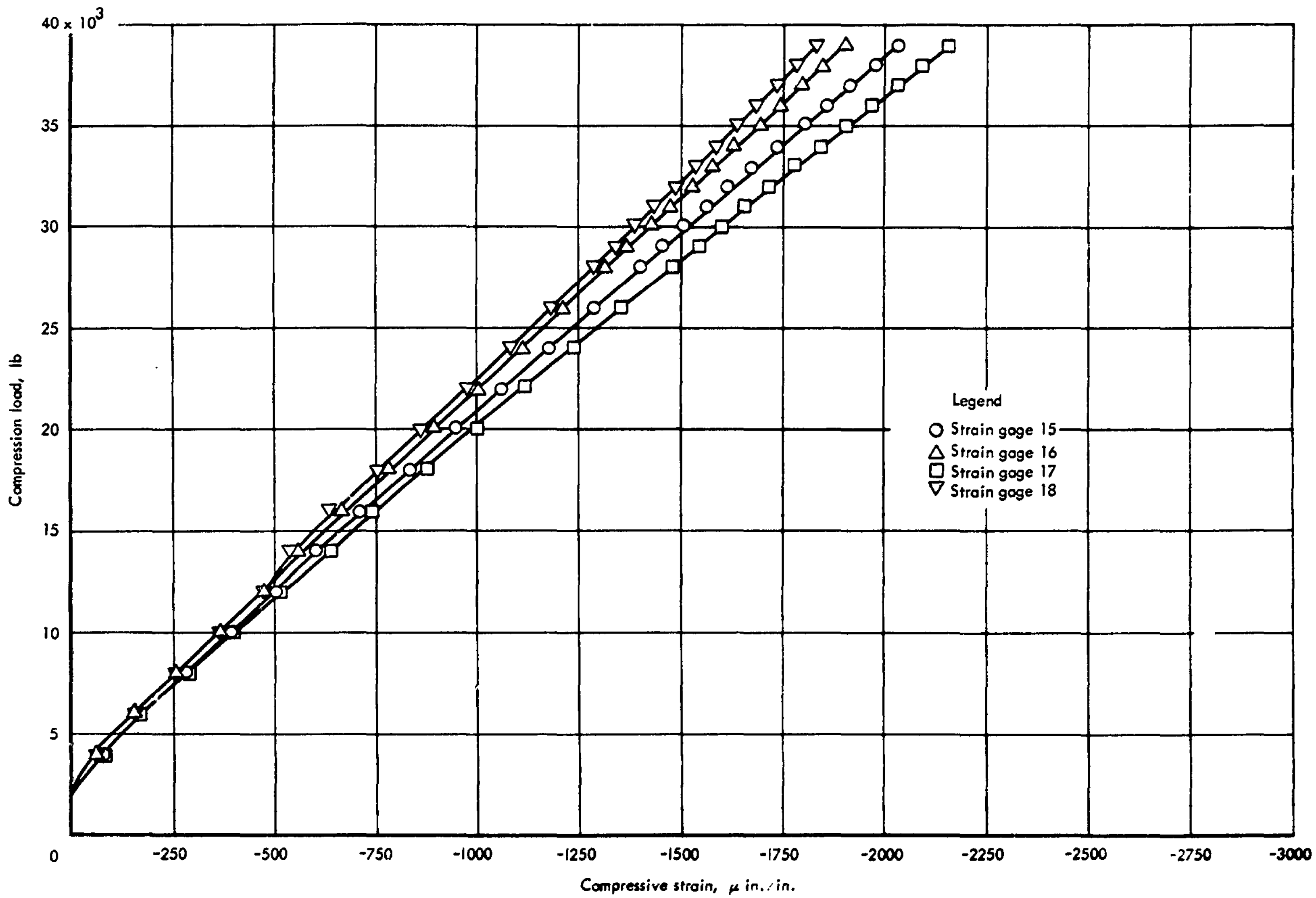

Figure 27-108 (Continued)

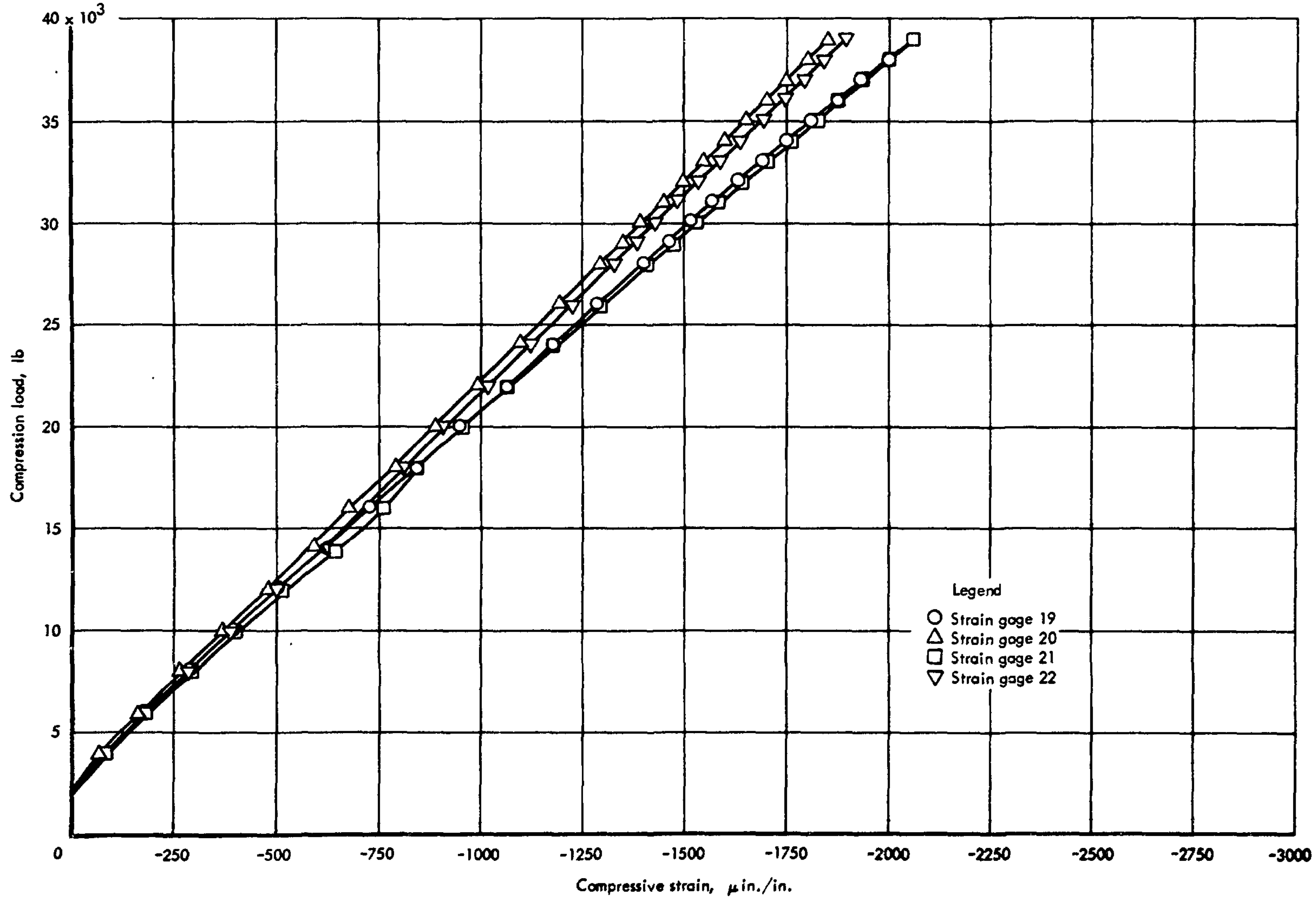

Figure 27-108 (Continued)

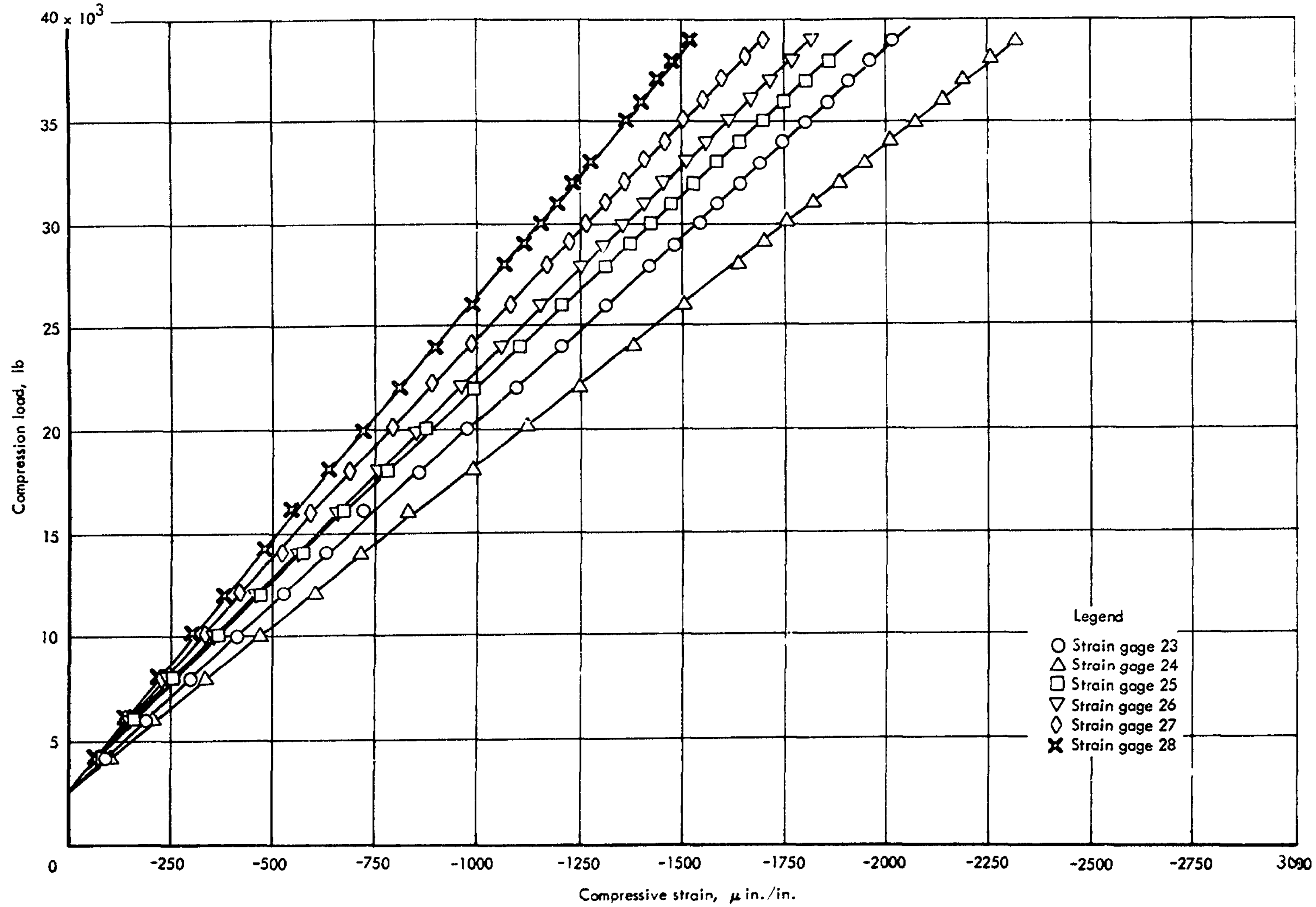

Figure 27-108 (Continued)

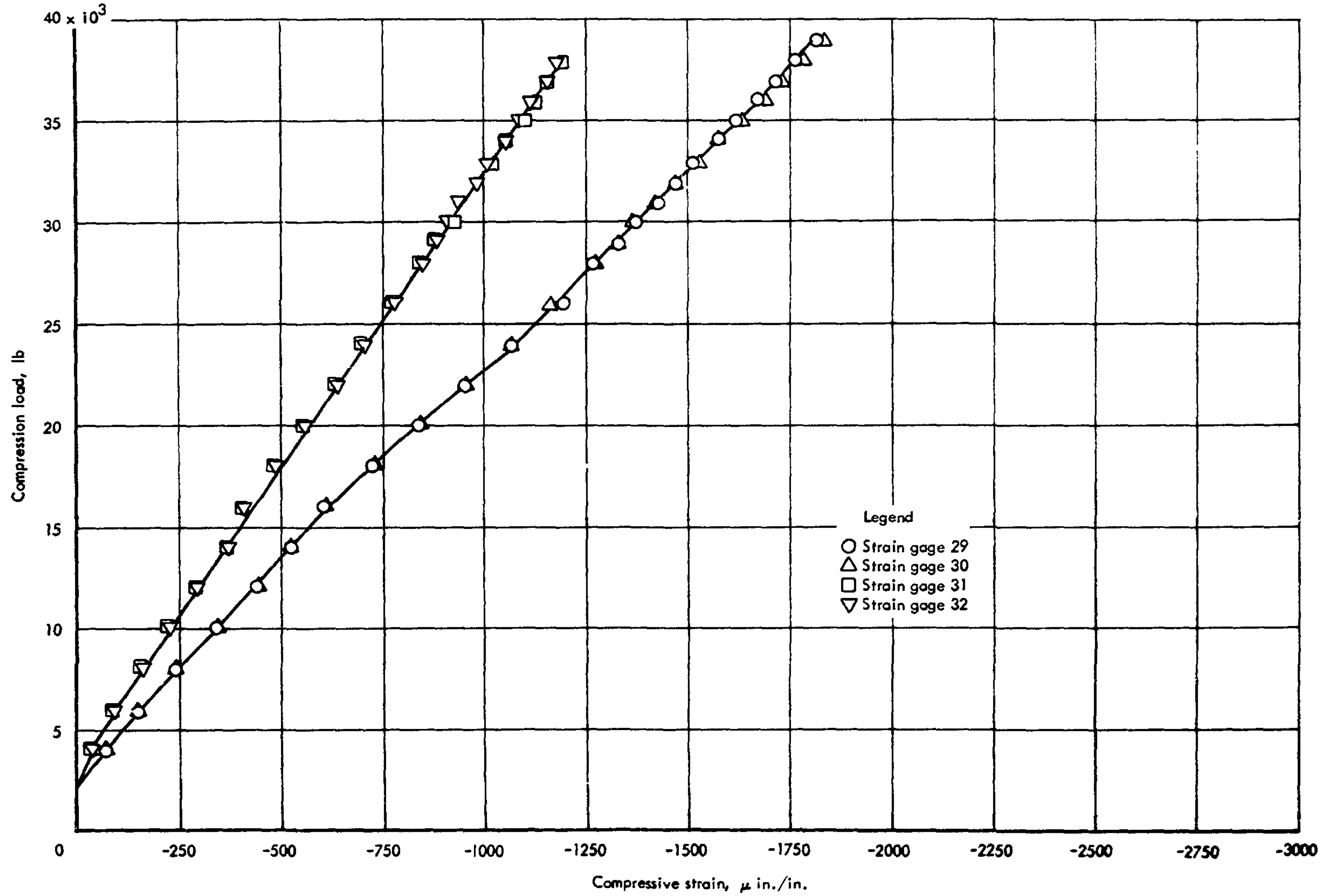

Figure 27-108 (Continued)

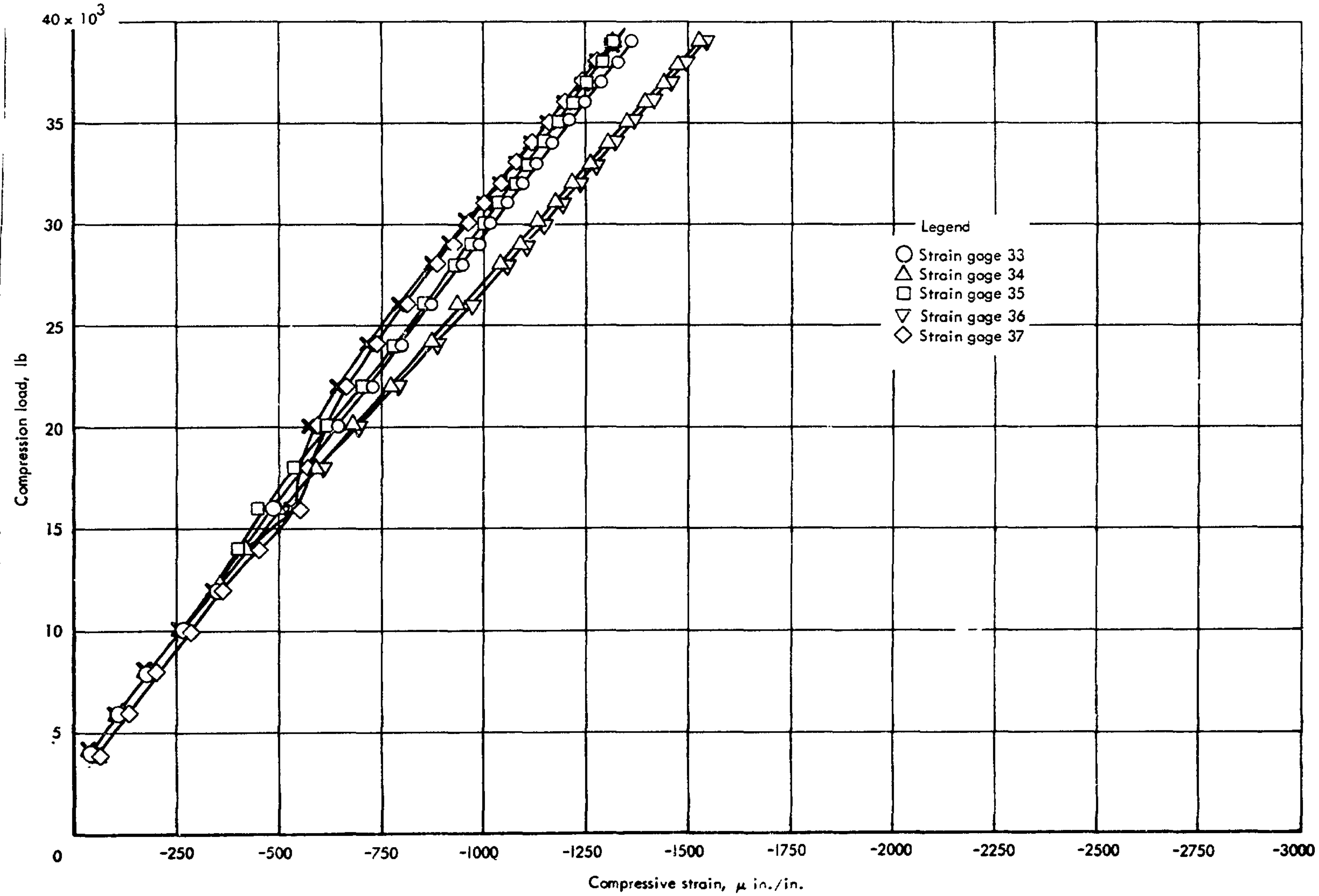

Figure 27-108 (Concluded)

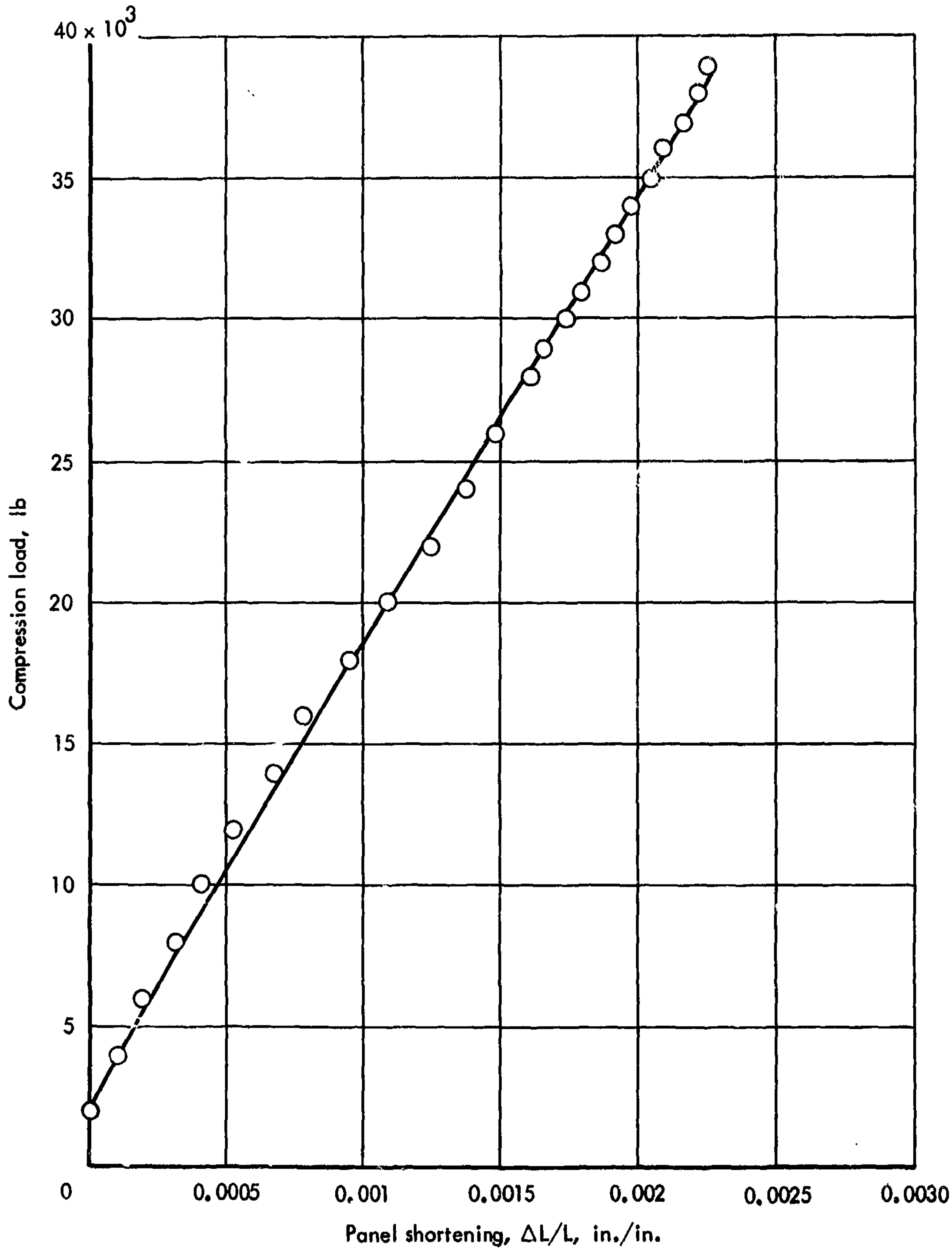

Figure 27-109 Panel shortening curve $\Delta L/L$ for tubular compression panel, room temperature

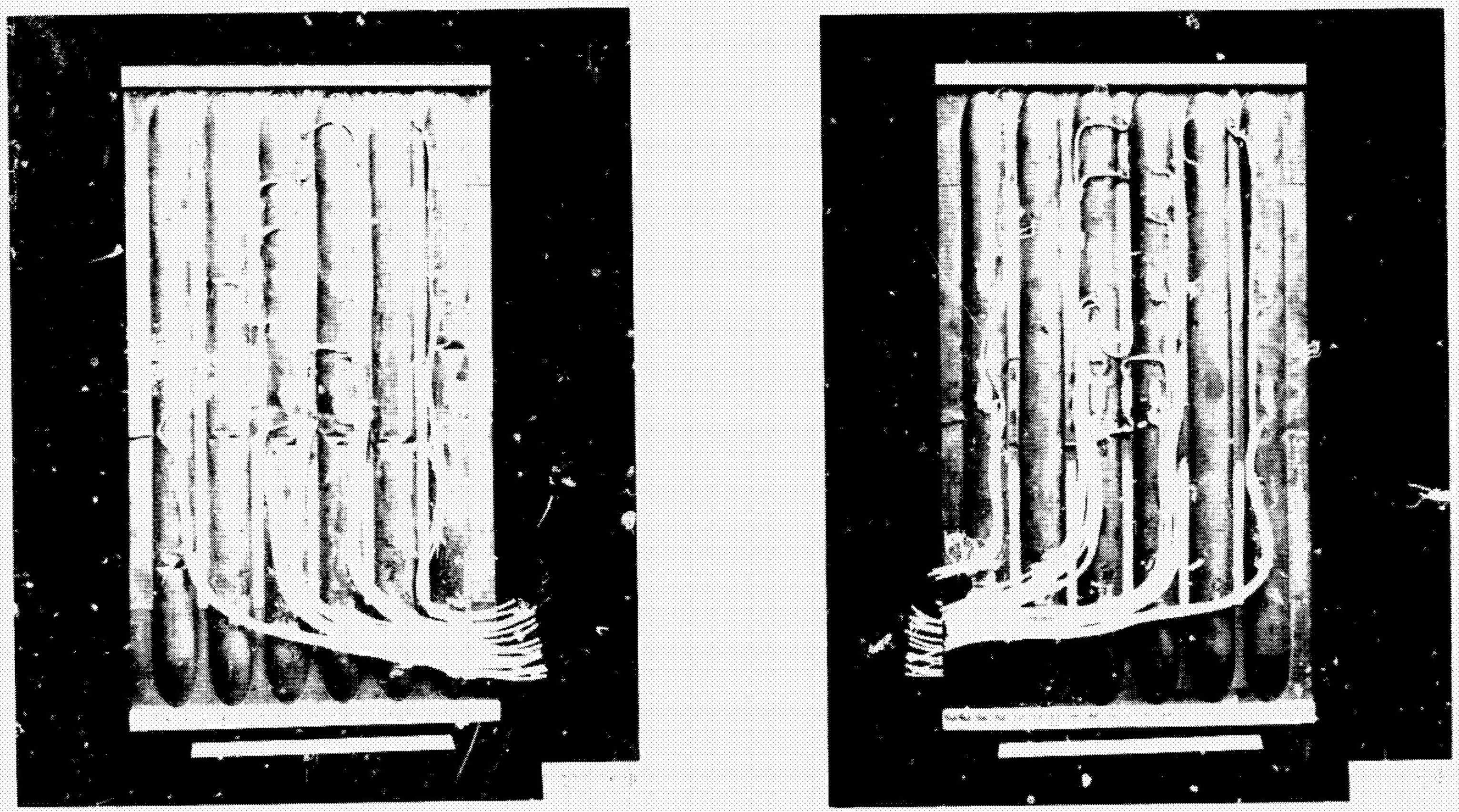

Front   Back

Figure 27-110 Tubular compression panel after failure, room temperature test

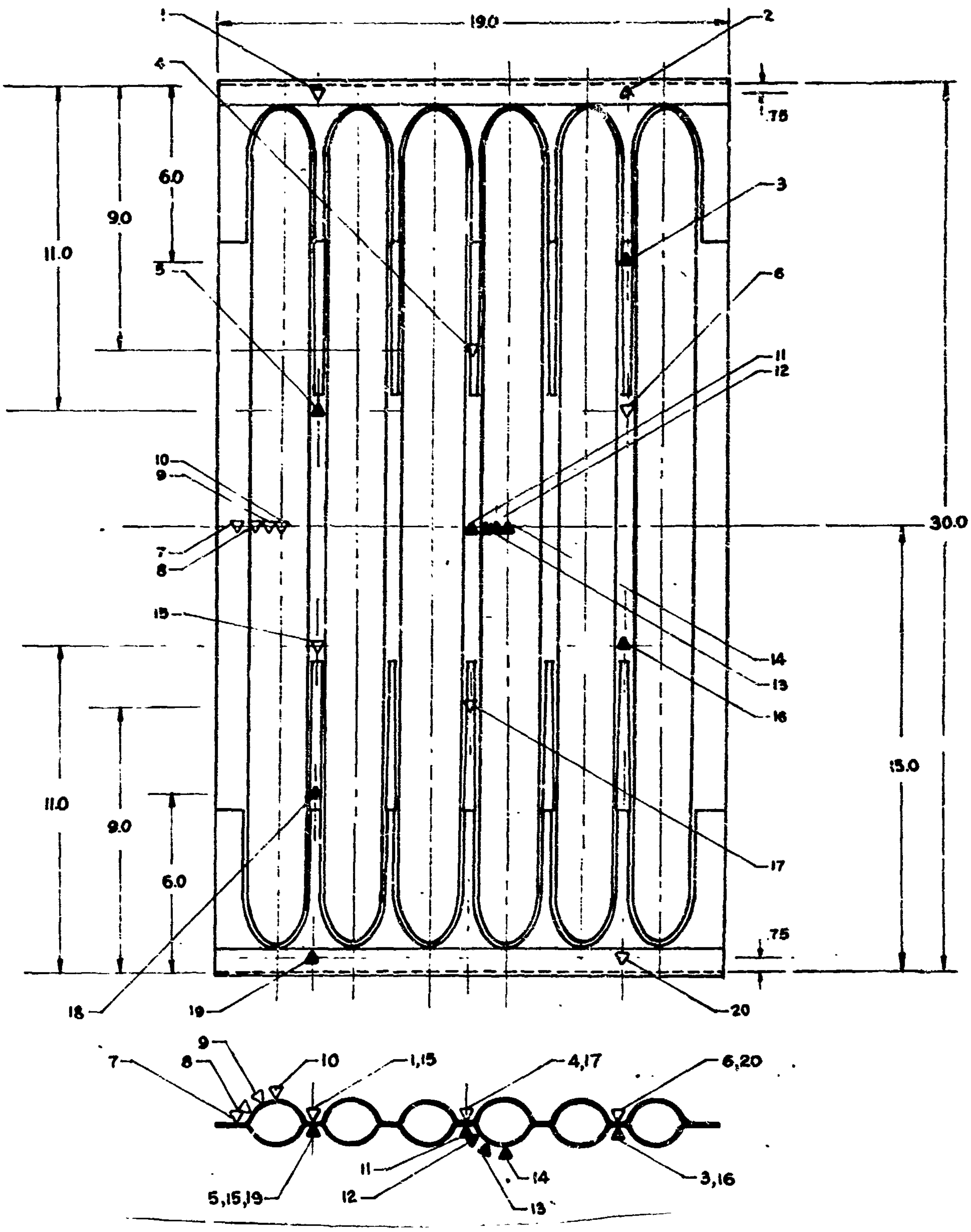

Figure 27-111 Thermocouple location for the tubular compression panel, 1400°F test

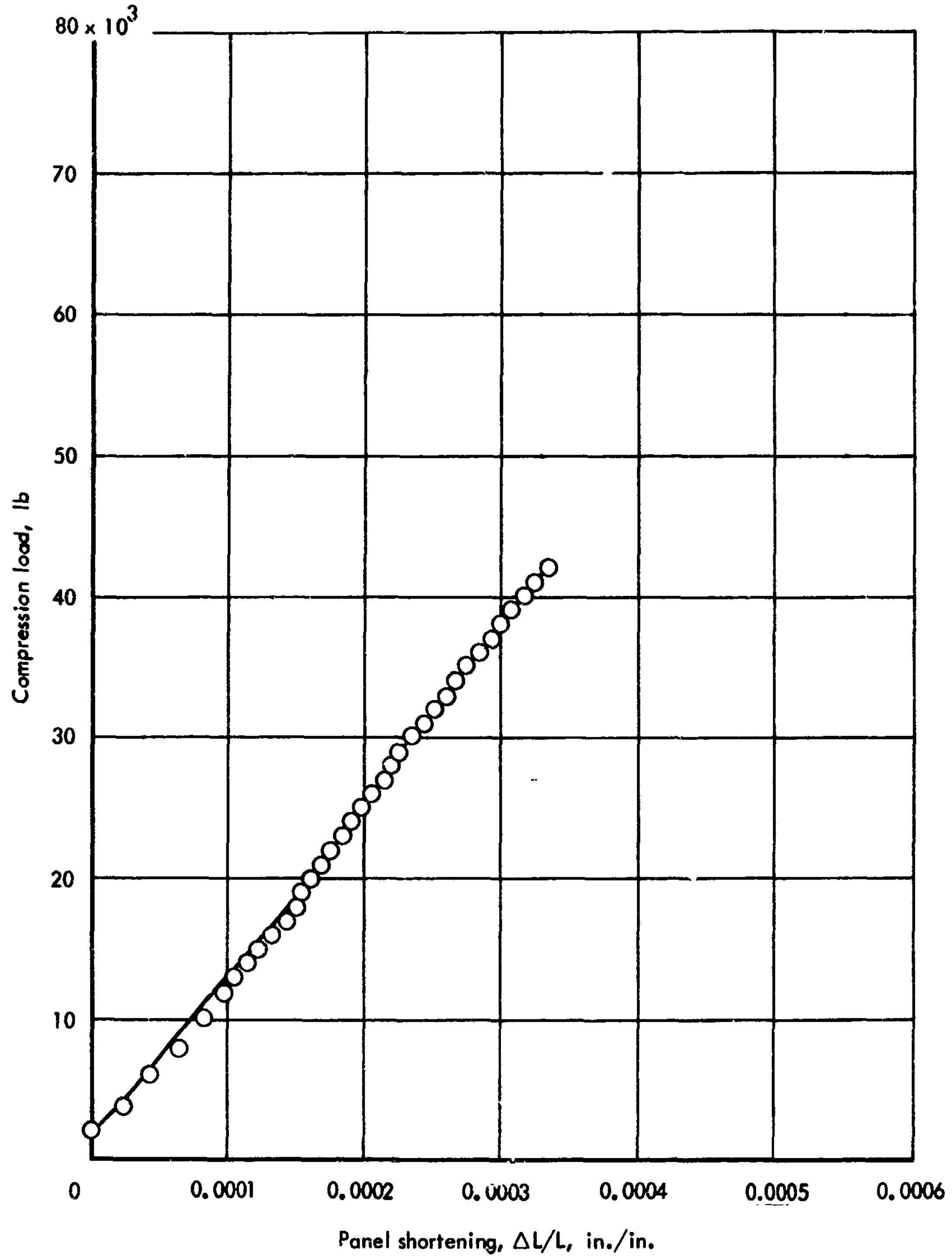

Figure 27-112 Panel shortening curve ΔL/L for tubular compression panel, 1400° test

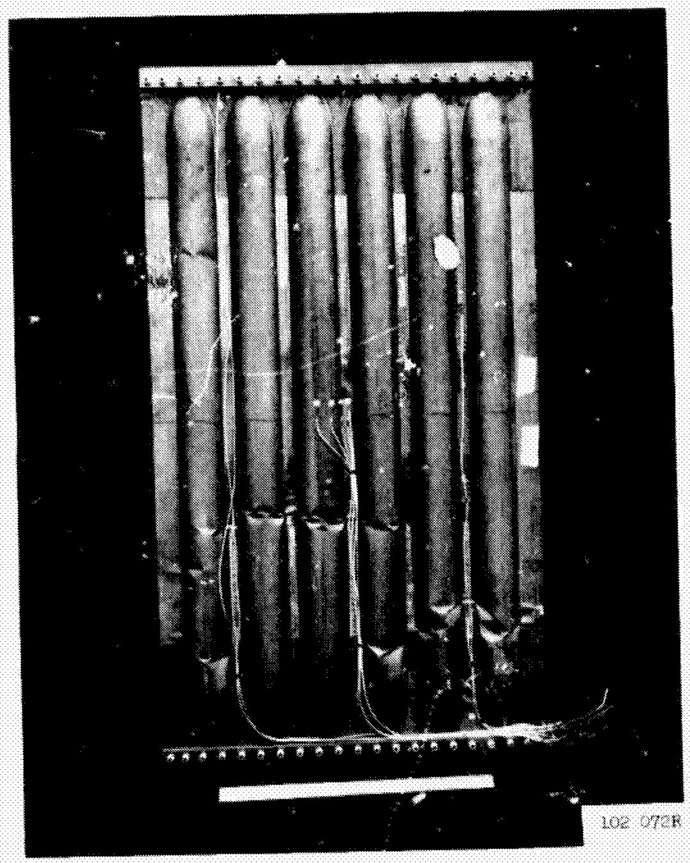

Front

Back

Figure 27-113 Tubular compression panel after failure, 1400°F test

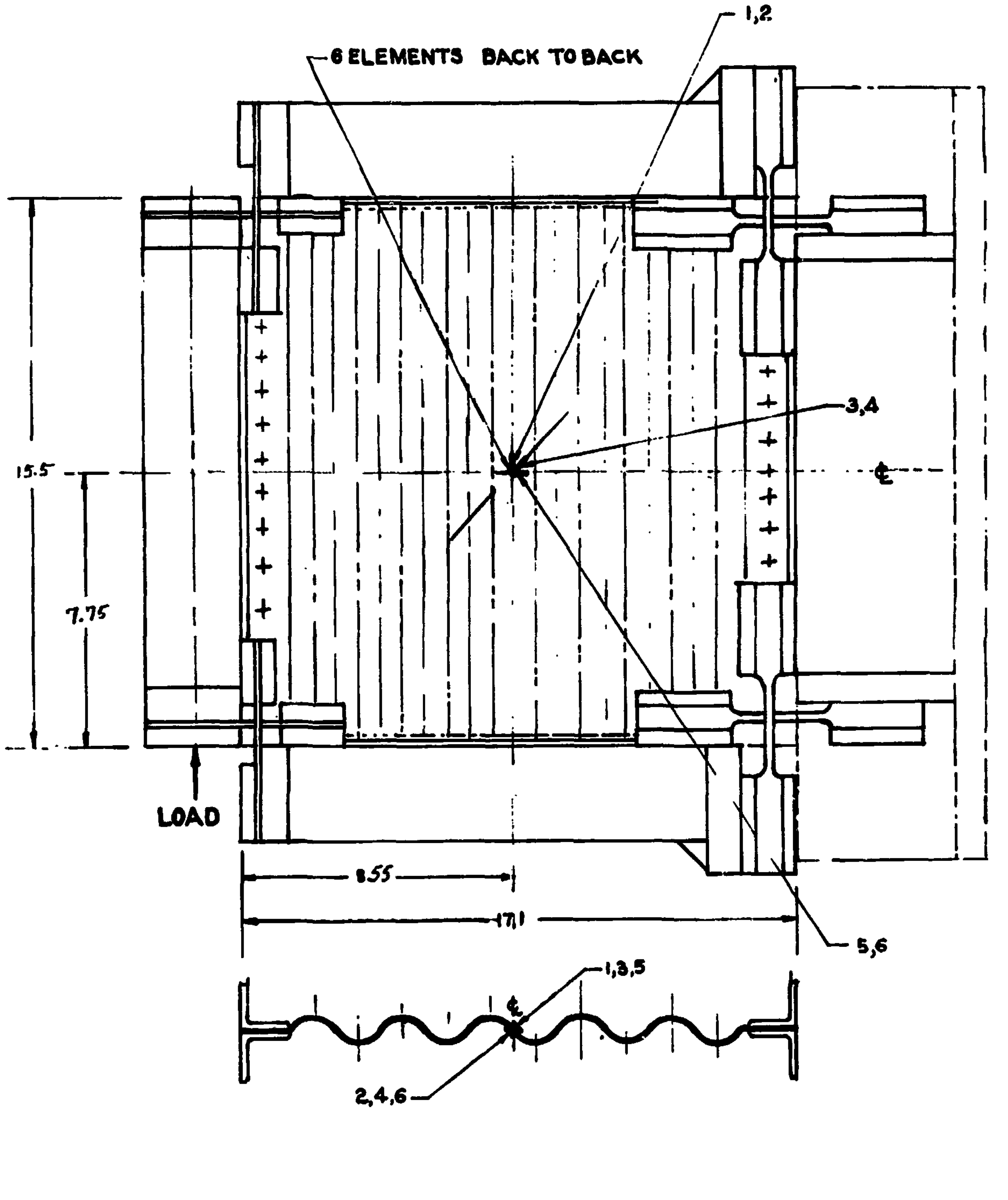

Figure 27-114 Strain gage locations for the circular arc corrugation shear panel

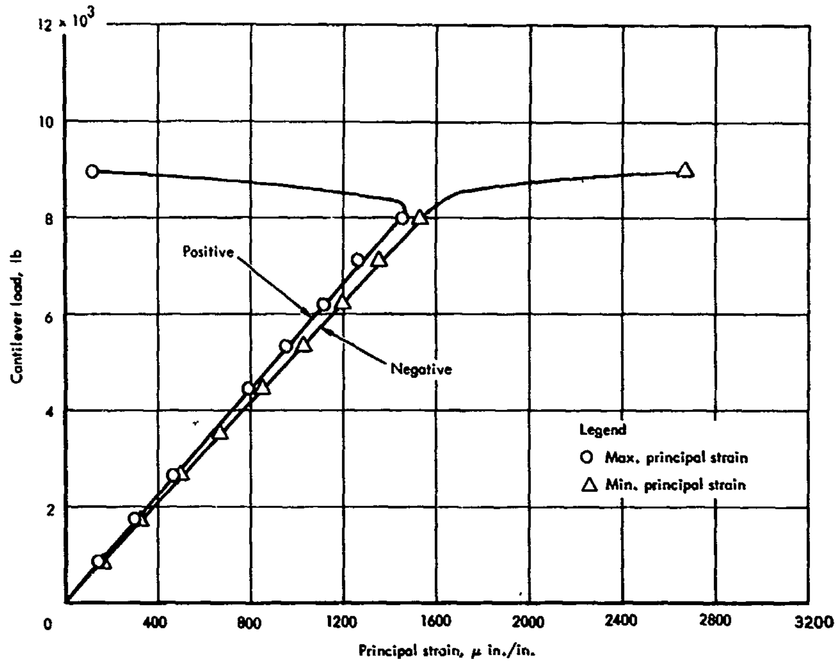

Figure 27-115 Relationship of principal strains and applied vertical cantilever loading for circular arc corrugation shear panel (TIG weld with Rene' 41 filler wire), room temperature

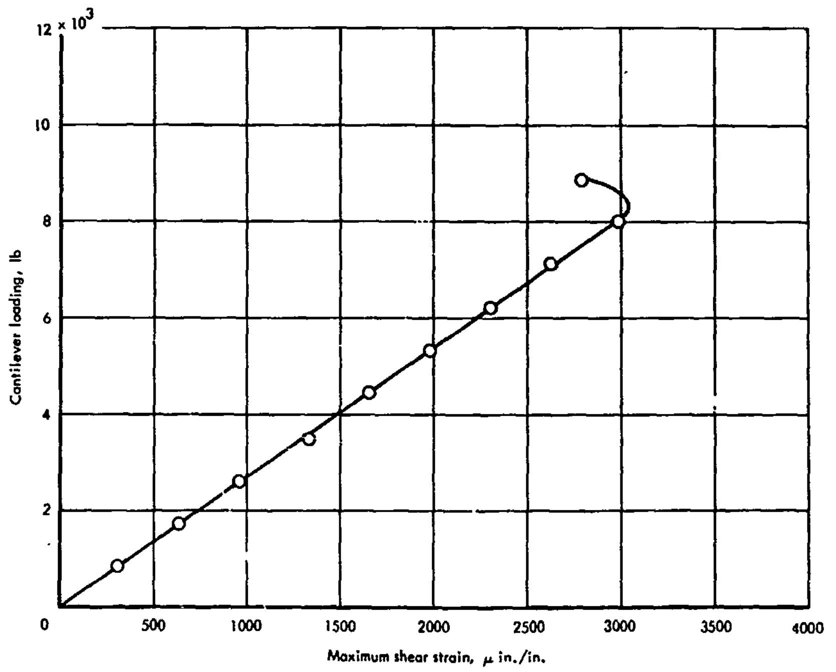

Figure 27-116 Relationship of shear strain and applied vertical cantilever loading for circular arc corrugation shear panel (TIG weld with Rene' 41 filler wire), room temperature

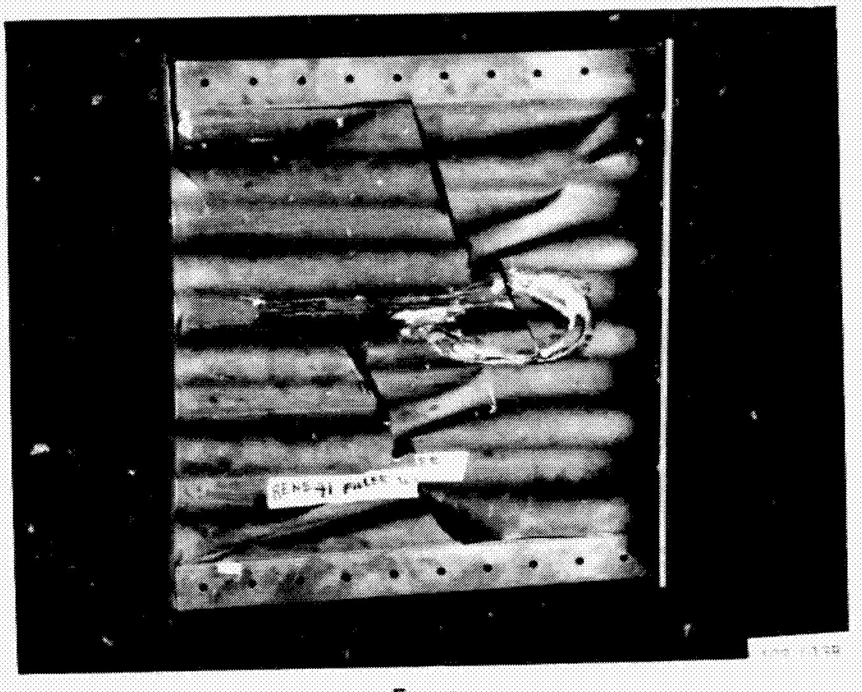

Front

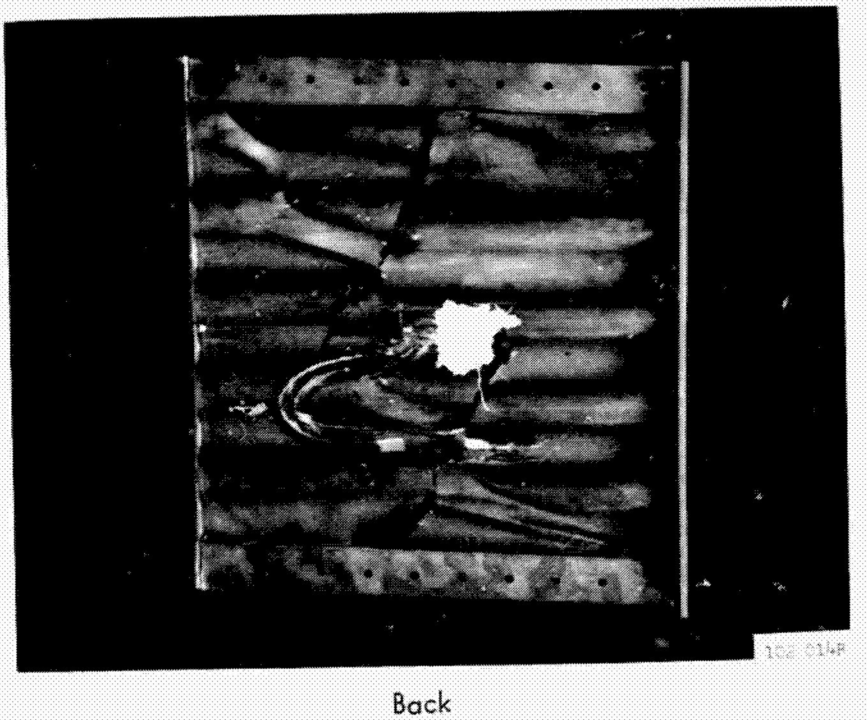

Back

Figure 27-117 Circular arc corrugation shear panel (TIG weld with Rene 41 filler wire) after failure, room temperature test

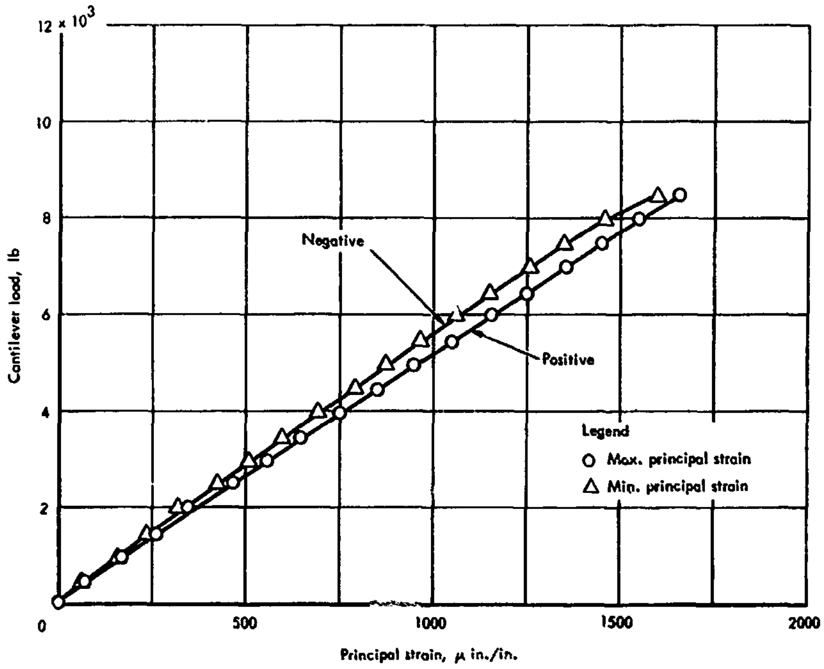

Figure 27-118 Relationship of principal strains and applied vertical cantilever loading for circular arc corrugation shear panel (TIG weld with Hastelloy W filler wire), room temperature

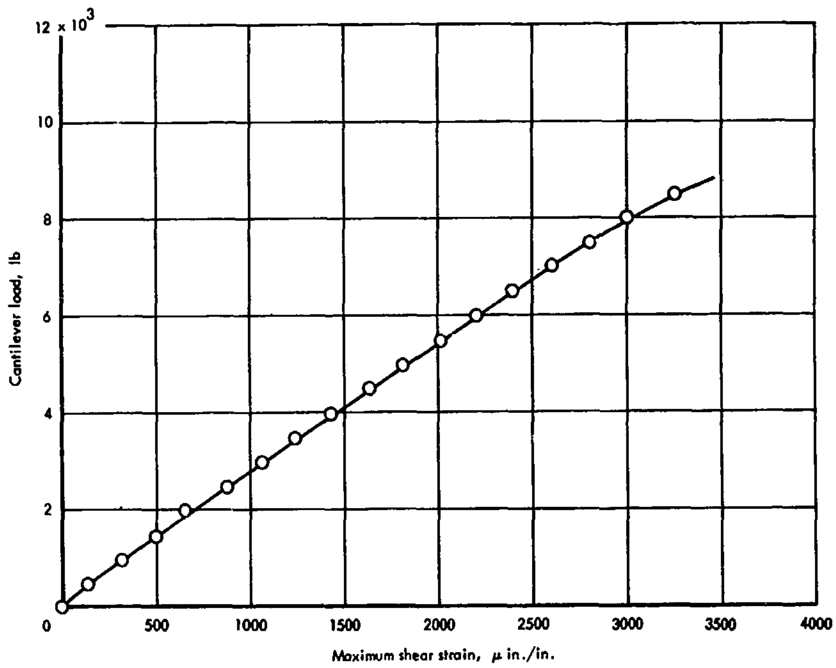

Figure 27-119 Relationship of shear strain and applied vertical cantilever loading for circular arc corrugation shear panel (TIG weld with Hastelloy W filler wire), room temperature

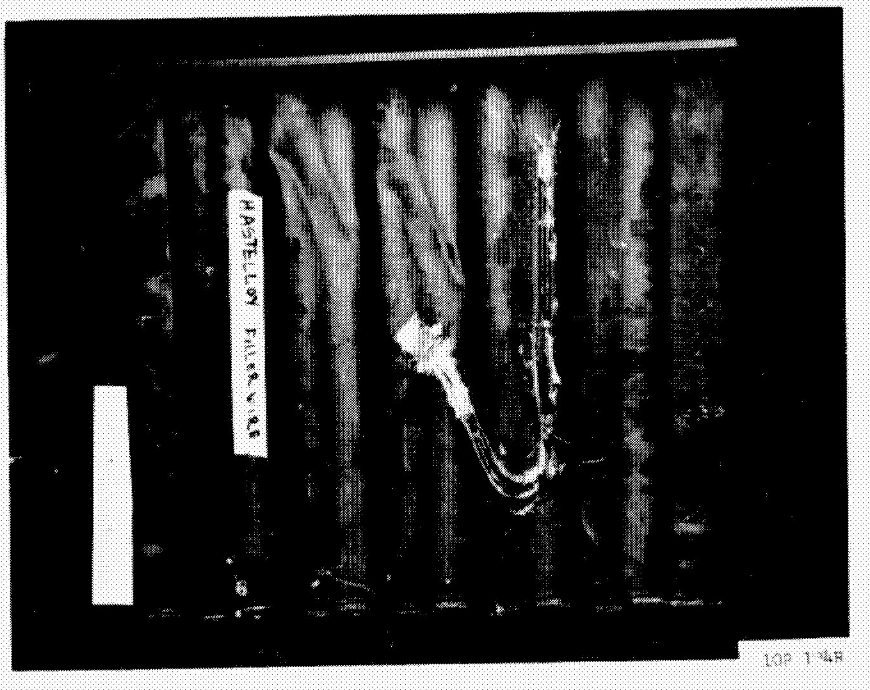

Front

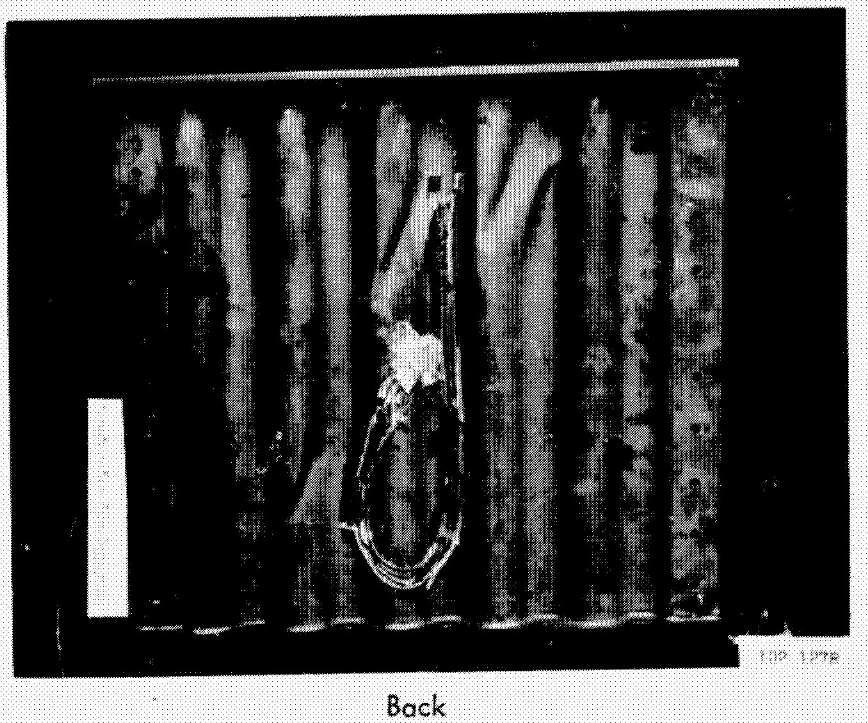

Back

Figure 27-120 Circular arc corrugation shear panel (TIG weld with Hastelloy W filler wire) after failure, room temperature

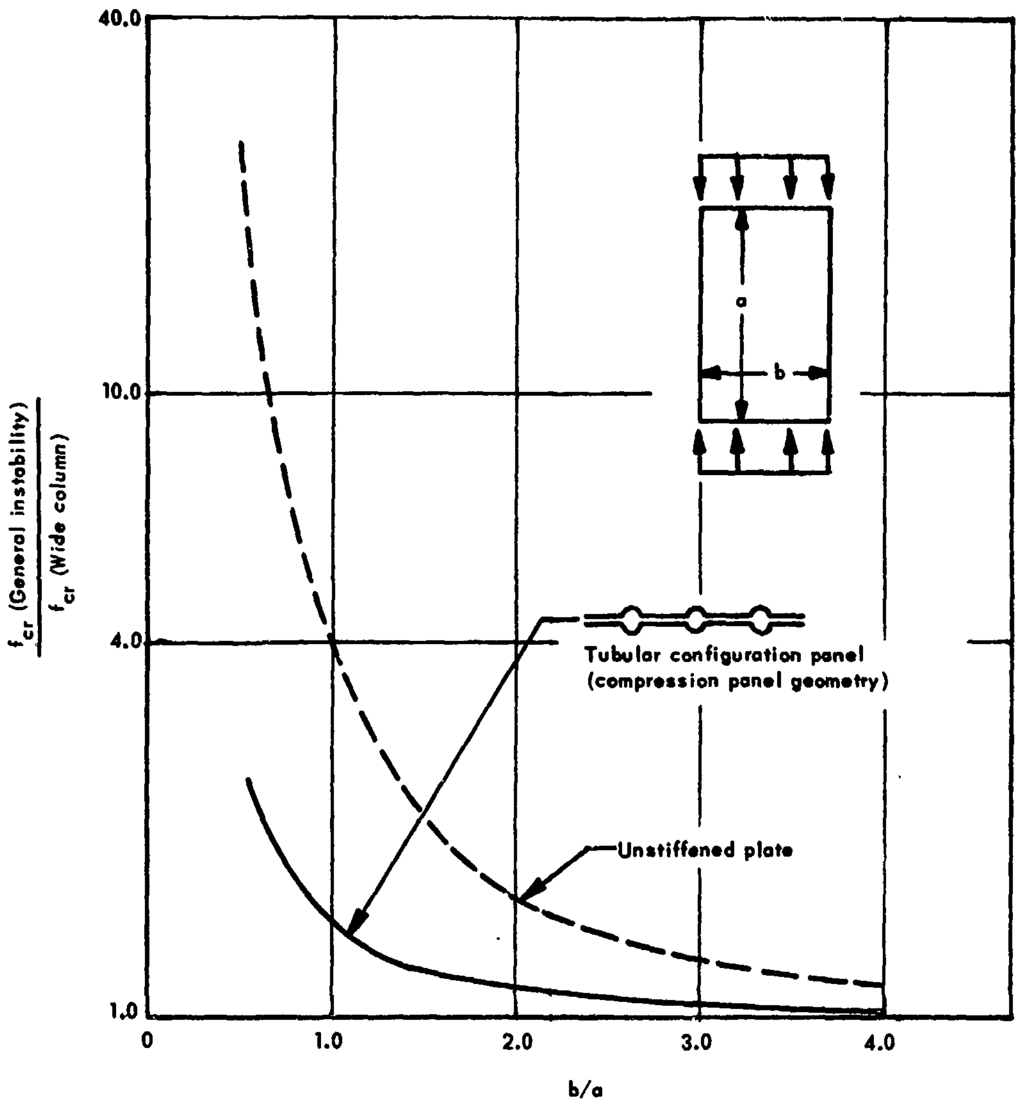

Figure 27-121 Degree of conservatism in the wide-column analysis as applied to compression panels vs. width-to-length ratio

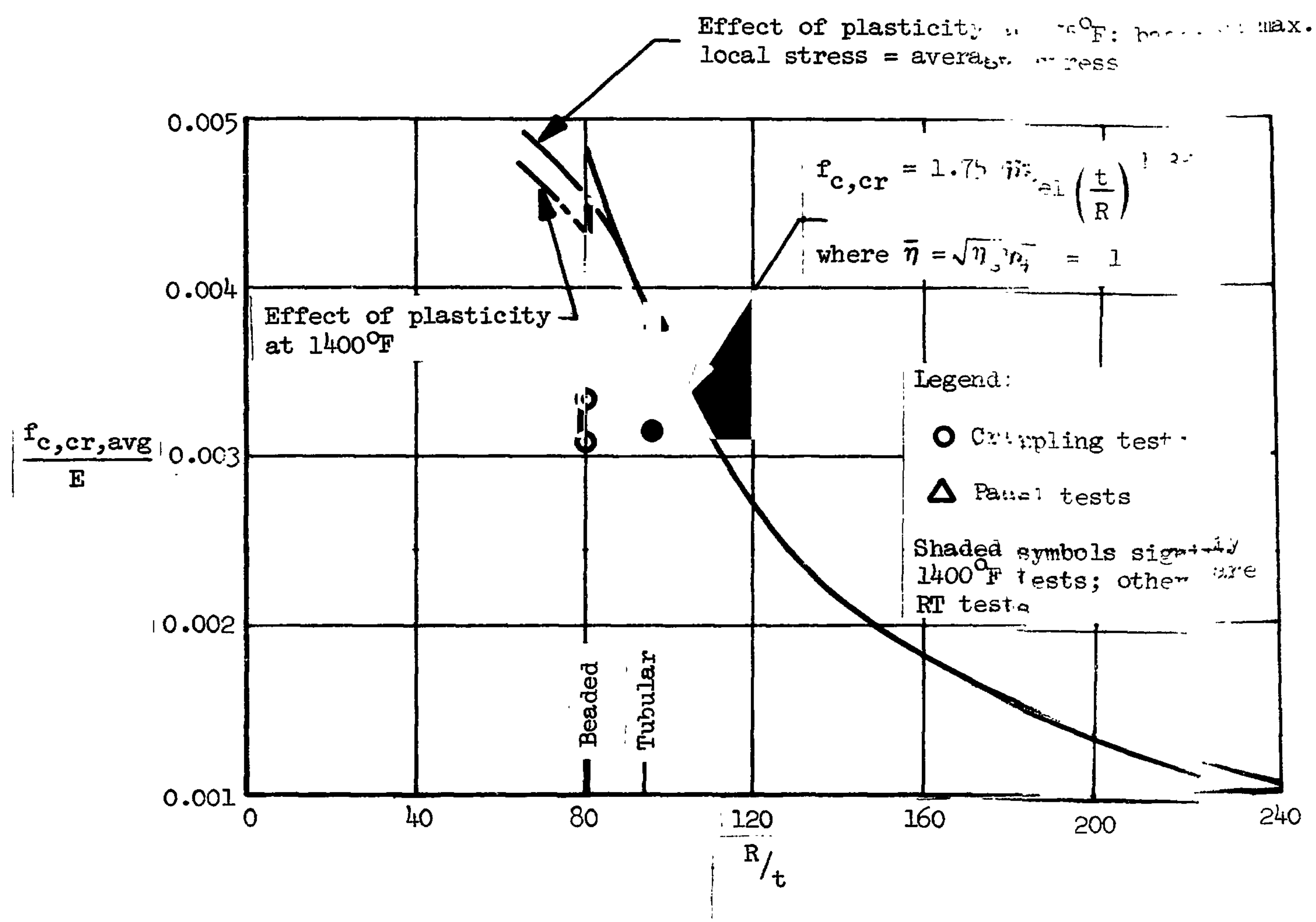

Figure 27-122. Comparison of tubular and beaded configuration ini[illegible] bucklin[illegible] test results with predictions

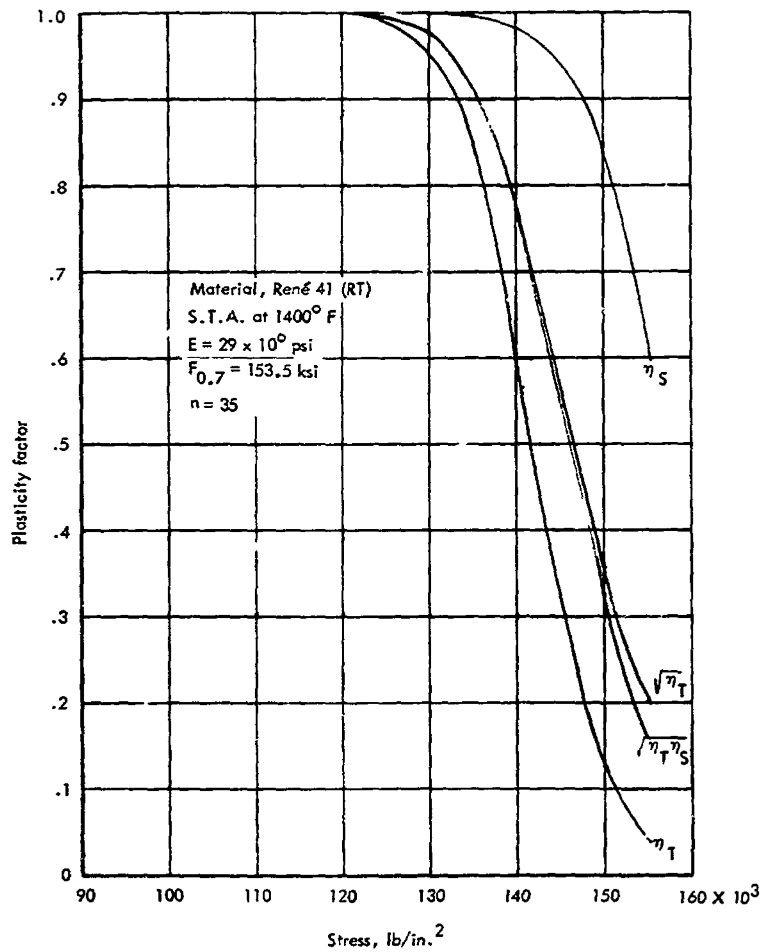

Figure 27-123 Plasticity factors for 0.016-in. René 41 sheet at room temperature

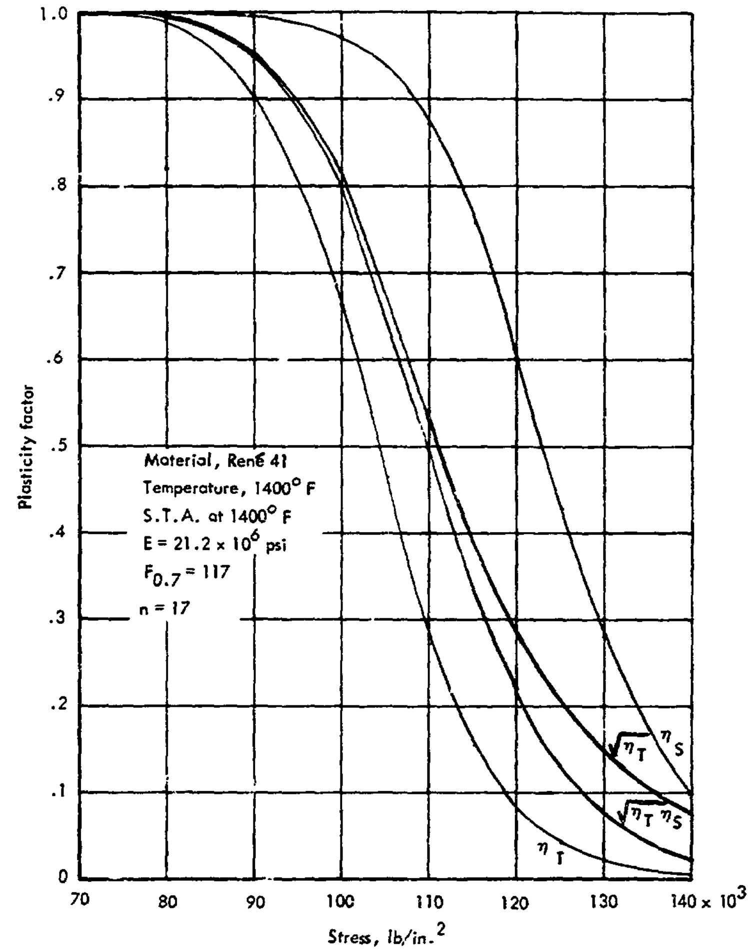

Figure 27-124 Plasticity factors for 0.016-in. - 0.019-in. René 41 sheet at 1400° F

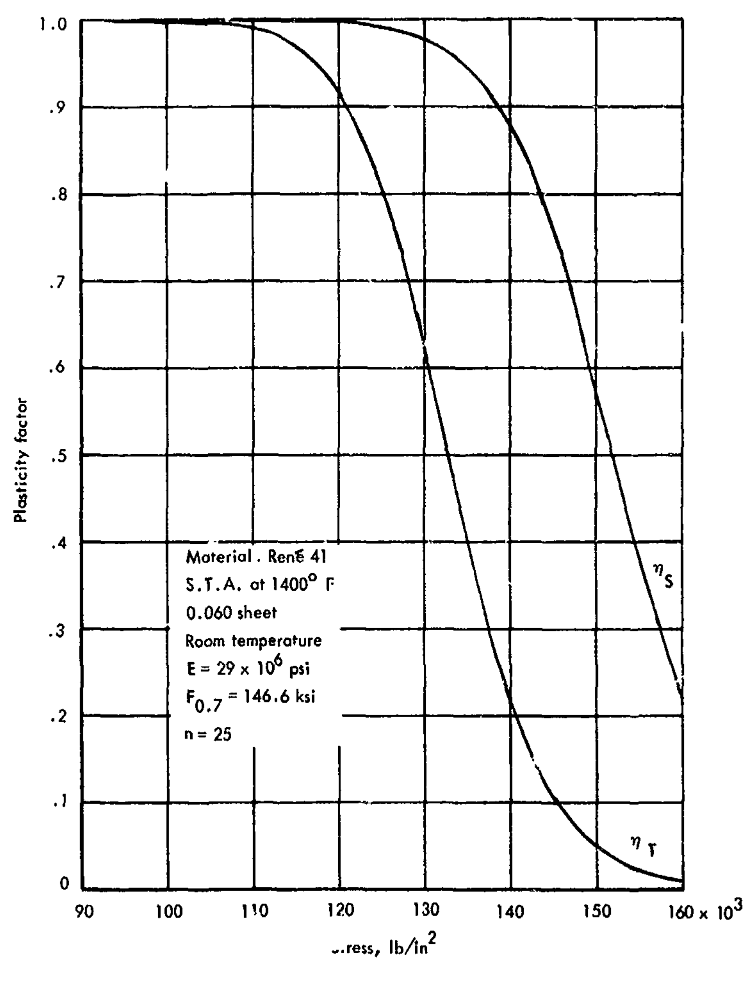

Figure 27-125 Plasticity factors for 0.060-in. Rene' 41 sheet at room temperature